A major purpose of the Technical Information Center is to provide the broadest dissemination possible of information contained in DOE's Research and Development Reports to business, industry, the academic community, and federal, state and local governments.

Although a small portion of this report is not reproducible, it is being made available to expedite the availability of information on the research discussed herein.

DISCLAIMER

ORNL--6120

DE85 006958

PHYSICS DIVISION

PROGRESS REPORT

for Period Ending September 30, 1984

J. B. Ball Director

S. Datz Section Head
E. E. Gross Section Head
C. M. Jones Section Head
J. B. McGrory Section Head
R. L. Robinson Section Head

Edited by: A. B. Livingston

Date Published: January 1985

OAK RIDGE NATIONAL LABORATORY
Oak Ridge, Tennessee 37831
operated by
MARTIN MARIETTA ENERGY SYSTEMS, INC.
for the
U. S. DEPARTMENT OF ENERGY
under Contract No. DE-AC05-84OR21400

Reports previously issued in this series are as follows:

ORNL-2718	Period Ending March 10, 1959
ORNL-2910	Period Ending February 10, 1960
ORNL-3085	Period Ending February 10, 1961
ORNL-3268	Period Ending January 31, 1962
ORNL-3425	Period Ending May 21, 1963
ORNL-3582	Period Ending January 31, 1964
ORNL-3778	Period Ending December 13, 1964
ORNL-3924	Period Ending December 31, 1965
ORNL-4082	Period Ending December 31, 1966
ORNL-4230	Period Ending December 31, 1967
ORNL-4395	Period Ending December 31, 1968
ORNL-4513	Period Ending December 31, 1969
ORNL-4659	Period Ending December 31, 1970
ORNL-4743	Period Ending December 31, 1971
ORNL-4844	Period Ending December 31, 1972
ORNL-4937	Period Ending December 31, 1973
ORNL-5025	Period Ending December 31, 1974
ORNL-5137	Period Ending December 31, 1975
ORNL-5306	Period Ending June 30, 1977
ORNL-5498	Period Ending December 31, 1978
ORNL-5787	Period Ending June 30, 1981
ORNL-6004	Period Ending September 30, 1983

Joseph Lee Fowler

Joe Fowler, director of the Physics Division from 1957 to 1973, died on June 3, 1984.

Moving from Los Alamos to Oak Ridge in 1950, Joe served as director of the high voltage laboratory from 1951 to 1953 and associate director of the Physics Division from 1954 to 1957 before becoming division director. In 1978, he retired from Oak Ridge National Laboratory but continued his appointment as professor of physics at the University of Tennessee. Joe's broad understanding of physics and his skill as an administrator served as an inspiration to all of those privileged to work with him.

SPECIAL DEDICATION

This issue of the Physics Division Progress Report is dedicated to the memory of two of our colleagues, James L. C. Ford, Jr., and Clyde B. Fulmer, who died during this past year.

Jim Ford joined the Physics Division in 1962. He played a lead role in nuclear structure studies with Coulomb excitation, inelastic scattering, and transfer reactions. He was especially active in the design and implementation of new experimental devices such as the time-of-flight facility, the gas-jet target, and a series of position sensitive focal-plane detectors. Since June 1983, Jim had served as Liaison Officer to the Holifield Facility Users Group.

Clyde Fulmer joined the Electronuclear Division (later to merge with the Physics Division) in 1958. Best known for his extensive studies of the elastic scattering process and its interpretation via the nuclear optical model, he also made significant contributions to measurement programs for accelerator shielding and residual radiation problems. For a number of years, Clyde served as the Division Safety Officer and as the Radiation Control Officer.

Both Clyde and Jim brought to the Division not only an ethic of hard work and dedication, but a special love of physics and an intense interest in their work. Between them, their studies resulted in more than two hundred published papers. Above all, their work was marked by an outstanding spirit of cooperation and good humor. They will be missed both as valued colleagues and as good friends.

CONTENTS

2. EXPERIMENTAL NUCLEAR PHYSICS

3. THE UNISOR PROGRAM

4. EXPERIMENTAL ATOMIC PHYSICS

ACCELERATOR-BASED ATOMIC PHYSICS

ATOMIC PHYSICS FOR FUSION PROGRAM

5. THEORETICAL PHYSICS

HEAVY-ION DYNAMICS

NUCLEAR STRUCTURE

THE UNISOR NUCLEAR STRUCTURE THEORY PROGRAM

RELATIVISTIC HEAVY-ION PHYSICS

THEORETICAL ATOMIC PHYSICS

INTRODUCTION

The reporting period covered by this progress report is the 1984 fiscal year beginning October 1, 1983, and ending September 30, 1984. This report marks a return by the Physics Division to issuing these reports on an annual cycle. The research activities of the Division are centered primarily in three areas: experimental nuclear physics, experimental atomic physics, and theoretical nuclear and atomic physics.

The largest of these efforts, experimental nuclear physics, is dominated by the heavy ion research program. A major responsibility under this program is the operation of the Holifield Heavy Ion Research Facility as a national user facility. During the period of this report, the facility has begun routine operation for the experimental program. The Holifield Facility and the internal experimental nuclear physics programs are described in Chapters 1 — 3 of this report.

The experimental atomic physics program has two components: the accelerator-based studies of basic collisional phenomena and the studies in support of the controlled fusion program. These efforts are described in Chapter 4. Also associated with the fusion-related studies are a plasma diagnostics program and the operation of an atomic physics data center. The former is described in Chapter 7, and the latter is discussed in Chapter 9, along with our effort in support of the nuclear data compilation effort.

The theoretical physics program, both nuclear and atomic, is covered in Chapter 5. This program has benefited this year from the success of the VAX-AP computer system and from the increase in manpower provided by the ORNL/University of Tennessee Distinguished Scientist Program.

Smaller programs in applications and high-energy physics are summarized in Chapters 6 and 8.

During the period of this report, we continued to explore possible future extensions of the Holifield Facility. We retain a strong interest in a relativistic heavy-ion collider in the 10 x 10 GeV/nuclear energy range. The ideas for such a facility, described in last year's report, have been modified to utilize the HHIRF 25 MV tandem accelerator as the first stage. This study is summarized in Chapter 10.

Finally, the report concludes with some general information on publications, Division activities, and personnel changes.

1. HOLIFIELD HEAVY ION RESEARCH FACILITY

OVERVIEW

R. L. Robinson J. A. Martin
C. M. Jones

Beginning January 19, 1984, the Holifield Facility began its first period of what is considered typical operation. Since that time, the division of time between beam available for research, development, maintenance, and tuning was near that projected for a normal year. Another indication of normality has been the scheduling of the Program Advisory Committee meetings on a six-month interval.

The three and one-half months prior to January 19 were devoted to (1) a major scheduled maintenance period in which 40 of 54 tandem acceleration tube units were removed, reconditioned, and replaced, and in which several major maintenance tasks were performed on the cyclotron, (2) repair and modification of several tandem accelerator column vacuum related components, and (3) initial conditioning of the tandem accelerator. Following a period of operation for the experimental program and another conditioning period in March, the tandem accelerator was operated with beam at a potential of 22.5 MV, a value which exceeds that achieved both at ORNL and at other laboratories by more than 2 MV. Since then, the facility has provided beams for several experiments at 20 MV or slightly above.

Refinements in the calculations used for determining cyclotron operating parameters have made it possible to increase the extraction radius from 77.5 to 79.2 cm. This seemingly modest change has the impressive effect of reducing power for the main cyclotron magnet at the maximum mass-energy product by 20%, resulting in a 15% reduction in total power use for cyclotron operation. This is especially significant because power is the major incremental cost for coupled operation and because coupled operation has and apparently will continue to be budget-limited.

A total of 3,177 research hours were provided during this one-year reporting period, of which 1,325 were in coupled-mode operation. Some statistics relating to research hours are given in Tables 1.1 – 1.3. Research hours/month are shown in Fig. 1.1. Research hours/month for three of the months in this reporting period exceeded that for any month prior to this period.

Table 1.1. Division of research hours by research activities for the period October 1, 1983 through September 30, 1984

Activity	Research Hours		
	Tandem	Coupled	Total
High-spin states	715	132	847
Fusion	291		291
Damped reactions		286	286
Incomplete fusion		274	274
Atomic	214		214
Charge exchange		171	171
Tests of apparatus	171		171
Pion production		168	168
Quasi-elastic	105	49	154
Giant resonances		123	123
Fission		98	98
Low-lying level properties	98		98
Tests of detectors	71	24	95
Applications	82		82
α-decay rates	56		56
Crystal blocking	49		49
Total	1,852*	1,325*	3,177*

*These numbers differ slightly from those in Tables 1.5 and 1.6 due to rounding errors.

The Spin Spectrometer has clearly proven to be the most popular research tool of this year (see Table 1.3). However, it was recently discovered that nearly half of the 70 NaI crystals have extensive cracks which have caused significant deterioration of the detector parameters. Although the Spin Spectrometer is still adequate for most experiments, those requiring high resolution (such as study of γ-ray emission from giant resonances) must be postponed or compromised.

The highlight for the experimental apparatus took place at UNISOR. The long-awaited atomic hyperfine structure spectrometer demonstrated its capability to investigate mass separated nuclei produced in heavy-ion induced reactions. This was tested with both the ground state and isomeric state in ^{192}Tl. (See Section 3.)

Table 1.2. Number of researchers from different institutions who participated in experiments at the HHIRF in the 12-month period October 1, 1983 through September 30, 1984

Institutions	Number of Researchers
UNIVERSITIES	
Eastern Kentucky Univ.	1
Emory Univ.	2
Georgia State Univ.	3
Georgia Inst. of Tech.	4
Indiana Univ.	2
Louisiana State Univ.	2
Massachusetts Inst. of Tech.	1
Michigan State Univ.	5
ORAU	3
Research Inst. of Physics (Sweden)	3
State University of New York	3
Tennessee Tech. Univ.	1
Texas A&M Univ.	6
Univ. of Claude Bernard Lyon (France)	1
Univ. of Florida	6
Univ. of Frankfurt (Germany)	2
Univ. of Houston	2
Univ. of Kentucky	3
Univ. of Köln (Germany)	1
Univ. of Maryland	7
Univ. of Michigan	1
Univ. of Pittsburgh	2
Univ. of Rochester	2
Univ. of South Carolina	3
Univ. of Tennessee	17
Univ. of Virginia	2
Univ. of Washington	5
Vanderbilt Univ.	10
Washington Univ.	5
Western Kentucky Univ.	1
Yale Univ.	1
	107
NATIONAL LABORATORIES	
Centro Atomico Baralache (Argentina)	1
LANL	5
NASA/Goddard	1
Naval Surface Weapons Lab.	2
ORNL	45
SANDIA	2
	56
INDUSTRY	
Aerospace Corp.	3
RCA	1
	4

Table 1.3. Use of experiment target stations for the period October 1, 1983 through September 30, 1984

	Research Hours (No. of Runs)		
Target Station	Tandem	Coupled	Total
γ-ray spectrometer (tandem)	221(3)	na	221(3)
γ-ray spectrometer (ORIC)	na	46(1)	46(1)
Velocity filter	189(4)	na	189(4)
Atomic physics (tandem)	263(4)	na	263(4)
Atomic physics (coupled)	na	0	0
Split-pole magnetic spectrometer	97(1)	na	97(1)
Applications (Beam line 31)	82(4)	na	82(4)
Beam line C-9	na	272(2)	272(2)
0.8-m chamber	na	0	0
Broad-range magnetic spectrometer	34(1)	244(4)	278(5)
Time-of-flight system	12(1)	189(2)	201(3)
1.6-m scattering chamber	25(2)	318(3)	343(5)
UNISOR	293(15)	0	293(15)
Spin spectrometer	636(7)	256(3)	892(10)
Total	1,852(42)	1,325(15)	3,177(57)

na = not accessible to beam

ACCELERATOR OPERATIONS AND DEVELOPMENT

OPERATIONS

G. D. Alton
J. A. Benjamin[1]
J. A. Biggerstaff
M. R. Dinehart
D. T. Dowling
H. D. Hackler
C. L. Haley
D. L. Haynes
D. E. Hoglund[2]
E. D. Hudson
C. A. Irizarry
C. M. Jones
N. L. Jones
R. C. Juras[3]
S. N. Lane
C. T. LeCroy
R. S. Lord[4]
C. A. Ludemann
J. E. Mann[4]
C. A. Maples
R. L. McPherson
P. Meszaros[5]
G. D. Mills
S. W. Mosko
S. N. Murray
E. G. Richardson
P. T. Singley[6]
C. L. Viar[7]
N. F. Ziegler

The first three and one-half months of this reporting period were devoted to a long scheduled maintenance period for both the

ORNL-DWG-83-17475R

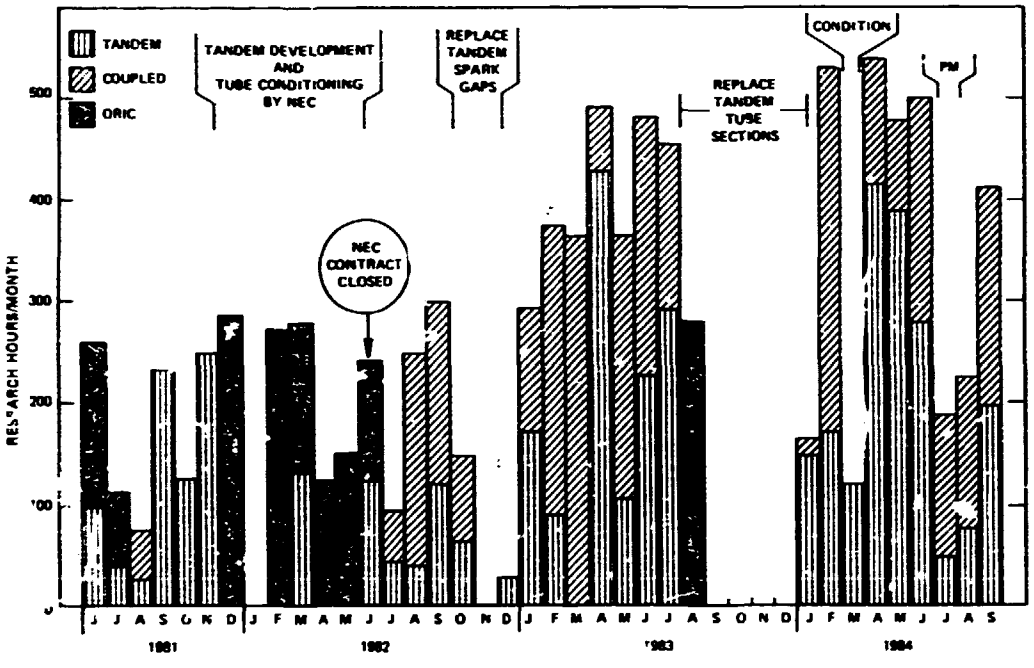

Fig. 1.1. Research hours per month for experiments utilizing the HHIRF accelerators. The interval denoted as PM was a programmed maintenance period.

tandem accelerator and the ORIC, repairs of vacuum related components in the tandem accelerator, and conditioning of the tandem accelerator. No beams were provided for research during this first period. Operation for the research program began in mid-January and continued until the end of this report period with interruptions only for a conditioning period in March, scheduled and unscheduled maintenance, and two major holidays. Thus, "typical" operation was provided for approximately the last three-fourths of the year.

The most striking feature of operation during this reporting period has been a further improvement in reliability and quality of operation. As shown in Fig. 1.1, we experienced three months in which over 500 hours of beam time were provided for research. We have also achieved a noticeable improvement in the degree to which our research schedule is maintained. Major contributors to these improvements were engineering modifications to both the tandem accelerator and the ORIC, installation of the improved radial geometry cesium plasma source described in the last progress report,[8] and increased experience of the operations staff.

A summary of beams provided during this reporting period is presented in Table 1.4. As noted in the table, four ion species (^{10}B, ^{45}Sc, ^{46}Ti, and ^{150}Nd) were provided for the first time. The most notable of these is probably ^{150}Nd which was provided with coupled operation using a separated isotopic sample in the negative ion source. As an illustration of the utility of the tandem accelerator, this beam was provided for a total of 45 hours while using only approximately 2 mg of separated isotopic material.

Table 1.4. Beams provided for research for the period October 1, 1983 through September 30, 1984

Ion Species	Maximum Energy (MeV)	Mode*	Provided for first time in this period
^{10}B	168	C	x
^{11}B	169	C	
^{12}C	135	T	
^{16}O	401	T,C	
^{18}O	352	T,C	
^{19}F	88	T	
^{24}Mg	178	C	
^{28}Si	240	T	
^{32}S	717	T,C	
^{34}S	155	T	
^{35}Cl	692	T,C	
^{45}Sc	200	T	x
^{46}Ti	184	T	x
^{48}Ti	581	T,C	
^{50}Ti	184	T	
^{56}Fe	842	C	
^{58}Ni	916	T,C	
^{64}Ni	290	T	
^{107}Ag	374	T	
^{116}Sn	684	C	
^{150}Nd	760	C	x
^{197}Au	591	T	

*T = Tandem alone; C = Coupled mode.

Utilization analyses for the tandem accelerator and cyclotron are presented in Tables 1.5 and 1.6, respectively. Electric power budgetary limitations continue to restrict cyclotron operation to about 2000 hours per year. Efficient accelerator utilization has been achieved by using the ORIC only in coupled mode and only for energies beyond the capability of the tandem accelerator.

1. Present address: Brookhaven National Laboratory, Upton, NY 11973.
2. Co-op student, Virginia Polytechnic Institute and State University, Blacksburg, VA 24061.
3. Instrumentation and Controls Division.
4. Consultant.
5. Computing and Telecommunications Division.
6. Energy Division.
7. Retired.
8. Physics Division Progress Report for Period Ending September 30, 1983, ORNL-6004 (1983).

Table 1.5. Tandem accelerator utilization for the period October 1, 1983 through September 30, 1984

	Hours	Percent
Beam available for research (tandem-alone and coupled operation)	3172	36
Beam available during ORIC tuning (coupled operation)	340	4
Accelerator tuning (includes scheduled startup-shutdown)	638	7
Machine studies (includes conditioning not required for specific experiments)	837	10
Unscheduled maintenance	1677	19
Scheduled maintenance	1816	21
Scheduled shutdown	304	3

Table 1.6. Cyclotron utilization for the period October 1, 1983 through September 30, 1984

	Hours	Percent
Beam available for research (coupled operation)	1331	15
Accelerator tuning (includes scheduled startup-shutdown and operation during tandem tuning)	494	6
Machine studies	130	1
Unscheduled maintenance	205	2
Scheduled maintenance	1376	16
Scheduled shutdown	5248	60

TANDEM ACCELERATOR

G. D. Alton
J. A. Benjamin[1]
J. A. Biggerstaff
D. L. Haynes
D. E. Hoglund[2]
C. M. Jones
R. C. Juras[3]
J. E. Mann[4]
E. G. Richardson
N. F. Ziegler

Voltage Performance

As discussed in the previous progress report,[5] initial voltage performance of the tandem accelerator was somewhat disappointing. Thus, a major maintenance period was planned for the period August through October 1983, with the primary motivation of improving tandem accelerator voltage performance. During this period, 40 of 54 acceleration tube units were removed, reconditioned at the National Electrostatics Corporation plant in Madison, Wisconsin, and reinstalled in the accelerator. Also during this period, all magnetic electron traps were removed and ports were installed for possible future hydrogen arc discharge cleaning of the accelerator.

Following repairs and modifications of vacuum related components in the column, conditioning of the accelerator began in mid-December 1983, and continued until mid-January 1984. Progress during this period was encouraging and the accelerator was operated at the end of the period with beam at a terminal potential of 20.2 MV, a new ORNL and world's record. This conditioning period was terminated in order to begin operation for the experimental program and to allow further improvement in vacuum. A second conditioning period was scheduled for March 1984. At the end of this period the accelerator was operated with beam at 22.5 MV, again a new record.

Although operation at unusually high terminal potentials was not a primary goal for our experimental program in FY 1984, voltage performance of the accelerator during this period was also encouraging. As shown in Fig. 1.2, six experimental runs have been performed at or above 19 MV and three experimental runs have been performed at or above 20 MV. The highest of these was 20.3 MV. During all operation in FY 1984 (both conditioning and operation for the experimental program) only 21 full column sparks occurred of which only two resulted in observable deconditioning. This low spark rate, the ease with which we have operated for experiments at or above 20 MV, and the absence of observed deterioration in voltage performance with time, all suggest that the voltage capability of the

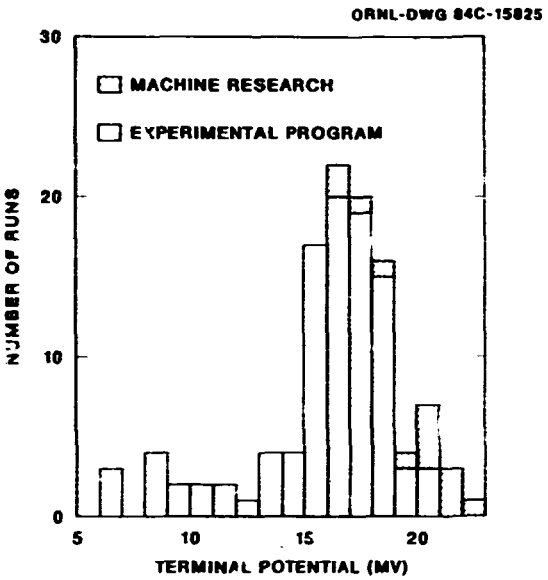

Fig. 1.2. The number of runs in 1-MV-wide intervals is shown as a function of tandem accelerator terminal potential for the period October 1, 1983 through September 30, 1984.

accelerator in its present configuration has not been fully exploited.

Two further initiatives to improve voltage performance are now planned. These are a hydrogen arc discharge cleaning or conditioning procedure and a modification of the present acceleration tube geometry which increases the active insulator length by 18%. Both are discussed in greater detail in other contributions to this report. The acceleration tube modification has been proposed as a FY 1986 AIM project.

Improvements and Modifications

Although our primary focus in this reporting period was on improved voltage performance and operation for the experimental program, a number of important improvements and modifications were also made to the accelerator system.

Within the column, ventilation and cooling were improved for both terminal and dead section electronics. Positive sublimator slug selection readout was provided for the terminal gas stripper pump and voltage monitoring was added for column ion pumps. Variable apertures, Faraday cups, and the terminal gas stripper were all modified to minimize motion feedthrough bellows failures. Three of six charging chains were removed to increase reliability and to provide an immediate source of spare parts in the unlikely event of chain breakage.

Outside the accelerator vessel, cryopumps were installed on both the low-energy and high-energy beam lines for maintenance use. In addition, a 3-foot diameter by 7-foot long pressure vessel was purchased to enable off-line pressure testing of accelerator components.

Control system improvements include expansion of the system to include additional injector parameters and all parameters on experimental beam line 2I. In addition to a number of detailed improvements to the control system operating program, two other important software tasks were completed. The automatic logging program was extensively revised so as to operate more easily and reliably. New programs were written to provide information on stripper foil parameters such as equilibrium thickness, angular dispersion, energy loss, and lifetime.

One of the most important improvements of FY 1984 was final commissioning and installation in the injector of the new radial geometry cesium plasma ion source described in the previous progress report.[5] While retaining the versatility and prolificacy of its predecessor, the "Mark I" ORNL version of the Aarhus radial extraction Penning Source,[6] the new source has proved to be more reliable, easier to service, and simpler to operate. It was used exclusively during FY 1984 and was a significant factor in the improvement in accelerator system utilization described above. The ion species provided during this period are listed in Table 1.4.

SF_6 System Operation

Operation of the SF_6 storage and recirculation system in FY 1984, including fifteen and one-half gas transfers to and from storage was without incident. Within the approximately 2% accuracy of the SF_6 weighing system, no SF_6 loss was observed.

---

1. Present address: Brookhaven National Laboratory, Upton, NY 11973.
2. Co-op student, Virginia Polytechnic Institute and State University, Blacksburg, VA 24061.
3. Instrumentation and Controls Division.
4. Consultant.
5. Physics Division Progress Report for Period Ending September 30, 1983, ORNL-6004, (1983).
6. G. D. Alton and G. C. Blazey, Nucl. Instrum. Methods 166, 105 (1979).

ORIC ACCELERATOR

D. T. Dowling R. S. Lord[1]
E. D. Hudson C. A. Ludemann
S. N. Lane J. A. Martin
S. W. Mosko

Coupled Operation

During the period of this report, 16 experiments have been completed using coupled operation of the cyclotron and tandem accelerator. Some details of coupled operation are given in Table 1.7. The heaviest ion accelerated was $^{150}Nd^{+33}$; the highest energy obtained was 916 MeV for $^{58}Ni^{+23}$. Beam currents obtained were generally consistent with predictions, taking into account the expected fraction of beam in the desired charge state and the buncher efficiency (~ 50%). The highest tandem voltage used was 18.8 MV.

Coupled operation was generally more reproducible and beam extraction efficiencies were higher than experienced last year. These improvements are a result of refined computational methods for beam setup and the use of

Table 1.7. Coupled operation for research for the period October 1, 1983 through September 30, 1984

Date	Ion	Desired Energy (MeV)	Actual Energy (MeV)	Extraction Efficiency (%)	Injected Ion	Injection Energy (MeV)	Tandem Voltage (MV)
2/5/84	$^{32}S^{+15}$	700	717	48	$^{32}S^{+6}$	122.8	17.5
2/19/84	$^{18}O^{+8}$	350	351.7	65	$^{18}O^{+3}$	67.9	16.9
4/7/84	$^{16}O^{+8}$	400	400.7	68	$^{16}O^{+3}$	67.5	16.8
4/9/84	$^{16}O^{+8}$	400	401.1	60	$^{16}O^{+3}$	67.5	16.8
5/8/84	$^{56}Fe^{+22}$	820	841.7	76	$^{56}Fe^{+8}$	170.0	18.9
6/15/84	$^{32}S^{+12}$	320	317.8	55	$^{32}S^{+3}$	66.9	16.6
6/19/84	$^{11}B^{+5}$	170	168.9	68	$^{11}B^{+2}$	38.4	15.9
6/22/84	$^{10}B^{+5}$	170	168.3	78	$^{10}B^{+2}$	39.6	16.0
6/27/74	$^{16}O^{+8}$	400	399.7	~100	$^{16}O^{+3}$	68.0	16.9
7/6/84	$^{35}Cl^{+16}$	700	692.1	75	$^{35}Cl^{+6}$	124.5	17.7
8/8/84	$^{16}O^{+7}$	208	206.6	61	$^{16}O^{+2}$	32.6	10.8
8/14/84	$^{24}Mg^{+8}$	180	177.6	64	$^{24}Mg^{+2}$	20.1	6.6
8/17/84	$^{150}Nd^{+33}$	750	760.7	67	$^{150}Nd^{+13}$	211.0	15.1
9/11/84	$^{58}Ni^{+23}$	900	916.0	68	$^{58}Ni^{+9}$	170.4	17.0
9/13/84	$^{48}Ti^{+17}$	576	581.4	56	$^{48}Ti^{+6}$	92.9	13.3
9/25/84	$^{116}Sn^{+29}$	700	684.1	78	$^{116}Sn^{+7}$	144.9	18.8

more systematic methods in tuning the beam through the extraction system.

It is well known that when the value of the radial focusing frequency, ν_r, is close to unity, the separation between orbits can be enhanced at a given azimuth by the introduction of a first harmonic component in the magnetic field. Such enhanced turn separation, if achieved at the electrostatic deflector entrance, normally leads to higher extraction efficiency, but, if it occurs at the wrong azimuth, it can drastically reduce the extracted beam. Turn separation enhancement would normally be achieved by the use of harmonic coils; however, essentially the full capacity of the harmonic coils is used in canceling the harmonics introduced by the extraction system.

By computation with the beam setup programs, it has been discovered (and confirmed by beam position measurements) that the compensated-iron extraction channel can produce a first harmonic component that suitably enhances turn separation when the channel currents are unbalanced. Using this technique, we have been able to: (1) extract beam at larger radii, reducing magnet power usage for a given energy; (2) improve average extraction efficiency from about 30% to about 70%; (3) improve the accuracy of the prediction of extracted beam energy; and (4) by careful adherence to the computer predicted settings, substantially reduce the time required to achieve extracted beam.

Cyclotron Development

Power Supplies. A program to upgrade dc power supplies throughout the Holifield facility is continuing. Several new SCR regulated power supplies, including those for the cyclotron harmonic coils and beam line bending magnets, were put in service during the past year. Thus far, our results with this type power supply have been very encouraging. The SCR regulated units rely upon high load reactance and the use of precision external sensing elements such as high voltage shunts (1 volt or greater) or dc current transformers (transductors) to achieve good regulation and low ripple. The motor generator set (two 1.75 MVA generators), which provides excitation for the cyclotron main field and compensated-iron magnetic channel outside coil, was overhauled. Its commutators were turned, ground, and undercut. This was the first major commutator servicing since the machine was installed about 24 years ago. Prior to the overhaul, we were experiencing magnet instability and short brush life (about 30 to 60 days). Stability has improved, and the brushes installed nearly a year ago are still in service.

RF System. The dee aperture was reduced from 2.5 cm to 2.2 cm in order to increase dee liner spacing on each side by 0.15 cm. The resultant reduction in dee to liner capacitance produced a slight shift in resonant frequency (an increase of ~ 0.2 MHz) and a reduction in excitation power at the upper end of the tuning range. The rf system is now operable over a 6.69 to 19.8 MHz tuning range. Previously it was tuneable but unstable above 18.0 MHz. An additional 0.2 cm aperture reduction is being considered with the hope of achieving a full 3:1 tuning range.

Vacuum System. Efforts by the manufacturer to achieve satisfactory performance from the 20-inch cryopump on the rf resonator tank were unsuccessful. The pump and compressor made several return trips to the factory for modifications and repairs, but were still showing symptoms of excessive heat loading. Consequently, we added a 16" aperture plate between the pump and gate valve which serves as a heat shield with only slightly increased pumping

impedance. The pump has now demonstrated several weeks of operation with acceptable pumping speed and base pressure.

New ORIC Control Computer

A MODCOMP Classic/55 has been purchased to replace the 12-year-old ORIC control computer. This processor was selected because approximately 90% of the existing control programming will operate on this software compatible machine. The new hardware will insure the long-range availability of spare components as well as reliability of the system. Of equal importance, the increased size of memory and disk storage will enhance the capability for software development. This will relieve the bottleneck that has been experienced in improving the operation monitoring software. Furthermore, operation parameter analysis programs will eventually lead to improved understanding of machine performance. This will be achieved by making detailed comparisons between parameters predicted by our mathematical cyclotron model and the actual settings used to produce an ion beam. Additional programs will be written that provide a data base for evaluating machine performance. This system is expected to be in operation by mid-1985.

Improved Beam Extraction Magnets

We have shown that it is possible to use the compensated-iron magnetic extraction channel to provide a desirable first harmonic in the cyclotron magnetic field to provide turn-spacing enhancement for improved beam extraction. However, the computations required to do this are tedious and very time-consuming and the derived settings usually require modification during cyclotron tuning.

The difficulty in accurately predicting settings of the cyclotron extraction system and harmonic coils results principally from the imperfect design of the compensated-iron magnetic channel and, to a lesser extent, of the coaxial magnetic channel. The arrangement of the beam extraction system is shown in Fig. 1.3. The beam extraction channels must provide magnetic field reductions of ~ 6 kG along the extracted beam path while producing very low external magnetic fields (ideally < 10 G) in the beam acceleration region. Presently, both channels produce excessive first harmonic external magnetic field components. Design improvements are now in progress which will result in a factor of 5 reduction in the harmonic contribution of the coaxial channel and an even greater reduction of the harmonic contribution of the compensated-iron channel. These improvements will effectively separate the function of field reduction for extraction from the function of turn separation enhancement, shifting the latter to the harmonic coils as was originally intended. Separation of functions should simplify computation and tuning procedures.

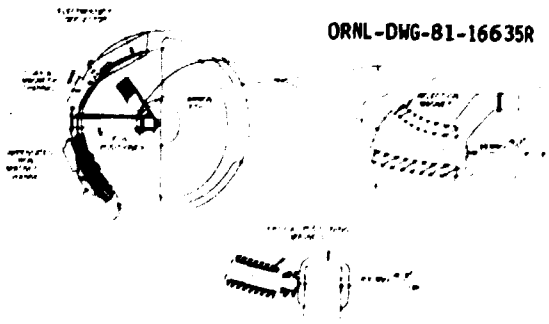

Fig. 1.3. Cyclotron beam extraction system.

Reduction of the external field of the coaxial magnetic channel can be accomplished by modifying only the portion of the channel known as the "insert." This is a removable section which contains the conductors closest to the beam. Reshaping the cross section and longitudinal configuration of these conductors, as shown in Fig. 1.4 (a) and (b), reduces the first harmonic coefficient of the external field close to the channel by factors of 5 to 9 depending on distance from the channel (Table 1.8). Design studies and computations for this change are complete and engineering drawings are being prepared.

The proposed new design for the compensated-iron channel (Fig. 1.5) is based on a cosine distribution of currents in two circuits inside and outside a cylinder of iron — with modifications to accommodate the realities of fabrication. The present design, in use since 1963, employs a linear distribution of currents about a rectangular iron box (Fig. 1.6). The external fields of the two channel designs are compared in Fig. 1.7. For this

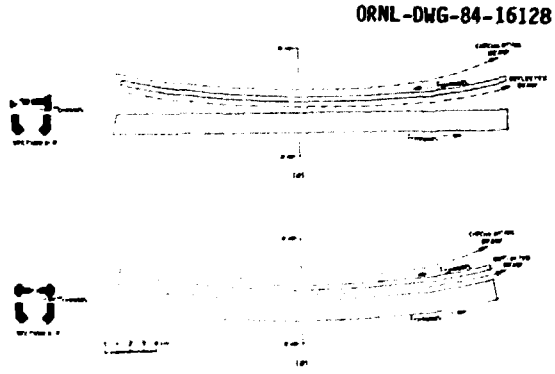

Fig. 1.4. Configuration of the present coax insert conductors (a), and of the proposed insert design (b). Both the detailed cross section and the longitudinal shape have been changed to achieve a lower field in the circulating beam region.

Table 1.8. External field of coaxial magnetic channel

Radius-centimeters	1st harmonic-gauss: Present coax	1st harmonic-gauss: Proposed coax
76.2	1.0	0.2
81.3 (coax entrance)	14.3	1.6

ORNL-DWG 84-16127

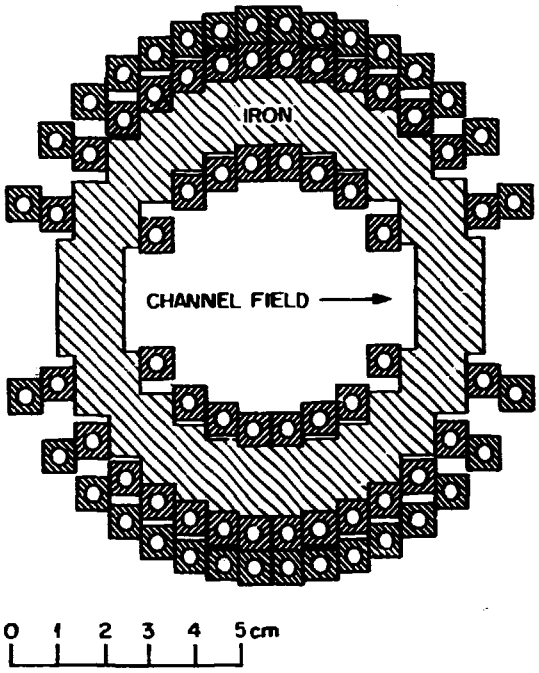

Fig. 1.5. Cross section of proposed new compensated-iron channel. Two layers of coils in one circuit are used inside the iron cylinder. The layer of coils outside the iron forms a second circuit.

ORNL-DWG 84-16125

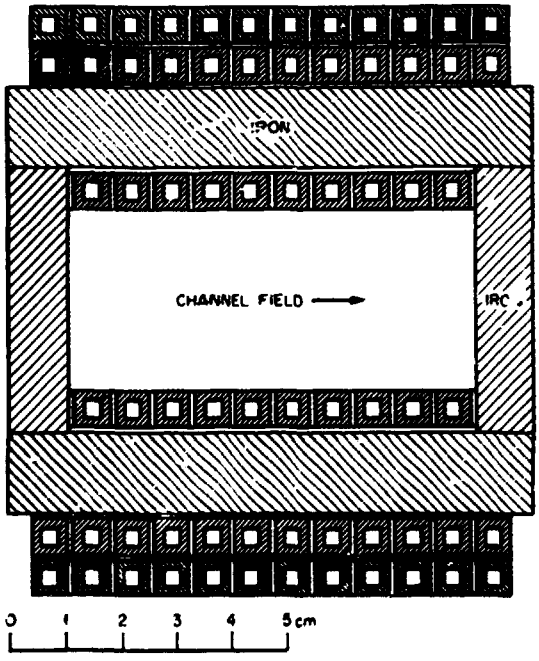

Fig. 1.6. Cross section of the existing compensated-iron channel with inside and outside coils.

ORNL-DWG-84-16126

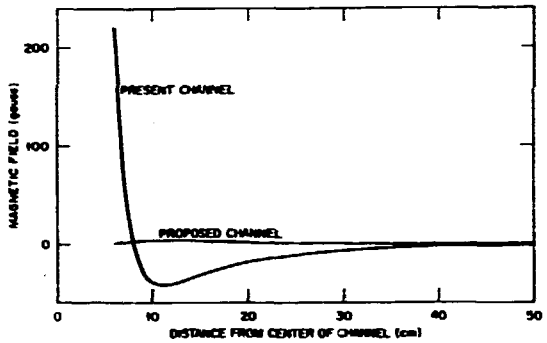

Fig. 1.7. External field of existing and proposed compensated-iron channels.

figure the currents of the proposed channel have been adjusted to produce zero field 6 cm from the center of the channel — approximately the location of the closest circulating beam orbit. Using the present channel, the best that can be achieved in minimizing the external field gives zero field at 8 cm and a substantial deviation from zero over a wide region. The external field of the present channel varies with the level of field reduction required for the extracted beams and must be largely compensated by the harmonic coils, leaving little or no ability to control turn separation with these coils.

Design studies for the new compensated-iron channel are nearly complete and engineering will begin soon.

Dual Arc Penning Ion Source Gas Flow Experiments

Previous experiments have shown that the addition of an easily ionized heavy gas (krypton or xenon) to the arc chamber of a Penning discharge ion source increases the output of multicharged lighter ions, for example, nitrogen and oxygen.[2,3] In a refinement of this technique, an auxiliary arc chamber, for support gas, was added to the ORIC internal ion source. This also results in an increase in the beam intensity for multicharged ions such as $^{16}O^{5+}$. To clarify the mechanism of this intensity increase, gas flow rates from the auxiliary chamber to the main chamber have been measured by using the ORIC cyclotron as a mass spectrometer. The results (Fig. I.8) show that only about three percent of the gas admitted to the auxiliary chamber reaches the main chamber. One can then infer that the improved operation probably results from the stabilizing effect of heating the common cathodes with the auxiliary arc and/or the more favorable distribution of the support gas to the part of the main arc close to the cathodes.

---

1. Consultant.

2. E. D. Hudson and M. L. Mallory, Nucl. Instrum. Methods, 141, 381 (1977).
3. E. D. Hudson and M. L. Mallory, IEEE Trans. Nucl. Sci. NS-24, No. 3, 1590 (1977).

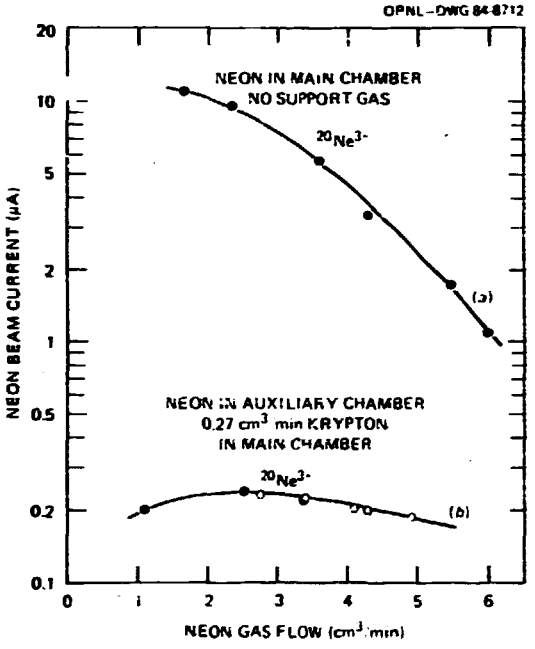

Fig. 1.8. Curve (a) is the intensity of $^{20}Ne^{3+}$ when neon is admitted to the main chamber with no support gas. Curve (b) is the $^{20}Ne^{3+}$ intensity with krypton support gas in the main chamber and neon in the auxiliary chamber.

NEGATIVE ION SOURCE DEVELOPMENT

Evaluation of the Axial Geometry Negative Ion Source

G. D. Alton

The radial geometry negative ion source[1] used in routine tandem accelerator operations can be readily converted to an axial geometry source by an almost trivial modification. The source, which has been briefly described previously,[1] is the second iteration of a similar source, designed and developed in 1978, with superior mechanical design features and rather different performance characteristics. The present source utilizes a solid tungsten annular ionizer with a noninductively-wound tungsten heater instead of the helically-wound tantalum heater which was incorporated in the original source for producing the positive cesium ion beam used to sputter the material of interest. This ionizer was chosen because it offers a simple but well-defined ion generation surface which is more amenable to numerical analysis than the conventionally used helical geometry ionizer. In the present design, ions are generated from the inner surface of the ionizer and all other heated surfaces are obscured from the electric field region of the source. Consequently, the sputter pattern exhibits only a weak halo surrounding the usual concentrated wear pattern located on axis.

The geometrical configuration is readily amenable to simulation by solving Poisson's equation numerically for the electrode system. Computer assisted design techniques were employed by performing detailed calculations of the positive and negative ion trajectories through the electrode system prior to expenditure of funds for engineering or construction of component parts of the source. An example of the positive ion optics of the ionizer/sputter probe region of the source is shown in Fig. 1.9. The computed positive ion current density resulting from the positive ion impact is shown in Fig. 1.10.

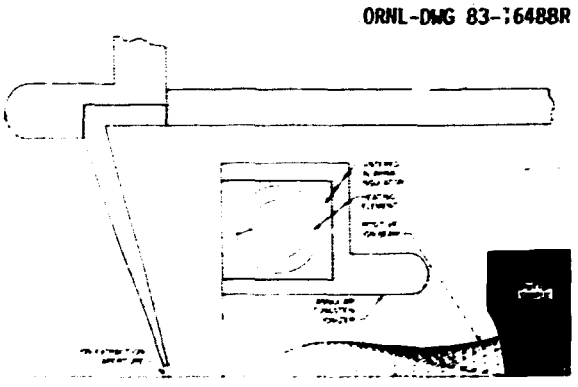

Fig. 1.9. Positive ion optics of the ionizer/sputter probe region of the axial plasma negative ion source.

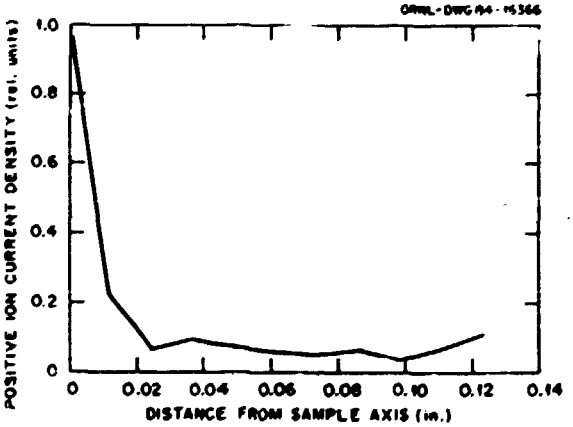

Fig. 1.10. Variation of the positive ion current density with distance from sample axis in the axial geometry negative ion source.

The source performed immediately and as predicted, without further development. For example, the observed sample wear pattern was found to be identical in almost all details with that predicted from Fig. 1.10.

Test stand operational experience with the source indicates that the source is reliable, long-lived, stably operating and a prolific producer of a wide spectrum of negative ions. The source has been used to produce beams of Ag^-, Au^-, Cu^-, Lu^-, Mo^-, Ni^-, Tm^-, and Yb^-, with respective total negative ion beam intensities of 16, 50, 57, 0.37, 1.4, 59, 0.10, and 5 μA when operated at optimum cesium oven temperatures and at 1000 volts dc impressed on the sputter probe. Negative ion yields exhibit maxima at an optimum cesium oven temperature of ~ 260°C. This behavior is identical to that observed for the radial geometry source. The total negative ion yields from this source increase strongly with voltage over a range of probe voltages up to 1100 V dc according to V^h where V is the probe potential and h is a number with value 3.5 to 4.0.

The source has been incorporated as an on-line source along with the radial geometry source for routine 25-MV tandem operation.

Pulsed Negative Ion Source Developments

G. D. Alton

Consideration of a synchrotron as an energy booster for HHIRF tandem accelerator ion beams and as a high energy, heavy ion collider for which the tandem accelerator would serve as an injector has stimulated interest in developing pulsed-mode negative ion sources. During the period of this report, a project was initiated to develop and evaluate negative ion sources and the associated pulsing technology required for injection into such accelerators. Typical pulse widths and repetition rates for synchrotron injection applications are ~ 100 μsec and a few Hz, respectively. Due to interbeam scattering effects in the synchrotron, maximum beam intensities will be limited to peak currents of ~ 200 μA at injection into the tandem accelerator — an intensity which, however, far exceeds the dc negative ion beam intensities of existing negative heavy ion sources. This requirement poses a challenge for the production of a wide variety of negative ion beams of this magnitude for pulsed-mode operation. However, it is known from previous work at the Brookhaven National Laboratory[2] that such pulsed beam intensities can be produced for a limited number of elements with high electron affinities and that such large, low duty-cycle beams can be injected into MP type tandem accelerators without detrimental effects to the operational stability of the accelerator. The pulsed source development project presently underway was initiated with the objectives of evaluating the performance of existing negative ion sources in pulsed mode and development of pulsed beams for tests using the HHIRF tandem accelerator.

An off-ground platform was acquired for housing standard power supplies as well as the special pulsed high-voltage power supply required for source operation in the pulsed mode. A pulsed high-voltage power supply with the desired output characteristics, in terms of voltage amplitude, pulse width and repetition rate, was located within the Physics Division.

Both the radial and axial geometry cesium plasma negative ion sources, described in the previous report,[1] were evaluated. A schematic diagram of the power supply arrangement utilized during testing is shown in Fig. 1.11.

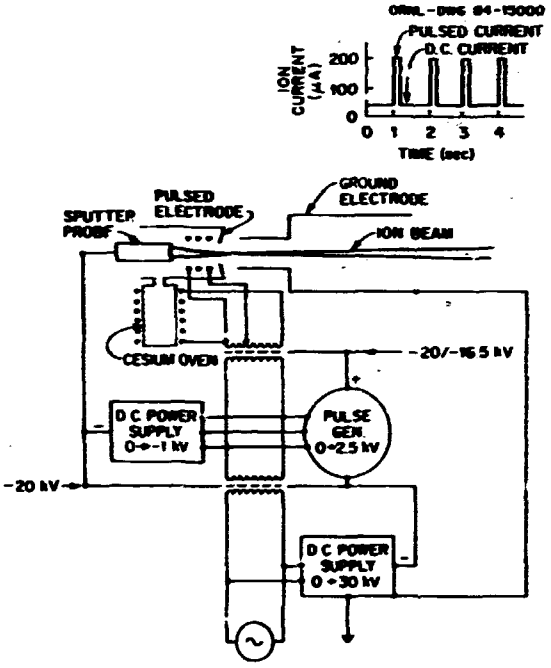

Fig. 1.11. Schematic electrical diagram of the power supply arrangement used during pulse testing of negative ion sources.

Negative ions are generated in these sources by cesium ion sputtering of a probe containing the material of interest which is biased negative by 1 → 3 kV relative to the source housing. The probe potential is maintained at a dc bias level for standard operation and a combination of a dc potential and superposed ac potential from the pulser power supply for pulsed operation. With the arrangement shown, a dc beam of modest intensity (< 1 μA typically) can be generated for use as a signal for tandem terminal voltage control and as a beam for optimization of beam line optical elements to assist in transmission of the superposed pulsed beam through the accelerator and beam transport system.

Preliminary comparative pulse testing of the radial and axial geometry sources showed the distinct superiority of the axial geometry

source for pulsed-mode generation of Au^-, Ni^- and Cu^- negative ion beams. During testing, the pulser amplitude voltage was operated at 1.2 kV with a pulse width of ~ 100 μsec and a repetition rate of 10 Hz. The negative ion yields from the radial geometry source for the indicated elements were typically ~ 60 μA/pulse while those from the axial geometry source were much higher. Negative ion yield spectra, shown in Fig. 1.12, from the indicated elements were 100, 250, and 350 μA peak pulse intensity for Au^-, Ni^-, and Cu^-, respectively.

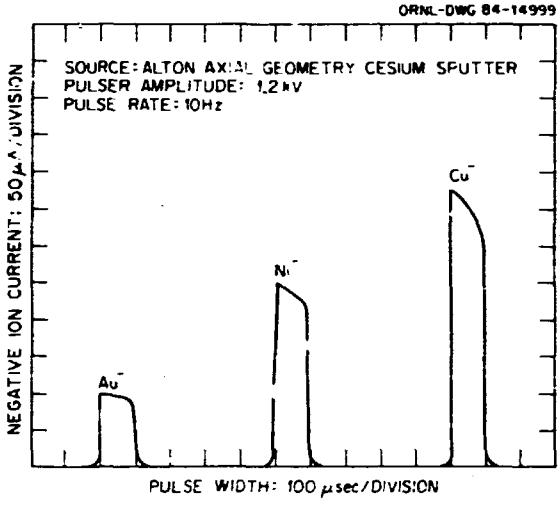

Fig. 1.12. Negative ion yields of Au^-, Ni^- and Cu^- from the axial geometry negative ion source operated in the pulsed mode.

The negative ion yields from the axial geometry source were found to vary linearly with pulse voltage amplitude and, in most cases, the pulsed amplitude and dc amplitude were found to be essentially independent of each other, i.e., the dc beam could be reduced without affecting the amplitude of the ac component. This independence is very important in practice because a weak dc beam component is desirable for control and monitoring of the accelerator while transmitting the largest possible ac beam component which is compatible with synchrotron requirements. The voltage amplitude from the pulsed power supply was limited to ~ 1.5 kV during testing due to stress limitations of the high-voltage cabling. Future tests will include operation of the source at pulse voltages up to 4 kV and injection through the 25-MV tandem accelerator. Much higher beam intensities are anticipated at the higher voltages and therefore we expect a wider range of negative ion species with intensities adequate for synchrotron utilization.

Production of Ca^- Through Double Charge Exchange With Li^+ Vapor

G. D. Alton T. J. Kvale[3]
D. J. Pegg[4]

Negative ion formation through sequential double charge exchange interactions between an initially positive energetic ion and a suitably chosen exchange vapor offers perhaps the most universal and efficient means of producing negative ions known to date. Production efficiencies depend primarily on ion energy, the electron affinity of the element under consideration, and the electron binding energy and density of the exchange vapor. This mechanism offers, as well, a practical and efficient means of producing useful negative ion beams from elements which have negative electron affinities. These ions often may be formed with relatively high efficiency in metastably-bound excited states which may live long enough to be of use for accelerator applications. The Group IIA elements are examples of ions that are well suited for charge exchange production since they are difficult to produce by other means.

The Group IIA elements (Be, Mg, Ca, Sr, and Ba) have negative ground-state electron affinities and thus do not form stable ground-state atomic negative ions. Therefore, other techniques must be employed for the production of these elements. For example, some of these elements (Be^- and Ca^-) can be formed through charge exchange in metastably-bound, autoionizing states which have lifetimes long enough to be of practical value.[5,6]

A major experimental effort has been initiated during this fiscal year using the Negative Ion Source Test Facility (NISTF)[7] and the universal charge exchange source.[1] These experimental investigations are designed to measure production efficiencies as a function of exchange vapor density and projectile energy as well as the atomic properties of the negative ions generated. Calcium was chosen as the first of the Group IIA elements to be investigated because of the considerable interest in this species for nuclear and atomic physics research. Production efficiencies as a function of exchange vapor density and projectile energy over an extensive energy range have never been reported for this ion.

The Negative Ion Source Test Facility has been extensively modified to accommodate research on the charge exchange mechanism and the properties of negative ions generated by this mechanism. In addition to the universal charge exchange source described previously, the facility has been equipped with a post momentum analysis charge exchange cell, the ancillary equipment necessary to perform such measurements, and a CAMAC-based data multichannel analysis/microprocessor system for data acquisition and analysis.

A schematic diagram of the experimental equipment used in measuring the production efficiency of Ca^- is shown in the accelerator-based atomic physics section of this report and therefore will not be included here. A momentum analyzed beam of Ca^+ is focused by means of a lens through the charge exchange cell and the emerging positive, neutral and negative ion components are separated by means of a specially designed electrostatic deflection system. The negative and positive ion beams are monitored in biased and shielded Faraday cups immediately following the deflection plate system. Two experiments

are in progress which deal with the measurement of the production efficiencies and auto- and collisional-detachment properties of Ca^- ions formed in double-charge exchange with neutral lithium vapor. The first of these experiments is described here; the latter experiment is discussed in the accelerator-based atomic physics section of this report.

Two principal determinations are of practical importance in the production of negative ions through charge exchange: (1) the measurement of the production efficiency as a function of target thickness, and (2) the dependence of the efficiency on projectile energy.

Preliminary results from these measurements for the production of Ca^- in lithium vapor are shown in Figs. 1.13 and 1.14. The optimum efficiency for this interaction occurs at a cell temperature of ~ 625°C for these data, as noted in Fig. 1.13. However, the optimum cell temperature is expected to be projectile energy dependent. This dependence is presently being investigated. The efficiency versus projectile energy is shown in Fig. 1.14. Work on this project will continue during the next fiscal year.

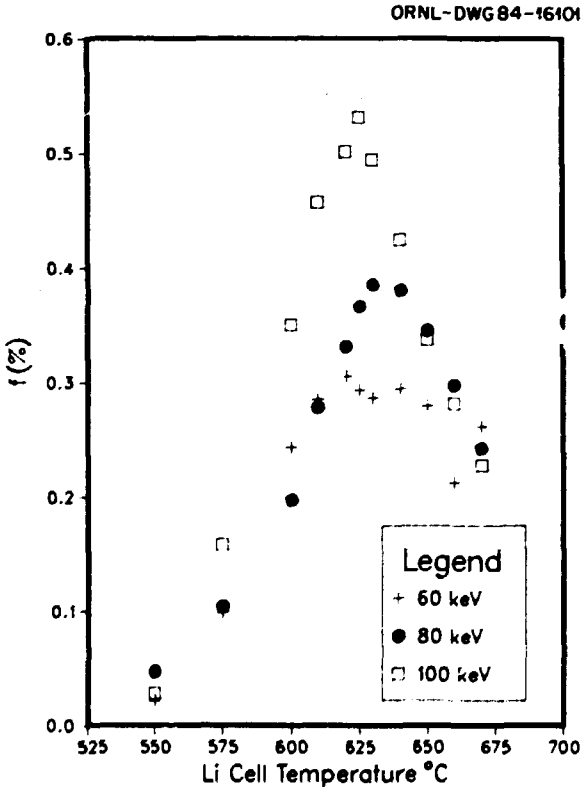

Fig. 1.13. Ca^- production efficiency of as a function of Li charge exchange cell temperature.

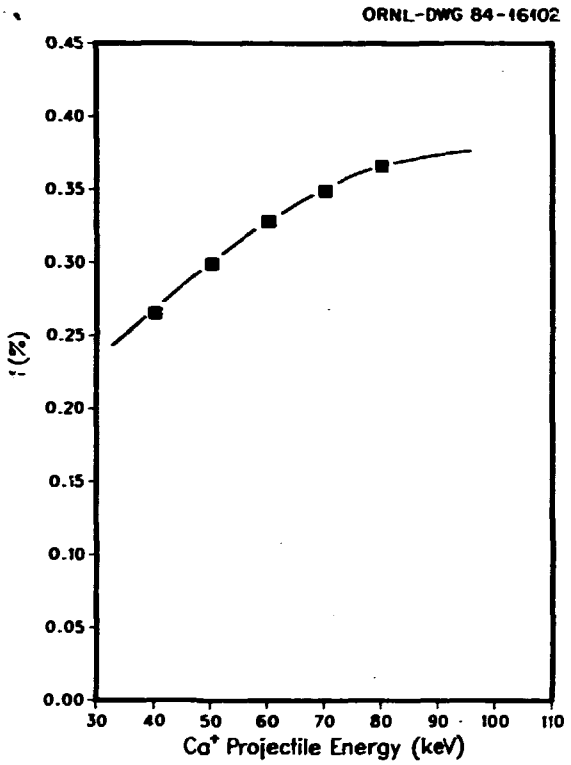

Fig. 1.14. Dependence of the optimum efficiency on Ca^+ ion energy.

Sputter Ratios for 0.4 - 50 keV Cs^+ Ions Using Sigmund Theory

G. D. Alton D. H. Olive[8]

In recent years, the sputter process has been utilized in positive ion source applications to provide vapor for subsequent electron impact ionization and in negative ion sources as a means of ejecting neutral particles through a surface covered with minute amounts of Group IA elements in the production of negative ions through surface ionization processes.

The type and quantity of secondary ions emitted as a consequence of sputtering is affected by the work function as well as by damage-induced effects. Positive surface ionization is enhanced by raising the surface work function, while negative surface ionization is enhanced by lowering the surface work function. In recent years, the sputter process, in combination with the work function lowering aspects of Group IA elements, has been utilized as a versatile and relatively efficient means of producing negative ions. In such sources, cesium is usually utilized because of ease of vaporization, high sputtering coefficient and greater work function lowering capabilities.

Although there is a considerable amount of experimental sputtering data available for a variety of energetic projectile-target combinations, there is little data available for the sputtering of solids with cesium ions. Such data is important to the negative ion source specialist who must estimate the lifetime of samples subjected to sputtering and minimize the amount of material required for a particular negative ion generation period. Hence, for such applications, there is a distinct need for a relatively accurate means of predicting cesium ion sputter coefficients — the primary objective of this report.

To date, the most widely accepted theory of sputtering is the Sigmund theory[9] which assumes that the sputtering of target atoms is a consequence of the formation of cascades of elastic atomic collisions set in motion by energetic ions as they slow down in a homogeneous medium.

By solving the Boltzmann transport equation and using results from linear cascade theory and elastic scattering theory, Sigmund was able to extract analytical formulas appropriate for low- and high-projectile energies.

The sputter coefficient, S, relations appropriate for the indicated ranges of projectile energies are

$$S(E,\theta) = \frac{3\lambda\alpha E}{\pi^2 4U_0(\cos\theta)^F} \quad \text{(for } E < 1000 \text{ eV)} \quad (1)$$

$$S(E,\theta) = \frac{0.042\alpha S_n(E)}{U_0(\cos\theta)^F} \quad \text{(for } E > 1000 \text{ eV)} \quad (2)$$

where,

α is a tabulated function of the ratio of the target mass M_2 to projectile mass M_1,

U_0 is the heat of sublimation of the target,

θ is the angle between the incident projectile and the surface normal,

F usually has values between 1 and 1.7, depending on the ratio of target to projectile masses.

$\lambda = 4M_1M_2/(M_1 + M_2)^2$,

$S_n(E) = 4\pi Z_1 Z_2 e^2 a_{12}[M_1/(M_1 + M_2)]S_n(\varepsilon)$,

Z_1, Z_2 are the respective projectile, target atomic numbers,

$a_{12} = 0.8853a_0(Z_1^{2/3} + Z_2^{2/3})^{-1/2}$,

a_0 is the radius of the first Bohr orbit,

$S_n(\varepsilon)$ is the projectile stopping power in the target,

$$\varepsilon = \frac{M_2E/(M_1 + M_2)}{Z_1Z_2e^2/a_{12}}$$

While the theory predicts shapes of target sputter coefficients versus projectile energy in good agreement with experimental data, calculated magnitudes are generally in poor agreement with experimental observation.

Experimentally, sputter coefficients are found to vary periodically while monitonically increasing with projectile mass.[10] These deviations are, in part, attributable to the many approximations and deletions made in the derivation and the assumption of a homogeneous distributed target when in reality most targets are polycrystalline.

A computer code,[11] based on Sigmund theory, was used to calculate sputter ratios for cesium projectiles and a variety of targets as a function of energy for an incident angle of $\theta = 0°$. A scaled version of the high-energy relation (Eq. 2) was selected as the more appropriate expression to cover the total range of interest. The expressions α and $S_n(E)$ were extrapolated to include the total array of naturally occurring projectile-target combinations.

Since there are few experimental data available for Cs^+ ions on arbitrarily chosen targets and since there is a pronounced dependence of the scaling factor on projectile, the task of determining the scaling factor was rendered more difficult. However, the ratios of scaling parameters determined for Cs^+ ions and those obtained for Xe^+ ions at a particular energy were found to be fairly constant from target to target where both sets of experimental data were available. Over the range of experimental data a mean value $\langle R \rangle$ of the ratio was found to be

$$\langle R \rangle = 0.83$$

with a standard deviation $\sigma = 0.1$.

This value of $\langle R \rangle$ was used to determine scaling factors for the Sigmund theory and, in turn, sputter coefficients for more than 20 targets over an energy range between 0.4 and 50 KeV. For targets where experimental data were available, scaling factors were determined by comparing experimental results with the unscaled theoretical results. Figure 1.15 makes comparisons between experimentally determined and calculated sputter ratios for cesium ions on Al and Cu targets.

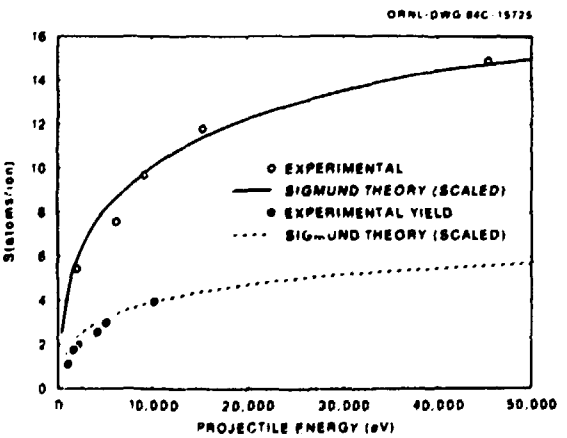

Fig. 1.15. Comparison of experimental and calculated sputter coefficients of normally incident ions on Al and Cu targets. (Calculated values are based on scaled Sigmund theory.)

Work continues on this project which is directed toward determining scaling parameters for arbitarily chosen projectile – target combinations.

---

1. Physics Division Progress Report for Period Ending September 30, 1983, ORNL-6004, (1983).
2. . Thieberger, M. McKeown, and H. E. Wegner, IEEE Trans. Nucl. Sci. NS-30, No. 4, 2746 (1983).
3. ORAU graduate laboratory participant from the University of Missouri-Rolla, Rolla, MO 65401.
4. Adjunct staff member from the University of Tennessee.
5. J. Heinemeier and P. Tykesson, Nucl. Instrum. Methods 141, 182 (1977).
6. W. Kutschera and G. Korschinek, Proc. Int. Conf. Ion Sources, 2nd, Vienna, 1972, p. 908 (1973).
7. G. D. Alton, et al., Physics Division Progress Report for Period Ending December 31, 1974, ORNL-5025, (1975), p. 192.
8. Summer research participant, Oak Ridge Associated Universities.
9. P. Sigmund, Phys. Rev. 184, 383 (1969).
10. O. Almen and G. Bruce, Nucl. Instrum. Methods, 11, 257 (1961).
11. G. D. Alton (unpublished).

BEAM BUNCHER DEVELOPMENT

J. A. Martin W. T. Milner
N. F. Ziegler

A new beam buncher-chopper system is being designed for the tandem accelerator which will provide pulsed beams for time-of-flight work in addition to bunching the beam for injection into ORIC. An improved rf control system will also be added. The chopper will operate at two discrete frequencies of 0.5 and 2.0 MHz providing beam pulses at intervals of 1.0 or 0.25 microseconds. Deflection plates for the chopper will be located i ..e low-energy beam line between the mass analyzing magnet and the buncher. A double-drift buncher similar to the present system will be used in the new design; however, three tube lengths will be provided for more efficient operation. An expanded frequency range of 4 to 16 MHz will be available in the buncher. With the chopper operating at 2.0 MHz, about 25 percent of the dc beam will be compressed into pulses of 1 to 3 ns while operation at 0.5 MHz will reduce the fraction of beam which is compressed to about 6 percent.

Engineering of the new pulsing system should be complete by December 1984, and installation will proceed in 1985.

EFFORTS TO IMPROVE TANDEM ACCELERATOR TUBE PERFORMANCE

In recent months the voltage performance of the tandem accelerator tubes has shown encouraging improvement. However, the accelerator tubes are still the principal limitation to achieving higher tandem voltages. In this section we summarize work done which could lead to eventual improved accelerator tube performance. Much of this work was inspired by the results obtained at the Munich MP Tandem Laboratory.

Hydrogen Arc Discharge Conditioning

P. H. Stelson J. R. Raatz[1]
R. D. Rathmell[1]

Korschinek et al.[2] have shown that NEC accelerator tubes can be more effectively conditioned by the use of a low-voltage hydrogen arc discharge than by the standard methods used previously. Results from tests in a small accelerator showed substantial improvements in voltage gradients from typical values of 20-25 kV/cm to values of over 40 kV/cm.

With Korschinek's advice and help, we assembled equipment to carry out hydrogen arc discharge conditioning at ORNL. After a period of familiarization, the equipment was transferred to the NEC 3-MV test accelerator where voltage tests could be carried out. However, the NEC accelerator could not achieve the column voltage gradient of 40 kV/cm of the Munich test accelerator but was limited to a maximum value of slightly under 30 kV/cm.

With the reservation that accelerator tube tests suffer from very limited statistics and many variables, we summarize our results with the following points.

1. The difference in the initial behavior of arc discharge conditioned tubes and normal tubes is striking. The familiar micro-discharges exhibited by normal tubes are largely eliminated in arc discharge conditioned tubes. There is essentially no vacuum activity.
2. The maximum voltage gradient is quickly achieved with tubes conditioned by the arc discharge. The column gradient proved to be the limitation.
3. Continuous X rays were frequently observed when high-voltage gradients were applied to arc discharge conditioned tubes. The intensity of these X rays could abruptly change. Once the continuous X rays were initiated, they persisted at lower voltage gradients, where they had not initially been observed. It is not clear whether these continuous X rays will prove to be troublesome in the use of arc discharge conditioned tubes to accelerate ions.

However, experience with operation of the HHIRF tandem accelerator, which is equipped with accelerator tubes which also show continuous x-ray activity, suggests that continuous x-ray activity does not adversely affect operation of the accelerator.

4. The deterioration of accelerator tube insulators by sputtering of electrode material by the arc discharge was very slight. It is important to operate the discharge at a pressure of about 100 mTorr in order to keep the mean-free path of the ion short so that they strike the electrodes with lower energies, thus reducing the sputtering yield.
5. Arc discharge conditioned tubes may be exposed to air with no obvious degradation of the voltage gradient performance.

An explanation for the effectiveness of the arc discharge in conditioning accelerator tubes is that it causes the inner parts of the tube electrodes to be heated to temperatures as high as 500-700°C, and that this promotes outgassing and cleaning of the electrode surfaces. However, based on our test results, we prefer a somewhat different explanation. The most clear-cut result from our tests is the almost complete elimination of microdischarges following arc discharge conditioning. Although hydrogen gas was originally chosen to minimize electrode sputtering, it has other important virtues. From Tokamak wall-cleaning research, it is known that the hydrogen discharge is a very effective way to clean carbon and heavy hydrocarbons from surfaces by chemically producing methane, whereas, simple heating of surfaces does not remove these substances. The good removal of carbon and hydrocarbons from the electrode surfaces eliminates the most likely source of negative ions needed to initiate the familiar microdischarge.

Compressed Geometry Accelerator Tube Tests

J. R. Raatz[1] R. D. Rathmell[1]
P. H. Stelson N. F. Ziegler

The success of the hydrogen low-voltage arc discharge conditioning of NEC accelerator tubes suggested to Assmann et al.[1] the possibility of using a "compressed geometry" by eliminating the heater plates previously used for tube conditioning. This compressed geometry provides about 18 percent more insulation length in NEC accelerators. Tests in the small Munich test accelerator with this new configuration were encouraging.

A somewhat similar "compressed geometry" accelerator tube was installed in the NEC 3-MV test accelerator. The tube was first subjected to the normal conditioning procedure of gradually increasing the voltage to gradually eliminate microdischarges. This procedure alone was quite successful and demonstrated that the tube would support total voltages which were about 18 percent higher than those for a tube of standard geometry. Since the accelerator tube had achieved a well-conditioned state without using a hydrogen arc discharge, the result from running an arc discharge in the tube is somewhat inconclusive. Nevertheless, the hydrogen arc discharge conditioning was carried out on this tube and we could conclude only that it did not in any way limit the tube's performance. A detailed account of these tests is given in NEC Internal Report No. 183, June 7, 1984.

The Munich MP Accelerator Arc Discharge Conditioning Tests

P. H. Stelson N. F. Ziegler

In December 1983, the Munich MP Laboratory performed a hydrogen arc discharge conditioning test on one section of the MP tandem accelerator. For this test they chose the section of the low-energy tube which is next to the terminal. This section had always been the weakest section for holding voltage gradients, typically supporting 3.5 MV. After conditioning by the hydrogen arc discharge, this section supported 3.9 MV, making it the strongest section in the accelerator. Encouraged by these results, plans were formulated to condition and test the whole accelerator during a four-week period beginning in July 1984. ORNL was invited to participate in this program.

The hydrogen arc discharge was run on one half of the MP accelerator tubes at a time. First, the low-energy tube was conditioned by operating a hydrogen arc of about 4 amperes for three hours. The high-energy tube was conditioned in a similar way. In both tubes the hydrogen gas was admitted at the opposite end of the tube from where the electron emitting filament and pump were located. During both discharge operations, an unanticipated difficulty was encountered. Gas which evolved from the tube during the initial operation of the discharge poisoned the filament. For the low-energy end, the cathode filament was replaced by a new one. For the high-energy end, the cathode was operated at a much higher than normal temperature to achieve a current of 4 amperes. In future conditioning of tubes, it would be advisable to admit the hydrogen gas at the end of the tube where the filament is located to avoid exposing the filament to the evolved gases.

After two weeks of testing the accelerator, the general concensus of the Munich accelerator staff was that the arc discharge conditioning had only slightly improved the accelerator tube performance. A possible reason for this disappointing result is that such a long accelerator tube system may require a proportionately longer time for operation of the arc discharge in order to clean the tube. In contrast to our results with much shorter tubes, the Munich tests showed that microdischarges were still encountered after the arc conditioning.

---

1. National Electrostatics Corporation, Middleton, WI 53562.

2. G. Korschinek, J. Held, A. Isoya, W. Assmann, and H. Münzer, Nucl. Instrum. Methods Phys. Res. 220, 82 (1984).
3. W. Assmann, G. Korschinek, H. Münzer, Nucl. Instrum. Methods Phys. Res. 220, 86 (1984).

FACILITY OPERATIONS AND DEVELOPMENT

EXPERIMENTAL APPARATUS

R. L. Auble — N. R. Johnson
E. E. Gross — F. E. Obenshain
M. L. Halbert — D. Shapira
J. W. Johnson — E. H. Spejewski[1]
P. D. Miller — H. J. Kim

The major experimental devices at HHIRF were described in detail in the previous Progress Report[2] and only those having significant changes in the past year are discussed in this section. For reference, the layout of the experimental facilities is given in Fig. 1.16.

Split Pole Magnetic Spectrometer

During the past year, a new dedicated power supply for the dipole magnet was delivered and installed. At present, the spectrometer scattering chamber and associated beam line serve as the staging area for a polarized target facility which is now nearing completion.

On-Line Isotope Separator

Since the last report, significant progress has been made on the He-jet and laser systems, both of which have been under development for several years. Briefly, tests of the He-jet successfully demonstrated the power of this device for studying short-lived (< 1 sec) activities. Further development is needed, however, to reduce the helium current in the separator and to improve the overall efficiency. The laser facility, which was developed to measure the atomic hyperfine structure (hfs) of separated isotope beams, was used successfully in a study of ^{192}Tl. In this case, a beam of about 10^5 atoms/sec allowed measurement of the hfs spectrum in a matter of minutes.

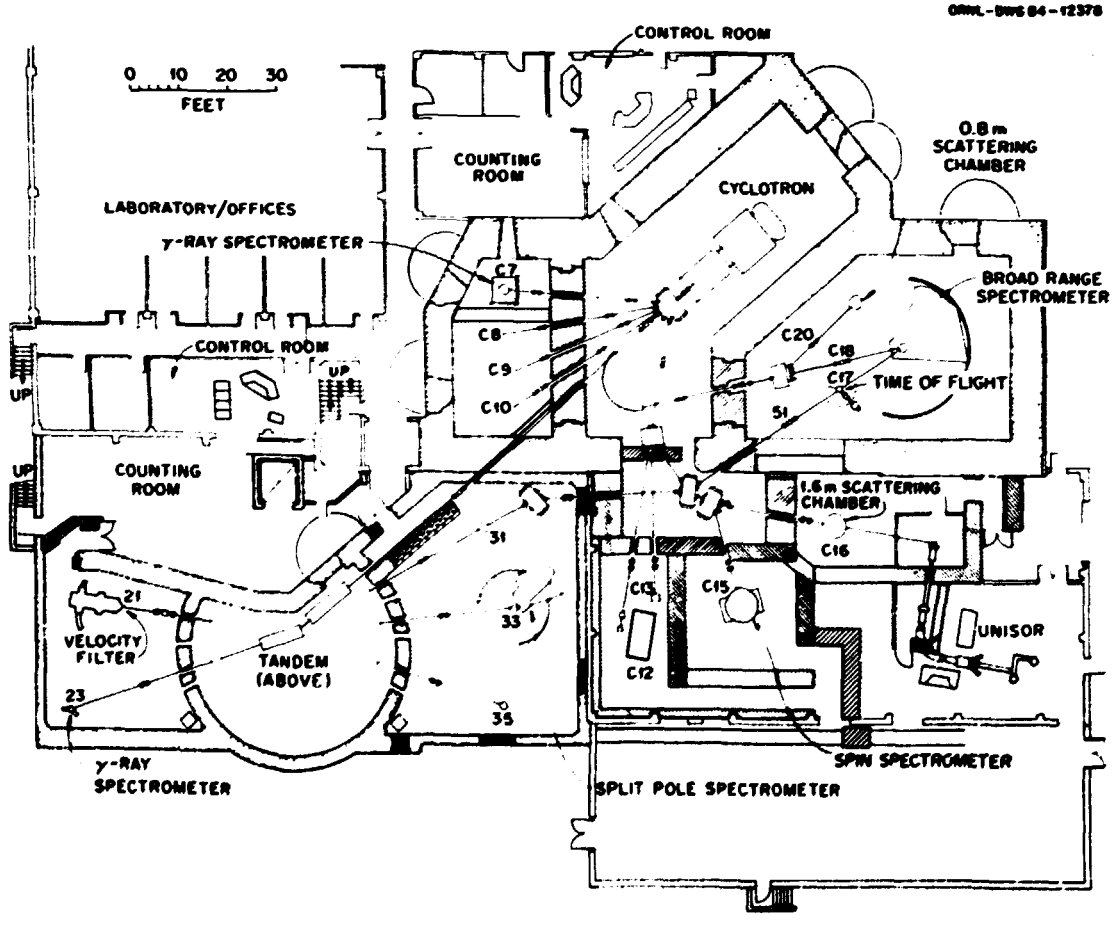

Fig. 1.16. Floor plan of the experimental areas at the HHIRF.

The results of the initial experiments on these devices are described in more detail elsewhere in this report.

Broad Range Magnetic Spectrometer

Improvements include the installation of a 1500 l/s cryopump on the magnet vacuum chamber and the addition of dedicated gas handling systems for the focal plane detectors. A test run has now been made to demonstrate the usefulness of the BRS for studying heavier particles. Normally, a parallel plate avalanche detector, located between the scattering chamber and the magnet, is used for time of flight measurements. However, for heavier projectiles, in this case ^{58}Ni, the energy loss in this detector becomes unacceptable. Therefore, the PPAD was replaced by a microchannel plate detector which detects secondary electrons from a 10 $\mu g/cm^2$ carbon foil located near the exit port of the scattering chamber. This detector, in conjunction with the large PPAD located at the focal plane, provides ~700 psec time-of-flight resolution and allows us to separate individual Ni isotopes.

The Spin Spectrometer

Improvements. The spin spectrometer, the HHIRF's "Crystal Ball," has undergone a number of improvements in the past year. The principal ones are as follows.

1. The electronics equipment has been moved to the new south counting room, which is described in this report. This has made experimental setup much more convenient.
2. Six pentagonal NaI Compton-suppression shields for Ge detectors are now available and have already been used in several experiments. Additional shields of both NaI and BGO, are under construction. A more complete description of these units is given elsewhere in this report.
3. The exit beam pipe has been modified to allow rotation of the scattering chamber and facilitate installation of auxiliary detectors.
4. The 15 radial rods supporting the NaI detector array from the outer dodecahedral frame were replaced by larger-diameter rods, and the mechanical coupling to the frame was improved. The result is a much stiffer and more accurate support system.

Problems. From October 1981 to May 1983 we observed a gradual deterioration of the resolution of the NaI detectors. During this time the average resolution over all units for 898-keV γ rays increased from 8.4% to 9.2%. However, from April to August 1984, a rapid degradation of performance was observed for most of the detectors. An inspection in August 1984 revealed that about 50 units show moderate to severe cracking of the NaI that appears to have originated at the interface between the NaI and the glass window.

It is likely that the cracks are the result of two factors, possibly acting synergistically, namely rapid thermal cycling and shrinkage with age of the epoxy-cement interface. Evidence for the thermal effect is based on the differing history and degree of cracking of the two halves of the spin spectrometer ball. During the winter, the NaI units from the beam-right segment were stored in an area which suffered a failure of the heating system. Nearly all the NaI units from this half were later found to be severely cracked. During this episode the beam-left half remained in the cave, well in the interior of the building, where the temperature fluctuations were smaller and slower. Only about 22% of the detectors on this half of the ball were severely cracked and 14% were moderately cracked.

Evidence for the importance of age is as follows. In the beam-right half of the ball, the two detectors that did not crack were both new or rebuilt within the previous year. Secondly, it took several months after the original assembly of the ball before an air conditioning unit was installed and during this time the temperature fluctuated with the seasons. Yet in the first two years of use, only one detector in the ball showed severe cracks; furthermore, its past performance suggested that it was already cracked before assembly of the ball. Also, at the NaI detector laboratory at Stanford University, this kind of cracking has occurred in all NaI detectors with hard-epoxy joints after they aged about five years.

Negotiations are in progress with three firms to replace or repair most of the detectors in the ball. The interface between the NaI and the glass will be a silicone-based elastomer instead of a hard-epoxy cement.

Velocity Filter

Calibration of the power supplies has been completed for the maximum deflection angle (10° electrostatic, 20° magnetic) using an α-particle source and beams of Ti and Zr. The electrostatic deflectors have also been tested at 250 kV (70% of the design limit) without breakdowns or excessive X-ray production. Hardware additions include a 10.2-cm x 12.7-cm Breskin-type start detector for making time-of-flight measurements, an ion chamber plus Si-detector counter telescope for ΔE-E measurement of the selected particles, and installation of new power supplies which make the RMS operation independent of shared supplies.

Neutron Chamber

A recent addition to the experimental apparatus available to HHIRF users is a chamber designed primarily for the study of neutrons emitted in heavy-ion reactions. The chamber, which was designed by G. R. Young with technical support from C. A. Reed, seeks to minimize the amount of material traversed by the neutrons before reaching the externally mounted neutron detectors. It consists of two spun aluminum hemispheres joined by an O-ring seal to form a sphere 80 cm in diameter with 0.3-cm wall

thickness. The chamber is shown in Fig. 1.17 with the back hemisphere removed to show the internal structure. Two independently rotatable rings are located inside the chamber to support charged particle detectors, and a target ladder is located on the vertical axis to provide space for mounting four targets. Several feedthrough and viewing ports are also available, and custom flanges can be readily fabricated. As is evident in the figure, the chamber has been used successfully in several experiments.

1. Oak Ridge Associated Universities.
2. J. L. C. Ford et al., Physics Division Progress Report, September 30, 1983, ORNL-6004, p. 20.

ORNL-PHOTO 6011-84

Fig. 1.17. Photograph of the 80-cm neutron chamber with the back hemisphere removed. Liquid scintillator neutron detectors are arranged around the outside of the chamber.

COMPUTER SYSTEMS

J. A. Biggerstaff
W. H. Atkins[1]
J. R. Beene
J. W. McConnell
J. B. McGrory
W. T. Milner
R. O. Sayer[1]
C. N. Thomas[2]

Data Acquisition/Reduction Computer System

The hardware configuration of the data acquisition/reduction system is essentially unchanged from that reported previously.[3] We have added a 6250-bpi tape drive (for a total of 7) and a color graphics terminal (for a total of 6). A monochrom. printer-plotter has been acquired and is dedicated to service of a new counting station in the "deep-south" annex.

We have fully commissioned a new data processing software package called "CHIL" (for Comprehensive Histogramming Instruction Language). CHIL provides major improvements in both the performance and the ease of use of our processing software without changing the basic structure of the system described previously.[3] Development of CHIL began with a description of a desirable machine instruction set for data processing with emphasis on tools for "gating" and "histogramming." These new instructions were implemented in microcode for our processors and assembly language routines generated to invoke them. A CHIL compiler was written to translate users' FORTRAN-like gating, histogramming and control (GOTO, IF, etc.) statements into a "machine-language" program using the new instruction set. An important feature of CHIL is its robustness. Responsibility for "crash-proofing" the system was divided into two areas. First, the microcode was hardened against unexpected (illegal) data values. Secondly, to eliminate the need for time-consuming run-time tests, the CHIL compiler was designed with thorough syntax and logic checking to insure that invalid instructions are never generated. User acceptance of the new package was so immediate and so trouble-free that CHIL has completely superseded all our older histogramming software.

The VAX-FPS Dual Processor Computer System

The VAX-FPS Dual Processor Computer System described in last year's report has become a widely used facility by both nuclear theorists and experimentalists to perform the extensive calculations needed to analyze and understand the heavy-ion physics experimental data produced on HHIRF. Several significant improvements have been made on the system in the past year. A new unibus adapter has been added to the VAX 11/780 to increase the number of ports available to users to 32, and the number of stations with direct access to the system has been increased accordingly. A new fast, sealed, 480-Mb disc has been installed, bringing the total disc storage capacity directly accessible from the VAX 11/780 to almost 1 billion bytes. The fast memory of the FPS-AP 164 attached processor has been increased from 2 Mb to 6 Mb. This will enable the system to handle much larger calculations, such as TDHF calculations for medium mass nuclei, and the heavy-ion coupled channels code ECIS will now fit on the AP 164. Hardware is now on order to provide ready access to the system from the Joint Institute for Heavy Ion Research.

1. Computing and Telecommuncations Division.
2. Oak Ridge Associated Universities.
3. J. A. Biggerstaff et al., Physics Division Progress Report, September 30, 1983, ORNL-6004 p. 24ff.

FACILITIES

R. L. Robinson M. L. Halbert
R. L. Auble D. Shapira
F. E. Bertrand C. M. Thomas[1]

JIHIR Building

The Holifield complex was enlarged by completion of the second building of the Joint Institute for Heavy Ion Research in April, 1984 (Fig. 1.18). This 6000-ft^2 building has 12 offices, 2 laboratories, and an 80-person conference room. Four offices in this building are occupied by the UNISOR staff. The two picturesque trailers which had served as their offices have been removed from the Holifield site.

Counting Rooms

The tandem counting room has been reconfigured to provide better access to the electronics racks and more work space. Patch panels linking the counting area with experimental stations 23, 31, 33, and 35 are presently in place and a panel for station 21 (velocity filter) will be installed in the near future.

A third counting room (south counting room) is now available. This counting room is located in the South Annex immediately outside the entrance to the spin spectrometer cave. Computer terminals, a graphics display unit, and a hard copy device are installed, and a link to the ORIC counting room provides access to the data acquisition computers. Cables connecting this area with the spin spectrometer are in place and the spin spectrometer electronics have been moved from the experiment room to this counting room. The new counting room has been used in several experiments on the spin spectrometer and has enormously improved the ease of experiment setup and data acquisition. Expansion of this counting room to service the 1.6-m scattering chamber is being considered.

A cable linking the tandem and ORIC counting rooms will soon be installed. This link will make it easy to connect any counting room with any of the three data acquisition computers, permitting rapid switching to another system in the event of computer problems.

---

1. Oak Ridge Associated Universities.

ORNL-PHOTO 4042-84

Fig. 1.18. View of the two buildings of the Joint Institute for Heavy Ion Research taken from atop the HHIRF tower. Building two is at the upper right with building one at the upper left.

USERS SUPPORT

R. L. Auble
J. A. Biggerstaff
R. P. Cumby
J. W. Johnson
R. W. Miles
C. A. Reed[1]
R. L. Robinson
C. M. Thomas[1]
W. T. Milner

Experimenters routinely call upon the resources of the Users Support Group in setting up their experiments. Normally, a technician (R. W. Miles or C. A. Reed) is assigned to a specific experiment when the run schedule is established. They assist the experimenters with hardware related matters such as installing alignment telescopes, diagnosing and overseeing repair of vacuum problems, and designing and supervising fabrication of parts which may be needed for a particular setup. On the electronics end, R. P. Cumby maintains the HHIRF electronics pool (consisting of nearly 1000 instruments and a multitude of cables), helps to locate modules needed for each experiment, diagnoses problems in the electronics, and tests the semiconductor and scintillation detectors to ensure that they meet specifications. Interfacing of the users electronics with the data acquisition system is handled by Charles Thomas. This includes connecting the CAMAC interface to the appropriate CPU, installing the Event-Handler and associated modules, and setting up peripherals (MTM terminals, Chromatics terminals, Trilogs).

In addition to these routine tasks, the technicians assist the mentors with maintenance and modification of the various experimental facilities and provide technical support to the research staff in the development of new equipment. Examples of the projects in which the technicians have been particularly active are: design of an improved collimator for the velocity filter (R. Miles), design of the 80-cm neutron chamber (C. Reed), development of an operating system for the 68000 Branch Driver (C. Thomas), and development of new high voltage supplies for the velocity filter (R. Cumby).

---

1. Oak Ridge Associated Universities.

JOINT INSTITUTE FOR HEAVY ION RESEARCH

R. L. Robinson L. L. Riedinger
J. H. Hamilton

Although the Joint Institute for Heavy Ion Research (JIHIR) legally became an entity with the signing on June, 1982, of the Agreement of Understanding by representatives of Union Carbide Corp. (then operating contractor of ORNL), the University of Tennessee, Vanderbilt University, and the Department of Energy, it did not become a fully operating Institute until it was provided operating funds July 1, 1984. The budget for the year beginning then is about $250,000. Two-thirds of this is from the State of Tennessee via a Centers-of-Excellence grant through the University of Tennessee - Knoxville. Contributors to the remaining one-third are ORNL, Vanderbilt University, and the Department of Energy.

Beginning a new Institute has required considerable involvement of the JIHIR Policy Council which is responsible for establishing policy and overseeing operation. These have included a myriad of mundane details: establishing utility, janitorial and telephone services by ORNL to a building not a part of ORNL; developing a mechanism for providing support to guests of the Institute; procuring furniture; assuring that minor building problems are rectified, etc. Members of the Policy Council are J. H. Hamilton (also serving as Director of JIHIR), L. L. Riedinger and R. L. Robinson.

The major portion of the budget is to support guests of the Institute with assignments ranging from a few days to a year. Persons already supported since July 1 are C. M. Ko, J. A. Maruhn, and J. Eberth. Thirteen others are expected before the end of this calendar year. The Institute has also hired a half-time secretary.

Initially the second building will provide offices for staff persons of UNISOR, of the University of Tennessee, and of Vanderbilt University, and in addition, offices for nine guests of the JIHIR. There are 12 desks for more Holifield users and JIHIR guests in the first building.

A dedication for the JIHIR is being planned for October 15, 1984. It will be followed by a one and one-half day symposium on Directions in Nuclear Structure Research.

The first building of the Joint Institute, which was opened for occupancy in May 1981, continues to meet needs by providing conveniently located dormitory accommodations for Holifield Users from outside the laboratory. During FY 1984, its eight dormitory beds accommodated 213 visitors with an average length of stay of 6.1 nights (1308 person-nights). The occupancy rate was strongly coupled to accelerator operation. Because of the frequent requests that could not be met when the accelerators were operating (22% of the time the dormitory rooms were full), we are adding two more dormitory rooms during the next month.

USERS GROUP ACTIVITIES

R. L. Auble and R. L. Robinson

The HHIRF Users Group presently includes nearly 500 members representing over 150 institutions. Members are represented by the Users Group Executive Committee, whose membership for 1983-84 is given in Table 1.9.

Two new members of the Executive Committee are elected each year by the Users Group from a slate of candidates selected by the Nominating Committee. For 1984, this committee consisted of L. Grodzins, M. Guidry, J. Hamilton, W. Lynch, L. Riedinger (Chairman), R. Stokstad, and K. Toth.

The Executive Committee normally meets about four times a year in order to provide input regarding facility operation, equipment needs, and other matters which impact the users.

Table 1.9. Users Group Executive Committee Members for 1983, 1984, and 1985.

1983	1984+	1985
H. C. Britt (LANL)	C. K. Gelbke	D. C. Hensley
C. K. Gelbke (Michigan SU)	D. C. Hensley	D. G. Sarantites
D. C. Hensley (ORNL)	J. B. Natowitz	S. G. Steadman*
J. B. Natowitz (Texas A&M)	D. G. Sarantites*	J. L. Wood**
D. G. Sarantites** (Washington U)	E. H. Spejewski	M. W. Guidry (U Tennessee)
E. H. Spejewski* (UNISOR)	S. G. Steadman** (MIT)	A. C. Mignerey (U Maryland)
	J. L. Wood (Georgia Tech)	

*Chairperson
**Chairperson-elect
+Seven members this year only due to change from 2 year to 3 year tenure

During the past year, the Committee met on October 14, 1983; May 3, 1984; June 23, 1984; and September 18, 1984; providing numerous recommendations which have been taken into consideration in the operation of HHIRF. Minutes of these meetings are available from the Liaison Office. The meeting of June 23, 1984 was notable in that it was the first on-site meeting of the Committee. This proved to be very informative for both HHIRF and the Committee and it is planned to hold similar meetings on an annual basis.

PROGRAM ADVISORY COMMITTEE

R. L. Robinson

Table 1.10 gives statistics on the PAC meetings held during FY 1984. The heavy oversubscription of research hours for PAC-3 is attributed to the long time (13 months) between this PAC and the preceding one. The requests shown for PAC-4 are suspected to be more typical since the time between meetings of PAC-3 and PAC-4 (5 months) is more nearly like the average 6 month interval that is planned between future PACs.

As outlined in the Users Handbook, the intent, normally, is to complete experiments within a year after their approval. Table 1.11, which summarizes status of the experiments recommended by all HHIRF PACs, indicates that, in practice, this objective is nearly being accomplished.

Table 1.10. Statistics on PAC-3 and PAC-4

	PAC-3	PAC-4
Meeting Dates	Apr. 5-6, 1984	Sept. 8-9, 1984
Number of Proposals Submitted	57	31
Requested Research Hours	5288	3272
Hours Recommended for Approval	2232	2043
Recommended Hours / Requested Hours	42%	63%
Participants on PAC	K. Gelbke E. Gross F. Iachello R. Nix P. Stelson F. Stephens	G. Bertsch E. Gross F. Iachello R. Nix P. Stelson D. Ward

Table 1.11. Status of experiments recommended by HHIRF PACs

	Dates Met	Hours Recommended	Hours Remaining
PAC-1	Nov. 10-11, 1984	2120	0
PAC-1A	June 5, 1981	1032	0
PAC-2	Feb. 28 – Mar. 1, 1983	1656	184
PAC-3	Apr. 5-6, 1984	2232	1184
PAC-4	Sept. 8-9, 1984	2048	2040
	Total	9088	3408

2. EXPERIMENTAL NUCLEAR PHYSICS

Our main research program in heavy-ion physics is carried out using the beams and equipment at HHIRF. Use is also made of heavy-ion facilities at LBL, Michigan State University and at Texas A&M. An extension of this program into the field of relativistic heavy-ion reactions is being pursued through a collaborative experiment to utilize 800 GeV to 3200 GeV ^{16}O beams at CERN. In addition, we continue to carry out a vigorous and productive program in medium energy physics using facilities at LAMPF, TRIUMF, and IUCF and a smaller program in neutron physics using the ORELA facility.

Noteworthy accomplishments for this period include: new results from the Spin Spectrometer on neutrons and γ decay from giant resonances; the appearance of a quasivibrational transition in ^{150}Yb above spin 24ħ; further measurements on π^0 production from heavy-ion collisions; and the measurement of time-delayed processes from ^{16}O + Ge reactions using the crystal blocking technique. This period has also been sadly marked by the losses of two long-time staff members, J. L. C. Ford, Jr. and C. B. Fulmer.

OPTICAL MODEL ANALYSIS OF 200-400 MeV PROTON ELASTIC SCATTERING ON ^{208}Pb

E. E. Gross D. Horen
F. E. Bertrand J. Lisantti[1]

Among the results of the Oak Ridge-Oregon-Oregon State proton inelastic scattering program conducted at TRIUMF are: (1) direct evidence for the excitation of the GDR by high energy proton inelastic scattering,[2] (2) confirmation[2] of L = 3 GDR resonances in ^{90}Zr and ^{120}Sn, (3) discovery of L = 4 GHR strength[3] in $^{206,208}Pb$, and (4) an improved understanding of the "background" underlying the giant resonance region in terms of quasifree scattering.[4]

In order to assign strengths (in terms of energy-weighted sum rule depletion) to the various giant resonances excited by 200-MeV proton inelastic scattering, we carried out DWBA calculations using an optical potential developed for proton elastic scattering in the 60-160 MeV range.[5] This analysis[2,3] led to strengths some 50% smaller than had been reported from previous lower energy measurements. Using the same analysis, the cross section for exciting the low lying 3^- state (2.61 MeV) in ^{208}Pb was also under-predicted by ~50% and we therefore renormalized the DWBA strength estimates for the observed giant resonances by a factor of about two.[2,3] This procedure is not entirely satisfactory and brings into question the applicability of the DWBA method for the higher proton energies.

Subsequently, we have measured[6] differential cross sections for 334-MeV proton elastic and inelastic scattering on ^{208}Pb using the HRS magnet facility at LAMPF. Rather than rely on optical model systematics developed at a lower energy,[5] we could use these new data to generate a more appropriate optical potential. Although covering a very limited angular range (2.5° to 13° c.m.), a coupled channels analysis[6] of the 334 MeV data yielded B(E3) values and giant resonance strengths for ^{208}Pb which were in excellent agreement with previous measurements.

More recently we have become aware of very extensive differential cross section and polarization measurements for 200-, 300-, 400-, and 500-MeV proton elastic scattering from ^{208}Pb performed by Hutcheon and collaborators.[7] These data have been subjected to an optical model analysis using the automatic search routine in the ECIS computer program.[8] The best fit parameters at each energy are summarized in Table 2.1. The best fit geometry parameters for the 200-, 300-, and 400-MeV analyses were averaged and the cross section and polarization data were again fitted by varying the optical potential strengths. The average geometry search results are also included in Table 2.1. The 500-MeV data could not be satisfactorily represented by an average geometry potential, especially the 500-MeV polarization data. The increasing importance of meson production and relativistic effects may account for the change in conventional optical model systematics in the 400-500 MeV range.

Figure 2.1 shows the average geometry fit to the 200-MeV elastic scattering data and Fig. 2.2 shows the same thing for polarization (solid curves). Also shown are predictions from the Nadesen et al.[5] potential (dotted curves). Using the new potential of Table 2.1 in an analysis of our previous 200-MeV-protons inelastic scattering data[3] from ^{208}Pb now provides agreement with previous results for B(E3) for the 2.613 MeV, 3^-, level. It is reassuring that the DWBA method can be safely applied in the

Table 2.1. Proton + ^{209}Pb optical parameters

	334 MeV		200 MeV		300 MeV		400 MeV		500 MeV
	Avg.geo.	Fit	Avg.geo.	Fit	Avg.geo.	Fit	Avg.geo.	Fit	Fit
V_R	4.452	12.4[illegible]	11.17	11.11	4.37	4.934	0.292	0.20	-10.11
r_R	1.315	1.121	1.315	1.299	1.315	1.304	1.315	1.341	1.103
a_R	0.599	0.770	0.599	0.623	0.599	0.606	0.599	0.568	0.489
V_I	19.67	30.00	21.17	20.38	25.19	24.48	34.12	33.49	30.81
r_I	1.149	1.090	1.149	1.167	1.149	1.165	1.149	1.116	1.157
a_I	0.799	0.765	0.799	0.827	0.799	0.762	0.799	0.808	0.597
V_{so}	2.11	1.89	2.20	2.65	2.32	2.105	2.211	2.230	2.972
r_{so}	1.104	1.138	1.104	1.095	1.104	1.098	1.104	1.123	1.008
a_{so}	0.689	0.777	0.689	0.685	0.689	0.651	0.689	0.730	0.874
V_I	-0.528	-0.770	-2.859	-2.88	-3.24	-3.314	-4.894	-3.630	-0.412
r_{Iso}	1.061	1.135	1.061	1.050	1.061	1.058	1.061	1.076	1.347
a_{Iso}	0.801	0.687	0.801	0.821	0.801	0.785	0.801	0.799	0.700
χ^2_σ	956	554	3710	1670	1530	2110	1580	1040	1420
χ^2_A	644	246	1820	2000	663	820	4150	3030	885

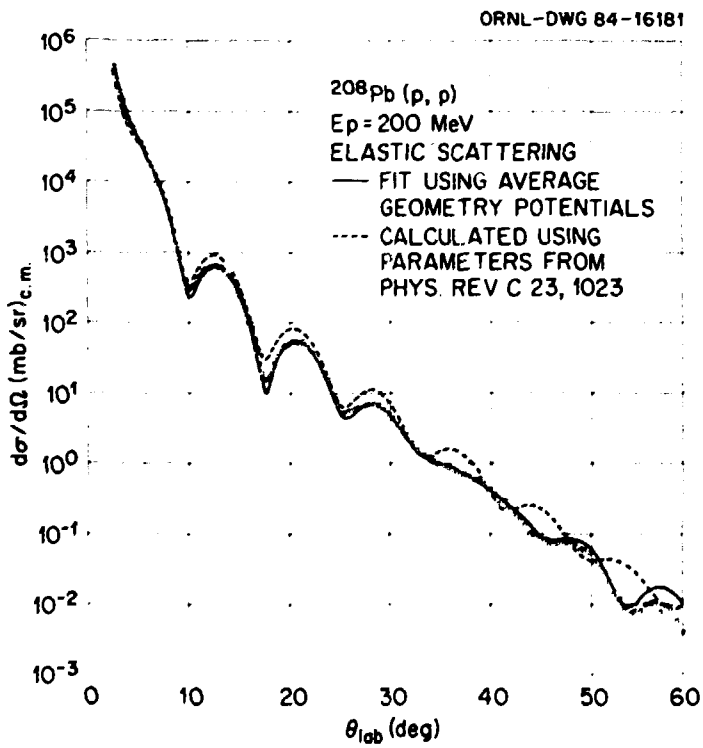

Fig. 2.1. Elastic scattering data[7] for 200-, 300-, and 400-MeV protons incident on a ^{208}Pb target. The solid curves are "average geometry" fits using the potenitals in Table 2.1. The dotted curves are predictions using the Nadasen et al. systematics.[9]

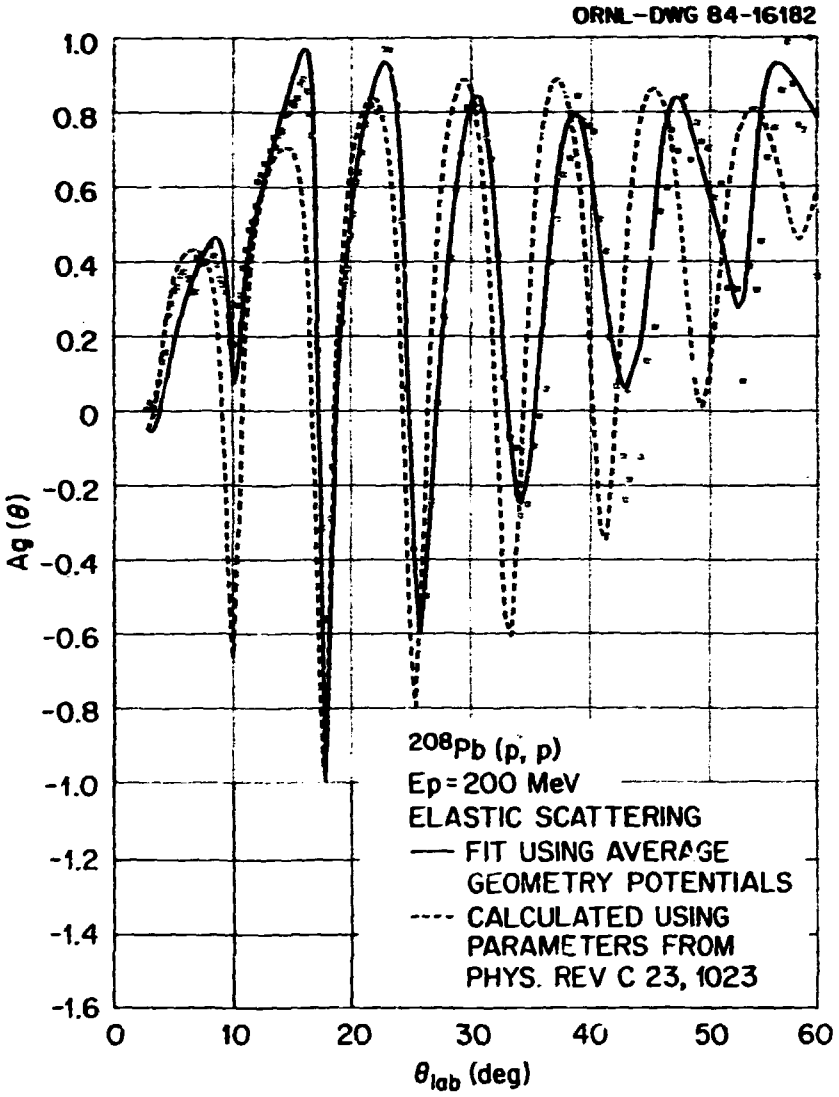

Fig. 2.2. Elastic polarization data[7] for 200-, 300-, and 400-MeV protons incident on a ^{208}Pb target. The solid and dotted curves correspond to those in Fig. 2.1 for the differential cross sections.

200-400 MeV proton energy range provided care is taken to determine the optical potential.

---

1. University of Oregon, Eugene, OR 97403.
2. F. E. Bertrand et al., Phys. Lett. 103B, 336 (1981).
3. J. R. Tinsley et al., Phys. Rev. C 28, 1417 (1983).
4. D. K. McDaniels et al., to be published.
5. A. Nadasen et al., Phys. Rev. C 23, 1023 (1981).
6. F. E. Bertrand et al., to be published and following contribution.
7. D. A. Hutcheon (private communication).
8. J. Raynal (private communication).

INELASTIC EXCITATION OF LOW-LYING STATES IN ^{208}Pb BY 334-MeV PROTONS

F. E. Bertrand
E. E. Gross
D. J. Horen
T. P. Sjoreen[1]
J. Lisantti[2]
J. T. Tinsley[2]
D. K. McDaniels[2]
L. W. Swenson[3]
T. Carey[4]
K. Jones[4]
J. B. McClelland[4]
S. Seestrom-Morris[4]

The strength of a giant resonance excitation is generally stated in terms of the percentage depletion of energy weighted sum rule (EWSR). The EWSR is directly associated with the transition rate [B(EL)] of the resonance as:

$$EWSR = B(EL)\,(E_f - E_i) = \frac{L(2L+1)\hbar^2}{4\pi 2m} A e^2 \langle r^{2L-2} \rangle$$

where E_f and E_i denote the energies of the final and initial states in the transition and $\langle r^L \rangle$ is the rms charge radius of the ground state. For electromagnetic interactions the determination of B(EL) is direct. However, in inelastic hadron scattering B(EL) is not directly obtained; rather, a deformation parameter, β_L, is deduced which is related to B(EL) in a model dependent way. In order to insure that the correct EWSR is being deduced for giant resonances excited in inelastic scattering, it is important to check the determination of B(EL) for low-lying nuclear states having known spin, parity, and transition rate.

In our recent, high resolution measurements of giant resonances in ^{208}Pb using inelastic scattering of 334-MeV protons, we obtained data for the elastic scattering and inelastic excitation of low-lying 3^-, 2^+, and 4^+ levels. The data have been compared with DWBA calculations which utilize optical model parameters from energy-dependent potentials obtained from fits to 200-, 300-, and 400-MeV proton elastic scattering on ^{208}Pb as described in the preceding contribution. Figure 2.3 shows the elastic scattering data (both differential cross section and analyzing power) and the optical model calculations for 334-MeV proton scattering from ^{208}Pb.

Figure 2.4 shows the differential cross sections for inelastic scattering to the 2.613-MeV, 3^-, 4.086-MeV, 2^+, and 4.323-MeV, 4^+, states in ^{208}Pb. The $\beta_L R$ values deduced by normalizing the calculations to the data are shown on the curves. From these $\beta_L R$ values we derive the B(EL) values shown in Table 2.2 compared with values adopted in the Nuclear Data Sheets.[5] It is clear from these results that results of inelastic scattering of medium energy protons can be used to deduce a correct B(EL) value. Through this comparison we gain confidence that our EWSR measurements for the giant resonance states in ^{208}Pb are reliable.

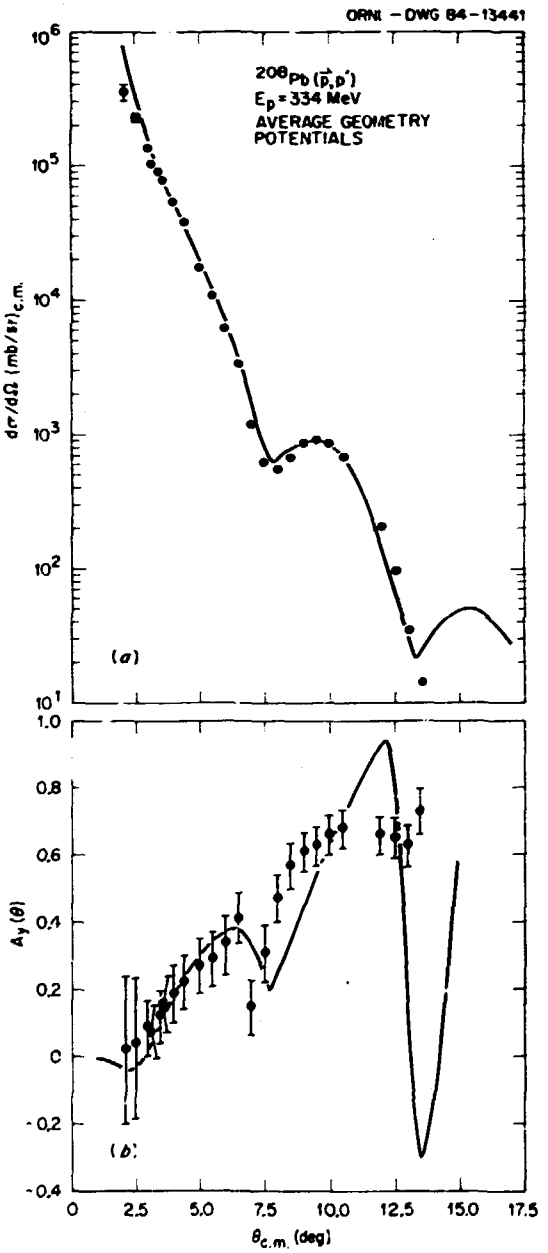

Fig. 2.3. Differential cross section and analyzing power for elastic scattering of 334-MeV protons from ^{208}Pb. The solid curve is an optical model calculation.

---

1. *Solid State Division, ORNL.*
2. University of Oregon, Eugene, OR 97403.
3. Oregon State University, Corvallis, OR 97331.
4. Los Alamos National Laboratory, Los Alamos, NM 87545.
5. M. J. Martin, Nuclear Data Sheets for ^{208}Pb, in preparation (private communication).

COMPARISON BETWEEN EXPERIMENTAL AND CALCULATED CROSS SECTIONS AND ASYMMETRIES FOR SPIN EXCITATIONS IN ^{40,48}Ca

D. J. Horen[1] — J. Lisantti[2]
F. E. Bertrand — L. W. Swensen[3]
E. E. Gross — J. B. McClelland[4]
T. P. Sjoreen[1] — T. A. Carey[4]
D. K. McDaniels[2] — S. J. Seestrom-Morris[4]
J. R. Tinsley[2] — K. Jones[4]

The ^{40,48}Ca($\vec{p}$,p') reaction has been studied utilizing the HRS facility at LAMPF. The incident protons had an energy of 334 MeV, and the overall resolution achieved was ~80 keV. Measurements included the angular region θ_{cm} ~2°-10°. The data were analyzed and differential cross sections and asymmetries were determined for spin-isospin excited states at 10.24 MeV ($J^\pi = 1^+$, T=4) in ^{48}Ca, 8.42 MeV ($J^\pi = 2^-$, T=1) and 10.31 MeV ($J^\pi = 1^+$, T=1) in ^{40}Ca. The experimental cross sections and asymmetries are shown in Figs. 2.5, 2.6, and 2.7.

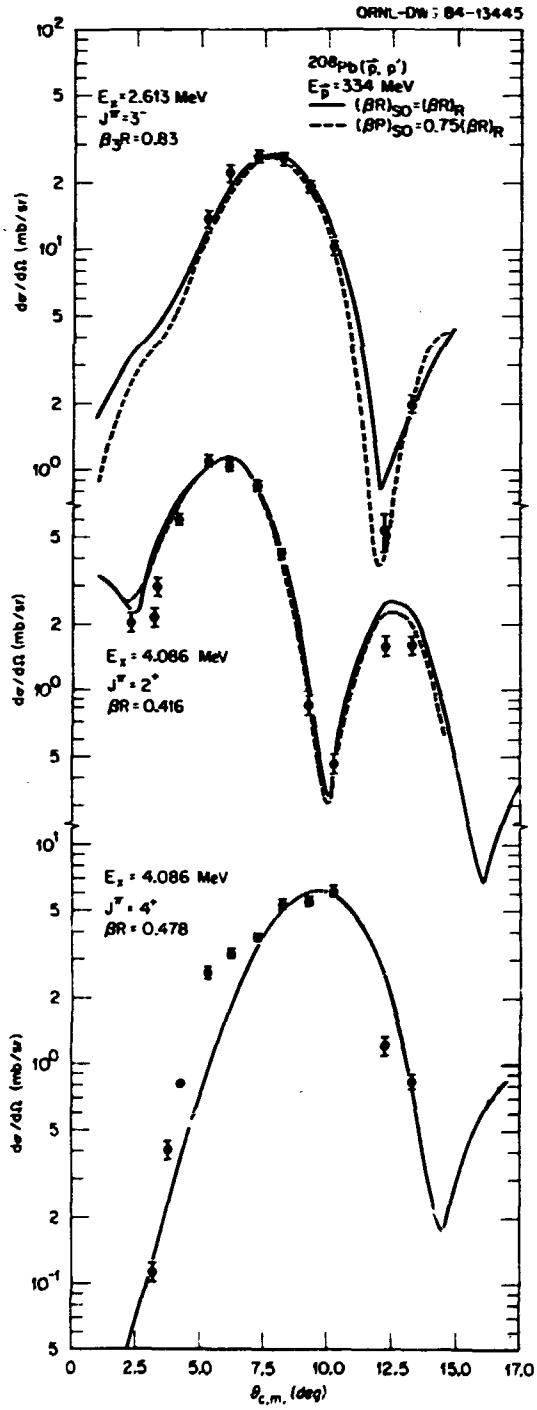

Fig. 2.4. Differential cross sections for inelastic scattering of 334-MeV protons to three low-lying levels in ^{208}Pb. The solid curves and dashed curves are from DWBA calculations.

Table 2.2. Properties of levels studied

Level Energy (Mev)	Level J^π	β$_L$R	B(EL) Deduced e^{2}b^L	B(EL) Nuclear Data Sheets
2.613	3$^-$	0.83	0.67[6]	0.611[9]
4.086	2$^+$	0.42	0.33[1]	0.318[16]
4.323	4$^+$	0.48	0.12[1]	0.135[11]

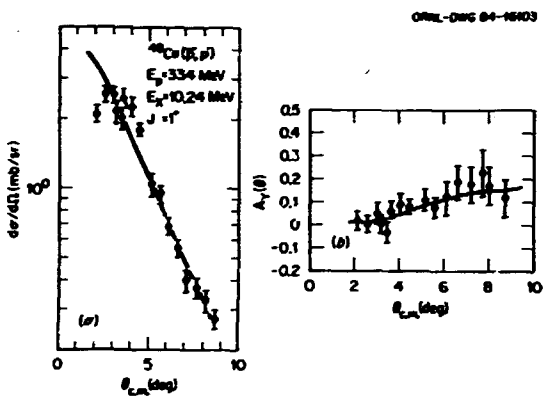

Fig. 2.5. Differential cross section and asymmetry for the 10.24-MeV 1$^+$ state in ^{48}Ca. The solid lines are from DWIA calculations.

Our measured cross section for the 10.24-MeV state in ^{48}Ca is in good agreement with that obtained by Nanda et al.[5] with protons of energy 319 MeV. However, we do not observe the sharp minimum at ~5° in the asymmetry as reported by those workers. Our data for the 10.31-MeV state in ^{40}Ca is consistent with the results obtained with 200-MeV protons.[6] Our asymmetry data are the first measured for this state at intermediate energies. The data at these energies for the 8.42-MeV state in ^{40}Ca is the first to our knowledge.

The quenching of spin transitions (e.g., M1, GT) is well established, although a complete understanding of its physical basis is still being debated. Two mechanisms which have been proposed to explain such quenching have been ground-state configuration mixing and mixing with ΔN$^-$ excitations. Both mechanisms would result in pushing some spin strength to the region of higher excitation. For $^{42-48}$Ca, McGrory and Wildenthal[7] have shown that an fp space can account for a considerable part of the

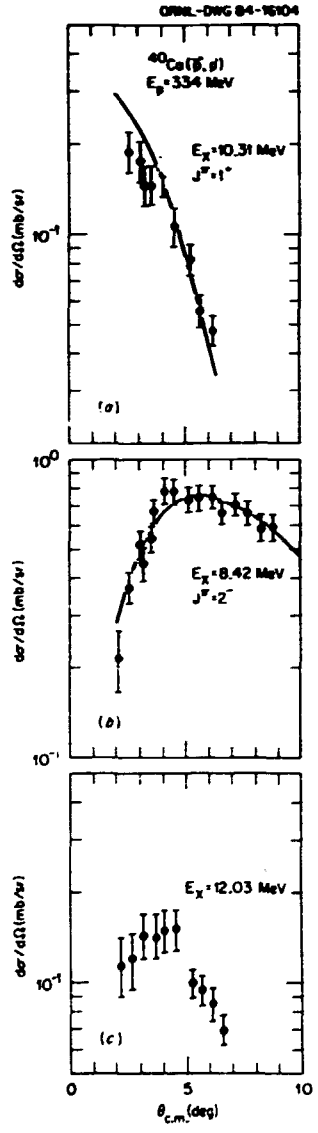

Fig. 2.6. Differential cross sections for excited states in ^{40}Ca. The solid lines are from DWIA calculations.

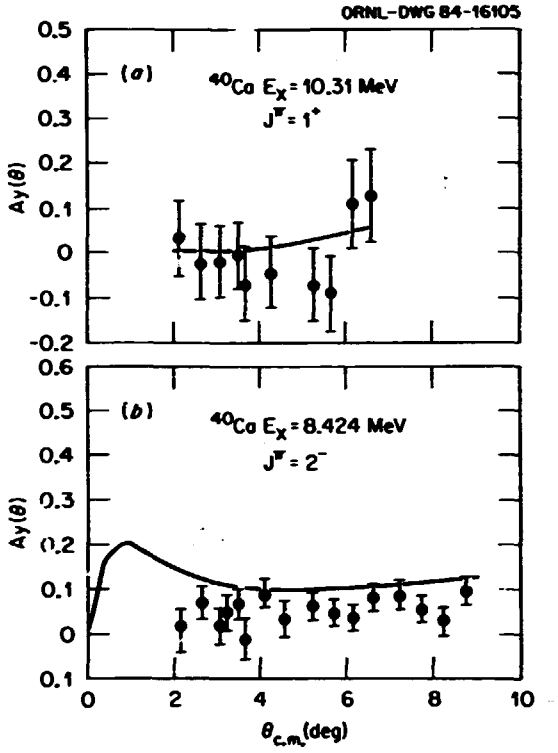

Fig. 2.7. Asymmetries for excited states in ^{40}Ca. The solid lines are from DWIA calculations.

quenching, but still have to quench the σ operator by ~80% as is needed to reproduce the ground-state magnetic moment of ^{41}Ca. Brown et al.[8] have discussed the qualitative aspects of core breaking.

We have performed microscopic DWIA calculations using the Love-Franey[9] interaction and the code[10] DWBA-81. For the 1$^+$ excitation in ^{48}Ca we have used a pure $f_{5/2}f_{7/2}$ neutron particle-hole transition. Our optical potential parameters were deduced by fitting our elastic cross section and polarization data over the angular range θ_{cm} ≈2°-15°. At 334-MeV, the reaction is dominated by the στ component of the interaction. We find that the calculated cross section must be multiplied by ~0.29 to fit the data. This is in good agreement with the results of Nanda et al.[5] who found a scaling factor of 28% at 319 MeV. The solid curves in Fig. 2.5 are the calculated values. Overall, the calculations reproduce the data quite well in the angular range considered. Nanda et al.[5] found that with the fp space model wave functions the normalization needed to get agreement with the data was ~47%. This is about the same ratio obtained from (e,e') results which is as expected for a pure neutron M1 excitation. From measurements at E_p = 201 MeV, Crawley et al.[11] deduced a normalization of only ~30%.

For the 10.31-MeV 1$^+$ state in ^{40}Ca, the ground state configuration was taken as $[(f_{7/2})^2(d_{3/2})^{-2}]_{0+}$; $f_{7/2}$→$f_{7/2}$ and $d_{3/2}$→$3/2$ transition densities provided by Brown[12] were used in a DWIA calculation. Normalization of the calculation to the data resulted in B(M1) = $(0.39 \pm 0.08)\mu_N^2$. This is in excellent agreement with a value of $0.55\mu_N^2$ deduced from B(GT) = 0.21 as reported by Taddeucci et al.[13] from (p,n) measurements. The calculated Ay(θ) for this transition is in good agreement with the data, as can be seen in Fig. 2.7.

The DWIA calculations for the 8.42-MeV 2$^-$ state were done with 1ħω particle-hole excitation transition densities provided by Brown.[12]

The calculated cross section was multiplied by 0.35 to normalize to the experimental data. This yields B(M2) = 281 μ_N^2 fm^2 which is in good agreement with a value deduced from excitation of the analogue state via the (p,n) reaction,[13] and also a value of 235 ± 20 μ_N^2 fm^2 measured[14] by inelastic electron scattering. The calculated Ay(θ) is in reasonable agreement with the data although it appears to be slightly high (see Fig. 2.7).

---

1. Solid State Division, ORNL.
2. University of Oregon, Eugene, OR 97403.
3. Oregon State University, Corvallis, OR 97331.
4. Los Alamos National Laboratory, Los Alamos, NM 87545.
5. S. K. Nanda et al., Phys. Rev. C 29, 660 (1984).
6. N. Anantaraman et al., Phys. Rev. Lett. 46, 1318 (1981).
7. J. B. McGrory and B. H. Wildenthal, Phys. Lett. 103B, 173 (1981).
8. B. A. Brown et al., Phys. Lett. 127B, 151 (1983).
9. W. G. Love and M. A. Franey, Phys. Rev. C 24, 1073 (1981); update, January 1984.
10. Program DWBA70, R. Schaeffer and J. Raynal (unpublished); extended version DW81 by J. R. Comfort (unpublished).
11. G. M. Crawley et al., Phys. Lett. 127B, 322 (1983).
12. B. A. Brown, private communication.
13. T. N. Taddeucci et al., Phys. Rev. C 28, 2511 (1983).
14. A. Richter, private communication in ref. 13.

A HIGH RESOLUTION STUDY OF GIANT RESONANCES IN ^{208}Pb USING INELASTIC SCATTERING OF 334-MeV PROTONS

F. E. Bertrand, E. E. Gross, D. J. Horen, T. P. Sjoreen[1], J. Lisantti[2], J. T. Tinsley[2], D. K. McDaniels[2], L. W. Swenson[3], T. Carey[4], K. Jones[4], J. B. McClelland[4], S. Seestrom-Morris[4], R.O. Sayer[5]

Even though giant multipole resonances have been studied for over a decade, there remain numerous uncertainties and discrepancies between measurements on some nuclei. One of these cases is a disagreement between inelastic electron scattering[6] and inelastic hadron scattering measurements on ^{208}Pb. The electron scattering results do not show the presence of a broad giant quadrupole resonance (GQR) peak as is observed in all hadron measurements,[7] but rather show a spectrum comprised of a large number of rather narrow peaks. Furthermore, the integrated E2 strength between 8 and 12 MeV of excitation energy is found to be 29^{+11}_{-8}% of the energy weighted sum rule (EWSR) via the electron work and 80 ± 15% in the hadron experiments. The electron experiments were performed with an energy resolution of 50-60 keV, considerably better than achieved with any of the hadron measurements.

In order to make a direct comparison with the electron measurements, we have studied giant resonances in ^{208}Pb using the high resolution spectrometer (HRS) at LAMPF. The resonances were excited using 334-MeV polarized protons and were detected in the spectrograph with an energy resolution of ~70 keV, comparable to that obtained in Ref. 1 using 50-MeV electrons.

Measurements were made at one degree intervals between 2.25 and 13.25 degrees. An inelastic excitation energy range in ^{208}Pb of 0-26 MeV was obtained by using three spectrograph magnetic field settings.

Figure 2.8 shows ^{208}Pb spectra at several angles. The spectra are dominated by several large and generally broad peaks. The various peaks have been fitted with Gaussian shapes and an estimate has been made for a smooth extrapolation of the nuclear continuum under the resonance peaks. At the smallest angles, 2.25 and 3.25 degrees, the spectra are dominated by a broad peak at 13.6 MeV. This peak arises from Coulomb excitation of the giant dipole resonance (GDR). At larger angles the GDR cross section falls off rapidly and a large peak is observed at 10.6 MeV. This peak is located at the energy where the GQR peak has been observed in other inelastic scattering work. The peak at ~14 MeV persists at larger angles but is likely to arise from excitation of both the GDR and giant monopole resonances (GMR). At 9.25 degrees, a peak centered at ~20 MeV is observed. This peak energy is in agreement with the location[8] of the giant octupole resonance. The spectrum at 10.25 degrees shows the need for inclusion of a peak located at 12.0 MeV. This result is in complete agreement with our work[9] at 200 MeV which showed the presence of L = 4 excitation at 12-MeV in both ^{208}Pb and ^{206}Pb. One of the more interesting features of the spectra in Fig. 2.8 is the large number of rather narrow peaks observed below the GQR excitation energy. These peaks are observed consistently at all angles of measurement.

Figure 2.9 shows the extracted angular distribution for the GQR peak (10.6 MeV). The cross sections are compared to a DWBA calculation for L = 2 transfer. The calculation uses optical model parameters obtained from a fit to the elastic scattering. Furthermore, as discussed in the preceding contribution to this report, use of the same parameters in DWBA calculations yield, when compared to angular distributions for low lying states in ^{208}Pb, excellent agreement with the known J^π and B(E2) for these states. From the comparison between the calculations and data shown in Fig. 2.9, we determine that 70% ± 14% of the EWSR is depleted in the 2.0-MeV-wide GQR peak. The lower part of Fig. 2.9 shows the measured analyzing power for the GQR peak. The comparison between the analyzing power calculation and data is rather good except near 11 degrees.

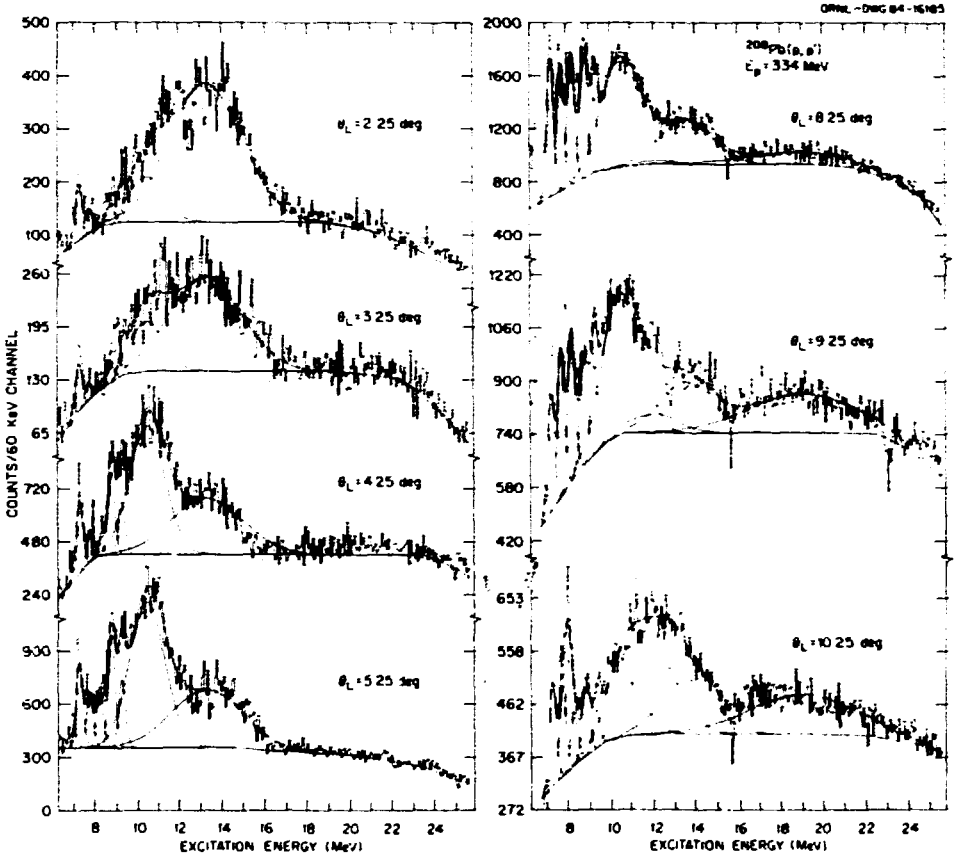

Fig. 2.8. Spectra at several angles from the reaction $^{208}Pb(p,p')$, for E_p = 334 MeV.

Figure 2.10 shows measured and calculated angular distributions for the narrow peaks found between ~7 and ~9.5 MeV of excitation energy. We find that most of the peaks are best described by L = 2 transfer although one L = 3 and one L = 4 peak has been identified. The four 2^+ states deplete a total of ~23% of the T = 0, L = 2, EWSR. This strength, when added to that found in the main GQR peak (Fig. 2.9) accounts for 93% ± 15% of the T = 0, quadrupole sum rule strength in ^{208}Pb.

It is clear from these measurements that the existence of a localized peak containing a large fraction of the quadrupole EWSR in ^{208}Pb persists in hadron scattering, even when studied with an energy resolution of 70 keV. Furthermore, these results indicate that ~90% of the L = 2, EWSR is located in the giant resonance region of ^{208}Pb. This result is in excellent agreement with that obtained from our recent measurements of the photon decay of the ^{208}Pb giant resonance region (discussed elsewhere in this report).

1. Solid State Division, ORNL.
2. University of Oregon, Eugene, OR 97403.
3. Oregon State University, Corvallis, OR 97331.
4. Los Alamos National Laboratory, Los Alamos, NM 87545.
5. Computing and Telecommunications Division, ORNL.

6. G. Kuhner et al., Phys. Lett. 104B, 189 (1981).
7. F. E. Bertrand et al., Phys. Rev. C 22, 1832 (1980).
8. F. E. Bertrand, Nucl. Phys. A354, 129c (1981).
9. J. R. Tinsley et al., Phys. Rev. C 28, 1417 (1983).

EXCITATION OF GIANT MULTIPOLE RESONANCES IN sd-SHELL NUCLEI VIA 500-MeV PROTON INELASTIC SCATTERING

B. L. Burks, F. E. Bertrand, R. L. Auble, E. E. Gross, D. J. Horen, R. O. Sayer[1], L. W. Swenson[2], D. K. McDaniels[3], J. Lisantti[3], J. R. Tinsley[3], K. W. Jones[4], J. B. McClelland[4], S. Seestrom-Morris[4]

Over the past few years considerable research effort has been expended toward the establishment of the location of various multipole giant

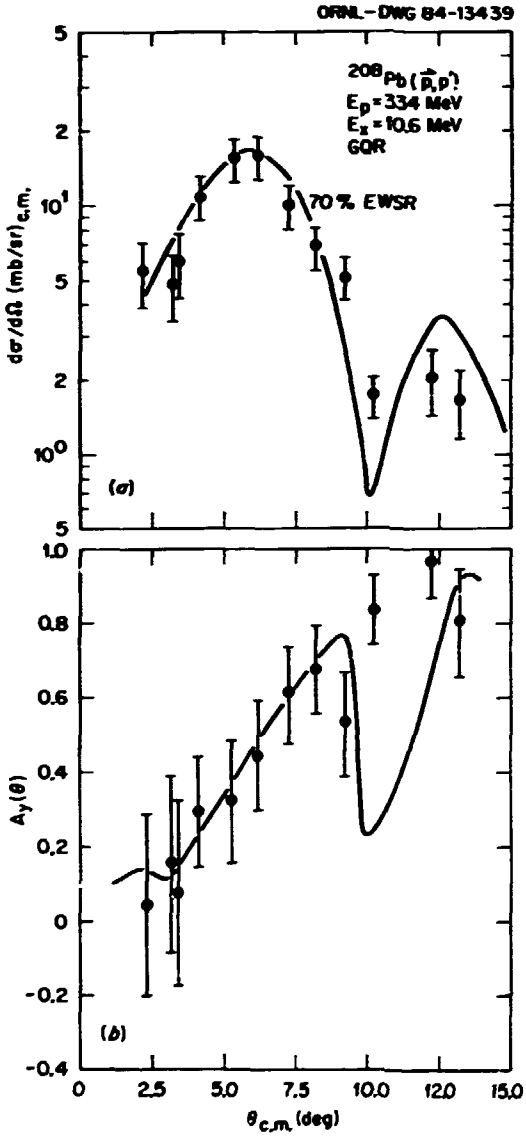

Fig. 2.9. Angular distributions and analyzing powers for the GQR in ^{208}Pb from inelastic scattering of 334 MeV protons.

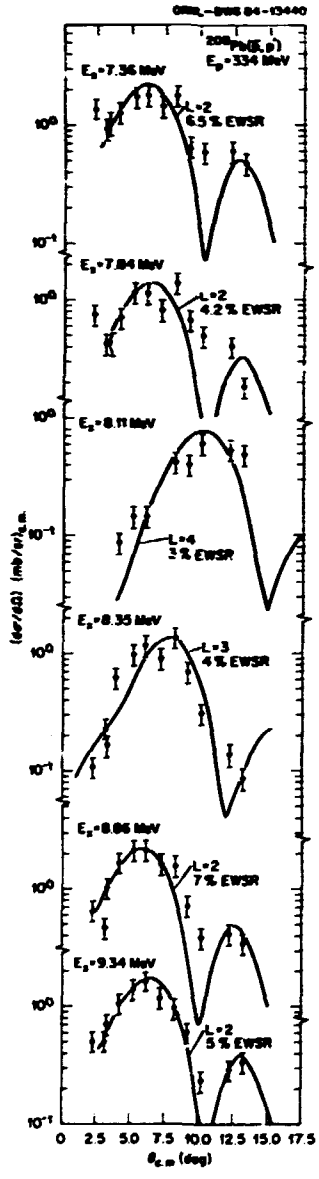

Fig. 2.10. Angular distributions for narrow states observed below the giant quadrupole resonance.

resonances. For nuclei having A > 40 systematics of the energy, width, and strength of isoscalar monopole, quadrupole, and octupole resonances have been rather well established.[5] For nuclei in this mass region the isoscalar giant resonances appear as broad (2-6 MeV FWHM) peaks rising above a generally flat nuclear continuum.

For nuclei lighter than A~40, specifically sd-shell nuclei, the character of the giant quadrupole resonance is dramatically different. No longer is a broad peak observed, but with adequate energy resolution many individual peaks are observed in the $2\hbar\omega$ - $3\hbar\omega$ region of excitation energy. This fine structure was initially observed via inelastic scattering of 60-MeV protons[6] and later using the (α,α') reaction[7] with 120-MeV alpha particles. The sd-shell offers a unique opportunity for comparison of GQR excitation via proton and alpha inelastic scattering, electron scattering,[8] and alpha capture reactions.[9] A comparison of giant resonance results from several different reactions is necessary to unfold the complicated observed resonance structures. Studies in the sd-shell offer the maximum number of reactions for comparison.

We report here a study of giant resonance states in sd-shell nuclei excited by inelastic scattering of 500-MeV polarized protons using

the HRS facility at LAMPF. Data were measured from 4° to 20° for scattering from ^{40}Ca and from 4° to 12° for scattering from ^{28}Si. We plan to request additional beam time to extend the ^{28}Si angular distribution and measure additional data for ^{24}Mg and ^{26}Mg. Two settings of the magnetic field were required to obtain composite spectra covering an excitation energy range from 0.5 to ~40 MeV. Elastic scattering data were measured separately at a third magnetic field setting. Figure 2.11 shows a spectrum obtained for the low excitation range in ^{40}Ca at a laboratory angle of 7°. Typical spectra have an energy resolution of 80 keV FWHM and show essentially no "bogus" background.

DWBA calculations (see Fig. 2.12) indicate that inelastic scattering of 500-MeV protons should be an effective probe for determining the multipolarity of the various observed peaks in the giant resonance region. Significant differences exist between the angular distributions of neighboring L-transfer values. For example, the GDR (L = 1) will be excited strongly and nearly exclusively for angles less than ~6 degrees and will provide almost no contribution to the spectra for angles greater than ~10 degrees. Previous measurements with 60-MeV protons and 120-MeV alphas yielded angular distributions which were not particularly discriminating between neighboring L-transfer values. With the high resolution of our proton scattering data and strong L-dependence of the cross section angular distribution, this analysis, when completed, should improve multipolarity assignments for peaks in the giant resonance region of the sd-shell nuclei.

In order to test the DWBA calculations, data must be taken for low-lying states of known spin and parity. A large number of low-lying states were well resolved in both the ^{40}Ca and ^{28}Si spectra, see, for example, Fig. 2.11(a). These data have been analyzed using the QSYSTEM replay package on the VAX computers at LAMPF. Peak-fitting and DWBA calculations for low-lying states and peaks observed in the giant resonance region are in progress at Oak Ridge.

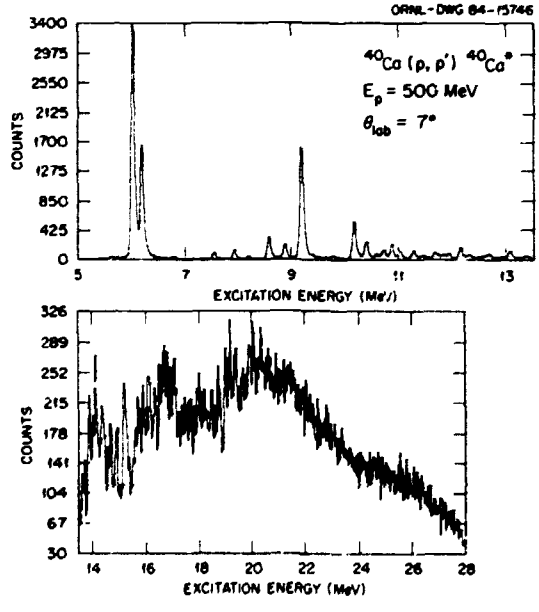

Fig. 2.11. An excitation energy spectrum for ^{40}Ca(p,p)^{40}Ca at E_p = 500 MeV and θ_{lab} = 7°. (a) shows low-lying discrete states in ^{40}Ca; excitation energies are labeled on the abscissa. (b) shows a compressed view of the giant resonance region in ^{40}Ca. Note in (b) that the efficiency of the focal plane detector at this magnetic field setting decreases for excitation energies above 25 MeV.

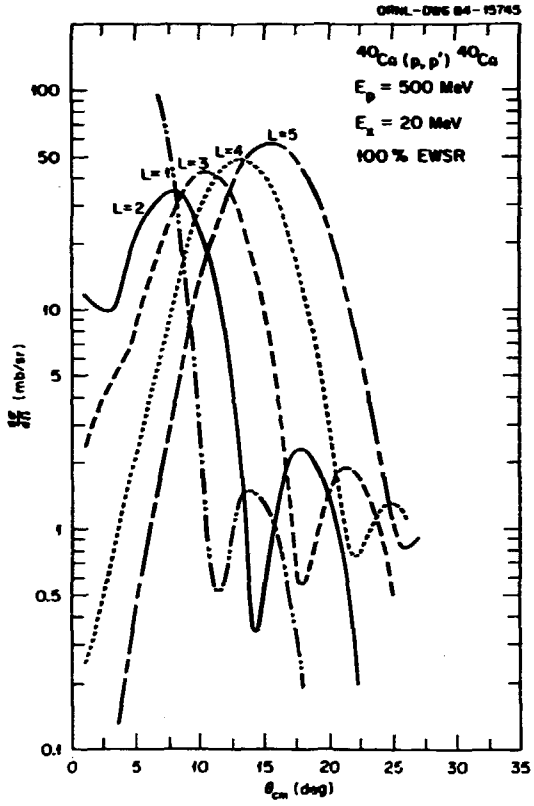

Fig. 2.12. DWBA calculations for excitation of various multipoles by the reaction ^{40}Ca(p,p')^{40}Ca for E_p = 500 MeV. Each calculation assumes 100% depletion of the energy weighted sum rule (EWSR).

---

1. Computing and Telecommunications Division, ORNL.
2. Oregon State University, Corvallis, OR 97331.
3. University of Oregon, Eugene, OR 9740[illegible].
4. Los Alamos National Laboratory, Los Alamos, NM 87545.
5. F. E. Bertrand, Nucl. Phys. A354, 129c (1981).

6. F. E. Bertrand et al., ORNL-5137, p. 63 (1975), unpublished.
7. F. E. Bertrand et al., Phys. Rev. Lett. 40, 635 (1978). K. Van der Borg et al., Phys. Lett. 67B, 405 (1977). K. Van der Borg et al., Nucl. Phys. A365, 243 (1981).
8. A. Richter, Lectures presented at "The International School on Nuclear Structure," Alushta, USSR, April 14-25, 1980, IKDA 80/4 (1980).
9. E. Kuhlmann et al., Phys. Rev. C 11, 1525 (1975).

ELECTROMAGNETIC DECAY OF GIANT RESONANCES

J. R. Beene R. L. Auble
F. E. Bertrand D. J. Horen
M. L. Halbert R. L. Robinson
D. C. Hensley T. P. Sjoreen[1]
R. O. Sayer[2]

Current theoretical investigations of giant resonances focus on efforts to understand the microscopic structure of the resonances and the damping of the resonance states into the continuum.[3] Experimental data required to guide and constrain these investigations include detailed studies of the decay of the resonances. Studies of electromagnetic decay are particularly appealing because of the relative simplicity of interpreting the results, and in the case of the direct decay of the resonances to the ground state, because of the intimate relationship of this process to the definition of the giant resonances.

We have carried out coincidence experiments to investigate photon and neutron emission from the giant resonance region in ^{208}Pb and ^{90}Zr using the ORNL Spin Spectrometer, a 72 segment, almost 4π NaI detector system. States in ^{208}Pb and ^{90}Zr were excited by inelastic scattering of 380-MeV ^{17}O. ^{17}O was chosen as a projectile because its low neutron binding energy (4.1 MeV) prevents projectile excitation from being an important source of background in the vicinity of the resonances.

Details of the experiment and the methods developed to analyze the data have been discussed extensively elsewhere.[4,5,6] In this report we will concentrate on results for ^{208}Pb. The ^{90}Zr experiment produced insufficient data to be useful in investigating the region of the giant quadrupole resonance (GQR), but will produce valuable results on decay of lower lying states, such as the low energy octupole resonance at ~7.5 MeV.

Table 2.3 summarizes current knowledge of strongly collective states in the 8-18 MeV region of ^{208}Pb, based largely on high resolution, medium energy proton scattering data.[7] The last two columns refer to the present experiment. The column labeled "Expected σ" gives the cross section for ^{17}O scattering calculated with the code ECIS, assuming the strengths from proton scattering. The last column gives the cross sections actually observed in the current experiment, obtained from fits to the ^{17}O inelastic spectrum with peak parameters fixed in accordance with the information from (p,p'). The ^{17}O data appear to be in excellent agreement with the proton data.

Table 2.3. Properties of states above 8 MeV in ^{208}Pb observed in ^{208}Pb(p,p'), from Ref. 7. The last two columns refer to the present ^{208}Pb(^{17}O,^{17}O') experiment. Expected σ is the cross section expected for ^{17}O scattering based on the proton results. Observed σ is the cross section which we observe. Uncertainties of about 15% apply to both the observed and expected cross sections.

Excitation Energy (MeV)	L	Γ (MeV)	EWSR Fraction %	For (^{17}O,^{17}O') Expected σ (mb/sr)	Observed σ (mb/sr)
8.11	4	0.4	3	9	13
8.35	3	0.4	4	5	
8.86	2	0.4	7	8	6
9.34	2	0.4	5	5	13
10.6	2	2	70	50	60
12.0	4	2.4	10	17	18
13.6	1	4.0	100	~4	20
13.9	0	2.9	100	10	

Figure 2.13 shows the relative ground state branching (i.e., ground state gammas/total gammas) as a function of excitation energy in ^{208}Pb. A rapid fall-off in ground state decay above the neutron binding energy (7.4 MeV) is evident, as is a strong clustering of ground state strength in the 9-15 MeV region. This provides a graphic illustration of the special relationship that states in this excitation energy region have with the ground state. This broad peak contains contributions from both the GQR and the giant dipole resonance (GDR), which though very weakly excited (see Table 2.3) has a much larger ground-state gamma decay width. The ground-state gamma decay spectrum was decomposed using the peak information from Table 2.3, assuming that only dipole and quadrupole states contribute. The decomposition was confirmed by gamma-ray angular distribution data which showed 70% of the ground-state radiation in the 9.6-11.6 MeV region to be quadrupole. The ground state decay and yields from the singles spectra provide an estimate of the ground-state gamma branch of the GQR:

$$\frac{\Gamma_{\gamma_0}}{\Gamma_T} = (3.27 \pm 0.45) \times 10^{-4}.$$

This result can be used to obtain an absolute value for $\Gamma_{\gamma 0}$ if we assume $\Gamma_T \approx \Gamma^{\uparrow}$ (where $\Gamma^{\uparrow}$ is the spreading width) and identify $\Gamma^{\uparrow}$ with the experimentally observed resonance width Γ_{EXP} from Table 2.3:

$$\Gamma_{\gamma 0} = \frac{\Gamma_{\gamma 0}}{\Gamma_T} \Gamma_{EXP} = 654 \pm 91 \text{ eV} \quad \text{(GQR)}$$

or, taking $E_{\gamma 0} = 10.6$

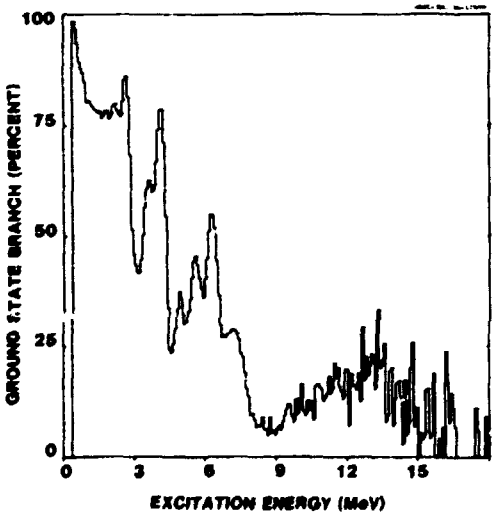

Fig. 2.13. The yield of gamma rays directly to the ground state divided by the total gamma-ray yield, as a function of ^{208}Pb excitation energy.

$$B(E2\uparrow) = (5.81 \pm 0.81) \times 10^3 \text{ e}^2 \text{ fm}^4.$$

This should be compared with the energy weighted sum rule (EWSR) value[8,9]

$$B(E2\uparrow)_{EWSR} = 49.9\ A^{5/3}/(5xE_{\gamma 0}) = 6.9 \times 10^3 \text{e}^2\text{fm}^4.$$

Therefore,

$$\frac{B(E2\uparrow)}{B(E2\uparrow)_{EWSR}} = 0.85 \pm 0.12.$$

The yield of dipole ground state transitions from the vicinity of the GDR is consistent within large uncertainties (~50%) with the pure Coulomb prediction of GDR excitation obtained from the direct reaction code ECIS, and a decay strength corresponding to 100% of the EWSR strength.

Gamma decay branches from the resonance region other than the ground state decay are also of great interest, in particular, direct decays to the low-lying collective states at 2.6 MeV (3^-) and 4.08 MeV (2^+). Figure 2.14 shows the relative strength of gamma ray branches to a number of low lying states: (a) is for the ground state, (b) the 2.6 MeV 3^-, (c) the 4.08 MeV 2^+, and (d) the 4.97 MeV 3^-. The yield distributions in (b)-(d) must be considered semi-quantitative, especially where they indicate small strengths, because adequate background subtraction has not been performed. Nevertheless they are valuable to indicate general features. One of the more striking aspects of these data is the marked absence of strength to the 2.61-MeV and 4.08-MeV states across the entire resonance region. Another interesting feature is the strong yield of decays to the 2.61-MeV state at ~5.2 MeV of excitation energy. This might be an indication of the long-sought, two-phonon octupole vibrational state. In contrast to the collective 3^- state, yield to the 4.97-MeV 3^- state (which is thought to be dominated by a single neutron particle hole configuration) is significant across the entire GQR resonance, but with its greatest yield ~1.5 MeV below the peak of the GQR. A very similar strength distribution is seen for population of a 5^- state at 3.97 MeV, which we take to indicate the presence of high spin (4^+ or 6^+) strength underlying the GQR.

A more quantitative analysis of the decay of an excitation energy bin centered on the GQR is given in Table 2.4. It should be noted that the absence of decay to the 2.6-MeV 3^- state, which appears remarkable at first sight, was predicted by Bortignon, Broglia, and Bertsch.[1]

The data presented in this report are only a sampling of a rich body of information now becoming available from Spin Spectrometer-based studies of giant resonance decay.

---

1. Solid State Division, ORNL.
2. Computing and Telecommunications Division, ORNL.

3. G. E. Bertsch, P. F. Bortignon, and R. A. Broglia, Rev. Mod. Phys. 5, 287 (1983).
4. J. R. Beene et al., Nuclear Physics with Heavy Ions, ed. P. Braun-Munzinger (Harwood Academic, N.Y., 1983).
5. F. E. Bertrand, J. R. Beene, and T. P. Sjoreen, Journal de Physique 45, C4-99 (1984).
6. J. R. Beene et al., Proceedings of Fifth International Symposium on Capture Gamma Ray Spectroscopy, Sept. 1984, to be published.

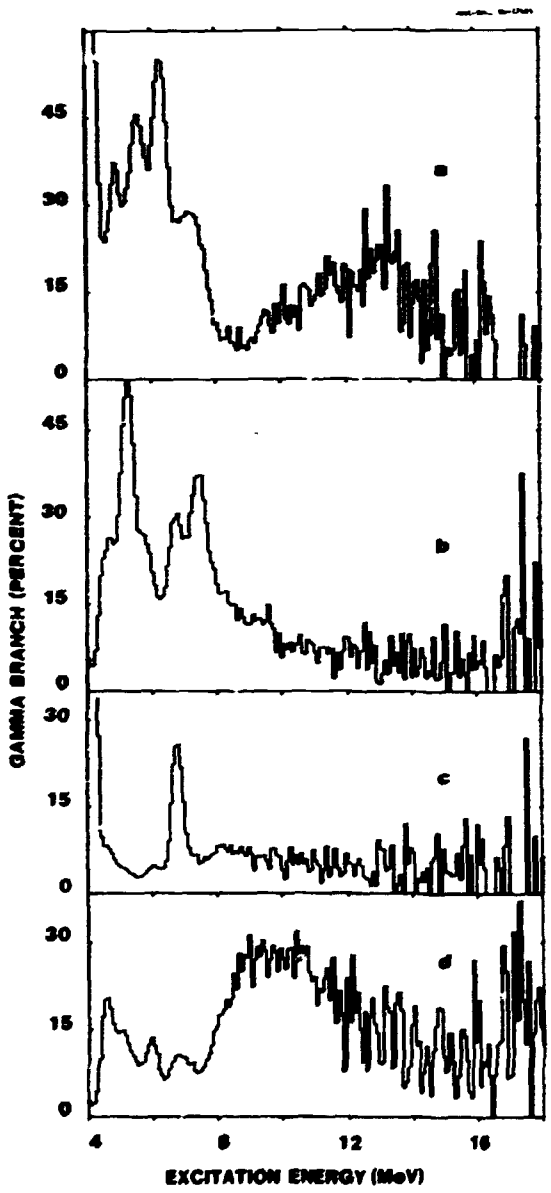

Fig. 2.14. The yield of gamma rays populating low-lying states in ^{208}Pb, relative to the total gamma-ray yield, as a function of excitation energy in ^{208}Pb. Figure 2a is for the ground state, 2b the 2.61 MeV 3$^-$, 2c the 4.08 MeV 2$^+$, and 2d the 3.97 MeV 3$^-$ state.

7. F. E. Bertrand et al., private communications.
8. F. E. Bertrand, Ann. Rev. Nucl. Sci 26, 457 (1976).
9. A. Bohr and B. Mottleson, Nuclear Structure, Vol. II (Benjamin, Reading Mass, 1975).
10. P. F. Bortignon, R. Broglia, and G. F. Bertsch, to be published.

Table 2.4. Relative gamma branching to low-lying states in ^{208}Pb from an excitation energy region 9.5-11.5 MeV [E(GQR) ± Γ(GQR)/2]. The 5-7 MeV 1$^-$ states refers to a group of 1$^-$ states in that region known from γ,γ' experiments.

Energy	J^π	Relative Gamma Branch (%)
0	0$^+$	2$\sim$ ± 2
2.61	3$^-$	0.8 ± 0.8
3.97	5$^-$	~5 - 10
4.08	2$^+$	0.$\sim$ $^{+1.0}_{-0.3}$
4.97	3$^-$	36 ± 5
5-7	1$^-$	23 ± 9

NEUTRON DECAY OF GIANT RESONANCES

J. R. Beene, F. E. Bertrand, M. L. Halbert, D. C. Hensley, R. L. Auble, D. J. Horen, R. L. Robinson, T. P. Sjoreen[1], R. O. Sayer[2]

Experimental studies of the decay of giant resonances are required to guide and constrain theoretical efforts to gain a more complete understanding of the microscopic structure of giant resonances and their damping into the underlying continuum of more complex states. We have performed experiments to study in detail all decay modes of the giant resonance region of ^{208}Pb and ^{90}Zr. Both ^{208}Pb and ^{90}Zr were excited by inelastic scattering of 381-MeV ^{17}O. Decay of the giant resonance region up to ~20 MeV was studied using the ORNL Spin Spectrometer.[3] The experimental techniques and methods of analysis employed in this study have been discussed in detail elsewhere.[4,5,6]

Neutron emission makes up the bulk of all decays in the 9-20 MeV region in both systems studied. The goal of the present study is to obtain as complete information as possible on the distribution of decay strength to low-lying states in ^{207}Pb and ^{89}Zr as a function of ^{208}Pb and ^{90}Zr excitation energy. The residual excitation energy in the daughter nucleus is

obtained from the total gamma-ray energy observed in the Spin Spectrometer in coincidence with a neutron (distinguished from gamma rays by its longer time of flight to the spectrometer). Neutron angular distributions can also be constructed, utilizing the almost 4π solid angle and relatively fine segmentation (70 elements in our case) of the Spin Spectrometer.[3] The kinetic energy of the emitted neutrons is obtained from the initial excitation energy in the parent nucleus (i.e., from the inelastically scattered ^{17}O energy), the residual excitation energy in the daughter nucleus (sum gamma-ray energy), and the neutron binding energy.

The analysis of neutron decay has, so far, concentrated on the ^{208}Pb data. We find neutron angular distributions up to about 12-13 MeV of excitation energy which are very nearly symmetric with respect to the ^{208}Pb recoil direction, suggesting the dominance of statistical or compound decay. The neutron energy spectra obtained from this excitation region, however, are significantly different from the Maxwellian shape normally associated with statistical decay. An apparent 10-15% excess of high energy neutron emission is observed, in agreement with earlier work.[7] It is dangerous, however, to conclude that these high energy neutrons represent a genuinely nonstatistical fraction without more careful investigation. The high energy neutrons result primarily from population of the ground state and the first two excited states in ^{207}Pb. The level density in this region is far too low to generate Maxwellian neutron spectra. Careful statistical model calculations, including explicitly the experimental level scheme of ^{207}Pb are required before a significant comparison can be made.[8] Such calculations are in progress.

The data show significant yield to high spin states of ^{207}Pb ($I > 9/2$) across the region dominated by the giant quadrupole resonance (9-12 MeV). This is in agreement with earlier work[7] and also supports evidence for high spin strength in this region found in the electromagnetic decay data.[4,5,6]

Above ~13 MeV of excitation in ^{208}Pb we see a rapidly rising (with increasing excitation energy) fraction of strongly forward peaked neutrons. These neutrons appear to be associated with processes which preferentially populate the $5/2^-$ and $3/2^-$ states at 570 and 898 keV in ^{207}Pb. At $E^* = 15$ MeV, approximately 30% of the population of the $3/2^-$, 898 keV, state corresponds to these forward peaked neutrons. Preliminary analysis indicates that these neutrons are more tightly correlated with the direction of detection of the ^{17}O ejectile than with the beam direction. It is likely that most of them arise from the reaction $^{208}Pb(^{17}O,^{18}O)^{207}Pb$, in which both the ^{207}Pb and the ^{18}O products are left excited, the ^{18}O having sufficient energy to decay in flight by neutron emission ($S_n = 8.04$ MeV for ^{18}O). This process has, of course, nothing to do with decay of the giant resonance region in ^{208}Pb. These and other interesting aspects of the data are under active study.

---

1. Solid State Division, ORNL.
2. Computing and Telecommunications Division, ORNL.

3. D. G. Sarantites, R. Lovett, and R. Woodward, Nucl. Instrum. Methods 171, 503 (1980), and M. Jääskeläinen et al., Nucl. Instrum. Methods 204, 385 (1983).
4. F. E. Bertrand, J. R. Beene, and T. P. Sjoreen, Journal de Physique 45, C4-99 (1984).
5. J. R. Beene et al., Nuclear Physics with Heavy Ions, ed. P. Braun-Munzinger (Harwood Academic, N.Y., 1983).
6. J. R. Beene et al., Proceedings of Fifth International Symposium on Capture Gamma Ray Spectroscopy, Sept. 1984, to be published.
7. H. Steuer et al., Phys. Rev. Lett. 47, 1702 (1981).
8. H. Dias and E. Wolynec, preprint IFUSP/P-469.

FISSION DECAY OF GIANT RESONANCES IN ^{238}U

J. R. Beene, B. L. Burks, C. E. Bemis, E. E. Gross, F. E. Bertrand, D. J. Horen, R. L. Auble, I. Y. Lee, R. O. Sayer[1]

In an earlier study[2] of the fission decay of the giant quadrupole resonance in ^{238}U, using the $^{238}U(\alpha,\alpha')$ reaction at 152 MeV, the data suggested that the fission branch was consistent with that of the underlying continuum and the GQR. A major shortcoming of that study was the limited angular range covered by the fission fragment detectors. This introduced a considerable uncertainty in the deduced fission branch due to the lack of information regarding the fission fragment angular distribution. A value $\Gamma_f/\Gamma = 0.25 \pm 0.10$ was obtained by assuming K was preserved in the decay process. This disagrees with an earlier measurement[3] which gave an upper limit of about 0.04. Thus, additional measurements were indicated to resolve this discrepancy.

The present measurements were performed using the $^{238}U(^{16}O,^{16}O')$ reaction at 400 MeV. This reaction was chosen on the basis of measurements on ^{208}Pb where a favorable peak/continuum ratio is obtained in GQR region using heavy ion inelastic scattering.[4] The scattered $^{16}O'$, and other reaction products, were detected in eight Si-detector telescopes oriented in a ring surrounding the beam line and at a scattering angle of 12 ± 1.5 degrees (a maximum of the GQR angular distribution). The fission fragments were detected by two 12 cm x 12 cm position sensitive avalanche detectors (PSAD's) located at 90° on either side of the beam line. The detector arrangement is shown in Fig. 2.15. The data will provide a measurement of the complete fission fragment angular distribution, relative to the recoil axis, and will answer the question regarding K conservation as well as provide a more precise measurement of the GQR fission

ORNL-Photo 2730-84

Fig. 2.15. Detector arrangement used to study the fission decay of the giant resonance region in ^{238}U. The parallel plate avalanche counters are located on either side of the beam line and a ring containing eight Si-detector telescopes is located near the center of the photograph. The target, which normally sits between the two avalanche detectors, has been removed.

branch. The PSAD position calibrations are now complete and the data analysis is in progress.

---

1. Computing and Telecommunications Division, ORNL.
2. F. E. Bertrand et al., Phys. Lett. 99B, 213 (1981).
3. J. van der Plicht et al., Phys. Rev. Lett 39, 1188 (1977).
4. T. P. Sjoreen et al., Phys. Rev. 29, 1370 (1984).

ELASTIC AND INELASTIC PROTON SCATTERING FROM ^{16}O AT 200 MeV

C. W. Glover

A growing number of nonrelativistic distorted wave approximation (DWA) analyses of elastic and inelastic proton scattering indicate that the effective free nucleon-nucleon interaction (t-matrix) must be modified to include effects due to the nuclear medium for proton bombarding energies below 400 MeV[1] and the need becomes essential for bombarding energies below 200 MeV.[2] The most sophisticated modifications to date have been those derived from G-matrices based on realistic NN potentials[3] and calculated in the presence of nuclear matter where one of the two interacting nucleons has an energy greater than the Fermi energy. The resulting G-matrices are local, energy- and density-dependent. In particular, the central isoscalar spin-independent component of the effective NN interaction is the most sensitive to these nuclear medium modifications.[2,3] These G-matrices are applied to transitions in finite nuclei by invoking the local density approximation (LDA).[2]

The study of proton induced elastic and inelastic isoscalar natural parity transitions has shown that these transitions are driven primarily by the central isoscalar spin-independent component of the effective NN interaction at small momentum transfer ($q \lesssim 1$ fm^{-1}), by the spin-orbit part of the effective interaction for intermediate q values (1 fm$^{-1} \lesssim q \lesssim 2.5$ fm^{-1}) and both components have roughly the same magnitude in the high-q region.[4,5,7] Calculations for these inelastic transitions in the 100-200 Mev energy regime which use the free t-matrix and phenomenological distorted waves indicate that the low-q cross section is overpredicted by typically 50% and the high-q part is underpredicted. The calculations using the G-matrix are in closer agreement with the cross section data because the low (high)-q components of the central isoscalar spin-independent part of the NN-interaction is reduced (enhanced) as compared to the free t-matrix.[2,5] Moreover, when analyzing power data are considered in addition to the cross section data, they appear to prefer distorted waves generated from a folding model optical potential using the G-matrix interaction over those generated from the phenomenological Woods-Saxon optical potentials which are fit to the elastic data.[2] However, the folded G-matrix optical potentials with the characteristic pocket of attraction in the nuclear surface do not adequately reproduce the elastic scattering data. Even so, all calculations (both elastic and inelastic) using the folded G-matrix are still far superior to those using the free t-matrix interaction.

An explanation, given by Kelly,[2] for this apparent lack of consistency in the G-matrix description of the elastic and inelastic data focuses on the radial localization of the transition.[4] Radial localization can be understood in the distorted wave approximation (DWA) by recalling that the inelastic transition amplitude is proportional to the average of the product of the transition density, distortion factor, and the effective NN-interaction. Inelastic natural parity transitions involving large angular momentum transfers (~2-4 ħ) tend to have transition densities which peak near the low density nuclear surface.[4] Monopole and isoscalar electric dipole transitions tend to peak more toward the high density nuclear interior.[2] Hence, the different inelastic transitions tend to weight different regions of the

distortion factor (i.e., optical potential), while elastic scattering is averaged over the entire nuclear volume. Thus, some inelastic transitions may be more sensitive to the interior properties of the optical potential than elastic scattering.

This can be realized by considering the fact that in fitting a phenomenological Woods-Saxon optical potential to elastic scattering data measured over small momentum transfers ($q \lesssim 3$ fm^{-1}) results in a potential which is biased toward the nuclear surface region and does not adequately reflect the contributions to elastic scattering from the nuclear interior. Hence, measurements to large q would constrain those partial waves emanating from the nuclear interior. Also, the Woods-Saxon shape presumes the optical potential remains constant in the nuclear interior and this is contrary to what is expected from the microscopic nuclear matter calculations.

An approach, the one to be reported here, to remedy this inconsistency is to measure elastic scattering data to large momentum transfer, so the contributions to the optical potential from the nuclear interior are reflected in the data. Then, fit the data by using a phenomenological parametrization for the real central optical potential that is flexible enough to reproduce those characteristics expected from microscopic derivations of the single-particle potential in nuclear matter. Finally, a comparison of the DWA analyses of the inelastic data for surface and interior states using these potentials for the distorted waves against those using the folded G-matrix optical potential should indicate to what extent our expectations from nuclear matter are borne out phenomenologically.

In Ref. 6, optical potentials were reported for $\vec{p}$ + ^{16}O at 200 MeV where the data were measured to q ~ 6 fm^{-1}. The standard single Woods-Saxon (SWS) and a nonstandard double Woods-Saxon (DWS) optical potential parametrizations were applied to the data, see Fig 2.16. In the DWS parametrization, the central real potential was modified to be the sum of two Woods-Saxon potentials, one attractive and one repulsive. The more flexible DWS parametrization reproduced all the data better than the SWS parametrization. The DWS parametrization proved to be so flexible that two vastly different optical potentials were found. These potentials are not related to one another through a phase-shift ambiguity. The best description of the data (including total and reaction cross sections) is obtained with the DWS(-) parametrization, where the real central potential is attractive over the entire radial range and exhibits an enhanced attraction inside 2 fm. The data are described nearly as well, however, by the DWS(+) representation in which the real central potential has an attractive pocket near the nuclear surface and a repulsive core inside 2 fm [hence the characterizations DWS(+) and DWS(-) with the (+) and (-) symbols obviously referring to the repulsive or attractive real central core]. The results of the latter parametrization are more in accord with expectations from various microscopic theories of nucleon propagation in a many-body nuclear

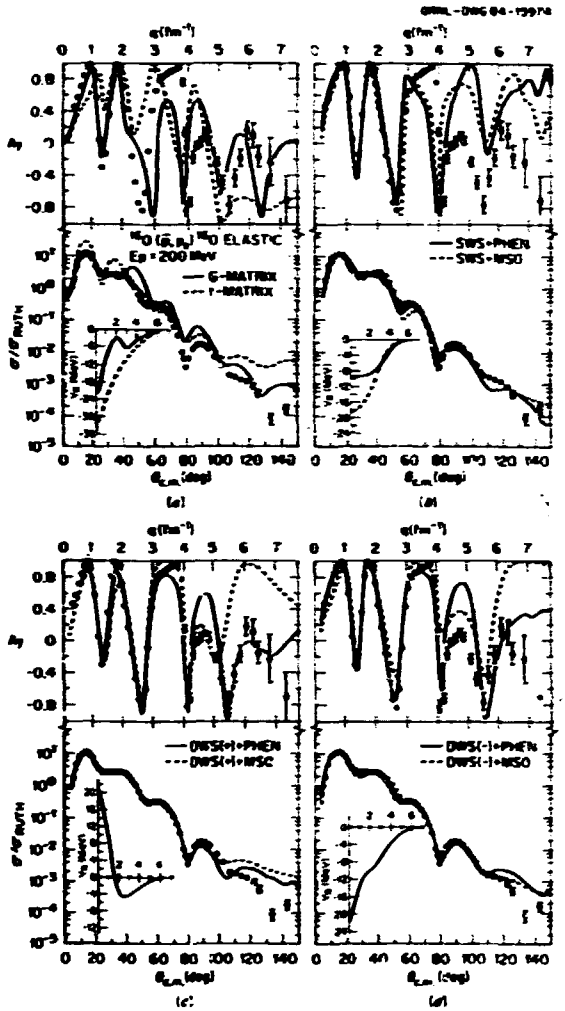

Fig. 2.16. The $\vec{p}$ + ^{16}O elastic scattering cross section and analyzing power data are compared with those microscopic and phenomenological optical potentials that are discussed in the text. The data are displayed as a function of center-of-momentum angle θ_{cm} on the bottom axis and as a function of momentum transfer q on the top axis. Inset in each figure are the resulting real central optical potentials. In Fig. 2.16(a), the G-matrix optical model calculation is based on the Paris NN interaction.

environment. Each potential implies that a different scattering mechanism is responsible for the increase in the elastic flux at large q; a particle can be scattered to large angles either from the near side of the nucleus by reflection from a strongly repulsive potential, or by a strongly attractive potential causing the particle to orbit around the far side of the nucleus. The results of the present analysis indicate that it is impossible to distinguish between these scattering mechanisms on the basis of the available elastic scattering data alone.

These phenomenological optical potentials have been used along with those generated by folding the G- and t-matrix NN interactions with the ^{16}O ground state density distribution in a DWA analyses for the inelastic transitions to the first 2^+ state (a surface state) and to the first 1^- state (an interior state). The ground state and inelastic transition densities were measured to ~3 fm^{-1} by electron scattering. (Hence, any critical assessment of the calculations will be limited to the data forward of 3 fm^{-1}). The free NN t-matrix comes from the parametrization of Love and Franey[7] at 210 MeV. The two G-matrix interactions come from the parametrizations of the Paris and Hamada-Johnson potentials by von Geramb.[3] The calculations were performed with computer code ALLWRLD-TAMURA as modified by Carr, Kelly, and Petrovich.[8] The results of these calculations are displayed in Fig. 2.17. The data were taken at the Indiana University Cyclotron Facility and the experimental procedure is described in Ref. 6.

In Fig. 2.16, one can see that the parameter-free microscopic optical potential derived from the G-matrix interaction does not reproduce all of the elastic data as well as the phenomenological potentials, but is in closer agreement with the forward angle cross section and analyzing power data than those from the t-matrix interaction. The dampening of the cross section at the first and second maxima and the enhancement of the third and fourth maxima in the G-matrix calculations over that from the t-matrix calculations is a result of the low-q (high-q) suppression (enhancement, of the isoscalar spin-independent NN interaction which was discussed above.

The consistent DWA analyses of the first 2^+ (surface) transition using the G-matrix interaction are in closer agreement with all of the data than the calculations using the free t-matrix interaction. This is quite evident in the analyzing power data (see Fig. 2.17a). (Here the term consistent means the optical potentials were calculated using the same NN interaction as that used in the inelastic form factor calculations.) Surface transitions, such as the 2^+, are sensitive to the low density part of the G-matrix interaction. The G-matrix calculation based on the Paris interaction is more representative of the 2^+ cross section data than the calculations using the Hamada-Johnson (HJ) interaction. This indicates that the magnitude of the low-density low-q component of the HJ interaction is too small and the low-density high-q component is too large, while the consistent calculation using the Paris (HJ) interaction under (over) predict the 1^- cross

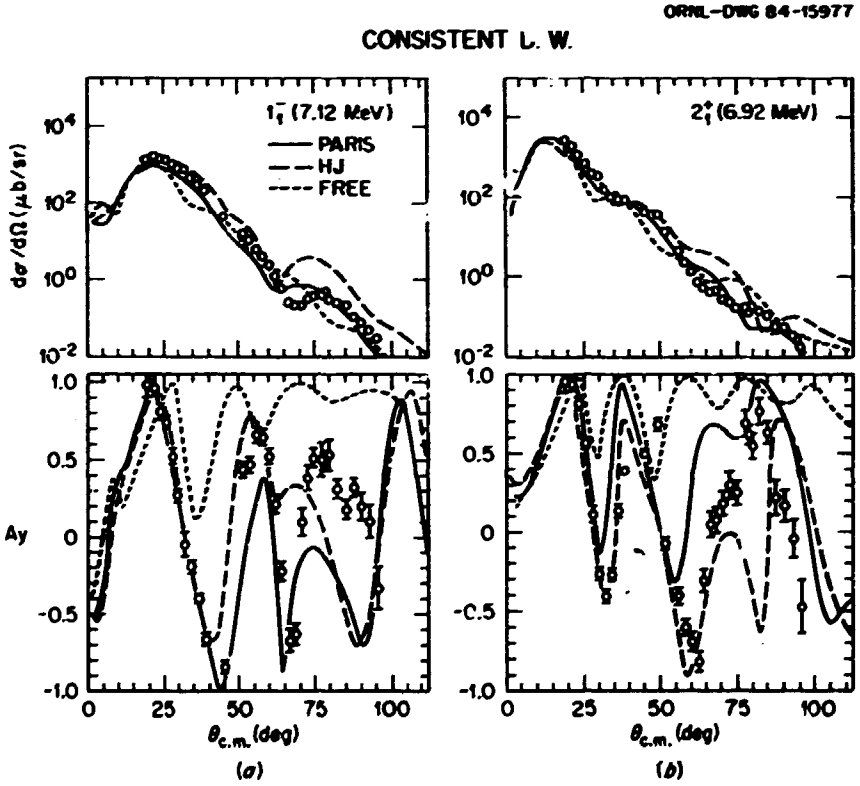

Fig. 2.17. The completely consistent microscopic calculations are compared with the 2^+(7.12 MeV) and 1^-(6.92 MeV) inelastic transition data in (a) and (b), respectively. Here the distorted waves were generated from a folding model optical potential which uses the same NN interaction as that used in calculating the inelastic form factor.

section (see Fig. 2.17b). This indicates the high-density component of the Paris (HJ) G-matrix is too small (large). However, all the analyzing power data appear to prefer the HJ interaction. It is apparent from these calculations that the data require the use of a modified NN interaction in the high density nuclear interior where Pauli blocking must be taken into account. Thus, in order to ascertain which phenomenological distorting potential the inelastic data prefer, we shall use only those form factors generated from the G-matrix interactions.

We shall use our arguments on the radial localization of the transition densities to infer the properties of the surface and interior forms of the optical potential. Displayed in Figs. 2.18a and 2.19a are the calculations for the 2^+ state employing the HJ and Paris G-matrix interactions for the form factor and the phenomenological distorting potentials. Their counterparts for the 1^- state are shown in Figs. 2.19b and 2.18b, respectively. One can see the effects of the different optical potentials by comparing the calculations using the consistent distorted waves with those using the phenomenological distorted waves. The first thing to be noticed is that the calculations using the SWS and DWS(-) optical potentials are not very different except at large q, where the calculations are more sensitive to the difference between the two potentials. Second, the calculations using the HJ form factor are in closer agreement with the analyzing power data for both transitions than those using the Paris based interaction. Third, the phenomenological optical potentials have little effect on the forward angle calculations and damp the oscillations at the larger angles. In the sense that the calculations for the cross section data are more sensitive to the imaginary central optical potential than the real central potential and the reverse is the case for the analyzing powers,[2] one would expect the high-q part of the analyzing power's angular distribution to be a very sensitive indicator as to which phenomenological real central optical potential is preferred by the inelastic data. From Figs. 2.16 and 2.19, one can see that the analyzing power data is best described by the DWS(+) optical potential, thus confirming our expectations from nuclear matter about the nature of the single particle potential.

This analysis, along with our understanding of the nuclear matter single particle potential, may indicate one possible source for the inconsistent G-matrix description of the elastic and inelastic data. A particle moving in the folded G-matrix real central optical potential sees a

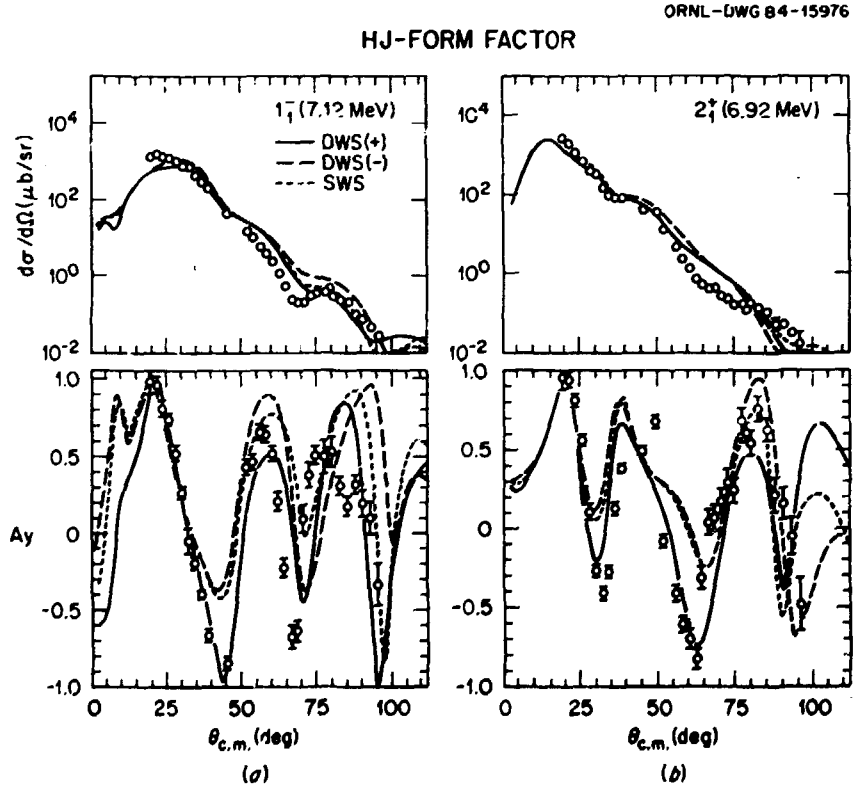

Fig. 2.18. The inelastic data are compared with calculations employing phenomenological optical potentials to generate the distorted waves and the form factor was calculated using the HJ based G-matrix.

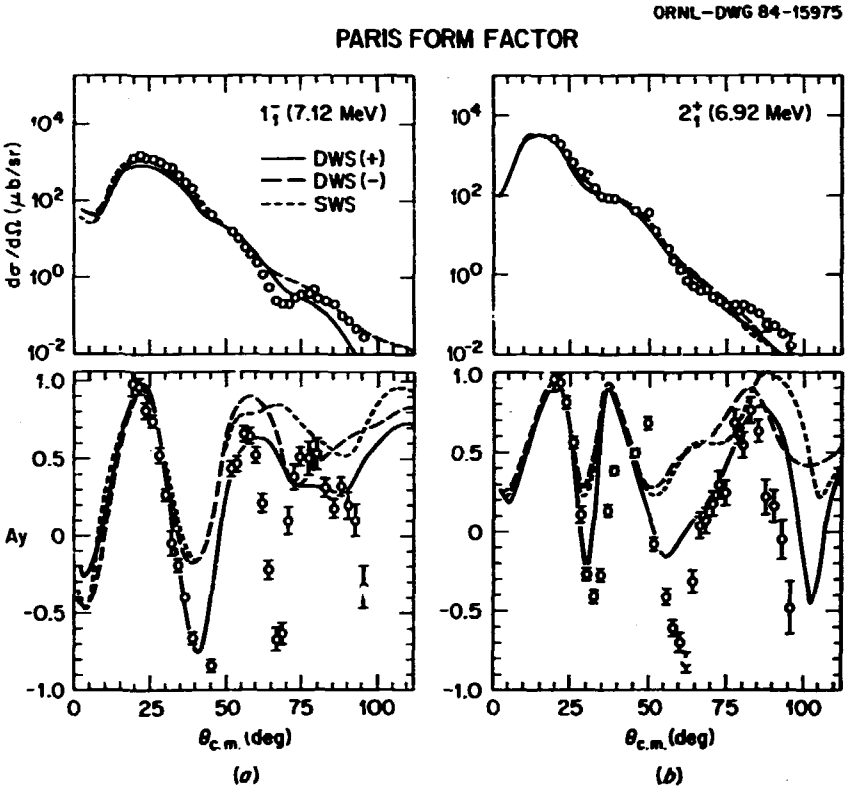

Fig. 2.19. This figure is the same as Fig. 2.18, except that the form factor was calculated using the Paris based G-matrix.

pocket of attraction near the nuclear surface. The attraction decreases as the particle approaches the nuclear interior. In the extreme nuclear interior the particle experiences a second pocket of attraction. This second pocket of attraction is contrary to what is expected from nuclear matter calculations. In the case of nuclear matter, as particles are added to the nuclear volume they attract each other until saturation is reached. Beyond this density the particles are squeezed so tight that the hard core repulsion of the NN interaction dominates. It is at this point the single particle potential becomes repulsive and stays repulsive. The phenomenological DWS(+) real central potential has this quality. Also, it provides a more consistent description of the elastic and inelastic data, especially in the back angle inelastic analyzing power data which is very sensitive to the interior of real central optical potential.

An alternate approach, successfully taken by Kelly,[9] to rectify this inconsistency is to parametrize the isoscalar spin-independent G-matrix and search on the parameters until a simultaneous description of the elastic and inelastic data can be found.

1. L. Ray, in The Interaction Between Medium Energy Nucleons in Nuclei - 1982, edited by H. O. Meyer (AIP Conf. Proc. No. 97), p. 121 and references cited within; in Studying Nuclei with Medium Energy Protons, edited by J. M. Green (Univ. of Alberta/TRIUMF Workshop - 1983), p. 101 and references cited within.

2. J. Kelly, in The Interaction Between Medium Energy Nucleons in Nuclei - 1982, edited by H. O. Meyer (AIP Conf. Proc. No. 97), p. 153 and references cited within.

3. H. Von Geramb, in The Interaction Between Medium Energy Nucleons in Nuclei - 1982, edited by H. O. Meyer (AIP Conf. Proc. No. 97), p. 1 and references cited within; in Studying Nuclei with Medium Energy Protons, edited by J. M. Green (Univ. of Alberta/TRIUMF Workshop - 1983), p. 44 and references cited within.

4. F. Petrovich et al., Phys. Lett. 91B, 27 (1980).

5. W. G. Love, in Studying Nuclei with Medium Energy Protons, edited by J. M. Green (Univ. of Alberta/TRIUMF Workshop - 1983), p. 29 and references cited within.

6. C. W. Glover et al., to be published in Phys. Rev. C.
7. W. G. Love and M. A. Franey, Phys. Rev. C 24, 1073 (1981).
8. J. C. Carr, J. Kelly, and F. Petrovich, the computer code ALLWRLD, to be published.
9. J. Kelly, private communication.

MEASUREMENTS OF GAMOW-TELLER STRENGTH DISTRIBUTIONS IN MASS 13 AND 15

D. J. Horen, C. D. Goodman[1], R. C. Byrd[1], I. J. Van Heerden[2], T. A. Carey[3], J. S. Larsen[4], C. Gaarde[4], J. Rapaport[5], T. P. Welch[5], E. Sugarbaker[6], T. N. Taddeucci[7]

The analysis of beta decay between mirror states has been used extensively for comparing shell model calculations with Gamow-Teller (GT) matrix elements extracted from measured decay rates. The essential simplicity of these transitions is that the parent and daughter states differ only in the isospin projection, T_z. The transition rate between mirror states is the incoherent sum of the rates for the Fermi and Gamow-Teller components. The Fermi (F) operator causes changes only in the isospin projection and converts the parent state exactly to the daughter state. Thus, the square of the Fermi matrix element is simply $2T_z$. The Gamow-Teller operator changes the projections of both isospin and spin. Due to the spin-orbit interaction, the GT strength is distributed between the spin-orbit pair states, and only a fraction of the GT strength is contained in the mirror state transition. In these cases, which can be explored through beta decay, the fraction of the total GT strength that appears in the mirror transition is typically very small, thereby making deductions about missing strength much more model-sensitive than would be the case if a large part of the sum rule strength were seen.

To investigate a possible A^j dependence of the GT quenching, we have studied the mass 13 and 15 systems. The cross sections and transverse spin-flip probabilities for $^{13}C(p,n)$ and $^{15}N(p,n)$ were measured at zero degrees using a 160 MeV polarized proton beam from the Indiana University Cyclotron Facility and a neutron polarimeter consisting of bars of plastic scintillator at the end of a 60-meter flight path. The polarimeter is described briefly elsewhere[8] and will be described more fully in a future publication. The targets were pressed wafers of carbon (>95% ^{13}C) and Melamine ($C_3H_6{}^{15}N_6$, >99% enrichment in ^{15}N).

The results of our measurements are displayed in Table 2.5 which gives the calculated and experimentally deduced values of B(GT). The shell model calculations are based on the assumption that these nuclei can be characterized as p-shell nuclei.[9] The ground state to ground state B(GT) values are deduced from beta decay ft values.

Excited-state transition strengths can be extracted by first decomposing the ground state cross section into Fermi and Gamow-Teller parts by using the observed relationship between GT and F transitions[10]:

$$\sigma_{GT}/\sigma_F = (E_p/55\pm1\ \text{MeV})^2[B(GT)/B(G(F))], \quad (1)$$

where B(F) = N-Z. Once the fraction $f_{GT} = \sigma_{GT}/(\sigma_{GT} + \sigma_F)$ of the cross section attributable to the GT part of the mirror transition has been determined, the cross section per B(GT) for that target is known. Values of B(GT) for excited states are then extracted with this proportionality factor.

The spin-flip probability measurements give a second (independent) determination of the GT fraction in the ground state cross sections, the spin-flip probability for these transitions is the weighted sum of the pure GT value of $S_{NN}(0°, GT) = 0.66 \pm 0.03$ and the Fermi value of zero. The "pure GT" value represents an average obtained from measurements of S_{NN} for many GT transitions at 160 MeV.[8] This value is consistent with the value 1/2 expected for a pure L=0 transition. The uncertainty represents not only experimental uncertainties, but also real deviations from the nominal value that can be attributed to L≠0 amplitudes in the transition.

The two procedures for extracting the GT fraction in the ground state and B(GT) for excited states can be summarized in the following formulas:

$$f_{GT} = [1 + B(F)/B_M(GT)R^2]^{-1} \quad (2)$$

Table 2.5. Cross sections, spin-flip probabilities, and GT transmission strengths for $^{13}C(p,n)^{13}N$ and $^{15}N(p,n)^{15}O$ at $\theta = 0°$ and E_p = 160 MeV.

Final state	$\sigma_{c.m.}(0°)$[a] (mb/sr)	$S_{NN}(0°)$	B(GT) expt.	B(GT) theory
^{13}N(0.00, 1/2⁻)	4.4	0.46	0.206[b]	0.323[e]
^{13}N(3.51, 3/2⁻)	11.1	0.66	0.83[c]	
			0.75[d]	
^{15}O(0.00, 1/2⁻)	4.7	0.53	0.261[b]	1/3
^{15}O(6.18, 3/2⁻)	11.5	0.70	1.00[c]	
			0.80[d]	
^{15}O(8-12, 3/2⁻)	3.4	0.68	0.30[c]	8/3
			0.26[d]	

[a]Statistical uncertainty only. Absolute normalization uncertainty is ±15%.
[b]Transition strength determined from beta-decay ft values.
[c]B(GT) determined from (p,n) data and Eqs. (2) and (4). Note that the value of B(GT) for ^{13}N(3.51 MeV) differs slightly from that in Ref. 10 because we have not averaged in values obtained from data at other energies.
[d]B(GT) determined from (p,n) data and Eqs. (3) and (4).
[e]Shell-model transition strengths, Cohen-Kurath "POT" wave functions, Ref. 9.

or

$$f_{GT} = S_{NN}(0°,M)/S_{NN}(0°,GT) \quad (3)$$

and

$$B_x(GT) = (\sigma_x/\sigma_M) f_{GT}^{-1} B_M(GT) F(q) \quad (4)$$

where R = E_p/(55 ± 1 MeV), M refers to the mirror (ground state) transition, and x refers to the excited state. The factor F(q) is a correction for the momentum transfer dependence of the differential cross section and is less than 1.10 for the cases studied here. The values of B(GT) for the excited states shown in Table 2.5 indicate that the methods of Eqs. (2) and (3) are more or less consistent. If anything, the spin-flip probability procedure makes the quenching of the 3/2⁻ transitions look even greater.

For the strongest transitions in both mass 13 and mass 15, the values of B(GT) extracted by the above procedures are reduced from the shell-model values by factors much larger then typical GT quenching. A striking feature is that the model predicts a ratio of 8:1 for the 1/2 → 3/2 to 1/2 → 1/2 transitions in mass 15, yet the observed ratio is only about 4:1. Similarly, in mass 13, a shell model calculation[9] predicts a ratio of 7.5:1 for the ratio of the strongest 1/2 → 3/2 transition to the mirror states 1/2 → 1/2 transition, while the observed value is about 4:1. Stated in other words, it appears that the major 1/2 → 3/2 transition is significantly more quenched than the 1/2 → 1/2 transition.

In summary, we have measured the cross sections and transverse spin-flip probability for $^{13}C(p,n)$ and $^{15}N(p,n)$ at E_p = 160 MeV. A surprising feature of the results is that the relative cross sections for the p1/2 → p1/2 and p → p3/2 transitions suggest that the 1/2 → 3/2 GT transitions are more quenched than the 1/2 → 1/2 transitions. It is not clear at this time whether the apparent extra quenching of the p1/2 → p3/2 transitions tends to favor explanations of GT quenching in terms of delta (3,3) coupling or in terms of configuration mixing with multiparticle-multihole states. In either case, some of the appealing simplicity of the nuclear shell model in providing a guide to a valid truncation of the space seems to be lost. Even for one of the simplest shell model nuclei, the simple version of the model seems to fail.

---

1. Indiana University, Bloomington, IN 47405.
2. Permanent address: University of Western Cape, Private Bag X17, Bellville, South Africa.
3. Los Alamos National Laboratory, Los Alamos, NM 87545.
4. Niels Bohr Institute, University of Copenhagen, DK-2100, Copenhagen, Denmark.
5. Ohio University, Athens, OH 45701.
6. Ohio State University, Columbus, OH 43214.
7. Ohio University, Athens, OH 45701 and Indiana University Cyclotron Facility, Bloomington, IN 47405.

8. T. N. Taddeucci et al., Phys. Rev. Lett. 52, 1960 (1984).
9. T.-S. H. Lee and D. Kurath, Phys. Rev. C 21, 293 (1980); S. Cohen and D. Kurath, Nucl. Phys. 73, 1 (1965); D. Kurath, private communication.
10. T. N. Taddeucci et al., Phys. Rev. C 25, 1094 (1981).

THE $^{19}F(p,n)^{19}Ne$ AND $^{39}K(p,n)^{39}Ca$ REACTIONS AT INTERMEDIATE ENERGIES AND QUENCHING OF THE GAMOW-TELLER STRENGTH[1]

D. J. Horen — C. D. Goodman[5]
J. Rapaport[2] — C. Foster[5]
C. Gaarde[3] — T. Masterson[6]
J. Larsen[3] — E. Sugarbaker[7]
C. Goulding[4] — T. N. Taddeucci[8]

Beta decay transitions between T = 1/2 ground states have a special simplicity because the initial and final states are isospin mirror images of each other. The T = 1/2 states, which have half-integral spins, can transform to their isospin mirrored states through either Fermi or Gamow-Teller transitions, and the observed beta decay is an incoherent sum of these two components. Since the Fermi operator transforms a T = 1/2 to its mirrored state, the Fermi matrix element is unity. This information allows one to decompose the total transition probability into its two components and to extract the GT matrix element from the ft value derived from the measured half-life and decay energy. The deduced empirical GT strength is 59% of the shell model value for the $^{19}Ne(\beta^+)^{19}F$ (gs) transition and 46% for the $^{39}Ca(\beta^+)^{39}K$ (gs) transition. Several authors have reported on the corrections needed to the calculated single particle GT matrix element. Recently Towner and Khanna[9] have done a very extensive study on these corrections; Brown and Wildenthal[10] have also reported on a comparison of shell-model predictions with sd-shell data.

In the case of mass 19 the model calculation shows that most of the strength should reside in the mirror transition. In the case of mass 39 only one-fifth of the sum strength is expected in the mirror transition, but the model is especially simple, that is, to first order the nucleus can be described as single $d_{3/2}$ hole in an L-S closed shell core.

The Indiana University Cyclotron and beam swinger facility[11] provided proton beams with energies E_p = 120 MeV and E_p = 160 MeV. The time of flight (t.o.f.) of neutrons was measured over a 100-m flight path with three large-volume time-compensated plastic scintillators.[12] Data were obtained for the angular range 0° < θ < 25° with a typical time resolution of 800-900 psec.

A commercially available teflon tape 35 mg/cm² thick was used as a ^{19}F target. A ^{nat}KF target 34.6 mg/cm² thick was used for the 120 MeV experiment and a nominal $^{39}KHF_2$ target, 28.7 mg/cm², 99.96% enriched in ^{39}K, was used for the

160 MeV run. The potassium targets were covered with a thin (about 1 mg/cm^2) double layer of polyethylene. Thus the $^{12}C(p,n)^{12}N$ (gs) transition is present in all the observed spectra which helped in determining possible target damage during the runs. A ^{12}C target, 34.9 mg/cm^2 and 99.9% enriched, was also run under identical experimental conditions.

The contribution from the C(p,n)N reaction was removed from the t.o.f. spectra taken with the teflon target at each angle, by substracting normalized observed t.o.f. spectra taken with the graphite target. In the case of the potassium spectra, subtractions had to be made for both ^{19}F and C(p,n) contributions. For the natural K target the neutron group representing the $^{39}K(p,n)^{39}Ca$ (gs) transition at 120 MeV has also contributions from the $^{41}K(p,n)^{41}Ca$ (IAS) transition. The difference in Q-value (8) between these two transitions is (259 ± 20) keV. A comparison of the spectrum at 120 MeV with the one at 160 MeV indicates a slight relative enhancement for the gs transition observed at the lower energy due in part to the $^{41}K(p,n)^{41}Ca$ (IA) contribution. Also the cross section value for the Fermi transition, which contributes to the gs transition, increases with decreasing energy with respect to the cross section value for the GT transition, which remains rather constant in this energy region.[13] The 120-MeV zero degree spectrum obtained with the thin (32 mg/cm^2) ^{nat}K target resulted in a better resolution and the 7% contribution of ^{41}K in the natural K target was resolved.

The analyzed spectra are shown in Fig. 2.20 for the $^{19}F(p,n)^{19}Ne$ reaction and in Fig. 2.21 for the $^{39}K(p,n)^{39}Ca$ reaction and the deduced cross sections are given in Tables 2.6 and 2.7.

For ^{19}Ne we observe that the gs transition carries about 84% of the total observed GT strength. The observed total GT strength is only 66% of the sum rule lower limit. In the case of ^{39}Ca, the observed sum GT strength up to 10 MeV excitation is only 36% of the sum rule lower limit. The distribution of GT strength among excited states agrees with the distribution of $d_{5/2}$ hole strength reported in neutron pick-up reaction studies. The relative ground state to excited states GT strength ratio agrees with the reported $d_{3/2}$ to $d_{5/2}$ hold strengths. The case of mass 39 represents the lowest quenching factor (i.e., 36%) for the total GT strength as reported from (p,n) reactions. This anomalously low value is also reported in the gs transition but calculated corrections to the shell model[9] are unable to predict the measured value. It is possible that weak transitions carrying additional GT strength are located above 9.0 MeV excitation energy in ^{39}Ca, which were not detected in the present experiment.

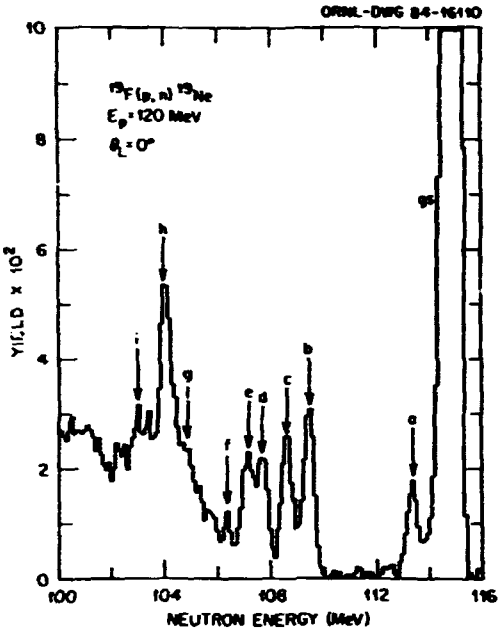

Fig. 2.20. Spectrum for the $^{19}F(p,n)^{19}Ne$ reaction at E_p = 120 MeV and θ = 0°. Cross sections for the labelled neutron groups are reported in Table 2.6.

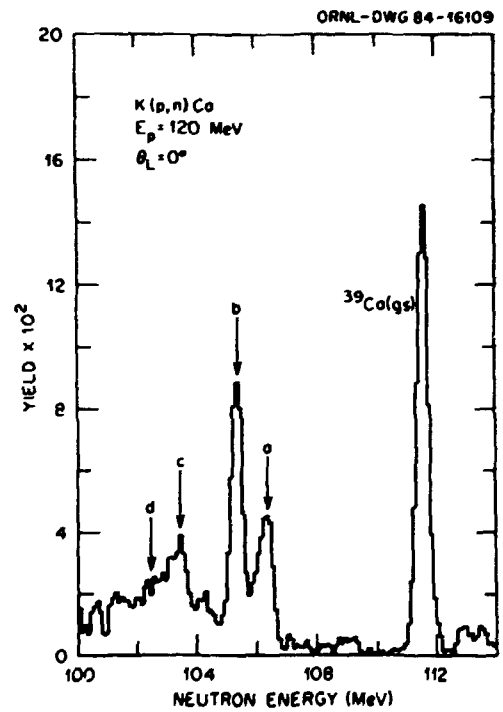

Fig. 2.21. Zero-degree spectrum for the $^{nat}K(p,n)Ca$ reaction at E_p = 120 MeV. Cross sections for the labelled neutron groups measured at E_p = 160 MeV are reported in Table 2.7.

---

1. Summary of paper submitted to Nuclear Physics.
2. Ohio University, Athens, OH 45701.
3. Niels Bohr Institute, Blegdamsvej 17, DK-2100 Copenhagen, Denmark.
4. Los Alamos National Laboratory, Los Alamos, NM 87545.

5. Indiana University Cyclotron Facility, Bloomington, IN 45405.
6. Colorado University, Boulder, CO 70309.
7. Ohio State University, Columbus, OH 43210.
8. Ohio University and Indiana University Cyclotron Facility.
9. I. S. Towner and F. C. Khanna, Nucl. Phys. A399, 334 (1983).
10. B. A. Brown and B. H. Wildenthal, Phys. Rev. C 28, 2397 (1983).
11. C. D. Goodman et al., IEEE Trans. Nucl. Sci. NS-26, 2248 (1979).
12. C. D. Goodman et al., Nucl. Instrum. and Methods 151, 125 (1978); C. D. Goodman, J. Rapaport and D. E. Bainum, IEEE Trans. Nucl. Sci. NS-25, 577 (1978).
13. T. N. Taddeucci et al., Phys. Rev. C 25, 1094 (1982).

Table 2.6. Summary of cross sections for the $^{19}F(p,n)^{19}Ne$ reaction

Neutron group E_x(MeV)	ΔL	E_p = 120 MeV $\sigma_{CM}(0°)$ mb/sr	B(GT)	E_p = 160 MeV $\sigma_{CM}(0°)$ mb/sr[a]	B(GT)
gs[b]	0	15.5±0.5[c]	1.64[d]	18.2±0.5[c]	1.64[d]
1.54	(0+2)	0.34±0.1	0.04	0.47±0.1	1.05
3.4	0	0.48±0.05	0.06	0.54±0.15	0.05
6.2	(0+1)	0.04±0.05	0.05	0.38±0.1	0.03
7.1	(0+1)	0.34±0.05	0.04	0.17±0.01	0.02
7.7	(0+1)	0.34±0.15	0.04	0.27±0.1	0.03
8.60	(0)	0.10±0.05	(0.01)	---	
10.2	(1)	0.15±0.05		0.2±0.05	
11.0	0	0.58±0.06	0.08	0.8±0.2	0.10
12.1	(0+2)?	0.18±0.03	0.03	0.25±0.05	0.03
		ΣB(GT) = 1.97±0.06			

[a]Relative uncertainties; to obtain absolute values add 15% in quadrature.
[b]At angles larger than 10°, the contribution of the 0.24 MeV (ΔL = 2) has been estimated.
[c]Includes cross section for Fermi transition, i.e., B(F) = 1.0.
[d]Normalized to β-decay value.

THE $^{51}V(p,n)^{51}Cr$ REACTION AT E_p = 160 MeV[1]

D. Horen — J. Larson[4]
J. Rapaport[2] — C. D. Goodman[5]
R. Alarcon[2] — C. C. Foster[5]
B. A. Brown[3] — T. Masterson[6]
C. Gaarde[4] — E. Sugarbaker[7]
T. N. Taddeucci[8]

The $^{51}V(p,n)^{51}Cr$ reaction has been studied at E_p = 160 MeV using the Indiana University beam swinger facility. Data have been obtained at several angles up to θ_L = 20°. The zero degree spectrum is used to obtain a ΔL = 0 response function from which Gamow-Teller strength is derived. A shell model calculation of the GT strength distribution is presented and compared with the experimental results. The M1 strength is also calculated and compared with available results from (e,e') and (p,p') experiment. A comparison is made with other N = 28 nuclei. Effects of a truncated shell model space are presented.

In a recent paper, Bender et al.[9] report on a search for M1 strength in ^{51}V via inelastic electron scattering. No strong M1 excitation was detected, in contrast to a $^{51}V(p,p')^{51}V$ experiment by Djalali et al.[10] in which a concentration of M1 strength was observed in the 10-MeV excitation energy region. This clear discrepancy has prompted us to report on the Gamow-Teller (GT) strength obtained via the $^{51}V(p,n)^{51}Cr$ reaction.

Here the experimental GT strength distribution is compared with that obtained in a shell model calculation done in a truncated model space. Using free nucleon g-factors, B(M1) values are calculated in the same model space and compared with available data.[11] The effects of a truncated shell model space are discussed by making an analogy between N = 14 (sd-shell nuclei) and N = 28 isotones nuclei. A full basis calculation can be done for the sd-shell nuclei as well as for ^{48}Ca but not for other N = 28 isotones. Data are presented for the $^{48}Ca(p,n)^{48}Sc$ reaction and the total GT strength is compared with the sum rule limit, 3(N-Z) = 24.

The Indiana University Cyclotron was used to obtain proton beams of 159.4 MeV. The data were obtained with the beam swinger facility.[12] A natural self-supported V target with a thickness of 50 ± 3 mg/cm^2 was used and an energy resolution of approximately 600 keV was achieved. The absolute values and energy dependence of the efficiency of the neutron detectors were obtained by taking data on a set of ^7Li and ^{12}C targets under identical experimental conditions.

Table 2.7. Summary of cross sections for the $^{39}K(p,n)^{39}Ca$ reaction E_p = 160 MeV

Neutron group (MeV)	ΔL	$\sigma_{CM}(0°)$ mb/sr[a]	B(GT)	B(F)
gs	0	3.6 ± 0.2	0.27[c]	1.0
5.3[b]	0	1.7 ± 0.1	0.19 ± 0.02	
6.2	(0+1)	2.8 ± 0.2	0.31 ± 0.03	
8.1	(0+1)	1.7 ± 0.15	0.20 ± 0.03	
9.0	(0+1)	0.9 ± 0.1	0.10 ± 0.02	
		ΣB(GT) = 0.27 + (0.8 ± 0.12)		
		shell model = 0.6 + 2.4		

[a]Relative uncertainties; to obtain absolute values add in quadrature 20%.
[b]Neutron groups corresponding to excitation energies of 5.1 MeV and 5.5 MeV are observed in the 120 MeV experiment; the relative strength of the 5.1 MeV state is about 30% larger than the strength of the 5.5 MeV.
[c]Normalized to β-decay value.

The $\Delta L = 0$ contributions to the zero-degree (p,n) spectra have been estimated in Fig. 2.22. The g.s. of the nucleus ^{51}V has $J^\pi = 7/2^-$, $T = 5/2$. Thus GT transitions will excite states in ^{51}Cr with $J^\pi = 5/2^-$, $7/2^-$, $9/2^-$ and $T = 3/2$, $5/2$, $7/2$ ($T_z = 3/2$). The IA of ^{51}V (g.s.) in ^{51}Cr occurs at $E_x = 6.61$ MeV and it has to be subtracted from the $\Delta L = 0$ spectrum in order to obtain the GT strength-function. The estimated total GT strength corresponds to $S_{\beta^-} = 12.6 \pm 2.5$ in units such that the free neutron has a GT strength, B(GT) = 3.

In order to interpret the experimental results, shell model calculations have been performed. Many of the low-lying levels of ^{51}V and ^{51}Cr are fairly well described with the simple $(1f_{7/2})^{11}$ model space[13] (model space A). However, this basis is clearly not adequate for the calculation of the GT strength distribution because of the importance of the $f_{7/2}$ to $f_{5/2}$ transition. The only model space truncation which is at present practical allows for at most one particle to be excited from the $f_{7/2}$ shell to the other fp shell orbitals and we refer to this as model space B.

In a full space calculation,[14] the Gamow-Teller sum rule $S(GT) = B(GT) - B(GT+) = 3(N-Z)$ must be obtained. In terms of the isospins of the final states, this sum rule in our case is

$$S(GT) = B(GT-) - B(GT+)$$

$$= B(GT-, T = 3/2) + B(GT-, T = 5/2) - 20\, B(GT-, T = 7/2) = 15.$$

The sum rule obtained in model space B is, in fact, 13.9 rather than 15. The reason for this is that the GT operator acting on the initial state can also go to a state with two particles excited into one of the $f_{5/2}$, $p_{3/2}$ or $p_{1/2}$ orbits and this state lies outside of model space B. Since we must make some truncation, it seems most consistent to restrict the ^{51}V, $J = 7/2$ ground state to the $(f_{7/2})^{11}$ (the model space A) configuration. Then the sum rule for the A → B type transitions is satisfied. The remaining discussion will be concerned only with A → B calculations.

The theoretical B(GT-) distribution is presented in Fig. 2.23 where it is compared with the empirical results (shaded). The histograms have been obtained by summing over 1 MeV intervals. The centroids and widths of the experimental and theoretical spectra are in excellent agreement with each other. The integrated experimental strength of 12.6 ± 2.5 is $(63 \pm 13)\%$ of the total theoretical strength of 20.14. This quenching factor is consistent with the global quenching factor of about 60% observed on a number of even-even targets in the region $40 < A < 208$. Within our model space there is essentially no GT strength above 20 MeV in excitation. This is consistent with the present multipole decomposition of the experimental strength above 20 MeV which shows

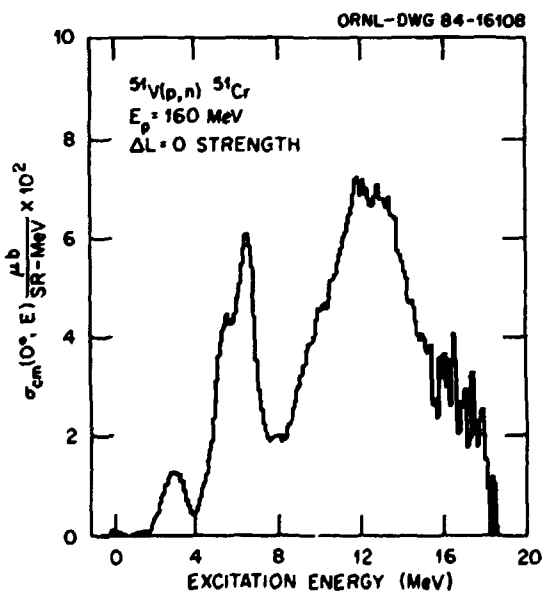

Fig. 2.22. $\Delta L = 0$ strength obtained at $\theta_L = 0°$ for the $^{51}V(p,n)^{51}Cr$ reaction at $E_p = 160$ MeV versus excitation energy in ^{51}Cr.

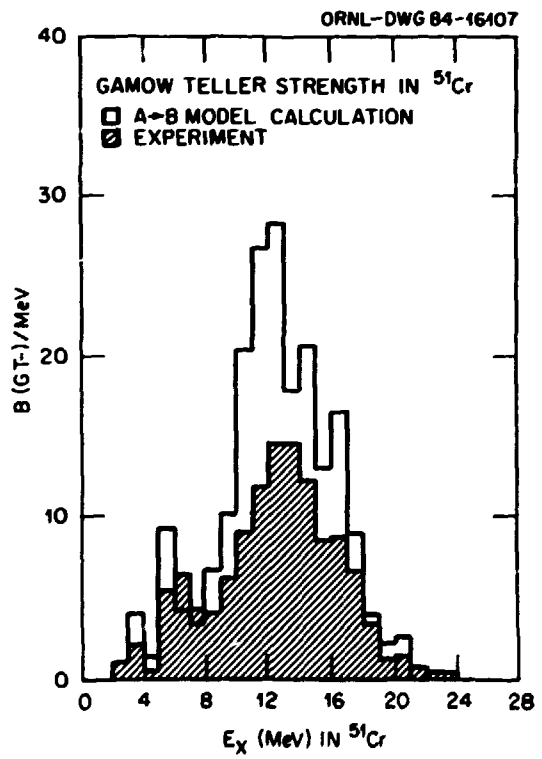

Fig. 2.23. Gamow-Teller strength in ^{51}Cr. The strength in energy bins of 1 MeV is presented versus excitation energy in ^{51}Cr. The experimental B(GT-) (integrated in 1 MeV bins), shaded area, is compared with shell model calculations.

$\Delta L = 1$ and $\Delta L = 2$ transitions to be dominant in this region.

The major effect of going from a truncated model A → B type calculation to a full fp shell model calculation is the admixture of two quasi-particle $f_{5/2}$ states in the ground state. The full fp shell model calculation is, in general, impossible to carry out. However, for the Ca isotopes, the full basis is tractible and the M1 strength have been calculated by McGrory and Wildenthal.[15] The ratio R (the sum in the full-basis calculation divided by the A → B calculation) varies monotonically from 0.62 to 0.75 on going from ^{42}Ca to ^{48}Ca.

Using an analogous argument for the N = 14 isotones in the sd shell going from ^{22}O to ^{28}Si, one can deduce a similar ratio for the $(f_{7/2})^{11}$ proton nuclei. We then find the quenching for B(GT-) in ^{51}V to be 0.70 ± 0.14.

The GT strength distribution obtained from the ^{48}Ca(p,n)^{48}Sc reaction has been reported[16] and has been the subject of several papers.[17,18,19] However, the value of the total GT strength normalized to beta-decay measurements has not been reported. We have measured a spectrum at $\theta = 0°$ were used to estimate the $\Delta L = 0$ cross section at $\theta = 0°$ for the ^{48}Ca(p,n)^{48}Sc reaction. From our analysis we find the quenching for B(GT) in ^{48}Ca to be $0.71^{+0.08}_{-0.15}$ in good agreement with that deduced for the ^{51}V.

B(M1) values were calculated from wave functions using free nucleon g-factors and a truncated model space. The summed M1 strength for ^{51}V, $\Sigma B(M1) = 20.19\ \mu_N^2$ is in disagreement with the experimental (e,e')[9] value $<1\ \mu_N^2$. A similar comparison with results obtained from the ^{51}V(p,p') experiment[20] indicates that only about 13% of the calculated strength has been observed. These results may be due to a high degree of fragmentation of M1 strength which may be difficult to detect above background.

---

1. Summary of paper to be published in Nuclear Physics.
2. Ohio University, Athens, OH 45701.
3. Michigan State University, East Lansing, MI 48824.
4. Niels Bohr Institute, University of Copenhagen, DK-2100 Copenhagen Ø, Denmark.
5. Indiana University, Bloomington, IN 47405.
6. University of Colorado, Boulder, CO 80309.
7. Ohio State University, Columbus, OH 43214.
8. Ohio University, Athens, OH 45701 and Indiana University, Bloomington, IN 47405.

9. D. Bender et al., Nucl. Phys A398, 408 (1983).
10. C. Djalali et al., Nucl. Phys. A388, 1 (1982).
11. G. M. Crawley et al., Proc. of the 1983 RCNP International Symposium on Light Ion React. Mech., edited by H. Ogata, T. Kammuri, I. Katayama, May 1983, p. 153.
12. C. D. Goodman et al., IEEE Trans. Nucl. Sci. NS-26, 2248 (1979)
13. W. Kutschera, B. A. Brown and K. Ogawa, Revista del Nuovo Cimento, Serie 3, Vol. 1, No. 12 (1978).
14. C. Gaarde et al., Nucl. Phys. A334, 248 (1980).
15. J. B. McGrory and B. H. Wildenthal, Phys. Lett. 103B, 173 (1981); Nucl. Phys. A399, 334 (1983); Phys. Rev. C 28, 2397 (1983).
16. B. D. Anderson et al., Phys. Rev. Lett. 45, (1980).
17. F. Osterfeld, Phys. Rev. C 26, 762 (1982).
18. F. Osterfeld et al., Phys. Rev. Lett. 49, 11 (1982).
19. W. Weise, Nucl. Phys. A396, 373c (1983).
20. C. Djalali et al., Nucl. Phys. A410, 399 (1983).

MEASUREMENT OF THE TRANSVERSE SPIN TRANSFER COEFFICIENT $D_{NN}(0°)$ FOR $(\vec{p},\vec{n})$ REACTIONS AT 160 MeV[1]

D. J. Horen — C. D. Goodman[5]
T. N. Taddeucci[2] — T. Masterson[6]
T. A. Carey[3] — J. Rapaport[7]
C. Gaarde[4] — T. P. Welch[7]
J. Larson[4] — E. Sugarbaker[8]

The first measurements of the transverse spin transfer coefficient $D_{NN}(0°)$ for intermediate energy (p,n) reactions to well resolved nuclear states are reported. Results are presented for $(\vec{p},\vec{n})$ reactions on ^{6,7}Li, ^{12,13,14}C, and ^{90}Zr at E_p = 160 MeV. The average value of $D_{NN}(0°)$ for pure Gamow-Teller transitions at this energy is shown to be close to the expected value of -1/3. The utility of spin transfer measurements for investigating aspects of the nuclear spin-dependent response not otherwise observable is pointed out.

Despite the successful use of (p,n) differential cross sections to identify and measure spin-flip strength, in some cases important details of the reaction are not adequately revealed by differential cross section measurements alone. In particular, there is the continuing problem of distinguishing giant resonances excited by the (p,n) reaction from the background of continuous excitations or competing giant resonances with which they are mixed.[9-13] This separation mainly depends upon distinguishing between components that have differing spin-flip characteristics.

A direct measure of the spin-flip character of a (p,n) transition is provided by the transverse spin transfer coefficient $D_{NN}(\theta)$ [or, equivalently, the transverse spin-flip probability $S_{NN} = (1 - D_{NN})/2$]. Measurements of $D_{NN}(0°)$ are potentially important tests of the effective nucleon-nucleon interaction as well as a means of investigating the nuclear spin-dependent response.

Data were obtained using the Indiana University cyclotron and beam-swinger facility.[14] Polarized protons with energy E_p = 160 MeV bombarded self-supporting targets

with thicknesses ranging from 107 mg/cm^2 to 232 mg/cm^2. The beam polarization was typically $0.65 < |p_i| < 0.75$ and was cycled between up and down orientations at two-minute intervals. The neutron polarimeter consisted of six 15 cm x 15 cm x 100 cm plastic scintillators arranged in two parallel stacks of three. The long axes of the scintillators were parallel to the horizontal plane and perpendicular to the incident neutron flux. The separation between stacks was approximately 1.4 m. The polarization of incident neutrons was determined by scattering from hydrogen [^{1}H($\vec{n}$,n')^{1}H] and carbon [^{12}C($\vec{n}$,n'x)] nuclei in one of the forward scintillators. The scattered neutrons (denoted as n') were subsequently detected by one of the trailing scintillators. A thin plastic scintillator between the stacks was used to veto events associated with forward-going protons. Time signals derived from each end of the detectors furnished both the TOF of the incident neutron and positron information from which the event geometry was reconstructed. Neutrons that scattered at polar angles of $14° < \theta < 31°$, at azimuthal angles ϕ within 45° of the horizontal plane, and with velocity $v_n'/\cos\theta > 0.91\ v_n$ were accepted as valid events. The measured instrumental analyzing power for these conditions (which includes the average value of $\cos\phi$) is $A_p = 0.34 \pm 0.02$ and is primarily due to scattering from hydrogen. The neutron-energy dependence of the analyzing power was calculated using the N-N phase shift solutions of Arndt[15] and amounts to a change of less than 5% in the magnitude of A_p for 140 MeV $< E_n <$ 160 MeV.

At $\theta = 0°$ the spin transfer coefficient is given by

$$D_{NN}(0°) = p_f/p_i \qquad (1)$$

(where p_i is the proton and p_f the neutron polarization), and may be defined in terms of measured quantities as

$$D_{NN}(0°) = (\bar{p}_i A_p)^{-1}(R-1)/(R+1) \qquad (2)$$

where $\bar{p}_i = (p_i^+ - p_i^-)/2$ is the average magnitude of the proton polarization, A_p is the instrumental analyzing power.

$$R = [(N_L^+ N_R^-)/(N_L^- N_R^+)]^{1/2}, \qquad (3)$$

and N_L^+ [N_R^+] is the number of neutrons that scatter to the left ($\phi = 0° \pm 45°$) [right ($\phi = 180° \pm 45$)] for positive incident proton polarization, etc. This definition of $D_{NN}(0°)$ is largely independent of false asymmetries caused by instrumental inefficiencies and misalignments or unequal beam current for spin up and spin down. The product $\bar{p}_i A_p$, which provides the absolute normalization of D_{NN}, was empirically determined by measuring R for the $0^+ \rightarrow 0^+$ ^{14}C(p,n)^{14}N (2.31 MeV) isobaric analog state (IAS) transition for which $D_{NN}(0°) = 1$.

Values of $D_{NN}(0°)$ determined in this work are given in Table 2.8. Significantly, the values of $D_{NN}(0°)$ for the pure GT transition are evenly distributed around the expected value of -1/3. The average for six strong transitions from ^{6}Li, ^{12}C, ^{13}C, and ^{14}C is $D_{NN}(0°) = -0.32 \pm 0.05$.

Table 2.8. Transverse spin transfer coefficient $D_{NN}(0°)$ for (p,n) reactions at 160 MeV. The quoted uncertainties are absolute and arise from the statistical uncertainty in the yields of double-scattered neutrons for each transition plus an uncertainty of about 6% owing to the statistical uncertainty in the yields for the ^{14}C(p,n)^{14}N (2.31 MeV) calibration reaction.

Reaction	E_x(MeV)	$D_{NN}(0°)$	Transition type
^{6}Li(p,n)^{6}Be	0.0	-0.37±0.04	GT
^{7}Li(p,n)^{7}Be	0.0±0.43	-0.28±0.06	GT + F
^{12}C(p,n)^{12}N	0.0	-0.24±0.03	GT
^{13}C(p,n)^{13}N	0.0	0.05±0.06	GT + F
"	3.51	-0.33±0.05	GT
"	15.1	-0.36±0.08	GT
^{14}C(p,n)^{14}N	0.0	-0.29±0.17	GT
"	2.31	1.0	F
"	3.95	-0.29±0.02	GT
"	13.72	-0.33±0.04	GT
^{90}Zr(p,n)^{90}Nb	4.3-6.3	0.24±0.17	F + GT background
"	6.4-13.1	-0.28±0.08	GT (Giant 1^+)
"	15.0-25.0	-0.17±0.09	?

Large systematic deviations from this value would be indicative of unexpectedly large L=2 (or tensor) amplitudes at 0° or failure of the assumed single-step direct-reaction mechanism.

1. Summary of paper: Phys. Rev. Lett. 52, 1960 (1984).
2. Ohio University, Athens, OH 45701 and Indiana University, Bloomington, IN 45405.
3. Los Alamos National Laboratory, Los Alamos, NM 87545.
4. University of Copenhagen, DK-2100 Copenhagen, Denmark.
5. Indiana University, Bloomington, IN 47405.
6. University of Colorado, Boulder, CO 80309.
7. Ohio University, Athens, OH 45701.
8. Ohio State University, Columbus, OH 43210.
9. G. Bertsch and I. Hamamoto, Phys. Rev. C 26, 1323 (1982).

10. F. Osterfeld, Phys. Rev. C 26, 762 (1982).
11. T. Izumoto, Nucl. Phys. A395, 189 (1983).
12. G. Bertsch, D. Cha, and H. Toki, Phys. Rev. C 24, 533 (1981).
13. O. Scholten, G. F. Bertsch and H. Toki, Phys. Rev. C 27, 2975 (1983).
14. C. D. Goodman et al., IEEE Trans. Nucl. Sci. 26, 2248 (1979).
15. R. A. Arndt and L. D. Roper, Scattering Analyses Dial-in (SAID) Program, phase shift solution FA83, Virginia Polytechnic and State University, unpublished.

$^{36}S(n,\gamma)^{37}S$ REACTION WITH THERMAL NEUTRONS AND DECAY OF ^{37}S TO LEVELS IN ^{37}Cl[1]

S. Raman
W. Ratynski[2]
E. T. Jurney[3]
M. E. Bunker[3]
J. W. Starner[3]

The $^{36}S(n,\gamma)^{37}S$ reaction with thermal neutrons has been studied utilizing a highly enriched ^{36}S target. Fifteen γ rays were observed which have been incorporated into a ^{37}S level scheme. The neutron separation energy of ^{37}S was determined to be 4303.52 ± 0.12 keV and the thermal neutron capture cross section of ^{36}S to be 230 ± 20 mb. The subsequent β^- decay of ^{37}S to levels in ^{37}Cl has also been studied. Seven γ rays were observed which have led to an improved ^{37}S decay scheme.

---

1. Abstract of paper: Phys. Rev. C 30, 26 (1984).
2. Institute for Nuclear Studies, Otwock-Swierk, Poland.
3. Los Alamos National Laboratory, Los Alamos, NM 87545.

$^{36}S(d,p)^{37}S$ AND $^{34,36}S(d,^3He)^{33,35}P$ REACTIONS[1]

C. E. Thorn[2]
E. K. Warburton[2]
J. W. Olness[2]
S. Raman

The $^{36}S(d,p)^{37}S$ reaction was studied at E_d = 25 MeV with an enriched ^{36}S target (81.1%) and momentum analysis of the protons. Twenty-six groups were identified with levels in ^{37}S. Excitation energies were obtained with an uncertainty of ≲3 keV and angular distributions yielded ℓ and S values for the transfer reaction. Comparison is made to local systematics and the ℓ = 1 strength is also compared to recent (n,γ) results. The $^{34,36}S(d,^3He)^{33,35}P$ reactions were also studied. A mass excess for ^{35}P of -24854(5) keV was obtained. $(d,^3He)$ proton pickup strength was observed to four states of ^{35}P and seven states of ^{33}P. These results are compared to predictions of Wildenthal.

---

1. Abstract of paper to be published.
2. Brookhaven National Laboratory, Upton, NY 11973.

DECAY SCHEME OF ^{116}Sn FROM $(n,n'\gamma)$ AND (n,γ) RESULTS[1]

Z. Gácsi[2]
J. Sa[2]
J. L. Weil[2]
E. T. Jurney[3]
S. Raman

A decay scheme for ^{116}Sn containing approximately 190 γ-rays and 112 levels below 6.0 MeV has been constructed by combining the results of $^{116}Sn(n,n'\gamma)$ and $^{115}Sn(n,\gamma)$ experiments.

---

1. Abstract of paper: Proc. Fifth Intern. Symp. Capture Gamma-Ray Spectroscopy and Related Topics, Knoxville, Tennessee, September 1984.
2. University of Kentucky, Lexington, Kentucky.
3. Los Alamos National Laboratory, Los Alamos, New Mexico.

OBSERVATION OF EXTREMELY LOW s-WAVE STRENGTH IN THE REACTION $^{136}Xe + n$[1]

B. Fogelberg[2]
M. Mizumoto[4]
J. Harvey[3]
S. Raman

The neutron cross section of ^{136}Xe has been investigated at the Oak Ridge Electron Linear Accelerator (ORELA). A sample of xenon gas, enriched to 93.6% in ^{136}Xe, was used as target. Measurements were made with an energy resolution of ~0.1%. The transmission data, which were analyzed for neutron energies below 500 keV, show 35 resonances in this region. Only four very weak resonances were found to be possibly due to s-wave neutron interactions, giving an extremely low value for the s-wave strength function in the analyzed region ($S_0 < 1.0 \times 10^{-6}$).

---

1. Summary of paper: Proc. Fifth Intern. Symp. Capture Gamma-Ray Spectroscopy and Related Topics, Knoxville, Tennessee, September 1984.
2. The Studsvik Science Research Laboratory, Nyköping, Sweden.
3. Engineering Physics and Mathematics Division.
4. JAERI, Tokai-Mura, Naka-gun, Ibaraki-ken, Japan.

ELECTRIC DIPOLE TRANSITIONS FROM NEUTRON CAPTURE IN ^{167}Er RESONANCES[1]

S. Kahane[2]
G. G. Slaughter
S. Raman
C. Coceva[3]
M. Stefanon[3]

Primary neutron capture γ rays have been studied from 86 neutron resonances in ^{167}Er in the energy range 5-600 eV. The spins of these resonances were assigned as I=3 or 4 on the basis of the intensity ratios of suitable pairs of low-energy γ rays. The measured intensities of the high-energy primary γ rays have been converted to partial radiation widths and further analyzed to obtain average E1 gamma strength. Individual γ

spectra from I=3 and 4 resonances have been summed separately after appropriate normalizations. The resulting average radiation widths (and hence the γ-ray strength function) were in good agreement with the Axel-Brink predictions based on a giant dipole resonance model. These widths were also consistent with the assumption that the γ-ray strength function is independent of the initial spin. The partial E1 radiation widths were subjected to a distribution analysis, revealing that these widths had a slightly narrower distribution than that predicted by the Porter-Thomas law. The ratio of the average population of a particular low-lying level from I=4 resonances to its population from I=3 resonances was found to be in good agreement with a five-step cascade model. The population of successive spins within a rotational band lay on smooth curves which, for different bands, were nearly parallel. A level scheme for ^{168}Er has been constructed, and the neutron separation energy for this nucleus was deduced as 7771.6 ± 1.0 KeV.

---

1. Abstract of published paper: Phys. Rev. C 30, 807 (1984).
2. Nuclear Research Centre-Negev, Beer-Sheva, Israel.
3. ENEA, CRE "Ezio Clementel," Bologna, Italy.

LOCATION OF A DOORWAY STATE USING THE CHANNEL n + ^{207}Pb[1]

L. C. Dennis[2] S. Raman

The location of a doorway state in the n + ^{207}Pb channel is established through a statistical analysis of the observed partial widths for gamma-rays and neutrons. Several statistical tests developed to help locate doorway states are presented. The statistical analysis focuses on the strong correlation between large partial widths in the two exit channels. Widths in both exit channels exhibit extremely large values in the energy region near E_n = 120 keV. This clustering of large widths, even when considered separately for each exit channel, is relatively unlikely to occur in a statistical sample. The strong correlation between channels decreases the likelihood for this clustering of large widths to occur in a statistical sample to less than 0.0003.

---

1. Abstract of paper: Proc. Fifth Intern. Symp. Capture Gamma-Ray Spectroscopy and Related Topics, Knoxville, Tennessee, September 1984.
2. Florida State University, Tallahassee, Florida.

THE (^{3}He,t) REACTION AT 197 MeV ON ^{12}C, ^{24}Mg, ^{28}Si AND ^{40}Ca[1]

S. L. Tabor[2] A. Guterman[3]
G. Neuschaefer[2] M. T. Collins[4]
J. A. Carr[2] D. L. Friesel[5]
F. Petrovich[2] C. Glover[5]
C. C. Chang[3] S. Y. van der Werf[6]
S. Raman

Spectra have been measured for the (^{3}He,t) reaction on ^{12}C, ^{24}Mg, ^{28}Si, and ^{40}Ca at E_{lab} = 197 MeV and θ_{lab} = 15°. The analog of the giant dipole resonance (GDR) is strongly populated in the charge-exchange reaction for each of the targets used in this study. Differences between the spectral shape of the GDR known in ^{12}C, ^{28}Si, ^{24}Mg, and ^{40}Ca from photonuclear work and their analogs in ^{12}N, ^{28}P, ^{24}Al, and ^{40}Sc are discussed. No evidence is seen for the population of a compact isovector giant quadrupole resonance (GQR) in any of these targets. Angular distributions have been measured at this energy for the ^{40}Ca(^{3}He,^{3}He), ^{40}Ca(^{3}He,^{3}He')^{40}Ca and ^{40}Ca(^{3}He,t)^{40}Sc reactions. The elastic ^{3}He scattering from ^{40}Ca is reasonably described by a volume Woods-Saxon optical potential that is very similar to one known from lower-energy studies. Collecative DWA calculations using this potential reproduce the inelastic scattering to the 3$^-$ and isoscalar GQR states of ^{40}Ca and an additional calculation using the Goldhaber-Teller model roughly reproduces the measured charge-exchange angular distributions of the GDR in ^{40}Sc. Data for the inelastic-scattering and charge-exchange reactions to a few low-lying discrete states and the region including the GDR in mass 40 have also been examined in DWA calculations using a microscopic double-folding model with a realistic effective interaction and particle-hole wave functions. Where possible these results are compared with results for other probes and rough consistency is found. The decomposition of the strength observed in the GDR region via (^{3}He,t) is considered in some detail and it is estimated that 30% of this strength is ΔS=1.

---

1. Abstract of published paper: Nucl. Phys. A422, 12 (1984).
2. Florida State University, Tallahassee, Florida.
3. University of Maryland, College Park, Maryland.
4. Brookhaven National Laboratory, Upton, New York.
5. Indiana University Cyclotron Facility, Bloomington, Indiana.
6. Kernfysisch Versneller Institute, Groningen, The Netherlands.

THERMAL NEUTRON CAPTURE GAMMA RAYS FROM SULFUR ISOTOPES: EXPERIMENT AND THEORY[1]

S. Raman J. C. Wells[3]
R. F. Carlton[2] E. T. Jurney[4]
J. E. Lynn[5]

We have carried out a systematic investigation of γ rays after thermal neutron capture by all stable sulfur isotopes (^{32}S, ^{33}S, ^{34}S, and ^{36}S). The measurements were made at the internal target facility at the Los Alamos Omega West Reactor. We detected a larger number of γ rays: ~100 in ^{33}S, ~270 in ^{34}S, ~60 in ^{35}S, and ~15 in ^{37}S. Before developing detailed level schemes, we culled and then consolidated the existing information on energies and J^{π} values for levels of these nuclides. Based on the current data, we have constructed detailed decay schemes, which imply that there are significant populations of 26 excited states in ^{33}S, 70 states in ^{34}S, 20 states in ^{35}S, and 7 states in ^{37}S. By checking the intensity balance for these levels and by comparing the total intensity of primary transitions with the total intensity of secondary γ rays feeding the ground state, we have demonstrated the relative completeness of these decay schemes. For strongly populated levels, the branching ratios based on the current measurements are generally better than those available from previous measurements. In all four cases, a few primary dipole (E1) transitions account for a large fraction of the capture cross section for that particular nuclide. To understand and explain these transitions, we have outlined ab initio a theory of potential capture. Toward this end, we reviewed the theory relating off-resonance neutron capture to the optical-model capture. We studied a range of model-dependent effects (nature and magnitude of imaginary potential, surface diffuseness, etc.) on the potential capture cross section, and we have shown how experimental data may be analyzed using the expression for channel capture suitably modified by a factor that takes into account the model-dependent effects. The calculations of cross sections for most of the primary transitions in the sulfur isotopes are in good agreement with the data. Some discrepancies for weaker transitions can be explained well by an interfering compound-nucleus contribution to capture. This contribution is of the magnitude expected from statistical surveys of resonance capture data. Estimates of the cross section due to the valence-capture mechanism in s-wave resonances show that this cross section should dominate the more complicated compound-nucleus contributions.

---

1. Abstract of paper to be published.
2. Middle Tennessee State University, Murfreesboro, TN 37132.
3. Tennessee Technological University, Cookeville, TN 38501.
4. Los Alamos National Laboratory, Los Alamos, NM 87545.
5. Atomic Energy Research Establishment, Harwell, England.

THE s- AND d-WAVE SCATTERING OF NEUTRONS ON ^{48}Ca

J. A. Harvey[1] C. H. Johnson
R. F. Carlton[2] Boris Castel[3]

Neutron total cross section measurements of ^{48}CaO up to 1.4 MeV reported by Seibel et al.[4] established the existence of one strong $d_{5/2}$ resonance at 0.956 MeV and no s-wave resonances were found. Although several other small resonances were observed, their spins and parities could not be determined. Divadeenam et al.[5] calculated the energies and strengths of possible 2p-1h states and predicted that the lowest s-wave resonance would be above 1.5 MeV with the majority of the s-wave strength at 3 MeV.

Neutron total cross section measurements of ^{48}Ca have been performed at ORELA over the energy interval from 10 keV to 4 MeV using a 200-m flight path. A $CaCO_3$ sample (1/N = 126 b/a) enriched to 96% ^{48}Ca was used. Neutrons from the Ta target were used at higher energies while water moderated neutrons were used below 500 keV. The energy resolution $\Delta E/E$ was $\sim 0.00025\,[1+25\,E]^{1/2}$ where E is in MeV. The experimental data after subtracting the oxygen and carbon cross sections are shown in Figs. 2.24 and 2.25. An R-matrix analysis using the code SAMMY[6] has been performed up to 4 MeV to obtain resonance parameters and potential scattering phase shifts for ℓ=0, 1 and 2 wave resonances. The resulting fits to the total cross section are shown in Figs. 2.24 and 2.25.

No resonances could definitely be assigned to s-wave neutrons. The nonresonant cross section for low energy neutrons (<400 keV) is very small ~0.5 b ($R' \sim 2.0$ fm). This can be described by scattering from a real Woods-Saxon potential with r_0 = 1.21 fm, a = 0.66 fm and V_0 = 48 MeV.

Three large $d_{5/2}$ resonances (at 0.960, 1.56 and 1.78 MeV) were identified up to 2 MeV whose

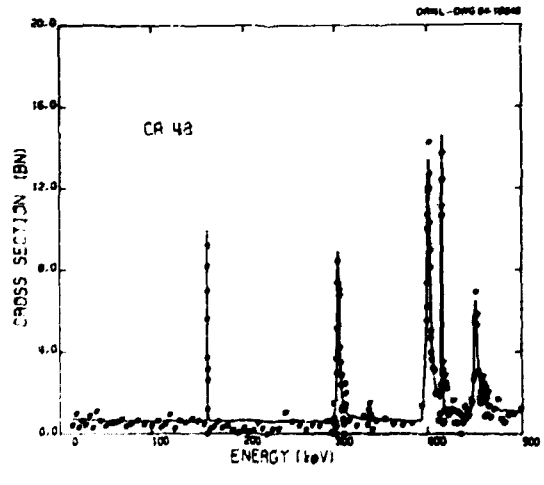

Fig. 2.24. Total cross section of ^{48}Ca obtained using water-moderated source. The curve is the R-matrix fit.

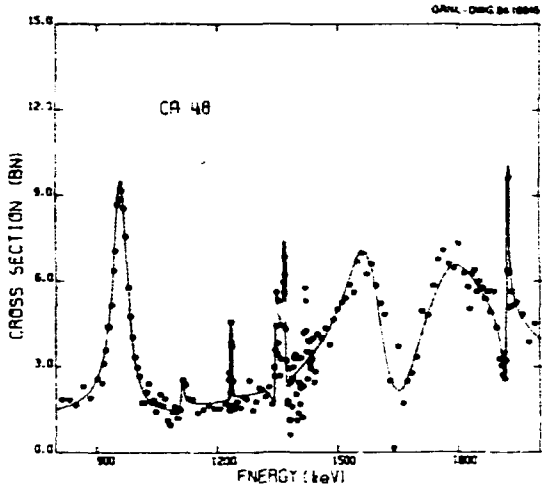

Fig. 2.25. Total cross section of ^{48}Ca obtained with neutrons from the Ta source.

combined strength (based on a radius of 5.27 fm) is ~45% of the single particle limit. The $d_{5/2}$ neutron strength function from 0.8 to 2.0 MeV is 14 x 10^{-4} in conventional units. The $d_{3/2}$ and p-wave strength functions are nearly 100 times smaller and the s-wave is approximately zero.

We have done a shell-model-in-the-continuum calculation[7] of the ^{48}Ca+n system. The $p_{3/2}$ ground state and the $p_{1/2}$ first excited state at 2.03 MeV of ^{49}Ca exhausts most of the p-strength in agreement with (d,p) data and little remains at higher energies. The positive parity states are calculated as a combination of $1g_{9/2}$, $2d_{5/2}$ and $2d_{3/2}$ s.p. states and $p_{3/2}$ and $p_{1/2}$ neutrons coupled to the 3$^-$ collective state in ^{48}Ca at 4.51 MeV. No significant J=1/2$^+$ states lie in the energy region from 0 to 3 MeV above the neutron separation energy and four J=5/2$^+$ states are predicted in this energy region. They represent a total of 60% of the available s.p. strength, fragmented by the particle-core interaction. The remainder of the strength is predicted to lie within the 3 to 5.5 MeV energy region.

---

1. Engineering Physics and Mathematics Division.
2. Middle Tennessee State University, Murfreesboro, TN 37132.
3. Queen's University, Kingston, Canada K7L 3N6.

4. F. T. Seibel, E. G. Bilpuch and H. W. Newson, Annals of Phys. 69, 451 (1972).
5. M. Divadeenam, W. P. Beres and H. W. Newson, Annals of Phys. 69, 428 (1972).
6. N. M. Larson and F. G. Perey, ORNL/TM-7485, 1980 and N. M. Larson, ORNL/TM-9179, 1984.
7. J. A. Harvey et al., Phys. Rev. C 28, 24 (1983); R. F. Carlton et al., Phys. Rev. C 29, 1980 (1984).

COUPLED-CHANNEL OPTICAL MODEL FOR 0-0.5 MeV NEUTRONS IN ^{60}Ni

A. D. MacKellar[1] C. H. Johnson
R. R. Winters[2]

In a previous report[3] averaged neutron scattering functions that had been deduced from high-resolution cross section measurements for various nuclei were compared to optical model potential (OMP) scattering functions for each partial wave. Assuming a spherical OMP a good fit to the average for 0-450 keV s-wave on ^{60}Ni was achieved for a real well depth of V_0 = 48 ± 5 MeV. (The model geometry was conventional with $r_0 = r_D$ = 1.21 fm, a_0 = 0.66 fm and a_D = 0.48 fm.) That value for V_0 is consistent with the known peak of the $3s_{1/2}$ size resonances. However, since an unusually large imaginary depth (namely W_D = 29 ± 5 MeV) was required, it was concluded that a non-spherical model should be considered for this vibrational nucleus.

To include the vibrational effects we used the coupled-channel formalism[4,5] with the target channel being the 0$^+$ ground state and the 2$^+$ state at 1.33 MeV with β = 0.211. (The 3$^-$ state at 4.04 MeV has negligible effects for s-wave neutrons.) Using the same geometry as for the spherical model we again fit the compound and shape elastic cross sections (σ_c and σ_{se}) by searching on V_0 and W_D and found V_0 = 50 ± 5 MeV, W_D = 24 ± 5 MeV. In other words, we found essentially the same well depths as for the spherical model.

Figures 2.26 and 2.27 illustrate the effects of V_0 and W_D in the two models. In both figures the abscissa is V_0 and the curves are calculated with various W_D for 0.2-MeV neutrons, i.e., at the midpoint of the experimental region. For that energy the horizontal lines give the experimental σ_c and σ_{se} with associated uncertainties, as indicated by the shaded areas. A good fit requires that W_D be chosen to fit both σ_c and σ_{se} for the same V_0.

In Fig. 2.26 which is for the spherical model, the observed σ_{se} restricts V_0 to about 48 MeV. At that V_0 the σ_c is at the peak of the $3s_{1/2}$ resonance; thus, W_D must be increased to about 29 MeV to reduce the peak to the observed value. (A small W_D of about 0.5 MeV would also fit at E_n = 0.2 MeV but not over the full 0-450 keV region.)

In Fig. 2.27, which is for the vibrational model, the σ_c curves exhibit two additional resonances arising from particle-core couplings of the bound 2d states with the 2$^+$ target state. The curve of σ_c for W_D = 1.5 MeV illustrates that the particle-core resonances are moved upward from their unperturbed energies (arrows) whereas the 3s resonance is moved downward from its position in the spherical model. The solid points indicate the fitted V_0 and W_D as stated above. The open symbols indicate an alternate solution with W_D only 1.5 MeV but with V_0 so large, namely 54.5 MeV, that the 3s size resonance would occur at A=44, far below the known peak near A=55.

1. Consultant from University of Kentucky, Lexington, KY 40506.
2. Consultant from Denison University, Granville, OH 43023.
3. A. D. MacKellar, B. Castel and C. H. Johnson, Physics Division Progress Report, ORNL-6004, 47 (1983).
4. T. Tamura, Rev. Mod. Phys. 37, 679 (1965).
5. J. Raynal, ECIS-79 (private communication).

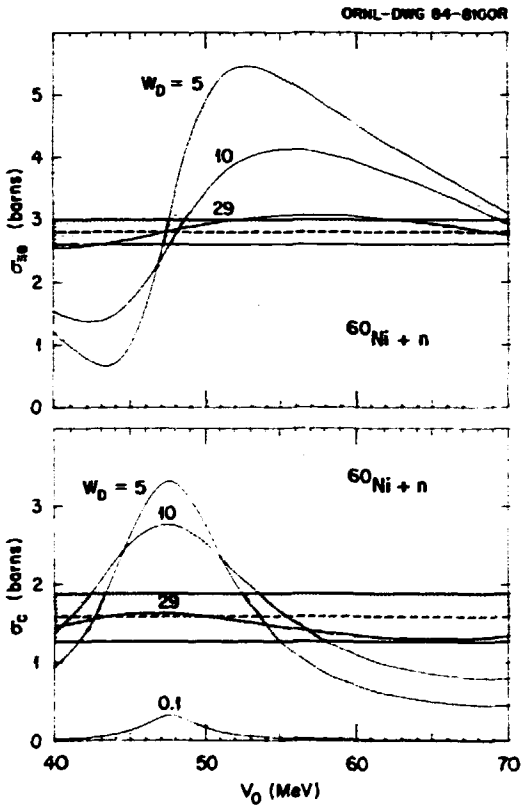

Fig. 2.26. Spherical OMP s-wave shape elastic and compound nuclear cross sections vs V_0 for various imaginary well depths at E_n = 200 keV. The horizontal lines indicate the experimental values and the shaded areas represent the associated uncertainties.

OPTICAL MODEL SCATTERING FUNCTIONS FOR 0-700 keV NEUTRONS ON ^{86}Kr

R. F. Carlton[1] J. A. Harvey[2]
C. H. Johnson

At low neutron energies parameters for an optical model potential (OMP) can be deduced from high resolution scattering measurements by first parametrizing the data in terms of an R-matrix and then averaging those scattering functions for each partial wave in order to compare to the OMP. In the preceding report[3] such analyses were given for ^{30}Si, ^{32}S, ^{34}S, ^{40}Ca, and ^{60}Ni. Here we present new measurements and preliminary analysis for ^{86}Kr. This nucleus has a closed neutron shell and its mass is just below the peak of the 3p size resonance.

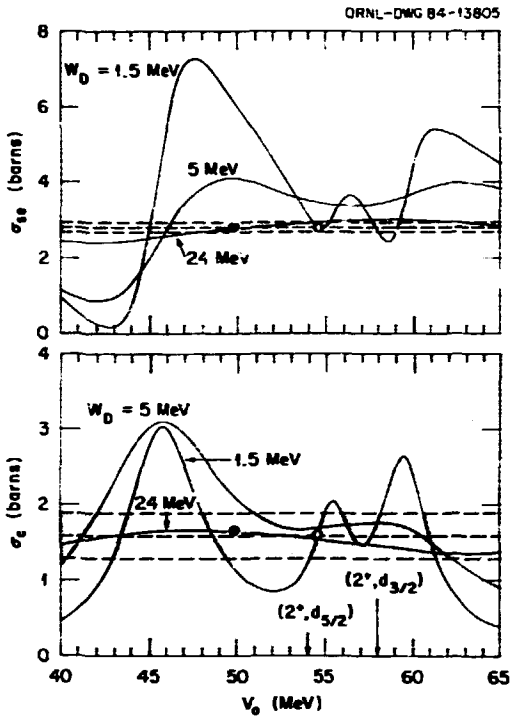

Fig. 2.27. Coupled channels OMP s-wave shape elastic and compound nuclear cross sections as for Fig. 2.26. THe 2^+ (1.33 MeV) target state is included with β = 0.211. Arrows indicate unperturbed energies of the $[2^+, 2d_{5/2}]$ and $[2^+, 2d_{3/2}]$ particle-core states. Solid points indicate the accepted model and the open points indicate a rejected solution.

Raman et al.[4] measured the transmission of a 99.5% enriched ^{86}Kr sample using the 80-m flight path at the ORELA facility. We repeated the measurement with the resolution of the 200-m flight path and 7 nsec burst width. With this resolution the resonances are well resolved such that definitive assignments of the important s- and p-wave resonances can be made for neutron energies up to about 400 keV. At higher energies the complicated structure makes assignments more difficult; nevertheless, our multilevel analysis is nearly complete for energies up to 700 keV.

In Fig. 2.28 the staircase plots show the cumulative sums of p-wave reduced widths for a 6.4-fm boundary radius. We see that the sum for $p_{3/2}$ is about three times that for $p_{1/2}$ and that the average slope or strength function, $\tilde{s} = \langle\gamma^2\rangle/D$, appears to be increasing in the region for $p_{3/2}$. These observations are consistent with a spin-orbit splitting of the 3p single-particle resonance. In our final analysis we

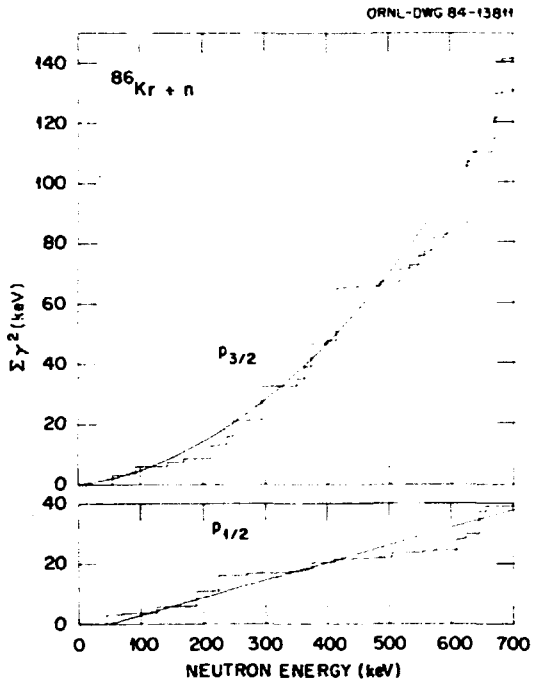

Fig. 2.28. Cumulative p-wave reduced widths.

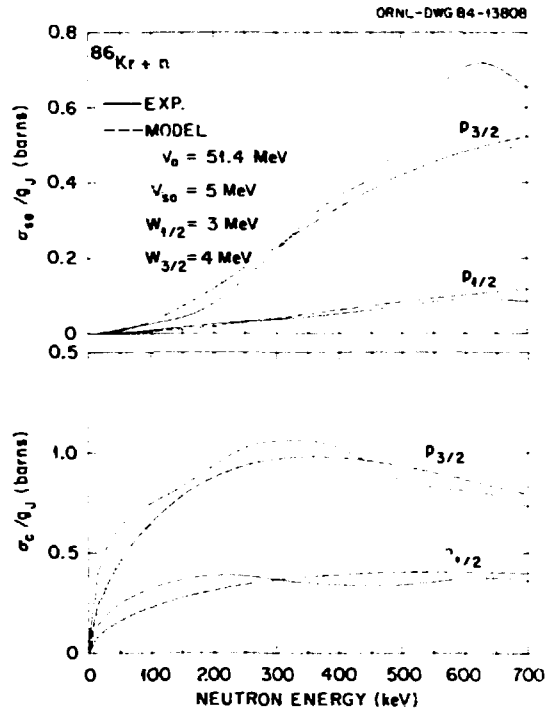

Fig. 2.29. Shape elastic and compound cross sections. Solid curves were deduced from the data by averaging the R-matrix scattering function with the averaging width 2I = 200 keV. Dashed curves are OMP fits with a given geometry and with the well depths adjusted as listed in the figure.

will introduce an energy dependence for the $p_{3/2}$ strength function, but here we assume each strength function to be constant within the region. Thus, we find $\tilde{s}$ = 0.022, 0.058 and 0.22, respectively, for $s_{1/2}$, $p_{1/2}$ and $p_{3/2}$.

Of equal importance for an OMP analysis is the external R-function which accounts for all levels outside the region from E_ℓ = 0 to E_u = 700 keV. For each partial wave it is parametrized by

$$R^{ext}(R) = \tilde{R}(E) - \tilde{s}\, \ell n\, [(E_u-E)/(E-E_\ell)]$$

where $\tilde{R} = a+b(E-E_m)$ and E_m is the midpoint of the analysis. The fitted (a,b) with b in MeV^{-1} are (-0.13,0.15), (0.60,0.14) and (0.58,1.74) for $s_{1/2}$, $p_{1/2}$ and $p_{3/2}$.

From the parametrized scattering functions we determined an average for each partial wave by use of an analytical approximation[5] with an averaging width of 2I = 200 keV. Figure 2.29 presents the p-wave average in terms of compound and shape elastic cross sections, σ_c and σ_{se}. The solid curves present the experimental values (divided by the statistical factors) and the dashed curves show the fit obtained by adjusting the well depths in an OMP of standard form with $r_0 = r_D = 1.21$ fm, $a_0 = 0.66$ fm and $a_D = 0.48$ fm. The fitted well depths are listed in the figure. We see that the imaginary well depths are essentially the same for both $p_{1/2}$ and $p_{3/2}$ and that the major part of the observed J-dependence in the p-wave cross sections is attributed to the real spin-orbit term. In other works, the spin-orbit splitting brings the $3p_{3/2}$ state down towards our region while pushing the $3p_{1/2}$ state upward. The proximity of the $3p_{3/2}$ state may account for the rising strength function in Fig. 2.28.

Table 2.9 lists the well depths deduced here for ^{86}Kr along with those reported[3] for the lighter nuclei. Some trends are apparent. For each nucleus the real well is deeper for p-waves than for s-waves. Coupled channel calculations[5] suggest that most, but not all, of this ℓ-dependence can be attributed to vibrational effects. For s-waves the smaller V_0 for ^{86}Kr is consistent with a relatively large symmetry term for this nucleus. The fact that the imaginary well depths have large fluctuations indicates the effects of nuclear structure for each nucleus.

---

1. Middle Tennessee State University, Murfreesboro, TN 37132.
2. Engineering Physics and Mathematics Division.

3. C. H. Johnson et al., Physics Division Progress Report, ORNL-6004, 47 (1983).
4. S. Raman et al., Phys. Rev. C 28, 603 (1983).
5. C. H. Johnson et al., Phys. Rev. C 27, 1913 (1983).
6. A. D. MacKellar, B. Castel and C. H. Johnson, Physics Division Progress Report, ORNL-6004, 48 (1983).

Table 2.9. Neutron optical model potential well depths

Nucleus	ℓ	V_0	V_{so}	W_D
^{30}Si	0	48 ± 1.7		4.5 ± 1.5
	1	62 ± 2.5	7[a]	4.5 ± 2.5
^{32}S	0	51.5 ± 0.4		6.0 ± 3.0
	1	61.4 ± 1.1	11 ± 3	2.7 ± 1.5
^{34}S	0	51.5 ± 1.1		3.0 ± 2.0
	1	58.5 ± 1.2	6 ± 3	3.5 ± 1.9
^{40}Ca	0	53.6 ± 1.0		6.7 ± 0.3
	1	56.1 ± 1.0	6 ± 7	0.6 ± 0.3
^{60}Ni	0	48 ± 5		29 ± 5
^{86}Kr	0	48.5 ± 1.0		
	1	51.4 ± 1.0	5 ± 1	3.5 ± 1.0

[a]Assumed value.

MEASUREMENTS OF THE NEUTRON TRANSMISSION AND CAPTURE CROSS SECTIONS IN ^{204}Pb[1]

D. J. Horen J. A. Harvey[2]
R. L. Macklin[2] N. W. Hill[3]

High resolution neutron transmission measurements have been performed on ^{204}Pb in the energy interval E = 0.4-105 keV. The transmission data were analyzed using a multilevel R-matrix code to deduce resonance parameters. Previously obtained neutron capture data were reanalyzed in the interval 2.6-86 keV. Values of $g\Gamma_n\Gamma_\gamma/\Gamma$ were determined from the capture data. For those resonances where Γ_n could be determined from the transmission data, the capture data were analyzed to extract Γ_γ. Our results yield an average capture for a stellar temperature kT = 30 keV of 89.5 ± 4.5 mb. The s-wave level density for ^{205}Pb corresponding to the neutron energy range investigated (i.e., E ~105 keV) relative to that for ^{207}Pb (which has about the same neutron separation energy) is greater by about a factor of 10. The average s-wave strength function in this energy region is determined as $S_0 = 0.93 \times 10^{-4}$. This is an order of magnitude greater than that for a similar energy region in $^{206}Pb+n$, where a doorway is observed at E ~ 500 keV. However, the strength function in the initial E ~ 0-100 keV in $^{204}Pb+n$ is almost identical to the average value of that for $^{206}Pb+n$ when the averaging interval for the latter is taken as E_n ~ 0-1000 keV (i.e., over the doorway state). This suggests that the s-wave doorway state observed in the higher mass lead isotopes is completely mixed with "background" states in ^{205}Pb, and most likely no intermediate structure will be observed in the s-wave strength function for the $^{204}Pb+n$ reaction.

1. Abstract of paper: Phys. Rev. C 29, 2126 (1984).
2. Engineering Physics and Mathematics Division.
3. Instrumentation and Controls Division.

SPHERICAL OPTICAL MODEL DESCRIPTION OF $^{208}Pb+n$ SCATTERING NEAR THRESHOLD

D. J. Horen C. H. Johnson

The spherical optical model potential (OMP) provides a good macroscopic description of nuclear scattering for energies for which the compound system can be treated statistically. The scattering of low energy neutrons by ^{208}Pb near threshold where the level density is quite small obviously does not satisfy these conditions. For example, there are only three $1/2^+$ resonances in the energy interval E_n = 0-1005 keV, and almost all of the s-wave strength is contained in a single resonance at 506 keV. Hence, it is clear that this energy regime is non-statistical and that standard averaging procedures would not be appropriate. However, it is still useful to attempt some sort of average description even at these energies in order to make comparisons to OMP predictions and, thereby, to relate to the OMP analyses which are made for higher energy data.[1]

As distinguished from higher energy studies (i.e., $E_n \gtrsim 3$ MeV), the low energy region which we study with ORELA is dominated by resonance structure. The data can be analyzed in terms of partial waves from which one can deduce information pertaining to possible ℓ-dependency of the spherical OMP. This is in contrast to work at higher energies where one is constricted to investigations of the average potentials.

We have analyzed our $^{208}Pb+n$ data utilizing the R-matrix formalism and deduced a parameter set that reproduces the differential elastic and total cross sections in the energy interval E_n = 40-1005 keV. The scattering function for each partial wave can be expressed in the form

$$S(E) = e^{-2i\phi(E)} \frac{1 + iP(E)R(E)}{1 - iP(E)R(E)},$$

where ϕ and P are the hardsphere phase shift and penetrability, respectively. R is the R-function which has been parametrized in terms of poles as

$$R(E) = R^{ext}(E) + \sum \frac{\gamma^2}{E\lambda - E}.$$

The function $R^{ext}(E)$ can be parametrized in a variety of ways, and we have chosen to do so by use of a distribution of poles outside of the region analyzed. For our choice of boundary radius, $R_0^{ext}(E)$ (i.e., for s-waves) is a smoothly varying function whose magnitude is small in our energy interval of analysis. Together with the hardsphere phase shift, it

determines the cross section which one would have in the absence of the observed resonances. This cross section is almost equivalent to the elastic cross section that one would calculate from a real potential. We find that the depth of the real well of a Wood-Saxon potential that fits the cross section calculated by setting the resonance part of the R-matrix to zero is very close to that required to yield the experimentally observed binding energy of the $4s_{1/2}$ neutron in ^{209}Pb.

We can write the OMP S-matrix in the same form as that for the R-matrix as

$$S^{OMP}(E) = e^{-2i\phi(E)} \frac{1+iP(E)[\bar{R}(E)+i\pi s(E)]}{1-iP(E)[\bar{R}(E)+i\pi s(E)]} .$$

For a real well (i.e., $W \equiv 0$), $s(E) \equiv 0$. Hence, we can see that what was done above is to assume that if we had averaged the experimentally determined S-matrix the resonance would not contribute significantly to the determination of $R(\bar{E})$. We have performed a numerical average[2] of $S(E)_{exp}$ and find this to be essentially so. Hence, we feel that our determination of the value of the real potential near threshold for a spherical potential model has validity.

The determination of the imaginary potential is more questionable. We have approached this in two ways. One is to ignore the fact that there are too few s-wave resonances to allow a reliable average and to perform a numerical calculation with a large averaging interval. The other is to consider the trend of the data for other isotopes of lead. From earlier works,[3] it has been shown that s-wave strengths in ^{206,207}Pb+n also have doorway structure in the energy interval E_n = 0-1000 keV. Recently, it has been found[4] that the s-wave strength in ^{204}Pb+n is much more fragmented, and has a value in the interval E_n = 0-100 keV that is essentially equal to that for the other lead isotopes when one averages the latter over a 1000 keV interval. This has been interpreted[4] as indicating that the compound system ^{204}Pb+n already is essentially statistical, and that the strength in the s-wave doorway states in ^{206,207,208}Pb is more or less uniformly distributed in ^{204}Pb+n. On this basis we would expect that if we uniformly distribute the strengths in ^{206,207,208}Pb we would find OMP parameters for all of the lead isotopes to be similar (except for an A dependence) as one might expect for a global model. The value of s obtained by averaging is not too different from that determined from a uniform distribution.

The values of the real, V_0, and imaginary, W_0, spherical OMP that we deduce with the geometry given by Finlay et al.[1] are shown in Fig. 2.30. The values of V_0 determined from our partial ℓ-wave analyses are in good agreement with the value of the average V_0 extrapolated downward from fits to higher energy data. Our indicated values for W_0 should be considered as tentative, with large error bars. Further consideration must be given to investigating the meaning of methods to deduce these. However, it is interesting to note that our tentative values at least appear reasonable. Since our intermediate structure can be explained in terms of a real resonance (i.e., particle-core excitation) within our region of analysis, it is clear that a spherical optical model description must contain a non-vanishing W_0. In another contribution we discuss a description of ^{208}Pb+n scattering in the s-wave channel in terms of a coupled-channel formalism with real potentials.

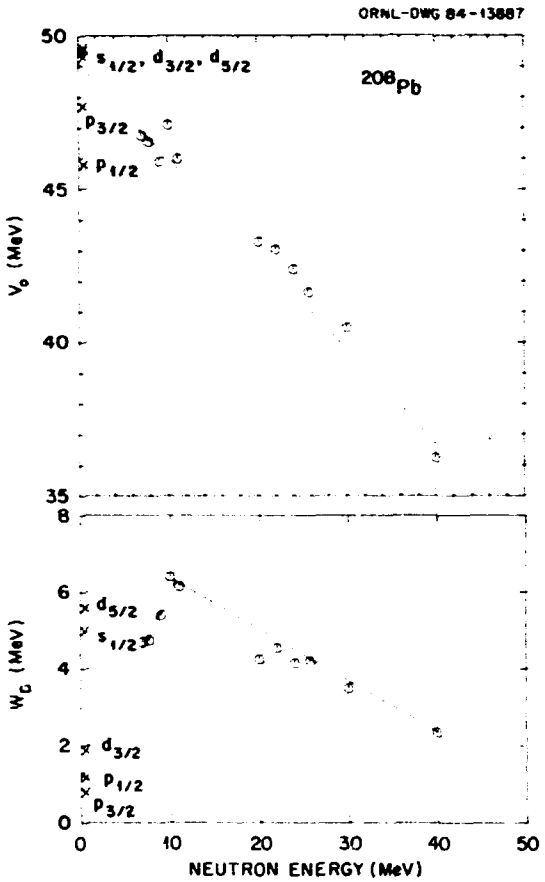

Fig. 2.30. Plots of the real, V_0, and imaginary, W_0, values for a spherical optical model description of ^{208}Pb+n scattering. The x's have been deduced from this work. The remaining points are from Ref. 1.

1. See for example, R. W. Finlay et al., Phys. Rev. C 30, 796 (1984).
2. C. H. Johnson et al., Phys. Rev. C 27, 1913 (1983).
3. D. J. Horen, J. A. Harvey and N. W. Hill, Phys. Rev. Lett. 38, 1344(1977); Phys. Rev. C 18, 722 (1978); 20, 478 (1979); 24, 1961 (1981).
4. D. J. Horen et al., Phys. Rev. C 29, 2126 (1984).

COUPLED-CHANNEL CALCULATION OF S-WAVE CROSS SECTION FOR ^{208}Pb+n: E_n = 40-1005 keV

A. D. MacKellar[1] D. J. Horen
C. H. Johnson

The s-wave channel for ^{208}Pb+n scattering in the energy range E_n = 40-1005 keV is essentially describable in an R-matrix analysis with

$$R(E) = R_{ext}(E) + \frac{\gamma^2}{(E_\lambda - E)}$$

where the resonance energy is 506 keV. Here we show that this intermediate structure can be reproduced using a coupled-channel calculation[2] with a simple particle-vibrator model.[3]

Experimentally it is found that the $4s_{1/2}$ single particle state lies at an excitation energy of 2.03 MeV in ^{209}Pb. The neutron separation energy is 3.94 MeV (which corresponds to the binding energy of the $2g_{9/2}$ ground state). The number of $1/2^+$ states that can be formed by particle-hole or particle-core excitations and which lie in the energy interval E_n = 0-1000 keV is very limited. One such state can be formed by coupling the $2g_{9/2}$ single particle to the 4^+ core excitation (i.e., 4.32 MeV in ^{208}Pb). Our initial calculations are being done with the coupled-channel code ECIS.[4] The coupling equations are of the form

$$\left[\nabla^2_{\rho_n} - \frac{\ell_n(\ell_n+1)}{\rho_n^2} - \frac{V_{diag}}{E_n} - 1\right] R_{J_n \ell_n j_n}(r)$$

$$= \frac{1}{E_n} \sum_{n' \ell_{n'} j_{n'}} \langle (Y_{\ell_n j_n}(x)\, \phi_{I_n} \mid V_{cpl} \mid (Y_{\ell_{n'} j_{n'}}(x)\, \phi_{I_{n'}}) JM \rangle R_{J_{n'} \ell_{n'} j_{n'}}(r),$$

where $\rho_n = k_N r$, k_N is the projectile wave number, and $E_n = E - \hbar\omega$. The scattered neutron has an energy, E_n, given by the incident energy minus the excitation energy of the core state. The central potential is purely real and of the Wood-Saxon form. The coupling potential can be expressed in terms of derivatives of a Wood-Saxon form and amplitudes for excitation of phonon modes of the target nucleus. Our preliminary calculations have used values of V_{diag} that result in binding the $4s_{1/2}$ and $2g_{9/2}$ single-particle states at their experimentally observed values. We used a value β_4 = 0.07 for the 4^+ core state.

In Fig. 2.31 we compare the coupled-channel calculated cross section with that calculated using our experimentally determined s-wave R-matrix. This preliminary comparison is quite good. The position of the resonance is close to that observed experimentally, but the width is somewhat broader. In this calculation, the resonance is shifted upward only about 130 keV from the sum of the experimentally observed (unperturbed values) $2g_{9/2}$ single particle state and 4^+ core excitation. This results partly because the coupling is weak and partly because the values of V_{diag} used are those that yield the observed rather than the unperturbed binding energies for the single particle states. A more correct calculation would utilize V_{diag} which give the unperturbed single particle binding energies, and then reproduce the distribution of single particle strength in the bound as well as the unbound region. Such an investigation is in progress.

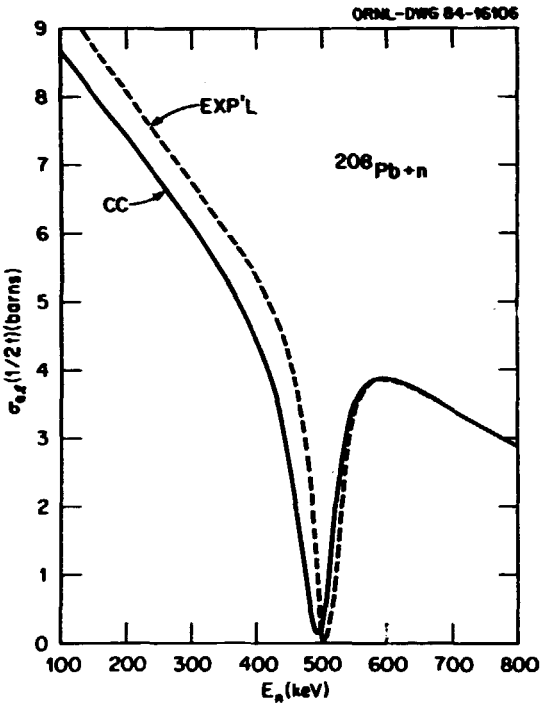

Fig. 2.31. Comparison of the experimental and coupled-channel calculated s-wave cross sections for ^{208}Pb+n.

---

1. Consultant from University of Kentucky, Lexington, KY 40506.
2. T. Tamura, Rev. Mod. Phys. 37, 679 (1965).
3. A. Landa and G. E. Brown, Nucl. Phys. 75, 344 (1966).
4. J. Raynal (unpublished).

ELASTIC AND INELASTIC SCATTERING OF ^{18}O FROM ^{28}Si AT 19.5 MeV/amu

B. L. Burks J. L. C. Ford, Jr.[1]
D. J. Horen E. E. Gross
R. L. Auble D. C. Hensley
F. E. Bertrand R. O. Sayer[2]
J. L. Blankenship D. Shapira
T. P. Sjoreen[3]

To date no global optical-model parametrization has been developed to adequately describe heavy-ion elastic scattering data for a large range of projectile energies and target-projectile combinations. Therefore, it is

necessary to measure elastic scattering data for incoming and outgoing heavy-ion reaction channels in order to determine reasonable optical-model potentials for use in direct reaction calculations such as DWBA. As a complementary measurement to a study[4] of reactions initiated by a 354-MeV ^{18}O beam incident upon a ^{28}Si target we have measured cross sections for $^{28}Si(^{18}O,^{18}O)^{28}Si$ elastic scattering and also inelastic scattering to the lowest 2^+ states in both the target and projectile, $^{28}Si(^{18}O,^{18}O)^{28}Si^*[1.78\ MeV,2^+]$ and $^{28}Si(^{18}O,^{18}O^*[1.98\ MeV,2^+])^{28}Si$, respectively.

The data described in this report were obtained using the coupled tandem and cyclotron machines and the broad range spectrograph (BRS) at HHIRF. Particle identification and focal plane position were determined using a multiparameter focal plane detector system which has been described elsewhere.[5] Scattering data were measured for a laboratory angle range of 2° to 15°, with a solid angle of 4.581 msr corresponding to an angular acceptance of ±2.0° horizontal and ±1.88° vertical at each magnetic field setting. Five magnetic field settings were required to provide ample overlap of scattering angle bite detected on the focal plane. The scattering yield has been analyzed by binning in 0.2 degree intervals, equivalent to approximately 0.33 degrees in the center of mass reference frame. Elastic scattering cross sections have been determined for an angular range of 3.5° to 20.9° c.m., as shown in Fig. 2.32. Inelastic scattering cross sections were determined for excitation of the 1.78-MeV state in ^{28}Si from 3.5° to 22.2° c.m., and for excitation of the 1.98-MeV state in ^{18}O from 3.5° to 16.0° c.m., as shown in Fig. 2.33.

An optical model fit to the elastic scattering data has been completed. The code PTOLEMY[6] was used to perform the optical model calculations and also automatic parameter searches for χ^2 minimization. Two sets of optical-model potentials were adopted as starting values for fitting the data; both taken from analysis of $^{16}O + ^{28}Si$ elastic scattering data.[7,8] Both parameter sets were derived from analysis of differential cross section angular distributions measured at 11 energies between 33 MeV and 215 MeV. The two parameter sets are summarized in Table 2.10 along with the parameters resulting from an optical model fit to the $^{18}O + ^{28}Si$ data presented here.

The potential labeled E18 is an energy-independent Woods-Saxon optical potential reported by Cramer et al.[7] The potential labeled A-type in Table 2.10 also uses a Woods-Saxon potential but includes a linear energy dependence of the diffuseness of the imaginary part of the potential. This potential along with a discussion of various other potential shapes was reported by Satchler.[8] Both starting parameter sets predicted angular distributions that were out of phase with the data. However, the shallow potential of Cramer et al. more nearly reproduced the amplitude of oscillation observed in Fig. 2.32 for the angular distribution of the cross section plotted as a ratio to the Rutherford scattering cross section. Although both parameter sets were

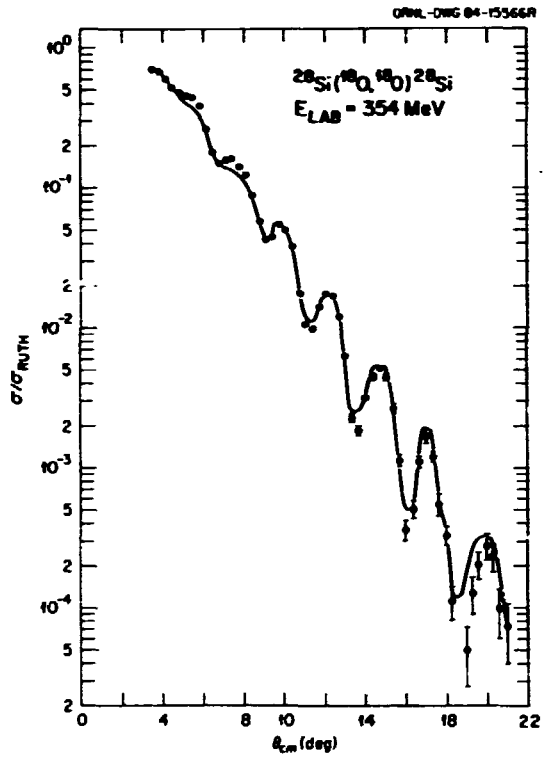

Fig. 2.32. Differential cross section data for $^{18}O + ^{28}Si$ elastic scattering at 354 MeV. The solid curve is the best optical-model fit to the data generated using the parameters labeled E-type given in Table 2.10.

searched for an optimum fit to the data, it was found that the phase and amplitude of oscillation of the data plotted in Fig. 2.32 could be reproduced more readily by modification of the shallow potential. The optical-model parameters which gave the best fit to the data are listed in Table 2.10, labeled E-type potential. Since the best fit was obtained by increasing the real well depth and decreasing the real well radius, the next step in this analysis is to explore the ambiguity in these parameters to see if a parameter set more closely resembling that of Cramer et al. could equally well reproduce the data.

A coupled-channels analysis of the elastic and inelastic scattering data shown in Figs. 2.32 and 2.33 is in progress using the E-type potential of Table 2.10 as a starting value. Initial calculations indicate that the best fit to the data will require significant reduction of the imaginary well depth so that the final parameter set will resemble the E18 potential of Cramer et al. even more closely. Although the coupled-channels analysis is still in progress, the calculations indicate that deformation parameters, β_2, required to fit the inelastic scattering cross sections are consistent with the values obtained by light ion scattering.

1. Deceased.
2. Computing and Telecommunications Division, ORNL.

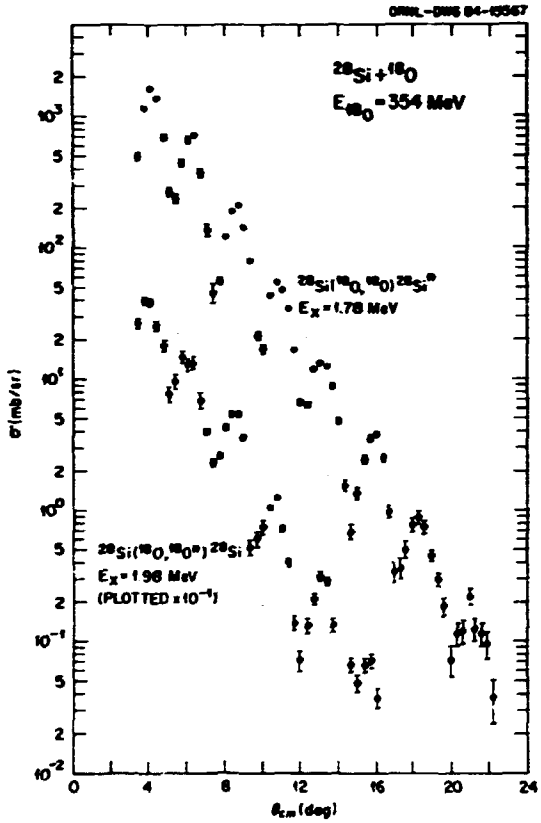

Fig. 2.33. Differential cross section data for ^{18}O + ^{28}Si inelastic scattering at 354-MeV populating the 1.78 MeV state in ^{28}Si and the 1.98 MeV state in ^{18}O. The latter angular distribution was multiplied by a factor of 0.1 before plotting.

3. Solid State Division, ORNL.
4. J. L. C. Ford, Jr. et al., ORNL-6004, p.147 (1983) unpublished. T. P. Sjoreen et al., ORNL-6004, p. 148 (1983) unpublished. M. W. Hynes et al., Nucl. Instrum. Methods Phys. Res. A224, 89 (1984). T. P. Sjoreen et al., Nucl. Instrum. Methods Phys. Res. A224, 421 (1984).
5. B. L. Burks et al., "Spectroscopy of ^{27}Al via the $^{28}Si(^{18}O,^{19}F)^{27}Al$ Reaction," this report.
6. M. H. Macfarlane, S. C. Pieper, and M. Rhoades-Brown, private communication, computer code PTOLEMY.
7. J. G. Cramer et al., Phys. Rev. C 14, 2158 (1976).
8. G. R. Satchler, Nucl. Phys. A279, 493 (1977).

SPECTROSCOPY OF ^{27}Al VIA THE $^{28}Si(^{18}O,^{19}F)^{27}Al$ REACTION

B. L. Burks, D. J. Horen, R. L. Auble, F. E. Bertrand, J. L. Blankenship, J. L. C. Ford, Jr.[1], E. E. Gross, D. C. Hensley, R. O. Sayer[2], D. Shapira, T. P. Sjoreen[3]

During a recent experiment studying the $^{28}Si(^{18}O,^{18}F)^{28}Al$ single charge exchange reaction, data were also obtained for the proton pickup reaction $^{28}Si(^{18}O,^{19}F)^{27}Al$. A 354 MeV ^{18}O beam was provided by coupled operation of the tandem and cyclotron machines at the Holifield Heavy Ion Research Facility (HHIRF) with a typical beam intensity of 3 to 4 pna incident on a 117 $\mu g/cm^2$ self-supporting ^{28}Si target. The reaction products were detected in the focal plane detector system of the broad range spectrograph (BRS).

At the beam energy used in this study, 19.5 MeV/amu, the proton pickup reaction channel is much stronger than the charge exchange reaction channel. Because of the 34 cm active length of the vertical drift chamber in the focal plane detector system of the BRS, position and particle-identification information were

Table 2.10. Optical model potential parameters deduced from ^{16}O + ^{28}Si elastic scattering data and used as starting values in the present analysis of ^{18}O + ^{28}Si elastic and inelastic scattering. The E-type potential is the result of an optical-model fit to the ^{18}O + ^{28}Si elastic scattering data in Fig. 2.32.

Potential	V (MeV)	r_0 (fm)	a_0 (fm)	W_0(volume) (MeV)	r_I (fm)	a_I (fm)	r_{Coul} (fm)
E18[7]	10.0	1.35	0.618	23.4	1.23	0.552	1.0
A-type[8]	100.0	0.967	0.745	44.1	1.073	1.009	1.3
E-type	15.0	1.30	0.710	42.0	1.19	0.707	1.0

obtained simultaneously for excitation energy ranges of approximately 0 to 70 MeV in ^{27}Al and 0 to 50 MeV in ^{28}Al. Other reaction products were also observed but will not be discussed in this report, see Fig. 2.34.

Figure 2.35 shows a focal plane position spectrum for the ^{28}Si(^{18}O,^{19}F)^{27}Al reaction measured at a laboratory angle of 2.1°. Prominent peaks corresponding to states in ^{27}Al or ^{19}F are labeled. The typical position resolution was approximately 1 mm FWHM, equivalent to an energy resolution of about 220 keV FWHM. The data have been analyzed in 0.2 degree bins for laboratory scattering angles from 2 to 8 degrees. Differential cross sections have been determined for many of the states labeled in Fig. 2.35. Further peak-fitting is under way for the remaining states. The resulting angular distributions will be compared to heavy-ion transfer reaction calculations performed using the code PTOLEMY.

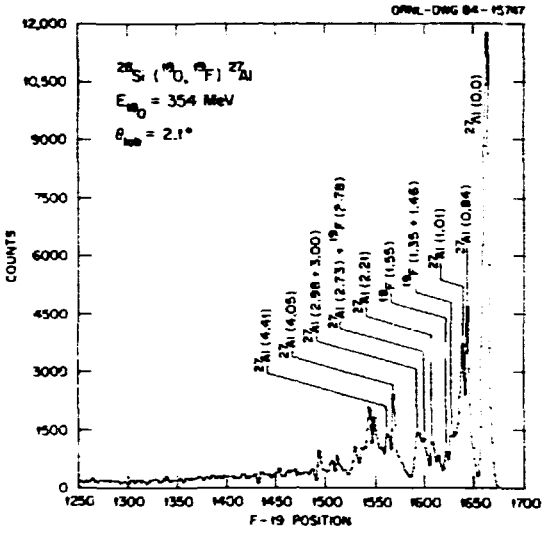

Fig. 2.35. A focal plane position spectrum for the ^{28}Si(^{18}O,^{19}F)^{27}Al reaction at θ_{lab} = 2.1°. Prominent peaks corresponding to states in ^{27}Al or ^{19}F are labeled with excitation energies in MeV.

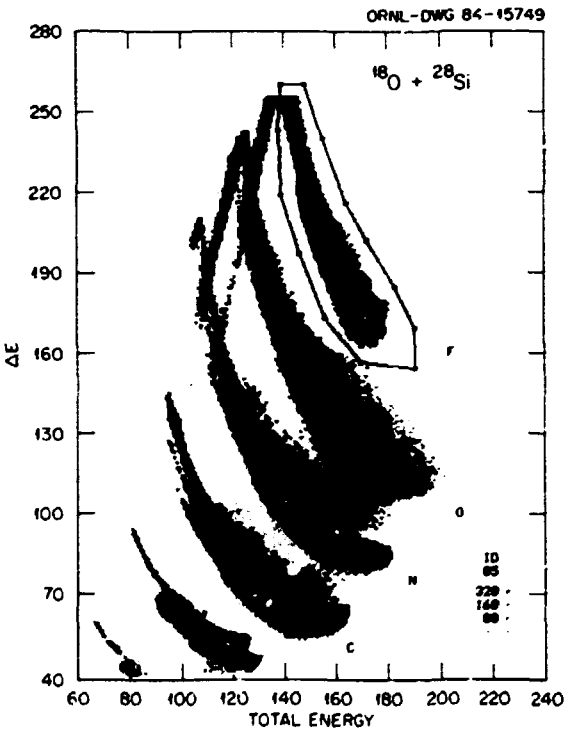

Fig. 2.34. An E-ΔE plot for light heavy ions emitted from the ^{18}O + ^{28}Si reaction. The solid line enclosing the Z = 9 distribution indicates the particle identification gate used to separate flourine (F) nuclei from other reaction products.

INCLUSIVE STUDIES OF HEAVY PRODUCTS FROM ^{28}Si + ^{12}C INDUCED REACTIONS WITH SINGLE UNIT MASS AND CHARGE IDENTIFICATION

D. Shapira M. Beckerman
J. Gomez del Campo B. A. Harmon[1]
S. T. Thornton[1]

Studies of orbiting and deep inelastic reactions with ^{28}Si + ^{12}C and other light systems have provided evidence for the presence of an upper limit to the orbital angular momentum stored in the dinuclear complex formed in deep inelastic collisions.[2] The value of this angular momentum limit can be related to a limit on the angular momentum in the entrance channel (with specific assumptions on the nature of nucleus-nucleus friction). In accordance with the model for nucleus-nucleus fusion put forth by R. Bass, it is expected that any limit on the formation of a dinuclear configuration will also prevent the fusion of the nuclei involved. We have therefore decided to investigate these effects and to demonstrate the presence of angular momentum limitations on nucleus-nucleus fusion in the ^{28}Si + ^{12}C system.

The effects of reaching an absolute limit on the angular momentum leading to fusion are twofold. (1) The magnitude of the cross section for complete fusion of projectile and target should become inversely proportional to the center-of-mass bombarding energy at energies beyond that for which this limit has been reached (see Fig. 2.36). (2) In addition, since complete angular momentum transfer to the composite system is no longer possible, we expect to observe the onset of processes where only part of the angular (and therefore linear)

---

1. Deceased.
2. Computing and Telecommunications Division, ORNL.
3. Solid State Division, ORNL.

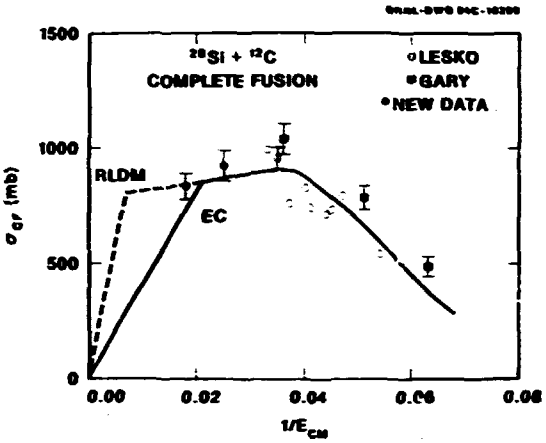

Fig. 2.36. Predictions for complete fusion of $^{28}Si + ^{12}C$ as a function of incident center-of-mass energy. The data shown as open circles and cross marks are from refs. 5 and 4 and the solid circles present new data acquired by the authors of this report.

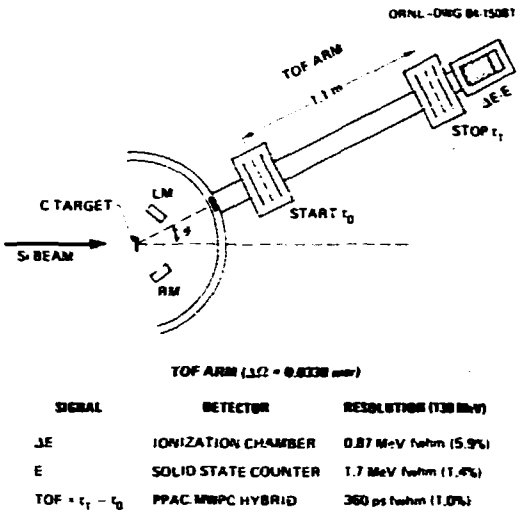

TOF ARM ($\Delta\Omega$ = 0.0338 msr)

SIGNAL	DETECTOR	RESOLUTION (130 MeV)
ΔE	IONIZATION CHAMBER	0.87 MeV fwhm (5.9%)
E	SOLID STATE COUNTER	1.7 MeV fwhm (1.4%)
TOF = $t_1 - t_0$	PPAC MWPC HYBRID	360 ps fwhm (1.0%)

Fig. 2.37. The experimental setup for time of flight, energy loss and total energy measurements reported here.

momentum of the projectile is transferred to the target (e.g., incomplete fusion). The predicted cross section for fusion of $^{28}Si + ^{12}C$ is shown in Fig. 2.36. This prediction is made in the spirit of the Bass model for nucleus-nucleus fusion but with a readjustment of the global parameters quoted by Bass[3] to fit fusion data measured at low energy.[4,5] The angular momentum limits are the values (E.C.) derived from the deep inelastic orbiting data[2] and the higher cutoff value corresponds to an assumed rotating liquid drop limit (RLDM).

It becomes increasingly complicated to identify evaporation residues from the collisions of light heavy-ions, particularly at higher energy. The data analysis involves careful studies of the energy and velocity spectra of heavy products and the identification of yields from processes where complete momentum transfer has occurred. Complete identification (mass and charge) of the products facilitates such analysis and renders it less ambiguous. It is also expected that the predominant incomplete fusion process in this system (^{28}Si beam with ^{8}Be target fragment) will be a process which is even more forward peaked than the complete fusion – evaporation yield.

We report here on measurements of reaction products from the bombardment of a ^{12}C target by a ^{28}Si beam. Angular distributions for all products were measured at angles ranging from 2 degrees to 13 degrees. The mass and charge of the products were identified by measuring their energy and time-of-flight as well as energy loss in a gas-filled ionization chamber. The setup used in the experiment is shown in Fig. 2.37. Angular distributions of the evaporation residues, measured at 130 and 180 Mev bombarding energies, are shown in Fig. 2.38. The fusion cross sections obtained from integrating the angular distributions shown in Fig. 2.38 are

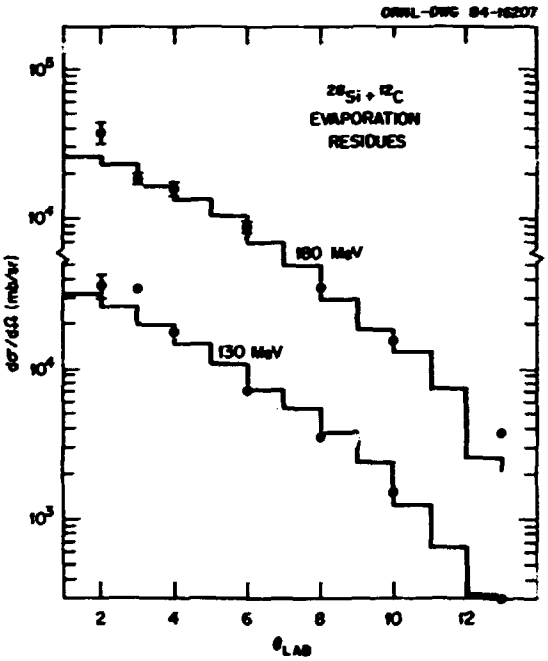

Fig 2.38. Angular distribution of evaporation residues from collisions of ^{28}Si and ^{12}C nuclei. The histograms are angular distributions predicted by the Monte Carlo evaporation code PACE (6).

shown (solid circles) in Fig. 2.36. Similar data at higher energies are clearly needed and we plan such measurements using a 260 MeV ^{28}Si beam from the HHIRF facility.

The velocity spectra shown in Figs. 2.39 and 2.40 serve to highlight the contribution of

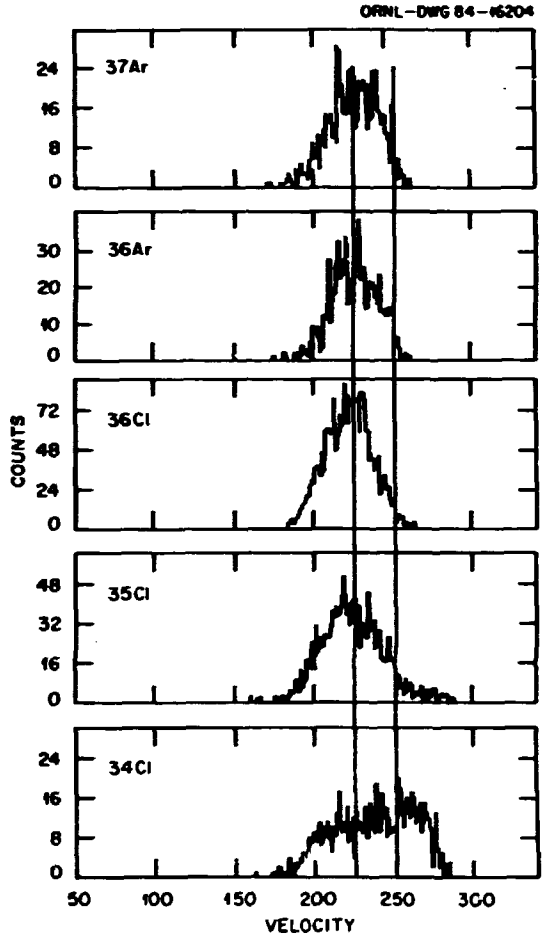

Fig 2.39. Velocity spectra for different evaporation residues meassured at a laboratory angle of two degrees.

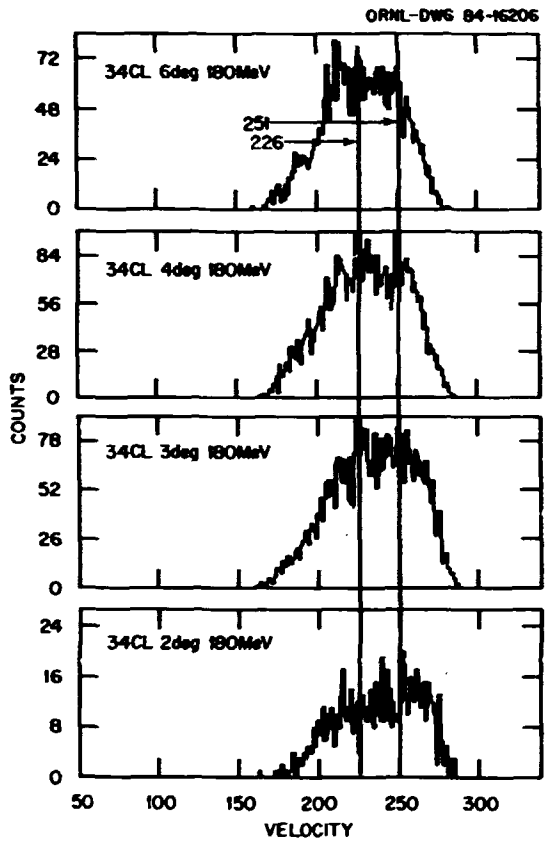

Fig 2.40. Velocity spectra for $^{35}Cl_{17}$ measured at four angles (2°, 3°, 4°, 6°, and 8°).

yields from the process of incomplete fusion of ^{28}Si with ^{12}C. The predominant incomplete fusion expected is that of ^{28}Si with a ^{8}Be fragment from the target. This results in higher velocities. Figure 2.39 shows the velocity spectra of $^{35,36}Cl$ and $^{36,37}Ar$ which are not likely to have contributions from an ^{36}Ar compound nucleus (^{28}Si + ^{8}Be). ^{34}Cl on the other hand shows some contributions from this process as do lighter elements. In Fig. 2.40 we see the evolution of the ^{34}Cl spectrum over the angular range of 2° to 6° as a shift from the velocity of incomplete fusion to that of products from complete fusion.

---

1. University of Virginia, Charlottesville, VA 22901.

2. D. Shapira et al., Phys. Rev. Lett. 53, 1634 (1984).
3. R. Bass, Nuclear Reactions Between Heavy Ions, Springer Verlag (1980).
4. S. Gary et al., Phys. Rev. C 25, 1877 (1982).
5. K. T. Lesko et al., Phys. Rev. C 25, 872 (1982).
6. A. Gavron, Phys. Rev. C 21, 230 (1980).

TWOFOLD AND THREEFOLD COINCIDENCE MEASUREMENTS OF COMPLEX FRAGMENT EMISSION IN $^{28}Si+^{12}C$ COLLISIONS

D. Shapira R. Novotny[1]
S. T. Thornton[2]

190 MeV ^{28}Si ions from the Heidelberg MPI Tandem + Linac Accelerator Complex were used to bombard natural carbon targets. Complex fragments ($Z > 2$) emitted in these collisions were identified in an array of five large volume ionization chambers (see Fig. 2.41). Each detector measures energy E, linear momentum $\vec{p}$ and the charge Z of an entering fragment.

This study is aimed at establishing the nature of the yield of recoiling target-like nuclei. Inclusive energy spectra and angular distributions of these target-like recoils were

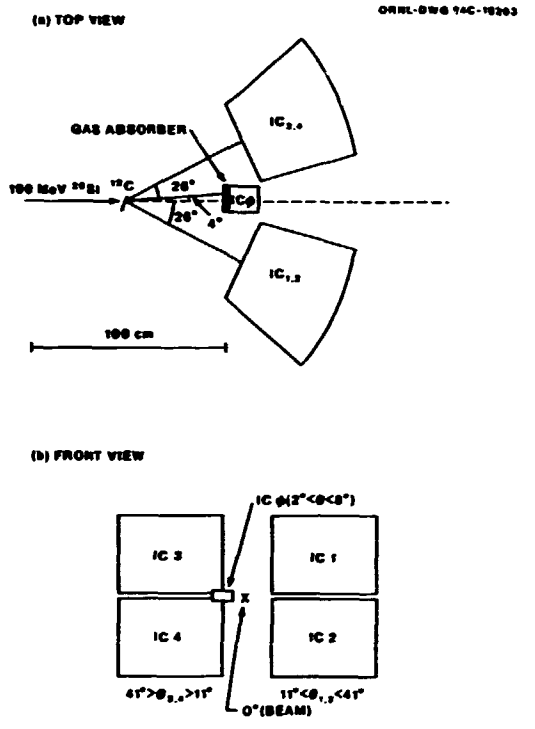

Fig. 2.41. Experimental arrangement of the three detectors: (a) top view, (b) front view.

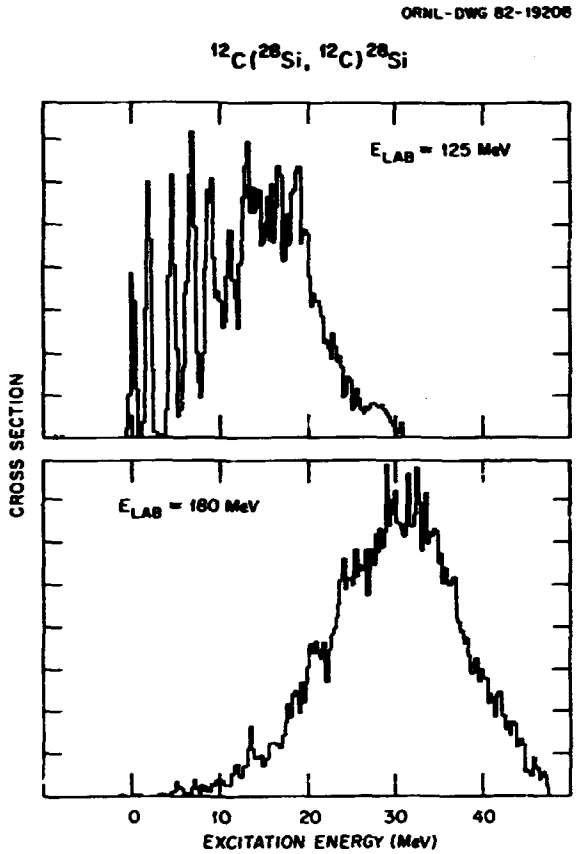

Fig. 2.42. Energy spectrum of recoiling ^{12}C nuclei from ^{28}Si + ^{12}C induced reactions.

studied extensively, over a wide range of bombarding energies in a series of measurements that confirmed the predominance of orbiting in collisions between light heavy nuclei.[3]

In particular, the continuum spectra of recoiling carbon nuclei of the type shown in Fig. 2.42 could originate in two different processes:

$$(1)\quad {}^{28}Si + {}^{12}C \rightarrow ({}^{28}Si^*) + {}^{12}C^* \rightarrow {}^{24}Mg^* + {}^{4}He + {}^{12}C^*$$

$$(2)\quad {}^{28}Si + {}^{12}C \rightarrow {}^{24}Mg^* + ({}^{16}O^*) \rightarrow {}^{24}Mg^* + {}^{4}He + {}^{12}C^*$$

Twofold coincidence measurements were aimed at separating these two most likely sources for carbon production and determining their relative contribution to the observed ^{12}C yield. In both cases the most likely end products of this chain is a combination of ^{4}He, ^{12}C, and ^{24}Mg nuclei.

The experiment was arranged in such a way that the ionization chamber placed at small angles had an absorber placed in front that served to keep any forward scattered beam particles and evaporation residues from reaching the active detector volume.[3] This enabled us to do the experiment with 100 na of ^{28}Si (14^+) but had the disadvantage that particles with $Z > 14$ could not reach the detector at all and only particles with $Z < 10$ could be detected over a sufficiently large range of kinetic energies.

The bottom part of Fig. 2.43 shows the distribution of missing charge $\Delta Z = 20 - Z_0 - Z_{1,2}$ for all two-body coincidences between IC0 (ionization chamber at forward angles) and $IC_{1,2}$. Clearly the most dominant coincidence channel is that with $Z_0 + Z_{1,2} = 18$ (two units of charge missing). The top part of the same figure shows the distribution of all those events with $Z_0 + Z_{1,2} = 18$. The majority of these events have carbon and magnesium detected in coincidence. The low yield of ions with $Z_0 > 9$ in IC0 is due to the high energy threshold for the heavier nuclei caused by the absorber placed in front of that counter.

Since we also have the information on angle and energy of the detected nucleus, and assuming $A = 2*Z$ also their approximate masses, we are able to calculate their momenta and from these deduce the total momentum of the missing particle(s). It is then possible to transform, event by event, the momentum of this missing particle to the center-of-mass system. The two-dimensional distribution of the momenta attributed to the missing particle(s) is shown on Fig. 2.44. This distribution serves as a clear indication that the dominant process producing carbon ions is the first chain indicated since the higher density of ^{4}He momenta point in the direction of the recoiling ^{28}Si. Monte Carlo

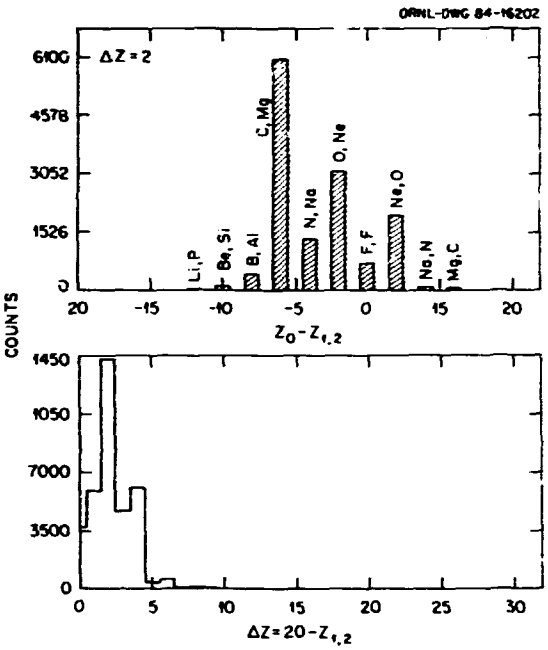

Fig. 2.43. Fragment abundance for two-body coincidences from ^{28}Si + ^{12}C collisions.

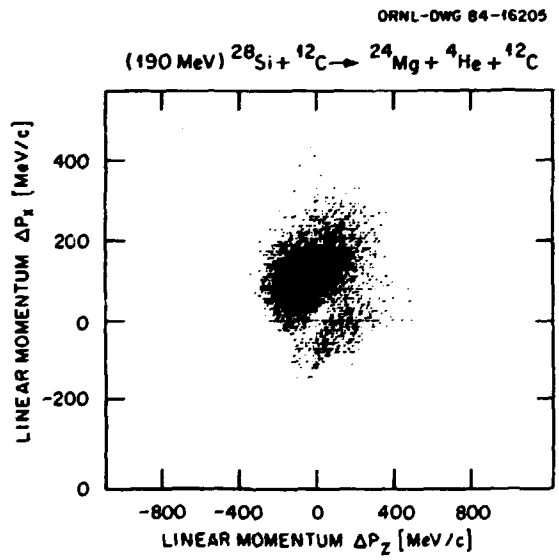

Fig. 2.44. Momentum of missing particle: components projected in the reaction plane.

simulation that take into account actual geometry and particle threshold will be employed in further ongoing quantitative analysis of these data.

---

1. II. Physical Institute, University of Giessen, Giessen, West Germany.

2. Physics Department, University of Virginia, Charlottesville, VA 22901.

3. Phys. Lett. 114B, 111 (1982).

MASS AND CHARGE FLOW DURING ORBITING OF LIGHT-HEAVY NUCLEI: STUDY OF THE ^{28}Si + ^{14}N SYSTEM

D. Shapira
J. Gomez del Campo
J. L. C. Ford, Jr.[1]
B. Shivakumar[2]
P. H. Stelson
B. A. Harmon[3]
R. A. Parks[3]
S. T. Thornton[3]

In a series of experiments performed at ORNL and elsewhere it has been demonstrated that colliding light heavy nuclei are likely to form a long-lived rotating dinuclear system which does not fuse.[4] The cross section for this process is tens of millibarns, a substantial magnitude for nuclear processes. The fact that such a process requires a precarious balance between attractive and repulsive forces in a nucleus-nucleus collision makes the existence and our understanding of this process important.

We focused on the study of backscattering of ^{12}C from ^{28}Si. Very large cross sections for emission of B, C, N and O isotopes to backward angles were measured. These particles emitted to the backward hemisphere were concentrated mostly at large negative Q value (corresponding to high excitation of the end fragments). The most probable kinetic energy (the peak of the Q value distribution) does not vary with angle of emission (completely relaxed), it does vary linearly, however, as a function of bombarding energy. It was also found that this particle yield at backward angle has a $1/\sin\theta$ dependence in the center of mass system. These results indicate that the two colliding nuclei (^{12}C and ^{28}Si) have formed a rotating dinuclear system. This complex subsequently decays with isotropic probability $d\sigma/d\theta = \sin\theta * d\sigma/d\Omega = \text{const}$) and the kinetic energy of the emitted fragments equals the energy stored in the rotating complex and does not depend on the angle of emission in agreement with the observed behavior.

A question that comes immediately to mind is how long is long-lived? This question cannot be answered directly but it can be answered relative to certain processes. For example the isotropic angular distribution requires rotation of at least 180° (that makes "long" about 10^{-21} sec!). We know that the dinuclear complex lives long enough for some mass and charge transfer to occur as well as complete equilibration of the energy degree of freedom, i.e., complete damping of the kinetic energy in the entrance channel has occurred and most of the excitation for a given exit channel is in the heavy fragment[4] (equal temperature). One could next ask the question: "Since we do have mass and charge flow, was there enough time for these degrees of freedom to equilibrate?" Figure 2.45 points out the inadequacy of the ^{12}C + ^{28}Si system for studying this question. The ^{12}C + ^{28}Si channel is bound to dominate under any assumption — since this is the entrance channel as well as the favored exit channel. The ^{28}Si + ^{14}N system

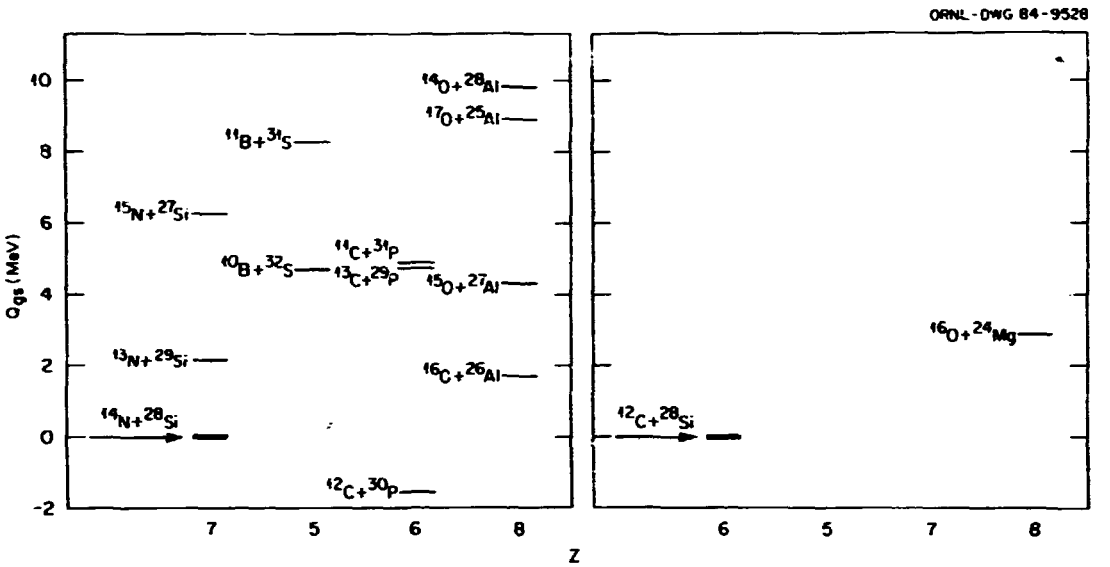

Fig. 2.45. Shifted energy level diagrams of different channels (partitions) of the $^{12}C + ^{28}Si$ (right side) and $^{14}N + ^{28}Si$ systems.

shown on the left side of Fig. 2.45 is much better suited for answering this question. While the $^{28}Si + ^{14}N$ exit channel would be favored with a fast process, the $^{12}C + ^{30}P$ channel would dominate if equilibrium emission took place. In order to bypass some of the difficulties enccuntered in backscattering experiments, all the measurements discussed here were done at forward angles, reversing the role of target and projectile. ^{12}C (or ^{14}N in the present experiment) were bombarded with energetic ^{28}Si beams and a study of the target-like nuclei, recoiling forward, was carried out. Natural nitrogen gas (99% ^{14}N) was used in the HHIRF supersonic gas jet target[5] to produce a 15 $\mu g/cm^2$ thick ^{14}N target. This target was bombarded with highly collimated (1/4 mm^2) 5 pnA 150 MeV ^{28}Si beam. The products were momentum analyzed in the spectrograph and identified (ΔE,E) in an ionization chamber. A two-dimensional energy vs. energy-loss map showing all the detected target-like products is shown in Fig. 2.46. The three other maps display focal plane position (momentum) vs. energy and show the mass and charge state distribution of the products. The projected energy spectra for products with Z = 6, 7 and 8 are shown in Fig. 2.47. These spectra are clearly dominated by ^{12}C, ^{14}N and ^{16}O (parts b, c and d of Fig. 2.46). Measurements at other angles have shown that the centroids of these energy spectra are unaltered and, as Fig. 2.48 shows, the emission probability for these products ($d\sigma/d\theta$) remains constant with angle. Therefore, these products come, in all likelihood, from the same orbiting process previously observed in $^{28}Si + ^{12}C$ and other systems.[6] The new information from these data is also obvious: a brief examination of the data in Figs. 2.46 and 2.47 shows that the dominant yield is in the $^{12}C + ^{30}P$ channel and not in the $^{14}N + ^{28}Si$ entrance-like channel.

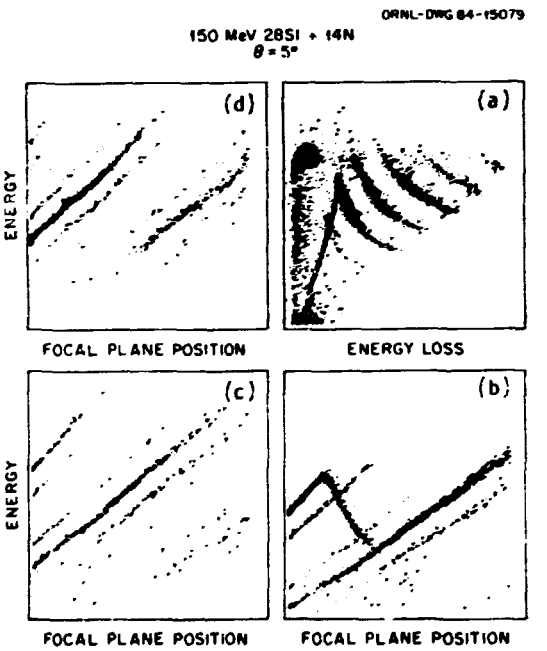

Fig. 2.46. (a) ΔE vs. E plot for target-like products reaching the counter; (b,c,d) Momentum (focal plane position) vs. energy plots for Z = 8, 7 and 6, respectively. These maps separate products according to charge state and mass.

The process therefore lasts long enough for energy, mass and charge flow to reach equilibrium. This still does not put an absolute time limit on the process but it is likely

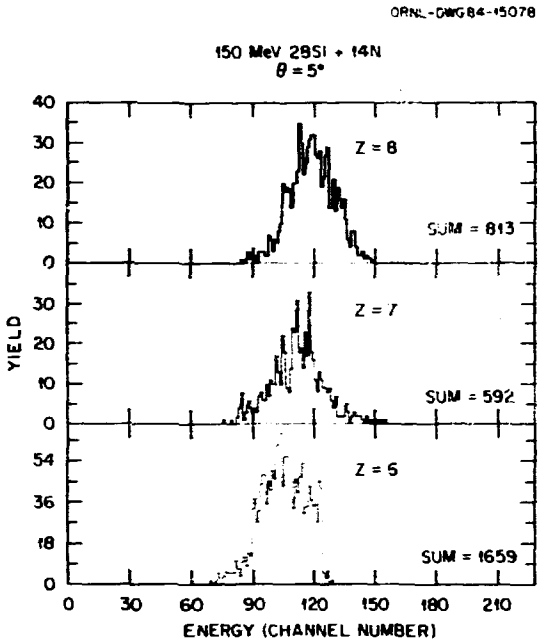

Fig. 2.47. Energy spectra for the carbon, nitrogen and oxygen ions seen in map (a) of Fig. 2.46.

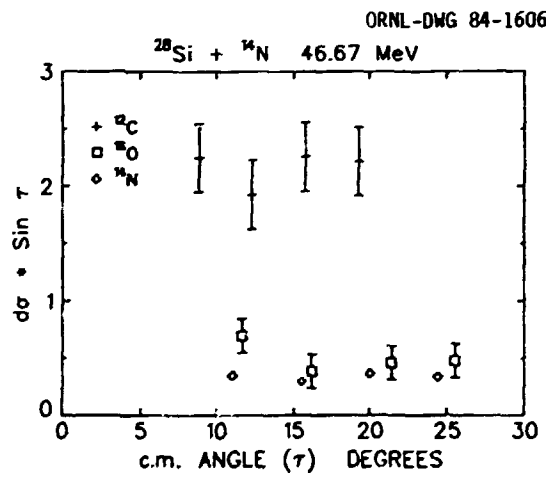

Fig. 2.48. Emission probability as a function of angle.

that more than the time needed for one rotation is involved. We are now actively engaged in calculations that assume equilibrium partitioning of the products and shall find out how these quantitative predictions compare with the observed data.

---

1. Deceased.
2. Permanent address: A. W. Wright Nuclear Structure Laboratory, Yale University, New Haven, CT 06520.
3. Physics Deparment, University of Virginia, Charlottesville, VA 22901.
4. D. Shapira et al., Phys. Lett. 114B, 111 (1982).
5. D. Shapira et al., to be published in Nucl. Instrum. Methods.
6. D. Shapira et al., to be published.

CRYSTAL BLOCKING MEASUREMENTS FOR THE ^{16}O + Ge AND ^{28}Si + Ge SYSTEMS

J. Gomez del Campo
R. Ribas[1]
D. Shapira
J. A. Biggerstaff
C. D. Moak
P. D. Miller
N. Neskovic[2]

The crystal blocking technique has been used successfully at HHIRF in the study of reaction mechanisms for the ^{16}O + ^{12}C reaction.[3,4] In this report new measurements are described for the ^{16}O + Ge and ^{28}Si + Ge reactions, that extend the technique to heavier systems.

In order to successfully utilize the crystal blocking technique to measure nuclear reaction times it is crucial to establish a zero time calibration curve. This is usually done through a careful study of the elastic scattering crystal blocking angular distribution. It is also important to have predictions of the blocking distribution which are based on theoretical calculations requiring a detailed knowledge of the properties of the crystal. All of the measurements on Ge discussed here were done along the Ge <110> axis, and the interaction potential used in the blocking distribution calculation was that of Doyle and Turner.[5] Thermal fluctuations were taken into account using an amplitude of 0.085 Å (see review of Ref. 6). Corrections due to crystal thickness and energy loss in the crystal were included in a manner similar to that used in the ^{16}O + ^{12}C study.[3] The thickness of the Ge crystal was 10 μm.

The data for the elastic scattering blocking distribution of ^{16}O on Ge <110> at 100 MeV bombarding energy are shown as crosses in Fig. 2.49(a). The detection angle was 22.5° and the rest of the experimental setup was the same as for the ^{16}O + ^{12}C study.[3] Two theoretical curves are shown in Fig. 2.49(a). The calculation shown as the light curve (σ = 0°) includes the effects of dechanneling and thermal fluctuations, but nevertheless fails to reproduce the data. Since elastic scattering is a fast process ($\tau < 10^{-21}$ sec), the discrepancy between the light curve and the data can be interpreted only as effects due to crystal imperfections which are not included in the σ = 0° curve. As discussed in Ref. 3, these effects can be evaluated by introducing a Gaussian smear (of standard deviation σ) to the theoretical distribution. A good fit to the data on Fig. 2.49(a) is obtained with σ = 0.08° (heavy curve). In order to check the consistency of these procedures, another blocking experiment was performed using a 120-MeV ^{16}O (collimated to 2 mm) from ORIC. The same Ge crystal was used and the results for the elastic scattering (circles) at θ_{lab} = 10° are shown in Fig. 2.49(b). Excellent

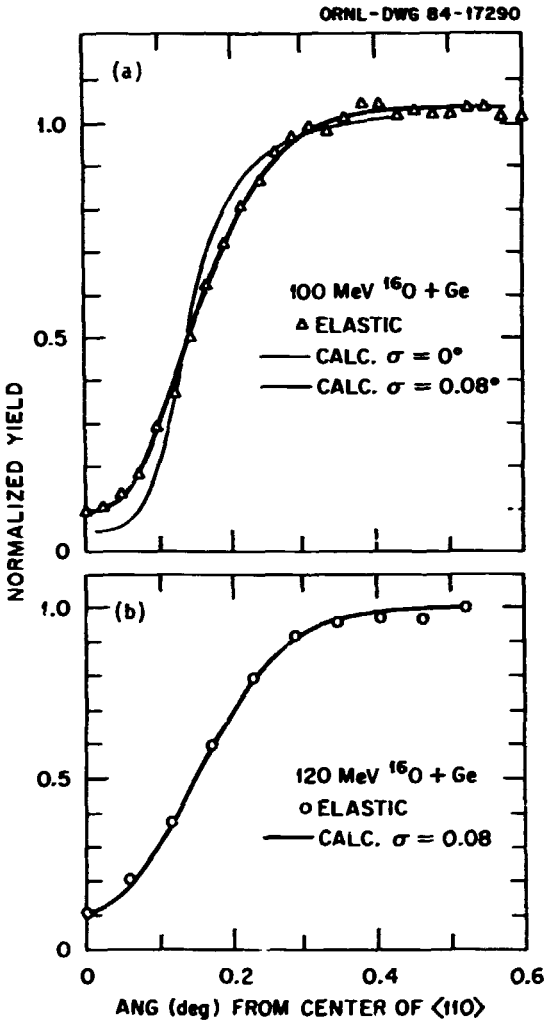

Fig. 2.49. (a) Blocking distribution for 100 MeV ^{16}O + <110> Ge. The effect of crystal imperfections is represented by σ = 0.08°. (b) Same as (a) for 120 MeV ^{16}O.

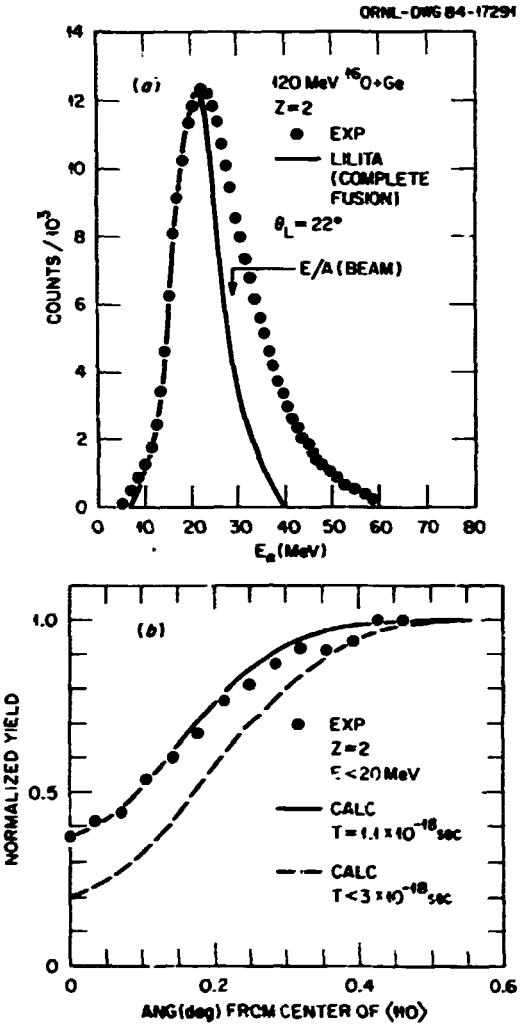

Fig. 2.50. (a) Energy spectrum (points) for the α particles emitted in the ^{16}O + Ge reaction. (b) Blocking angular distribution.

agreement with the data is obtained with a calculation using σ = 0.08°, the same value as for 100 MeV.

Products from the ^{16}O + Ge reaction were detected for Z = 9 to Z = 2 using a ΔE-E position sensitive telescope.[3] The analysis of the Z = 6 to Z = 8 reaction products is given elsewhere[4] and confirms the idea that these nuclei are produced as the result of direct (fast) processes. However, detailed analysis of the emitted alpha particles shows significant time-delay effects. Figure 2.50(a) shows an energy spectrum of the alpha particles emitted at 22° for the 120-MeV ^{16}O + Ge reaction. This spectrum was obtained with a solid state counter telescope (E = 2000 μm, ΔE = 300 μm). The solid line, normalized to the data at the maximum, is the result of a complete fusion calculation from the computer code LILITA[7] and shows that nearly 50% of the alpha particles can be accounted for by a compound nucleus process. Figure 2.50(b) shows the "blocking curve" for alpha particles below 20 MeV emitted from the ^{16}O + Ge reaction. The 20 MeV energy limit assures that most of the alpha particles are from compound nucleus emission. Under the assumption of compound nucleus emission, the recoil velocities were calculated and the extracted decay time (for multiple particle emission) was 1.1×10^{-17} sec (solid line). The dashed curve in Fig. 2.50(b) is the lower limit for the time that can be measured with the present Ge crystal for the compound emission process. The result of 1.1×10^{-17} sec agrees well with a Monte Carlo calculation of multiparticle equilibrium emission which yields 2×10^{-17} sec.

The ^{28}Si + Ge reaction was used to study de-excitation times for deep inelastic collisions (DIC). Usually for DIC reactions the only

reference to time is the reaction time (primary time) which is the time needed for formation and separation of the dinuclear complex after large amounts of energy dissipation and mass exchange have occurred. Although considerable time delays are expected for DIC, most experimental and theoretical estimates predict values $T < 10^{-20}$ sec,[8] too fast to be measured directly. Nevertheless, the blocking technique will be sensitive to the secondary time, which reflects the time delay of the particle decay process (whether in equilibrium or not) of the primary reaction fragments. It is in this regard that the blocking measurement can provide unique information for the DIC process. Coincidence experiments between the emitted light particles and fragments have been carried out in the past to study the equilibration effects of energy and mass transfer, but this is the first experiment in which a direct measurement of the secondary time is attempted.

The ^{28}Si + Ge reaction was studied by bombarding the same Ge crystal used previously with a ^{28}Si beam of 220 MeV extracted from the HHIRF tandem. The detector was placed at an angle of 16.2°, and energy spectra and blocking angular distributions were measured for nuclear reaction fragments of Z = 16 to Z = 6. The analysis of the energy spectra show large energy dissipation (Q = -70 to -100 MeV) which is typical for DIC reactions in this mass region. We also observe a small quasi-elastic component for Z = 12 and Z = 13 fragments. The results for the blocking angular distributions are shown on Fig. 2.51 for some of the DIC fragments. The theoretical fits (solid lines) were calculated using the value $\sigma = 0.08°$ (see Fig. 2.49) and a value for the recoil distance D(Å) was indicated for each case. The fact that $D \neq 0$ for all cases given in Fig. 2.51 indicates that sizable time-delay effects are present in the DIC reaction. In order to extract the de-excitation time, δ, ($\delta = D/v_R \cdot \ln\theta_{lab}$) the recoil velocities V_R have to be determined. There are two values of V_R possible for a DIC reaction, depending on whether the time delay responsible for the observed displacement, D, takes place during the collision (primary time) or is due to the decay of the fully accelerated fragments (secondary time). For the first case $V_R = V_{c.m.}$ and the extracted times will be $\sim 10^{-17}$ sec, too long to be consistent with previous experimental observations. The second assumption, commonly used in the analysis of fragment-particle correlation data, is that the fragments decay after scission, in which case the recoil velocities are those of the primary fragments (about 0.1c for the present experiment). These velocities have been determined by a Monte Carlo calculation in a way similar to that of Ref. 9, and the resulting δ values are given in Fig. 2.52(a). On Fig. 2.52(b) we show the differential cross sections (points) measured at 16.2° and the result (histogram) of the Monte Carlo simulation (the primary distribution is a Gaussian centered at Z = 14 and $\sigma^2 = 2$). The main conclusion to

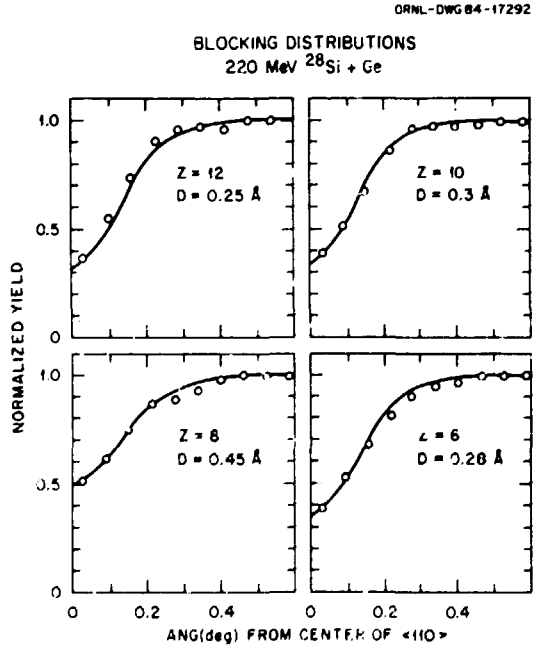

Fig. 2.51. Blocking angular distribution for DIC fragments resulting from 220 ^{28}Si + Ge. The Ge crystal is the same as for the data on Figs. 1 and 2.

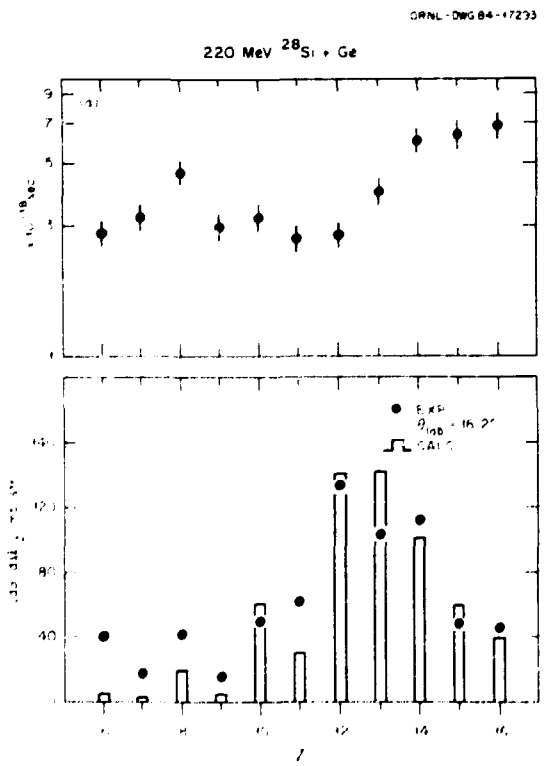

Fig. 2.52. (a) Results of the deexcitation time δ for DIC fragments. (b) Measured and predicted cross sections for DIC of ^{28}Si + Ge.

be drawn from Fig. 2.52 is that for all Z fragments the time delay is large and this result can be interpreted only as due to a multiparticle evaporation process similar to the one observed for the evaporation residues of $^{16}O + ^{12}C$ (Ref. 3). Of course the data of Fig. 2.52 needs a good theoretical calculation that could explain both the δ_Z and $(d\sigma/d\Omega)_Z$ distributions. Further analysis of these effects are in progress.

1. On leave from Instituto de Fisica University of Sao Paulo, Brazil.
2. On leave from Boris Kidric Institute, Belgrade, Yugoslavia.
3. J. Gomez del Campo et al., Phys. Rev. Lett. 51, 401 (1983).
4. J. Gomez del Campo et al., Notas de Fisica, Vol. 6, No. 1, 115 (1983), Proceedings of the 6th Oaxtepec Symposium on Nuclear Physics.
5. P. A. Doyle and P. S. Turner, Acta Crystallogr., Sec. A24, 390 (1968).
6. D. S. Gemmell, Rev. Mod. Phys. 46, 129 (1974).
7. J. Gomez del Campo and R. G. Stokstad, ORNL Report TM-7295 (1981).
8. R. A. Dayras et al., Phys. Rev. C 22, 1485 (1980).
9. J. Gomez del Campo, Proc. Symposium on Heavy-Ion Physics, edited by J. Barrette and P. D. Bound, BNL-51115, 93 (1979).

REMOVING SURFACE ABSORPTION FROM THE OPTICAL MODEL: CCA FITS TO $^{60}Ni + ^{60}Ni$ ELASTIC AND INELASTIC DATA

K. A. Erb M. J. Rhoades-Brown[1]

The imaginary component (W) of the optical potential is intended to account, in an average way, for the absorption of flux into channels that are not treated explicitly in a given model calculation. Conceptually, the short-range portion of W corresponds to compound nucleus formation, while the longer-range pieces reflect reactions that are localized in the nuclear surface. It has long been hoped that in a sufficiently complete model calculation, which treated all the important direct reaction channels explicitly, the need for optical model surface absorption could be eliminated. If such a situation could be realized, without sacrificing quantitative reproduction of the measured yields, a major source of ambiguity would be removed. Then, models for the real part of the optical potential, for transition densities, and for direct reactions in general, could be tested cleanly.

We have noted previously[2] that our measurements of yields from $^{60}Ni + ^{60}Ni$ and $^{60}Ni + ^{56}Fe$ interactions determined that the 2^+-inelastic cross sections nearly exhaust the total reaction cross section. We argued[3] that the coupling evidenced by these magnitudes implies the existence of strong non-local effects which are difficult to mimic in standard one-channel models, and which thus could account for the failure of simple penetrability calculations to reproduce the Ni + Ni fusion data.[4] Rhoades-Brown and Braun-Munzinger subsequently reported a coupled-channel calculation[5] that used a short-range imaginary plus standard real potential, with explicit 2^+ and 3^- inelastic coupling to achieve improved agreement with a portion of the fusion data. Such a calculation of fusion, although conceptually appealing, makes sense only if fits to elastic and inelastic yields can be achieved simultaneously.

We have recently succeeded in fitting our $^{60}Ni + ^{60}Ni$ elastic and inelastic data reasonably well using an optical potential with W=0 in the surface region. The results are shown in Fig. 2.53. The coupled-channels program, Ptolemy, was used, with measured B(E2) and B(E3) values and a standard real potential. The scattering calculation was insensitive to the details of W in the interior region. This work raises the possibility of fitting quasielastic and fusion data simultaneously.

1. Present address: SUNY at Stony Brook, NY.

2. K. A. Erb, in Resonances in Heavy Ion Reactions (Springer-Verlag, 1982), p. 204.

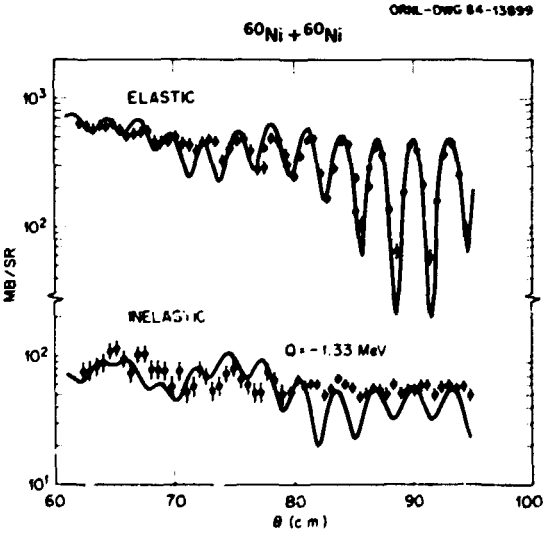

Fig. 2.53. Measured and calculated (CCA, Ptolemy) elastic and inelastic yields for $^{60}Ni + ^{60}Ni$ collisions of E(lab) = 228 MeV. The lowest 2^+ and 3^- levels of ^{60}Ni were coupled with measured B(Eλ) values. The real potential was a Woods-Saxon with V = 73 MeV, r_0 = 1.177 fm, a = 0.67 fm, while the imaginary potential was a Woods-Saxon squared with parameters W = 10 MeV, r_0' = 1.0 fm, a' = 0.4 fm.

3. Physics Division Progress Report for Period Ending September 30, 1983, ORNL-6004 (1983), p. 42.
4. M. Beckerman, et al., Phys. Rev. Lett. 45, 1472 (1980).
5. M. J. Rhoades-Brown and P. Braun-Munzinger, Phys. Rev. Lett. 136B, 19 (1984).

FUSION CROSS SECTIONS FOR BEAMS OF ^{46,50}Ti ON TARGETS ^{90}Zr AND ^{93}Nb

P. H. Stelson M. Beckerman[1]
H. J. Kim D. Shapira
R. L. Robinson

The ^{50}Ti nucleus has a closed neutron shell of 28, and as a result, its first 2^+ state has an energy of 1.55 MeV and β_2 = 0.173. On the other hand, ^{46}Ti (four neutron holes away from n = 28) has a 2^+ state at 0.89 MeV and a β_2 = 0.314. Theoretical estimates[2,3] of subbarrier fusion cross sections based on the couplings to inelastic channels suggest a factor of 20 difference in subbarrier fusion cross sections when beams of ^{46}Ti and ^{50}Ti are incident on targets such as ^{90}Zr or ^{93}Nb. We used the velocity filter to measure these cross sections. The analysis of the data has not yet been completed. Preliminary analysis confirms the theoretical prediction. At energies well below the barrier ($E_B - E_{CM}$ = 12 MeV), the ratio of the fusion cross sections, ^{46}Ti + ^{93}Nb/^{50}Ti + ^{93}Nb, is approximately a factor of 30.

---

1. Guest scientist from Massachusetts Institute of Technology, Cambridge, Massachusetts.
2. C. H. Dasso, S. Landowne, and A. Winther, Nucl. Phys. A405, 837 (1983).
3. R. A. Broglia et al., Phys. Lett. 133B, 34 (1983).

INELASTIC SCATTERING OF ^{28}Si ON ^{208}Pb

D. C. Hensley F. E. Bertrand
J. R. Beene M. L. Halbert
G. Vourvopoulos[1]

Heavy ion inelastic scattering has been shown to be a useful tool in providing collective nuclear structure properties.[2,3] Analyses using the coupled-channel rotational model formalism can provide information on deformation parameters β_2 and β_4, static quadrupole moments of 2^+ states, triaxial shape parameters, and the relative phases of matrix elements.

Previous heavy ion studies based their results on the analysis of elastic scattering data and data for the excitation of the first 2^+ collective state. It has been shown in the scattering of ^{20}Ne[2] and ^{28}Si,[4] however, that the 2^+ angular distribution in the region of the grazing angle is very sensitive to the addition of β_4 deformation. Furthermore, for the case of ^{28}Si it was found that a range of values for the hexadecapole deformation parameter β_4 gave excellent fits to both the elastic and 2^+ inelastic angular distributions. From an experimental point of view, due to the existence of overlapping groups of states in the vicinity of the excitation of the 4^+ state, it has not been possible to extract reliable values for the 4^+ cross section for the cases studied.

During a short run with the HHIRF Tandem in July 1984, we were able to demonstrate that this difficulty can be overcome if the Spin Spectrometer is operated in coincidence with position-sensitive charged particle detectors. In studying the reaction ^{208}Pb(^{28}Si,^{28}Si*), we identified the ^{28}Si 4^+ state by its gamma-ray cascade $4^+ \rightarrow 2^+ \rightarrow 0^+$. At the same time, the gamma-ray angular correlations for both the 2^+ and 4^+ states were measured. Preliminary analysis of the data indicates that we will be able to map out the angular distribution for the 4^+ state within one or two shifts of beam time without requiring excessive rates in either the Spin Spectrometer detectors or in the position sensitive detectors. Because several reaction channels have larger cross sections than does the inelastic scattering to the 4^+ state, we found that charged particle resolution on the order of 0.5 MeV, in addition to the resolution of the Spin Spectrometer, will be required to separate unambiguously the various reactions.

---

1. Western Kentucky University, Bowling Green, KY 42101.
2. E. E. Gross et al., Phys Rev. C 17, 1665 (1978).
3. E. E. Gross et al., Nucl. Phys. A401, 362 (1983).
4. J. J. Kolata et al., Phys. Rev. C 30, 125 (1984).

MASSES OF ^{77}Kr AND ^{75}Kr

D. M. Moltz[1] R. E. Tribble[2]
K. S. Toth C. A. Gagliardi[2]
J. P. Sullivan[2] F. T. Avignone, III[1]

Direct mass measurements[3] have recently been made for most of the known rubidium isotopes. To supplement and complement these data, we have been involved in a systematic program to determine masses of extremely neutron-deficient rubidium and krypton nuclides via β-endpoint measurements[4] and transfer reactions[5] induced by light ions. Herein we report our latest work, i.e., the determination of the ^{77}Kr and ^{75}Kr masses by means of the ^{80}Kr(^{3}He,^{6}He) and ^{78}Kr(^{3}He,^{6}He) reactions, respectively.

Helium-3 particles from the Texas A&M University 224-cm cyclotron were allowed to impinge upon an isotopically enriched gas target statically pressurized in a cell to ~ 50 Torr. Reaction products were detected at the focal plane of an Enge split-pole spectrograph with a single-wire proportional ΔE counter and a 1.0 cm x 5.0 cm x 600 μm silicon surface barrier E

detector. Particle time-of-flight information was also obtained relative to the cyclotron rf signal.

A 70-MeV bombarding energy and a scattering angle of θ_L = 7.25° were chosen by comparison with prior[6] (^{3}He,^{6}He) studies. The spectrograph was calibrated by $^6He^{2+}$ particles from the $^{18}O(^3He,^6He)^{15}O$ reaction. The existence of two prominent ^{15}O excited states at approximately the same Q-value as predicted for the ground state of ^{75}Kr made this an ideal calibrant. After calibration, successive enriched isotope samples of ^{82}Kr, ^{80}Kr, and ^{78}Kr were introduced into the gas cell and bombarded by 21.8, 30.0, and 34.0 mC of $^3He^{2+}$ beam, respectively. The $^{82}Kr(^3He,^6He)$ reaction was used to measure the mass excess of ^{79}Kr, a nucleus whose mass is known[7] to 8.6 keV, to demonstrate the validity of both our experimental technique and data analysis procedure.

Table 2.11 summarizes our mass excesses and compares them with values found in the compilation of Wapstra and Bos.[7] One sees that the two values for ^{79}Kr are in excellent agreement. The ^{75}Kr mass was previously unknown (the literature value given in Table 2.11 is deduced from systematics). There is a discrepancy between our ^{77}Kr mass and the adopted number based[7] on the precise ^{77}Br mass and the β-decay energy of ^{77}Kr (Ref. 8). It would appear that the β-decay scheme of ^{77}Kr is not well understood.

We are also in the process of completing the analysis of the ^{75}Rb positron endpoint spectrum. With the newly determined ^{75}Kr mass this endpoint will provide us with the ^{75}Rb mass. Overall then, our investigation will have yielded masses for $^{75,76,77}Rb$ and $^{74,75,76,77}Kr$. We plan to compare these measurements with mass formula predictions.

---

1. University of South Carolina, Columbia, SC.
2. Texas A&M University, College Station, TX.
3. M. Epherre et al., Phys. Rev. C19, 1504 (1979); G. Audi et al., Nucl. Phys. A378, 443 (1982).
4. D. M. Moltz, K. S. Toth, F. T. Avignone, III, H. Noma, B. G. Ritchie and B. D. Kern, Phys. Lett. 113B, 16 (1982).
5. D. M. Moltz, K. S. Toth, R. E. Tribble, R. E. Neese and J. P. Sullivan, Phys. Rev. C26, 1914 (1982).
6. R. C. Pardo et al., Phys. Rev. C18, 1249 (1978).
7. A. H. Wapstra and K. Bos, At. Data Nucl. Data Tables 19 175 (1977).
8. S. Thulin, Ark. Fysik 9, 137 (1955).

DELAYED PROTON DECAY OF ^{145}Dy AND OF THE NEW ISOTOPE ^{151}Yb

K. S. Toth
F. T. Avignone[1]
D. M. Moltz[2]
R. S. Moore[1]

We recently completed a study[3] of the β-delayed proton spectra of ^{147}Dy and the hitherto unknown isotope ^{149}Er. The purpose was twofold: (1) to provide decay energy data for comparison with the predictions of available mass formulae, and, (2) to identify ^{149}Er so that its β-decay properties could be studied in detail to obtain information concerning the single-neutron and single-proton levels in ^{149}Er (N = 81) and ^{149}Ho (N = 82), respectively.

The investigation has now been expanded to include a search for the delayed-proton branch of ^{145}Dy and an attempt to identify ^{151}Yb the next N = 81, even-Z, isotone above ^{149}Er. As before, thin targets were bombarded with heavy ions accelerated in the Lawrence Berkeley Laboratory 88-inch cyclotron. A helium gas-jet apparatus was used to transport radioactive products to a shielded area and assayed with a Si-particle telescope and a Ge detector. The telescope, consisting of a 20-μm ΔE detector combined with a 300-μm E detector, was necesary for the selective detection of low-energy protons in the presence of intense β radiation and a profusion of α particles emitted in the decay of nearby nuclides. The Ge detector was of the γ-x variety, suitable for detecting both low- and high-energy photons. Events registered in each detector were tagged with a time signal for half-life information.

In a series of ^{12}C + ^{142}Nd bombardments (from 135 to 195 MeV) we looked for delayed protons from the β decay of ^{145}Dy, an isotope whose half-life has been reported to be 18 ± 3 sec (Ref. 4) and 13.6 ± 1.0 sec (Ref. 5). Yields

Table 2.11. Summary of mass measurements (all values are in MeV)

	^{79}Kr	^{77}Kr	^{75}Kr
Reaction Q-value	-8.977	-10.646	-12.970
Mass Excess	-74.441(31)	-70.155(25)	-64.231(16)
Literature (Ref. 7)	-74.4389(86)	-70.231(30)	-64.162(SYST)

were measured for γ rays belonging to ^{146}Dy, ^{146}Tb, ^{145}Dy, ^{145}Tb, and ^{144}Tb. An energy of ~188 MeV was then selected to emphasize the ^{142}Nd (^{12}C,9n) reaction. Figure 2.54 shows the accumulated proton spectrum. We assign these β-delayed protons to ^{145}Dy on the basis of excitation function data and on the fact that they decayed with a (15 ± 4)-sec half-life. High-energy endpoints of delayed-proton spectra are fixed by differences between the electron-capture (EC) decay energies of the parents and the proton binding energies in the corresponding EC daughters. The predicted $Q_{EC} - B_p$ value from the 1977 Atomic Mass Evaluation[6] for ^{145}Dy is 5.70 MeV. (Note the EC decay energy for ^{145}Dy is not given in Ref. 6; based on decay energies for nearby isotopes we estimated it to be 7.24 MeV.) This prediction is consistent with our data (Fig. 2.54).

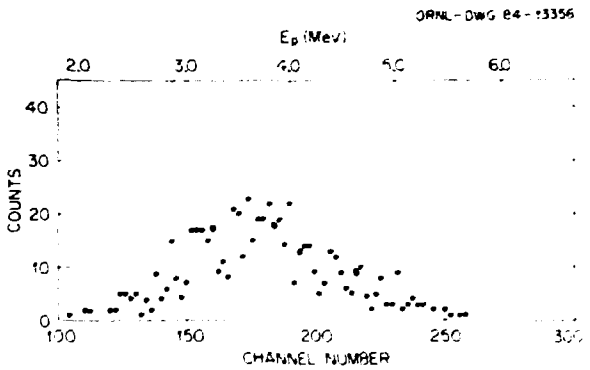

Fig. 2.54. Delayed-proton spectrum observed in 188-MeV ^{12}C bombardments of ^{142}Nd; it is assigned to the β-decay of ^{145}Dy.

In the attempt to identify ^{151}Yb, proton and γ-ray spectra were investigated in ^{160} + ^{144}Sm irradiations. Yields as a function of incident energy for γ rays known to follow the β decays of ^{152}Yb, ^{152}Tm, and ^{151}Tm were used to select the peak of the (^{160},9n) excitation function. Preliminary analyses indicate the existence of a delayed-proton emitter with a half-life of ~0.5 sec which we tentatively assign to the new isotope ^{151}Yb.

---

1. University of South Carolina, Columbia, SC.
2. Lawrence Berkeley Laboratory, Berkeley, CA.
3. K. S. Toth et al., Phys. Rev. C30, 712 (1984).
4. G. D. Alkhazov et al., Z. Phys. A305, 185 (1982).
5. E. Nolte et al., Z. Phys. A306, 223 (1982).
6. A. H. Wapstra and K. Bos, At. Data Nucl. Data Tables 19, 175 (1977).

SINGLE-NEUTRON AND SINGLE-PROTON STATES IN ^{149}Er AND ^{149}Ho

K. S. Toth
Y. A. Ellis-Akovali
R. S. Moore[1]
D. M. Moltz[1]
R. L. Mlekodaj[2]
D. C. Sousa[3]

The investigation of levels in nuclei with single particles (or holes) plus closed-shell configurations is of considerable interest since it provides data for comparison with calculations based on Hartree-Fock and independent-particle models. These models have sets of phenomenological parameters which can be improved by being fit to experimental results. The goal is to arrive at a universal description of single-particle properties throughout the periodic table.

We have been involved in studying decay properties of short-lived, proton-rich isotopes near the 82-neutron shell to obtain structure information for even-Z nuclei with N = 81 and N = 83, and, for odd-Z nuclei with N = 82. Of relevance to the present investigation was our study of ^{147}Dy^{m} and ^{147}Dy^{g} decays wherein we identified the $s_{1/2}$, $d_{3/2}$, and $h_{11/2}$ neutron states in ^{147}Dy,[4] and, the $s_{1/2}$, $d_{3/2}$, $d_{5/2}$, and $g_{7/2}$ proton states in ^{147}Tb.[5] The immediate interest was to extend these single-particle level systematics to ^{149}Er and ^{149}Ho and a search was begun for the unknown nuclide ^{149}Er. In a series of ^{12}C + ^{144}Sm bombardments we identified[6] ^{149}Er via its β-delayed-proton activity to be a (9 ± 1)-sec isotope. With this half-life information in hand we now have investigated its β-decay properties.

As in the earlier study,[6] ^{149}Er was produced in the ^{144}Sm (^{12}C, 7n) reaction. Irradiations were made with 135-MeV ^{12}C ions from the Holifield Heavy Ion Research Facility tandem accelerator. The target was a 2.1-mg/cm^2 thick samarium metal foil enriched in ^{144}Sm to 96.5%. A helium gas-jet apparatus thermalized products recoiling out of the target and transported them to a counting station for assay with γ- and x-ray detectors. Singles and coincidence data were taken simultaneously.

Transitions were assigned to ^{149}Er decay on the basis of measured half-lives, γ-ray coincidence relationships, and energies of K X rays observed in coincidence with the γ rays. The ^{149}Er^{m} and ^{149}Er^{g} decay schemes were found to be similar to those of ^{147}Dy^{m} and ^{147}Dy^{g} (see Refs. 4 and 5). A cascade of three transitions (171.2, 343.9, and 435.9 keV) is assigned to follow ^{149}Er β decay; they depopulate and connect the following single-proton states in ^{149}Ho: $g_{7/2}$ → $d_{5/2}$ → $d_{3/2}$ → $s_{1/2}$. Two γ rays (111.0 and 630.5 keV) in coincidence with one another are ascribed to ^{149}Er^{m}; this isomeric deexcitation connects the $h_{11/2}$, $d_{3/2}$, and $s_{1/2}$ single-neutron levels in ^{149}Er.

The order of the single-proton states in ^{147}Tb and in ^{149}Ho is very different from those in odd-Z N = 82 nuclei with Z < 63 where the $g_{7/2}$ and $d_{5/2}$ orbitals are below the $s_{1/2}$, $d_{3/2}$ and $h_{11/2}$ states. One must remember, however, that the $g_{7/2}$ orbital is a hole state for Z > 59 and

that the $d_{5/2}$ orbital becomes a hole state in ^{147}Tb. With this in mind, we show in Fig. 2.55 the proton level systematics for N = 82 isotones. Hole states are indicated as having negative energies with the ^{147}Tb and ^{149}Ho $s_{1/2}$ orbitals shown as being close to the $h_{11/2}$ ground states. One then sees that the ^{147}Tb and ^{149}Ho levels are not discontinuous with respect to the energies of the same orbitals in the lower-Z isotones. We noted in Ref. 5 that the two hole states appeared to be more tightly bound in ^{147}Tb. Now that the investigation has been extended to ^{149}Ho, the extra binding in ^{147}Tb does seem to exist due to the influence of the Z = 64 subshell on the quasiparticle energies.

Excitation energies of the $h_{11/2}$, $d_{3/2}$, and $s_{1/2}$ neutron states in N = 81 isotones are shown in Fig. 2.56. One sees that the ^{149}Er level data fit the systematics for the nuclei with lower atomic numbers. Overall our results for ^{147}Dy and ^{149}Er clearly establish the trend predicted by Silverberg.[7] His calculations showed that the $h_{11/2}$ - $d_{3/2}$ splitting with increasing Z would first increase, reach a maximum at around ^{139}Ce, and then begin to decrease. Included in Fig. 2.56 are the M4 transition rates, expressed in Weisskopf units, where the isomeric decay branchings are known. We utilized the constancy of these transition rates for Z > 58 (also predicted in Ref. 7) and estimated the isomeric branch for ^{149}Er^{m} to be 2.7%. Note that while $h_{11/2}$ level in ^{131}Sn has been located[8] the M4 transition has not been observed. By using an extrapolated Weisskopf factor of 7.5 units we calculated the isomeric decay branch to be 0.057%, or only 0.0087% for the unobserved 241.8-keV photon.

We plan to extend this investigation to levels in ^{151}Yb and ^{151}Tm. Preliminary data[9] from delayed proton studies indicate that ^{151}Yb has a half-life of ≈ 0.5 sec.

1. University of South Carolina, Columbia, SC.
2. UNISOR, Oak Ridge, Tennessee.
3. Eastern Kentucky University, Richmond, KY.

4. K. S. Toth, et al., Phys. Letters 56B, 29 (1975).
5. K. S. Toth, et al., Phys. Rev. C25, 667 (1982).
6. K. S. Toth, et al., Phys. Rev. C30, 712 (1984).
7. L. Silverberg, Nucl. Phys. 60, 483 (1964).
8. B. Fogelberg and J. Blomquist, Phys. Lett. 137B, 20 (1984).
9. K. S. Toth, et al., contribution submitted to the 7th International Conference on Atomic Masses and Fundamental Constants, Darmstadt, West Germany, September 3-7, 1984; to be published in conference proceedings.

INITIAL RESULTS WITH THE USE OF THE UNISOR GAS-JET ION SOURCE; ELECTRON-CAPTURE DECAY PROPERTIES OF ^{154}Tm

K. S. Toth, D. M. Moltz[1], R. L. Mlekodaj[2], H. K. Carter[2], E. H. Spejewski[2], C. R. Bingham[3]

The first on-line test of the coupled helium-jet UNISOR separator system was done. Overall, the progress that had been accomplished was very encouraging. There was no problem with the high-voltage transition through the pumping line. The ion-source filament operated throughout the testing without failure. Targets withstood ~ 150 pnA of ^{16}O beam and the four-position target wheel made changing targets a

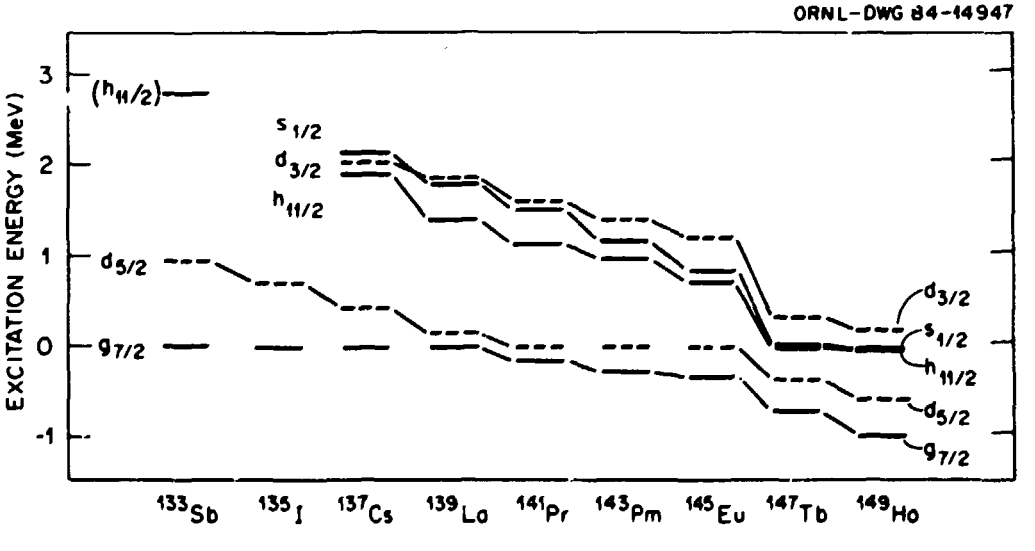

Fig. 2.55. Energy systematics of single-proton states in N = 82, odd-Z isotones. Hole states are indicated as having negative energies.

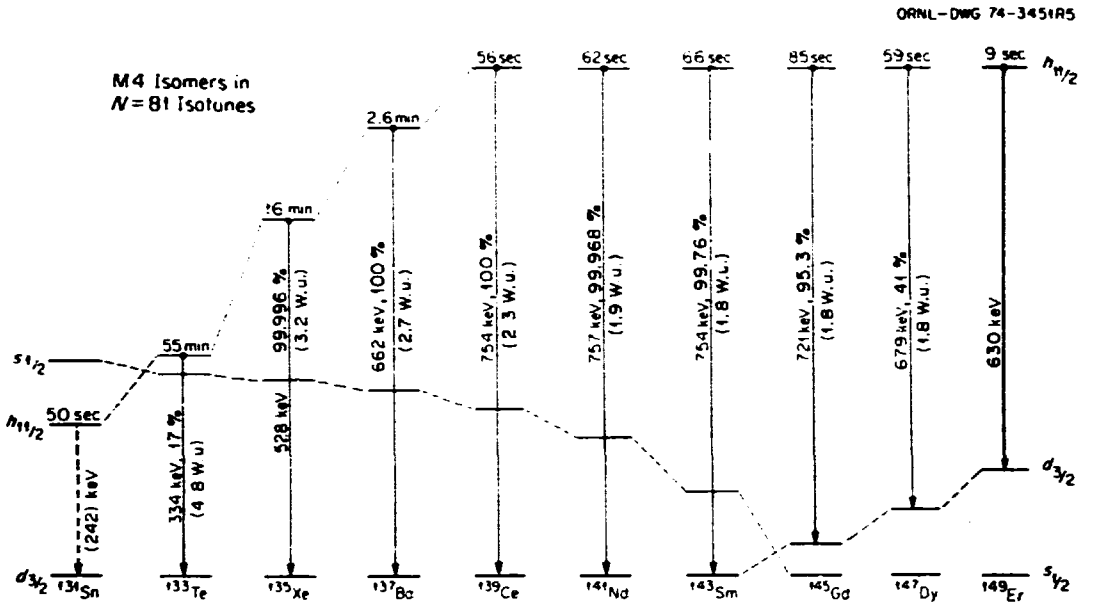

Fig. 2.56. Energy systematics of single-neutron states in N=81, even-Z isotones. Included are the rates, expressed in Weisskopf units, for the M4 transitions connecting the $h_{11/2}$ and $d_{3/2}$ levels.

trivial operation. One major problem encountered was poor mass resolution which caused significant cross-contamination in the separator beams. This was almost certainly due to a combination of the ac heating of the filament and to the large output current (mostly helium) of the ion source. A ripple, and sometimes a serious overload, in the separator high-voltage supply resulted. The test run involved ^{16}O bombardments of ^{92}Mo, ^{nat}Ag, ^{142}Nd, and ^{144}Sm. Based on estimated production cross sections, the total efficiencies were in the range of 0.01-0.04% for non-alkali metals and ~ 4% for cesium. There was no dependence of the yield on half-life down to 400 msec.

The hollow-cathode ion source was modified to operate with a dc filament so as to remove the ripple on the separator power supply. This modification was tested in an experiment in which ^{144}Sm was bombarded with ^{16}O ions to search for the β-decay branches of the well-known α emitters, ^{154}Yb ($T_{1/2}$ = 400 msec) and ^{154}Tm ($T_{1/2}$ = 3.4 sec). The change made the helium-jet system much more manageable. The separator beam stability during this run was exceptional. Gamma rays from ^{154}Yb β decay were not observed; the isotope's α/total branching ratio must therefore be close to unity. The $8^+ \rightarrow 6^+ \rightarrow 4^+ \rightarrow 2^+ \rightarrow 0^+$ transitions in ^{154}Er, the ^{154}Tm β-decay daughter were seen, however. ^{154}Tm β-decay scheme is being put together, following which the nuclide's α/total branch will be determined.

These initial on-line tests indicate: (1) The efficiencies are about a factor of three lower than had been expected. (2) Improvements to the system should first focus on the ion source. (3) The ion source hold-up time is substantially less than those of the standard UNISOR ion sources and experiments involving isotopes with half-lives much less than a second can now be done.

---

1. University of South Carolina, Columbia, SC.
2. UNISOR, Oak Ridge Associated Universities.
3. University of Tennessee, Knoxville, TN.

EVIDENCE FROM α DECAY THAT Z = 82 IS NOT MAGIC FOR LIGHT LEAD ISOTOPES[1]

K. S. Toth
Y. A. Ellis-Akovali
C. R. Bingham[2]
D. M. Moltz[3]
H. K. Carter[4]
R. L. Mlekodaj[4]
E. H. Spejewski[4]
D. C. Sousa[5]

Alpha-decay transitions between ground states of doubly-even nuclei are taken to represent unhindered decays. Reduced widths for these s-wave transitions behave in a regular fashion as a function of both neutron and atomic number. They are largest for nuclei two or four particles beyond a closed shell (with sharp minima at the shell) and they then decrease as the next closure is approached. The s-wave widths for ^{186}Pb, ^{188}Pb, ^{190}Pb, and ^{192}Pb, however, have been reported[6] to behave anomalously, i.e., they purportedly increase by a factor of 30 between

^{186}Pb (N = 104) and ^{192}Pb (N = 110) instead of decreasing as one nears N = 126.

The [electron-capture (EC) + β^+] strengths were deduced in Ref. 6 from K x-ray intensities. A number of corrections are involved in such determinations. We undertook the investigation of the (EC+β^+) decay schemes of these neutron-deficient lead isotopes, in conjunction with studies of their α-decay properties, to obtain more reliable α-branching ratios. Results for ^{192}Pb, ^{190}Pb, and ^{188}Pb have been summarized[7] earlier.

More recently we produced ^{186}Pb in the ^{160}Dy(^{32}S,6n) reaction by bombarding a (2.92-mg/cm^2-thick) dysprosium metal foil enriched in ^{160}Dy to 78.9% with 200-MeV ^{32}S ions from the Holifield Heavy Ion Research Facility tandem accelerator. Reaction products were mass-separated with the UNISOR on-line isotope separator. Our γ-ray and α-particle data yield a ^{186}Pb α branching of 100%, a value which is much larger than the 4.8% branch used by Hornshoj et al.[6] in their analysis of α widths.

In considering α-decay rates we consider them within the theoretical formalism developed by Rasmussen[8] wherein decay probabilities are represented by a reduced width, δ^2. Decay energies, half-lives, and α branches are needed to compute the reduced widths. In comparing these quantities for ^{186,188,190,192}Pb as obtained in our current investigations with earlier data, large discrepancies were found, not only for the ^{186}Pb branching ratio, but for the ^{188}Pb and ^{190}Pb α branches as well. As a result, the corresponding widths are increased by factors of 32, 7, and 4.5. Our width for ^{192}Pb, on the other hand, is less than the value based on the earlier data because the nuclide's half-life is 3.5 min, rather than 2.3 min used in Ref. 6.

Figure 2.57 shows s-wave reduced widths for nuclei with Z from 78 to 100 plotted as a function of N. One sees the regularity of the reduced widths as a function of neutron number with the extremely sharp break at N = 126. This discontinuity has been shown to be a shell structure effect. A less pronounced minimum is seen at the subshell closure at N = 152. The lead anomaly[6] is indicated by the dashed line which connects the ^{186,188,190,192}Pb widths calculated from earlier data. The widths for ^{186,188,190,192}Pb, computed from our data are shown by the open points. It is clear that they have a dependence on N which is similar to that observed for other elements. However, these new data indicate neutron deficient lead isotopes to be less hindered toward α decay than mercury isotopes, contrary to the expectation of a shell effect at Z = 82.

Our results seem to be related to the disappearance of the Z = 82 gap in the vicinity of N = 114 which has been predicted[9] on the basis of Hartree-Fock-Bogoliubov calculations of proton single-particle energies, and, to the existence of varying shapes in mercury and platinum isotopes in this mass region. In ^{182,184,186,188}Hg it has been shown[10] that well-deformed prolate bands cross the slightly oblate ($\epsilon \sim 0.1$) ground-state bands. Platinum nuclei with A < 190, on the other hand, are believed[11] to be prolate in their ground states. If one supposes that ^{186,188,190,192}Pb also have slightly oblate ground states then α transitions from oblate mercury to prolate platinum isotopes would be expected to be hindered whereas lead α decays, which do not involve shape changes between the parent and daughter nuclei, would not be. (Low-lying 0^+ excited states in ^{192,194,196,198}Pb have been described[12] by oblate two-particle, two-hole configurations; their ground states, however, have been assumed to be spherical.) Further detailed calculations of α-decay rates incorporating shape changes are needed. If such theoretical results do indeed agree with our experimental observations, then the study of α-decay rates may prove to be a useful tool to deduce information concerning nuclear shapes.

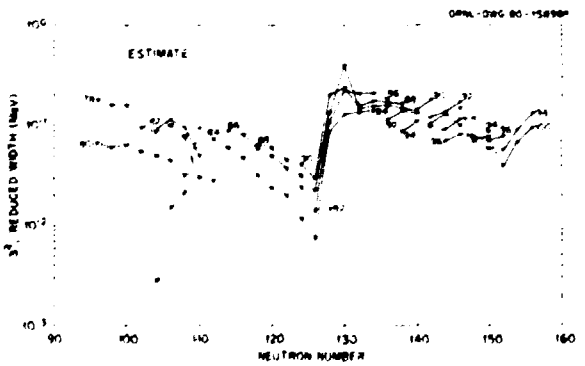

Fig. 2.57. Reduced widths for s-wave α transactions plotted as a function of N for isotopes with Z from 78 to 100. The dashed line connects widths for ^{186,188,190,192}Pb calculated from earlier data. Open points for Z = 82, connected by the full line, as widths for ^{186,188,190,192}Pb calculated from our experimental results.

---

1. Summary of a paper: Phys. Rev. Lett. 53, 1623 (1984).
2. University of Tennessee, Knoxville, TN.
3. University of South Carolina, Columbia, SC.
4. UNISOR, Oak Ridge, TN.
5. Eastern Kentucky University, Richmond, KY.
6. P. Hornshoj et al., Nucl. Phys. A230, 365 (1974).
7. K. S. Toth et al., Proc. of the 4th International Conference of Nuclei Far From Stability, Helsingor, Denmark, 7-13 June 1981, p. 174, CERN Report 81-09 (July 1981).
8. J. O. Rasmussen, Phys. Rev. 113, 1593 (1959).
9. R. A. Sorensen, p. 498 in Proceedings 4th International Conference on Nuclei Far From Stability, CERN 81-09 (1981); Nucl. Phys. A420, 221 (1984).
10. R. V. F. Janssens et al., Phys. Lett. 131B, 35 (1983); W. C. Ma et al., Phys. Lett. 139B, 276 (1984), and references therein.

11. M. Finger et al., Nucl. Phys. A188, 369 (1972); F. R. May et al., Phys. Lett. 68B, 113 (1977); J. Sauvage-Letessier et al., Nucl. Phys. A370, 231 (1981); B. Nerlo-Pomorska, Z. Phys. A293, 9 (1979).

12. P. Van Duppen et al., Phys. Rev. Lett. 52, 1974 (1984).

BETA-DELAYED PROTON ACTIVITIES: ^{147}Dy AND ^{149}Er[1]

K. S. Toth
Y. A. Ellis-Akovali
F. T. Avignone, III[2]
D. M. Moltz[2]
E. C. Schloemer[3]
M. D. Cable[3]

The β-delayed proton spectra of ^{147}Dy and the hitherto unknown isotope, ^{149}Er, were investigated at the Lawrence Berkeley Laboratory 88-inch cyclotron in ^{12}C bombardments of ^{142}Nd and ^{144}Sm, respectively. A helium gas-jet system was used to transport product nuclei to a shielded area where they were assayed with a ΔE-E particle telescope and a Ge γ-x detector.

The ^{12}C + ^{142}Nd proton data [see Fig. 2.58 (a)] confirm preliminary results of Klepper et al.[4] that the ^{147}Dy delayed-proton spectrum has a high-energy cutoff at about 4.5 MeV and is dominated by distinct peaks below 4 MeV in excitation. The proton spectrum following ^{149}Er decay [see Fig. 2.58 (b)] has a half-life of 9 ± 1 sec and extends from about 2.0 to 6.5 MeV; it has less of the sharp structure observed for ^{147}Dy.

The intrinsic structure of delayed-proton spectra that accompany heavy mass precursors usually is not resolved due to the large density of states in the excitation energy range fed by the β decay. In Fig. 2.58 (a), however, the peaks have full widths at half-maximum which are on the order of the ΔE-E detector resolution, i.e., ~ 60 keV. The indication is that the ^{147}Dy β decay is sampling either selected ^{147}Tb states or else an energy region in ^{147}Tb where the level density is not high. The reader is reminded that ^{147}Tb consists of a single proton coupled to the doubly-closed core of ^{146}Gd (N = 82 and Z = 64). In Fig. 2.58 (b), while there are peaks in the lower half of the spectrum, the structure is much less distinct than in Fig. 2.58 (a). This could be due to a larger level density in ^{149}Ho, a nucleus still with 82 neutrons but now having three protons beyond Z = 64.

High-energy endpoints of delayed-proton spectra are fixed by differences between the electron-capture (EC) decay energies of the parents and the proton binding energies in the corresponding EC daughters. Predicted $Q_{EC} - B_p$ values from the 1977 Atomic Mass Evaluation[5] for ^{147}Dy and ^{149}Er are 4.42 and 6.44 MeV, respectively. These predictions are consistent with our data, see Figs. 2.58 (a) and (b).

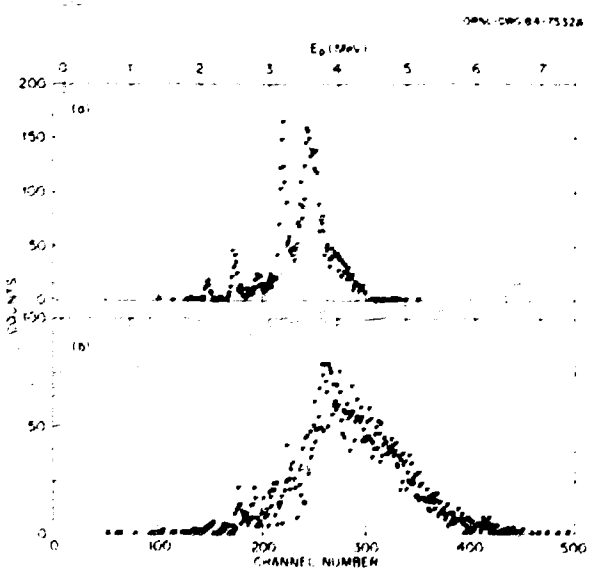

Fig. 2.58. Delayed-proton spectra observed in ^{12}C + ^{142}Nd[part (a)] and ^{12}C + ^{144}Sm [part (b)] irradiations made at an incident energy of ~ 135 Me; they are assigned to ^{147}Dy and ^{149}Er, respectively.

---

1. Summary of paper: Phys. Rev. C30, 712 (1984).
2. University of South Carolina, Columbia, SC.
3. Lawrence Berkeley Laboratory, Berkeley, CA.
4. O. Klepper et al., Z. Phys. A305, 125 (1982).
5. A. H. Wapstra and K. Bos, At. Data Nucl. Data Tables 19, 175 (1977).

GAMMA-RAY DECAY PATHWAYS OF A COMPOUND NUCLEUS WITH HIGH ANGULAR MOMENTUM AND HIGH EXCITATION ENERGY[1]

I. Y. Lee
C. Baktash
J. R. Beene
H. Kim
R. O. Sayer
M. L. Halbert
N. R. Johnson
F. K. McGowan
W. T. Milner
D. G. Sarantites[2]
M. P. Fewell[3]

The γ-rays emitted from a high-spin compound nucleus consist mainly of many stretched low multipolarity (λ = 1, 2) transitions which remove most of the angular momentum of the nucleus. The starting point of this γ-ray cascade is usually referred to as the entry point which is distributed over a wide region in the (E*,I) plane centered at about one neutron binding energy above the yrast line.[4] Initially, the γ-ray decay follows a path through regions of high level density and this leads to a large number of possible decay pathways resulting in an unresolved continuum of γ-rays. Near the end of the continuum cascade, all the pathways converge into the yrast band. A few bands just above the yrast band (< 1 MeV), as well as the yrast band itself, usually can be observed as discrete γ-ray lines.

Knowledge of the decay route from the entry states to the yrast line is necessary in order to extract information on nuclear structure from the associated continuum γ-ray spectrum. This route determines the region in the (E,I) plane from where the γ-rays are emitted, allowing us to associate the measured nuclear properties with the proper nuclear spin and excitation energies (temperature). So far, there is no direct determination of the decay pathways from the entry states to the yrast states. Models for the decay pathways have been proposed[5-8] based on indirect information such as yrast-state side-feeding intensities, γ-ray multiplicity distributions, and continuum γ-ray spectra. Therefore, an experimental determination of the decay pathways is not only necessary for an understanding of the continuum γ-ray results but it is also necessary if we are to make any meaningful comparison of these high-spin properties with theoretical calculations.

In the present experiment the entry states in ^{130}Ce were populated in the reactions of 144-MeV ^{34}S with ^{100}Mo. The spin spectrometer was triggered with two Ge counters. The continuum spectra (from the NaI detectors) coincident with ^{130}Ce discrete lines (from the Ge detectors) were constructed as a function of total pulse height, H, and fold, k. These were then unfolded to remove the detector response and trigger bias. The spectra from each (H,k) bin represent all the γ-rays emitted in the cascade from a given entry point to the ground state, but the order of emission of these γ-rays cannot be determined directly from a spectrum.

The decay pathway can be determined, however, by using a differential method as described in the following. Assume that from a state (E,M), the nucleus emits a γ ray with energy E_γ and ends in a state (E-E_γ,M-1). From the state (E-E_γ M-1), the rest of the cascade is identical to the cascade with entry point (E-E_γ M-1). Therefore, if we subtract the spectrum with entry point (E-E_γ M-1) from the spectrum with entry point (E,M), we will obtain a difference spectrum with only one γ ray of energy E_γ. On the other hand, the spectra from entry point (E_2,M-1) with $E_2 \neq$ E-E_γ is different from the spectrum of (E-E_γ,M-1). Thus, in the difference spectrum there is no complete cancellation of γ rays. In fact, the difference spectrum will contain negative counts in some channels, although the net counts still correspond to one γ ray. Therefore, the method of determining the decay pathway is to subtract from the spectrum with (H_1,k) the spectra with (H_2,k-1) for all possible H_2 values. The difference spectrum with the least amount of negative counts gives the H_2 value to which the state (H_1,k) will most likely decay. To measure the negative counts in the spectrum, we can define a parameter F as $F = \sum C_i / \sum |C_i|$, where C_i is the counts at channel i. For spectra with only positive counts, F = 1, whereas spectra containing some negative counts will have F smaller than 1.

The difference spectra obtained are shown in Fig. 2.59. These are the differences of the k = 22, H* = 7.5 MeV spectrum (H* is the excitation energy above the yrast line) and the K = 21, H* = 3, 6, 9, and 12 MeV spectra. We see

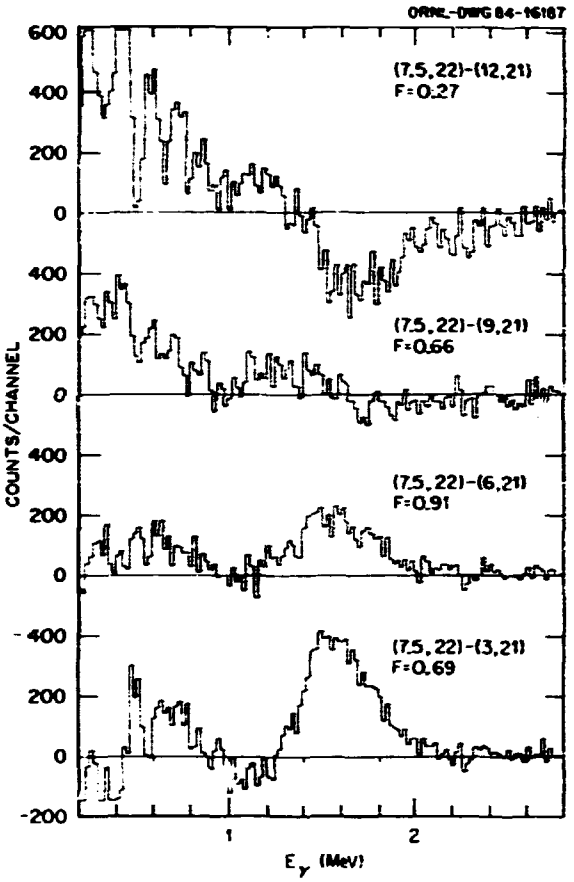

Fig. 2.59. Difference spectra of k = 22, H* = 7.5 MeV and k = 21.

clearly that only the middle spectrum, i.e., (H* = 7.5 MeV, k = 22) - (H* = 6 MeV, k = 21) had mostly positive counts. This indicates that the most probable path from H* = 7.5 MeV and k = 22 is through states with almost the same H* value. Similar features are seen for the decay of (H* = 13.5 MeV, k = 22) states. The F values from such difference spectra have been calculated and they are shown in Fig. 2.60 for the decay of the k = 22, H* = 7.5 MeV region. These results track the decay path from k = 22 to k = 14. The peak of the F value distribution is at about the same energy above the yrast line. This indicates that nuclei most likely decay along bands parallel to the yrast line.

The above results show that the decay pathways in the high spin and high excitation energy regions are mainly parallel to the yrast line, contrary to early predictions that nuclei with high excitation energy will decay toward the yrast line through statistical (mainly E1) γ-decay. This dominance of collective E2 decay in the high-spin regions was in fact suggested recently by Newton.[9] This is due to the increase of the γ-ray energy for rotational collective E2 transitions as a function of spin which can be shown to vary approximately as with the fifth power of (4I-2). The present results

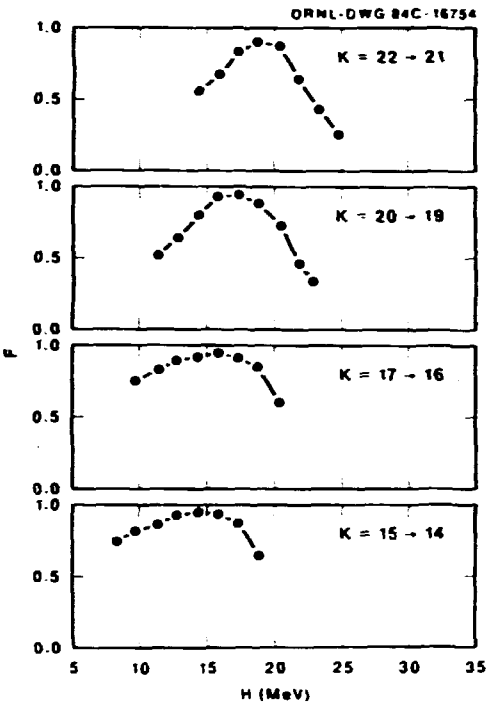

Fig. 2.60. The distribution of decay probability F in excitation energy as function of k.

also show that the nuclear deformation and collective motion still exist at high excitation energy, and therefore the nuclear shell effects are not completely attenuated at these excitations.

Since the continuum γ-rays are emitted from regions with a broad distribution in excitation energy rather than from a narrow region near the yrast line, it is mandatory that we measure both the spin and the excitation energy of the continuum γ-rays. In the cases where only the multiplicity (spin) is used for selection, one should recognize that the spin-dependent nuclear properties are averaged over a wide region of excitation energy. On the other hand, when the total γ-ray energy is used in selecting spectra for study, it selects an unknown mixture of spin, excitation energy and decay pathways. Therefore, the interpretation of such data can be highly ambiguous.

---

1. Summary of paper to be published.
2. Washington University, St. Louis, MO.
3. Australian National University, Canberra, Australia.
4. D.G. Sarantites et al., Phys. Lett. 115B, 441 (1982).
5. J.O. Newton et al., Nucl. Phys. A141, 631 (1970).
6. E.J. Liotta and R.A. Sorensen, Nucl. Phys. A297, 162 (1978).
7. M. Wakai and A. Faessler, Nucl. Phys. A307, 307 (1978).
8. G. Leander, Y.S. Chen and B.S. Nilsson, Phys. Scr. 24, 164 (1981).
9. J.O. Newton, Phys. Scr. 24, 83 (1981).

AN INVESTIGATION OF THE COLLECTIVITY IN THE YRAST BAND OF ^{158}Er BY LIFETIME MEASUREMENTS[1]

M. Oshima[2] N. R. Johnson
F. K. McGowan I. Y. Lee
C. Baktash R. V. Ribas[4]
Y. Schutz[3] J. C. Wells[5]

Both experimental and theoretical investigations of deformed rare-earth nuclei have shown that the interplay between collective rotations and single-particle excitations determines the structure of these nuclei at high spins. From the macroscopic point of view, the Coriolis force which comes into play at high rotational frequencies causes alignment of the single-particle angular momenta along the axis of the collective rotation. Such an alignment of single particles will result in a deformation change from prolate to triaxial or oblate shapes. Furthermore, centrifugal force can cause stretching of the nucleus. The E2 matrix elements along the yrast line should reflect such deformation changes. Indeed, recent lifetime measurements in the s-bands of $^{156-158}$Dy (Ref. 6) and $^{159-163}$Yb (Refs. 7,8), which lie near the N = 90 region, indicate a significant reduction in the E2 matrix elements and suggest that these nuclei undergo a deformation change from prolate to triaxial shape at high angular momentum. In order to extend our understanding of the evolving pattern of shapes and the forces that determine these deformation changes in soft transitional nuclei (near N = 90), we have carried out lifetime measurements on all states in the yrast sequence of ^{158}Er from $I = 2^+$ through $I = 24^+$.

Lifetimes of these high spin states in ^{158}Er have been measured by means of the recoil-distance method. Excited ^{158}Er nuclei were produced via the reaction ^{128}Te(^{34}S,4n)^{158}Er at a bombarding energy of 155 MeV. Deexcitation γ rays were detected in a Compton-suppressed Ge detector positioned at 0° and gated by five germanium detectors at 90° to the incident beam. The recoil-distance device used in the experiment has been described[9] previously. Coincidence counts were recorded event by event on magnetic tape for fourteen recoil-flight distances ranging from 20 μm to 2.515 mm. In addition, a lead-backed target was used to get the spectrum at zero separation.

From the coincidence data, three types of decay curves were obtained for each state: (1) one from the total projected coincidence spectra; (2) one from the spectra generated by gating on all transitions below the state of interest; and (3) one from the spectra gated by the next transition above the state of interest. A few comments about these three types of spectra are in order. Total projected coincidence spectra provide data of improved statistical quality for weak transitions, but can lead

to difficulty in fitting the decay curve due to added complexity in treating side feeding. A decay curve obtained from the summed spectra gated on transitions below the state of interest includes essentially the same fraction of side feeding as the one obtained from "singles" spectra. The major difference is that the gated spectra contain fewer γ rays, thus making the analysis simpler and more reliable. In principle, the third type of decay curve produces by far the simplest case for extraction of lifetimes since the data are unencumbered with the problems of sidefeeding into the state of interest. This approach is limited only by the statistical quality of the data that can be collected for high-spin states. In all of these coincidence spectra, events of low γ-ray multiplicity which correspond to Coulomb excitation or residual decay are considerably reduced.

The three types of decay curves were obtained for transitions from the 2^+ through 24^+ member of the yrast band. Lifetimes were extracted by a computer code[10] which applies all of the usual corrections to the data and handles the problem of feeding by direct solution of the Bateman equations.

A summary of lifetimes for members of the yrast sequence is given in Table 2.12. The lifetimes in the table are weighted averages of values extracted from the different types of analyses described above. Reduced transition probabilities were extracted from the lifetimes, and transition quadrupole moments, Q_t, were calculated according to the expression

$$B(E2;I\to I-2) = \frac{5}{16\pi} \langle I\ 2\ 0\ 0 \mid I-2\ 0 \rangle\ {}^2Q_t{}^2.$$

In Fig. 2.61, the Q_t values are plotted as a function of spin. In this figure two important features are conspicuous: The Q_t values of the g-band appear to increase with spin up to 8^+, and, after the backbending which occurs at about 14^+, the Q_t values become smaller compared with the g-band and even decrease at higher spins.

It is interesting that many nuclei lying at or near the 90-neutron transitional boundary show, at least qualitatively, similar behavior.

Table 2.12. Lifetimes of yrast states in ^{158}Er

I^π	E_γ(keV)	τ(ps)	B(E2;I→I-2)	Q_t(eb)
2	192.1	371(37)	0.65(6)	5.7(3)
4	334.8	19.2(18)	0.96(9)	5.82(27)
6	442.8	3.7(4)	1.27(14)	6.37(34)
8	522.7	1.33(26)	1.55(30)	6.9(7)
10	576.8	1.13(45)	1.10(44)	5.7(11)
12	607.9	1.2(6)	0.81(41)	4.9(12)
14	509.5	3.1(4)	0.76(10)	4.7(3)
16	472.6	3.48(24)	0.97(7)	5.26(18)
18	566.0	1.82(13)	0.76(5)	4.64(17)
20	659.4	1.16(7)	0.57(3)	4.01(12)
22	740.1	0.96(17)	0.38(7)	3.3(3)
24	805.7	0.43(14)	0.56(18)	4.0(6)

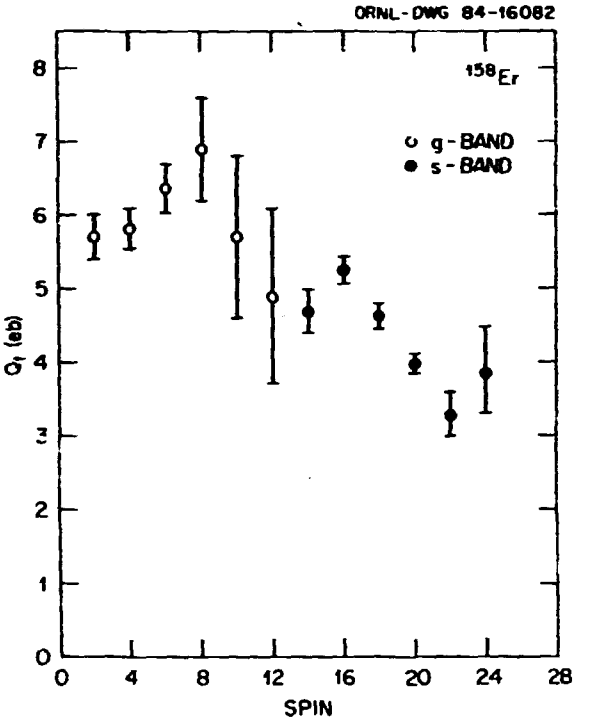

Fig. 2.61. Transition quadrupole moments of yrast states in ^{158}Er plotted as a function of spin.

Several theoretical calculations have been performed in order to understand these phenomena. Recently, a group at Lund has reported preliminary results[11] of some self-consistent cranked Hartree-Fock-Bogoliubov (HFB) calculations of the shape of the ^{158}Er as a function of angular momentum. They find that, in the g-band, variation of γ is rather small (within 2°) while ε_2 shows a steady increase, ranging from 0.20 at ground state to 0.24 at 10^+. This result accounts qualitatively for our observed behavior except for the 10^+ state, where we see significant reduction in the collectivity. Furthermore, in a similar calculation for the s-band in ^{160}Yb it has been shown[12] that ^{160}Yb undergoes a triaxial deformation at high spins. The similar tendency of the experimental Q_t values were observed in ^{158}Er and it could be attributed to the polarizing effect on the core caused by the high-j aligned quasiparticles.

---

1. Summary of paper to be published.
2. On leave from Japan Atomic Energy Research Institute, Tokai, Ibaraki 319-11, Japan.
3. Present address: University of Sao Paulo, Sao Paulo, Brazil.
4. On leave from CRN, Strasbourg, France.
5. Tennessee Technological University, Cookeville, TN.

6. H. Emling, et al., Nucl. Phys. A419, 187 (1984).
7. N. R. Johnson, Proc. of 1982 INS International Symposium on Dynamics of Nuclear Collective Motion, ed. by K. Ogawa and K. Tanabe (Inst. for Nuclear Study, University of Tokyo, 1982) p. 144.
8. M. P. Fewell, et al., Proc., Conf. on High Angular Momentum Properties of Nuclei, Oak Ridge, Tennessee, Nov. 1982, Vol. 4 of Nuclear Science Research Conference Series. ed. by N. R. Johnson (Harwood Academic Publishers, New York, 1983) p. 69.
9. N. R. Johnson, et al., Physics Division Progress Report for Period Ending June 30, 1981, ORNL-5787 (1981).
10. J. C. Wells and M. P. Fewell, to be published.
11. R. Bengtsson and S. Aberg, private communication.
12. R. Bengtsson, et al., Nucl. Phys. A405, 221 (1983).

QUASIVIBRATIONAL BANDS AT HIGH SPINS IN ^{158}Yb[1]

C. Baktash — L. Courtney[4]
Y. Schutz[2] — A. J. Larabee[4]
I. Y. Lee — L. L. Riedinger[4]
F. K. McGowan — A. W. Sunyar[5]
N. R. Johnson — E. der Mateosian[5]
M. L. Halbert — O. C. Kistner[5]
D. C. Hensley — D. G. Sarantites[6]
M. P. Fewell[3] — I. Ragnarsson[7]

Rare-earth nuclei with neutron numbers $N \lesssim 90$ offer a unique opportunity to study spin induced nuclear shape transitions. Being situated between the nearly doubly magic ^{146}Gd "core" at one end, and the well-deformed nuclei at the other, they span a variety of shapes which range from moderately oblate to prolate. In particular, the transitional nuclei ($N \approx 88$) which have soft potential energy surfaces are predicted to experience large changes in their shape parameters as the angular momentum is increased and high-j quasiparticles are excited. Study of these shape transitions and the associated excitation modes provides valuable insight into the question of the interplay between collective and single-particle degrees of freedom in nuclear systems.

To investigate these effects, we have studied the high spin states in ^{158}Yb, which were populated using ^{20}Ne ($E \approx 115$ MeV) and ^{64}Ni ($E \approx 285$ MeV) beams. The ^{20}Ne run utilized an array of six Ge counters along with two 25cm x 25cm NaI crystals which served as a total energy spectrometer. More than 100 million events, defined by coincidence firing of both NaI detectors and a minimum of two Ge counters, were collected in this mode. The ^{64}Ni run was carried out in the Spin Spectrometer by replacing six of the NaI elements with Ge detectors. By demanding a coincidence firing of a minimum of two Ge and 22 NaI detectors, collection of those events with rich multiplicity content was emphasized. Off-line analysis of these data started with separate gain matching of all Ge and NaI detectors and removal of the neutron-induced signals. The corrected data were then scanned to generate several E_γ-E_γ matrices that were gated with various two-dimensional cuts in the total pulse-height vs coincidence fold map to enhance the 4n-channel. A recently developed background subtraction technique was used to remove nearly 90% of the Compton events present in these matrices before generating gated coincidence spectra.

On the basis of the γ-γ coincidence data from these runs, we established the positive- and negative-parity yrast states up to $I^\pi = (40^+)$ and (31^-), respectively (Fig. 2.62). Figure 2.63 compares the kinematical moments of inertia, $\mathcal{J}^{(1)}$, of these two bands with similar bands in ^{160}Yb (full and open circles, respectively). A noteworthy feature is the

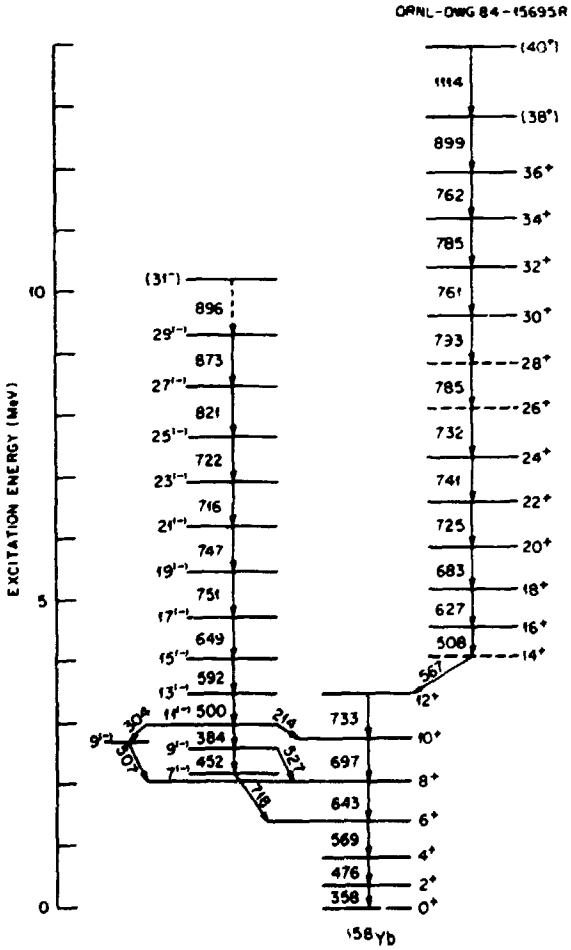

Fig. 2.62. Partial decay scheme for ^{158}Yb. Gamma ray energies are given in keV. Dashed horizontal lines indicate uncertain ordering of the transition of γ rays. Parentheses indicate uncertain spin-parity assignment.

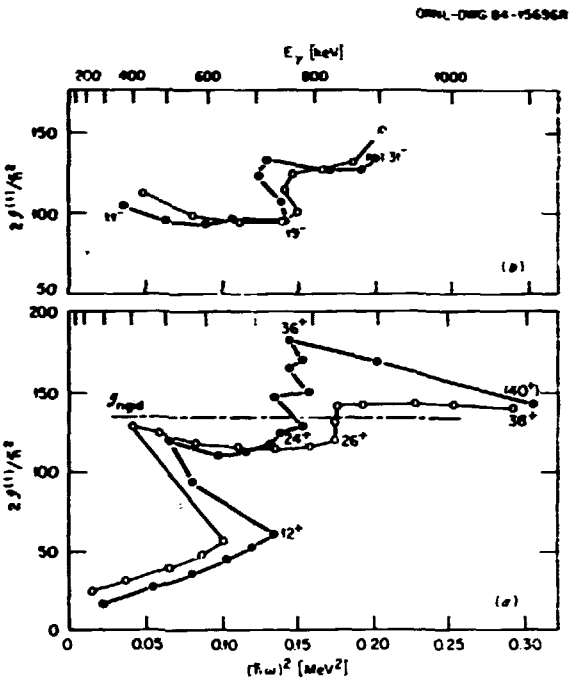

Fig. 2.63. Plots of moments of inertia $2\mathcal{J}^{(1)}/\hbar^2$ vs $(\hbar\omega)^2$ for (a) positive bands, and (b) negative parity bands in ^{158}Yb (full circles) and ^{160}Yb (open crosses).

contrasting behavior of the two bands in ^{158}Yb. In the case of the negative-parity band (Fig. 2.64), which consists of $i_{13/2}\ h_{9/2}$ neutron orbitals, we observe its first band crossing at an angular frequency of $\hbar\omega$ = 0.36 MeV, close to that of the ^{160}Yb. Both nuclei exhibit an upbending in the frequency range of $\hbar\omega$ = 0.44 MeV, which has been shown to be due to Coriolis alignment of an $h_{11/2}$ proton-pair in N = 90 isotopes. The overall behavior of this band is not very different from other odd-spin odd-parity bands in the neighboring collective nuclei.

The low and medium spin states in the positive parity band show a similar collective behavior up to spin 24. At higher spins, however, this band shows an excitation pattern which is quite different from that of the negative parity band or other positive-parity bands in neighboring nuclei. In particular, the stretching of $\mathcal{J}(1)$ resumes past spin 20 and assumes an extreme form, namely, a vertical ascent, after the second discontinuity at spin I = 24. The resulting moment of inertia exceeds the rigid rotor value by nearly 40%. Such a large $\mathcal{J}(1)$ has not been observed previously and is a consequence of the quasivibrational excitation mode. (The energies of the γ rays deexciting the states with spin $24<I<36$ remain within a 730-790 keV interval.) Rotational alignment effects cannot explain this sharp rise in $\mathcal{J}(1)$, nor the near constancy of the gamma ray energies. (Alignment of proton $h_{11/2}$ is expected to occur at higher rotational frequencies, and that of the $h_{9/2}$ neutron orbital can at best account for only half of the observed gain in alignment.) A likely explanation is that the nuclear shape gradually evolves from being prolate at $I^\pi = 24^+$ to oblate at $I^\pi = 36^+$. Indeed, on the basis of cranked shell model calculations, Ragnarsson et al. have recently suggested that these states belong to an yrast band which continuously minimizes its energy by adjusting its shape parameters and acquiring larger γ values, where γ is the asymmetry parameter. This band finally terminates on the oblate axis upon reaching spin 36, which is obtained by aligning the angular momentum of its valence particles along the oblate axis. Although such terminating bands have long been observed in very light nuclei, the positive parity band in ^{158}Yb is the first evidence for the existence of such bands in a heavy nucleus.

---

1. Summary of paper to be published.
2. On leave from CRN, Strasbourg, France.
3. The Australian National University, Canberra, Australia.
4. University of Tennessee, Knoxville, TN.
5. Brookhaven National Laboratory, Upton, NY.
6. Washington University, St. Louis, MO.
7. Lund Institute of Technology, Lund, Sweden.

COULOMB EXCITATION OF ^{160}Dy WITH LEAD IONS

R. V. Ribas[1] L. L. Riedinger[3]
N. R. Johnson R. M. Diamond[4]
I. Y. Lee F. S. Stephens[4]
D. R. Haenni[2] S. Shi[4]
H. Kluge[4]

Coulomb excitation of ^{160}Dy was carried out with a ^{208}Pb beam from the Lawrence Berkeley super HILAC. This was done in order to study the changing collectivity at high spins by measuring the reduced transition probabilities between states in the yrast sequence. Gamma rays emitted following Coulomb excitation were detected by two Ge(Li) detectors in coincidence with scattered projectiles and recoiling nuclei. These particles were detected in a pair of two-dimensional position-sensitive parallel-plate avalanche detectors. The target was 0.5 mg/cm^2 (99% enriched) ^{160}Dy deposited onto a 0.7 mg/cm^2 Ni foil.

The Coulomb Excitation Data Analysis Code (GOSIA) obtained from D. Cline[5] was used to determine the set of matrix elements that best account for the experimental γ-ray yields by means of a least squares fitting. Eight sets of data, corresponding to four different regions of the scattering angles for two bombarding energies (942 and 1035 MeV) were used in order to obtain unambiguously the complete set of transition matrix elements up to spin 20$^+$. The initial set of matrix elements used in the

fitting were those of the symmetric rigid rotor model. Since the β-band and the K = 2 and 4 band heads in ^{160}Dy have rather high excitation energies (> 1.5 MeV) and since no transitions associated with these bands were observed in the spectra, only the g-band, the γ-band and the s-band were included in the level scheme. The s-band was assumed to have the same intrinsic quadrupole moment as the g-band, and interband matrix elements were taken only at the crossing point. The diagonal elements were kept fixed during the analysis and were calculated using an intrinsic quadrupole moment that reproduces the $2^+ \rightarrow 0^+$ transition probability. This value, which is well known from previous measurements,[6] was allowed to vary only in a narrow range around the known value.

The reduced transition probabilities obtained from the present experiment are shown in Table 2.13. As seen, these results are consistent with the previous Coulomb excitation data of Sayer, et al.[7] at lower spins, with the exception of the $8^+ \rightarrow 6^+$ transition, where the present result is ~ 15% higher than that of Ref. 7.

We have used our B(E2) values in Table 2.13 to calculate transition quadrupole moments (Q_t) according to the following expression

$$B(E2;\ I \rightarrow I-2) = \frac{5}{16\pi} \langle I\ 2\ 0\ 0 \mid I-2\ 0 \rangle^2 Q_t^2 .$$

Table 2.13. Reduced E2 transition probabilities for transitions in ^{160}Dy.

Transition	Present Results	Sayer, et al.[7]
4→2	$3.33^{+0.10}_{-0.05}$	3.53±0.18
6→4	$3.91^{+0.3}_{-0.2}$	4.00±0.10
8→6	$5.85^{+0.3}_{-0.2}$	5.16±0.16
10→8	$7.30^{+0.8}_{-0.6}$	6.81±0.34
12→10	$7.33^{+0.6}_{-0.2}$	8.2±1.8
14→12	$7.90^{+0.6}_{-0.4}$	
16→14	$5.59^{+0.2}_{-0.7}$	
18→16	$7.70^{+1.3}_{-1.0}$	
20→18	$8.73^{+2.4}_{-2.0}$	

These values along with those for ^{156}Dy and ^{158}Dy from Emling et al.[8] are shown in Fig. 2.64. The same pattern observed for the spin dependence of the reduced transition probabilities for the g-band in the lighter ^{156,158}Dy isotopes is also present in ^{160}Dy. The B(E2) value for the $10^+ \rightarrow 8^+$ transition is about 40% above the rotational model prediction and corresponds to a transition quadrupol moment of ~ 8.6 eb, still larger than the maximum for the less deformed ^{156}Dy as seen in Fig. 2.64. Although the error extracted for two transition probabilities in the s-band ($20^+ \rightarrow 18^+$ and $18^+ \rightarrow 16^+$) are quite large, the data in Fig. 2.64 do not seem to indicate evidence for a decreasing collectivity in these higher-spin members of the rotation-aligned band as is observed[8] for ^{156,158}Dy.

---

1. On leave from University of Sao Paulo, Brazil. (Fellow of Fundacás de Amparo à Pesquisa de Sao Paulo.)
2. Present address: Texas A&M University, College Station, Texas.
3. University of Tennessee, Knoxville, Tennessee.
4. Lawrence Berkeley Laboratory, Berkeley, California.
5. D. Cline, private communication; for details of the code, see T. Czosnyka et al., Publ. of University of Rochester, UR-NSRL 263 (to appear in Nucl. Phys.)
6. P. C. Lopiparo, R. L. Rasera and M. E. Caspari, Nucl. Phys. A178, 577 (1972).
7. R. O. Sayer et al., Phys. Rev. C9, 1103 (1974).
8. H. Emling, et al., Nucl. Phys. A419, 187 (1984).

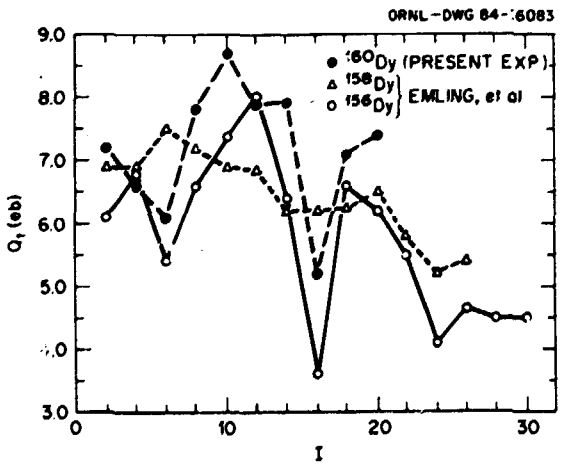

Fig. 2.64. Plot of transition quadrupole moments (Q_t) for states in ^{156,158,160}Dy.

DISCRETE AND CONTINUUM γ RAY STUDY OF ^{154}Er AT HIGH SPINS[1]

C. Baktash — A. J. Larabee[5]
I. Y. Lee — Y. Schutz[6]
N. R. Johnson — M. Oshima
O. C. Kistner[2] — E. der Mateosian[2]
D. Horn[2] — A. W. Sunyar[2]
C. Y. Chen[2] — C. J. Lister[2]
J. X. Saladin[3] — O. Dietzsch[4]
D. G. Sarantites[4] — K. Honkanen[4]
T. Semkov[4]

Study of the interplay between the macroscopic and microscopic effects in nuclei as a function of angular momentum has become the focus of nuclear structure studies in recent years. Theoretically, cranked shell model calculations by several groups predict shape transition patterns in the light rare-earth nuclei which depend sensitively on the neutron number.[7,8] For example, the Er isotopes with $N \lesssim 86$ are predicted to have nearly spherical shapes at low spins and gradually become oblate at higher angular momenta (Fig. 2.65). In contrast, for neutron number $N > 88$, the equilibrium shapes are expected to change from prolate at spins $I \lesssim 40$ to triaxial at $I \gtrsim 50$. Of particular interest is the predicted transition to superprolate ($\beta \approx 0.6$) shapes for $N \approx 82$ isotopes at very high spins. Such large deformations correspond to a major-to-minor axis ratio of nearly 2:1 and have been observed only in the fission isomers. Experimental verification of these predictions provides a very stringent test of the validity of these calculations, which have been very successful in describing the nuclear behavior at high angular momenta. To investigate these predicted spin induced shape changes in ^{154}Er, we used the ^{124}Te (^{34}S, 4n) reaction to populate the high spin states in this nucleus. The ^{34}S beam (170 MeV) was obtained from the double tandem facility at Brookhaven National Laboratory. The experimental setup consisted of six Ge and eleven NaI detectors which served as a multiplicity filter. Four of the Ge detectors were surrounded by annular NaI Compton-suppression shields which gave a suppression factor of better than 2.5 for the ^{60}Co source. By demanding a coincidence of at least two Ge and two NaI detectors, high multiplicity events were emphasized. Nearly 140 million such events were collected on an event-by-event basis.

In the off-line analysis, the gains of all Ge detectors were equalized and the Ge-Ge coincidence data were scanned to generate an Eγ-Eγ matrix. This matrix contained nearly 12 million photo peak-photo peak counts before symmetrization, of which approximately 40% belong to ^{154}Er. These data formed the basis for a revised and expended decay scheme of ^{154}Er shown in Fig. 2.66. Angular correlation information were used to deduce the multipolarity of the newly found transitions. The noteworthy features of the decay scheme include:

(1) The level scheme shows a shell model structure up to the maximum observed spin of 38.

(2) All of the expected optimal states generated by the alignment of the valence nucleons around the oblate symmetry axis are clearly established in the decay scheme (bold horizontal lines in Fig. 2.66). The configurations of these states (11^-, 21^-, 27^-, 33^-, 36^+) are indicated in this figure.

(3) Existence of high energy γ rays feeding the highest optimal sate, $I^\pi = 36^+$, reflects the fact that above this state core excitation becomes necessary. Consistent with this picture

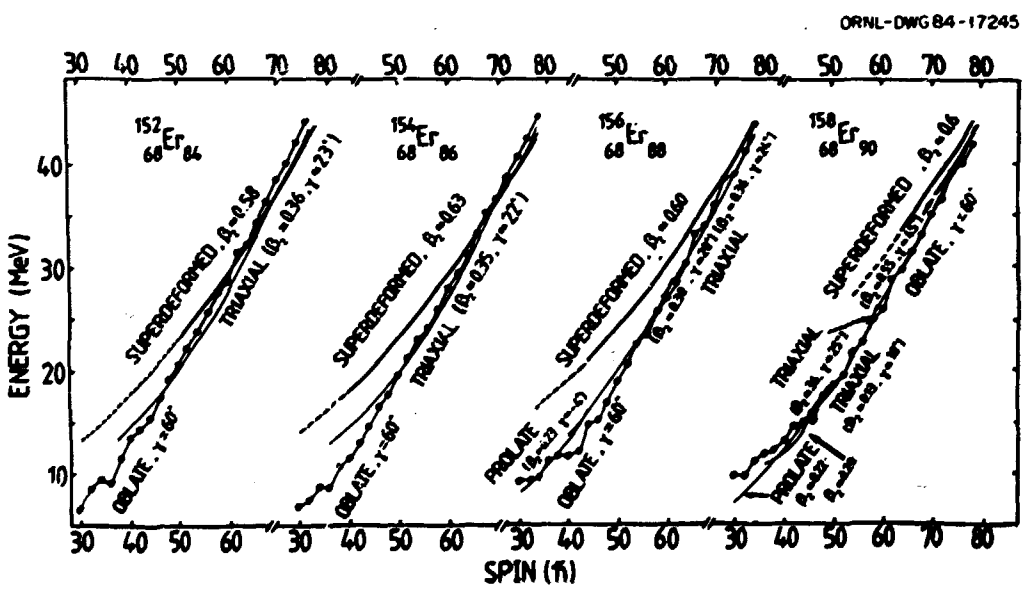

Fig. 2.65. Predicted equilibrium shapes as a function of angular momentum and excitation energy for erbium-isotopes (Ref. 8).

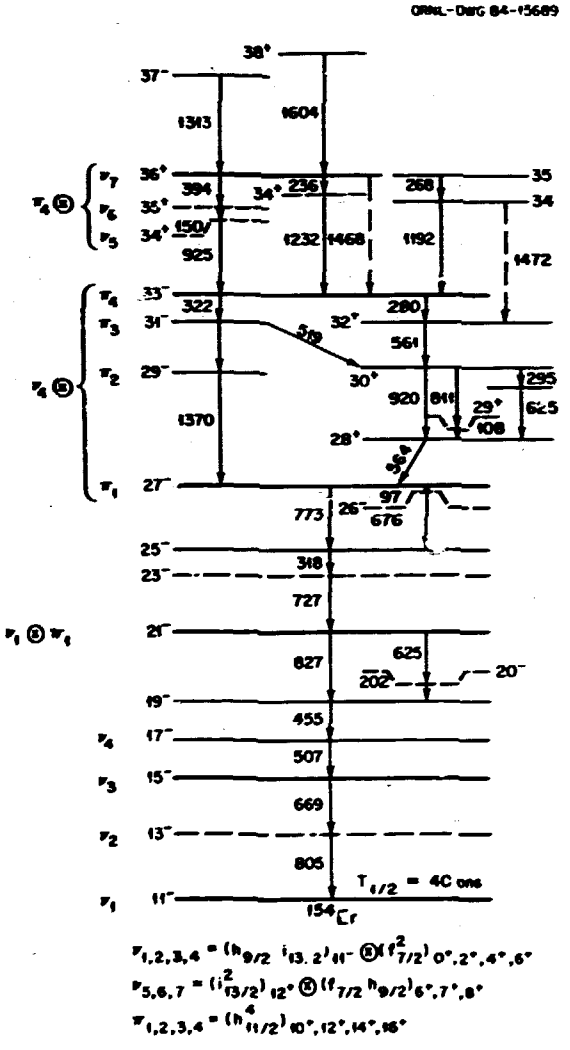

Fig. 2.65. Partial decay scheme of ^{154}Er showing levels above the $I^{\pi} = 11^-$ isomeric state. Dashed horizontal lines indicate uncertainty in the level ordering. Neutron (ν) and proton (π) configurations are indicated for several states.

is the fragmentation of the feeding into this state that was experimentally observed.

(4) The level spacings of states with $I^{\pi} = 27^-$, 29^-, 31^-, and 33^- closely resemble those of the $I^{\pi} = 10^+$, 12^+, 14^+, and 16^+, states in ^{150}Dy formed by $(h^4_{11/2})$ proton-excitation. Also, the 1467 keV γ ray between $I^{\pi} = 36^+$ and 33^- optimal states is very similar to the octupole transition that connects the corresponding optimal states in ^{153}Ho. They both arise from $i_{13/2} \rightarrow f_{7/2}$ neutron transition, and reflect the *excitation energy of the* $i_{13/2}$ *neutron orbital.*

The above observations are in good agreement with theoretical predictions that noncollective excitations dominate the yrast structure of ^{154}Er below spin 50. To verify the predicted onset of collectivity at higher spins, we have searched for the ridge-valley structure in the unfolded $E\gamma$-$E\gamma$ correlation maps. Such a structure has been observed in ^{152}Dy,[9] and interpreted to arise from collective rotation of a superdeformed shape. We have found no evidence for such structures in the $E\gamma$=1000-1400 keV range, where a strong quadrupole structure has been observed in the energy spectrum. This implies that contrary to the ^{152}Dy case, either the collective bands in ^{154}Er are not fed even at the highest angular momentum populated in this reaction (60h), or the interband transitions divert the population away from these bands. Either possibility is in conflict with the theoretical predictions.

---

1. Summary of a paper to be published.
2. Brookhaven National Laboratory, Upton, NY.
3. University of Pittsburgh.
4. Washington University, St. Louis, MO.
5. University of Tennessee, Knoxville, TN.
6. On leave from CRN, Strasboug, France.
7. I. Ragnarsson et al., Nucl. Phys. A347, 287 (1980).
8. J. Dudek, Private Communication.
9. B. M. Nyako et al., Phys. Rev. Lett. 52, 507 (1984).

^{158}Yb GAMMA RAY SPECTROSCOPY AS A FUNCTION OF SPIN AND TEMPERATURE[1]

Y. Schutz[2] M. L. Halbert
C. Baktash D. C. Hensley
I. Y. Lee L. Courtney
F. K. McGowan A. J. Larabee[3]
N. R. Johnson L. L. Riedinger[3]
D. C. Sarantites[4]

Discrete-line spectroscopy in ^{158}Yb suggests coexistence of two different band structures at high spins. While the energies of the positive-parity band up to $I \approx 24$ and the negative-parity band up to its maximum observed spin of $I = 31$ show collective rotational patterns, γ rays de-exciting states with $I^{\pi} = 24^+ - 36^+$ have nearly equal energies. The latter behavior is interpreted as due to termination of a band wherein the nucleus continuously adjusts its shape parameters while gradually evolving toward an oblate shape. To ascertain which band structure dominates above the yrast line and beyond spin 40, we have examined the continuum γ ray data. The experimental setup consisted of six Ge detectors placed in the Spin Spectrometer as described in Ref. 5. Following removal of neutron signals on an event-by-event basis, all singles spectra were corrected for double-hit events and unfolded using measured response *functions of the individual NaI elements. The* response functions also were used to effect the transformation of total pulse-height (H) into excitation energy (E), and coincidence fold (K) to multiplicity (M). The use of the Spin

Spectrometer allows a detailed characterization of the quasicontinuum γ rays. In the following we shall examine the evolution of these continuum γ ray spectra with spin and excitation energy, their multipolarity composition, and their E_γ-E_γ correlation patterns.

Spin and Temperature Dependence. Singles γ ray spectra were generated by gating simultaneously on the strong discrete transitions in ^{158}Yb, and various (H, K) cuts. Typical spectra for two H and two E values are shown in Fig. 2.67 (a) and (b). The narrow peak around E_γ = 750 keV contains mainly yrast transitions deexciting states in the I = 26-36 spin range. The higher energy edge of this peak falls rapidly and does not move noticeably with increases in the multi-plicity or the excitation energy. Instead, a second and much broader structure gradually develops around 1.15 MeV at higher multiplicity and excitation energies. The number of transi-tions in the lower energy part of the spectrum increases also with increasing multiplicity but decreases with increasing excitation energy. This behavior indicates that the low-energy transitions and the transitions in the high-energy bump originate from different regions of the (E,I) map and may be due to different modes of excitation of the nucleus.

Multipolarity Decomposition. The angular distribution has been measured at seven angles using single NaI detectors of the spin spectrometer. A sample A_2/A_0 spectrum obtained from a Legendre polynomials analysis is displayed in Fig. 2.67 (c) for H=29. The decomposition of the energy spectrum into stretched quadrupoles and stretched dipoles is shown in Fig. 2.67(d). One observes a strong quadrupole peak at 750 keV on top of a weaker dipole peak and a second quadrupole bump centered at 1.15 MeV. The intensity of these three structures increase with increasing multiplicity. The higher energy quadrupole bump can be interpreted in terms of a collective rotation of the deformed nucleus and may indicate the onset of a triaxial deformation of ^{158}Yb at high spin and temperature.

Correlation Patterns. Two-dimensional E_γ-E_γ coincidence spectra have been constructed for different (H, K) bins using all possible coincidences between any two NaI detectors in the Spin Spectrometer. A two-dimensional unfolding method was used to yield photo-peak-photopeak coincidence spectra. Fig. 2.68 displays such a spectrum corresponding to the difference between two (H, K) bins for a constant H. The spectrum is dominated by coincidences with transitions in the 750 keV energy region. One recognizes the

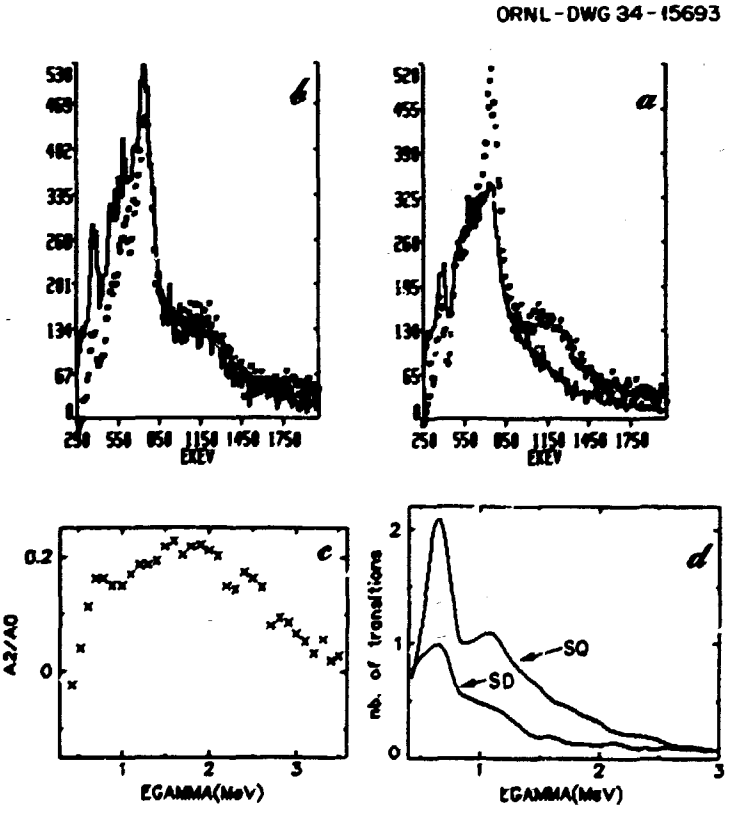

Fig. 2.67. Unfolded energy spectra for: (a) H = 23, E = 3.2 MeV (full line); H = 31, E = 32 MeV (square). (b) H = 31, E = 3.2 MeV (full line); H = 31, E = 9.4 MeV (square). (c) Angular distribution coefficient for H = 29. (d) Stretched dipole and stretched quadrupole spectra for H = 29.

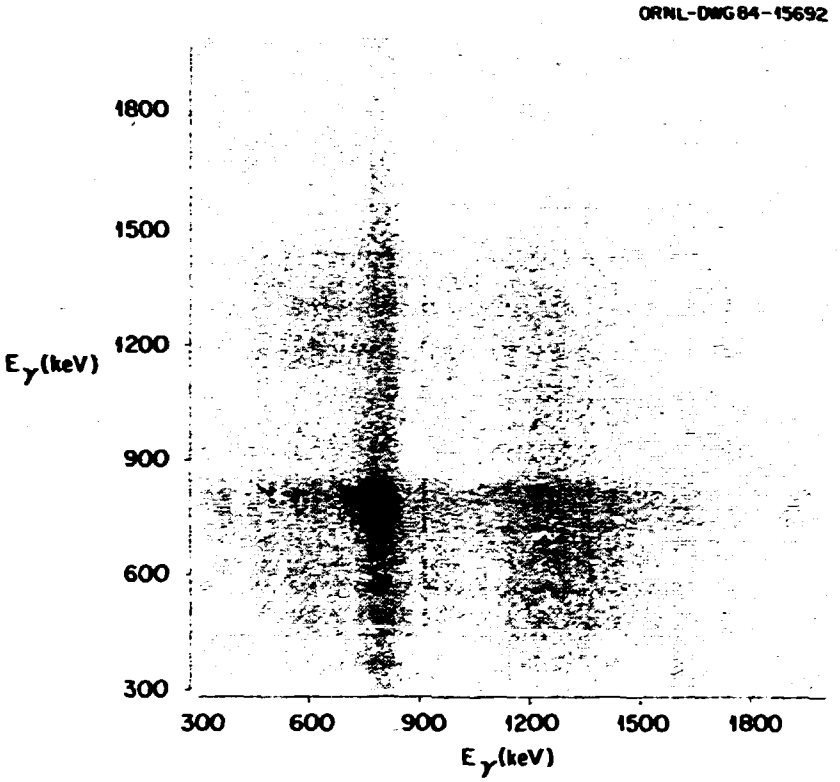

Fig. 2.68. Unfolded coincidence-spectrum corresponding to the difference of two (H, K) binds: (12 MeV, 31) - (12 MeV, 23).

coincidence pattern of the discrete yrast transitions with the first backbending at 570 keV. Above E_γ= 850 keV one observes a cut-off of the valley-ridge structure, which indicates absence of collective rotational bands beyond an angular frequency of $\hbar\omega$=0.45 MeV. The quadrupole bump observed at 1.15-MeV in the single energy spectra originates mainly from coincidences with the 750 keV transitions; only 20% of the transitions in the 1.15 MeV region are in coincidence with transitions from the same energy region. This fact indicates that only a few transitions decay along rotational bands built on possible triaxial deformations which might exist at high spin and temperature.

Using the code GAMBLE, we are now carrying out simulations of the deexcitation pattern of *high spin-high energy* states in ^{158}Yb. This will aid in the interpretation of the origin of various components in the energy spectrum, especially the low energy dipole component.

1. Summary of paper to be published.
2. On leave from CRN, Strasbourg, France.
3. University of Tennessee, Knoxville, TN.
4. Washington University, St. Louis, MO.
5. C. Baktash et al., "Quasivibrational Bands at High Spins in ^{158}Yb", this section.

E2 AND E4 DETERMINATIONS IN ^{233,234,235,238}U[1]

J. D. Zumbro[2] R. A. Naumann[2]
E. B. Shera[3] M. V. Hoehn[3]
Y. Tanaka[4] W. Reuter[3]
C. E. Bemis, Jr. R. M. Steffen[4]

Precise intrinsic quadrupole, Q_0, and hexadecapole moments, H_0, of ^{233,234,235,238}U have been determined from muonic K, L, M, and N X rays. The charge distribution parameters are listed in Table 2.14, together with the derived intrinsic moments. For ^{233,235}U, seven E2 matrix elements were independently determined. These E2 matrix elements are in good agreement with the adiabatic rotational model; this agreement is further improved if a correction for $\Delta K = 1$ band mixing is included, as indicated in Table 2.15. The measured hexadecapole moments are in good agreement with shell-correction calculations and Hartree-Fock calculations, as shown in Fig. 2.69.

1. Summary of paper: Phys. Rev. Lett. 53, 1888 (1984).
2. Princeton University, Princeton, New Jersey.
3. Los Alamos National Laboratory, Los Alamos, New Mexico.

Table 2.14. Uranium charge parameters. The parameters c, a, and $\langle r^2 \rangle^{1/2}$ are given in units of fm; Q_0 in units of eb; and H_0 in units of eb^2.

	Nucleus	^{233}U	^{234}U	^{235}U	^{238}U
This work	c*	6.9518 (16)	6.9703 (13)	6.9859 (17)	7.0110 (12)
	a*	0.5125 (12)	0.5089 (10)	0.5029 (13)	0.5046 (9)
	Q_0†	10.294 (59)	10.610 (57)	10.630 (59)	11.188 (58)
	H_0†	2.55 (30)	2.49 (14)	2.64 (10)	2.28 (11)
	β_2*	0.2431 (40)	0.2507 (18)	0.2485 (13)	0.2653 (14)
	β_4*	0.091 (15)	0.0843 (71)	0.0913 (45)	0.0572 (49)
	$\langle r^2 \rangle^{1/2}$*	5.8158 (66)	5.8289 (31)	5.8343 (28)	5.8604 (23)

*Model-dependent analysis (statistical uncertainties only).
†Q_0 and H_0 include 0.5% and 2.0% model uncertainty, respectively.

Table 2.15. Spectroscopic quadrupole moments and B(E2) values for $^{233,235}U$. Spectroscopic and intrinsic (q and Q, respectively) are given in units of eb, and the B(E2) values are given in $(eb)^2$. Errors do not include model uncertainties.

	^{233}U (I = 5/2)			^{235}U (I = 7/2)		
	Present experiment	Theory		Present experiment	Theory	
		Adiabatic rotation	Rotation +ΔK = 1 mixing		Adiabatic rotation	Rotation +ΔK = 1 mixing
q(I)	3.663 (8)	3.677	3.666	4.936 (6)	4.955	4.939
B(E2; I→I+1)	5.041 (16)	5.020	5.034	4.834 (16)	4.757	4.816
q(I+1)	0.642 (30)	0.686	0.649	1.870 (30)	1.931	1.851
B(E2; I→I+2)	1.756 (26)	1.757	1.781	1.189 (41)	1.223	1.267
B(E2; I+1→I+2)	3.969 (37)	3.993	3.973	4.653 (73)	4.611	4.613
B(E2; I+1→I+3)	2.729 (41)	2.683	2.720	2.120 (51)	2.117	2.193
B(E2; I+2→I+3)	2.974 (60)	2.948	2.905	3.778 (96)	3.842	3.789
Q_{20}		10.295 (12)	10.303 (13)		10.619 (10)	10.651 (12)
ζ		0.0	-1.4 (6)x10^{-3}		0.0	-2.5 (5)x10^{-3}
χ^2/DF		1.5	0.5		6.4	1.6

4. Purdue University, West Lafayette, Indiana.
5. C. E. Bemis, Jr., et al., Phys. Rev. C 8, 1466 (1973).
6. D. A. Close, J. J. Malanify, and J. P. Davidson, Phys. Rev. C 17, 1433 (1978).
7. M. Brack et al., Nucl. Phys. A234, 185 (1974).
8. J. Libert and P. Quentin, Phys. Rev. C 25, 571 (1982).

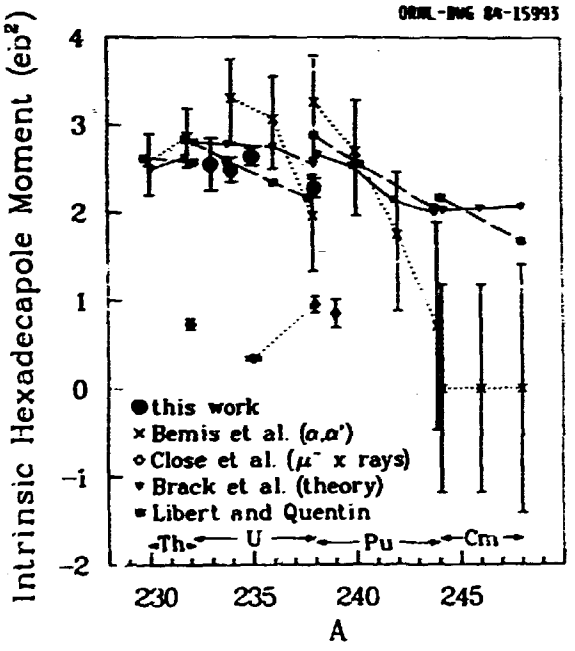

Fig. 2.69. The intrinsic hexadecapole moment vs. A, for thorium, uranium, plutonium, and curium isotopes. The legend indicates the sources of the data plotted. Values for isotopes of the same element are connected by dashed or solid lines. (Bemis et al., Ref. 5; Close et al., Ref. 6; Brack et al., Ref. 7; Libert and Quentin, Ref. 8).

LIFETIMES OF HIGH-SPIN STATES IN ^{162}Yb

F. K. McGowan, I. Y. Lee, N. R. Johnson, C. Baktash, Y. Schutz[1], A. J. Larabee[2], J. C. Wells[3]

The interplay of collective rotations and single-particle excitations determines the structure of neutron-deficient rare-earth nuclei at high spins. It is generally thought that many nuclei which have prolate shapes in their ground states will have a tendency to move toward oblate shapes at higher spins in part due to the alignment of angular momentum along the rotation axis. The discontinuities observed in the yrast sequence of even-A nuclei near N = 90 around spins of 14 or 16 are mainly due to the alignment of an $i_{13/2}$ neutron pair. These changes in the single-particle structure are expected to influence also the collective properties of the nucleus. The alignment of the nucleon orbits and its polarizing effect on a soft nuclear core should result in a deformation change and in particular in a loss of the axial symmetry of the nucleus. Additional deformation changes may be caused by the centrifugal force acting in fast rotating nuclei. Therefore, E2 matrix elements along the yrast line should provide information on the two parameters ϵ_2 and γ describing the quadrupole deformation of a nucleus as a function of rotational frequency.

To search for possible shape changes, we have measured the lifetimes of high-spin states in ^{162}Yb by means of the recoil-distance method. The nuclei were populated by the reaction ^{116}Cd (^{50}Ti, 4n) at a center-of-mass energy of 150 MeV. The recoil distance device was designed to fit in the annular opening of a 25-cm and 25-cm NaI crystal which acts as a total-energy filter and thus provides some selectivity of reaction channel. The recoil velocity v = 7.177 ± 0.048 μm/ps (v/c = 2.394%). Spectra were obtained at 13 recoil distances ranging from 16 to 5000 μm. The complexity of the γ spectra limits the number of useful decay curves extracted from the data. For example, the γ spectra of $^{161-163}$Yb contain ≈150 γ rays or 300 peaks (shifted + unshifted). In addition there are γ rays from the (n,nγ) reaction on the materials in the recoil distance device (F, NaI, Al, Fe, Ni). For instance, the 439.7 keV γ ray from ^{23}Na (n,nγ) matches the $10^+ \rightarrow 8^+$ transition of 439.2 keV in ^{162}Yb. Four multiplets (γ rays of equal energy) exist in ^{162}Yb. Also, the upbend in the continuation of the ground-state band at the 18^+, 16^+, and 14^+ states gives rise to 3 transitions of nearly equal energy.

The time dependence of any decay curve is determined by the lifetime of the initial state of the observed transition and by the time structure of the cascades feeding into this initial state. The feeding of a particular level, in general, proceeds via experimentally observed discrete transitions. However, a fraction of the intensity is fed into the level through many complex paths (side feeding). The side feeding from the quasi-gamma continuum into a particular level was modeled either by the decay of two states which share the feeding intensity or by the time distribution of a rotational cascade with parameters based on an effective moment of inertia, an average transition moment Q_t, and an average γ-multiplicity (number of steps in the feeder cascade).

The transition quadrupole moments Q_t, extracted from the reduced transition probabilities along the yrast line

$$B(E2;I\rightarrow I-2) = \frac{5}{16\pi} \langle I\ 2\ 0\ 0 \mid I-2\ 0 \rangle^2 Q_t^2,$$

are plotted versus the rotational frequency which is obtained from $\hbar\omega = E\gamma/2$ for $I\rightarrow I-2$ transitions of K = 0 bands. Although the uncertainties are large, the data shown in Fig. 2.70 for the ground band of ^{162}Yb are not inconsistent with an enhancement of collectivity for rotational frequencies $\hbar\omega < 0.27$MeV. The Q_t for

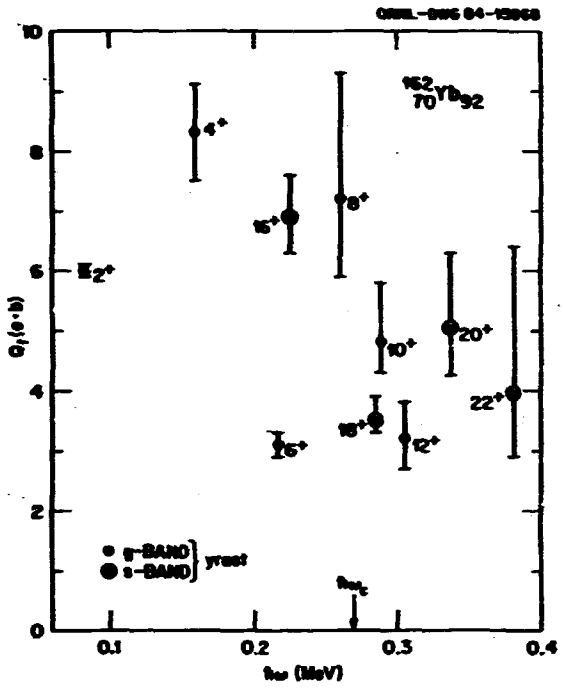

Fig. 2.70. Transition quadrupole moments of some yrast states of ^{162}Yb as a function of the rotational frequency.

the 6^+ state is anomalously small and difficult to understand (the $6^+ \rightarrow 4^+$ transition in ^{156}Dy was observed to be low). Bochev et al.[4] published Q_t values for the 2^+, 4^+, 6^+, and 8^+ states of 6 e-b based on a very limited knowledge of the level scheme of ^{162}Yb. An analysis of our data with this level scheme yields Q_t values in agreement with values given by Bochev et al., but the quality of fit is poor because of the intensity imbalance of the intraband transitions $I \rightarrow I-2$.

Above $\hbar\omega$ = 0.27 MeV, the crossing frequency at which a pair of $i_{13/2}$ quasineutrons align, there appears to be a significant decrease of Q_t to a value of 4.5 e-b in both the g- and s-bands. The missing interband yrast transition $14^+ \rightarrow 12^+$ implies a very weak interaction strength between the 0-quasiparticle g-band and the 2-quasiparticle s-band. One might consider the yrast band as the continuation of the g-band. However, its g-band character does not prevail; instead, upbending occurs at $\hbar\omega$ = 0.31 MeV. The extracted aligned spin $i(\omega)$ is about 8$\hbar$ compared to 10$\hbar$ at the first backbend. This upbending could be attributed to the alignment of a second less favored $i_{13/2}$ quasineutron pair.

The level structure in ^{162}Yb is very similar to ^{156}Dy, i.e., backbend at $\hbar\omega$ = 0.29 MeV followed by an upbend at $\hbar\omega$ = 0.34 MeV. Emling et al.[5] at GSI have already published an extensive set of quadrupole transition moments Q_t between states whose structure is influenced mainly by quasiparticle excitations. Therefore, it is of interest to compare the limited results from ^{162}Yb with those from ^{156}Dy. Below the first backbend in ^{156}Dy the Q_t values increase from 6 to 7.5 e-b with increasing rotational frequency. The Q_t values are clearly retarded at $\hbar\omega$ > 0.29 MeV compared with $Q_t \approx$ 7.5 e-b reached in the g-band just below the onset of quasiparticle alignment. The overall trend of Q_t from the less extensive results of ^{162}Yb with $\hbar\omega$ is similar to the results from ^{156}Dy. The loss of collectivity could indicate either a decrease of ε_2 deformation or a positive γ deformation or a combination of both. Self-consistent HFB calculations by Bengtsson et al.[6] for the N = 90 nucleus ^{160}Yb suggest potential-energy surfaces which are very flat in the vicinity of the minimum. Therefore, aligned quasiparticles moving in oblate orbitals can easily polarize the nuclear core, i.e., change the mass distribution in the equatorial plane of the prolate core yielding a triaxial shape. However, the observed reduction of collectivity at the larger rotational frequencies implies a greater degree of triaxiality than recent calculations predict.

---

1. On leave from CRN, Strasbourg, France.
2. University of Tennessee, Knoxville, TN.
3. Tennessee Technological University, Cookeville, TN.

4. B. Bochev et al., Nucl. Phys. A267, 344 (1976).
5. H. Emling et al., Nucl. Phys. A419, 187 (1984).
6. R. Bengtsson et al., Nucl. Phys. A405, 221 (1983).

SPIN AND TEMPERATURE DEPENDENCE OF THE MULTIPOLARITY OF THE γ-RAY CONTINUUM

D. G. Sarantites[1] J. J. Gaardhoje[2]
F. A. Dilmanian[1] J. D. Garrett[2]
M. Rajagopalan[1] S. Pontoppidan[2]
M. Jääskeläinen[1,3] P. J. Nolan[5]
H. Puchta[1,4] Th. Lindblad[6]
R. Woodward[1] J. R. Beene
K. Honkanen[1] M. L. Halbert
T. Semkow[1] D. C. Hensley
B. Herskind[2] I. Y. Lee
G. B. Hagemann[2] W. T. Milner
G. Sletten[2] F. Plasil
J. Hattula[3]

Previous studies of the multipolarity of the γ-ray continuum from rotational nuclei, based either on angular distributions or on internal-conversion coefficients, have led to conflicting results. In particular, some data on internal conversion[7] indicate that the high-energy continuum is purely E1 while results obtained at the Holifield laboratory[6] show that there are significant M1 or E2 contributions. We present here preliminary results from the Spin Spectrometer in which γ-ray angular distributions were obtained with respect to the spin direction of the emitting nucleus.

The method of determining the spin alignment was first used in Ref. 9, and may be outlined briefly as follows. The γ-ray cascade from decay of rotational nuclei is dominated by stretched E2 transitions (i.e., ΔI = -2) which have a toroidal intensity pattern about the axis of the emitting nucleus. By searching for the plane of maximum γ-ray intensity, a computer program can deduce the most probable direction of the spin alignment for each event. Applying this method to a sequence of events, the program builds up the angular distribution of the γ rays as a function of β, the angle between the observed γ ray and the nuclear spin.

The data presented here are from reactions of 230-MeV ^{50}Ti on ^{124}Sn, one of 49 targets bombarded in a survey experiment.[10,11] The compound nucleus is ^{174}Hf and the high-spin entry states selected here belong mainly to ^{171}Hf. Similar data have been obtained for other targets of the survey.

The full analysis involved several steps before the angular distributions could be generated. First, 15 regions of (H,k) space were defined (H = sum of NaI pulse height, k = number of responding detectors per event). These correspond to average γ-ray multiplicities M_γ = 16, 20, 23, 27, and 30, and to three cuts in excitation energy above the yrast line. Next, the raw NaI spectra for each (H,k) region were unfolded (i.e., corrected for detector response, including scattering and summing effects, on the basis of measurements with γ-ray sources). The lower part of Figs. 2.71 and 2.72 give examples of E_γ spectra for low and high excitation in the M_γ = 27 region.

The spectrum in Fig. 2.71 shows a sharp drop in intensity at E_γ ~1.3 MeV, the upper edge of the so-called yrast bump known to consist of stretched E2 transitions. At higher E_γ, the characteristic statistical spectrum can be observed. It can be represented by $N_\gamma = C\,E_\gamma^3 \exp(-E_\gamma/T)$, where T is the nuclear temperature. The three cuts in excitation energy chosen for this analysis correspond to T = 0.4, 0.7, and 1.0 MeV. For the T = 1.0 cut (Fig. 2.72), the edge of the yrast bump occurs at higher E_γ, as expected for a rotational nucleus. However, an unexpected feature is the slow approach to the $E_\gamma^3 \exp(-E_\gamma/T)$ shape seen well above the yrast bump. The excess transitions in the intermediate region amount to 0.5 to 1.5 per cascade.

The next step was to create angular distributions, as outlined above, for the 80-keV E_γ bins shown in Figs. 2.71 and 2.72. (At high E_γ adjacent bins were combined to maintain reasonable statistics.) Examples for two E_γ bins are shown in Fig. 2.73 for the highest region in (T, M_γ) space.

The angular distribution for stretched dipoles (ΔI = -1) is readily distinguishable from that for stretched quadrupoles (ΔI = -2), allowing the quadrupole fractions shown in the upper part of Figs. 2.71 and 2.72 to be deduced. The yrast bump, as expected, is 100% quadrupole. At low E_γ there is a dipole component that we have reported earlier[12] in the light Yb isotopes. A new feature is that the quadrupole-like angular distribution extends beyond the upper edge of the yrast bump and seems to be

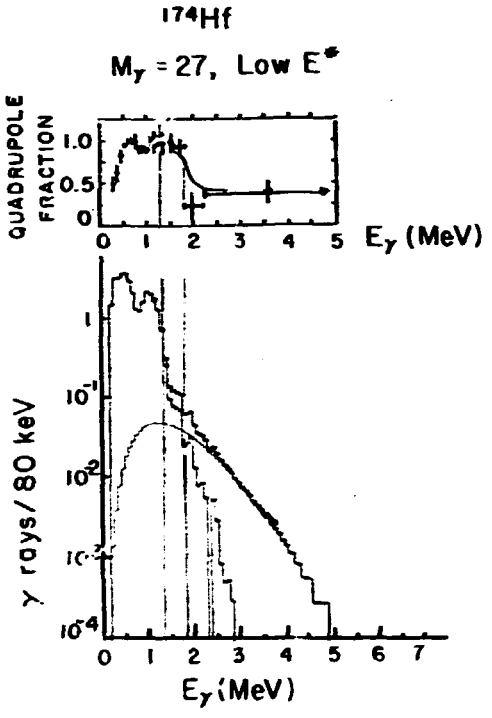

Fig. 2.71. Energy spectrum (lower part) and quadrupole fraction (upper part) as a function of E_γ for the region with average M_γ = 27 and low excitation. The yrast bump ends at 1.3 MeV but the stretched quadrupole-like character continues to about 1.6 MeV. The curve with the broad peak at about 1 MeV is a fit to the expression $CE_\gamma^3 \exp(-E_\gamma/T)$ with T = 0.4 MeV.

associated with the excess yield noted in Fig. 2.72. Unstretched dipoles (ΔI = 0) have an angular distribution similar to that of stretched quadrupoles. They can be distinguished by the sign of the A_4 coefficient, but A_4 is not defined adequately with the present data. If the excess transitions were due to collective quadrupoles, their yield and energy would increase with I for a given T; the data do not show this feature. The other possibility, that they are unstretched dipoles, is consistent with our conversion-electron results.[8] The two pieces of data taken together indicate that the excess yield centered at E_γ ~2.2 MeV is due to unstretched M1 transitions. It is interesting to note that Chen and Leander[13] have predicted the existence of ΔI = 0 M1 transitions at ~2.3 MeV in similar nuclei for bands with small signature splitting.

---

1. Washington University, St. Louis, MO 63130.
2. Niels Bohr Institute, Copenhagen, Denmark.
3. Present address: University of Jyväskylä, Finland.

4. Present address: Sektion Physik, Universität München, 8046 Garching, West Germany.
5. Liverpool University, Liverpool, U.K.
6. Research Institute for Physics, Stockholm, Sweden.
7. S. J. Feenstra et al., Phys. 80B, 183 (1979).
8. L. Westerberg et al., Phys. Rev. Lett. 41, 96 (1978).
9. F. A. Dilmanian et al., Phys. Rev. Lett. 49, 1909 (1982).
10. D. G. Sarantites et al., ORNL-6004, 110 (1983).
11. J. J. Gaardhøje et al., Phys. Scripta T5, 178 (1983).
12. M. Jääskeläinen et al., Phys. Rev. Lett. 49, 1387 (1982); Phys. Lett. 119B, 65 (1982).
13. Y. S. Chen and G. A. Leander, Proc. Conf. on High Angular Momentum Properties of Nuclei, ed. N. R. Johnson, pp. 327-338 (1982).

ORNL-DWG 84-17213

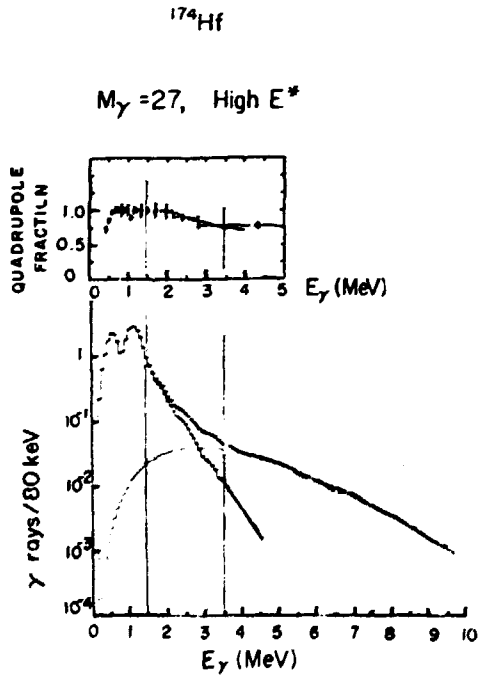

Fig. 2.72. Same as Fig. 2.71 for high-excitation region (T = 1.0 MeV). The upper edge of the yrast bump occurs at E_γ ~1.4 MeV, but the quadrupole-like character of the radiation persists to considerably higher E_γ than in Fig. 2.71. The excess yield of γ rays above the yrast bump that is not accounted for by the $E_\gamma^3(-E_\gamma/T)$ shape is larger than in Fig. 2.71.

ORNL-DWG 84-17684

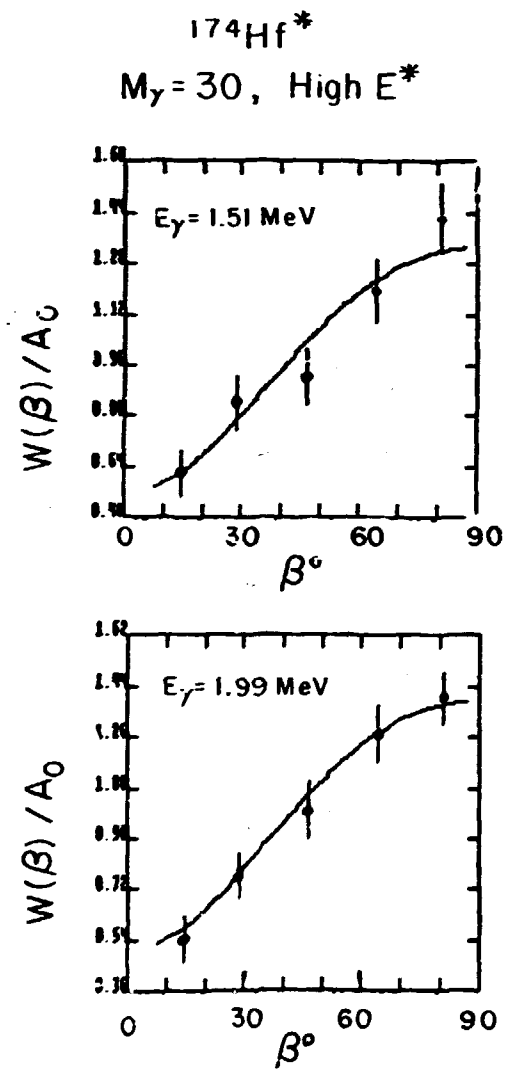

Fig. 2.73. Gamma-ray angular distributions with respect to the spin direction of the emitting nucleus for the (H,k) region corresponding to T = 1.0 MeV, M_γ = 30. Data are shown for two bins of γ-ray energy.

REACTION MECHANISM FOR ONE AND TWO PARTICLE TRANSFER WITH VERY HEAVY IONS

M. W. Guidry[1]
S. Juutinen[1]
X. T. Liu[1]
C. R. Bingham[1]
A. J. Larabee[1]
L. L. Riedinger[1]
L. H. Courtney[1]
C. Baktash
I. Y. Lee
M. L. Halbert
M. P. Fewell
D. Cline[2]
B. Kotlinski[2]
A. Bäklin[2]
D. Sarantites[3]
T. M. Semkow[3]
K. Honkanen[3]
M. Rajagopalen[3]

It has been suggested that transfer reactions with very heavy ions (A > 40) might hold

considerable promise as a tool for studying nuclear structure.[4,5] Resolution of the closely spaced collective states excited by heavy ions is achieved most easily using high resolution Ge γ-ray detectors to observe the deexcitation gamma rays in coincidence with the scattered ions. To reconstruct the initial distribution one needs the γ-ray feeding pattern. The non-yrast portion of the transfer population will decay to the yrast line by emission of a quasi-continuum cascade of γ rays, with individual transitions difficult to resolve. Both the population of discrete states on or near the yrast line, and the population of the quasicontinuum present unique opportunities to study nuclear structure. However, to fully exploit these opportunities it is necessary to separate these two portions of the population. To do so requires both total energy and angular momentum information for the states populated.

Here, we report on the use of the ORNL Spin Spectrometer[6] to measure total γ-ray energies and multiplicities for heavy-ion transfer reactions populating high spin states in the reaction ^{161}Dy (^{58}Ni, ^{59}Ni) ^{160}Dy, with the E_{lab} = 270 MeV ^{58}Ni beams (giving $\theta_{LAB} \sim 130°$) produced by the Holified Heavy Ion Research Facility.

The experimental procedure involves detection of γ rays by Ge detectors in coincidence with scattered beam-like and projectile-like fragments which are observed using large solid angle position-sensitive parallel-plate avalanche detectors. Each particle-particle-γ coincidence triggers the Spin Spectrometer, which is used to determine the total energy and multiplicity of the resulting γ-ray cascade in the standard manner.[6]

Figure 2.74 shows the total energy-multiplicity (E,M) spectrum gated on the strong ground-band transitions in ^{160}Dy. In addition, we show as a dashed line the lowest contour only for the corresponding inelastic excitation of ^{161}Dy. The (E,M) distribution is clearly quite different for the two reactions.

The yrast line sketched in Fig. 2.74 is that for ^{160}Dy. It represents the total energy and multiplicity expected if the yrast line of ^{160}Dy and ground state of ^{59}Ni were populated in the transfer, and is deduced from the known energies in the ^{160}Dy yrast band by assuming that the transitions are stretched E2's near the yrast line, and that the spin spectrometer multiplicity is corrected to account for the trigger γ ray, and the mostly internally converted $2^+ \rightarrow 0^+$ transition. In addition, ~ 400 KeV is added to the total energy to account for these missing γ-rays. This prescription is consistent when checked against the expected results for the Coulomb excitation reaction ^{162}Dy(^{58}Ni, ^{58}Ni') ^{162}Dy, and is expected to be most reliable near the bottom of the distribution in Fig. 2.74. The narrow width of the distribution of total energy with multiplicity leaves little room for statistical transitions. Therefore, the prescription relating multiplicity to spin for the yrast line may be applied to the whole distribution of Fig. 2.74 with an error not much beyond the resolution in M (typically 1-2 units). With this assumption, Fig. 2.74 becomes a map of the cross section for populating a

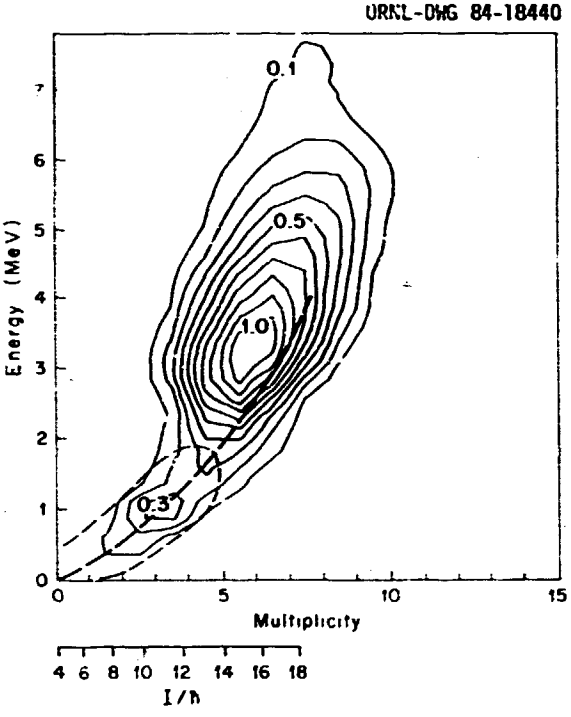

Fig. 2.74. The total energy - multiplicity (E,M) distribution for the transfer reaction ^{161}Dy(^{58}Ni,^{59}Ni)^{160}Dy (solid lines) and the inelastic reaction ^{161}Dy(^{58}Ni,^{58}Ni')^{161}Dy (dashed line, outer contour only). The distributions are gated on the strong ground band transitions in ^{160}Dy and ^{161}Dy respectively, as observed by the Ge detectors. The heavy dashed line represents the ^{160}Dy yrast line. Events below it reflect finite resolution. The estimated resolution in E and M is about 40%.

given differential element of total energy and angular momentum in the internal structure of the ^{59}Ni and ^{160}Dy product nuclei.

Figure 2.75 shows a cranked shell model calculation[7] for bands near the yrast line in ^{160}Dy. The average alignment is ~ 6 ħ for the low lying bands in this region. A theoretical model for transfer to the quasicontinuum will be discussed separately.[8] Essentially kinematic effects associated with Q-windows, L-windows, and binding energies of the transferred particles conspire in the reaction ^{161}Dy(^{58}Ni,^{59}Ni) ^{160}Dy to limit strong transfer to a band of states lying within 1-2 MeV of the yrast line (inset to Fig. 2.75). The dominant factor in this case is that excitation above the yrast line requires the removal of more tightly bound particles from ^{161}Dy. This strongly suppresses the form factor for transfer greater than 1-2 MeV above the yrast line, unless particles are transferred between heated nuclei with particles excited before transfer to less tighly bound states. The population pattern seen in Fig. 2.74 provides direct evidence for a cold mechanism giving large cross sections for

ORNL-DWG 84-18441

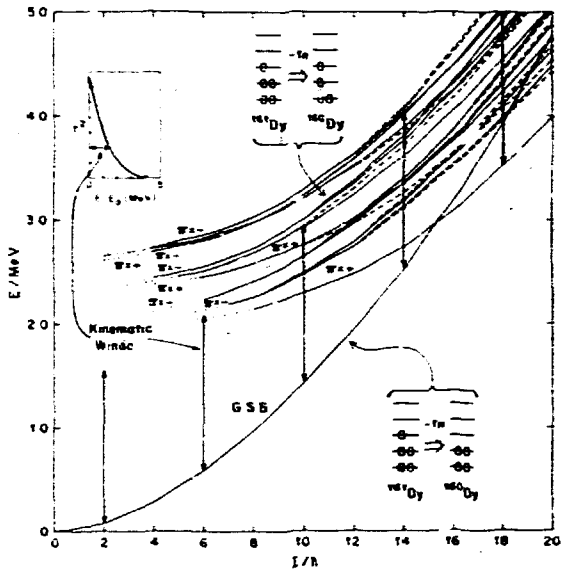

Fig. 2.75. Low-lying bands in ^{160}Dy calculated using the cranked shell model with parameters reflecting the standard systematics in this region. The kinematic window discussed in the text is indicated by the inset and the arrows, and strongly suppresses transfer to states lying outside the window. The other insets indicate schematically the kind of pickup process populating the bands.

transfer between very heavy ions if ground-state Q-values are chosen properly. This cold transfer mechanism is obviously significant for using these reactions as spectroscopic tools, and for a general understanding of heavy-ion reaction mechanisms. In addition, it raises interesting possibilities for populating states and nuclei inaccessible to other reactions.

The qualitative and even quantitative features of the population distribution are easily understood. Because of the pairing gap, at low angular momenta (I < 10) only the ground band, and possibly a few collective bands, lie in the kinematic window. The population in the lower maximum of Fig. 2.74 primarily represents direct population of the ground band. The width of the lower portion of the distribution is consistent with the inherent total energy resolution of the experiment. As the angular momentum is increased the 2-quasiparticle states come down relative to the yrast line. Above I ~ 10 the 2-quasiparticle bands begin to fall within the kinematic window, and the sudden broadening of the total energy distribution represents the kinematic accessibility of those non-yrast bands. The peak in this non-yrast population lies ~ 500-1000 keV above the yrast line at I ~ 14-16. This is where, naively, one would expect the aligned bands to be strongly populated, that is, 8-10 units of collective angular momentum (peak of the lower minimum) plus ~ 6 units of aligned angular momentum gives the angular momentum of the upper maximum, and the excitation above yrast coincides quantitatively with the level density of aligned bands in Fig. 2.75, weighted by a kinematic factor decreasing approximately exponentially with energy above the yrast line. This qualitative discussion neglects the differences among spectroscopic factors for different aligned bands. This should be included to provide more stringent tests of high-spin models.

This analysis assumes that the amount of collective angular momentum is the same for transfer to the ground and aligned bands. This is not generally true, due to the angle dependent form factor discussed theoretically in Refs. 4 and 5, and for which we provide experimental evidence below. However, it should be a good assumption for the average properties of a group of bands.

These simple considerations account for all the basic features of the quasicontinuum spectra in a natural way. This implies that the data of Fig. 2.74 are related directly to the density of 2-quasiparticle states as a function of energy and angular momentum, and provides clear evidence for a gap between the ground and excited 2-quasiparticle states which decreases with angular momentum.

---

1. University of Tennessee, Knoxville, TN.
2. University of Rochester, Rochester, NY.
3. Washington University, St. Louis, MO.
4. M. W. Guidry, T. L. Nichols, R. E. Neese, J. O. Rasmussen, L. F. Oliviera, and R. Donangelo, Nucl. Phys. A361, 275 (1981).
5. C. H. Dasso, T. Dossing, S. Landowne, R. A. Broglia, and A. Winther, Nucl. Phys. A389, 191 (1982).
6. M. Jääskeläinen, et al., Nucl. Inst. and Meth. 204, 385 (1983).
7. R. Bengtsson and S. Frauendorf, Nucl. Phys. A327, 139 (1979).
8. M. W. Guidry, G. Leander and W. Kincaid, to be published.

CROSS SECTION FOR POPULATION OF HIGH SPIN STATES IN TRANSFER REACTIONS

M. W. Guidry[1] — M. L. Halbert
S. Juutinen[1] — M. P. Fewell
X. T. Liu[1] — D. Cline[2]
C. R. Bingham[1] — B. Kotlinski[2]
A. J. Larabee[1] — A. Bäklin[2]
L. L. Riedinger[1] — D. Sarantites[3]
L. H. Courtney[1] — T. M. Semkow[3]
C. Baktash — K. Honkanen[3]
I. Y. Lee — M. Rajagopalen[3]

We report on the use of the ORNL Spin Spectrometer[4] to measure total γ-ray energies and multiplicities for heavy-ion transfer reactions populating high spin states in the reaction ^{161}Dy(^{58}Ni, ^{59}Ni)^{160}Dy, with the E_{lab} = 270 MeV ^{58}Ni beams (giving θ_{LAB} ~ 130°) produced

by the Holified Heavy Ion Research Facility. Relating the total γ-ray energies and multiplicities to the energy and angular momentum of the states populated allowed separation of the direct population of the yrast line from that feeding the yrast line by quasicontinuum transitions. Moreover, cross sections for one-particle transfer to yrast high-spin states and the near-yrast quasicontinuum were determined.

The experimental procedure involves detection of γ-rays by Ge detectors in coincidence with scattered beam-like and projectile-like fragments which are observed using large solid angle position-sensitive parallel-plate avalanche detectors. Each particle-particle-γ coincidence triggers the Spin Spectrometer, which is used to determine the total energy and multiplicity of the resulting γ-ray cascade in the standard manner.[4]

Discrete lines up to the $18^+ \rightarrow 16^+$ yrast transition are seen for the reaction product ^{160}Dy. Peak intensities range from ~ 200 counts for the $18^+ \rightarrow 16^+$, to ~ 30,000 counts for the $4^+ \rightarrow 2^+$ transition. No strong channels other than inelastic scattering and 1-neutron pickup are seen, and the spectrum quality is comparable to that for sub-barrier reactions. In a separate contribution in this report we show the total energy-multiplicity (E,M) spectrum gated on the strong ground-band transitions in ^{160}Dy. There, the general features of the quasicontinuum transfer population are discussed. In this contribution we discuss the population of the discrete states.

For the discrete yrast states observed in the transfer spectrum it is possible to be more specific than in the case of the quasicontinuum. By gating in the (E, M) plane to exclude the feeding from the quasicontinuum, a Ge spectrum may be constructed for direct population of the yrast states. The cross sections for direct population of individual yrast states may be deduced from this Ge spectrum by correcting for feeding. The results are shown in Fig. 2.76, along with the corresponding cross sections for the inelastic scattering reaction ^{162}Dy(^{58}Ni, ^{58}Ni')^{162}Dy, which should be quite similar to that expected for the inelastic reaction ^{160}Dy (^{58}Ni,^{58}Ni')^{160}Dy. No special provision was made in the experiment to detect the low energy and highly converted $2^+ \rightarrow 0^+$ transition, so only states with $I^\pi > 4^+$ are shown. Note that because the total energy resolution is several hundred keV, and the multiplicity resolution is 1-2 units, such (E, M) gating also might include some non-yrast states. However, a detailed comparison of the yrast gate in the transfer data to the corresponding gate in the inelastic scattering (assumed mostly yrast) shows that up to $I \sim 12^+$ the transfer yrast gate contains less non-yrast population than the experimental uncertainty in the population. This conclusion is buttressed by the absence of any strong peaks representing decay of non-yrast to yrast states. Within the yrast gate below spin 12 the level densities should be sufficiently low that, if non-yrast states are populated, the deexcitation γ-rays should be resolved. Above 12^+ the statistics are not good enough to rigorously exclude non-yrast contributions from the cross

ORNL-DWG 84-18442

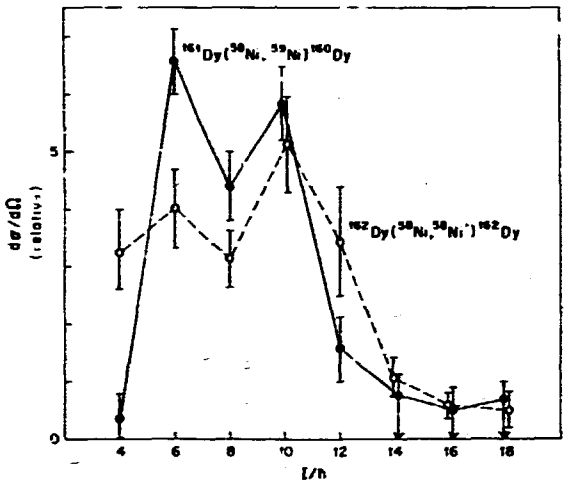

Fig. 2.76. Differential cross sections (arbitrary scale) at the grazing angle for population of ground band states in the transfer reaction ^{161}Dy(^{58}Ni,^{59}Ni)^{160}Dy (solid) and the inelastic scattering reaction ^{162}Dy(^{58}Ni,^{58}Ni')^{162}Dy (dashed).

sections, meaning that the small cross sections for direct population of the 14^+ - 18^+ actually represent upper limits.

The most striking feature of the transfer cross sections is the dramatic suppression of the 4^+ state relative to that seen in inelastic scattering. Such a minimum is too deep to be explained by the standard interferences giving the oscillating cross sections for inelastic scattering, but has a simple explanation in terms of the geometrical surface form factors for transfer discussed in Refs. 5, 6. Population of the ground band of ^{160}Dy requires pickup of the [642] $5/2^+$ neutron from ^{161}Dy if we assume a Nilsson model. For maximum transfer from this orbit, the combination of damping by the imaginary potential, barrier penetration effects, and distribution of the single particle wavefunction on the surface, favors a collision between the heavy ions with approximately a 45° angle between the symmetry axis of the rotor and the line joining the ions at closest approach. This condition favors high collective angular momentum transfer.[5] This is precisely what is suggested in Fig. 2.76, and is the most likely explanation for the extremely low 4^+ cross section.

---

1. University of Tennessee, Knoxville, TN.
2. University of Rochester, Rochester, NY.
3. Washington University, St. Louis, MO.

4. M. Jääskeläinen, et al., Nucl. Inst. and Meth. 204, 385 (1983).
5. M. W. Guidry, T. L. Nichols, R. E. Neese, J. O. Rasmussen, L. F. Oliviera, and R. Donangelo, Nucl. Phys. A361, 275 (1981).

6. C. H. Dasso, T. Dossing, S. Landowne, R. A. Broglia, and A. Winther, Nucl. Phys. A389, 191 (1982).

ANGULAR MOMENTUM TRANSFER IN VERY HEAVY ION DIRECT REACTIONS

M. W. Guidry[1] R. W. Kincaid[1]
R. Donangelo[2]

One- and two-particle transfer reactions with very heavy ions (A>40) provide a unique opportunity to obtain information about single particle wavefunctions and particle-particle correlations for states which are highly collectively excited. The results of several recent experiments[3-6] indicate that large cross sections are being observed for the direct, cold population of collective states in such transfer reactions. Given that these experiments are feasible, it becomes important to realistically estimate how much collective excitation can be present in such systems when the transfer takes place, since the more collective the excitation at the time of transfer, the more sensitive the data is likely to be to the interplay of collective, single-particle, and pairing modes.

We have specifically addressed the case of rotational excitation to determine the amount of angular momentum in the region of the classical turning point, where the transfer is most likely. The reaction is viewed as a process in which there is strong collective inelastic excitation of the entrance channel as the nuclei approach each other, transfer of one or two particles near the distance of closest approach, and strong inelastic excitation in the exit channel as the ions recede from each other.[7] Although the nuclei may be highly collectively excited at the time of transfer, experimental data near the barrier[3] suggest them to be cold (near the yrast line). We presume that for collisions near the barrier it is necessary to describe the inelastic excitation in entrance and exit channels by coupled channels methods, while the transfer itself might be subject to a low order perturbation approach. For present purposes, however, a purely classical calculation may be used to provide a good estimation of the angular momentum transfer near the classical turning point (close agreement of predictions by classical and quantum mechanical coupled channels calculation has been verified for a representative test case.)

Exact classical trajectories for head-on collisions were calculated using a complex Woods-Saxon potential which is a function of the radial separation of the ions r and the angle x between the symmetry axis of the rotor and the line of centers between the ions. For the Coulomb excitation, well-known parameters from the literature were used. A series of inelastic scattering experiments using ^{40}Ar on rare-earth targets[8,9] was used to determine the nuclear potential parameters. The energies for the collision were chosen to bring the ions to a nearest radial separation of $\sim 1.5\ (A_1^{1/3} + A_2^{1/3})$ fm, where the data indicate the transfer cross sections are largest.

Figure 2.77 shows calculations of the collective angular momentum in the classical rotor near the turning point, weighted by the transfer form factor, for several heavy ions on a representative rare earth target and a representative

ORNL-DWG 84-18443

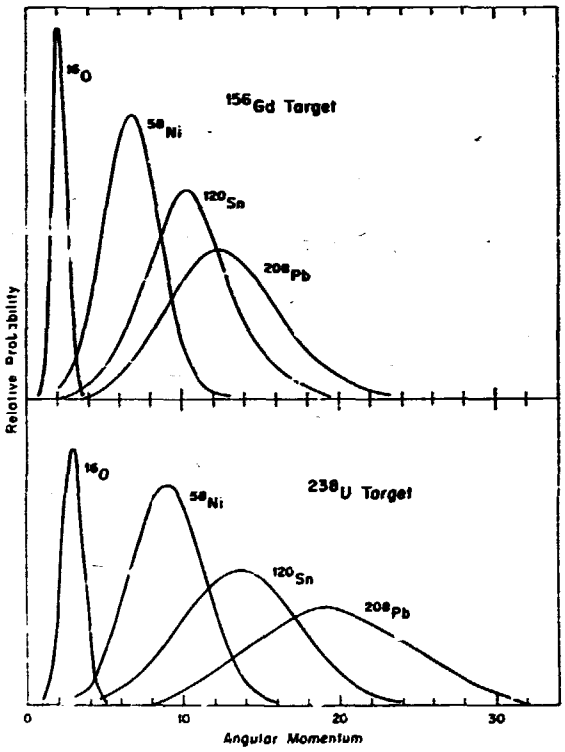

Fig. 2.77. Most likely collective angular momentum when particles are transferred for some representative heavy ion systems.

actinide target. The calculation assumes the transfer probability to be proportional to the square of a form factor, dropping exponentially to one-half of its value at the turning point when the ions are 1 fm outside the turning point. Whereas with oxygen ions we may expect rather small angular momentum transfer, with Sn or Pb the transfer between states with collective angular momenta in the range I ≈ 10-25 h appears quite feasible. These calculations consider only the collective excitation of angular momentum. The transferred particle(s) may also carry angular momentum, which would further increase the angular momentum populated directly by the transfer. Since large nuclear structure modification by collective angular momentum in this angular momentum regime is expected, these reactions hold considerable promise as a spectroscopic tool.

1. University of Tennessee, Knoxville, TN.
2. Niels Bohr Institute, Copenhagen, Denmark.

3. M. W. Guidry, et al., to be published.
4. P. A. Butler, et al., private communication and to be published.
5. A. Machiavelli, et al., private communication and to be published.
6. C. Lauterbach, et al., private communication and to be published.
7. M. W. Guidry, et al., Nucl. Phys A361, 275 (1981).
8. R. E. Neese, et al., Phys. Lett. 85B, 201 (1979); R. E. Neese, Ph.D. Thesis, University of Tennessee, 1981 (unpublished).
9. M. W. Guidry, et al., Nucl. Phys. A430, 485 (1984).

A MODEL FOR HEAVY ION TRANSFER TO THE QUASICONTINUUM

M. W. Guidry[1] R. W. Kincaid[1]
G. A. Leander[2]

In recent experiments we have observed large cross sections populating the region within a few MeV of the yrast line and extending up to I ~ 15-20 by heavy ion transfer reactions on rare-earth nuclei.[3] Since little direct information exists on the structure for nuclei in this regime of temperature and angular momentum, a theoretical understanding of the data being obtained could provide insight into the way nuclei accommodate internal excitation energy and angular momentum. Such information is significant in its own right, but also is important for a detailed understanding of more complicated processes such as deep inelastic collisions, since such reactions may proceed through an initial doorway involving energy transfer by inelastic and few-particle transfer mechanisms.

As a first approximation we might separate the reaction mechanism into that part responsible for the angular momentum, and that part giving rise to internal excitation (heating). Then, since such a separation is surely unrealistic, we may consider the interplay of these effects in the overall reaction mechanism in further work. The beginnings of such an approach are outlined in this report.

We first assume that, for the strongly deformed nuclei and very heavy ions under consideration, the dominant transfer mechanism involves strong inelastic excitation up to the turning point region, transfer of a particle or two, and strong inelastic excitation as the nuclei recede from each other.

With these assumptions, the average angular momentum transfer may be described by inelastic excitation in the entrance and exit channel [illegible] with a spread in angular momentum transferred by the particle. The latter can be estimated from the distribution of single-particle angular momenta available in the excitation region of interest (e.g., using the Cranked Shell Model), and by imposing an L-matching window for the particle transfer. Analytical formulae have been given for such L-windows, and methods for calculating the inelastic excitation have been amply described in the literature.

Here we ignore the angular momentum transferred by the particles and concentrate on the factors governing the total energy of the states populated in the transfer reactions. The yrast lines are taken to define zero temperature for the system and excitation energy is measured from there. To avoid unnecessary confusion, it is assumed for the remainder of the discussion that the reaction involves transfer of one nucleon from a deformed target nucleus to a spherical projectile, and that the spherical projectile accepts the transferred particle in its ground state. All excitations may then be discussed relative to the yrast line of the deformed nucleus.

Then, the probability for the transfer reaction to populate an energy interval lying a distance δ above the yrast line may be expected to depend on three important factors: (1) An optimum Q-window resulting from momentum matching considerations. For neutron transfer the Q-window is approximately a Gaussian centered at a distance from the yrast line given by the ground-state Q-value. Analytical formulas have been obtained for the width. For the heavy nuclei we consider here, the Gaussian Q-window has a full width of ~5 MeV. (2) A radial form factor f(r) which decreases for higher excitation δ above the yrast line as a penalty for transferring more and more tightly bound particles. The square of the form factor may be approximated by

$$f^2(r) \sim \exp\left[-2\sqrt{2m'\hbar^2(S+\delta)}\, r\right]$$

where S is the separation energy for a particle, and δ is the excitation energy relative to the yrast line. Unless the Q-window is shifted far above or below the yrast line, the form factor dependence on excitation energy tends to dominate the Q-window factor. (3) A strength function describing the density of states with suitable structure to be populated in the transfer reaction. This function will depend on energy and angular momentum.

Figure 2.78 compares the square of the product of the Q-window and radial form factors for both the one-particle transfer ^{161}Dy(^{58}Ni,^{59}Ni)^{160}Dy and the two-particle transfer ^{162}Dy(^{58}Ni,^{60}Ni)^{160}Dy. The difference between the two primarily reflects a higher-lying Q-window in the 2-particle transfer reaction. The data[3] indicate that states further from the yrast line are populated in the reaction ^{162}Dy (^{58}Ni,^{60}Ni)^{160}Dy than in ^{161}Dy(^{58}Ni, ^{59}Ni)^{160}Dy. This would be expected from purely kinematic considerations (Fig. 2.78).

Although only a rather idealized model has been outlined here, the kinematical factors (1) and (2) should be amenable to precise calculation in a more realistic model. Comparison of the expected kinematical weighting to the measured distribution of the transfer population might then allow extraction of strength functions as a function of both energy and angular momentum of the states populated in the transfer reaction.

1. University of Tennessee, Knoxville, TN.

2. UNISOR, Oak Ridge Associated Universities.

3. M. W. Guidry, et al., separate contributions to this progress report, and to be published.

ORNL-DWG 84-18444

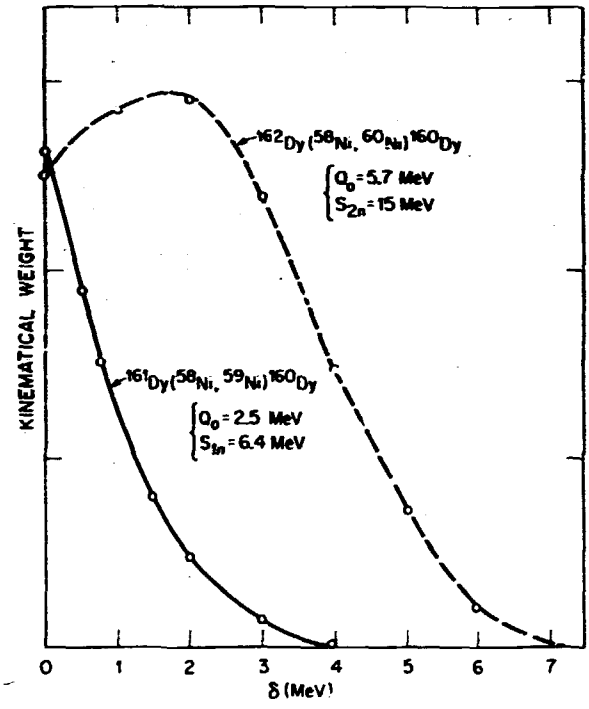

Fig. 2.78. Comparison of the square of the product of the Q-window and radial form factors for both the one-particle transfer ^{161}Dy(^{58}Ni, ^{59}Ni)^{160}Dy and the two-particle transfer ^{162}Dy(^{58}Ni, ^{60}Ni)^{160}Dy.

FISSION FRAGMENT ANGULAR DISTRIBUTIONS FROM ^{12}C- AND ^{16}O-INDUCED REACTIONS[1]

A. Gavron[2]
P. Eskola[3]
A. J. Sierk[2]
J. Boissevain[2]
H. C. Britt[2]
K. Eskola[4]
M. M. Fowler[2]
H. Ohm[5]
J. B. Wilhelmy[2]
S. Wald[6]
R. L. Ferguson

The study of fission fragment angular distributions from heavy-ion-induced fission has been a very active field of investigation during the last two years.[7-16] The interest has been kindled in part by the observation[9] that for very heavy fissioning systems, the fission anisotropy is, as expected, consistent with compact saddle-point shapes provided that light heavy ions (e.g., ^{16}O) are used to induce fission, but that when heavier projectiles (e.g., ^{32}S) are used, the anisotropy is larger than expected, indicating that the fissioning systems are unexpectedly elongated at the time that the angular distribution is determined. Back et al.[9] have suggested that the explanation lies in extra push effects and that the increased anisotropy constitutes a signature for "quasi fission."

We have made fission fragment angular distribution measurements[7,8] for ^{16}O-induced reactions on ^{142}Nd, ^{170}Er, ^{192}Os, and ^{238}U and for ^{12}C-induced reactions on ^{174}Yb, ^{198}Pt, and ^{238}U. The oxygen energies were 140, 250, and 315 MeV, and the carbon energies were 95, 188, and 291 MeV. The standard transition-state model, together with the saddle-point moments of inertia from the rotating finite-range model (RFRM),[7,8] was used to analyze the angular distributions. The number of particles (neutrons) emitted before fission plays an important role in this analysis, and since there is considerable uncertainty associated with this question, the data were analyzed under two extreme assumptions: (1) all neutrons are emitted prior to fission, and (2) no neutrons are emitted before fission. In cases of agreement between theory and experiment, the measured values are expected to fall between the two calculated extremes. This was, in fact, found to be the case for all reactions, except those involving ^{238}U targets, as can be seen in Fig. 2.79. From this and from an examination of other data,[8] it was concluded that the transition-state model (together with RFRM saddle-point shapes) is valid only when the fission barrier is higher than the temperature at the saddle point for a significant number of the partial waves that contribute to fission.

---

1. Summary of paper: Phys. Rev. Lett. 52, 589 (1984).
2. Los Alamos National Laboratory, Los Alamos, New Mexico.
3. Present address: Theoretical Physics Department, University of Helsinki, Helsinki, Finland.
4. Present address: Physics Department, University of Helsinki, Helsinki, Finland.
5. Chemistry Department, Mainz University, Mainz, West Germany.
6. Lawrence Berkeley Laboratory, Berkeley, California.
7. A. Gavron et al., submitted to Physical Review C.
8. A. Gavron et al., Phys. Rev. Lett. 52, 589 (1984).
9. B. B. Back et al., Phys. Rev. Lett. 50, 818 (1983).
10. K. T. Lesko et al., Phys. Rev. C 27, 2999 (1983).
11. H. Rossner et al., Phys. Rev. C 27, 2666 (1983).
12. L. C. Vaz and J. M. Alexander, Phys. Rep. 97, 1 (1983).
13. L. C. Vaz and J. M. Alexander, Z. Phys. A312, 163 (1983).
14. M. B. Tsang et al., Phys. Lett. 129B, 18 (1983).
15. M. B. Tsang et al., Phys. Rev. C 28, 747 (1983).
16. P. D. Bond, Phys. Rev. Lett. 52, 414 (1984).

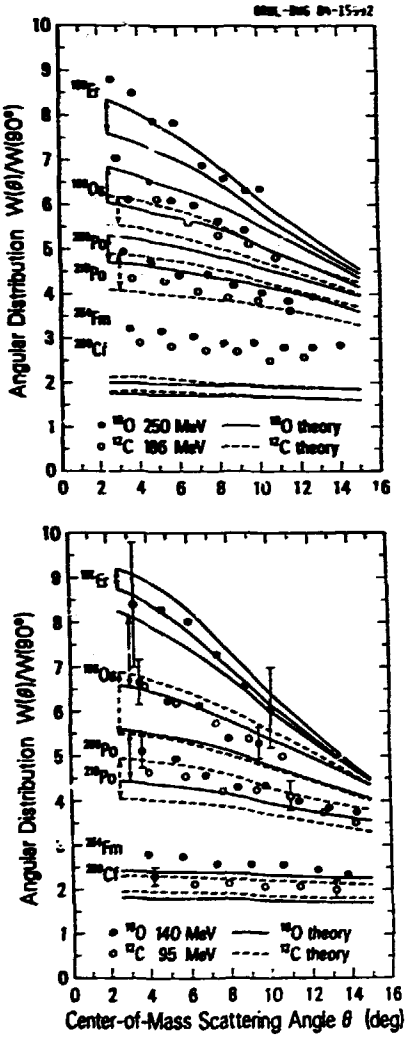

Fig. 2.79. Experimental results of anisotropy in fission-fragment yields. The curves correspond to calculations for each set of data under two extreme assumptions (see text). The full curves are calculations for ^{16}O-induced reactions and the dashed curves are calculations for ^{12}C-induced reactions.

COINCIDENCE MEASUREMENTS BETWEEN EVAPORATION RESIDUES AND LIGHT PARTICLES PRODUCED IN $^{16}O + ^{40}Ca$ AND $^{28}Si + ^{40}Ca$ REACTIONS

C. Maguire[1] H. Ikezoe[2]
Z. Kui[1] D. G. Kovar[2]
W. C. Ma[1] G. Rosner[2]
S. Robinson[1] G. Stephans[2]
D. Watson[1] E. Ungricht[2]
G. Word[1] B. Wilkins[2]
T. C. Awes
G. R. Young

The experimental evidence that preequilibrium or incomplete fusion processes occur in light and medium weight heavy-ion-induced reactions at higher bombarding energies (E_{lab} > 6-3 MeV/amu) comes from the observation of energetic nonstatistical light particles in coincidence with fusionlike products[3,4] and the observation that full linear momentum has not been transferred to the compound nucleus (i.e., the evaporation residues show a velocity deficit[5] and the fission fragments too large a folding angle[6]). At present the details of the reaction mechanism giving rise to the incomplete fusion process are not well understood, and progress has been hindered by the experimental difficulties in quantitatively distinguishing between the contributions from incomplete and complete fusion to the evaporation residue (fission fragment) yields. In the present study the velocity (energy) spectra of evaporation residues and coincident light particles are measured with the motivation of better establishing the kinematics and, hopefully, better understanding the reaction mechanism. Two projectiles, ^{16}O and ^{28}Si, were used to investigate the projectile dependence.

Coincidence measurements of evaporation residues with light particles ($1 < A < 6$) were performed for the reactions $^{16}O + ^{40}Ca$ and $^{28}Si + ^{40}Ca$ with beams of $^{16}O(E_{lab} = 157$ MeV) and $^{28}Si(E_{lab} = 252$ MeV) obtained from the Argonne National Laboratory Superconducting Linac. The masses of the evaporation residues produced at $\theta_{lab} = 9°$ were identified, and their velocity spectra were measured in a channel plate start detector/Si stop detector time-of-flight system with a flight path of ~1.2 m. An example of the mass resolution obtained is shown in Fig. 2.80. The light particles were identified and their energy spectra were measured in six triple-Si detector-telescopes located at $\theta_{lab} = +59°, +28°, -15°, -25°, -40°$, and $-70°$, where the negative angles are on the opposite side of the beam from the time-of-flight detector.

The results of the measurements are presently in the process of being analyzed. The preliminary results from the $^{16}O + ^{40}Ca$ measurement show that the singles evaporation residues ($40 < A < 52$) have velocity centroids 9.4% lower than expected for complete fusion, consistent with the previously reported results of Chan et al.[7] The coincidence measurements show that the foward-angle alpha particles in coincidence with the evaporation residues have energy spectra with a significant high-energy (≈beam velocity) component (see Fig. 2.81), while no such component is apparent in the coincidence proton spectra. The dependence of the evaporation residue velocity spectra and light-particle energy spectra with coincidence angle are not well reproduced by LILITA calculations for complete fusion, and indicate the presence of significant contributions from a reaction process consistent with the kinematics for fusion of $^{12}C + ^{40}Ca$ [assuming $^{16}O + ^{40}Ca \rightarrow ^{12}C + ^{40}Ca + \alpha$ (beam velocity)]. More complete calculations are under way to further substantiate the interpretation suggested by these preliminary calculations.

---

1. Vanderbilt University, Nashville, Tennessee.

2. Argonne National Laboratory, Argonne, Illinois.
3. P. Gonthier et al., Phys. Rev. Lett. 44, 1387 (1980).
4. J. Wilczynski et al., Phys. Lett. 80B, 41 (1979).
5. H. Morgenstern et al., Phys. Lett. 113B, 463 (1982).
6. B. Back et al., Phys. Rev. C 22, 1927 (1980).
7. Y. Chan et al., Phys. Rev. C 27, 447 (1983).

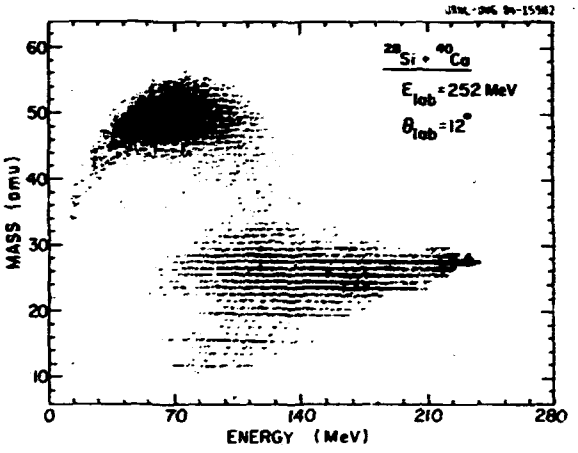

Fig. 2.80. Example of mass resolution attained in the $^{28}Si + ^{40}Ca$ reaction at E_{lab} = 252 MeV.

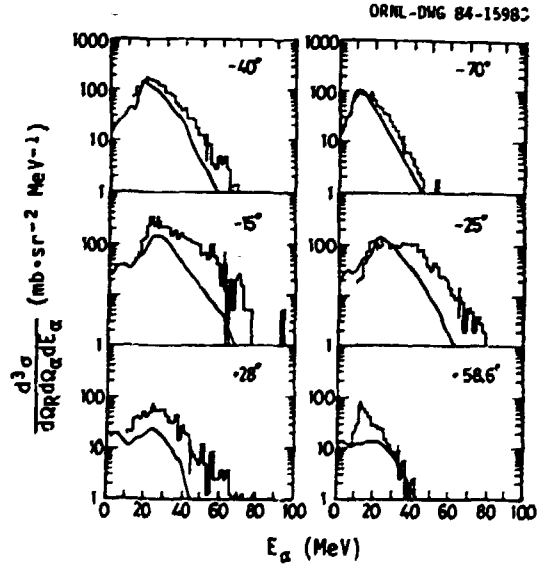

Fig. 2.81. Evaporation residues (mass > 40) observed at 9° in the reactions of 157-MeV ^{16}O with ^{40}Ca. Error bars represent the statistical errors.

NEUTRON EMISSION IN INELASTIC REACTIONS $^{12}C + ^{158}Gd$ AND $^{20}Ne + ^{150}Nd$

G. A. Petitt[1] F. E. Obenshain
A. Gavron[2] F. Plasil
J. R. Beene G. R. Young
B. Cheynis[3] M. Jääskeläinen[4]
R. L. Ferguson D. G. Sarantites[4]
C. F. Maguire[5]

Spectra and angular distributions of neutrons in coincidence with light fragments produced in inelastic collisions of ^{12}C on ^{158}Gd at 192 MeV and of ^{20}Ne on ^{150}Nd at 176 and 239 MeV have been measured. The data were analyzed to determine if the neutron spectra could be explained entirely on the basis of emission from the projectilelike fragments (PLF) and targetlike fragments (TLF) after the fragments have reached the asymptotic velocity due to their mutual Coulomb repulsion or whether there is evidence for some kind of nonequilibrium emission mechanism. No evidence for nonequilibrium neutron emission is found for the Ne + Nd reaction at either energy. For the C + Gd reaction, a small fraction of neutrons (5%) are due to nonequilibrium emission.

For the $^{12}C + ^{158}Gd$ reaction, the small nonequilibrium component appears to be concentrated on the opposite side of the beam from the detector telescope used to measure the energy and charge state of the PLF, although a small component, hidden by the large numbers of neutrons emitted by the PLF and kinematically focused in its direction of travel, may be present on the same side of the beam.

Some of the results of the analysis are given in Figs. 2.82 and 2.83, which show the neutron energy spectra recorded by the neutron detectors on the opposite side of the beam from the telescope. In both figures the uppermost spectrum is closest to the beam (15°), and the bottom spectrum is at the largest angle (140°). The data points (triangles) are shown along with the results of a procedure in which the events recorded in two reference neutron detectors were transformed into the other neutron detectors. One of the reference detectors was located at a back angle and was assumed to detect only neutrons emitted by the TLF. The other detector was directly behind the fragment telescope and was assumed to detect only neutrons emitted by the PLF. The results of the transformation are shown as dots in the figures. As can be seen in the figures, for the Ne + Nd reaction the transformed spectra agree well with the data, whereas for the C + Gd reaction, the data points at forward angles and high neutron energies lie well above the transformed spectra, indicating the presence of nonequilibrium emission in this reaction.

---

1. Georgia State University, Atlanta, Georgia.
2. Los Alamos National Laboratory, Los Alamos, New Mexico.
3. Institut de Physique Nucleaire de Lyon, Villeurbanne, France.

4. Washington University, St. Louis, Missouri.
5. Vanderbilt University, Nashville, Tennessee.

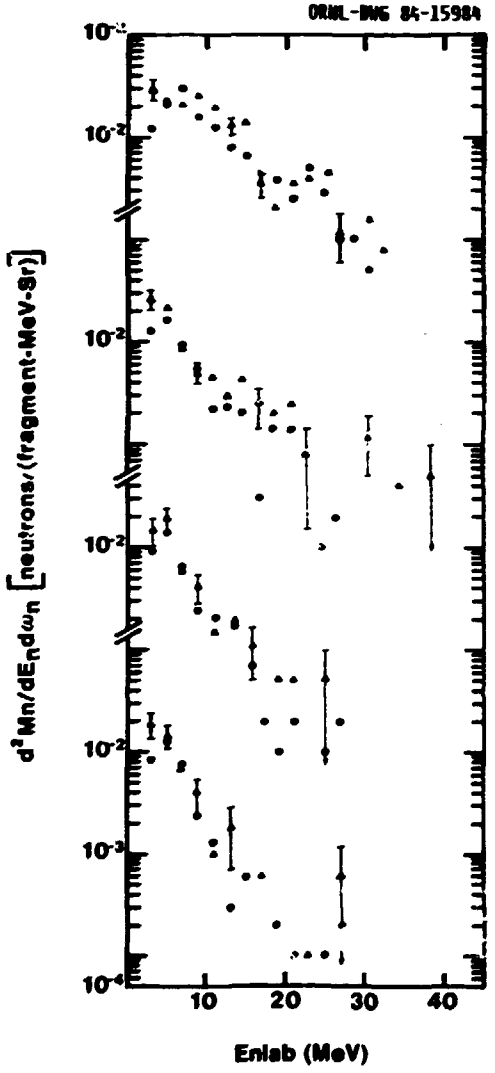

Fig. 2.82. Neutron energy spectra recorded in detectors on the opposite side of the beam from the heavy-ion detector telescope in the reaction $^{20}Ne + ^{150}Nd$ at 239 MeV. The data points (Δ) are shown along with the results of the transformed spectra (•) described in the text.

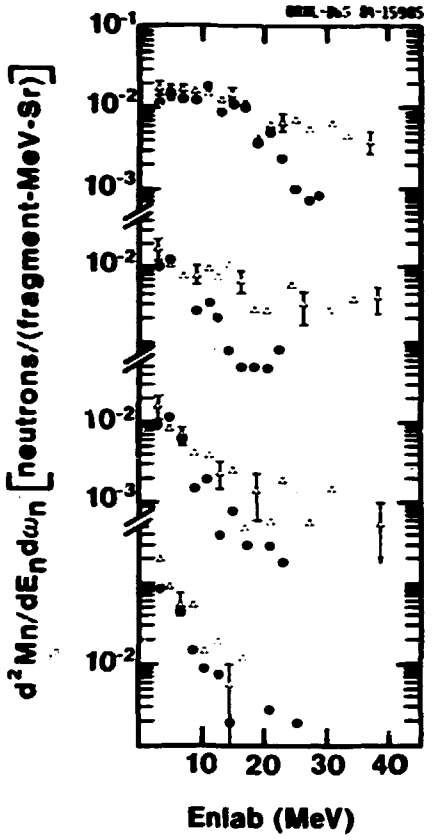

Fig. 2.83. Same as Fig. 2.82, but for the $^{12}C + ^{158}Gd$ reaction at 192 MeV.

AZIMUTHAL CORRELATIONS BETWEEN LIGHT PARTICLES EMITTED IN ^{16}O-INDUCED REACTIONS ON ^{12}C AND ^{197}Au AT 400 MeV

M. B. Tsang[1]
W. G. Lynch[1]
C. B. Chitwood[1]
D. J. Fields[1]
D. R. Klesch[1]
C. K. Gelbke[1]
G. R. Young
T. C. Awes
R. L. Ferguson
F. E. Obenshain
F. Plasil
R. L. Robinson

For intermediate-energy nuclear collisions, particle emission prior to the attainment of full statistical equilibrium of the emitting nucleus is expected to provide information about the early stages of the reaction. The global trends of single-particle inclusive cross sections can be rather well described in terms of the concept of local statistical equilibrium.[2-4]

Recent results from two-proton correlation measurements at small relative momenta are consistent with the emission of energetic light particles from a localized region of high excitation.[5] Additional information about the dynamical and geometrical aspects of the reaction may be obtained from investigations of light-particle correlations. In order to search for such dynamical correlations and to assess the importance of phase-space constraints for small nuclear systems, we have measured azimuthal angular correlations between energetic light particles emitted in ^{16}O-induced reactions on a light (^{12}C) and a heavy (^{197}Au) target at an incident energy of 400 MeV.

Prescaled singles and coincident light particles (p,d,t) were detected using seven telescopes with solid angles between 13 and 40 msr. Three of these telescopes were mounted at the polar angles, measured with respect to the beam axis, of $\theta = 40°$, 70°, and 130° and the azimuthal angle of 0°. The remaining four telescopes were positioned at the polar angles of $\theta = 40°$, 70°, 130°, and 160°; their azimuthal angle was varied between 50° and 130°.

The inclusive energy spectra of protons, deuterons, and tritons detected at $\theta = 40°$ and 70° have been measured. For reactions induced on ^{197}Au, estimated upper limits for emission from the compound nucleus were determined by assuming that the energy spectra measured at $\theta = 160°$ are entirely due to isotropic evaporation from the compound nucleus. The energy spectra at 40° and 70° are dominated by noncompound emission processes. For reactions on ^{12}C, on the other hand, the shapes of the energy spectra are consistent with evaporation from the compound nucleus.

In order to reduce systematic errors, the azimuthal correlation is defined by the ratio of the coincidence cross section divided by the singles cross sections $\sigma_{xy}/\sigma_x\sigma_y$. A low-energy threshold of 36 MeV was applied in computing the cross section. For reactions on ^{197}Au, that threshold strongly reduces contributions from compound nucleus decay. Figure 2.84 shows the azimuthal correlations of two coincident light particles emitted at $\theta = 40°$ and 70°. For reactions on ^{12}C, there is a clear enhancement for the emission of two coincident light particles to opposite sides of the beam axis, Fig. 2.84a. These correlations may be understood in terms of the phase-space constraints imposed by momentum conservation.[6] To illustrate the effect of momentum conservation, we performed schematic calculations[6] for a source of $A_s = 28$ nucleons and temperature $T = 7.1$ MeV moving with the velocity of the compound nucleus, $v_0 = 0.13$ c. To conserve total linear momentum, in these calculations the entire residual source is assumed to recoil after the emission of the first particle. These schematic calculations reproduce the overall trends of the data rather well, indicating that the preferential emission of coincident light particles to opposite sides of the beam axis may be explained in terms of the phase-space constraints imposed by momentum conservation on finite nuclear systems.

Entirely different azimuthal correlations are observed for reactions on ^{197}Au, Fig. 2.84b.

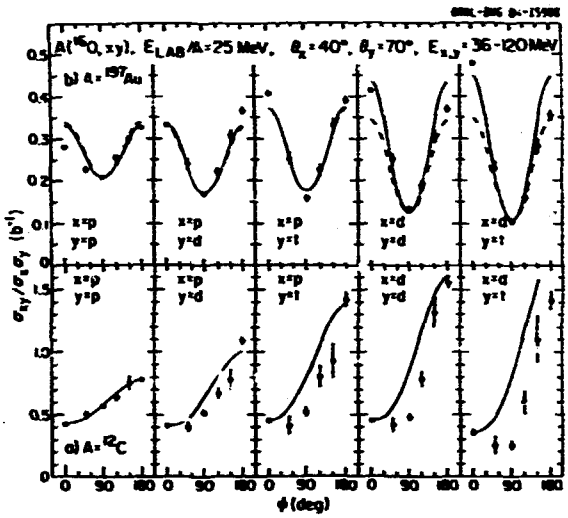

Fig. 2.84. Azimuthal angular correlations between coincident light particles emitted at $\theta = 40°$ and 70° with respect to the beam axis for ^{16}O-induced reactions on ^{12}C (a, lower part) and ^{197}Au (b, upper part) at 400-MeV incident energy. A low-energy threshold of 36 MeV was applied. See text for explanation of solid and dashed curves.

These correlations are nearly left-right symmetric about the beam axis and exhibit a characteristic "V" shape corresponding to the preferential emission of energetic light particles in a plane which contains the beam axis. Close inspection of the coincidence cross sections at $\phi_x = 0°$ and 180° shows a small enhancement for the emission of coincident protons to opposite sides of the beam axis. Coincident deuterons and tritons, on the other hand, are preferentially emitted to the same side of the beam axis.

The preferential emission of coincident light particles in a plane containing the beam axis is consistent with the recent observation[7] that noncompound light particles are preferentially emitted in the entrance-channel scattering plane (defined as the plane which contains the beam axis and which is perpendicular to the semiclassical orbital angular momentum vector for the relative motion between the projectile and target nuclei). These observations could be described by assuming the superposition of a collective motion in the reaction plane on the random motion of the individual nucleons.

The calculations with the rotating hot source parameterization are shown by the solid curves in Fig. 2.84b; they were performed with the parameters $T = 5.6$ MeV, $v_0 = 0.09$ c, $E_C = 10$ MeV, and $R_\omega = 0.1$ c. The calculations for two sideward moving sources are shown as dashed curves in Fig. 2.84a; they were performed with the parameters $T = 6$ MeV, $v_0 = 0.12$ c, $E_C = 10$ MeV, and $\theta_0 = 35°$. Both of these schematic calculations can reproduce the overall trends of the azimuthal correlations rather well.

Except at very forward angles, the emission of energetic light particles is largely associated with fusionlike reactions[7,8] in which the major part of the projectile is absorbed by the target nucleus. Therefore, the above parameterizations must not be interpreted in terms of the emission from one or two hot sources which exist separately from the composite system. In particular, the two-source parameterization should not be interpreted in terms of the sequential decay of excited projectile and target residues. We introduce these parameterizations solely to illustrate the effects which may arise from the superpositions of random and ordered velocity components. The relative success of the two parameterizations may be understood in terms of the relative importance of these two velocity components. The random component decreases for heavier particles, but the ordered velocity component remains constant. As a consequence, heavier particles are more sensitive to the collective motion of the emitting system. Both of these rather simple parameterizations describe the qualitative trends of the data, but they are not unique, and similar agreement may be obtained by other models which superimpose collective and statistical velocity components.

To provide a quantitative comparison of the cross sections corresponding to the emission of coincident light particles to the same (ϕ_x = 0°) and to opposite (ϕ_x = 180°) sides of the beam axis, Fig. 2.85 shows the ratios of these coincidence cross sections, $\sigma_{xy}(\phi_x = 180°)/\sigma_{xy}(\phi_x = 0°)$. For reactions on ^{197}Au this ratio decreases with increasing mass of the two coincident light particles, in contrast to the strong increase measured for reactions on ^{12}C. The dot-dashed and dashed lines in the figure illustrate the effects due to momentum conservation for the case that the momentum of the emitted particle is shared by A_S = 28 and A_S = 40, 60, 90, and 213 nucleons, respectively. (The number A_S should not be identified with the number of "participant" nucleons since momentum may also be transferred to the cold spectator matter.) For these calculations, particles were assumed to be emitted with Maxwellian distributions corresponding to a temperature of T = 7.1 MeV and initial mean velocity parallel to the beam axis of v_0 = 0.13 c (dot-dashed line) and v_0 = 0.11 c (dashed lines). After the emission of a particle of mass number A_x and velocity $\vec{v}_x$, the mean velocity of the second particle was assumed to be changed by $\Delta\vec{v}_0 = A_x \vec{v}_x/(A_S - A_x)$. (The parameters for the source consisting of A_S = 28 nucleons are identical with the parameters used for the calculations shown in Fig. 2.84a.)

Qualitatively, the ratios $\sigma_{xy}(\phi = 180°)/\sigma_{xy}(\phi = 0°)$ might be explained in terms of the competing effects caused by shadowing[9-11] and momentum conservation, although different interpretations may be possible. If preequilibrium emission originates from a localized region of high excitation,[5] absorption or rescattering by the adjacent spectator nuclear matter will enhance emission to the same side of the beam axis. Momentum conservation, on the other hand, will favor emission to opposite sides of the beam axis. Whether coincident light particles

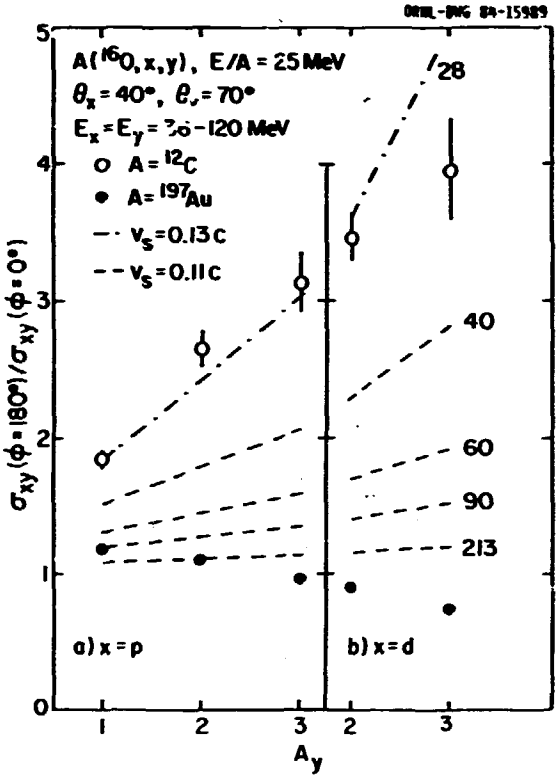

Fig. 2.85. Ratio of cross sections corresponding to emission of coincident light particles to opposite sides and to the same side of the beam axis for ^{16}O-induced reactions on ^{12}C (open points) and ^{197}Au (full points) at 400-MeV incident energy. The dashed and dot-dashed curves illustrate the effects of momentum conservation for systems with finite number of nucleons. The calculations are explained in the text.

are preferentially emitted to the same or to opposite sides of the beam axis will depend on the relative magnitude of these two opposing effects. Absorptive effects are expected to be more pronounced for the emission of composite light particles than for the emission of nucleons. This is in qualitative agreement with the trends measured for reactions on ^{197}Au where it is observed that coincident protons have a slight preference to emerge at opposite sides of the beam axis, whereas coincident composite light particles have a slight preference to emerge at the same side of the beam axis.

---

1. National Superconducting Cyclotron Facility, Michigan State University, East Lansing, Michigan.

2. T. C. Awes et al., Phys. Lett. 103B, 417 (1981).

3. T. C. Awes et al., Phys. Rev. C 25, 2361 (1982).

4. G. D. Westfall et al., Phys. Lett. 116B, 118 (1982).

5. W. G. Lynch et al., Phys. Rev. Lett. 51, 1850 (1983).
6. W. G. Lynch et al., Phys. Lett. 108B, 274 (1982).
7. M. B. Tsang et al., Phys. Rev. Lett. 52, 1964 (1984).
8. T. C. Awes et al., Phys. Rev. C 24, 89 (1981).
9. P. A. Gottschalk and M. Westrom, Nucl. Phys. A314, 232 (1979).
10. I. Tanihata et al., Phys. Lett. 97B, 363 (1980).
11. W. A. Friedman, Phys. Rev. C 29, 139 (1984).

FINAL-STATE INTERACTIONS BETWEEN NONCOMPOUND LIGHT PARTICLES FOR ^{16}O-INDUCED REACTIONS ON ^{197}Au AT E/amu = 25 MeV

C. B. Chitwood[1] M. B. Tsang[1]
J. Aichelin[1] J. C. Shillcock[2]
D. H. Boal[1] T. C. Awes
G. Bertsch[1] R. L. Ferguson
D. J. Fields[1] F. E. Obenshain
C. K. Gelbke[1] F. Plasil
W. G. Lynch[1] R. L. Robinson
G. R. Young

Two-particle correlations at small relative momenta may contain information about the space-time characteristics of the emitting source because of their sensitivity to final-state interactions[3] and quantum statistical effects.[4,5] Previous investigations of the space-time characteristics of highly excited nuclear systems were based on analyses of two-pion[6-9] and two-proton[10-12] correlations. In the only case which allows a direct comparison,[9,10] different source dimensions were extracted from the two measurements. The interpretation of light-particle correlations may be complicated by sensitivities to ensemble averaging,[13] reaction dynamics,[13] momentum conservation,[11] and sequential decay of particle unbound resonances.[14-16] Since correlations between different light particles are expected to exhibit different sensitivities to these effects, we have measured correlations between noncompound protons, deuterons, and tritons emitted in ^{16}O-induced reactions on ^{197}Au at E/amu = 25 MeV. The observed two-deuteron correlations, for example, cannot be interpreted in terms of the decay of particle unstable resonances.

The experiment was performed at the Holifield Heavy Ion Research Facility. A gold target of 9.7 mg/cm^2 was bombarded with ^{16}O ions of 400-MeV incident energy. Small-angle correlations between coincident light particles were measured with six ΔE-E telescopes consisting of silicon ΔE and NaI(Tl) E detectors. The detectors were mounted in a closely packed hexagonal array that was centered at the scattering angle of 15°. Each telescope subtended a solid angle of 7.6 msr; the angular resolution and angular separation between adjacent telescopes were 1.6° and 5.1°, respectively. For a quantitative presentation of the data, we define the correlation function, $R(\vec{p}_1,\vec{p}_2)$, in terms of the singles cross sections, $\sigma(\vec{p}_1)$, $\sigma(\vec{p}_2)$, and the coincidence cross section, $\sigma(\vec{p}_1,\vec{p}_2)$,

$$\sigma(\vec{p}_1,\vec{p}_2) = \sigma_0\, \sigma(\vec{p}_1)\sigma(\vec{p}_2)[1 + R(\vec{p}_1,\vec{p}_2)] , \quad (1)$$

where $\vec{p}_1$ and $\vec{p}_2$ denote the momenta of particles 1 and 2. The normalization constant, σ_0 (used for all correlations shown in Fig. 2.86), was determined previously[11] by requiring the two-proton correlation function to vanish for sufficiently large relative momenta at which final-state interactions are negligible. The experimental correlation functions shown in Fig. 2.86 were obtained by inserting the measured cross sections into Eq. (1) and by summing both sides of the equation over all energies and angles corresponding to a given momentum of relative motion, $\Delta p = \mu|\vec{p}_1/m_1 - \vec{p}_2/m_2|$, where m_1 and m_2 denote the masses of particles 1 and 2 and μ is the reduced mass. This procedure corresponds to a significant averaging process and tends to reduce the measured correlation function.[11]

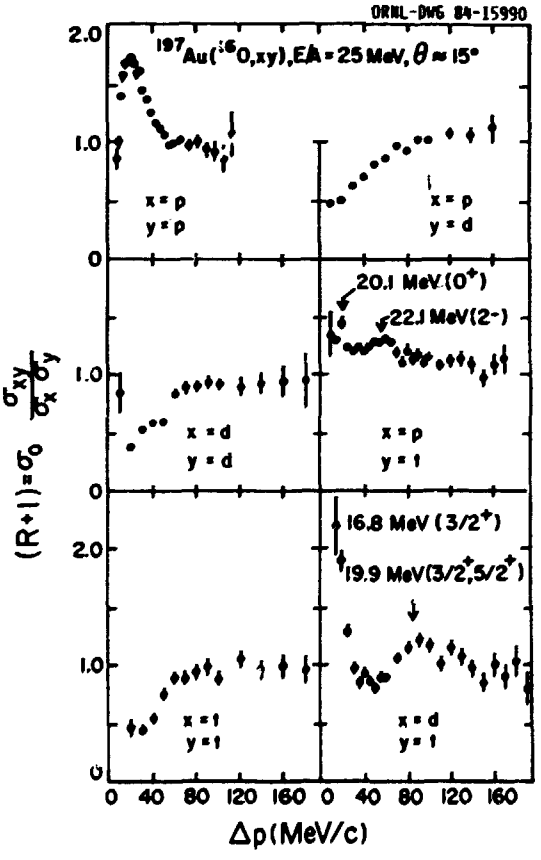

Fig. 2.86. Experimental correlation functions, 1 + R(Δp), plotted as a function of the momentum of relative motion. The locations of several known particle unstable resonances are indicated by arrows. The errors are purely statistical.

The two-proton correlations have been discussed previously.[11] Because of the dominance of the attractive s-wave interaction, correlations arising from the emission and decay of unbound ^{2}He nuclei can be very similar to those caused by final-state interactions between protons randomly emitted from a source of small space-time extent.[14-16] More generally, light-particle correlations resulting from final-state interactions should be more pronounced for systems with sharp resonances. The locations of several known particle unbound states of ^{4}He and ^{5}He, decaying into p + t and d + t, respectively, are indicated by arrows in Fig. 2.86. The enhanced correlations at these locations may be interpreted in terms of final-state interactions or, alternatively, in terms of emission of particle unstable nuclei. However, the strong suppression of the p + d, d + d, and t + t coincidences at small relative momenta cannot be interpreted in terms of the emission and decay of particle unstable nuclei.

In order to illustrate that nonresonant final-state interactions between composite light particles contain useful information about the space-time characteristics of the emitting system, we have extended the treatment of hadron interferometry previously applied to two-proton[3] and two-pion[4,5] correlations to two-deuteron and two-triton correlations. In previous investigations, the emitting region was assumed to be of Gaussian form in space and time, characterized by the parameters r_0 and τ, respectively. In order to reduce the ambiguities resulting from the unknown value of τ and to obtain an upper limit for r_0, we used $\tau = 0$ corresponding to a source of negligible lifetime.

Correlations calculated for $r_0 = 8$ fm are shown in Fig. 2.87a. The attractive potential set (RG) predicts enhanced correlations at Δp = 30 MeV/c. This enhancement becomes more pronounced as r_0 is decreased. In contrast, the repulsive potential set (RM) predicts a suppression of the correlation function at these values of Δp. The data clearly favor the phase shifts extracted by the coupled-channels R-matrix method. (For comparison we also show the correlations predicted for the case of pure Coulomb interaction between the two deuterons; see dot-dashed curve.) In order to illustrate the sensitivity of the calculations to the source radius, we show two calculations for the repulsive potential set (RM) corresponding to $r_0 = 8$ and 4 fm, respectively. Although the two-deuteron correlations appear to be less sensitive to the source dimensions than two-proton correlations, they indicate a large source radius of $r_0 = 8$ fm, compared to the values $r_0 \lesssim 4$ fm extracted from two-proton correlations.[11]

For large source dimensions, the neglect of the short-range nuclear interaction might be a satisfactory approximation. Because of difficulties in obtaining appropriate t-t phase shifts, we have calculated two-triton correlations only for the simplifying case of pure Coulomb interaction. In Fig. 2.87b, these calculations are compared to the measured two-triton correlations. Although we cannot make a definitive statement, the size of the emitting

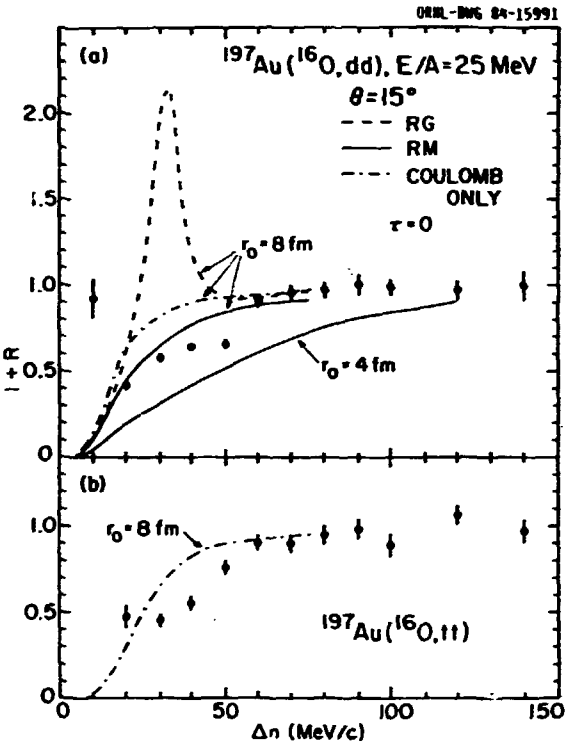

Fig. 2.87. (a) Comparison of d-d correlation function data with calculations based on phase shifts of Refs. 17 (RG) and 18 (RM). The dot-dashed curve neglects the nuclear part of the potential. (b) Comparison of t-t correlation function data with a calculation using only the Coulomb part of the potential. The radius parameter r_0 is indicated in the figure. The experimental correlation functions were normalized to R(Δp) = 0 at large relative momenta.

region appears to be large, just as observed for the two-deuteron correlations.

The difference between source sizes extracted from the analyses of the two-proton and the two-deuteron and two-triton correlations could indicate uncertainties in the interpretation of these correlations. Future investigations should clarify this point. However, larger source radii for composite particles might not be unreasonable. In terms of a thermal model, final-state interactions were suggested[19] to keep light fragments close to equilibrium for a longer period of time than nucleons. The freeze-out densities for nucleons and light fragments were estimated[19] to be of the order of 0.5 ρ_0 and 0.05 ρ_0, respectively. While the corresponding change in scale of $10^{1/3} \approx 2.15$ should not be directly equated with the approximate factor of 2 obtained from the analysis of the correlation measurements ($r_0 \lesssim 4$ fm for p-p, $r_0 \approx 8$ fm for d-d and t-t), the scale change is suggestive.

Significant correlations, with different qualitative shapes, were measured for all combinations of p, d, and t for ^{16}O-induced reactions on ^{197}Au at 400 MeV. Our analysis of the

two-deuteron correlations favors phase shifts obtained from the R-matrix approach, consistent with a repulsive interaction between two deuterons at small relative momenta. The emitting source radii extracted from two-deuteron and two-triton correlations appear to be roughly twice as large as the ones obtained from two-proton correlations. This presents an intriguing puzzle which must be addressed by reaction models of nucleon and light-fragment production.

1. National Superconducting Cyclotron Facility, Michigan State University, East Lansing, Michigan.
2. Simon Fraser University, Burnaby, B.C., Canada.
3. S. E. Koonin, Phys. Lett. 70B, 43 (1977).
4. G. I. Kopylov and I. M. Podgoretskii, Sov. J. Nucl. Phys. 18, 336 (1974); G. I. Kopylov, Phys. Lett. 50B, 472 (1974).
5. F. B. Yano and S. E. Koonin, Phys. Lett. 78B, 556 (1978).
6. S. Y. Fung et al., Phys. Rev. Lett. 41, 1592 (1978).
7. D. Beavis et al., Phys. Rev. C 27, 910 (1983).
8. D. Beavis et al., Phys. Rev. C 28, 2561 (1983).
9. W. A. Zajc et al., Phys. Rev. C 29, 2173 (1984).
10. F. Zarbaksh et al., Phys. Rev. Lett. 46, 1268 (1981).
11. W. G. Lynch et al., Phys. Rev. Lett. 51, 1850 (1983).
12. H. A. Gustafsson et al., Phys. Rev. Lett. 53, 544 (1984).
13. M. Gyulassy, Phys. Rev. Lett. 48, 454 (1982).
14. M. A. Bernstein et al., Phys. Rev. C 29, 132 (1984), and to be published.
15. P. D. Bond and R. J. de Meijer, Phys. Rev. Lett. 52, 2301 (1984).
16. W. G. Lynch et al., Phys. Rev. Lett. 52, 2302 (1984).
17. F. S. Chwieroth et al., Nucl. Phys. A189, 1 (1972).
18. G. M. Hale and B. C. Dodder, Few-Body Problems in Physics, ed. B. Zeitnitz, Elsevier, Amsterdam, Vol. II, p. 433.
19. D. H. Boal, Phys. Rev. C 30, 749 (1984).

STRUCTURE IN THE ASYMMETRIC REACTION $^{56}Fe + ^{238}U$ AT 15 MeV/amu

A. Weston-Dawkes[1] V. E. Viola, Jr.[2]
A. Mignerey[1] H. Breuer[1]
C. Merouane[1] D. Benton[1]
S. Bradley[1] F. E. Obenshain
K. Kwiatkowski[2] R. L. Ferguson

One of the goals of this experiment was the search for structure in the kinetic energy spectra of the Fe-like reaction products. Structure has previously been observed for the symmetric reaction $^{56}Fe + ^{56}Fe$ in this energy range,[3] and recent results from the group of Frascaria et al. show clear structures excited in asymmetric reactions of ^{36}Ar and ^{20}Ne beams with ^{208}Pb targets.[4] It has been suggested that these structures arise from excitation of the target nucleus. This interpretation is able to explain the relatively narrow widths observed at high excitation energy.

The 15-MeV/amu ^{56}Fe beam from the MHIRF was used to study the reaction $^{56}Fe + ^{238}U$. The projectilelike products were measured with discrete charge and mass resolution by means of the time-of-flight technique. The start and stop detectors were of the Breskin design and were manufactured by the Oak Ridge detector laboratory under the direction of J. Blankenship. The stop detector was a large x-y position-sensitive device which permitted position correction of time-of-flight and energy signals. The energy and charge of the fragments were determined by a large-area segmented ΔE-E ion chamber. The 150-torr pressure of CF_4 provided sufficient stopping power to measure all projectilelike fragments down to $Z \sim 10$. The best time resolution achieved by the double Breskin system was ~300 ps. This necessitated using a 2.5-m flight path to obtain a mass resolution of ~0.8 mass units for the elastically scattered ^{56}Fe. The energy resolution from the Snell chamber was ~1% for elastically scattered ^{56}Fe at 5°.

At the time of this report, only charge data are available from the $^{56}Fe + ^{238}U$ reaction. Results from the previously studied $^{56}Fe + ^{56}Fe$ system[3] indicate that the Z = 27 (cobalt) spectrum shows qualitatively the same structure as the isotopically separated ^{57}Co spectrum. This is because the dominant cobalt isotope is A = 57. Separation into individual isotopes serves to sharpen structure already evident in the inclusive spectrum. Figure 2.88 shows the low excitation energy (high total kinetic energy) region of the cobalt total kinetic energy spectrum obtained from 15-MeV/amu ^{56}Fe on ^{238}U. Shown for comparison in Fig. 2.89 are the results obtained at 14.6 MeV/amu for the symmetric reaction $^{56}Fe + ^{56}Fe$. The distinct structures in the cobalt spectrum from the ^{238}U target are in qualitative agreement with those obtained for asymmetric reactions with ^{208}Pb targets.[4] The peak corresponding to a total kinetic energy loss, E_{loss}, of ~25 MeV probably comes from the direct one-proton transfer and can be compared to the most prominent peak in Fig. 2.89. The next major rise at E_{loss} = 50-60 is probably the sequential one-particle evaporation, primarily from ^{58}Co neutron emission. This is consistent with the second major peak observed in the $^{56}Fe + ^{56}Fe$ reaction at $E_{loss} \sim$ 50 MeV. However, for the ^{238}U reaction there appears to be a substructure with possible peaks at $E_{loss} \sim$ 50 and 65 MeV superimposed on the broader underlying structure.

The overwhelming conclusion from all evaporation calculations is that it is difficult to produce or preserve structure at large energy losses. The widths of narrow peaks in primary spectra are broadened by the assumptions of isotropic particle emission and of distributions in excitation energy division. Hence, when clear structure is observed at large energy

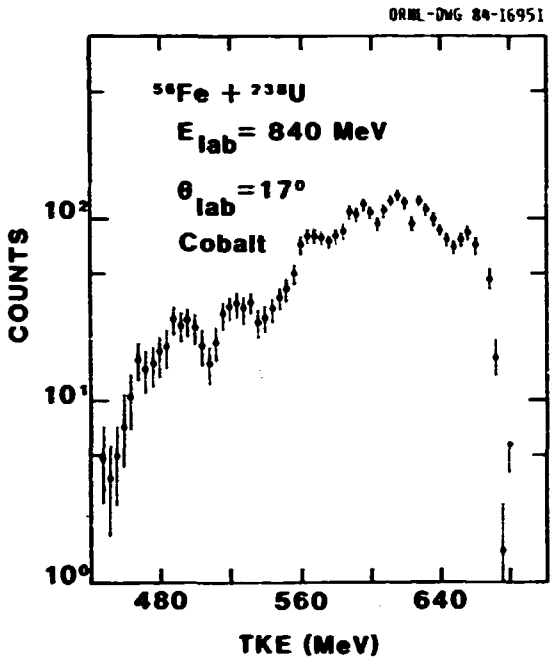

Fig. 2.88. Total kinetic energy spectrum of the cobalt product (Z = 27) measured at a laboratory angle of 17° in the reaction of 840-MeV ^{56}Fe with ^{238}U.

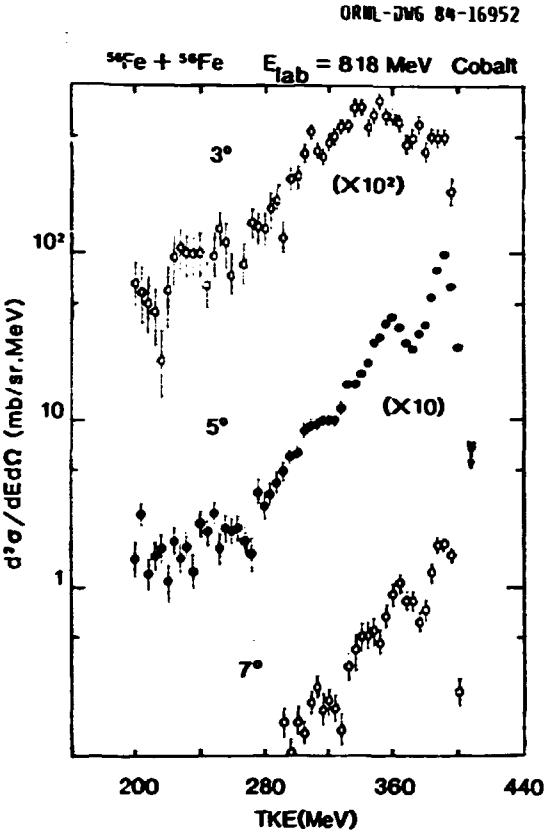

Fig. 2.89. Total kinetic spectra of the cobalt products (Z = 27) measured at laboratory angles of 3°, 5°, and 7° in the reaction of 818-MeV ^{56}Fe with ^{56}Fe.

losses, processes other than evaporation would appear to be responsible. In the $^{56}Fe + ^{238}U$ reaction, four additional peaks may be identified, centered at E_{loss} = 85, 115, 155, and 190 MeV. As energy loss increases, the width and energy spacing of the structures also increase. This trend is the same as that observed in the reaction of 11-MeV/amu ^{36}Ar on ^{208}Pb (Ref. 4). The explanation of target excitations producing the structure is attractive since the cobalt product remains relatively cold and sequential particle emission will not wash out any structure produced in the primary reaction.

Attempts have been made to deduce excitation energy sharing in asymmetric damped reactions by fitting the shape of secondary energy spectra using excitation energy division as a parameter.[5] The underlying envelope of yield is surely fed by sequential decay, which gives this method some validity. However, care must be taken to recognize the possibility of other mechanisms, even at high energy losses, which could make deconvolution of the spectra difficult.

This is the first time our group has identified structure in an asymmetric system. Several factors are probably responsible for this. The increased bombarding energy may have increased the cross section for these processes or decreased that for the competing damped reaction mechanism, which dominates the energy spectra at lower bombarding energies. Also, the increase in solid angle subtended by the time-of-flight system, due to the use of large-area Breskin detectors, made study of the $^{56}Fe + ^{238}U$ reaction experimentally feasible.

---

1. University of Maryland, College Park, Maryland.
2. Indiana University, Bloomington, Indiana.
3. A. Mignerey et al., Proc. Workshop on Nuclear Dynamics III, Copper Mountain, Colo., March 1984, p. 76.
4. Ph. Chomaz et al., preprint (1984).
5. H. Sohlbach et al., Proc. Workshop on Nuclear Dynamics III, Copper Mountain, Colo., March 1984, p. 72.

INCLUSIVE CROSS SECTIONS FOR π^0 EMISSION IN 25-MeV/amu HEAVY-ION REACTIONS

P. Braun-Munzinger[1] F. E. Obenshain
R. Freifelder[1] F. Plasil
J. Stachel[1] G. R. Young

We have studied production of neutral pi mesons using heavy ion beams at energies per

nucleon well below the value required for free nucleons to interact and produce a pion. The experiment used the 25-MeV/amu ^{16}O beam from the ORNL Holifield complex to bombard ^{27}Al and ^{nat}Ni targets. The purpose of the experiment was, after establishing a nonzero value for the pion-production cross section at such low bombarding energies, to obtain energy distribution, angular distribution, and target mass-dependence data which might allow one to learn what mechanism is responsible for concentrating so much of the kinetic energy of the projectile into creation and ejection of one outgoing particle. Theorists have provided a range of explanations from "ordinary" (involving coupling of relative and Fermi momenta of individual nucleons to give energies in excess of the nucleon-nucleon threshold) to "exotic" (involving very short-range clustering of nucleons to form a massive hard scattering center, or involving a nuclear counterpart to the familiar electromagnetic bremsstrahlung emission of photons). One of the fascinations of such measurements is the concentration of over half of the center-of-mass energy to produce a pion (m_{π^0} = 135 MeV/c^2, $m_{\pi^\pm}$ = 139 MeV/c^2). While the emission of very energetic nucleons is familiar from the observation of nucleons in the high-energy region of evaporation spectra from compound or composite systems of nuclei, the particles emitted were present in the entrance channel. If emission of a quark-antiquark pair (i.e., meson, here a pion) requires large momentum transfer in the scattering of the constituents, one wishes to inquire as to what constitutes such scattering, or who the participants are, in such low-energy experiments.

The experimental method used in the present work consisted of detecting the two energetic photons emitted in decay of a π^0, in an array of Cerenkov detectors. A π^0 decays 98.8% of the time into two equal energy (in the π^0 rest frame) photons with a lifetime of 8.3 x 10^{-17} secords. The photons emitted in the decay have energies of the order of 70 MeV or larger, increasing with increasing π^0 kinetic energy. The photons tend to cluster about a laboratory opening angle $\theta_{12} = 2\cos^{-1}(\beta_\pi)$, where $\beta_\pi = v_\pi/c$. Low-energy or nearly stopped π^0's decay into two correlated gamma rays which are near 180° separation in the laboratory system. This makes the π^0's easier to identify than charged pions. At low energies the charged-pion lifetime approaches the proper lifetime of 26 ns, and consequently, the pions decay before detection.

Lead-glass Cerenkov shower counters were used to detect the decay photons. These detectors are large rectangular blocks of optical glass loaded with ~55% by weight lead oxide. Cerenkov light emitted by electrons and positrons as they pass through the glass is detected with photomultiplier tubes attached to the glass blocks. The detectors used were arranged as 20 pairs of detectors, with each telescope placed either 15° above or below a plane containing the beam, at 30° intervals in polar angle. The beam pipe occupied the 0° and 180° positions. The front, or converter, block of each telescope was a 10 cm x 10 cm x 5 cm thick block of F2-type glass viewed on a side edge (10 cm x 5 cm) by a fast 5-cm, 14-stage phototube. The rear, or absorber, block of each telescope was a 15 cm x 15 cm x 34 cm thick block of SF5 glass viewed from the rear 15 cm x 15 cm face by a 12.5-cm, 10-stage phototube. Pulse heights and time of arrival relative to the cyclotron RF for all good events were recorded on magnetic tape and analyzed off line.

A Monte Carlo code was used to simulate π^0 decay in the laboratory for kinetic energies between 0 and 110 MeV and for all emission angles (polar and azimuthal). The geometric acceptance of the detector array was 2.9% of 4π and decreased with increasing π^0 kinetic energy to a value of 0.3% at T_π ~ 100 MeV. The detection efficiency of the converters was taken from the measurements of C. Michel.[2]

Neutral pions were tagged by calculating the invariant mass of a detected photon pair and searching for events where this was clustered about 135.6 MeV, the π^0 rest mass. A scatter plot of invariant mass vs. detector pair opening angle shows a distinct cluster of events is found near 135 MeV for $\theta_{12} > 90°$. A projection onto the invariant mass axis is given in Fig. 2.90. By recasting the invariant mass equation in the form

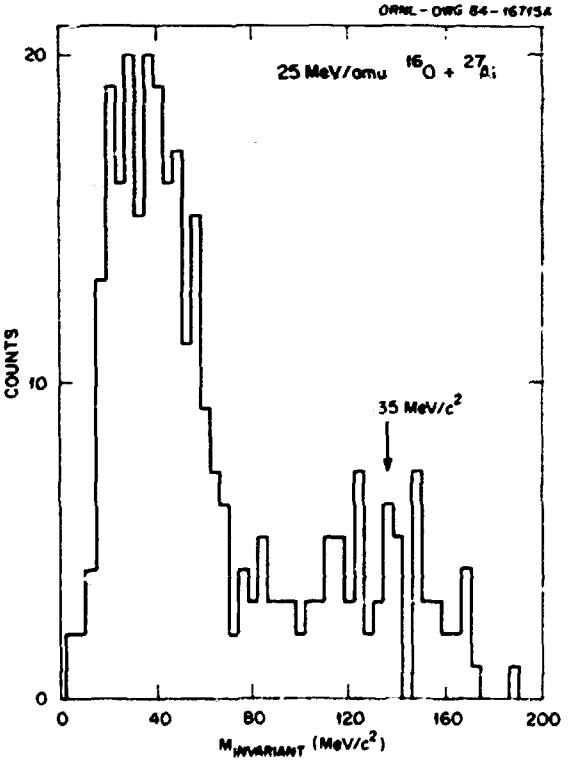

Fig. 2.90. Invariant mass spectrum of two-photon events produced in reactions of 25-MeV/amu ^{16}O + ^{27}Al.

$$T_\pi = m_\pi c^2 \frac{2}{(1 - \cos\theta_{12})(1 - X^2)} - 1 \quad ,$$

where $X = (E_{\gamma 1} - E_{\gamma 2})/(E_{\gamma 1} + E_{\gamma 2})$, the kinetic energy T_π can be obtained. The resulting energy and angular distributions for the Al target are shown in Fig. 2.91.

The difficult background arises from penetrating cosmic-ray muons and products of cosmic-ray hadron showers. Since energetic muons do not interact (except by electroweak processes, which have very small cross sections) in the glass, they penetrate the array in a more or less straight line, and thus tend to be concentrated near the horizontal plane. Showers and muons are suppressed by the invariant mass cut, a prompt cut on the event time relative to the beam RF timing, and by requiring a multiplicity of exactly four hit counters. This last requirement was checked to cause only an ~1% loss in real π^0 events (due to, for example, random coincidences between a π^0 and beam-related γ background).

Even with these precautions, for $\theta_{12} < 110°$ a large contamination of cosmic rays in the invariant mass spectrum is found. To tag these cosmic rays, 2.5-cm-thick plastic paddles were placed in front of telescopes to veto cosmic rays hitting the arrays by detecting their Cerenkov light. As plastic has a 48-cm radiation length, only <4% of the photons convert in the paddle, resulting in small efficiency loss but a very large reduction in cosmic-ray background for $\theta_{12} < 120°$.

An integrated π^0 production cross section of 5.9 ± 2.4 nb is found for the reaction 25-MeV/amu ^{16}O + Al. Scaling according to our earlier prescription[3] to the value for the ^{12}C + ^{12}C system, a cross section of 2.8 nb results, which is an order or magnitude less than the result at 35 MeV/amu (Ref. 3). It was pointed out earlier[4] that "Fermi-gas" type production models[5] fail to reproduce the observed cross sections by three orders of magnitude at 35 MeV/amu; this failure is expected to be much worse at 25 MeV/amu.

However, a model[6] based on cooperative action of several target and projectile nucleons ("clusters") yields fair agreement with production cross sections and spectral shapes for the 35-MeV/amu results. When the curve of cross section vs. beam energy for ^{12}C + ^{12}C is extrapolated to 25 MeV/amu, it appears to give agreement within a factor of 2 with the present total cross section result. It will be interesting to compare our spectral shapes with the predictions of this model when these calculations become available for our case. The energy distributions are concentrated at lower kinetic energies than the 35-MeV/amu data and have an exponential slope of ~17.5 MeV. The angular distributions are somewhat forward peaked, as are those for the intermediate-energy ($24 < T_\pi < 80$ MeV) pions observed at 35 MeV/amu. Unlike the latter results, the present results do not show an obvious decrease at $\theta = 90°$.

A completely different model based on pionic bremsstrahlung[7] predicts a π^0 cross section for ^{12}C + ^{12}C at 25 MeV/amu of 2.5 nb, similar to the observed value. This model has provided good agreement with energy and angular distributions measured for ^{12}C + ^{12}C at 60-85 MeV/amu. Predictions for these quantities for asymmetric systems such as ours are eagerly awaited.

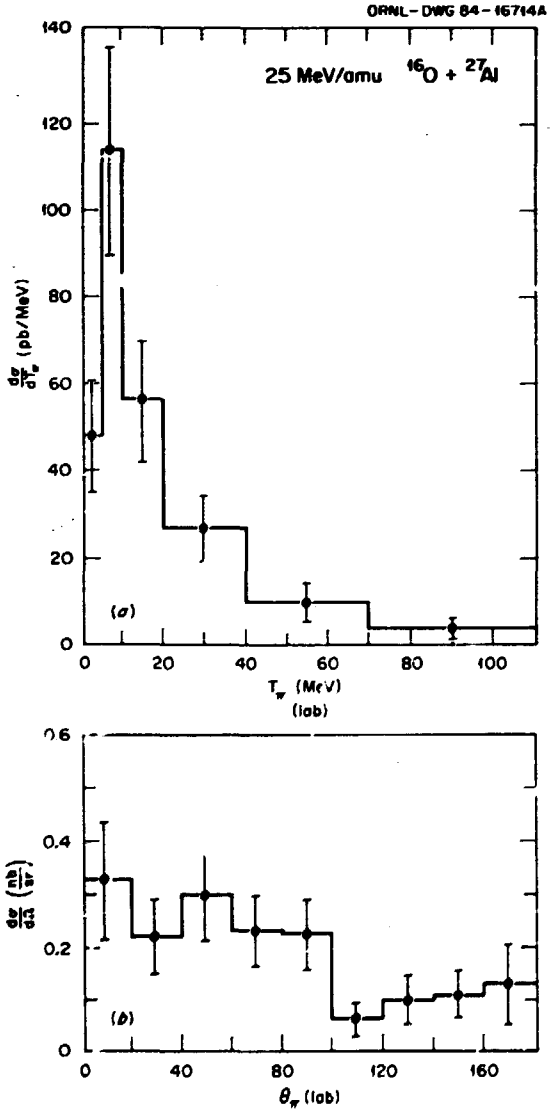

Fig. 2.91. (a) Laboratory kinetic energy spectrum of π^0's produced in reactions of 25-MeV/amu ^{16}O + ^{27}Al. (b) Laboratory angular distribution of π^0's produced in the same reaction.

1. State University of New York, Stony Brook, New York.
2. C. Michel, Saclay (to be published).
3. P. Braun-Munzinger et al., Phys. Rev. Lett. 52, 255 (1984).

4. R. Shyam and J. Knoll, Phys. Lett. 136B, 221 (1984).
5. G. Bertsch, Phys. Rev. C 15, 713 (1977).
6. R. Shyam and J. Knoll, Nucl. Phys. A426, 606 (1984).
7. D. Vasak et al., Phys. Lett. 93B, 243 (1980).

DETERMINATION OF THE REST FRAME FOR NEAR-THRESHOLD π^0 EMISSION IN HEAVY-ION REACTIONS

J. Stachel[1] T. C. Awes
P. Braun-Munzinger[1] F. E. Obenshain
P. D. Young[1] F. Plasil
P. Paul[1] G. R. Young

Pion production in heavy-ion collisions at energies below the free nucleon-nucleon threshold, i.e., at energies where the pion mass exceeds the kinetic energy of a projectile nucleon in the zero momentum frame, has been discussed for a long time in terms of probing the intrinsic Fermi motion in the projectile and target nuclei. However, as the beam energy is lowered, this process gets more and more unlikely, and below a certain energy it should not be observed anymore. In a sharp cut-off Fermi-gas model, this occurs[2] at E_{lab} = 54 MeV/amu. However, as long as the total center-of-mass energy exceeds the pion mass, pions still can be produced by a cooperative sharing of the beam energy of several (or all) projectile nucleons. The experiments presented here are meant to extend the experimental information into that kinematic domain.[3] The production of a pion of 100-MeV kinetic energy with a 35-MeV/amu ^{14}N beam requires Fermi momenta as high as ~380 MeV/c or, alternatively, 60% of the total beam energy. The information from the present experiments, combined with the results of previous experiments at higher beam energies of 44 MeV/amu and 60-84 MeV/amu (Refs. 4 and 5), enables us to determine which of the alternative production mechanisms is dominant at a given beam energy.

In the experiments presented here, neutral pions have been detected through their predominant fast decay into two high-energy γ rays. These two γ rays were observed in coincidence in an annular array (coplanar with the beam axis) of lead glass Cerenkov detector telescopes. Each telescope consists of a converter and an absorber section with respective depths of 1.6 and 15 radiation lengths (for details see Ref. 3). The measurement of the two γ energies and angles (given by the opening angles of the separate telescopes) allows a reconstruction of the pion invariant mass, its kinetic energy, and emission angle.

In a first experiment,[3] data from ten of these telescopes, which covered a solid angle of about 8.5% of 4π, were combined. A 35-MeV/amu ^{14}N beam of the K = 500 superconducting cyclotron at Michigan State University was used to bombard targets of natural Al, Ni, and W. In the present experiment, using the same beam and the Ni target, we aimed at obtaining very detailed information on one particular target and combined data from 20 Cerenkov telescopes. Because of the finer granularity of this setup, the γ-ray angular resolution improved from 24° to 17°, thus providing a significantly better pion angle and kinetic energy resolution. The solid angle covered by this setup was somewhat smaller (about 6% of 4π).

The probability that the two decay γ rays of a pion entered our detectors is obtained from Monte Carlo simulations which take into account the pion decay kinematics. The response of the converter sections to 125-MeV electrons has been measured to be 75%. This provides an upper limit for the response to γ rays. The energy dependence of this response is obtained from Monte Carlo simulations[6] that include the conversion of a γ ray into an electromagnetic shower, the subsequent Cerenkov light emission and collection probability, and the photomultiplier response. The resulting detection probability increases monotonically with increasing γ energy until it levels off at ~150 MeV at 68%, in good agreement with our measured value.

The very intense background of beam-correlated γ radiation and neutrons and the background due to cosmic rays is effectively reduced by (1) our coincidence technique, which requires a four-fold trigger of two absorber signals together with the corresponding two converter signals; (2) the ~2-ns time resolution of the setup, which allows the application of narrow gates on the various detector-detector and detector-beam time differences; (3) a software threshold on low γ energies (30-40 MeV) and small opening angles ϕ between the two γ rays (a minimum ϕ is kinematically determined by the pion kinetic energy); and (4) a gate on the pion invariant mass. The effects of the different cuts on the data were investigated by Monte Carlo simulations, and if necessary, corrections were applied to the results.

Figure 2.92 shows the experimental invariant mass spectrum. It exhibits a clear peak around the π^0 invariant mass of 135 MeV. Approximately 900 pions were detected in a beam time of one week. Also displayed in Fig. 2.92 is the result of a Monte Carlo simulation. Its good agreement with the data shows that effects of the geometry, the γ-ray energy and angular resolution, and of the various cuts on the data were treated properly. An effective background suppression is also apparent.

There is one piece of experimental information that can provide information on the velocity of the source that emits the pions. Figure 2.93 shows a plot of the double differential cross section versus the rapidity y and the momentum perpendicular to the beam direction $p_\perp$ for the present experiment at 35 MeV/amu. It can be seen that the experimental cross sections are symmetric around $y = 0.01 \pm 0.05$, which indicates that the pion source is moving very slowly. This again is a strong hint that single nucleon-nucleon collisions are not the origin of the presently observed pion cross sections. For this process a source velocity of half the beam rapidity (labeled $\rightarrow$ 1/2 p in Fig. 2.93) is expected, in clear contradiction to the experimental results. On the other hand, pion

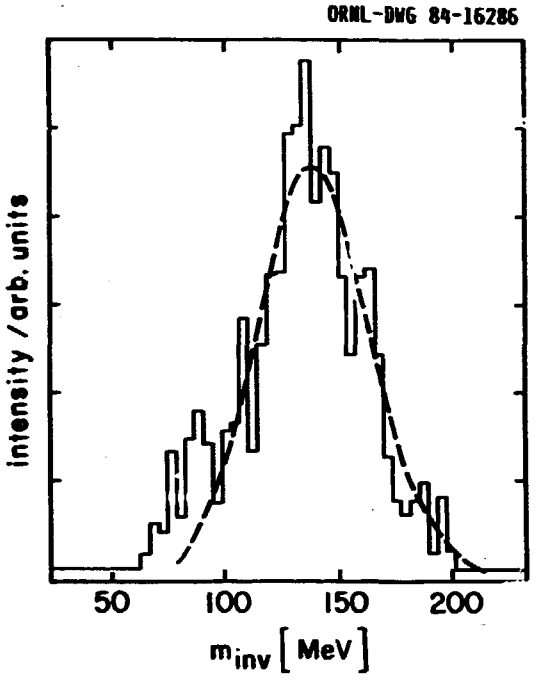

Fig. 2.92. Experimental invariant mass spectrum for 35-MeV/amu ^{14}N on Ni, together with the result of a Monte Carlo simulation (dashed line).

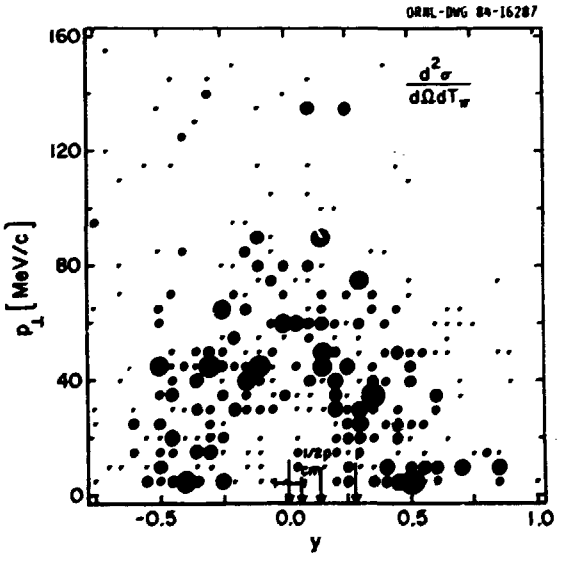

Fig. 2.93. Double differential cross sections $d^2\sigma/d\Omega dT_\pi$ versus rapidity, $y = 1/2 \log[(E + p_\parallel)/(E - p_\parallel)]$, and momentum perpendicular to the beam axis $p_\perp$ for 35-MeV/amu ^{14}N + Ni. The arrows indicate the projectile rapidity, half the projectile rapidity, the rapidity of the ^{14}N + Ni center-of-mass system, and the centroid of the experimental cross sections, $\langle y \rangle = 0.01 \pm 0.05$.

emission from the N + Ni composite system is compatible with the data. Monte Carlo simulations indicate, however, that pion reabsorption effects play an important role. For example, for a pion source located near the edge of the combined N + Ni system, corresponding to the complete stopping of the projectile, a considerable reduction in the apparent source velocity is expected, due to these effects. The low average rapidities are in accordance with similar information[5] for the asymmetric systems ^{12}C + ^{238}U and ^{12}C + ^{56}Ni at E_{lab} = 60-84 MeV/amu, where the pion source also was found to move significantly more slowly than the nucleon-nucleon center-of-mass system. This source velocity can be interpreted in terms of the size of the system emitting the pions. At 60-84 MeV/amu it has been concluded[5,7] that if the whole projectile nucleus is active, then the system involves 14-15% of the U nucleus and 34-41% of the Ni.

The experimental data collected so far can be interpreted as displaying a transition in the pion production mechanism from nucleon-nucleon collisions at high beam energies, with increasing importance of high Fermi momenta as the energy is lowered, to a cooperative sharing of the beam energy of several projectile nucleons, e.g., via multiple quantum mechanical off-shell collisions, and finally towards a collective production mechanism dominated by the mean field.

---

1. State University of New York, Stony Brook, New York.
2. G. Bertsch, Phys. Rev. C 15, 713 (1977).
3. P. Braun-Munzinger et al., Phys. Rev. Lett. 52, 255 (1984).
4. H. Heckwolf et al., Z. Phys. A315, 243 (1984).
5. H. Noll et al., Phys. Rev. Lett. 52, 1284 (1984).
6. C. Michel, to be published.
7. E. Grosse, Proc. VI High Energy Heavy Ion Study, Berkeley (1983).

HEAVY-ION-INDUCED FISSION AT ENERGIES UP TO 20 MeV/amu

T. C. Awes — M. M. Fowler[1]
J. Boissevain[1] — F. E. Obenshain
H. C. Britt[1] — H. Ohm[4]
K. Eskola[2] — F. Plasil
P. Eskola[3] — J. B. Wilhelmy[1]
R. L. Ferguson — G. R. Young

During the past year we have published our extensive studies of angular-momentum-dependent fission barriers.[5,6] This work, carried out at energies up to 10 MeV/amu, led to the conclusion that calculated barriers from the rotating-finite-range model (RFRM)[7] adequately describe the measurements over a large range of excitation energy, angular momentum, and mass of the fissioning system. The statistical model, together (in some cases) with calculated Bass

fusion cross section,[8] was used in the data analysis. Encouraged by our success, we extended our fission studies into the energy range between 10 and 20 MeV/amu. To the extent to which it was possible, we have studied the same compound (or composite) systems, i.e., ^{158}Er, ^{186}Os, and ^{208,210}Po. In addition, we made measurements on a ^{238}U target. The target and projectile combinations were as follows: ^{12}C on ^{174}Yb, ^{198}Pt, and ^{238}U; ^{16}O on ^{142}Nd, ^{170}Er, ^{192}Os, and ^{238}U; ^{32}S on ^{126}Te, ^{144}Nd, and ^{238}U; and ^{58}Ni on ^{96}Zr, ^{116}Cd, and ^{238}U. The energies ranged from 95 to 291 MeV for ^{12}C, 140 to 315 MeV for ^{16}O, 350 to 700 MeV for ^{32}S, and 352 to 875 MeV for ^{58}Ni. The data included measurements of angles and velocities of coincident fission fragments, from which the linear momentum transfer to the fissioning system could be deduced. Fission following incomplete momentum transfer was found to be substantial only in reactions on ^{238}U targets. In our cross section analysis, we have included only events with complete and nearly complete momentum transfer.

We had expected at these higher energies to observe limitations resulting from various dynamical processes such as incomplete fusion and/or extra push effects. This, indeed, turned out to be the case, since it was no longer possible to describe the measured cross sections in terms of statistical model calculations with RFRM fission barriers and with Bass model fusion cross sections. It was expected that in reactions with ^{12}C and ^{16}O ions, incomplete fusion would result in lower observed fission cross sections, except in the case of the ^{238}U target, where even partially fused systems are highly fissile. Results of ^{12}C and ^{16}O bombardments of ^{238}U are shown in Fig. 2.94a for the near full momentum transfer component, together with calculations using the Bass model. On the basis of the good agreement between theory and experiment, we conclude that the Bass model constitutes a reasonable parametrization of fusion (complete and incomplete) in this energy range. This situation did not prevail in the case of reactions of ^{32}S and ^{58}Ni with ^{238}U, as can be seen from Fig. 2.94b. The discrepancy between the Bass model results and the measured fission cross sections for the near full momentum transfer component can be attributed to higher Coulomb repulsion between target and projectile nuclei, resulting in the need for an additional energy (extra push) to achieve fusion.[9]

In Fig. 2.94c we show the fission excitation functions for the ^{16}O + ^{142}Nd and the ^{12}C + ^{174}Yb systems, together with statistical model calculations in which the Bass model fusion cross sections and the RFRM fission barriers have been incorporated. It can be seen that, at the highest energies, calculated cross sections are three to five times higher than measured cross sections, which saturate at a level consistent with a maximum angular momentum of the fissioning system of about 65 ħ. This observed saturation in the fission excitation function may, presumably, be attributed to incomplete fusion, and the implication is that collisions with partial waves beyond ~65 ħ involve processes that result in residual nuclei with reduced angular momenta. While incomplete

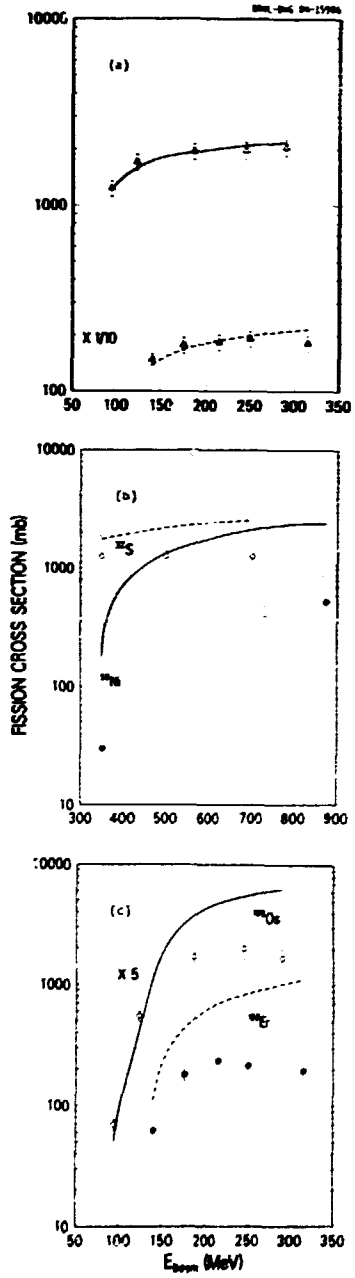

Fig. 2.94. Fission cross sections for reactions of ^{238}U with ^{12}C (open triangles), ^{16}O (closed triangles), ^{32}S (open circles), and ^{58}Ni (closed circles) are shown in (a) and (b). In (c), cross sections are shown for the ^{16}O + ^{142}Nd (open circles) and the ^{12}C + ^{174}Yb (closed circles) systems. The solid and dashed lines depict Bass fusion cross sections in (a) and (b) and statistical model calculations using the Bass model in (c).

fusion is the most likely explanation, our results cannot be accounted for quantitatively on the basis of the Wilczynski model.[10] This is because partial waves of only up to 60 ħ (for

^{16}O + ^{142}Nd at 315 MeV) are expected to contribute to complete fusion,[10] which would account for only 10% of our observed fission cross section. Furthermore, based on our measured momentum transfer distributions, fission following incomplete fusion does not contribute significantly to the fission cross sections in the ^{158}Er and ^{186}Os cases. Thus, it appears that fusion with nearly full momentum transfer must be taking place with partial waves above the limit predicted by the Wilczynski sum-rule model.[10]

We may proceed with a schematic description of the implications of our findings for the incomplete fusion process by restricting ourselves to situations in which alpha particles (or larger nuclei) escape absorption by the target, and by assuming that the angular momentum imparted to the residual system scales with the mass of the fraction of the projectile absorbed. As was stated above, for the ^{16}O + ^{142}Nd reaction, complete fusion, accompanied by some fission, accounts for partial waves up to 65 ħ. The first alpha particle emitted in the incomplete fusion process will leave the residual system with 75% of the incoming angular momentum, and since the nucleus does not decay predominantly by fission, this angular momentum must be $\lesssim$65 ħ. Thus, the partial waves associated with single alpha-particle emission must lie between 65 and about 87 ħ (i.e., 65/0.75 ħ). In addition, the Bass model, which describes the ^{238}U data adequately, predicts that partial waves of up to 105 ħ (at 315 MeV) contribute to fusionlike reactions. If this is the case, we must also attribute the reactions in this angular momentum window (between ~87 ħ and ~105 ħ) to situations that leave the residual nucleus with an angular momentum of $\lesssim$65 ħ. The emission of ^{8}Be (two alpha particles) is consistent with the above requirement. Obviously, further experiments are necessary to clarify the picture. In particular, measurements of evaporation residue products, both inclusive and in coincidence with alpha particles, are needed to confirm the above conjecture.

For systems with high values of the Z_pZ_t product, we expect that an additional energy (extra push)[9] is needed for fusion to take place. It was already indicated in Fig. 2.94b that this effect is likely to play a role in our reactions with ^{32}S and ^{58}Ni projectiles. However, even for reactions with ^{16}O ions, at energies above about 120 MeV, the highest partial waves involve angular momenta that are sufficient to increase the effective fissility to the point where extra push[9] effects are expected. Calculations with the parameters of Bjornholm and Swiatecki[9] (with the exception of our use of a = 10, which is within their limits of uncertainty) are compared with measurements in Fig. 2.95. For the ^{16}O-induced reactions (Fig. 2.95a), agreement between experiment and theory at the higher energies is much better than that which was obtained with the Bass model, except for the case of ^{238}U. We conclude that, even with ^{16}O ions, there is some evidence

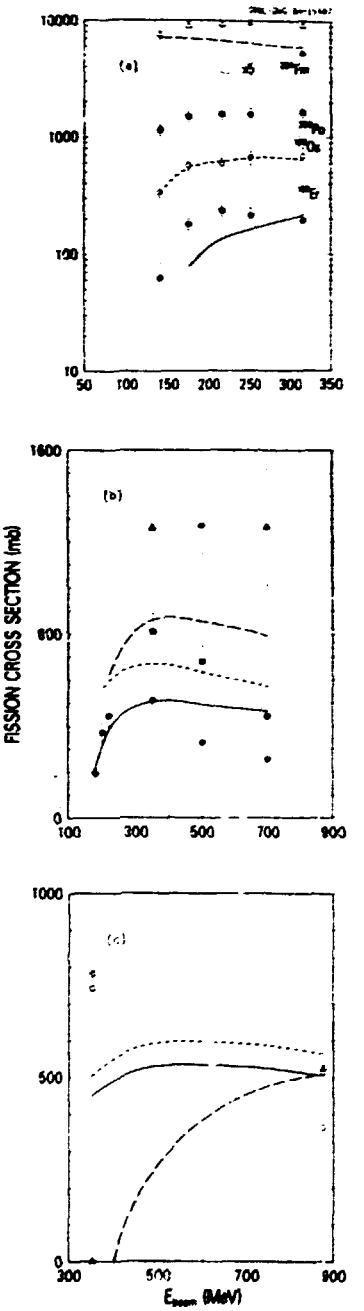

Fig. 2.95. Comparison of measured fission cross sections with extra push model cross sections (curves). In (a), reactions with ^{16}O are shown, and the labels indicate the composite systems. In (b), ^{32}S-induced reactions on ^{126}Te (circles, solid curve), ^{144}Nd (squares, short-dashed line), and ^{238}U (triangles, long-dashed line) are shown. Reactions of ^{58}Ni with ^{96}Zr (circles, solid line), with ^{116}Cd (squares, short-dashed line), and ^{238}U (triangles, long-dashed line) are shown in (c).

for a dynamical limitation to the fusion process and that the extra push model[9] determines the highest partial waves for which complete fusion takes place.

In Figs. 2.95b and 2.95c similar comparisons are shown for reactions with ^{32}S and ^{58}Ni. There does not appear to be a consistent quantitative agreement between experiment and theory, although it is clear that some kind of dynamical limitation plays a role in the cases that we have studied. Best agreement was found in the case of ^{58}Ni-induced reactions at the highest energy (875 MeV). In addition, a clear cut illustration of the extra push threshold effect is provided by the 352-MeV $^{58}Ni + ^{238}U$ result, where our measured fission cross section is 0^{+50}_{-0} mb and where a threshold of 460 MeV is predicted by the extra push model.

---

1. Los Alamos National Laboratory, Los Alamos, New Mexico.
2. Present address: Physics Department, University of Helsinki, Helsinki, Finland.
3. Present address: Theoretical Physics Department, University of Helsinki, Helsinki, Finland.
4. Chemistry Department, Mainz University, Mainz, West Germany.

5. J. van der Plicht et al., Phys. Rev. C 28, 2022 (1983).
6. F. Plasil et al., Phys. Rev. C 29, 1145 (1984).
7. M. G. Mustafa, P. A. Baisden, and H. Chandra, Phys. Rev. C 25, 2524 (1982); A. J. Sierk, unpublished results.
8. R. Bass, Phys. Rev. Lett. 39, 265 (1977).
9. W. J. Swiatecki, Nucl. Phys. A376, 275 (1982); S. Bjornholm and W. J. Swiatecki, Nucl. Phys. A391, 471 (1982).
10. J. Wilczynski et al., Phys. Rev. Lett. 45, 606 (1980).

NUCLEUS-NUCLEUS REACTIONS AT ENERGIES UP TO 200 GeV•amu — PLANS FOR AN EXPERIMENT AT CERN

T. C. Awes, C. Baktash, J. R. Beene, R. L. Ferguson, T. A. Gabriel[1], E. E. Gross, J. W. Johnson, I. Y. Lee, F. E. Obenshain, F. Plasil, G. R. Young

In early 1984 a major commitment was made to participate in the PS 190 collaboration at CERN. This new initiative is expected to be an important research activity of the Physics Division during the next three to four years. The CERN experiment PS 190 is an approved experiment to be run in late 1986 and again in early 1987. The Gesellschaft fUr Schwerionenforschung (GSI), Darmstadt, West Germany, and the Lawrence Berkeley Laboratory (LBL), Berkeley, California, will provide the means necessary to accelerate ^{16}O ions in the PS and SPS accelerators at CERN by building an ECR source and an RFQ injector. The ^{16}O energies will be 800 GeV and 3200 GeV. It is possible that nuclei in the energy range between 10 and 50 GeV•amu will also be available.

Currently, the PS 190 collaboration consists of two totally independent experiments that have recently been assigned separate SPS experiment numbers. The first, WA 37, is centered about a streamer chamber, with R. Stock as spokesman. The second, WA 80, makes use of the GSI/LBL plastic ball, and H. H. Gutbrod of GSI is the spokesman. ORNL is associated with the WA 80 collaboration. Other institutional members of this collaboration, in addition to GSI, LBL, and ORNL, are the Universities of Lund, Sweden, and of Münster, West Germany. The experiment is to be performed in the west experimental hall of the SPS. The author list of this contribution to the Physics Division Progress Report includes only the ORNL members of the WA 80 collaboration, since the list of all collaborators from the various institutions is not as yet final.

The plastic ball, currently located at LBL, will be moved to CERN. It will be suitable only for the study of the target rapidity region, including: (1) determination of matter flow from a global analysis approach; (2) determination of the extent of spectator drag from determinations of the average value of p_t in this rapidity region; (3) determinations of pertinent temperatures from inclusive energy spectra; (4) determinations of entropy from d/p ratios; and (5) determinations of source sizes from two-particle correlations. More pertinent to the type of physics to be addressed at SPS energies is the mid-rapidity region, encompassing most of the participant region as well as the region in which the effects of the quark-gluon plasma may manifest themselves. A key question to be considered here is the determination of conditions under which maximum baryon density buildup can be attained (stopping versus transparency). Energy flow questions, as determined from global analysis, also play a major role in this region. In recent cosmic-ray data, unexplained fluctuations in pseudo-rapidity were observed. Search for such effects can also be carried out. The observation of direct gamma production may be one of the signatures of the quark-gluon plasma. Thus, the measurement of these gamma rays and their identification in the presence of a large background of gammas from π^0 decay are an important aspect of the experiment.

As was stated above, the plastic ball is adequate to cover the target rapidity region. For the mid-rapidity region, three new devices are needed: (1) a 6-m^2 array of sampling calorimeters, each calorimeter consisting of a hadronic and an electromagnetic portion, (2) a multiplicity array of about 10^4 cells, and (3) a finely segmented 1000-element lead glass electromagnetic calorimeter capable of distinguishing between intrinsic gammas and the decay of neutral pions. Finally, the projectile rapidity (trigger) devices will consist of a "bull's-eye" scintillator to determine the projectile charge and a uranium calorimeter to determine the projectile energy. The responsibility for the various devices was assigned as follows: plastic ball, LBL/GSI; multiplicity array, GSI;

6-m^2 array of calorimeters, ORNL; electromagnetic, γ/π^0 calorimeter, University of Münster; "bull's-eye" scintillator, LBL/GSI; and zero-degree calorimeter, ORNL. Work is in progress at ORNL to design and build the two types of calorimeters listed above. The calorimeters are funded jointly by LBL and by ORNL.

The mid-rapidity calorimeters are based on the design of Fabjan, Willis, and their co-workers at CERN. Like the CERN calorimeters, the ORNL/LBL version consists of modular stacks, each covering an area of 20 cm by 120 cm. The mechanical design is such as to allow the stacks to be closely packed with a minimum of dead space between them. Each stack consists of six 20-cm by 20-cm towers; each tower is read out separately. Again, as in the CERN design, each tower consists of an electromagnetic section in which primarily π^0, gamma rays, and electrons are detected, followed by a hadronic section for the detection of charged pions, protons, neutrons and other hadrons. While both the electromagnetic and the hadronic sections of the CERN calorimeters contain uranium, because of funding and procurement constraints, the ORNL/LBL design will consist of a lead/plastic electromagnetic section and a stainless steel/plastic hadronic section. Twenty-five stacks covering 6 m^2, with a total of 150 towers of 20 cm by 20 cm, are to be built. The high-granularity GSI charged-particle multiplicity array will be placed in front of the calorimeters.

The crucial parameters in calorimeter design are the e/p ratio (the ratio of the average effective energy deposited in the plastic by an electron to the average effective energy deposited in the plastic by a proton of the same energy) and the energy resolution, σ/E, expressed as a percentage of E. It is desirable for the e/p value to be as close to 1.0 as possible, and σ/E to be as low as possible. For a calorimeter consisting entirely of interleaved sheets of iron and plastic, typical e/p and σ/E values are 1 4 and 25%, respectively, at E = 5 GeV. For a uranium/plastic calorimeter, the corresponding values are about 1.1 and about 15%. Extensive Monte Carlo simulation calculations were performed to optimize the ORNL/LBL mid-rapidity calorimeter design, with regard to both e/p, σ/E, and overall containment. It was decided that the length of the lead/plastic electromagnetic section will be 15 radiation lengths and that the hadronic section will be sufficiently long to contain 96% of the energy of a 50-GeV proton. Both of these lengths are considerably greater than those of the CERN calorimeters. For each stack, the electromagnetic section will thus consist of 27 lead sandwiches (consisting of 1-mm Al + 3-mm Pb + 1-mm Al), interleaved with 27 plastic sheets (3 mm thick). The length of the section is 21.6 cm, and the weight is 280 kg. The hadronic section will consist of 122 stainless steel plates of 8-mm thickness, interleaved with 122 scintillator plates of 3-mm thickness. The length of this section is 134 cm, and the weight is 1947 kg. The overall length of each stack will thus be 156 cm, and the overall weight will be 2227 kg. The calculated e/p ratio for the above design is 1.5 at 5 GeV. However, by balancing the electromagnetic and hadronic signals, the effective e/p values are 0.91 at 1 GeV and 1.01 at 5 GeV. The calculated resolution values are 26% at 1 GeV and 17% at 5 GeV. Thus, the overall performance of our design is expected to be only marginally worse than that of a uranium calorimeter.

Since the energy resolution requirements for the zero-degree trigger calorimeter are higher than those of the mid-rapidity calorimeters, and since only one has to be built, it was decided to build it entirely from a uranium/plastic combination. Monte Carlo calculations were performed for a 70-cm by 70-cm array of 10-cm by 10-cm cells, with an electromagnetic section consisting of 32 uranium sheets (each 0.2 cm thick) interleaved with 32 plastic sheets (each 0.3 cm thick) and with a hadronic section consisting of 275 uranium/plastic cells with the same dimensions as those of the electromagnetic section, except that the uranium sheets will be 0.3 cm thick. The output events were analyzed to determine the effects of calorimeter size on resolution and on containment. 30 cm x 30 cm, 50 cm x 50 cm, and 70 cm x 70 cm calorimeters were considered. The performance of the 50 cm x 50 cm calorimeter was deemed to be marginal. For example, its containment for a 50-GeV proton was 97% of the containment of a 70 cm x 70 cm device. The resolution was also degraded. It was thus decided to build a 60 cm x 60 cm zero-degree calorimeter.

Both the mid-rapidity calorimeters and the zero-degree calorimeters will be built during 1985 and will be available for tests and calibrations in mid-1986.

---

1. Engineering Physics and Mathematics Division.

PERFORMANCE OF RECOIL MASS SEPARATOR

H. J. Kim C. E. Bemis, Jr. P. H. Stelson

The ability of the recoil mass separator (RMS) to perform the separation of evaporation residues has been studied in detail for a number of target-projectile combinations. 0° excitation functions and angular distributions of evaporation residues induced by fusion of O, F, and Ti beams with Ti, Zr, Ta, and W targets near and below the Coulomb barrier were investigated. Calibrations of the RMS acceptance were made using both the 180° backscattering of light-ion projectiles and alpha particles from a ^{244}Cm source. The acceptance was established as a function of ion velocity and charge to obtain absolute fusion cross sections. The fraction of residues collected by the RMS at 0° ranges from less than 1% for such asymmetric systems as O + W to more than 30% for symmetric systems (e.g., Ti + Ti). Although with lower collection efficiencies, the residues from asymmetric systems are separated much more cleanly from the energy degraded incident particles. Because

observed results depend on kinematics of particular reaction as well as on the quality of incident beam, deducing a simple figure of merit regarding the filtering power of the RMS is not uniquely possible. But, our study indicates that fusion cross sections down to the few hundred microbarn level should be obtainable for most target-projectile combinations using the RMS. Preparations are in progress to study nuclei far from stability, which are generally produced with very small cross section in fusion reactions, by observing decay of separated residues or coincidences between prompt gamma rays and the residues.

As an example of our calibration experiments and tests, we mention here our experiments with monoenergetic ^{208}Pb ions, which served as a model for our evaporation residue experiments for the ^{16}O + ^{182,184,186}W Pb compound systems. Monoenergetic ^{208}Pb ions in the specific energy range 25-40 keV per amu were generated from 180° Rutherford backscattering of 25- to 40-MeV ^{12}C ions from ^{208}Pb. Incident beam fluence was simultaneously determined using a monitor detector at ~30° with a well-defined solid angle. The velocity acceptance window, charge-state acceptance window, and absolute efficiency of the RMS as a function of Pb ion energy was determined. The backscatter kinematics determine a unique energy for ^{208}Pb, with a nearly flat angular distribution across the RMS aperture when the RMS is at 0°. Our calibrations indicate that for 35 keV per amu, Pb recoils from ^{16}O on W, the charge-state acceptance is ~20%; velocity acceptance is ~60%; and the angular distribution acceptance is ~4%. For this very asymmetric projectile (^{16}O), target (^{182,184,186}W) system, the relatively broad angular distribution is clearly the limiting RMS efficiency factor. The overall efficiency is ~0.5% in these cases. The kinematically reversed conditions, W projectile + O target, would dramatically improve the efficiency.

DEVELOPMENT OF A POLARIZED Eu TARGET

B. Shivakumar C. E. Bemis, Jr.
J. R. Beene D. Shapira

As part of the development of a polarized Eu target, the gas jet apparatus[1] has been modified to facilitate operation at high temperatures. The existing nozzle assembly has been replaced by one capable of being heated to 900°C. The assembly is connected to a high temperature feedthrough which takes the gas line at high temperature from a region of high vacuum to a region at atmospheric pressure. A similar feedthrough then connects to the oven/seeder assembly which has also been designed to operate up to 900°C. The oven/seeder contains two reservoirs, one for heating Eu and the other for heating the Ar carrier gas. The heating of the two reservoirs is done in an Ar atmosphere. The temperature of the apparatus is controlled at the Ar and Eu reservoirs and at the nozzle. An Ar gas jet has been operated successfully at 850°C. The apparatus is currently being setup to test the seeding of Eu atoms into the Ar jet. Measurements will be made of the Eu target thickness (using elastic scattering of an ^{16}O beam) at temperatures around 800°C. Once the target has been optimized, we intend to proceed with the optical pumping of the Eu atoms in the jet and the full implementation of the polarized target facility.

---

1. J. L. C. Ford, Jr. et al., Phys. Div. Prog. Rep. Sept. 30, 1983, ORNL-6004, p. 153 (1983).
2. B. Shivakumar et al., Phys. Div. Prog. Rep. Sept 30, 1983, ORNL-6004, p. 154 (1983).

A LOGARITHMIC TOTAL EVENT COUNTER SYSTEM FOR THE STUDY OF HEAVY ION INDUCED REACTIONS

D. Shapira J. L. Blankenship[1]
B. L. Burks

The products from a reaction induced by energetic heavy ions are in general highly excited. The particles that are eventually detected are fragments that have cooled down by emission of γ radiation, neutrons, protons, alpha particles or heavier nuclei.

A measurement of observables associated with the primary reaction products requires kinematic reconstruction of the initial event based on simultaneous detection of all (or most of) the decay products and their residues. While this approach is typical in the study of high energy nuclear collisions, it has usually been bypassed in low energy nuclear physics. At bombarding energies below a few MeV/amu, excitation of the primary outgoing fragments is limited and very few products emerge. Furthermore, the cross sections for the processes studied are quite large in general, so that limited measurement of a few final products and some correlation studies usually suffice. At energies above 10 MeV/amu one expects that processes where the two outgoing products are highly excited will dominate. Also, processes where the incoming projectile or target nuclei themselves break up become important. As the excitation energy of the products increases and as fragmentation becomes more probable, the number of final products emerging from the collision increases rapidly. Extraction of the observables associated with the primary process from measurement of individual products then becomes increasingly dependent on conjecture and modeling of the reaction process.

We propose to build a multiparticle counter system that will measure a large fraction of the products emerging from a collision between energetic heavy ions. Practicality dictates that such a device cannot address all reactions but it should address a wide range of nuclear physics phenomena.

We will limit the study to systems of nuclei lighter than A ~ 100. Heavier systems decay predominantly via γ and neutron emission or fission, and the 4π γ-ray spectrometer addresses

similar inclusive measurements for these heavy systems. For the lighter systems the principal decay mode is light particle emission: neutron, proton and α particles; the emission of γ rays and symmetric fission, although present, are not dominant for this mass range.

The detector we plan to build will be designed primarily to detect the residue of a fast moving heavy fragment and all, or most, of the light particles emitted from it.

Figure 2.96 is a simulated density contour for alpha particles emitted in the forward hemisphere from collisions of 890 MeV ^{58}Ni particles with ^{12}C nuclei. The density contour shows only alpha particles that emerge in coincidence with a $^{62}Sc_{21}$ ion detected at $\theta = -4°$ $\phi = 180°$ (in plane). There is a strong concentration of α particles in the direction of the emitted Sc fragment. The α particles evaporated from a large, fast-moving fragment are emitted, moving approximately in the same direction as the heavy fragment because their most probable velocity in the rest frame of the emitting nucleus is small (only a few MeV/amu). With a counter system that covers the approximate area shown in the box on Fig. 2.96 one can capture, therefore, most of the emitted light particles together with the heavy residue.

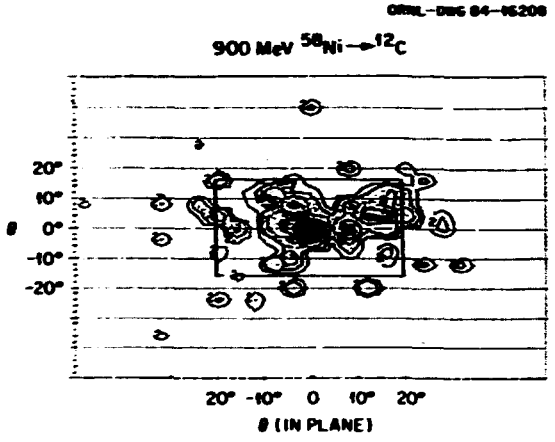

Fig. 2.96. Density contours for α particles emitted in correlation with scandium nuclei detected at $\theta = 4°$ and $\phi = 180°$.

The counter system we are proposing is shown, schematically, in Fig. 2.97. The front portion consists of a large area, gas-filled ionization chamber. The 30-cm-deep ionization chamber will stop the heavy residue and provide an event trigger. The detector will yield energy (<1% resolution), energy loss (~2% resolution) and spatial position (x,y) signals. The multi-electrode design will permit identification of heavy ions over a wide dynamic range (better than 1:20 in ion ranges) but light particles will deposit a negligible amount of energy in the gas counter. An array of 96 scintillation counter telescopes arranged in a 6 x 16 array behind the gas counter will yield the spatial position (2.4° x 2.4° granularity), energy and identity of light particles. Each element of the scintillation counter array will include a 1-mm-thick ΔE and an approximately 10-cm-thick E detector. Charged light particles will be identified by the ΔE-E technique and this design

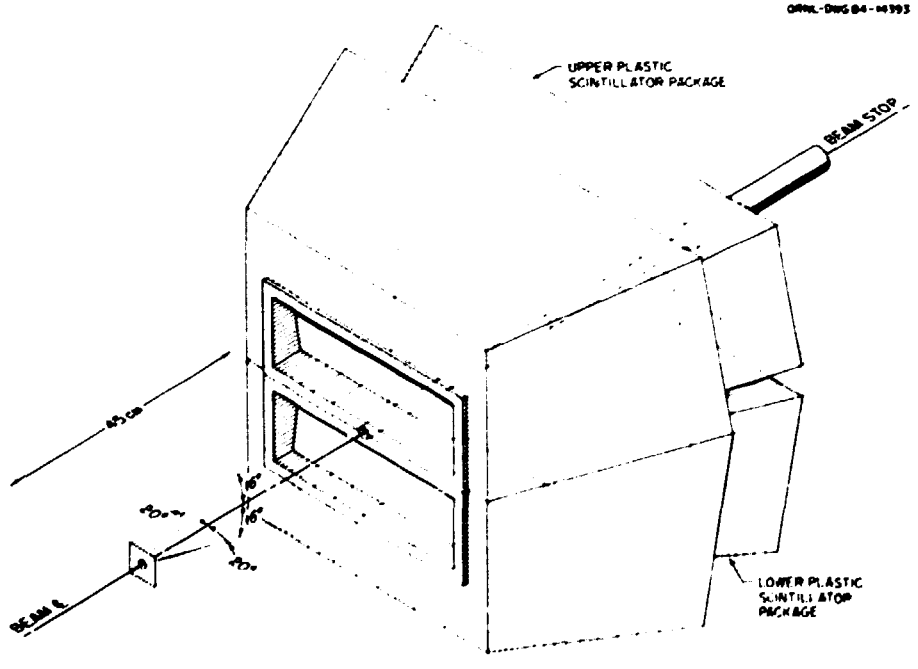

Fig. 2.97. Schematic drawing of the HILI detector.

should identify protons with energies ranging from 10 to 140 MeV and alpha particles with energies ranging from 30 to 400 MeV. The neutrons will leave a signal only in the thicker scintillator. Crude TOF information will be used to get the neutron energy (~10-15% resolution).

The ionization counters straddle the reaction plane and are organized in two separate volumes. They can be operated at different pressures and can thus detect and identify two fragments for an asymmetric mass split. Each half of the detector has a split anode structure that allows the simultaneous study of two heavy fragments, one in each half. Provision is also made for the beam to exit the chamber and be stopped downstream far from any of the light-ion detectors.

---

1. Instrumentation and Controls Division, ORNL.

LARGE IONIZATION DETECTORS FOR HEAVY ION REACTIONS

J. L. Blankenship[1] F. E. Obenshain
A. H. Snell

Several design changes for this time-of-flight (TOF) facility were reported in the previous progress report.[2] Additional design modifications to the 80-cm ion chamber have been made. Curved anodes and Frisch grid were used in the original design to provide maximum rigidity, and therefore minimum microphonics. However, the Frisch grid curvature introduces a variation in the electric field strength from center to outside extremes of the drift space, which causes variations in the drift velocity and drift time as a function of out-of-plane angle.

The new design shown in Fig. 2.98 incorporates flat aluminum plates for the anodes, guard bars on the sides for field grading and electrostatic shielding from housing ground, and a flat Frisch grid structure. Two grid structures have been fabricated. The first design employs stainless steel wire of 280-μm diameter in a woven wire mesh spaced 8 x 8 cm^2 and provides good shielding and fair reach-through-field charge collection behavior. The second design consists of a plane of phosphor bronze wire of 114-μm diameter spaced 1.59 mm on center. This second design has not been tested in the 80-cm ion chamber, but has been used with success in the 40-cm ion chamber used in the broad range spectrometer.

---

1. Instrumentation and Controls Division, ORNL.
2. ORNL Progress Report for period ending September 30, 1983, ORNL-6004, p. 152.

ORNL Photo 6271-84

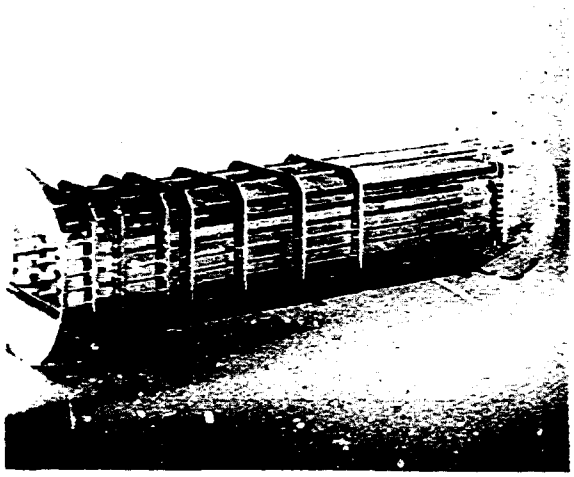

Fig. 2.98. The electrode assembly of the 80-cm-deep ion chamber. The four planar anodes are shown at the top, and the Frisch grid is below the anode assembly. Field shaping is facilitated by the guard bars which are on each side and uniformly spaced from the Frisch grid to the cathode at the bottom.

DESIGN OF AN EVAPORATION RESIDUES DETECTOR

J. L. Blankenship[1] F. E. Obenshain

A gas-filled detector system for measuring ΔE, E, θ, and φ, and velocity of evaporation residues has been designed and is shown in Fig. 2.99. Velocity is determined by measuring

ORNL Photo 6148-84

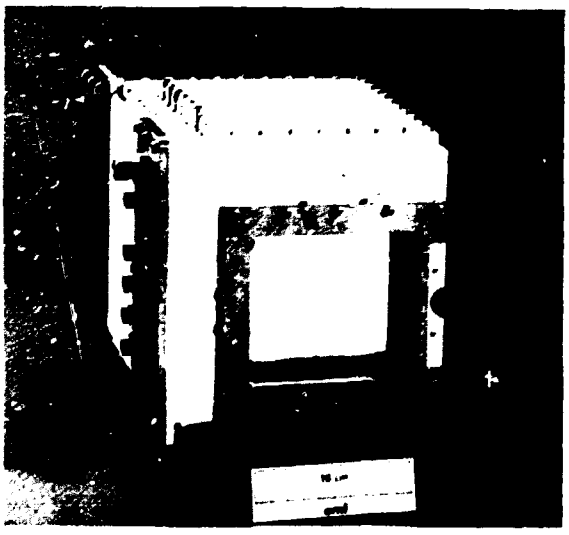

Fig. 2.99. Front view of evaporation residue detector showing gas inlet and outlet.

the time of flight over a 20-cm path using Breskin-type multiwire, position-sensitive proportional counters as start and stop detectors. The entrance window is made of ~55 μg/cm² polypropylene and has an 8.5 x 10.5 cm² opening. The start detector has an 8 x 10 cm² sensitive area, and the cathodes are constructed of 90 percent transparency, 45 x 45 lines/inch nickel mesh.

A conventional, Frisch grid ionization chamber is located between the start and stop detectors, in the same gas volume. The anode is 8-cm-long and is a segment of a circular band whose inner and outer radii are selected to match the target-to-anode distances. This design provides a ΔE signal which is independent of in-plane angles. The stop detector has aluminum-striped cathodes for θ and φ readout and has an 8 x 14-cm² working area. The detector system is designed to fit inside the 1.6-m chamber against the outside wall.

At the rear of the detector, a 1-mm-thick sheet of NE-102 plastic scintillator, enclosed in a light pipe and pressure bearing window, provides a measure of the residual energy. The chamber design incorporates a semicircular segment of a 1.9 cm i.d. pipe in the sidewall to permit the closest possible approach to the beam center line. After the detector design has been demonstrated as satisfactory, a second detector, which is a mirror image of the first, will be built. This detector pair will then span the beam.

---

1. Instrumentation and Controls Division, ORNL.

AFTERPULSES FROM RESIDUAL GASES IN PHOTOMULTIPLIER TUBES

N. W. Hill[1] J. A. Harvey[2]
D. J. Horen C. H. Johnson

At the ORELA time-of-flight facility we have extended the energy for neutron detection down to about 10 keV for liquid and plastic scintillators by accepting pulses corresponding to a few photoelectrons. At such low levels there is a background of afterpulses which originate either in the scintillator or in the photomultiplier, a 5-inch RCA-8854 PMT, but appear several μsec after the earlier detection of a neutron or γ-ray.

In our previous study[3] of the afterpulsing phenomenon we observed pulses originating from electron-atom collisions in various residual gases in the PMT and we made the conventional[4] assumption that most of that ionization occurred in the large region between cathode and first dynode. However, our subsequent calculations on that assumption gave spectral shapes inconsistent with those observed. Therefore, we have extended the measurements in an effort to find the points of origin of most of the ions.

For this study we irradiated various new RCA-8854 tubes with light pulses from a Monsanto MV52 green LED. Each pulse ejected about 600 electrons from the cathode. Afterpulse time spectra were recorded in 1-nsec channels out to 6 μsec and in 25-nsec channels at later times. Spectra were recorded with a multistop per start-time digitizer with a 1.1-μsec deadtime and corrected for deadtime losses. Figure 2.100 shows for one tube the spectrum in units of afterpulses per photoelectron per μsec. We attribute the narrower peaks to backstreaming ions from localized surfaces and the broader peaks to ions from residual gases. Figure 2.101

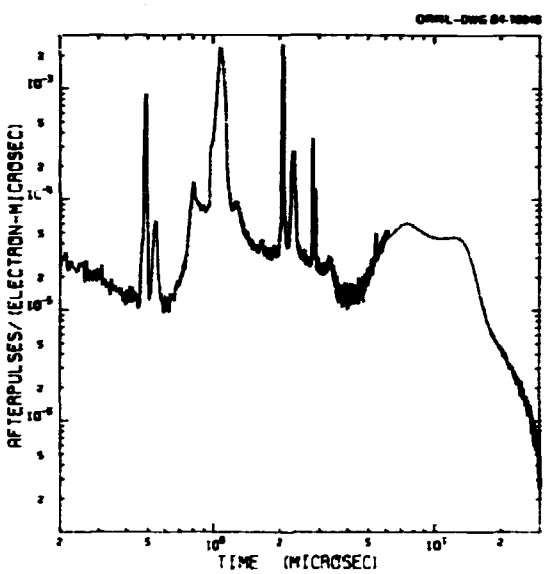

Fig. 2.100. Afterpulse spectrum for an RCA-8854 photomultiplier tube.

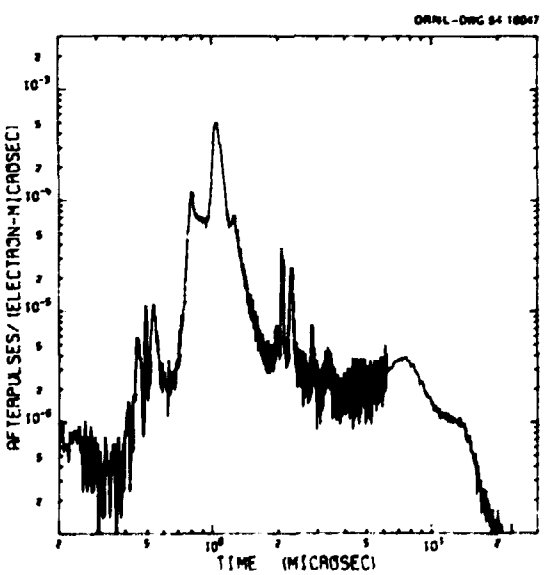

Fig. 2.101. Afterpulse spectrum for the PMT of Fig. 2.100 with the 2nd dynode gated off during the initial pulse.

shows the spectrum for this tube with the 2nd dynode gated off during the initial pulse. Gating eliminates most ion formation in the dynode region. A comparison with Fig. 2.100 shows that most ions in the ungated mode originate in the dynode region. The exception is the "pedestal" between 0.8 and 1.2 μsec. In fact, our calculations predicted this "pedestal" arises from the residual He gas between cathode and first dynode.

Also observed is a pronounced peak on top of the pedestal at 1.1 μsec. Previously[3] we assumed this peak also arises from ions in the cathode-dynode region but now we conclude that it arises from ionization of the He gas in the region between the 1st and 2nd or 3rd dynodes. It is more intense because the 1st dynode has high gain. In an auxiliary experiment we measured the spectrum for an RCA-4522 PMT, which does not have the high gain dynode, and we found a much smaller peak relative to the pedestal. To further check this conclusion on the origin of the pedestal-peak we varied the PMT grid voltage relative to the cathode and first dynode. As expected, a change in voltage such as to decrease grid-to-cathode acceleration but to increase extraction from the dynodes resulted in a later pedestal but earlier peak.

In addition to the 1.1-μsec He^+ peak, Figs. 2.100 and 2.101 also show broad spectra of pulses due to ions originating somewhere in the dynode region. If such a PMT is used with a scintillator for neutron detection, little can be done to eliminate the afterpulses from a detected neutron. However, when used at a facility such as ORELA, the serious afterpulses from the γ-burst can be eliminated by gating of the dynode during the burst. Further improvement can be obtained by the use of 2 PMT's in fast coincidence on the same scintillator.

---

1. Instrumentation and Controls Division.
2. Engineering Physics and Mathematics Division.
3. N. W. Hill et al., Physics Division Progress Report, ORNL-6004, 155 (1983).
4. G. A. Morton, H. M. Smith, and R. Wasserman, IEEE Trans. on Nucl. Sci. NS-14, 443 (1967).

PREPARATION OF TARGETS FOR NUCLEAR PHYSICS RESEARCH

D. K. Galbraith F. K. McGowan

The preparation of targets for nuclear physics research by the SPUTTERBELL (focused ion beam sputtering system) has continued to be extremely useful. Thin targets from materials with very high melting points, such as refractory metals, are easily produced. Self-supporting targets of Si as thin as 30 μg/cm² have been produced. Since ion beam sputtering is a "cool" process, thin targets of Pb evaporated on carbon foil backings have been covered with 5 μg/cm² carbon by sputtering successfully.

Table 2.16 contains examples of targets prepared by ion beam sputtering and by evaporation.

Table 2.16. Targets for nuclear physics research

Element	Weight	Backing	Method	Remarks
Si	30-120 μg/cm²	None	Sputtering	
^{74}Ge	500 μg/cm²	None	Sputtering	
^{90}Zr	50-150 μg/cm²	30 μg/cm² C	Sputtering	Recoil mass spectrometer
^{93}Nb	50-150 μg/cm²	30 μg/cm² C	Sputtering	Recoil mass spectrometer
^{181}Ta	50-75 μg/cm²	30 μg/cm² C	Sputtering	Recoil mass spectrometer
^{238}U	1 mg/cm²	None	Sputtering	
^{27}Al	30-50 μg/cm²	None	Evaporation	
Ag	1 mg/cm²	None	Evaporation	
In	160 μg/cm²	None	Evaporation	
^{124}Sn	1.0-1.5 mg/cm²	None	Evaporation	
^{128}Te	0.8 mg/cm²	1 mg/cm² Au	Evaporation	Recoil distance device
Sb	1 mg/cm²	0.5 mg/cm² Au	Evaporation	
^{197}Au	150 μg/cm²	10 μg/cm² C	Evaporation	Line shaped target
^{197}Au	170 μg/cm²	None	Evaporation	
^{197}Au	40 μg/cm²	0.8 mg/cm² ^{128}Te	Evaporation	Covered to contain ^{128}Te target in recoil distance device
^{197}Au	150 μg/cm²	1 mg/cm² Sb	Evaporation	Covered to contain Sb
^{208}Pb	50 μg/cm²	20 μg/cm² C	Evaporation	Recoil mass spectrometer
Pb	2-3 mg/cm²	1 mg/cm² ^{122}Sn	Evaporation	Pb-backed target for γ-ray spectroscopy
Pb	30 mg/cm²	2.5 μm Ni	Evaporation	Stoppers for recoil distance device
^{208}Pb	50-200 μg/cm²	20 μg/cm² C	Evaporation	

Many productions of detector windows and planes for avalanche counters were done. Carbon stripper foils for ORIC and tandem are now being produced routinely.

SPECIAL ENHANCEMENTS TO THE EVENT HANDLER

D. C. Hensley

The Event Handler[1,2] is a programmable CAMAC based processor with auxiliary crate controller capability and is the major control device for data acquisition at the HHIRF. Because of the success of this device in managing the front-end data acquisition electronics, special emphasis has been placed on making it as general as possible without degrading its basic performance.

One particular problem to be faced in data acquisition is what to do with 24 bit devices when the principle data stream is only 16 bits wide. CAMAC supports 24 bit devices, principally scalers, but most data acquisition is based on 16 bits due to the 32 bit structure of typical data acquisition computers. The Event Handler already had special instructions for setting the top 4 bits of a 16 bit word (useful when 11 and 12 bit ADCs are used), but it lacked any general way to transmit the full 24 bits from the CAMAC dataway over a 16 bit path.

The following enhancements help to overcome this difficulty. It has always been possible to transmit the 16 bottom bits of a CAMAC word, but it is now possible to transmit the 8 top bits of the same CAMAC word. This byte is placed in the position of the 8 bottom bits (the 8 top bits are set to zero) of the 16 bits of the transmitted word. This top byte can be transmitted at any time, either before or after the 2 bottom bytes are transmitted. If the upper byte needs to be communicated over the CAMAC dataway, but in the position of the lowest byte, this can be done by first writing the top byte of the Event Handler CAMAC data register (CDR) into the 2 lower bytes of the same register (essentially shifting the top byte down 2 bytes). Then the newly formed CDR can be written out over the CAMAC dataway to whichever module requires it. Since this operation destroys the original 2 lower bytes, one would presumably transfer these bytes first.

The handling of the Event Handler Save Register was made more symmetric. Not only can one store a 24 bit CAMAC data word in this register, but now one can either transmit the 16 bottom bits or move them to the CDR. This latter capability allows one to move a 16 bit word from one crate to another, moving it through the Event Handler.

Provisions have been made for enhancing the speed of the Event Handler – special "hooks" have been provided which allow an external device to specify the unconditional branch address in a branch operation. A particular external device would be one which could look ahead to determine which of many possible routines needed servicing next.

In order to protect the integrity of the final data stream, the Event Handler has been changed so that it will wait forever to transmit a word into a full FIFO. Formerly it would wait about 4 ms before it would proceed to its next operation. While it is recommended that the Event Handler not be used in this way, in the event that a FIFO should manage to become totally full, a requested transmission will not get lost.

Finally, the auxiliary crate controller part of the Event Handler, which previously could generate normal CAMAC cycles or "short" CAMAC cycles (terminated at the end of timing strobe S1), can now generate even shorter cycles in which timing strobe S1 is not generated on the CAMAC dataway.

In addition to their use at the HHIRF, Event Handlers are being implemented at the University of Notre Dame in conjunction with a project at Argonne National Laboratory and at Texas A & M University. Use of the device is also being considered for projects at ANL, Princeton, Chalk River, and Kansas State.

---

1. D. C. Hensley, IEEE Trans. Nucl. Sci. NS-26, 710 (1979).
2. D. C. Hensley, IEEE Trans. Nucl. Sci. NS-26, 4454 (1979).

3. THE UNISOR PROGRAM

The University Isotope Separator - Oak Ridge is a consortium of eleven academic institutions, Oak Ridge Associated Universities and Oak Ridge National Laboratory. It operates an isotope separator installed on-line to the accelerators within the Holifield Heavy Ion Research Facility. The accounts which follow describe work at the UNISOR facility or work associated with UNISOR research performed principally by investigators outside of the Physics Division. Research and development performed at UNISOR principally by Physics Division staff members are included in the Nuclear Physics section of this report.

In addition, theoretical research performed by UNISOR staff and collaborators is included in the Theoretical Physics section.

THE UNISOR MASS SEPARATOR

R. L. Mlekodaj[1] H. K. Carter[1]
E. H. Spejewski[1] J. D. Cole[2]

The vacuum system of the mass separator has been completely converted to turbomolecular pumps in order to provide a relatively oil-free vacuum. This change was implemented to cut down on problems caused by deposits of cracked diffusion pump oil on lenses, insulators and other critical surfaces. This changeover was coupled with a complete cleaning and realignment of all internal surfaces.

In order to accommodate a rearrangement of the experimental space in the south addition of Building 6000, the high-voltage rack with all of the ion source supplies has been relocated in a new dehumidified room constructed above the off-line ion source area. The control console and the power distribution cabinet also are in new positions.

In order to facilitate the tuning of beams down the sensitive laser facility, several new aids have been built into the separator ion-optical system. A new horizontal and vertical deflection system has been installed at the exit of the first lens box to precisely align the beam entering the second lens box. This eliminates steering introduced when the beam is not correctly centered. A vertical deflection adjustment has been built into the 30° deflectors to correct any vertical error at that point.

In addition, a new Faraday cup located on a moveable carriage in the focal plane allows the monitoring of a beam at any position along the focal plane and has been useful for continuously monitoring one beam while transmitting another mass through one of the beam lines.

Several new developments are helping to carry out the defocussing of the tandem beams which is necessary to avoid the target-destroying tight focus attainable from the tandem. Highly damage-resistant phosphors of Al_2O_3 have been produced and installed in the UNISOR beam handling box as well as a two-dimensional beam scanner which is integrated into the MHIRF beam-scanning system. These aids, along with operator experience, enable uniform defocussing of the beam spot up to the optimum size of about 8 mm diameter while retaining greater than 90% of available beam intensity.

The last section of beam line to UNISOR from the 1.6-m scattering chamber to the He-Jet box has now been upgraded to the new all stainless-steel contruction and should result in much improved vacuum quality in that region.

A new, faster stepping-motor controller and a higher torque motor have been installed on one of the UNISOR tape transport systems. With this system and a simple loop of tape, a source can be moved to a counting station in about 0.15 sec. Because of built-in acceleration and deceleration, longer distances can be covered in proportionately shorter times.

---

1. UNISOR, Oak Ridge Associated Universities.
2. Louisiana State University; present address: Idaho National Engineering Laboratory, Idaho Falls, Idaho.

NUCLEAR ORIENTATION FACILITY

E. H. Spejewski[1] J. H. Hamilton[3]
F. T. Avignone, III[2] K. S. Krane[4]

Funding has been obtained for a nuclear orientation facility to be installed in the UNISOR laboratory. It will consist of a helium dilution refrigerator and superconducting magnet to provide orientation at temperatures ≈ 10 mK. The final design of the system is nearing completion. It is expected that a purchase order will be placed for the major equipment early in 1985, with construction of the separator beam-transport, and support mechanisms initiated thereafter.

This facility will allow the measurement of angular distributions of nuclear radiations and, therefore, a determination of multipole mixing ratios of the radiations and of spin-parity changes between the nuclear levels. A nuclear magnetic resonance capability will be added to allow the measurement of the nuclear g-factor of

ground and isomeric states, and thus a direct determination of spin.

---

1. UNISOR, Oak Ridge Associated Universities.
2. University of South Carolina, Columbia, South Carolina.
3. Vanderbilt University, Nashville, Tennessee.
4. Oregon State University, Corvallis, Oregon.

SEARCH FOR DEFORMATION IN THE VERY LIGHT SAMARIUM ISOTOPES

R. L. Mlekodaj[1] P. Semmes[2]
G. A. Leander[1] R. W. Fink[2]
R. A. Braga[2] K. S. Toth
B. D. Kern[3]

The possibility of a new region of stable nuclear deformation around the neutron-deficient Sm isotopes has recently been discussed in the literature.[4] These calculations of intrinsic equilibrium deformations indicate that these nuclei should be rotational at A ~ 135. The determination of the rotational properties of this region, as well as the characteristics of the adjacent transition region coupled with the possibility of observing beta-delayed proton emission, promises a rich area for many future experiments.

Recent on-line ion source test runs have shown that Eu and Sm isotopes around this region can be made in good yields using a ^{35}Cl or ^{32}S beam on a natural Ag target. All known gamma lines from the decay of Sm isotopes from mass 135 to 140 and Eu isotopes of mass 139 and 140 were observed in a few minutes running time at each mass. Longer experiments are being planned.

---

1. ORAU, Oak Ridge Associated Universities.
2. School of Chemistry, Georgia Institute of Technology, Atlanta, Georgia.
3. Department of Physics and Astronomy, University of Kentucky, Lexington, Kentucky.
4. G.A. Leander and P. Möller, Phys. Lett. 110B (1982) 7.

THE DECAY OF MASS-SEPARATED ^{191m}Hg AND ^{191g}Hg TO ^{191}Au AND ODD-MASS Au SYSTEMATICS

J. L. Wood[1] E. F. Zganjar[2]
C. D. Papanicolopulos[1] E. Van Walle[3]
R. L. Mlekodaj[4]

In the studies of the $^{191m}Hg \rightarrow {}^{191}Au$ and $^{191g}Hg \rightarrow {}^{191}Au$ decay schemes at UNISOR and at KOOL/LISOL (see the report here on dynamical supersymmetries in ^{191}Au) we have obtained very detailed information on the structure of ^{191}Au. In particular, we believe the $^{191m}Hg(J^\pi = 13/2^+)$ and ^{191g}Hg ($J^\pi = 3/2^-$) decays, together, populate all states of spin 1/2 - 17/2 below 1 MeV. This, in combination with the unique level spin and transition multipolarity assignments made possible by the nuclear orientation data, provides an exacting test of the scheme of systematics that we have proposed[5,6,7] for the odd-mass Au isotopes. This is a crucial step in the chain of level scheme studies that we have made to probe the structure of nuclei far from β stability in the Pt, Au and Hg isotopes. Without the use of systematics, elucidating nuclear structure far from β stability is, in our opinion, impossible. These data are in the process of being analyzed.

---

1. School of Physics, Georgia Institute of Technology.
2. Louisiana State University.
3. Catholic University of Louvain, Louvain, Belgium.
4. UNISOR, Oak Ridge Associated Universities.
5. E.F. Zganjar, et al., Phys. Lett. 58B, 159 (1975).
6. E.F. Zganjar, in Future Directions in Studies of Nuclei Far From Stability, ed. J.H. Hamilton, et al. (North Holland, Amsterdam, 1980), p. 49-62.
7. J.L. Wood, ibid., p. 37.

DYNAMICAL SUPERSYMMETRIES AND THE POSITIVE-PARITY STATES IN ^{191}Au

J. L. Wood[1] L. Vanneste[6]
C. D. Papanicolopulos[1] E. Van Walle[6]
E. F. Zganjar[2] M. Huyse[6]
J. D. Cole[3] A. V. Ramayya[7]
K. S. Krane[4] J. H. Hamilton[7]
R. L. Mlekodaj[5] J. Vervier[8]

It has been suggested that dynamical supersymmetries may be present in the spectra of complex nuclei.[9] The particularly simple supersymmetric structure of Ref. 9 is generated by a single particle with j = 3/2 and L = 0,2 bosons with O(6) symmetry. The nuclide ^{191}Au, which has a j = 3/2 ground state and lies in a region of even-even nuclei with O(6) symmetry,[10] is under study to determine whether its low-lying spectrum can be described by this classification scheme. This is an extension of the study of ^{193}Au described in Ref. 11.

High statistical quality γ-γ-t data for the $^{191m}Hg \rightarrow {}^{191}Au$ and $^{191g}Hg \rightarrow {}^{191}Au$ decays, taken at UNISOR, have been analyzed and a level scheme for ^{191}Au has been constructed. The next step is the assignment of level spins and transition multipolarities to the scheme. This is being done using low-temperature nuclear orientation data taken at the KOOL facility operated on-line to the Leuven-Isotope-Separator-On-Line (LISOL) at the CYCLONE cyclotron in Louvain-la-Neuve, Belgium. These data are being analyzed.

---

1. School of Physics, Georgia Institute of Technology.
2. Louisiana State University.

3. Louisiana State University; present address: Idaho National Engineering Laboratory, Idaho Falls, Idaho.
4. Oregon State University, Corvallis, Oregon.
5. UNISOR, Oak Ridge Associated Universities.
6. Catholic University of Louvain, Louvain, Belgium.
7. Vanderbilt University, Nashville, Tennessee.
8. University of Louvain-la-Neuve, Louvain-la-Neuve, Belgium.
9. F. Iachello, Phys. Rev. Lett. 44, 772 (1980).
10. R.F. Casten and J. Cizewski, Nucl. Phys. A309, 477 (1978).
11. J.L. Wood, Phys. Rev. C24, 1788 (1981).

GROUND STATE SHAPE AND CROSSING OF NEAR SPHERICAL AND DEFORMED BANDS IN ^{182}Hg[1]

W. C. Ma[2] K. Zhao[2]
A. V. Ramayya[2] J. D. Cole[3]
J. H. Hamilton[2] E. F. Zganjar[3]
S. J. Robinson[2] E. H. Spejewski[4]
M. E. Barclay[2]

The energy levels of ^{182}Hg have been identified for the first time through comparison of in-beam studies of the reactions ^{156,154}Gd (^{32}S,4n) ^{184,182}Hg and γ-X-ray coincidences. Levels up to 12^+ in ^{182}Hg were established from γ-γ coincidences and singles measurements. The data establish that the ground state shape is near spherical, and that the ground band is crossed by a well-deformed band at 4^+. In contrast to IBA model predictions that the deformed band will rise in energy in ^{182}Hg compared to ^{184}Hg, the energies of the deformed levels in ^{182}Hg continue to drop.

---

1. Abstract of paper: Phys. Lett. 139B (1984) 276.
2. Vanderbilt University, Nashville, Tennessee.
3. Louisiana State University, Baton Rouge, Louisiana.
4. UNISOR, Oak Ridge Associated Universities.

SHAPE COEXISTENCE IN ^{187}Au AND ^{185}Au

E. F. Zganjar[1] M. A. Grimm[3]
J. L. Wood[2] H. K. Carter[4]

We are exploring the possibility that the low-energy structure of ^{187}Au and ^{185}Au contains four families of states, via:

^{186}Pt(0_1^+,2^+,....)$\otimes\nu^{+1}$, $\pi = h_{9/2}, i_{13/2}$
^{186}Pt(0_2^+,2^+,....)$\otimes\nu^{+1}$, $\pi = h_{9/2}, i_{13/2}$
^{188}Hg(0_1^+,2^+,....)$\otimes\nu^{-1}$, $\pi = d_{3/2}, h_{11/2}, d_{5/2}, s_{1/2}$
^{188}Hg(0_2^+,2^+,....)$\otimes\nu^{-1}$, $\pi = d_{3/2}, h_{11/2}, d_{5/2}, s_{1/2}$

This involves analysis of γ-γ-t and e-γ-t data for the decays of ^{187m}Hg($J^\pi = 13/2^+$), ^{187g}Hg($J^\pi = 3/2^-$), ^{185m}Hg($J^\pi = 13/2^+$) and, ^{185g}Hg($J^\pi = 1/2^-$).

The level density in ^{187}Au at low energy is very high, resulting in an extremely high density of lines in the γ-ray and conversion-electron spectra. We have developed techniques of running coincidence gates to elucidate the ^{187m,g}Hg decay schemes and to extract γ-ray and conversion-electron line intensities for closely spaced multiplets. The technique, as applied to the determination of α_k values, is shown schematically in Fig. 3.1. In addition, to check that multiplet structure has not been missed, we are in the process of exhaustively extracting absolute coincidence intensities for both γ-γ and e-γ data. So far, we have established 48 excited states below 1150 keV in ^{187}Au (cf. 27 excited states reported in Ref. 5). Further, we have been able to establish a number of E0+M1(+E2) transitions which we interpret to connect the ^{186}Pt(0_1^+) $\otimes$ $h_{9/2}$ and ^{186}Pt(0_2^+) $\otimes$ $h_{9/2}$ bands. These are listed in Table 3.1. In particular, transitions of 270.71 and 272.19 keV should be noted. These transitions form a multiplet of five lines, the other three having energies of 271.0, 271.47 and 271.67 keV.[5] This quintuplet is clearly established by the coincidence data (which shows the 271.47 and 271.0 keV lines to be in coincidence with lines at 298.57 and 299.4 keV, respectively--other coincident lines and the running gate technique separate these pairs).[6] We have levels which are candidates for ^{188}Hg(0_2^+) $\otimes$ π^{-1} band(s). Further analysis of the ^{187m,g}Hg $\rightarrow$ ^{187}Au decay data are necessary before the picture is complete, but already the scheme that we have constructed points to the (co)existence (in a geometrical picture) of four different "shapes" in ^{187}Au.

The complexity of ^{187}Au suggests that the data we obtained on the ^{185m,g}Hg $\rightarrow$ ^{185}Au decays are inadequate for completely elucidating the ^{185}Au level scheme. This is particularly significant since it has been reported[7] that very converted transitions in ^{185}Au have M1 multipolarity (with abnormal penetration factors).

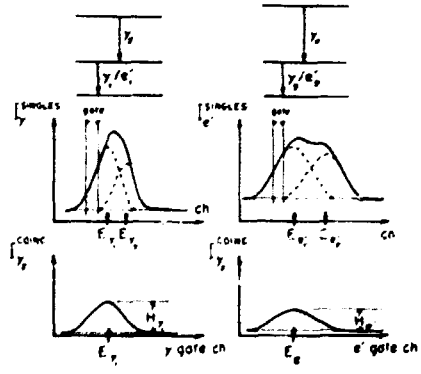

Fig. 3.1. A schematic description of the technique used to determine a_k values for closely spaced doublets (or multiplets). A coincidence gate is advanced across the doublet and, for example, the "coincidence response" of γ_2 to γ_1 and e_1 (H_{γ_1} and $H_{e_1^-}$, respectively) is extracted from γ-γ and e-γ coincidence data, respectively. α_k is determined from H_{e_1}/H_{γ_1} with correction for detection efficiency for γ_1, e_1 and normalization using α_k's (determined in this manner) for transitions of known multipolarity.

Table 3.1. Transitions and their α_k values and γ multipolarities, between states of the same spin in the two $h_{9/2}$ bands in ^{187}Au.

$J_i^\pi \rightarrow J_f^\pi$	E_{trans}(keV)	α_k^{expt}	α_k(M1)th	γ-mult.
$1/2^- \rightarrow 1/2^-$	270.71	1.15^{25}	0.372	E0+...
$3/2^- \rightarrow 3/2^-$	not found	-	-	-
$5/2^- \rightarrow 5/2^-$	284.35	0.29^{11}	0.329	M1+E2
$7/2^- \rightarrow 7/2^-$	272.19	0.81^{19}	0.372	E0+...
$9/2^- \rightarrow 9/2^-$	322.92	0.30^{4}	0.233	E0+...
$11/2^- \rightarrow 11/2^-$	332.42	0.22^{8}	0.215	M1
$13/2^- \rightarrow 13/2^-$	388.19	0.62^{7}	0.142	E0+...

We plan a restudy of these decays to resolve this abnormality and to ascertain if ^{185}Au also exhibits four "shapes".

1. Louisiana State University, Baton Rouge, Louisiana.
2. Georgia Institute of Technology, Atlanta, Georgia.
3. Georgia Institute of Technology, Atlanta, Georgia; present address University of Louisville, Louisville, Kentucky.
4. UNISOR, Oak Ridge Associated Universities.

5. C. Bourgeois, et al., Nucl. Phys. A295, 424 (1978).
6. E.F. Zganjar, et al., in Proc. 4th Int. Conf. on Nuclei Far From Stability, CERN 81-09, p. 630.
7. C. Bourgeois, et al., Nucl. Phys. A386, (1982) 308.

A NEW CLASS OF LOW-ENERGY STRUCTURE AT CLOSED SHELLS: LEVELS IN $^{187-191}$Tl

E. F. Zganjar[1] L. L. Riedinger[5]
J. D. Cole[2] C. R. Bingham[5]
J. L. Wood[3] G. Campbell[5]
G. M. Gowdy[4] E. H. Spejewski[6]

The mechanism of pair excitation across a shell gap to produce shape coexistence now appears to be fairly well established.[7] Recent evidence[8] for low-lying 0^+ states in $^{192-198}$Pb indicates that the excitations are due to a proton 2p-2h configuration. Since the π(2p-2h) excitation in the neutron-deficient even-A Pb isotopes occurs at low energy, one expects to see a new class of low-energy structure in the neutron-deficient Tl, Bi and odd-Pb isotopes. In particular, levels due to the coupling $\pi^{-1} \otimes \pi$(2p-2h) should appear at low energy in the neutron-deficient odd-mass Tl isotopes.

A major puzzle in our studies of excited states in ^{189,191}Tl has been the observation of a considerable number of levels "extra" to those expected from systematic trends in the heavier odd-mass Tl isotopes. We are investigating the possibility that these extra states are due to the couplings $\pi^{-1} \otimes \pi$(2p-2h), π = $s_{1/2}$, $d_{3/2}$. This has necessitated a restudy of the ^{191m}Pb → ^{191}Tl and ^{193m}Pb → ^{193}Tl decay schemes. These data are in the process of being analyzed. There is also evidence[9] for some "extra" states in ^{187}Tl. An attempt to make a detailed study of the ^{187m}Pb → ^{187}Tl decay scheme was unsuccessful, probably because of a long hold-up time in the catcher of the target/ion source (the half life of ^{187m}Pb is 18s).

Our interpretation of the lowest-lying extra states in ^{187,189,191}Tl is shown in Fig. 3.2.

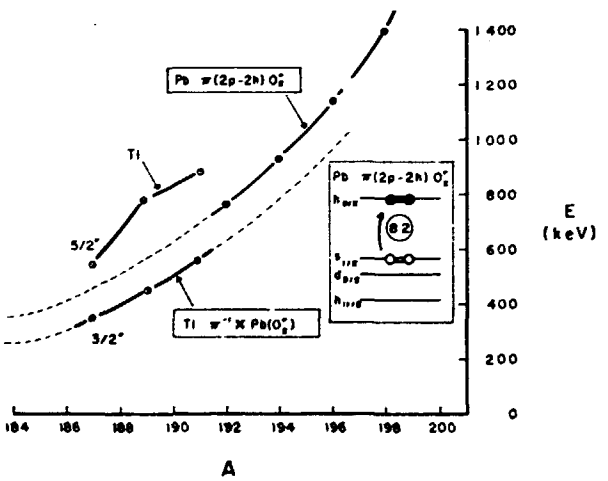

Fig. 3.2. The 0_2^+ energies in $^{192-198}$Pb from Ref. 8, and the new low-lying states in $^{187-191}$Tl. The 0_2^+ states in the Pb isotopes have been argued[8] to be due to the π(2p-2h) configuration. Based on the present systematics, it is suggested that these new low-lying bands in $^{187-191}$Tl are due to the $\pi^{-1} \otimes$ Pb(0_2^+) configuration. The pair excitation leading to the Pb(0_2^+) core state results in a lowering of the Fermi energy from $s_{1/2}$ to $d_{3/2}$ (in a deformed field, this corresponds to a lowering from $1/2^+$ 400↑ to $3/2^+$ 402↑): this is consistent with the tentative spin assignment.

The task for the immediate future is to identify the corresponding states in ^{193}Tl and to make reliable spin-parity assignments.

1. Louisiana State University, Baton Rouge, Louisiana.

2. Louisiana State University; present address: Idaho National Engineering Laboratory, Idaho Falls, Idaho.
3. Georgia Institute of Technology, Atlanta, Georgia.
4. GSI Darmstadt; present address: SCGE Co., Columbia, South Carolina.
5. University of Tennessee, Knoxville, Tennessee.
6. UNISOR, Oak Ridge Associated Universities.

7. K. Heyde et al., Phys. Repts. 102, 291 (1983).
8. P. Van Duppen et al., Phys. Rev. Lett. 52, 1974 (1984).
9. P. Misaelides et al., Z. Phys. A311, 199 (1981).

MEASUREMENT OF THE ISOTOPE SHIFTS AND HYPERFINE STRUCTURES OF ^{192m}Tl AND ^{201}Tl AT THE UNISOR LASER FACILITY

J. A. Bounds[1] R. L. Mlekodaj[2]
H. K. Carter[2] E. H. Spejewski[2]
C. R. Bingham[1] W. M. Fairbank, Jr.[3]
P. Juncar[4]

The laser facility on line to the UNISOR separator has successfully measured the atomic hyperfine structure of an on-line produced isotope, ^{192}Tl. Using the laser facility essentially as reported previously,[5] the first on-line data are shown in Fig. 3.3.

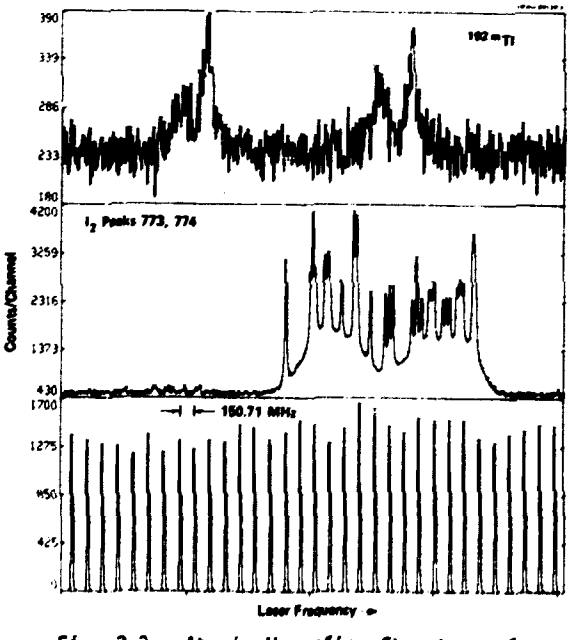

Fig. 3.3. Atomic Hyperfine Structure of ^{192}Tl obtained in 45 minutes at a rate of 1 x 10^5 atoms/sec. The middle section is a portion of the saturated absorption spectrum of I_2 and the bottom section shows frequency markers.

The difficulties reported last year, i.e., Na deposition on the fiber optic detector, high PMT background due to radioactivity, and low ion beam transmission through the laser line, have been resolved. The Na deposition problem was solved by increasing the separation between the charge exchange cell and the fiber optic detector. The resulting increase in optical pumping is prevented by introducing a magnetic field in the space which Zeeman shifts the levels out of resonance until the atom reaches the detection region. The PMT background was reduced by shielding of the beam collimators and the laser line transmission was improved by realignment of ion optics and more careful control of ion source parameters. With the new experimental conditions, the efficiency of the detection system was carefully studied using the medical isotope ^{201}Tl in an off-line mode. Using standard gamma-ray spectroscopy, we could accurately determine the Tl beam intensity through the laser line. From these data we determined our system detection efficiency to be 9 x 10^{-4}, in good agreement with our value of 6 x 10^{-4} obtained last year[5] by neutral current measurement techniques. These data enabled us to obtain an improved isotope shift and hyperfine structure for ^{201}Tl as shown in Tables 3.2 and 3.3.

With the improved laser system, the improved target/ion source arrangement and improved beams from the tandem accelerator, beams of approximately 10^5 atoms/sec of ^{192}Tl were obtained through the laser line. The hfs spectrum of ^{192}Tl shown in Fig. 3.3 was obtained in 45 minutes at an average beam intensity of 1 x 10^5 atoms/sec. Our preliminary analysis of these data and gamma-ray spectra taken simultaneously suggest we have observed the hfs of the high spin state of ^{192}Tl. The initial results are given in Tables 3.2 and 3.3.

---

1. University of Tennessee, Knoxville, Tennessee.
2. UNISOR, Oak Ridge Associated Universities.
3. Colorado State University, Ft. Collins, Colorado.
4. Laboratoire Aime Cotton, Orsay, France.
5. H.K. Carter et al., Physics Division, Prog. Rept. ORNL-6004 (1983), p. 169.

NEW METHOD TO MEASURE RELATIVISTIC DOPPLER SHIFT: FIRST RESULTS AND A PROPOSAL[1]

P. Juncar[2] C.R. Bingham[4]
H.K. Carter[3] D.J. Pegg[4]
R.L. Mlekodaj[3] J.D. Cole[5]
J.A. Bounds[4]

Utilizing a newly derived relativistic relation, $\sigma_0=\sqrt{\sigma_+ \sigma_-}$, the collinear-laser/fast-atom beams technique has been used to measure the relativistic Doppler effect to an accuracy comparable to the best previous experiments (5 parts in 10^3). Improved calibration data and a similar technique, but employing two

Table 3.2. Measured hfs level splitting in the Tl 535.2 nm transition (in MHz).

Tl	$\Delta\nu(6^2P_{3/2})$			$\Delta\nu(7^2S_{1/2})$		
	this work	others	method	this work	others	method
205	529.3(1.6)	530.076546(3)[a]	ABMR	12292.4(8.3)	12291(15)[c]	optical
203	524.6(2.0)	524.059953(3)[a]	ABMR	12179.7(5.6)	12184(15)[c]	optical
201	510.0(10.0)	510(120)[b]	optical	12045.3(9.4)	12052(120)[b]	optical
192	-	-	-	2071(65)	-	optical

[a]F.R. Petersen, H.G. Palmer, J.H. Shirley, Bull. Am. Phys. Soc. 13, 1674 (1968).

[b]R.J. Hull and H.H. Stroke, J. Opt. Soc. Am. 51, 1203 (1961).

[c]A.I. Odintsov, Opt. and Spec. IX, 2, 75 (1960).

Table 3.3. Isotope shifts of the 535.2 nm line in ^{201,203,205}Tl (in GHz).

	this work	others
Δ(203-205)	-1.758(18)	-1.766(21)[a]
Δ(201-205)	-3.537(15)	-3.72(12)[b]
Δ(192-205)	-10.75(25)	-

[a]A.I. Odintsov, Opt. and Spec. IX, 2, 75 (1960).

[b]R.J. Hull and H.H. Stroke, J. Opt. Soc. Am. 51, 1203 (1961).

lasers, is proposed which should improve the test of time dilation by at least another factor of ten.

---

1. Abstract of paper submitted to Phys. Rev. Letters.

2. University of Tennessee and Laboratoire Aimé Cotton, Orsay, France.

3. UNISOR, Oak Ridge Associated Universities.

4. University of Tennessee, Knoxville, Tennessee.

5. Louisiana State University, Baton Rouge, Louisiana; present address: Idaho National Engineering Laboratory, Idaho Falls, Idaho.

4. EXPERIMENTAL ATOMIC PHYSICS

The experimental atomic physics program within the physics division is carried out by two groups, whose reports will be given in this section. Work of the accelerator atomic physics group is centered around the 6.5-MV EN tandem accelerator; consequently, most of its research is concerned with atomic processes occurring to, or initiated by, few MeV/amu heavy ions. Other activities of this group include higher energy experiments at the Holifield Heavy Ion Research Facility (HHIRF), studies of electron and positron channeling radiation, and collaborative experiments at other institutions. The second experimental group concerns itself with lower energy atomic collision physics in support of the Fusion Energy Program. During the past year, the new Electron Cyclotron Resonance Source has been completed, and some of the first data from this facility will be presented here. In addition to these two activities in experimental atomic physics, other chapters of this report will describe progress in theoretical atomic physics, experimental plasma diagnostic development, and atomic data center compilation activities.

CORRELATED TWO ELECTRON EFFECTS IN HIGHLY CHARGED ION-ATOM COLLISIONS

S. Datz
C. Bottcher
L. H. Andersen[1]
M. Frost[1]
P. Hvelplund[1]
H. Knudsen[1]

We have studied the fate of electrons released in collisions between highly charged Au^{q+} ions (20 MeV) and He atoms and find that the large transfer ionization (TI) cross section observed can be accounted for by transfer of two electrons to a highly correlated state on the Au projectile followed by the loss of one electron to the continuum. Autoionization lines are also observed, but they are attributable to electron transfer accompanied by core excitation (TE).

In these experiments, we collide Au^{q+} at 100 keV/u (i.e., at $2v_0$ = orbital velocity of the He electrons) with He atoms and measure the spectrum of ejected electrons moving in the rest frame of the Au ion projectile, in coincidence with the charge state of the emergent Au ion.

Figure 4.1 shows electron spectra obtained with Au^{15+} ions. The singles spectrum at the top of the figure displays two features: a peak at 54 eV made up of electrons with velocities corresponding to zero velocity in the rest frame of the 20-MeV Au ions and a symmetric set of small peaks with corresponding low energy autoionizing electrons leaving the Au core in the forward and backward laboratory directions.

From the coincidence spectra, it can be seen that the observed autoionizing electrons are all associated with Au^{15+} and hence with transfer plus excitation (TE), i.e.,

$$Au^{15+} + He \rightarrow [Au^{14+}]^{**} + He^{+}$$
$$\downarrow$$
$$Au^{15+} + e.$$

Transfer ionization is defined as the loss of a larger number of electrons from the target than are transfered to the projectile. In the case of a helium target

$$Au^{15+} + He \rightarrow Au^{14+} + He^{++} + e$$

the occurrence of a free electron in coincidence with a bound state capture implies the formation of He^{++}. The spectrum of these electrons is shown in the bottom portion of Fig. 4.1. In a separate experiment, we showed that the yield of these electrons corresponds to a formation cross section of 6×10^{-16} cm^2, a number equal to the entire measured TI cross section.

ORNL-DWG. 84-18343

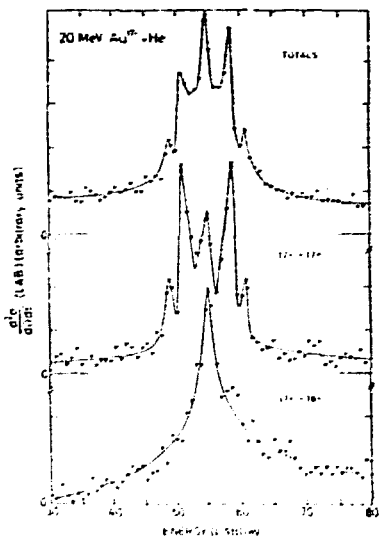

Fig. 4.1. Double-differential cross section in the laboratory frame as a function of electron energy.

Much can be learned from a study of the detailed shape of this spectrum, and to do this we transform coordinates from laboratory system to the rest frame of the ion (Fig. 4.2). The upper portion showing the singles spectrum is dominated by electron capture to the continuum, as evidenced by the asymmetric distribution with enhanced density in the backward hemisphere ("negative energy"). The 15+14 TI coincidence spectrum is seen to be symmetric, a shape characteristic of electrons which have been released from the pro-jectile, otherwise known as "electron loss to the continuum" (ELC).

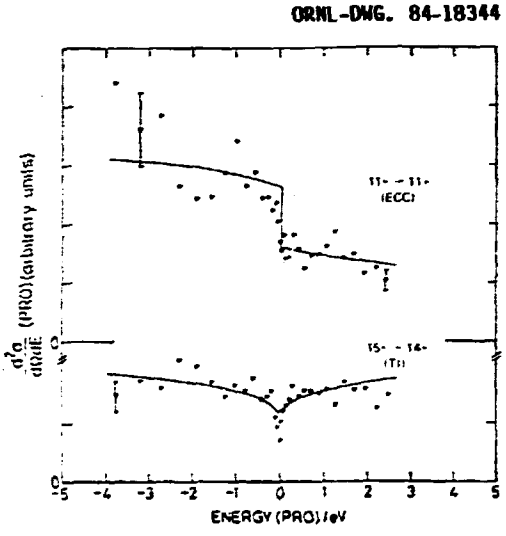

Fig. 4.2. Double-differential cross section in the projectile rest frame as a function of electron energy. Negative energies correspond to emission in the backward hemisphere.

The flatness of the distribution suggests a similarity to the process of ionization near threshold (e,2e) wherein two electrons share the total available energy in a so-called Wannier state. The electrons dispose themselves on opposite sides of the nucleus and move apart along a line.[2] In our case, we use a two-dimensional model to obtain an insight into the four-body Coulomb problem, i.e., two electrons in the field of two nuclei. To illustrate, we consider the potential surface for two electrons confined to the line of joining nuclei of charges 2+ and 16+ separated by a distance 10 a_0. In Fig. 4.3 is plotted a contour map of this surface in the plane generated by the coordinates of the two electrons relative to the helium nucleus; this represents a natural generalization of the hyperspherical plane used in discussions of threshold phenomena.

The quadrant IV contains the saddle point X associated with single-electron capture, but two-electron capture would more likely proceed via the ridge R over the pass P in quadrant I. In the latter case, the electrons would

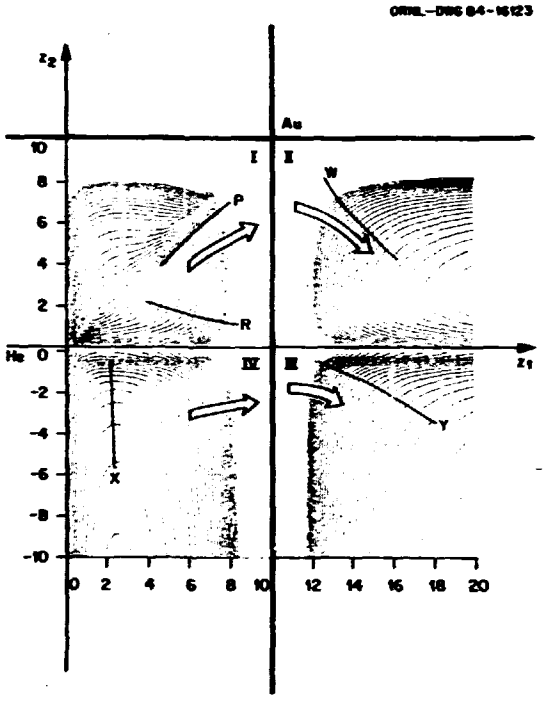

Fig. 4.3. Potential energy contours at 0.3 a.u. (8.1 eV) intervals for two electrons in the field of charges 2+ and 16+ separated by 10 a_0. The coordinates z_1 and z_2 represent distances of the electrons from the 2+ nucleus. Thus, the points He' represents both electrons on the He nucleus and Au' both electrons on the Au nucleus. The quadrants correspond to the linear configurations: I(He-e-e-Au), II(He-e-Au-e), III(e-He-Au-e), and IV(e-He-e-Au).

plausibly end up on the ridge W (quadrant II) which is the Wannier ridge associated with an almost isolated Au nucleus. On these grounds, we can conjecture that the energy distribution of cusp electrons should be predicted by Wannier theory which should apply whether both electrons are free or bound. It should be emphasized that this model, as yet, contains no dynamics, i.e., quasiadiabatic motion on the potential surface is assumed. The feasibility of numerical solutions to the model is being assessed.

---

1. Physics Institute, University of Aarhus, DK-8000, Aarhus C, Denmark.
2. C. Bottcher et al., this report.

ELECTRON AND POSITRON CHANNELING RADIATION

S. Datz R. H. Pantell[2]
B. L. Berman[1] J. U. Upphart[2]
H. S. Park[2] R. H. Pin[2]

The study of channeling radiation has now proceeded past the point of quantitative proof

of principal. In the case of simple single component crystals, higher-lying line energies may now be predicted to within a percent using Hartree-Fock atomic wave functions (for spherically symmetric atoms) with proper planar or axial averaging in a many-beam calculation.

Diamond

Perhaps the best crystal with which to study channeling radiation is diamond, because of its high Debye temperature and its low Z. Indeed, the first measurement of channeling radiation from diamond showed remarkably sharp structure.

Our recent results for the (110) channeling-radiation spectra at three incident electron-beam energies are shown in Fig. 4.4, together with the many-beam calculation of transition energies and strengths from the "standard" Hartree-Fock potential. It can be seen that there is agreement between experiment and theory, although there is a slight tendency for the calculated transition energies to lie higher than the experimental spectral peaks (this is attributable to simple kinematic effects from multiple scattering). For the (111) plane, however, this tendency is much exaggerated, as shown in Fig. 4.5. Both a (111) potential obtained from x-ray-diffraction data and an empirical potential fitted to the data are shallower than the standard potential and both fit the data better. We believe the fact that significant charge in the diamond crystal is distributed along the <111> valence-bonding

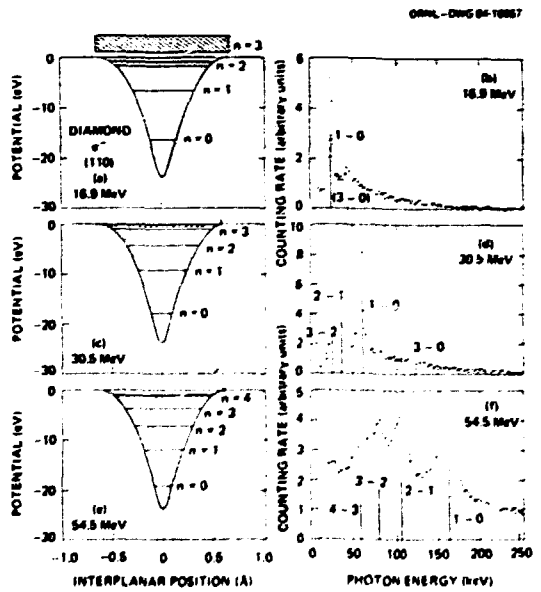

Fig. 4.4. The (110) potential and eigenvalues [parts (a), (c), and (e)] and channeling-radiation spectra [parts (b), (d), and (f)] for 16.9-MeV, 30.5-MeV, and 54.5-MeV electrons, respectively, channeled in diamond. Note the increase with electron-beam energy of the line energies and linewidths.

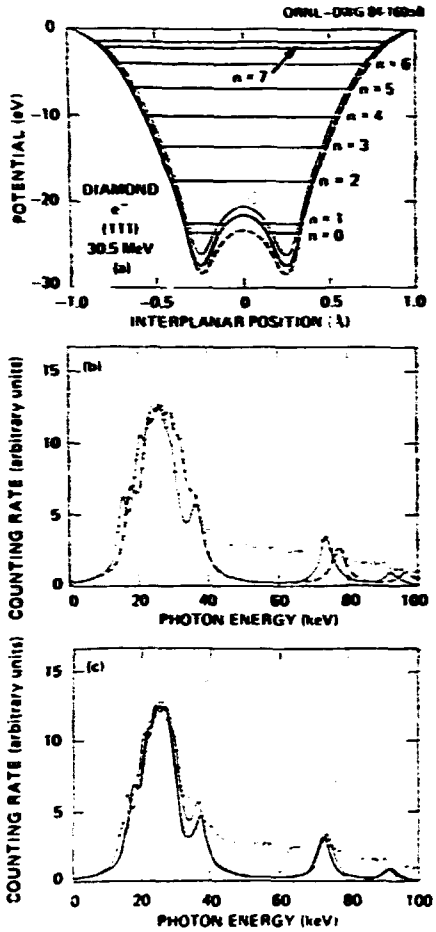

Fig. 4.5. (a) (111) potentials for diamond: the "standard" many-beam potential dashed curve); a potential based upon x-ray-diffraction data (light solid curve); and an empirical potential based upon the best fit to the 30.5-MeV data (heavy solid curve), together with the corresponding eigenvalues. (b) The (111) spectrum for 30.5-MeV electrons, together with the calculated spectra obtained from the standard (dashed curve) and x-ray-diffraction (light solid curve) potentials. (c) The same spectrum, together with the spectra calculated from the x-ray-diffraction (light solid curve) and empirical (heavy solid curve) potentials.

direction alters the (111) interplanar potential as shown in the figure. In fact, the data shown in Fig. 4.5 can serve as a quantitative measure of this asymmetric charge distribution.

Platelet Defects in Diamond

Platelets in diamond [nitrogen mono- or di-layers precipitated along the (100) planes] influence the channeling radiation dramatically. In particular, they cause an energy shift in the (100) spectral lines, as shown in Fig. 4.6. We have shown recently that these lineshifts can be accounted for by equating the lattice distortion

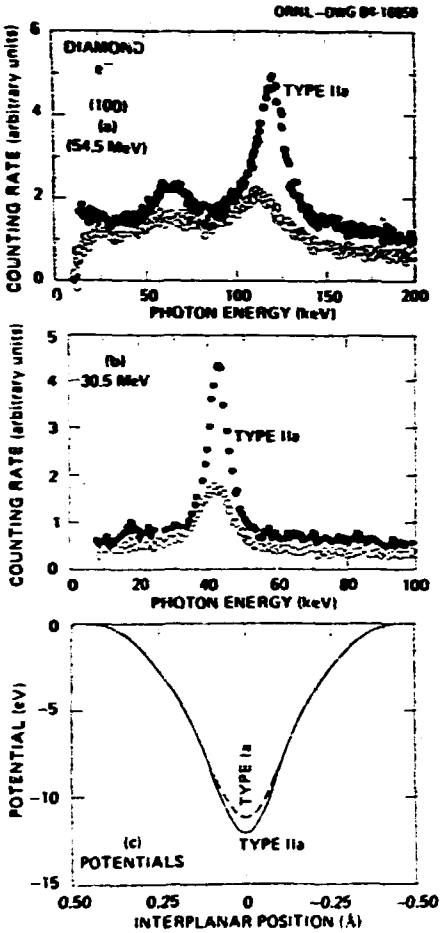

Fig. 4.6. (100) channeling-radiation spectra from both Type-Ia (with platelets; open data points) and Type-IIa (without platelets; closed data points) diamonds for (a) 54.5-MeV and (b) 30.5-MeV incident electrons. Note in particular the energy shift for the 1 → 0 transition. (c) (100) potentials for diamond: the one which uses the accepted value of 0.040 Å for the thermalvibration amplitude, as is appropriate for the Type-IIa diamond (solid curve) and the one which uses the value of 0.055 Å, which arises from the best fit to the data for the Type-Ia diamond (dashed curve).

caused by the platelets with a large average thermal-vibration amplitude perpendicular to the (100) planes and hence to the platelets. The (100) potential so altered is also shown in Fig. 4.6. These results also serve to show that channeling radiation can be used as a diagnostic probe of impurities and defects in crystals.

Temperature Effects

The bottom of the planar or axial averaged potential is affected by lattice vibrations. This is taken into account by introducing a Debye-Waller factor into the potential. Larger vibrational amplitude raises the bottom of the potential and shifts the eigenstates upward, with the lowest state being most affected and the upper states hardly affected at all.

As the crystal temperature is decreased, one expects a lowering of the well bottom and an increase in the energy of photons arising from transitions to lower states. This is demonstrated in Fig. 4.7 where spectra of radiation from 54-MeV electrons channeled in the (100) and (110) planes of Si are shown for two temperatures. The temperature dependence of the transition energies for the lowest-lying energy levels (the 1 → 0 transitions), shown in Fig. 4.8, is sensitively dependent on the Debye temperature. These data consistently yield a value of the Debye temperature of silicon of 495 ± 10 K in agreement with shell model calculations, but in sharp disagreement with the value of 543 K obtained from previous x-ray diffraction studies. The cause of this discrepancy is not yet understood.

Isotope Effects: LiH and LiD

Our recent results for LiH and LiD show two interesting effects for these lowest-Z crystals.

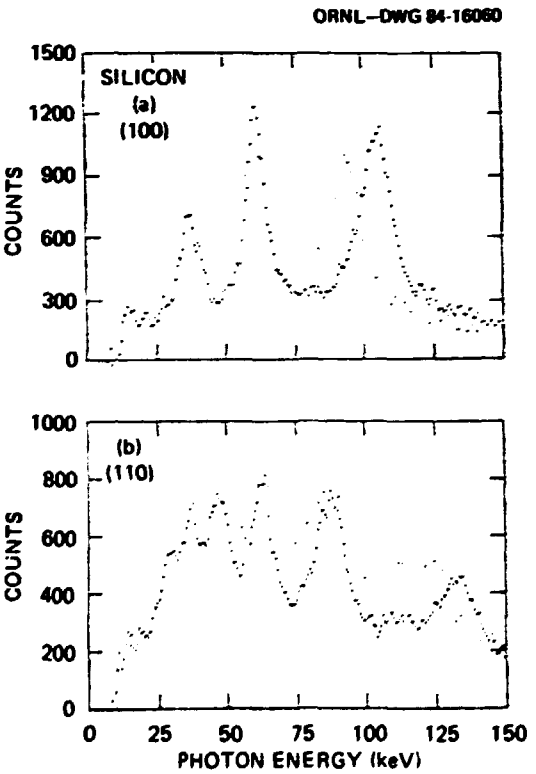

Fig. 4.7. Superposed channeling-radiation spectra for 54.5-MeV electrons incident along the (a) (100) and (b) (100) planes of silicon for two different temperatures: (a) -190°C (heavy data points) and +5°C (light data points); (b) -180°C (heavy data points) and +7°C (light data points). Note the large energy shifts of the 1 → 0 transitions.

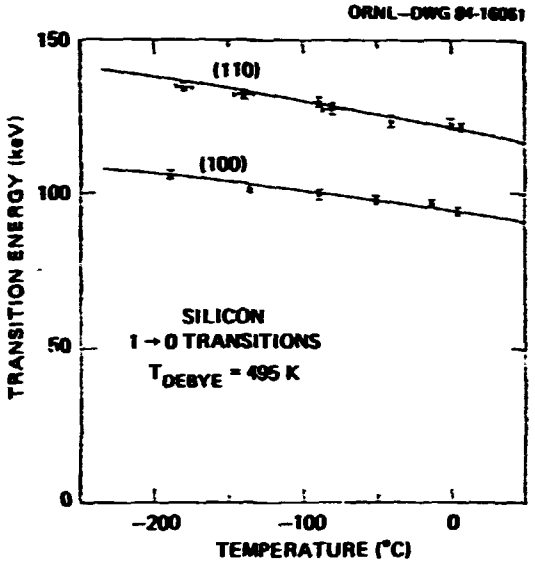

Fig. 4.8. Temperature dependence of the channeling-radiation transition energies for the 1 → 0 transitions of 54.5-MeV electrons channeled along the (100) and (110) planes in silicon. The fits to these data (solid curves) yield a consistent value of 495 K for the Debye temperature of silicon.

One is the largest disagreement to date between measured and calculated transition energies, as shown, for example, in Fig. 4.9 for the case of 54.5-MeV positrons and electrons incident along the (100) and (110) planes of LiH. The other can be seen in Fig. 4.10, where (110) channel-

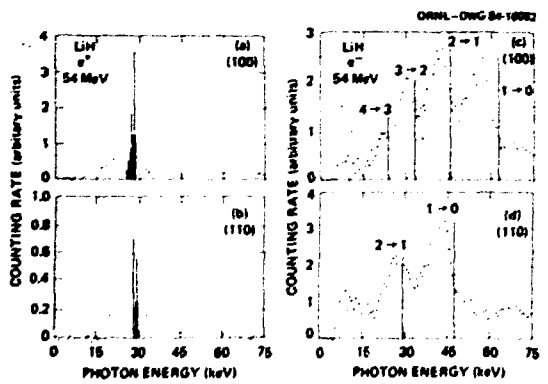

Fig. 4.9. Channeling-radiation spectra for LiH, both for 54.5-MeV positrons incident along the (a) (100) and (b) (110) planes and for 54.5-MeV electrons incident along the (c) (100) and (d) (110) planes, together with the calculated transition energies and strengths (vertical lines) obtained from the standard many-beam theoretical treatment. Note the very large discrepancies between experiment and theory.

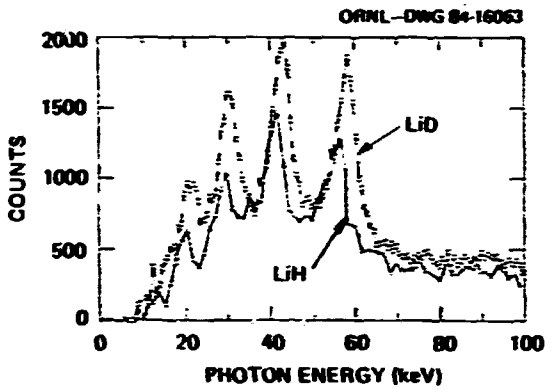

Fig. 4.10. Superposed channeling-radiation spectra for 54.5-MeV electron incident along the (110) planes of LiH (triangles) and LiD (squares). Note that the LiD spectrum resembles a spectrum that one might expect to obtain from the cooled LiH crystal.

ing radiation spectra from LiH and LiD (both obtained at room temperature) are superposed.

In general, the LiD lines lie at higher energies than the LiH lines and reflect the smaller vibrational amplitudes of the D ions in the lattice, as one would expect from the fact that deuterons are heavier than protons. This would cause LiD to appear as a low-temperature version of LiH. The line energies are listed in Table 4.1. The largest effect is the 10% shift seen in the 1→0 transition in the (110) plane. This plane has the most weakly bound states and the effect of lattice vibrations on the bottom of the potential well is most significant. The thermal vibration amplitudes required to fit the data are totally at variance with those listed in Crystallographic Data but lie close to those recently calculated by M. Mosteller.[3]

I. Department of Physics, Lawrence Livermore National Laboratory, Livermore, CA 94550.

Table 4.1. Channeling radiation line energies (keV) for LiH and LiD crystals

		LiH	LiD
(100)	1 → 0	57.0 ± 0.6	58.3 ± 0.4
	2 → 1	41.8 ± 0.4	43.6 ± 0.3
	3 → 2	29.6 ± 0.4	29.3 ± 0.3
	4 → 3	21.1 ± 0.5	21.2 ± 0.4
(110)	1 → 0	41.3 ± 0.5	45.3 ± 0.4
	2 → 1	26.3 ± 0.5	28.1 ± 0.3
(111)	1 → 0	52.0 ± 0.4	52.8 ± 0.4
	2 → 1	36.5 ± 0.4	37.4 ± 0.3
	3 → 2	26.0 ± 0.4	25.1 ± 0.3

2. Department of Electrical Engineering, Stanford University, Stanford, CA 94305.
3. Solid State Division, ORNL, private communications.

RESONANT COHERENT EXCITATION OF HEAVY IONS MOVING IN CRYSTALLINE CHANNELS

C. D. Moak
J. A. Biggerstaff
O. H. Crawford[1]
S. Datz
P. F. Dittner
J. Gomez del Campo
H. F. Krause
P. D. Miller
P. L. Pepmiller
M. D. Brown[2]

Figure 4.11 illustrates the phenomenon called resonant coherent excitation. In this example, a fast one-electron ion is moving in a crystalline channel. The ion is shown moving nearest the middle string of atoms which lies just above the ion path; the smaller black circles illustrate another string outside the plane of the figure. The six atoms schematically represented by the large black circles are closest to the ion path and they give rise to an electric field which acts upon the ion as shown by the sine wave. The space variation of this field is, for the ion, a time-varying field of frequency $\nu = v/d$ where v is the ion velocity and d is the distance between the atoms. The field is never a pure sine wave and its wave-shape depends sensitively upon the ion path, the type of crystal lattice and the particular channel axis being used in that lattice. In general, the field is rich in harmonics of the fundamental string frequency and, as shown in the figure, a more appropriate expression is $\nu = K\,v/d$ where K is an integer. Resonant excitation of the projectile can occur whenever one of these frequencies happens to match the frequency of some transition $(\Delta E)_{ij}$ where i and j denote the initial and final state of the system being excited. In Fig. 4.11, we have a one-electron ion and the transition is from the hydrogenic ground state to the first excited state. Of course, ΔE could have been the energy for nuclear excitation of the first excited level of a bare nucleus. In the one-electron case, the numerical example is carried further for the one-electron ion C^{5+} in the <100> axis of a gold crystal, and it can be seen that the fundamental frequency occurs for an ion energy of 6.8 MeV/amu and the second harmonic occurs at 1/4 as much energy (half the velocity). The numerical examples are helpful for scaling to other ions with different energy levels. Once the ion is in an excited state, its electron is less tightly bound and it moves in a larger region around the nucleus; thus, it is more likely to be ionized. When the ion velocity is tuned to a resonance, there is a drop in the population of the one-electron fraction and a peak in the bare-ion fraction. Detailed features of these resonances can be seen in Refs. 3-7.

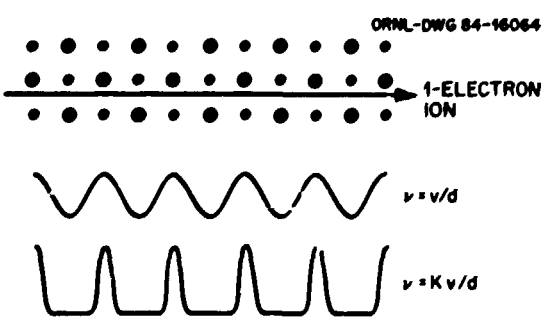

Fig. 4.11. Conditions for resonant coherent excitation of channeled ions.

An additional complication is that some of the oscillating fields are along the ion path and some field components are perpendicular to the ion path; generally, there is a mixture. Longitudinal oscillating fields are superimposed on the steady braking field which is also longitudinal, and the result is that resonances with longitudinal fields are split by a Stark effect; transversely oscillating fields do not produce such splittings. All of these phenomena have been seen and they are illustrated in the references.[3-7] An example of resonant coherent excitation with a Stark mixed level is shown in Fig. 4.12. The level positions deduced from the resonances observed, as in Fig. 4.12, have been compared with theory[4] and the results are not very satisfactory as shown in Fig. 4.13; similar results are shown for N^{6+} in Fig. 4.14. Here, open circles are theoretical predictions and experimental points are full circles. For odd harmonics (K = 3 for example), the fields are mostly transverse, no splitting is found and theory and experiment are in excellent agreement. For even harmonics, splittings are predicted and found but although the $2sp_z^*$ component occur at the expected energy, the $2sp_z$ component is shifted in energy with respect to the expected position. Certain ions at higher energies from the Holifield accelerator might provide the data to explain the difference. As shown in Fig. 4.12, the resonances are not sharp enough to provide very high accuracy in the

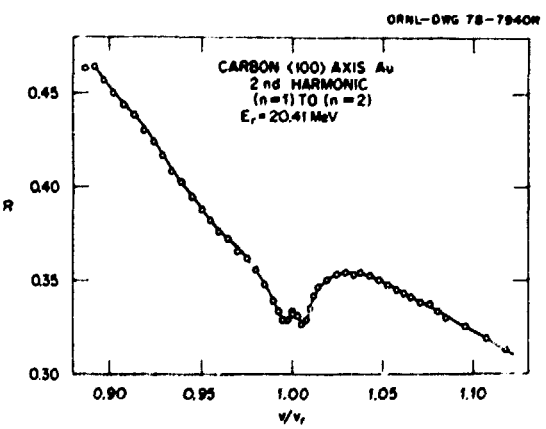

Fig. 4.12. Ratio of counts, R, $C^{5+}/(C^{5+} + C^{6+})$ as a function of velocity divided by the resonant velocity for the vacuum state.

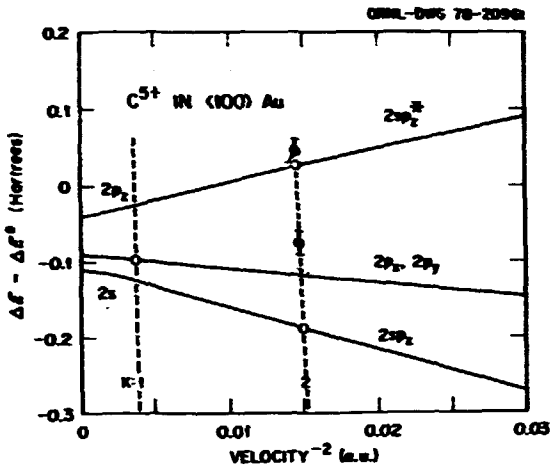

Fig. 4.13. Velocity dependence of energy shift from vacuum levels for C^{5+}. The open circles are expected energy shifts from theory, and solid circles are experimentally observed shifts.

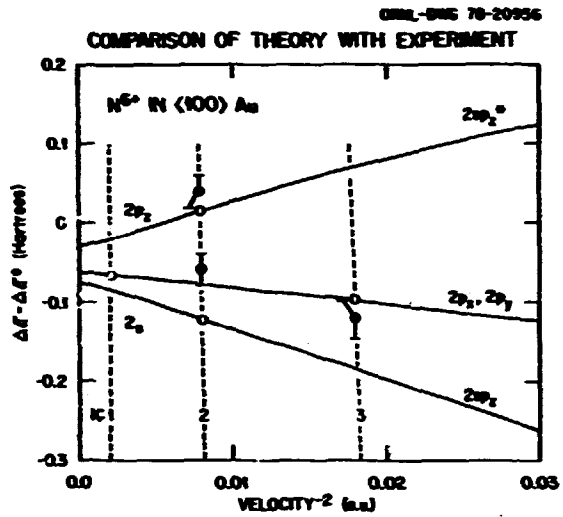

Fig. 4.14. Velocity dependence of energy shift from vacuum levels for N^{6+}. The open circles are expected energy shifts from theory, and solid circles are experimentally observed shifts.

estimate of the Stark level splittings. One reason is that the ion energy changes as it slows down inside the crystal; this means that the ion cannot remain at resonance throughout the crystal regardless of the bombarding energy setting. To avoid smearing the resonance, $\Delta v/v_0$ should be as small as possible, where $\Delta v/v_0$ is the percentage velocity change in passing through the crystal. In Tables 4.2 and 4.3, we show some cases which illustrate the improved resolution to be expected using the Holifield accelerator. The tables illustrate, for our thinnest crystal, the energy loss in the <100> channel expressed as a fraction of the resonance energy and the fractional velocity change in passing through the crystal for K = 1, the fundamental frequency (odd harmonic, predominantly transverse oscillating fields). For C^{5+} we see that $\Delta v/v_0$ is 0.551%. In Fig. 4.12 we see that 0.551% (or 0.00551 in abscissa units) is enough to limit the resolutic... Another example, N^{6+}, has a $\Delta v/v_0$ of 0.277% and, as we can see in Fig. 4.15, the resonances show up more clearly. The next improvements would come with O^{7+} and F^{8+}. The K = 2 resonances for O^{7+} and F^{8+} would lie at 86.0 MeV (tandem terminal voltage 10.7 MV)

Table 4.2. Resonance parameters for one-electron ions using the fundamental frequency (K = 1) for ions traversing the <100> channel in a Au crystal 1470 Å thick. The resonant energy is given by $E_0 = 0.00524\ Z_1^{\ 4}$ in MeV.

	Z	MeV/amu	E_0, MeV	V(MV)	Random Loss ΔE MeV	$\frac{1}{2}\Delta E/E_0$	$\Delta v/v_0$	MPC†
Be^{3+}	4	1.34	12.1	3.02 (EN)	0.240	0.99%	0.50%	
B^{4+}	5	3.28	32.8	6.56 (EN)	0.260	0.40%	0.20%	
C^{5+}	6	6.79	81.6	13.59 (H,T)	0.257	0.16%	0.08%	6^+
N^{6+}	7	12.58	176.2	25.17 (H,T)	0.235	0.07%	0.03%	7^+
O^{7+}	8	21.47	343.4	(42.92) Coupled	0.210	0.03%	0.02%	8^+

†MPC: Most Probable Charge

Table 4.3. Resonance parameters for one-electron ions using the second harmonic frequency (K = 2) for ions traversing the <100> channel in a Au crystal 1470 Å thick. The resonant energy is given by $E_0 = 0.00131\ Z_1^{\ b}$ in MeV.

	Z	MeV/amu	E_0, MeV	V(MV)	Random Loss ΔE MeV	$\frac{1}{2}\Delta E/E_0$	$\Delta v/v_0$	MPC†
C^{5+}	6	1.70	20.4	3.40 EN	0.449	1.10%	0.55%	5.5^+
N^{6+}	7	3.15	44.0	6.29 EN	0.489	0.56%	0.28%	6.5^+
O^{7+}	8	5.37	85.9	10.74 (H,T)	0.505	0.29%	0.15%	7.7^+
F^{8+}	9	8.60	163.3	18.14 (H,T)	0.487	0.15%	0.08%	8.8^+
Ne^{9+}	10	13.10	---	---	---	---	---	Becoming
Na^{10+}	11	19.18	441.2	(40.11) Coupled	0.428	0.05%	0.02%	more
Mg^{11+}	12	27.17	652.0	(54.34) Coupled	0.396	0.03%	0.02%	totally
Al^{12+}	13	37.42	1010.4	---	---	---	---	stripped
Si^{13+}	14	50.33	1409.4	---	---	---	---	+

†MPC: Most Probable Charge

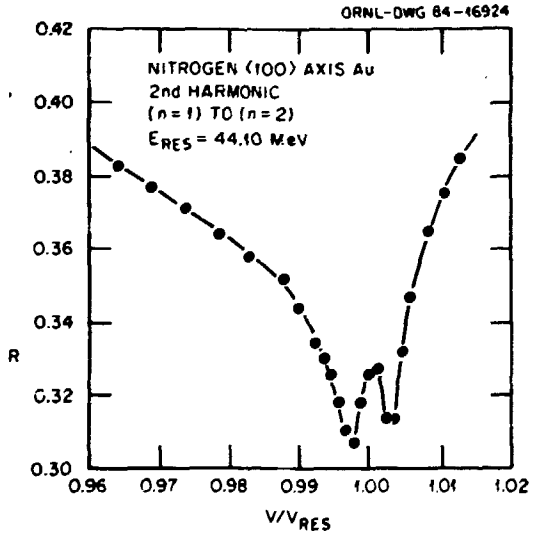

Fig. 4.15. Ratio of counts, R, $N^{6+}/(N^{6+} + N^{7+})$ as a function of velocity divided by the resonant velocity of the vacuum state.

and 163.6 MeV (tandem terminal voltage 18.1 MV), respectively.

These latter two experiments have just been completed. The anticipated sharpening is, indeed, observed but the Stark split double-peak structure is entirely absent in both cases. In another experiment, we investigated the K = 1 resonance in C^{5+} at 81.6 MeV. The depth is enormous, a factor of at least 4 below the secular trend, but the resonance is very broad. Perhaps this is a sign of power broadening or saturation. In any case, these entirely new results require some time for interpretation.

1. Chemistry Division, ORNL.
2. Naval Surface Weapons Laboratory, Silver Spring, MD 20910.

3. S. Datz et al., Phys. Rev. Lett. 40, 843 (1978).
4. C. D. Moak et al., Phys. Rev. A19, 977 (1979).
5. O. H. Crawford and R. H. Ritchie, Phys. Rev. A20, 1848 (1979).
6. S. Datz et al., Nucl. Instr. Meth. 170, 15 (1980).
7. C. D. Moak et al., Nucl. Instrum. and Methods 194, 327 (1982).

ION-ION COLLISION STUDY USING THE FOLDED BEAM APPARATUS

H. J. Kim

We have observed the formation of Ar^{4+} from $Ar^{3+} + Ar^{3+}$ collisions and N^{4+} from $N^{3+} + N^{3+}$ collisions at C-M energies of 120 keV using the

folded beam apparatus. Although we were successful in separating signal events from backgrounds, much work remains to be done before absolute charge-changing cross sections for ion-ion collisions can be reliably and routinely deduced from observed results. Making reasonable assumptions and using the previously measured Ar^{3+} Ar → Ar^{4+} cross sections to calibrate our beam overlap and target length, we obtained approximate cross sections for the multicharged ion collisions, i.e.,

$$\sigma(Ar^{3+} + Ar^{3+} \rightarrow Ar^{4+}) \sim 5 \times 10^{-16}\ cm^2$$
$$\sigma(N^{3+} + N^{3+} \rightarrow N^{4+}) \sim 1 \times 10^{-16}\ cm^2.$$

These numbers appear large but they are commensurate with 5fσ promotion for the Ar^{3+} and curve crossing for N^{3+} case.

Recently, our main effort has been directed toward rendering the results obtained with the folded beam apparatus more amenable to absolute cross section determinations by making the separation of reaction products from the tail of the main beam cleaner and by simplifying the selective detection of reaction products.

DIELECTRONIC RECOMBINATION: A STATUS REPORT

P. F. Dittner, S. Datz, C. M. Fou[1], P. D. Miller, C. D. Moak, P. L. Pepmiller

Following the publication of our measurements [Ref. 2] on the dielectronic recombination (DR) of B^{2+} and C^{3+}, we modified the analysis section of our merged beam apparatus. Previously the initial charge state (q+) beam and the $(q-1)^+$ beam were magnetically deflected through ~6° resulting in a motional emf of ~40,000 volts/cm. This high field had the disadvantage that it caused recombined $(q-1)^+$ ions in high n states to be Stark-stripped back to q+, thus resulting in a loss of DR signal, e.g., for C^{3+} all n > 27 were lost. The charge state analysis is now done by electrostatic deflection (E ~4000 V/cm) through ~0.6° (see Fig. 4.16) resulting in a larger signal, e.g., for C^{3+}, all n > 45 are lost. In addition, the flight distance between the interaction region and the charge state analyzer was decreased from 2.5 m to 25 cm, but the hoped for decrease in noise due to charge-changing collisions with the background gas was not realized. We think that the dominant part of the noise arises from slit edge scattering and has only a minc dependence on the flight distance. Nevertheless, the overall signal-to-noise ratio was improved by a factor of ~2 for the C^{3+} DR experiment.

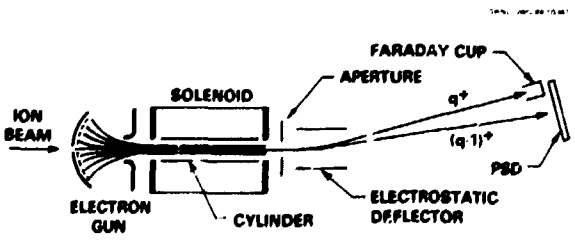

Fig. 4.16. Schematic diagram of merged beam apparatus.

In order to decrease the uncertainty in the background subtraction needed to extract the DR rate from the total rate of $(q-1)^+$ ions, we now modulate the electron energy at each ion energy (E_i) step.[3] This modulated electron energy method (MEEM) works as follows: (1) The electron gun is operated with a fixed cathode voltage, $-V_C$. (2) The relative energy (E_r) is varied, by stepping through a range of E_i's from 0 to E_r above the Rydberg limit of the DR resonance energy (E_S). (3) An ~10 Hz square-wave modulated voltage having two values, 0 and V_T, is applied to the cylinder surrounding the electron beam. (4) The events ($(q-1)^+$ ions) accumulated when V_T is on, N_T, are background and are subtracted from the number of events, N_0, accumulated when the cylinder voltage equals zero. Ideally, the events, due to DR, N_S, should be given by $N_S = N_0 - N_T$. However, at $E_r > E_S$, where $N_S = 0$, we found that $N_0 \neq N_T$ because when the electron velocity is changed the outgassing (due to the electron beam) changes and, in turn, the number of noise events changes. In view of the aforementioned, our procedure for extracting N_S is to construct a smoothed E_i dependent N_T (from the N_T data), multiply it by a constant α determined by insisting that $N_S = N_0 - \alpha N_T' = 0$ when $E_r > E_S$, and continuing the subtraction where $0 < E_r < E_S$ to yield $N_S = N_0 - \alpha N_T'$. Current integration of the initial q+ beam gives the number of q+ ions, N_i, and the ratio $R_S = N_S/N_i$ and, as heretofore, [Ref. 3].

$$R_S = \frac{\rho_e L}{v_i} \int f(v_r)\, v_r\, \sigma\, dv_r \qquad (1)$$

where ρ_e is the electron density, L is the length of the interaction region, v_i is the ion velocity, v_r is the relative velocity, σ is the DR cross section, and $f(v_r)$ is the v_r distribution due to the velocity distribution of the electron beam.

Using the MEEM, we have measured R_S over a wide range of E_i ($0 < E_r < 25$ eV) for the Li-like ion, C^{3+} and O^{5+}, and for the Na-like ions P^{4+}, S^{5+}, and Cl^{6+} having the resonant transition 2s-2p and 3s-3p, respectively. According to theory, the DR cross section of these ions (except C^{3+}) has, as its most prominent feature, a very narrow peak at E_S and, if $f(v_r)$ were narrow, Eq. (1) predicts large values of R_S only near $E_r = E_S$. Our measurements show non-zero values of R_S over a wide range of E_r, peaking a little below E_S and a highly asymmetric (higher yield towards lower E_r) shape. We believe that our electron beam has a broad energy (hence velocity) distribution which we are currently trying to determine from our data and the theoretical values of σ.

1. Department of Physics, University of Delaware, Newark, DE 19711.
2. P. F. Dittner et al., Phys. Rev. Lett. 51, 31 (1983).
3. For the former experimental procedure, see pp. 188-192 in Physics Division Progress Report, ORNL-6004 (1983).

CHARGE TRANSFER TO MULTICHARGED RECOIL IONS IN A PENNING TRAP[1]

D. A. Church[2] S. Berry[3]
R. A. Kenefick[2] M. Breinig[5]
W. S. Burns[2] S. B. Elston[5]
C. S. O[3] J.-P. Rozet[3]
R. Holmes[3] I. A. Sellin[5]
S. Huldt[4] D. Taylor[3]
B. Thomas[3]

Low-energy neon recoil ions with charges ranging from +2e to +8e were produced by impact of 35-MeV Cl ions foil stripped to a mean charge near 11e. The recoil ions ($3e < q < 6e$) were confined for times of 100 msec to several seconds in a Penning trap. Charge transfer from neon atoms to the ions reduced the stored ion number exponentially with storage time. Measurements of the stored ion number versus time, following deflection of the fast ionizing beam, yielded storage time constants, which were measured at several pressures. Pressures were determined with a calibrated nude ion gauge, and with a quadrupole residual gas analyzer. Flow of gas through the vacuum system to the pump required additional calibration of pressure gradients. Using the target gas density obtained from the pressure measurements, and the storage time constant, rate coefficients for low energy electron transfer were calculated for each neon charge state. The mean energies of the ions were estimated by reducing the confining axial dc potential of the Penning trap, and observing the ion number stored versus trap depth. It was found that, above a certain depth, the number of stored ions maximized. Below this depth, the ion number for a fixed storage time was reduced due to loss from the trap of the highest energy ions. From the measurement, a mean ion collision energy of 2q eV was obtained.

Work continued on charge transfer from water vapor to the neon ion charge state. The choice of water vapor as a target arose from theoretical predictions about the charge and temperature dependence of the rate coefficient, plus the ubiquitous presence of water vapor in most vacuum systems. The principal difficulty with these measurements, as it was for neon, lies in the target density determination. Due to the polar nature of the H_2O molecule, the surface attracting force, plus dissociation of the molecule on the surfaces, can lead to errors in partial pressure determinations. Final pressure calibration measurements based on known singly-charged ion rate coefficients are now underway. Of course, since the measurements must be made in target gas mixtures, the neon ion rate coefficients are required to obtain the final results.

Following the successful demonstration of recoil ion storage in the Penning trap, work has been initiated on the use of a radio-frequency trap. This trap does not utilize a magnetic field, but the low measured energy of the recoils in the Penning trap implies that the magnetic field, used for strong radial ion confinement, is not essential. The absence of a magnetic field has two important implications: higher precision in spectroscopic measurements can be obtained, and the experimental configuration is open to permit easy introduction of atomic or laser beams. Of course, the operation of the rf trap is more involved, and the device is not a replacement of the Penning trap for collision measurements. Following initial tests using electron impact ion production, the rf trap has been mounted on the beam line in series with the Penning trap, so that simultaneous operation is feasible in principle. It is expected that the m/q resolution of the Penning trap is superior, so this can be used to identify ions in cases of uncertainty in the rf trap.

1. D. A. Church et al., Phys. Rev. Lett. 51, 636 (1983).
2. Department of Physics, Texas A&M University, College Station, TX 77843.
3. Department of Physics, University of Tennessee, Knoxville, TN 37996.
4. Department of Physics, University of Lund, Lund, Sweden.
5. Adjunct staff member from the University of Tennessee, Knoxville, TN 37996.

THE EFFECT OF TRANSVERSE CORRELATIONS IN ION-CHANNELING IN VERY THIN CRYSTALS: EXPERIMENTAL AND THEORETICAL RESULTS

H. F. Krause P. D. Miller
S. Datz C. D. Moak
P. F. Dittner N. Nešković[1]
J. Gomez del Campo P. L. Pepmiller

Considerable effort has been directed toward a detailed understanding of the transmitted angular distribution of ions channeled along the axial directions of single crystals.[2] When the projectile energy is low and/or when the crystal is thick enough to cause significant multiple-scattering effects, the transmitted beam becomes concentrated along the chosen axis with lower intensity arms extending radially outward along the principal planar directions. Under these conditions, the characteristic star pattern observed is well understood, and it provides a useful aid in determining the crystal orientation in channeling experiments. For a very thin crystal and a swift projectile, the pattern of transmitted particles is somewhat more complex and not so well understood. Under these conditions, the projectile scatters as if it has undergone a single collision with the strings of

atoms adjacent to the axial channel. Previous experimental single-collision investigations of the axial channeling pattern have been directed toward understanding the angular distributions produced when the projectile direction deviates from the crystal's axial direction. Systematic single-collision studies have not been performed when the projectile and axial directions are aligned. We have performed such studies in an attempt to observe theoretically predicted rainbow scattering effects[3] in single-collision channeling patterns. Our results, consisting of both measured and theoretical angular distributions, suggest that the predicted rainbow effect occurs in channeling.

Swift protons (3-7 MeV) produced by the EN tandem Van de Graaff accelerator were narrowly collimated (angular divergence <0.012° FWHM) before illuminating a small portion of a very thin silicon single crystal. The crystal thickness was 1400 Å in the <100> direction; this thickness corresponds to an atomic string length of about 520 atoms along the <110> axis. Axially channeled particles that emerged from the crystal were detected by a two-dimensional position sensitive proportional counter.[4] The overall detector angular resolution measured in the horizontal and vertical laboratory directions was 0.012° and 0.008° (FWHM), respectively. Detector spatial resolution and the angular extent of the illuminated target as viewed from the detector contributed about equally to the overall angular resolution.

The experimental 2D angular distribution for 7-MeV protons channeled in the <110> axial direction of silicon is shown in Fig. 4.17. Particle intensity cuts through the distribution at several levels (percentage of the peak count) show that the particle intensity decreases monotonically and very rapidly from that in the undeflected beam direction. Fig. 4.17 also shows the angular locations of the last atom in each atomic string adjacent to the channel as viewed from the center of the axial channel at a longitudinal location halfway through the crystal (i.e., the location of the center-of-mass for each atomic string). The narrow [100] and wide [111] planar channels that intersect at the <110> axis are also shown. Under our experimental conditions, we see that (a) arms in the angular distribution appear to point toward the nearest atomic strings (evidence of a transverse correlation effect) and (b) the scattered protons avoid the wide [111] planar channels. It is clear that 7-MeV protons do not undergo significant multiple scattering in such a short channel length. Multiply scattered projectiles would statistically fill available phase space in planar channels, giving rise to a large number of trajectories in the [111] planar directions and a comparatively smaller number of trajectories in the [100] planar directions. More importantly, we show that the binary collision regime was reached to good approximation at 7 MeV by comparing the measured angular distribution (Fig. 4.17) to one obtained in a binary collision Monte Carlo trajectory calculation shown in Fig. 4.18.

In the Monte Carlo simulation, each projectile entered the axial channel at a randomly

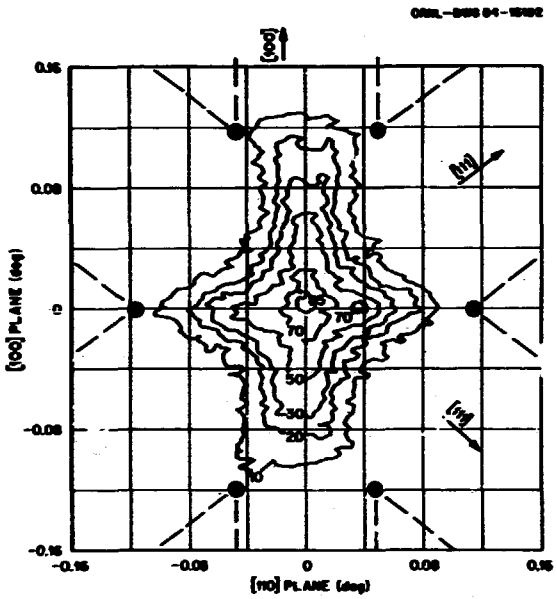

Fig. 4.17. Measured angular distribution for 7-MeV protons axially channeled along the <110> axis of a silicon crystal (thickness = 2000 Å). Particle intensity contours at 10, 20, 30, 50, 70, and 85 percent of the peak intensity are shown. The transverse location of atomic strings and the [100], [111] planar channeling directions are identified (see text).

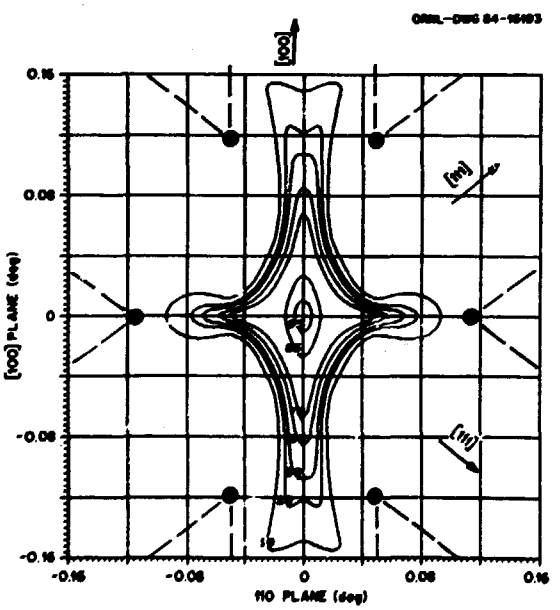

Fig. 4.18. Calculated angular distribution for 7-MeV protons axially channeled along the <110> axis of a silicon crystal (thickness = 2000 Å). Particle intensity contours at 10, 20, 30, 50, 70, 85, and 95 percent of the peak intensity are shown. The transverse location of atomic strings and the [100], [111] planar channeling directions are identified.

selected location traveling parallel to the axial direction (no beam divergence). The ionic projectile inter-acted with each atomic string adjacent to the channel through a transverse electric field that was calculated using the Lindhard potential.[5] The Lindhard potential constant used (C = 4.00) gives rise to a transverse electric field that is in excellent agreement with that given by the Molier potential over the impact parameter range of interest for <110> axial channeling. Thermal vibration effects were simulated. The transverse momentum imparted to the projectile in a binary collision with each string was assumed to occur at the string's center-of-mass. The net transverse momentum imparted to the projectile from all strings determined the overall deflection. The deflection of each particle in the horizontal and vertical directions were graded using a bin size (0.002°) much smaller than the measured experimental resolution, and these results were later averaged over the experimentally determined angular resolution functions (see Fig. 4.18).

The measured angular distribution for 7-MeV protons (Fig. 4.17) is in excellent agreement with the binary collision simulation calculated at the same energy (Fig. 4.18). The unaveraged Monte Carlo results (angular resolution = 0.002°) showed a well resolved ridge (maximum) whose shape is similar to the 20% contour shown in Fig. 4.18 and a minimum halfway between the ridge and the unde-flected beam position (height about 50% of the ridge height in a vertical cut across the [110] planar direction). The ridge has been shown analytically to be the consequence of rainbow scattering within the crystal.[3] From the similarity of measurements and the averaged Monte Carlo results, we conclude that the experimental angular resolution was insufficient to resolve the predicted rainbow scattering ridge. An angular distribution measurement at 7 MeV in the <100> axial channel (not shown) appears to confirm this conclusion. Here, the averaged Monte Carlo calculation indicated that four maxima should be observed at about 0.03° in the direction of the closest atomic strings (different from <110> axial symmetry). Two maxima in the correct location were observed. Slight misalignment of the crystal and the beam in one direction is probably the reason for incomplete resolution of the peaks in the <100> rainbow ridge.

ANOMALOUS MEAN-FREE PATHS OF CONVOY ELECTRONS PRODUCED BY 25 a.u. HIGHLY STRIPPED Ni IONS IN C AND Al TARGETS[1]

C. Bottcher
R. Latz[2]
M. Burkhard[2]
H. J. Frischkorn[2]
K.-O. Groeneveld[2]
D. Hofmann[2]
P. Koschar[2]
S. D. Berry[3]
M. Breinig[4]
I. A. Sellin[4]

Considerable evidence has accumulated over the past decade suggesting that unbound electrons associated with the passage of fast ions through foils may be correlated with their parent ions over distances an order of magnitude larger than the mean free path for free electrons of the same velocity.

We have measured the yields of convoy electrons associated with Ni^{24+} and Ni^{26+} traversing polycrystalline C and Al foils of thickness 3-500 $\mu g/cm^2$ at energies of 15.2 MeV/amu. These foils are thin enough that mean free paths of a few hundred Å may be inferred from a growth curve, such as that shown in Fig. 4.19. The mean free path for convoy electrons is 2000 ± 200 Å in contrast to the free electron value of ~100 Å.[1]

We have sought to explain this effect in terms of Coulomb focusing. As the electron moves through the foil, it is subjected to repeated scatterings, but between scatterings it is pulled back towards the parent ion by Coulomb attraction. A very simple model of the competition between scattering and focusing suggests that for ionic velocities $\gtrsim q^{1/2}$ Bohr velocities, an enhancement of the mean free path by a factor of ~10 is reasonable.

It is possible to write down a Boltzmann equation which describes the random walk of the electron under repeated scatterings in the presence of a Coulomb field. If this equation can be solved numerically without too drastic

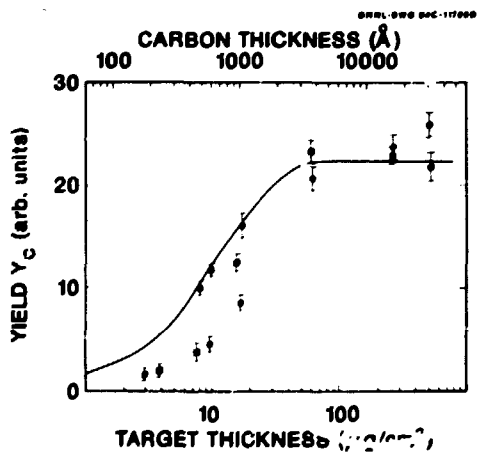

Fig. 4.19. Convoy electron yield versus target thickness. The open circles and squares refer to Ni^{24+} ions at 15.2 MeV/amu in Al and C foils, and the closed circles to Ni^{26+} in Al. The full line is a fit to the data of the form: $1 - \exp(-x/\lambda)$.

1. Boris Kidrič Institute of Nuclear Sciences, Belgrade, Yugoslavia.
2. D. S. Gemmel, Rev. Mod. Phys. 48, 129 (1984).
3. N. Neskovič, pp. 203-206 in Physics Division Progress Report, ORNL-6004 (1983).
4. R. W. Fearick et al., summary of paper to be published.
5. J. Lindhard, Mat. Fys. Medd. Dan. Vid. Selsk., 34, No. 14 (1965).

approximation, it may be possible to put the heuristic model on a firm footing.

---

1. Summary of paper submitted to the Symposium on the Physics of Electron Ejection in Ion-Atom and Ion-Solid Interactions held at the Institute of Physics, University of Aarhus in Denmark, June 29-30, 1984.
2. Universität Frankfurt/M, D6 Frankfurt am Main, Federal Republic of Germany.
3. Department of Physics, University of Tennessee, Knoxville, TN 37996.
4. Adjunct staff member from the University of Tennessee, Knoxville, TN 37996.

THE NEGATIVE ION SOURCE TEST FACILITY AS A NEGATIVE ION ATOMIC PHYSICS RESEARCH FACILITY

G. D. Alton T. J. Kvale[1]

We have made major modifications to the Negative Ion Source Test Facility[2] during the fiscal year in order to perform negative ion source research and the proposed Be^- and Ca^- experiments. The Negative Ion Source Test Facility, shown schematically in Fig. 4.20, is a multiple-purpose facility with emphasis placed on extending our knowledge of methods and mechanisms involved in the generation of negative ions and of the structure and properties of these ions.

Figure 4.20 illustrates the basic components which make up the facility. The facility can be operated for the generation and acceleration of positive ions which can be double charge-exchanged to produce negative ions prior to or following momentum analysis. In the former case, positive ions produced in a hollow cathode positive source are accelerated to energies up to 30 keV for singly charged particles. These are then focused through a recirculating Li charge-exchange cell where they are converted to negative ions through double charge exchange. Negative ions, thus created, are post-accelerated by the accelerator tube assembly and injected into the analyzing magnet at energies up to 150 keV. Post-momentum analysis charge-exchange can also be effected by reversing the polarities of the ion source housing and magnet, and focusing the analyzed positive ion beam through the Li charge-exchange cell situated immediately before the experimental chamber. In this way, positive ion beam energies up to 150 keV for singly charged particles can be obtained. The experimental arrangement should permit observation of very short-lived negative ion states.

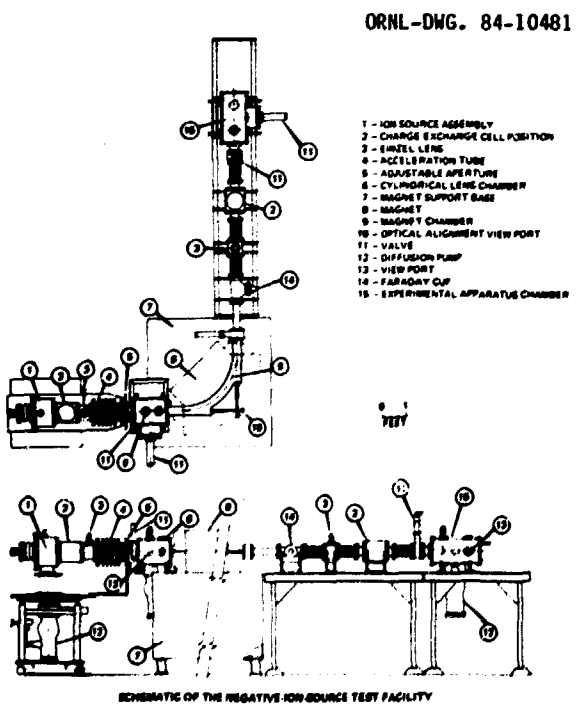

Fig. 4.20. The modified negative ion source test facility.

The facility can also be equipped with direct extraction-type negative ion sources for producing extensive numbers of high-intensity negative ion beams. Specifically, we have fabricated, installed, and tested a universal charge-exchange negative ion source which is presently being used to generate positive and negative ions.[3] The charge-exchange source consists of a positive ion hollow cathode source, ion extraction electrode system, einzel lens, and recirculating type Li charge-exchange cell. Negative ions can be formed in either of two cells located prior to or following magnetic analysis. The post-analysis charge-exchange cell is located in close proximity to the experimental chamber so that we can study metastably bound negative ions with lifetimes as short as a few tens of nanoseconds.

In addition to the previously described modifications to the facility, we have converted the magnetic mass analysis system so that circularly symmetric beams can be formed at the plane of analysis. (This modification was necessary in order to optimally transport the ion beam to our experimental chamber.) We have, as well, fabricated and installed beam transport components (lenses, magnetic steerers, valves, drift tubes, and apertures), a postanalysis charge-exchange cell and an experimental chamber which houses a specially designed electrostatic deflection system, Faraday cups, and electrostatic energy analyzer for performing the intended research.

In addition to the rather extensive changes in the Negative Ion Source Test Facility, we have converted our data acquisition system from analog to digital. The data acquisition system, shown schematically in Fig. 4.21, centers around a LeCroy 3500c CAMAC based data acquisition and control microcomputer and/or multichannel analyzer system. The system has available 64 kB of RAM and 30 kB of PROM firmware for data acquisition, manipulation, and experimental apparatus control. The data acquisition time for accumulation in a particular channel is determined by monitoring the transmitted ion beam in the Faraday cup after the electrostatic analyzer and

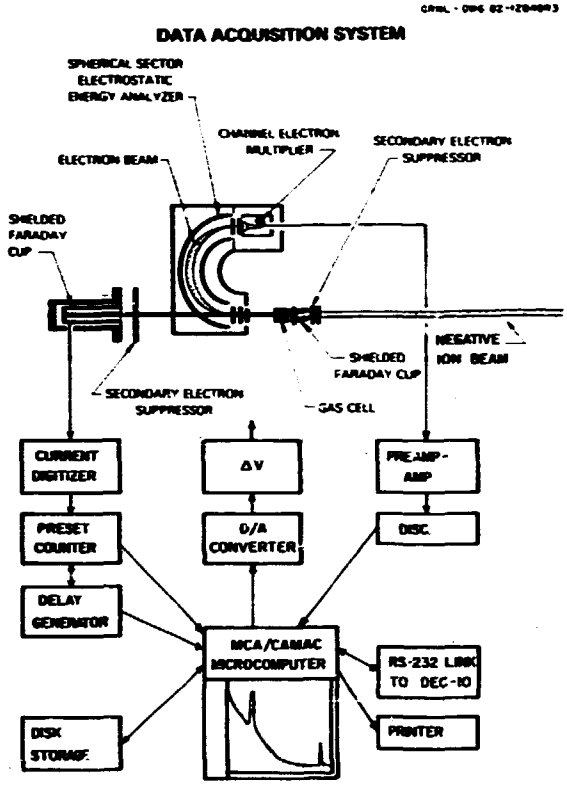

Fig. 4.21. A schematic diagram of the data acquisition system for measuring auto- and collisional-detachment properties of negative ions.

digitizing the analog signal which is fed into a preset scaler. After accumulation of a predetermined amount of charge, a signal from the preset scaler is used to inhibit further data acquisition, to store acquired data, and to advance a multichannel scaling unit to the next channel where the process is repeated. Signals derived from the CAMAC based multichannel scaling unit are used to advance a locally constructed external DAC which drives a bipolar operational amplifier used to change the voltage on the electrostatic energy analyzer. The electron signal, which is transmitted through the spectrometer, is detected with a conventional channel electron multiplier/amplifier circuit and fed into a CAMAC based ADC where it is stored in the memory of the multichannel analyzer. A typical electron energy spectrum obtained by this method is shown in this section of this report.

---

1. Postdoctoral Fellowship through Oak Ridge Associated Universities with the Physics and Health and Safety Research Divisions, ORNL.
2. G. D. Alton et al., p. 192 in Physics Division Progress Report, ORNL-5025 (1974).
3. G. D. Alton et al., p. 14 in Physics Division Progress Report, ORNL-6004 (1983).

PROGRESS TOWARD MEASUREMENT OF THE PROPERTIES OF METASTABLY BOUND NEGATIVE IONS

G. D. Alton T. J. Kvale[1] R. N. Compton[2]
D. J. Pegg[3] J. S. Thompson[4]

The present report deals with progress made toward measurement of the auto- and collisional-detachment properties of negative ions of the Group IIA elements (Be^- and Ca^-) using electron spectroscopic techniques. The experimental techniques and procedures utilized in the present investigations are similiar in many respects to those described in previous reports concerning H^- and He^- negative ions.[5,6] However, the present experiments are being performed at the Negative Ion Source Test Facility[7,8] which has been extensively modified in order to generate negative ions through charge exchange and perform ion source related experiments as well as interesting negative ion atomic physics experiments. In addition to the rather extensive changes in the Negative Ion Source Test Facility, we have converted our data acquisition system from analog to digital. The data acquisition system centers around a LeCroy 3500c CAMAC based data acquisition and control microcomputer and/or multichannel analyzer system. The modified facility, thus, is a multiple purpose facility which can be used to extend our knowledge of methods and mechanisms involved in the generation of negative ions, as well as to study their interesting atomic structure properties. The reader is referred to the description given in this section of this report for more details on the facility.

A schematic drawing of the experimental apparatus is shown in Fig. 4.22. The post-analysis charge-exchange cell is located in close proximity to the experimental chamber so that we can study metastably bound negative ions with lifetimes as short as a few tens of nanoseconds. The negative, positive, and neutral components which leave the charge-exchange cell are separated by a computationally designed deflection system. After electrostatic deflection through 10°, the negative and positive beams are monitored in shielded and biased

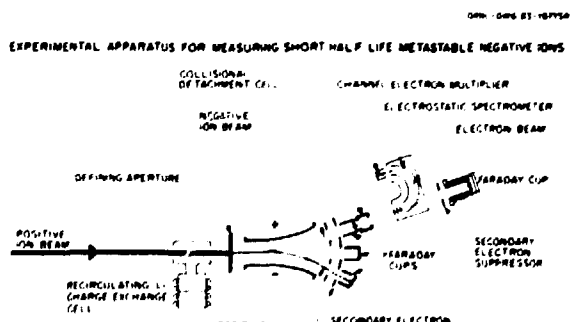

Fig. 4.22. Schematic drawing of the experimental arrangement for performing electron spectroscopic measurements of short half-life metastable negative ions.

Faraday cups. A portion of the negative ion beam is allowed to pass through a small aperture located in the center of the first Faraday cup and enters a gas cell which is used to collimate the beam and produce collisionally detached electrons which are used to calibrate the energy scale of our measurements. The ion beam then passes through a spherical sector electrostatic analyzer and is monitored in the rear Faraday cup. Detached electrons accompanying the ion beam are energy analyzed with the spherical sector electrostatic energy analyzer in the fixed-pass energy mode. In this mode of operation, electrons moving slower than the pass energy of the spectrometer are accelerated, while those moving faster than this pass energy are decelerated. In this way, our spectrometer resolution function remains approximately constant.

An energy spectrum resulting from the auto- and collisional-detachment of He^- which was produced by doubly charge exchange using the previously described experimental apparatus and the digital data acquisition system is shown in Fig. 4.23. Our present efforts are concentrated on measurements of the production efficiencies as a prelude to performing spectroscopic measurements similiar to those described previously for He^- which are designed to identify energy levels of the auto-detaching states of Ca^-. Calcium was chosen over beryllium as the element to study first because of the ease of generation of Ca^+ beams relative to those of Be^+. Experience with this ion will enable improvements to be made in the hollow-cathode source before studying Be^-. (Beryllium is highly toxic and will require special handling during periods of source maintenance.) In fact, during preliminary studies of the Ca^- ion, the hollow cathode source proved to be very unreliable with many internal electrical connections, filament, and oven related problems. Substantial progress has been made in reducing the number of failures and, therefore, significantly improving the reliability of the source. Extensive modifications to the ionization chamber and oven were required which has led to a more reliable source. These modifications will be the subject of a forthcoming report.

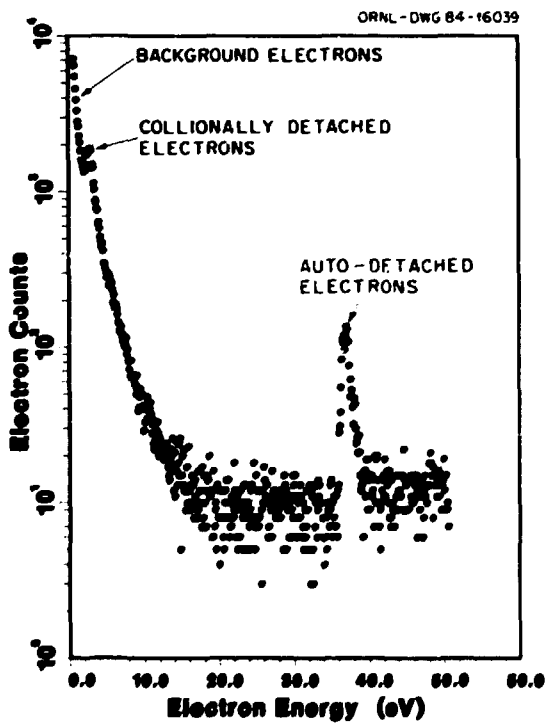

Fig. 4.23. Electron energy spectrum for metastable He^- interaction with Ar.

Calculations by Bunge et al.[9] predict that the Ca^- ion exists in metastable $[Ar]\ (4s4p^2)^4P$ states which are bound by ~0.55 eV with respect to the metastable $(4s4p)^3P^o$ state of the Ca atom. The J = 5/2 level of this state should, for example, autodetach via a forbidden process driven by magnetic interactions between the electrons in a manner analogous to the decay of the metastable quartet J = 5/2 state of He^-. The energy of these autodetached electrons should be 1.34 eV relative to the rest frame of the moving ion based on an electron affinity value of 0.55 eV. The lifetimes of the three levels associated with the $(4s4p^2)^4P$ state have not, as yet, been calculated. One can expect a differential metastability among the levels as in the case of He^- due to the different strengths of their couplings with doublets of the same configuration. In He^-, the lifetimes are in the approximate range of 10^{-5} to 10^{-3} sec. For a heavier ion such as Ca^-, one might expect stronger magnetic interactions between electrons and which might lead to a breakdown of LS coupling resulting in somewhat shorter lifetimes than in a light ion such as He^-. This being the case, our present experimental arrangement should permit observation of such short-lived decaying states. For extremely long-lived states, however, another procedure may be necessary to determine the energy levels of Ca^-, such as using laser photodetachment techniques, or extending the decay length at our experimental chamber.

We have recently obtained preliminary results on Ca^- ions in the energy range from 60-120 keV produced by sequential charge-exchange interactions with Li vapor. At 120 keV, the laboratory frame energies at the collisional- and auto-detachment peaks in Ca^- are 1.6 eV and 6.0 eV, respectively. We are continuing our work on Ca^- by investigating the production process, methods of reducing the background, and the effects of stray magnetic fields on the intensity and resolution of low-energy electron peaks. The collisional- and auto-detachment spectroscopic portion of this work is expected to be completed in the near future, at which time we will direct our attention toward measurements of similiar properties of the Be^- negative ion.

---

1. Postdoctoral Fellowship through Oak Ridge Associated Universities with the Physics and Health and Safety Research Divisions, ORNL.

2. Health and Safety Research Division, ORNL.
3. Adjunct staff member from the University of Tennessee, Knoxville, TN 37996.
4. Graduate Student from the University of Tennessee, Knoxville, TN 37996.
5. G. D. Alton, R. N. Compton, and D. J. Pegg, Phys. Rev. A28, 1405 (1983).
6. G. D. Alton, R. N. Compton, and D. J. Pegg, summary of paper submitted to Physical Review A.
7. G. D. Alton et al., p. 192 in Physics Division Progress Report, ORNL-5025 (1974).
8. G. D. Alton et al., p. 14 in Physics Division Progress Report, ORNL-6004 (1983).
9. C. F. Bunge et al., Nucl. Instr. Meth. 202, 299 (1982).

SHAPE OF THE ELECTRON CAPTURE TO THE CONTINUUM CUSPS FOR H, H_2, AND He TARGETS IN THE VELOCITY RANGE 6.3 TO 18.0 a.u.[1]

S. D. Berry[2] S. B. Elston[4]
G. A. Glass[3] P. Engar[2]
I. A. Sellin[4] N. Stolterfoht[7]
K.-O. Groeneveld[5] H. Schmidt-Böcking[7]
D. Hofmann[5] G. Nolte[7]
L. H. Andersen[6] G. Schiwietz[7]
M. Breinig[4]

The velocity spectrum of electrons ejected into the forward direction in energetic ion-atom collisions exhibits a cusp-shaped peak when the emergent electron velocity $\vec{v}_e$ matches that of the outgoing ion velocity $\vec{v}_p$ in both speed and direction. For projectile ions with few electrons, the electrons predominately arise from transfer of a target electron to a low-lying projectile-centered continuum state (ECC), whereas if there are *many* projectile electrons, those electrons can be lost to similar low-lying continuum states. This process is termed electron loss to the continuum (ELC). For several years, there has been much interest in both the experimental and theoretical aspects of this problem;[8,9] we are concerned here with only ECC.

In early theories, a first-order perturbative treatment of the charge-exchange amplitude was used to explain the ECC cusp, with the final electronic state described in terms of a simple Coulomb wave centered on the projectile, leading to a cusp nearly symmetric in $(\vec{v}_e - \vec{v}_p)$. However, later experimental results for both heavy and light bare projectiles showed a skewness of the ECC peak shape toward lower electron velocities.

To account for this asymmetry, the distortion of the outgoing electron by the interaction between it and the residual ion must be considered, but in a way which goes far beyond a simple postcollision interaction description. In 1978, Shakeshaft and Spruch (SS) included a second-order term in the Born expansion[10] to approximate this effect upon the ECC shape while Chan and Eichler (CE) proposed that slightly extending the first Born approximation could account for the cusp skewness.[11] Subsequent experiments[12,13] showed an asymmetry more similar to that predicted by SS than that by CE, but the strong dependence of the asymmetry upon projectile Z and velocity of the SS theory was not found. More recently, Jakubassa-Amundsen[14] has calculated the shape of the ECC cusp within the semiclassical impact approximation (SCIA) for the case of argon projectiles and helium targets; the resulting shape compares well with experiment.

Here, we present a summary of results, obtained from accelerator runs at Brookhaven National Laboratory (BNL), Lawrence Berkeley Laboratory (LBL), Hahn-Meitner-Instutut (HMI), and Oak Ridge National Laboratory (ORNL), contained in our paper recently accepted for publication.[15] By using a general, model-independent method of describing the cusp shape that explicitly takes into account the effect of a given experimental choice of analyzer geometry, resolution, and angular acceptance, we can compare spectra from different experiments directly and extract the basic underlying shape of the ECC cusp.

To accurately describe that shape, the cross section was expanded over two of the projectile frame variables $v_e' = |\vec{v}_e - \vec{v}_p|$ and θ_e' (angle with respect to the projectile direction). This expansion is then transformed to the laboratory frame and integrated over the velocity and angular acceptance of the spectrometer to yield:

$$Q(v_e,\theta_e) = C \sum_{n,\ell} B_{n,\ell}(v_p) \times \int_{v_e} \int_{\Omega_e} (v_e)^2 (v_e')^{n-1} P_\ell(\cos\theta_e') \; S(v_e,\Omega_e) dv_e d\Omega_e .$$

Here Q is the measured spectral function, C is an overall amplitude, $B_{n,\ell}$ are the coefficients for each term, P_ℓ are Legendre polynomials, and S is the function describing the acceptance of the particular spectrometer arrangement used.

By making some reasonable assumptions as to the functional form of S, we are able to perform the integration above and thereby make direct comparisons with the experimental data using standard fitting techniques. The results of these comparisons are values of the coefficients $B_{n,\ell}$ which, to the degree the assumptions in making this expansion are valid, are independent of the experimental arrangement. The term with $n = \ell = 0$ is that commonly known as the "Dettmann" cusp.[16]

A summary of the fit results is presented in Table II of Ref. 15, and a complete discussion of the results appears there. Here, we briefly review those conclusions.

The most striking feature of the fit results is the consistency of the value of the B_{01} coefficient ($n = 0$, $\ell = 1$), which is also the major source of the asymmetry found in the cusp shape at these energies. The value of this coefficient, relative to the leading term B_{00}, remains constant at ~.45 for projectile Z_p values between 6 and 18, projectile velocities between 6 and 18 a.u., and target Z_t values of 1 and 2. As noted by Macek et al.,[17] the presence of this term implies the necessity of second Born terms in any theoretical treatment

of the problem, as in the approach of Shakeshaft and Spruch.[10] However, the SS theory has a strong dependence on Z_p, v_p, and Z_t not found here. The results of Jakubassa-Amundsen[14] are very promising, but we presently lack a detailed understanding of the dependence on Z_p, v_p, and Z_t predicted by her approach.

Also evident from the fit results is the very small contribution of terms with $\ell = 2$. This suggests, at least for the combinations of Z_p, v_p, and Z_t used here, that the expansion may be limited to the lowest four terms $n = 0,1$ and $\ell = 0,1$.

In addition, the data collected using atomic hydrogen targets suggests that the shape is substantially similar to that found for helium targets.

Finally, we reproduce here in Fig. 4.24 some representative fit results. The top half of the drawing contains comparisons of the expansion of the equation above with the data, and the bottom half of the figure contains the component parts of the fit (summed over $n = 0,1$) for ℓ values of 0, 1, and 2 (termed S, P, and D, respectively).

In summary, we hope that by analyzing our data in a model independent, apparatus independent manner, we can provide insight into the ECC process at high velocities, and thereby stimulate further theoretical investigation.

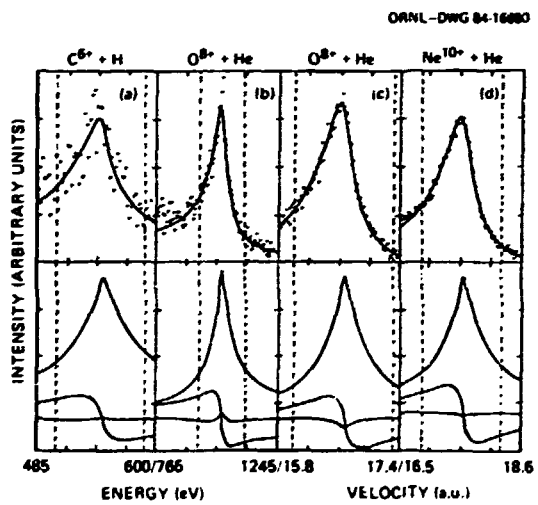

Fig. 4.24. The top row shows four comparisons between fitted spectra (solid lines) and data (dots) incorporating background subtraction where appropriate for: (a) 12-MeV bare carbon projectile, (b) 30-MeV bare oxygen projectiles, (c) 110-MeV bare oxygen projectiles, and (d) 155-MeV bare neon projectiles. The vertical dashed lines indicate equivalent arbitrary $(1 \pm .04)v_p$ limits for each of four spectra. The bottom row displays S, P, and D components of the fitted function (summed over both $n = 0,1$ components) and the corresponding fitted function shown above. The bottom spectra have been displayed with a δ-functional line width, to remove the dependence of the cusp shape on the particular experimental line width, allowing for a more direct comparison of the results.

---

1. Summary of paper to be published in Physical Review A.
2. University of Tennessee, Knoxville, TN 37996.
3. Naval Surface Weapons, Silver Spring, MD 20910.
4. Adjunct staff member from the University of Tennessee, Knoxville, TN 37996.
5. Institut für Kernphysik, Universität Frankfurt, August-Euler-Strasse, D 6 Frankfurt am Main, Federal Republic of Germany.
6. Institute of Physics, University of Aarhus, DK-8000, Aarhus C, Denmark.
7. Hahn-Meitner-Institut für Kernforschung, D 1000 Berlin 39, Federal Republic of Germany.
8. W. Meckbach and R. A. Baragiola, in Inelastic Ion-Source Collisions, edited by N. H. Tolk, J. C. Tully, W. Heiland, and C. W. White (Academic Press, New York, 1977);, p. 283;
I. A. Sellin, J. Phys. (Paris) 40, C1-255 (1979);
C. R. Vane, IEEE Trans. Nucl. Sci. NS-26, 1078 (1979);
M. W. Lucas, Proceedings of the Workshop on Physics with Fast Molecular-Ion Beams, edited by D. S. Gemmell, Argonne National Laboratory Report No. ANL/PHY79-3, p. 291;
V. H. Ponce and W. Meckbach, Comments At. Mol. Phys. 10, 231 (1981);
I. A. Sellin, Proceedings of the XII International Conference on the Physics of Electron and Atomic Physics, edited by S. Datz (Amsterdam, 1982);
K.-O. Groeneveld et al., Comments on Atomic and Molecular Phys. 14, 187 (1984).
9. M. Breinig et al., Phys. Rev. A25, 3015 (1982).
10. R. Shakeshaft and L. Spruch, Phys. Rev. Lett. 41, 1037 (1978).
11. F. T. Chan and J. Eichler, Phys. Rev. A20, 367 (1979); R. Shakeshaft and L. Spruch, ibid. 20, 376 (1979).
12. S. D. Berry et al., IEEE Trans. Nucl. Sci. NS-30, 902 (1983).
13. M. Breinig et al., Phys. Rev. Lett. 45, 1689 (1980).
14. D. H. Jakubassa-Amundsen, J. Phys. B16, 1767 (1983).
15. S. D. Berry et al., Phys. Rev. A (to be published.
16. K. Dettman, K. G. Harrison, and M. W. Lucas, J. Phys. B7, 269 (1974).
17. M. W. Lucas et al., J. Phys. B13, 4833 (1980);
J. Macek et al., Phys. Rev. Lett. 46, 1571 (1981).

EN TANDEM OPERATIONS

P. L. Pepmiller G. F. Wells
P. D. Miller

The beginning of this report period found us in the midst of a major tank opening. During

the summer of 1983, machine performance had degraded substantially so a decision was made to go in for major maintenance. The acceleration column was stripped of all nonessential pieces before doing a complete washdown with soap and water. After drying out, the graded resistor chain was reinstalled. Then we tried using a new belt material, Poly-C, instead of our standard belt. This type of belt had been used previously in vertical machines with great success. It costs considerably less than the standard belt, does not produce dust, and can be bought as a long strip and assembled in the machine. After installation and initial tensioning, we closed the machine and began voltage tests without tubes. We experienced tank sparks at voltages above 5 MV, however, their frequency was no higher at 7.3 MV than at 5 MV. After about 50 hours of voltage tests, we re-entered the machine for inspection and reinstallation of tubes. At this point, it was noticed that the Poly-C belt had failed. There were multiple puncture holes through the belt, which resulted in longitudinal splits. The causes of the spark holes are not clear at this time. Fortunately, we were able to borrow a standard belt from Kansas State University to replace ours. The tank opening was concluded with the installation of rebuilt tubes. The machine resumed normal operation in late December 1983. Since that time, it has logged over 1700 hours in support of basic atomic physics research. During the first five months of operation, there were numerous tank openings, mainly due to problems with belt guides. However, the generator has now operated for four months without a failure. Major projects begun during this reporting period include installation of a new ion source, replacement of magnet power supplies, upgrading of various outdated or unreliable power supplies throughout the laboratory, and a new operator's training guide and schedule.

ATOMIC PHYSICS FOR FUSION PROGRAM

ECR MULTICHARGED ION SOURCE

F. W. Meyer J. W. Hale
J. W. Johnson

Construction and installation of the Electron Cyclotron Resonance (ECR) multicharged ion source was completed on schedule early in FY 1984. Although the ECR ion source was designed for operation at 10.6 GHz, initial source testing was carried out at 2.45 GHz in order to gain experience in source operation while awaiting delivery of the 10.6 GHz microwave amplifier scheduled for June 1984.

During the initial testing phase at 2.45 GHz, X-ray measurements of the bremsstrahlung spectrum produced by the source provided evidence of ECR heating of electrons. A calibrated Si-Li X-ray detector indicated electron energies up to 160 keV. Following construction and installation of the beam line and charge analyzer in March 1984, source performance could be assessed more directly by measuring charge state distributions of extracted beams. Even at the lower microwave frequency, fully stripped C beams were obtained, which were used to initiate the first planned experiment involving the new source, total cross sections measurements of electron capture by fully stripped light ions incident on atomic hydrogen. Operation of the source at its design frequency of 10.6 GHz started on schedule in June 1984. Since that time efforts toward source optimization have been ongoing, in parallel with the above-mentioned cross section measurements.

The salient features of the ECR ion source, shown in Fig. 4.25, are summarized in Table 4.4. The source consists of two stages, and is quite similar in size to MINIMAFIOS.[1] The first stage, which supplies plasma to the second stage to facilitate startup, is operated in overdense mode.[2] A helical slow-wave launcher[3] is used to inject 2.45 GHz microwaves into the first stage which is located in an axial magnetic field of 5-7 kG. Plasma density is controlled by the microwave power level and gas pressure, which varies in the 10^{-3} - 10^{-4} torr range. Since microwave absorption in the first stage is nonresonant, the magnetic field can be tuned to optimize second stage performance. The second stage is separated from the first stage by two stages of differential pumping, which is sufficient to maintain low 10^{-6} torr pressure in the second stage during source operation.

In the second stage, electrons confined in a minimum-B configuration are heated by resonant absorption of 10.6 GHz microwaves that are injected radially immediately following the differential pumping section. The minimum-B structure is produced by a superposition of an axial mirror field and a radial hexapole field. Three conventional water-cooled solenoids are used to establish the axial magnetic field.[4] The hexapole field is produced by a compact assembly[4,5] of $SmCo_5$ permanent magnets positioned around the cylindrical vacuum wall of the second stage. Cooling of the permanent magnet assembly is achieved by water circulation through the voids created between the cylindrical vacuum wall and the duodecagon defined by the placement of the $SmCo_5$ bars.

As regards the mechanical design, care was taken to ensure ease of assembly and access. The source divides into three sections, each of which is separately supported by, and can be rolled freely on, precision tracks. The three solenoidal field coils are supported by a similar track structure, and can be moved freely about to expose otherwise inaccessible source parts during source disassembly, or to change the axial mirror ratio in the second stage while the source is fully assembled.

Ion extraction is accomplished by a three-element extraction electrode, the first two elements of which can be biased independently for ion focussing and prevention of electron backstreaming. The position of the anode and the extraction electrode, and the extraction gap itself can be varied by the use of shims. An electrostatic unipotential lens operated in "accel" mode[6] images the extracted beam onto the entrance slit of a stigmatic 90° magnetic charge

ORNL Photo 6434-84

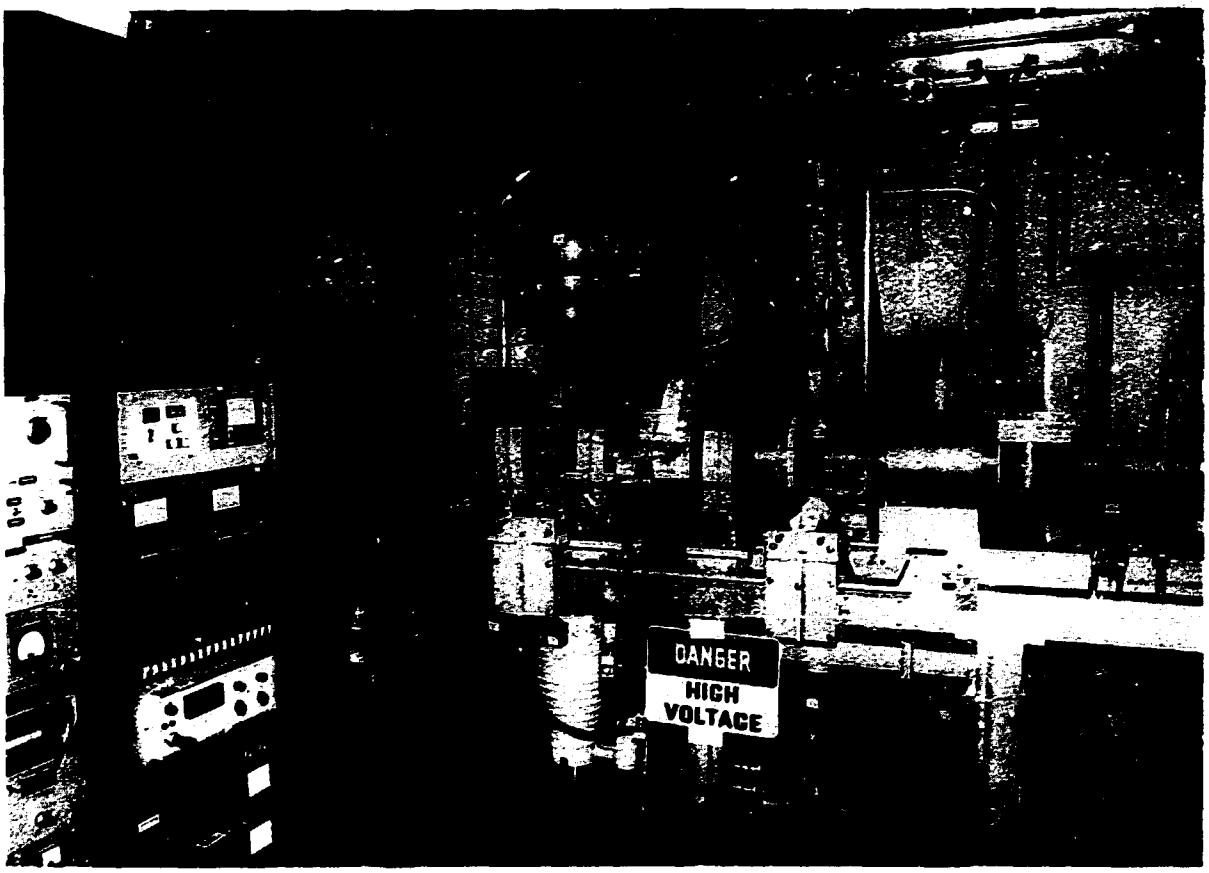

Fig. 4.25. The ORNL ECR multicharged ion source.

analyzer having a 40-cm radius of curvature. The entrance slit assembly is located about 100 cm downstream of the source anode; object and image distances for the 90° magnet are 80 cm. Retractable Faraday cups located immediately after the entrance and exit slits are used to measure total extracted beam currents, and charge-selected beam intensities, respectively. Both entrance and exit slit assemblies feature independently adjustable horizontal and vertical slit jaws, to which current can be measured. An electrostatic quadrupole lens located downstream of the exit slits can be used to transport the charge-selected beam to those experiments requiring maximum beam intensities.

Prior to delivery of the 10.6-GHz microwave system, the ECR ion source was operated at an interim frequency of 2.45 GHz. In order to maintain roughly the same ratio of hexapole-to-axial magnetic field strength at the lower frequency, only 6 of the 12 $SmCo_5$ bars were used, reducing the strength of the hexapole by a factor of two. An additional 25% decrease in hexapole strength was obtained by shimming out the bars to their maximum radius determined by adequate clearance to the solenoidal field windings.

Operation of the source at the lower frequency was far from optimum, due mainly to poor coupling between the second stage plasma and the 2.45 GHz microwaves. Due to their longer wavelength, only a few modes propagated in the second-stage cavity; microwave absorption seemed to occur preferentially on the microwave injection side of the second stage which is furthest removed from the extraction region. Even in this mode, the high-charge-state capability of the new source significantly exceeded that of the ORNL PIG ion source. Figure 4.26 shows a typical charge stage distribution for Ar source gas obtained at this frequency. For light ion production, beams up to fully stripped ^{13}C (10^{-14} el. A) and up to H-like O (10^{-12} el. A) were produced at the lower frequency.

Significant improvement in source performance was obtained, as expected, after installation of the 10.6 GHz microwave system, both in terms of total extracted beam intensity and mean charge state of the extracted beams. Microwave absorption increased dramatically, as evidenced by very low reflected power (typically less than 10%) during source operation. Optimum charge-state distributions were obtained for a second-stage mirror ratio of about 1.6, significantly

Table 4.4 ORNL ECR source parameters

Microwaves	
First stage 2.45 GHz (300 W max)	50 - 200 W
Second stage 10.6 GHz (2.2 kW max)	20 - 800 W
Magnetic Fields	
Mirror ratio	1.6
Hexapole field at vacuum wall	4.0 kG
Field in extraction plane	4.5 kG
Field in first stage	5 - 7 kG
Total solenoid power	60 kW
Vacuum (operating condition)	
First stage	10^{-3} - 10^{-4} T
Second stage (1×10^{-7} torr base)	$1 - 6 \times 10^{-6}$ T
Extraction	1×10^{-7} T
Beamline (2×10^{-9} torr base)	2×10^{-8} T
Dimensions	
Solenoids ID	18 cm
Solenoids OD	40 cm
Hexapole ID	9.5 cm
Hexapole length	33 cm
Vacuum wall ID second stage	8.6 cm
Anode aperture	0.5 cm
Extraction aperture	0.8 cm
Extraction gap	2.6 cm

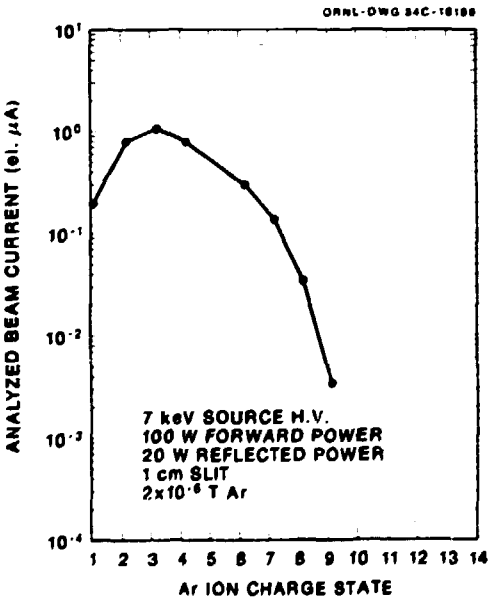

Fig. 4.26. Ar charge state distribution from ECR ion source — 2.45 GHz source operation.

below the 2.1 mirror ratio attainable at maximum second-stage field coil separation. Figure 4.27 shows a measured charge state distribution obtained for Ar with the source operating at 10.6 GHz. As has been noted by other workers,[7,8] an admixture of O_2 was found to significantly increase the Ar high-charge-state

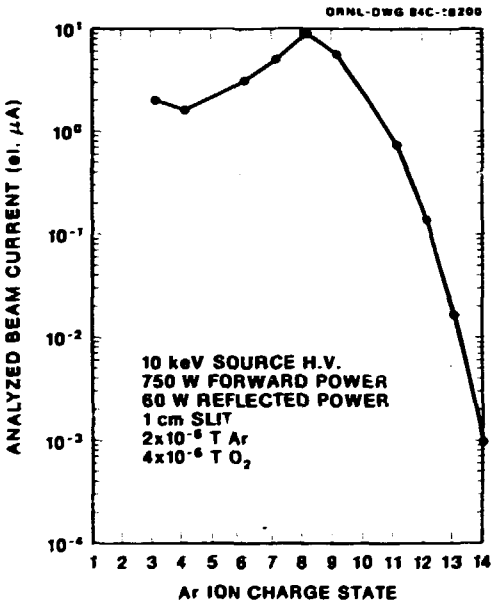

Fig. 4.27. Ar charge state distribution from ECR ion source — 10.6 GHz source operation.

output of the source. Production of light ion beams has yet to be optimized. So far ^{13}C, ^{15}N, ^{18}O, ^{19}F, and ^{22}Ne beams have been obtained, with intensities varying from a few μA for charge states up to and including He-like, about 0.1-1 μA for H-like, and 1-50 nA for fully stripped ions.

1. R. Geller, B. Jacquot, and C. Jacquot, Proceedings of the 7th Symposium (1983 International) on Ion Sources and Ion Assisted Technology - ISIAT 1983, p. 187, Kyoto, Japan.
2. G. Lisitano, M. Fontanesi, and E. Sindoni, Appl. Phys. Lett. 16, 122 (1970).
3. D. P. Grubb and T. Lovell, Rev. Sci. Inst. 49, 77 (1978).
4. Physics Division Progress Report, Oak Ridge National Laboratory report ORNL-6004, December 1983.
5. K. Halbach, Nucl. Inst. Meth. 169, 1 (1980).
6. Operation in "decel" mode is not possible in the present application due to the favorable conditions for Penning discharge produced by the combination of ion source magnetic fringe field and lens electrostatic field.

7. H.-G. Mathews, H. Beuscher, R. Fiedler, and W. Krauss-Vogt, IKP - Annual Report 1983, KFA Julich.

8. D. J. Clark, Y. Jongen, and C. M. Lyneis, p. 133 in Proceedings of the 10th International Conference on Cyclotrons and their Applications, April 30-May 3, 1984, East Lansing, MI, IEEE Conference Record 84CH1996-3 (1984).

ELECTRON CAPTURE CROSS SECTION MEASUREMENTS

F. W. Meyer C. C. Havener
A. M. Howald R. A. Phaneuf

Measurements of total electron capture cross sections for fully stripped and H-like C, N, O, F, and Ne ions incident on H and H_2 have been performed in the energy range 0.2 to 10 keV/amu using ion beams produced by the new ECR multicharged ion source. While straightforward experimentally, these measurements are of significant current interest both from a basic and applied scientific perspective, and also provide a convenient mechanism for exploring the range of operating parameters and capabilities of the new source.

The experiment employed the ORNL atomic hydrogen gas target, a directly heated tungsten tube in which molecular hydrogen is thermally dissociated. A collimation section preceding the target limited the magnetically charge analyzed incident beam to a divergence of ±1.7 mr, and 1-mm cross section inside the target. Immediately downstream of the collision target cell, charge analysis occurred in an electrostatic parallel-plate analyzer. A single CEM operated in pulse-counting mode was employed for particle detection. The electron-capture signal and primary beams were measured alternately for a preselected number of cycles under computer control; the total electron capture cross sections were deduced from the fraction of ions which capture an electron at a known (calibrated) target thickness.

Figures 4.28-4.32 show the experimental electron capture cross section results obtained for the measured fully stripped and H-like light ions incident on atomic and molecular hydrogen. The error bars shown reflect random uncertainty in terms of reproducibility of the measurements at two standard deviations. Systematic uncertainties are estimated to be ±9% for both the H and H_2 cross sections.

In the case of the fully stripped C, N, and O projectiles incident on H, the present measurements can be compared to theoretical calculations. Very good agreement is found between the present results for C^{6+}, N^{7+}, and O^{8+} incident and H, and the close-coupling calculations of Fritsch and Lin[1] employing a modified atomic-orbital (AO) expansion. While falling systematically below the AO calculations, the discrepancy is less than 20% at energies above 1.5 keV/amu, and approaches 40% at the lowest energies measured. For C^{6+} and O^{8+} incident on H, close coupling calculations by Green et al.[2] and Shipsey et al.[3], respectively, employing a molecular-orbital (MO) expansion are also in

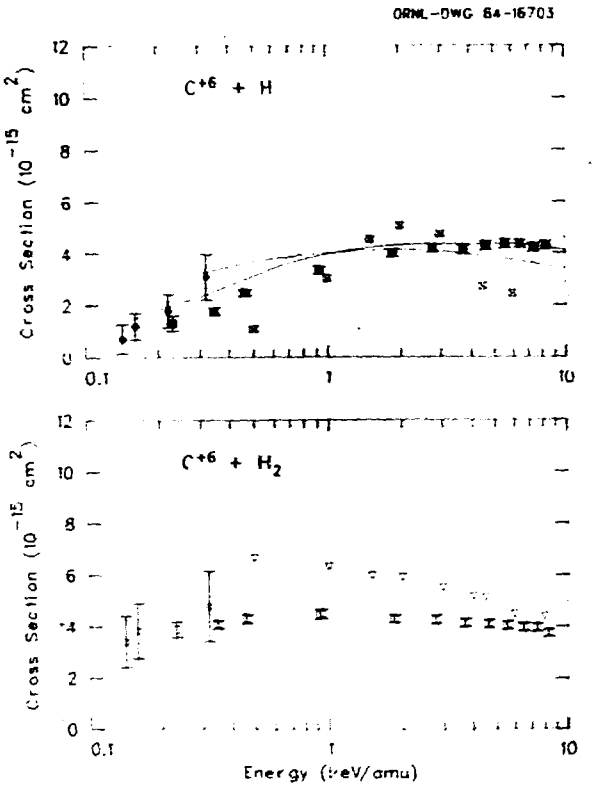

Fig. 4.28. Total electron capture cross sections for C^{6+} incident on H and H_2 vs energy; solid and open squares — present results for H and H_2 targets, respectively; solid and open diamonds — measurements of Phaneuf et al. (ref. 5); cross hatched boxes and inverted triangles — measurements of Panov et al. (ref. 6). Curves represent theoretical results for C^{6+} + H. Solid line — AO calculation by Fritsch and Lin (ref. 1); dashed line — MO calculation by Green et al. (ref. 2); chain dashed curve — multichannel Landau Zener calculation by Janev et al. (ref. 4).

reasonable accord with the present results. The MO results lie systematically above the AO calculations by about 10% above 1.0 keV/amu, and by as much as 40% at 0.2 keV/amu.

An interesting comparison can be made between the total electron capture cross sections for fully stripped projectiles of nuclear charge Z, and those for H-like projectiles of nuclear charge Z+1. It is observed that the cross sections for the pairs of ions C^{6+} and N^{6+}, N^{7+} and O^{7+}, O^{8+} and F^{8+}, and F^{9+} and Ne^{9+} are nearly identical over the entire energy range covered, indicating that the projectile charge is the prime determinant of the total electron capture cross section for these highly stripped systems. This finding is consistent with the theoretical results[2,3] that, for the fully stripped ions, electron capture occurs preferentially into high n-levels ($n > 4$). The presence of a tightly

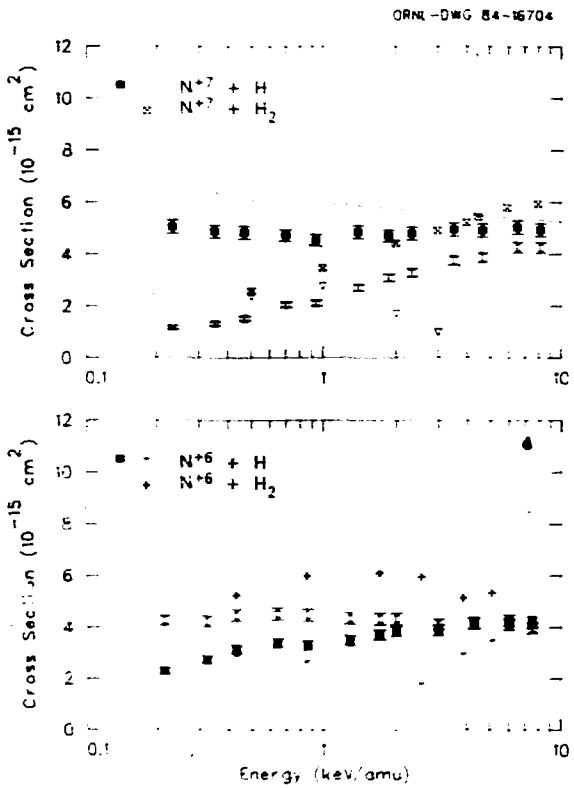

Fig. 4.29. Total electron capture cross sections for N^{7+} and N^{6+} incident on H and H_2 vs energy; solid and open squares — present results; data points without error bars — measurements by Panov et al (ref. 6); solid line — AO calculation by Fritsch and Lin (ref. 1); dashed curve — multichannel Landau Zener calculation by Janev et al. (ref. 4).

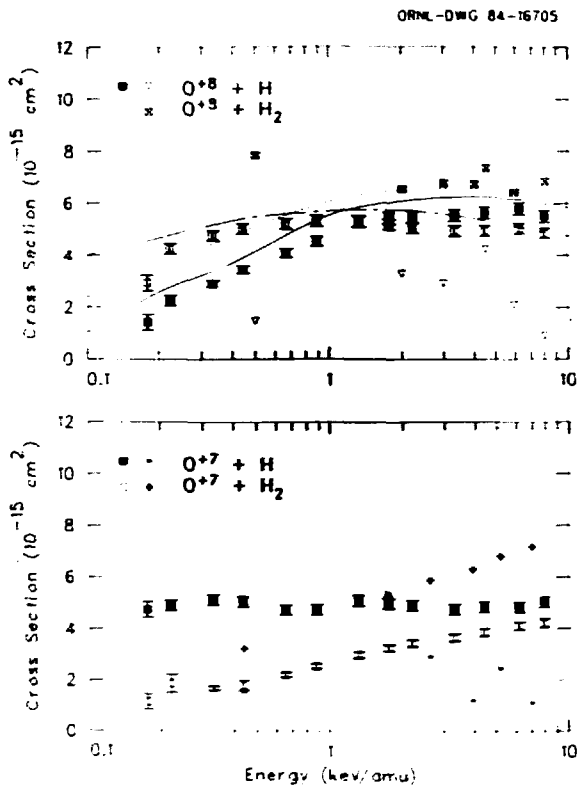

Fig. 4.30. Total electron capture cross sections for O^{8+} and O^{7+} incident on H and H_2 vs energy; solid and open squares — present results; data points without error bars — measurements by Panov et al. (ref. 6); solid line — AO calculation by Fritsch and Lin (ref. 1); dashed line — MO calculation by Shipsey et al. (ref. 3); dashed curve — multichannel Landau Zener calculation by Janev et al. (ref. 4).

bound electron in the ionic core should have only a minimal effect on the behavior of the electronic wavefunction of these highly excited states. The interesting question of how many electrons can be added to the core before an effect is observed in terms of the total electron capture cross section will be addressed in future experiments.

ION-ATOM MERGED-BEAMS EXPERIMENT

C. C. Havener H. F. Krause
R. A. Phaneuf

An ion-atom merged beam experiment has been developed to measure the total electron capture cross sections for collisions of multicharged ions with H at energies in the range 1-500 eV/amu. Our aim is to extend to lower energies previous measurements made at ORNL using a pulsed laser source.[1] At such low energies, theoretical models remain essentially untested. In some multiply ionized systems, an orbiting mechanism is predicted to give very large electron capture cross sections with a 1/v velocity dependence.

The current arrangement of the apparatus is shown in Fig. 4.33. A 2-5 kV, mass-analyzed beam of H^- from a duoplasmatron ion source passes through the optical cavity of a 1.06-μm Nd:YAG laser where up to 1 kW of circulating intracavity power is maintained. Up to 1%

1. W. Fritsch and C. D. Lin, Phys. Rev. A 29, 3039 (1984).
2. T. A. Green, E. J. Shipsey, and J. C. Browne, Phys. Rev. A 25, 1364 (1982).
3. E. J. Shipsey, T. A. Green, and J. C. Browne, Phys. Rev. A 27, 821 (1983).
4. R. K. Janev, D. S. Belic, and B. H. Brandsen, Phys. Rev. 28, 1293 (1983).
5. R. A. Phaneuf, I. Alvarez, F. W. Meyer, and D. H. Crandall, Phys. Rev. 26, 1892 (1982).
6. M. N. Panov, A. A. Basalev, and K. O. Lozhkin, Phys. Scr. T3, 124 (1983).

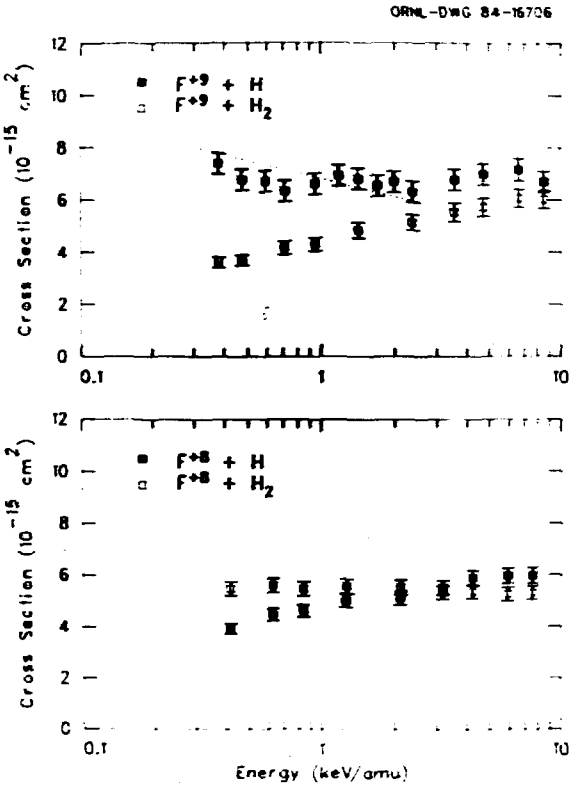

Fig. 4.31. Data points — present measurements of the total electron capture cross section for F^{9+} and F^{8+} incident on H and H_2 vs energy; dashed curve — multichannel Landau Zener calculation by Janev et al. (ref. 4).

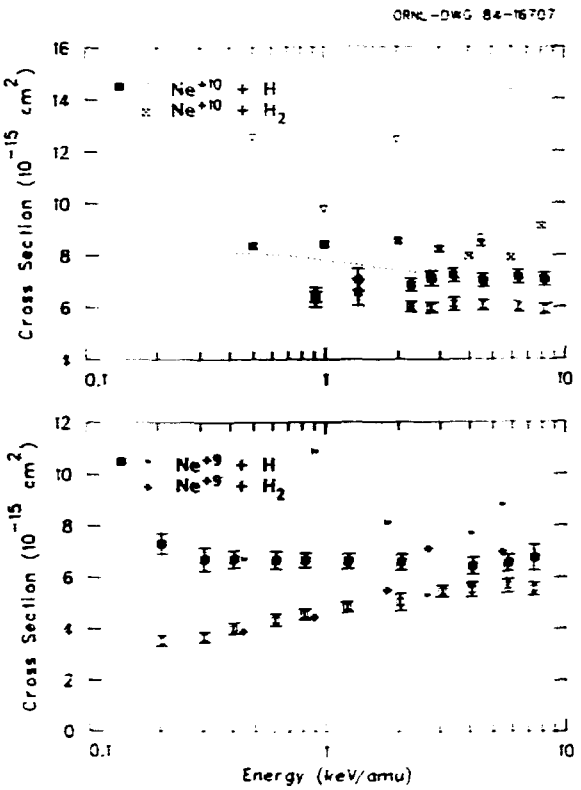

Fig. 4.32. Solid and open squares — present measurements of the total electron capture cross section for Ne^{10+} and Ne^{9+} incident on H and H_2 vs energy; data points without error bars — measurements by Panov et al. (ref. 6); cashed curve — multichannel Landau Zener calculation by Janev et al. (ref. 4).

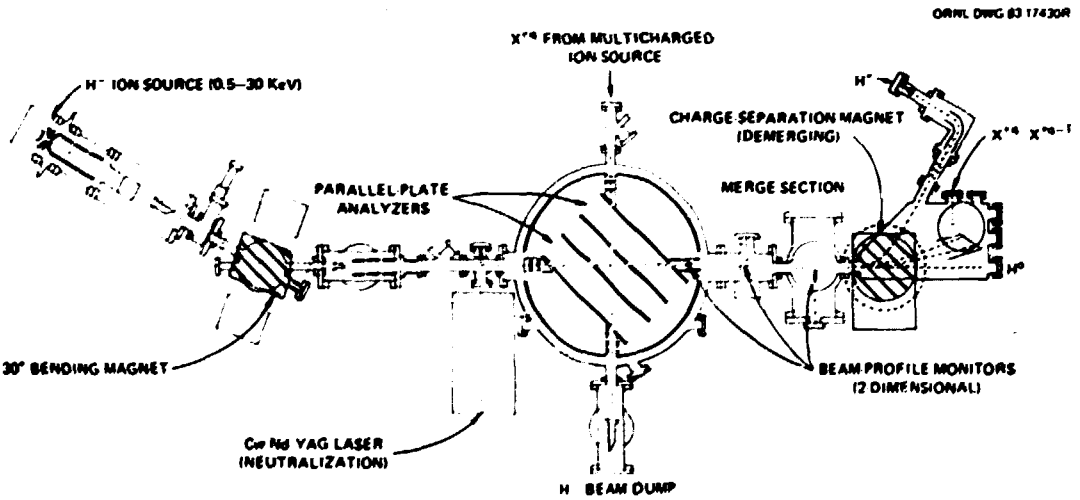

ION-ATOM MERGED-BEAMS EXPERIMENT

Fig. 4.33. Schematic of the ion-atom merged beam apparatus.

photodetachment has been achieved, producing a collimated flux of up to 2×10^{12} neutral H per second. The undetached H^- beam is electrostatically separated from the neutrals and collected in a differentially pumped beam dump. The apparatus has been operated on-line using the ORNL-PIG multicharged ion source, which has produced a highly collimated 200 nA beam of N^{3+} at 30 keV. This N^{3+} beam has been successfully merged with the neutral H beam in the 70 cm ultrahigh vacuum merge path ($P \approx 5 \times 10^{-10}$ torr). A two-dimensional scan of the spatial beam overlap at one position in the merge path, shown in Fig. 4.34, is generated by a commercial rotating-wire beam-profile monitor. Additional scans at different positions along the merged path must be made before the spatial overlap over the entire merged section can be accurately quantified. The ions are then magnetically demerged, separating the H^+ from the N^{3+}, N^{2+}, and the neutrals. Signals in the H^+ detector resulting from the beam-beam interaction have been observed above background by modulating both the N^{3+} and H^0 beams. These beam-beam signals are only about 10 Hz compared to 8 kHz due to the H^0 being stripped on background gas and 1 kHz due to photons emerging from the N^{3+} Faraday cup.

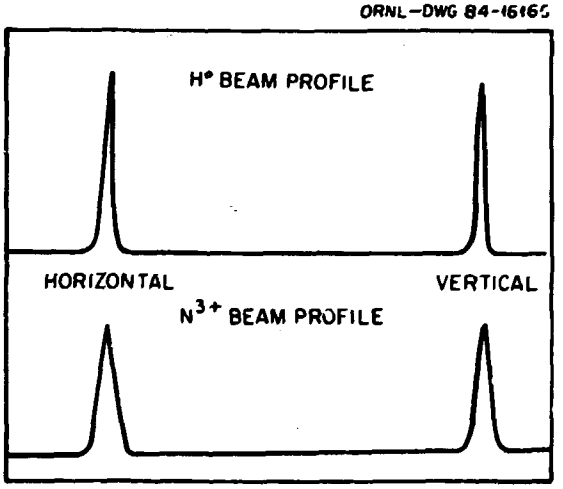

Fig. 4.34. The left and right portions of the upper trace show the respective horizontal and vertical profiles of a 20 nA H^0 beam. The bottom trace shows the profiles of a 120 nA N^{3+} beam and its relative position with the H^0 beam.

Modifications are under way which are expected to significantly improve the signal-to-noise ratio. The gas load from the duoplasmatron ion source will be further decoupled, reducing the pressure in the merge path, and therefore the 8 kHz background signal due to stripping, by at least a factor of two. The H^+ signal beam will be focused and electrostatically deflected out of the plane of magnetic dispersion, assuring detection of all the signal and eliminating the 1 kHz background due to photons produced in the multicharged ion cup. With this decoupling of the H^+ detector from the photon background, only the N^{3+} beam need be chopped to separate the signal from the background, thereby halving the time required to acquire reasonable statistics. Within a few months these modifications will be complete and the apparatus will be ready for more definitive cross-section measurements.

---

1. R. A. Phaneuf et al., Phys. Rev. A 26, 1892 (1982).

ELECTRON-IMPACT IONIZATION OF MULTICHARGED METALLIC IONS: Cu^{2+}, Cu^{3+}, Ni^{3+}, Sb^{3+}

D. C. Gregory A. M. Howald

The present study is part of our continuing effort to provide accurate cross section data for metallic ions of interest in controlled thermonuclear fusion research.

Details of the electron-ion crossed-beams apparatus have been published.[1,2] Ion beams were obtained from the ORNL-PIG multicharged ion source. All measurements are independently absolute, and a typical absolute uncertainty at good confidence level (equivalent to two standard deviations for statistical uncertainties) near the peak cross section is ±8%. Typical relative uncertainties (due mainly to signal counting statistics) are shown in the figures.

The cross section for ionization of Cu^{2+} (Fig. 4.35) is typical of the measurements for Cu and Ni reported here. The data are compared to predictions of the three-parameter Lotz semiempirical formula[3] and distorted-wave calculations.[4] The latter provide a reasonable prediction for the single ionization cross sections for Cu^{2+}, Cu^{3+}, and Ni^{3+}. In each case, the Lotz prediction for total ionization is somewhat higher than the measurement, even taking into account the expected effects of multiple ionization. At high energies, the two calculations converge with the data in each case. In the Cu^{2+} measurements, a significant contribution to the cross section is observed below the ground state ionization threshold due to the presence of metastable ions in the beam. In fact, significantly different metastable contents were observed from day to day, and near-threshold measurements for two ground state/metastable ratios are plotted. In general, for ionization of Cu^{2+}, Cu^{3+}, and Ni^{3+} we conclude that distorted-wave direct ionization calculations give a reasonably accurate representation of single ionization. No large indirect ionization contributions are observed. The three-parameter Lotz formula, although not as reliable as distorted-wave calculations, is observed to be well within its predicted factor-of-two accuracy in each case.

In contrast to the above examples, electron impact ionization of Sb^{3+} has a considerable

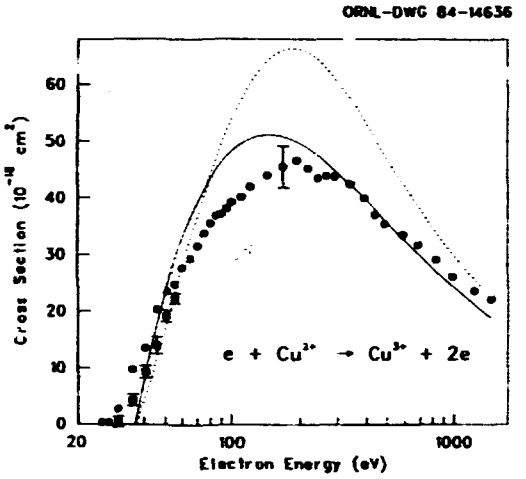

Fig. 4.35. Electron impact ionization of Cu^{2+}. The circles and squares present near-threshold data with ion beams having different metastable ion content. A typical absolute uncertainty at good confidence level is plotted near 200 eV. The theories are from the three-parameter Lotz formula for 3d ionization (dashed curve — ref. 3) and distorted wave calculations of Pindzola et al. (ref. 4).

contribution from indirect effects (Fig. 4.36). The indirect ionization, contributing up to 45×10^{-18} cm^2 to the total cross section, is mainly due to non-dipole-allowed excitation of inner-shell electrons to autoionizing states. The cross section for this type of transition increases abruptly to a maximum at or just above its threshold energy but has a much faster fall-off with increasing energy ($\sigma \propto 1/E$) than does direct ionization ($\sigma \propto \ln E/E$), so that its signature is a "hump" superimposed upon the direct cross section curve. This measurement was undertaken as a check of detailed distorted-wave indirect-ionization calculations which predicted the observed feature.[5] Good agreement is found with the calculations and predictions of that study.

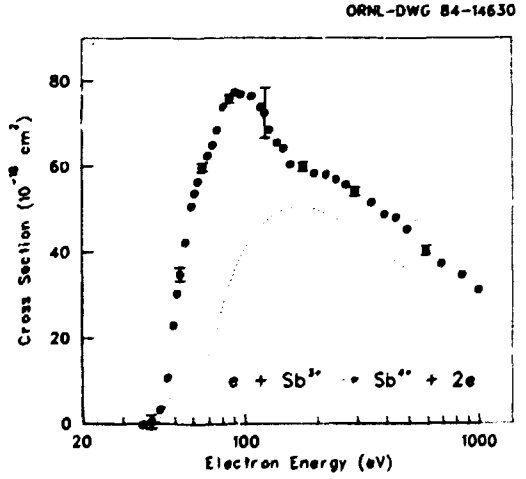

Fig. 4.36. Electron impact ionization of Sb^{3+}. Typical relative uncertainties are plotted, and the absolute uncertainty at good confidence level is shown near 100 eV. The dashed curve is from the Lotz formula for 4d and 5s ionization (ref. 3).

The examples discussed illustrate two goals of our current research efforts: First, selected measurements are made to provide specific data requested by the fusion community for electron-impact ionization of multicharged ions. Second, cooperative studies involving experiment and detailed calculations provide our best means of understanding the relative importances of the many possible mechanisms which can lead to ionization by electron impact.

1. D. H. Crandall, R. A. Phaneuf, and D. C. Gregory, Electron Impact Ionization of Multicharged Ions, ORNL/TM-7020, Oak Ridge Natl. Lab., September 1979.
2. D. C. Gregory et al., Electron Impact Ionization of Multicharged Ions at ORNL, 1980-1984, ORNL/TM-9501, Oak Ridge Natl. Lab., 1985.
3. Wolfgang Lotz, Z. Physik 220, 466 (1969).
4. M. S. Pindzola et al., Survey of Experimental and Theoretical Electron-Impact Ionization Cross Sections for Transition Metal Ions in Low Stages of Ionization, ORNL/TM-9436, Oak Ridge Natl. Lab., 1985.
5. M. S. Pindzola, D. C. Griffin, and C. Bottcher, Phys. Rev. A 27, 2331 (1983).

SINGLE, DOUBLE, AND TRIPLE ELECTRON-IMPACT IONIZATION OF Xe^{6+}

A. M. Howald
D. C. Gregory
D. H. Crandall
R. A. Phaneuf

Electron impact ionization of Xe ions has been studied previously at Oak Ridge National Laboratory from several different perspectives. Experimentally, the ORNL-PIG ion source and electron-ion crossed beams apparatus have been used to study single ionization of Xe ions from Xe^{2+} to Xe^{6+} (Ref. 1), and Sb^{3+} (Ref. 2), which is isoelectronic with Xe^{6+}. The Xe isonuclear sequence and In^+, Sb^{3+}, Xe^{6+} isoelectronic sequence have also been studied theoretically,[1,3] and comparisons made with experiment.

During the past year, electron-impact ionization of Xe^{6+} was studied from yet another point of view. Measurements were made of the cross sections for double and triple ionization of this ion. The processes are

$$e + Xe^{6+} \rightarrow Xe^{8+} + 3e,$$

and

$$e + Xe^{6+} \rightarrow Xe^{9+} + 4e$$

and the cross sections are denoted by σ_{68} and σ_{69}, respectively.

The results of these measurements are shown in Figs. 4.38 and 4.39, with the previously measured cross section[4] for single ionization of Xe^{6+} (denoted by σ_{67}) shown in Fig. 4.37 for comparison. The peak of σ_{67} is roughly an order of magnitude larger than the peak of σ_{68}, which in turn is roughly an order of magnitude larger than the peak of σ_{69}. As expected, the successive ionization thresholds increase along this sequence.

The dashed line in Fig. 4.37 is an estimate of the cross section for direct single ionization of Xe^{6+} from the semiempirical formula of

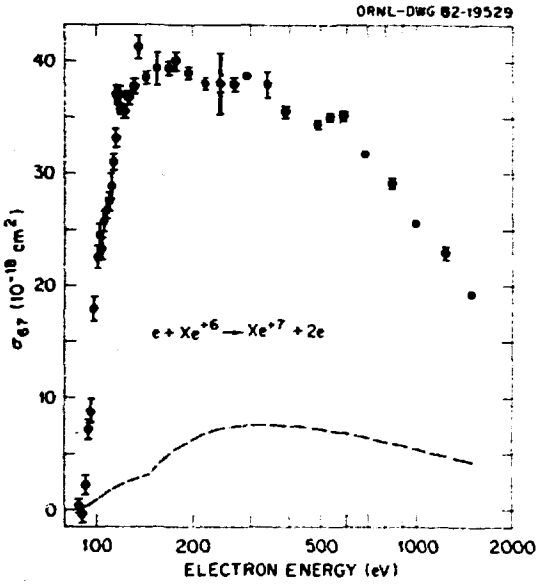

Fig. 4.37. Measured cross section for single ionization of Xe^{6+} by electron impact. The dashed line is the Lotz formula estimate for direct ionization of an outer shell 4s electron.

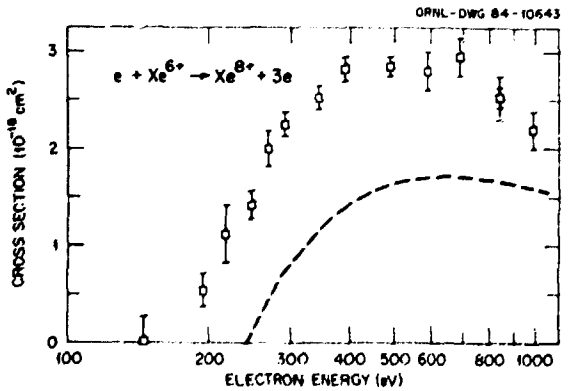

Fig. 4.38. Double ionization of Xe^{6+} by electron impact. The dashed line is the Lotz formula estimate for direct single ionization of an inner shell 4p or 4s electron.

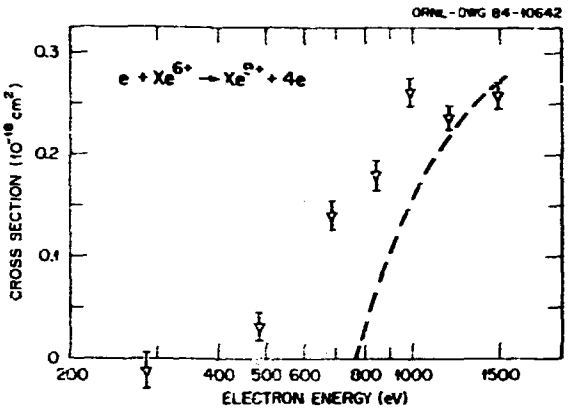

Fig. 4.39. Triple ionization of Xe^{6+} by electron impact. The dashed line is the Lotz formula estimate for direct single ionization of an inner shell 3d electron.

Lotz. The actual cross section is much larger due to ionization by mechanisms other than direct ionization, especially electron-impact excitation of an inner-shell electron followed by autoionization.

Single direct ionization of an inner-shell electron of Xe^{6+} can also lead to production of Xe^{8+} or Xe^{9+} if the Xe^{7+} is produced in a multiply excited autoionizing level. For example, collision of an electron with Xe^{6+} ($4p^6 4d^{10} 5s^2$) can remove an inner-shell 4p electron to form Xe^{7+} ($4p^5 4d^{10} 5s^2$) which can subsequently autoionize to form Xe^{8+} ($4p^6 4d^{10}$). A number of calculated energy levels of various ionization stages of Xe are shown in Fig. 4.40 along with some autoionizing transitions.[5]

In Fig. 4.38 the dashed line is the sum of the Lotz estimates for direct single ionization of Xe^{6+} 4p and 4s electrons. The resulting Xe^{7+} ions are in autoionizing levels. Hence (assuming a branching ratio near unity for autoionization versus radiative stabilization), this gives an estimate of the double ionization cross section due to the process of single direct ionization followed by autoionization. Similarly, the dashed line in Fig. 4.39 is the Lotz estimate for single direct removal of a 3d electron from Xe^{6+}. In this case the resulting excited Xe^{7+} has sufficient potential energy to doubly autoionize to form Xe^{9+}.

The double ionization (Fig. 4.38) cross section calculated for this mechanism is similar in magnitude to the measured cross section (within a factor of 2) but has a threshold value that is higher than the experimentally-observed ionization onset. For triple ionization (Fig. 4.39) the Lotz estimate of the cross section for the mechanism of single direct ionization followed by double autoionization also has the correct magnitude and also has a predicted threshold that is higher than observed.

Other higher-order mechanisms must be responsible for the observed non-zero cross sections below 240 eV and 760 eV in Figs. 4.38 and 4.39,

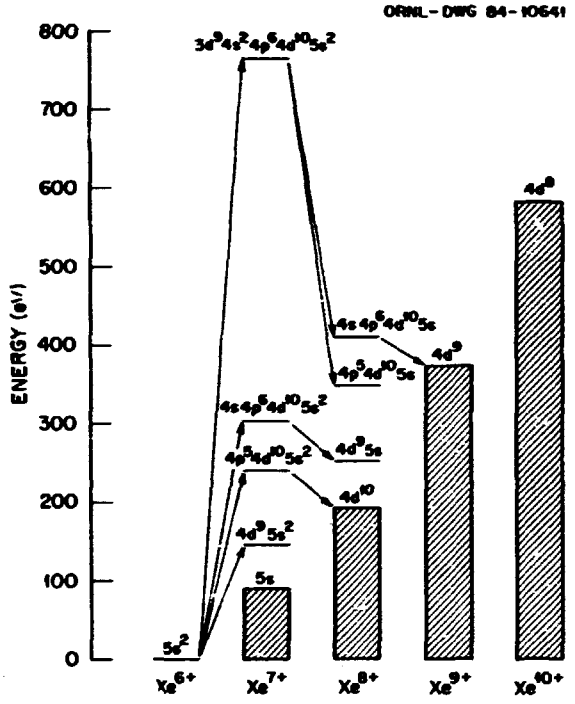

Fig. 4.40. Calculated energy levels (from ref. 5) of Xe ions, showing some electron-impact and autoionizing transitions.

respectively. There are at least four possibilities: direct multiple ionization; electron-impact excitation followed by double or triple autoionization; direct single ionization accompanied by the simultaneous excitation of a second electron; or multiple excitation in a single collision, followed by autoionization. Direct multiple ionization of Xe^{6+} is expected from the classical Binary Encounter Approximation (BEA) model to be of negligible importance. The other three processes have not been studied in detail and are not yet well understood. Our experimental results offer intriguing evidence that one or more of them can play a significant role in electron-impact multiple ionization of multiply charged ions.

1. D. C. Griffin, C. Bottcher, M. S. Pindzola, S. M. Younger, D. C. Gregory, and D. H. Crandall, Phys. Rev. A. 29, 1729 (1984).
2. D. C. Gregory and A. M. Howald (unpublished).
3. M. S. Pindzola, D. C. Griffin, and C. Bottcher, Phys. Rev. A 27, 2331 (1983).
4. D. C. Gregory and D. H. Crandall, Phys. Rev. , 27, 2338 (1983).
5. S. Pindzola, private communication (1984).

NEW ELECTRON-ION CROSSED-BEAMS APPARATUS

D. C. Gregory F. W. Meyer

Since 1977, electron-impact ionization cross section measurements have been completed at ORNL for some 44 different ions with initial charges ranging from +2 through +6 and spanning the periodic table from boron to tantalum.[1,2] These total cross section measurements for single, double, and triple ionization have all utilized the ORNL-PIG ion source and crossed ion-electron beams apparatus.[3,4] With the completion of the new ORNL-ECR ion source, our capabilities for producing multicharged ion beams now extend to considerably higher ionization stages. Since some aspects of the existing apparatus are inadequate for operation with more highly charged ions, the experiment has been redesigned.

Electrostatic separation of ion beams by charge state is difficult to achieve. In a crossed-beams ionization experiment, as little as 1 part in 10^8 cross-talk between exit channels produces an intolerable background level, and separation becomes progressively more difficult as the charge increases and the initial-to-final charge ratio approaches unity. In addition, low-noise electrostatic analyzers must usually be mechanically modified for each charge ratio under study. To overcome both of these difficulties, a magnetic spectrometer is being constructed for product charge-state analysis.

The modified apparatus is shown in Fig. 4.41. The ion-beam optics and ultra-high vacuum system will remain much the same as in the present arrangement through the interaction volume in the center of the electron gun. The combined beam containing the primary ions and further-ionized signal ions then enters a double-focusing analyzing magnet which disperses the beam components by charge state. Signal ions are deflected through 90° and focussed into a channel electron multiplier. The ion optics are designed such that the crossed-beams interaction region is imaged onto the signal detector with unit magnification. The primary ion beam is trapped in one of two movable, guarded Faraday cups, depending on the initial-to-final charge ratio for that particular experiment. Deflection plates and einzel lenses are provided as diagnostic tools both in the main interaction chamber and immediately before the signal ion detector.

The apparatus is designed to allow measurements ranging from initial-to-final charge state ratios of 4/5 to 15/16. Initial tests of the completed apparatus are planned for early 1985. The next phase in the development of the crossed-beams apparatus will involve redesign or replacement of the existing magnetically-confined electron gun to extend the available range for reliable measurements to electron energies greater than 1.5 keV.

1. D. H. Crandall, R. A. Phaneuf, and D. C. Gregory, Electron Impact Ionization of Multicharged Ions, ORNL/TM-7020, Oak Ridge Natl. Lab., September 1979.

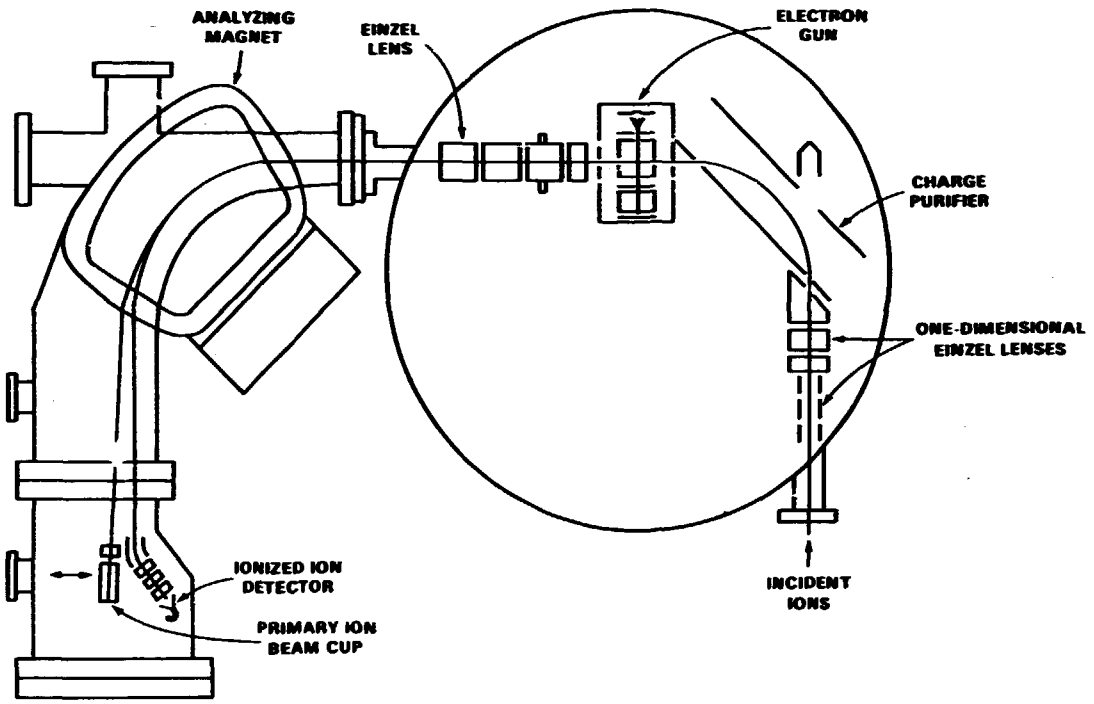

Fig. 4.41. New electron-ion crossed beams apparatus with post-collision charge-analyzer magnet. Measurements will include single and multiple ionization of a wide range of highly ionized ($6 < q < 15$) target ions.

2. D. C. Gregory et al., Electron Impact Ionization of Multicharged Ions at ORNL, 1980-1984, ORNL/TM-9501, Oak Ridge Natl. Lab., 1985.

3. D. C. Gregory, P. F. Dittner, and D. H. Crandall, Phys. Rev. A. 27, 724 (1983); D. H. Crandall et al., Phys. Rev. A. 25, 143 (1982).

4 P. O. Taylor et al., Rev. Sci. Instrum. 45, 588 (1975).

RADIOMETRIC STANDARD FOR THE EXTREME ULTRAVIOLET

P. M. Griffin C. C. Havener
J. W. Johnson

A light source utilizing bremsstrahlung and transition radiation[1,2] generated by keV electron impact on metals is being investigated. This low power, compact, simple lamp has potential as a secondary-standard radiometric source for the soft x-ray (SXR) and extreme ultraviolet (EUV) spectral region. Its spectral radiance is being characterized by a few easily measurable and controllable electrical, mechanical, and chemical parameters.

The essential elements of the lamp are the straight edge of a 0.12-mm-thick, ohmically heated, tungsten cathode and a flat metal anode. A well-defined thin sheath of keV electrons is electrostatically drawn from the hot edge of the cathode located ~0.18 mm from and perpendicular to the anode target. At the intersection of the flat sheath of impinging electrons and the flat anode, a 6-mm-long, narrow, luminous line is generated.

An example of spectrometric measurements of radiation generated by the prototype source is shown in Fig. 4.42. It should be noted that at each spectrometer setting corresponding to a given value of $m\lambda$, several discrete portions of the output spectrum are simultaneously sampled. The emissions from wavelength intervals $(\Delta m\lambda/n)$ Å wide, centered at wavelengths $(m\lambda/n)$ Å, contribute to the measured signal at that setting. Relatively high spectral order-numbers n must be considered since, for high Z metals, bremsstrahlung and transition radiation intensities vary as λ^{-3} and λ^{-2} respectively. The number of spectral orders observed is limited by the product of the short wavelength cutoffs of the grating and detector efficiencies. The undulations in the data in Fig. 4.42 are accounted for in terms of the dropping-out rate of the highest integral spectral orders in proceeding to smaller values of $m\lambda$.

As this source is operated, bremsstrahlung, generated as the penetrating electrons are decelerated or deflected below the surface of the target, is the principle light emitting

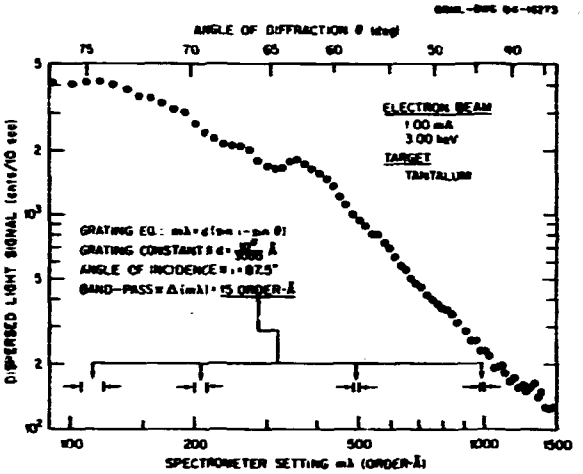

Fig. 4.42. Spectrometric measurement of the SXR and EUV light generated by 1.00 mA of 3.00 keV electrons incident on a tantalum target in the prototype radiometric source. Data are from a step-wise scan with a 2.2 meter, grazing-incidence spectrometer. The dispersed light was detected with a ZnO-TiO_2 ceramic channel-electron-multiplier. The spectrometer entrance slit subtended a 0.005 steradian solid angle at the source.

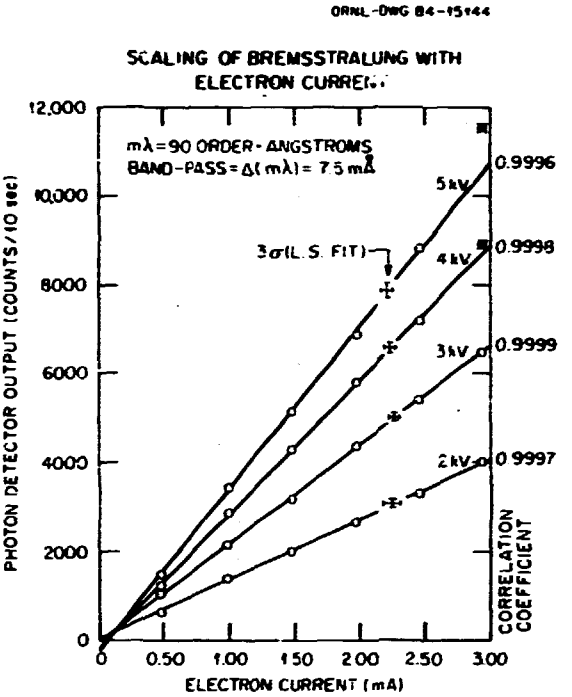

Fig. 4.43. Dependence of bremsstrahlung signal strength on electron beam current for accelerating voltages of 2.00, 3.00, 4.00, and 5.00 kV. The least-squares fits of the signals with current had standard deviations of 32, 31, 49, and 61 counts/10 sec, respectively. The highest current measurements at 4.00 and 5.00 kV were excluded in the fits since their deviations were greater than the 3σ error-bars which are shown for each line.

mechanism for the continuum shortward of ~450 Å. Of particular interest is the lamp's scalable emission in the overlapping SXR and EUV spectral regions as displayed in Fig. 4.43. The aforementioned spectrometer was set to simultaneously sample the emissions from 7.5, 3.8, and 2.5 Å intervals in the continuum observed at 90, 45, and 30 Å, respectively. As expected according to the theory of bremsstrahlung, the combined signals scale with electron current at four representative electron energies. The utility of this lamp as a practical standard is indicated in that statistically acceptable data were obtained with only 10 sec integration times and electron beam powers of only 2 to 15 watts.

At wavelengths longer than ~450 Å, transition radiation should be the dominant light-emitting mechanism in the lamp. Phenomenologically, this radiation is a consequence of the collapse of the dipole field, produced by the approaching electron and its positive image charge in the metallic target, as the electron "transits" through the vacuum-target interface. The Fourier transform of the resulting electromagnetic pulse is a "white" frequency spectrum. The optical constants of whatever material exists at the surface characterize this radiation, rather than the bulk properties of the target. A reproducible surface is self-maintained if the source is operated at an adequate electron-beam areal power-density.

Investigations of the transition radiation component of the lamp's emission have been hampered by the overlapping of high spectral orders of shorter wavelength bremsstrahlung. Solutions to this problem are being sought through the use of combinations of thin metal-foil spectral filters which effect appropriate transmission "windows."

An improved model of the source and vacuum system have been designed and built which should permit operation at electron energies greater than 10 keV. This will permit generation of transition radiation of much longer wavelength. In addition, with the resulting greater electron penetration depths, the bremsstrahlung will be completely absorbed before it can emerge from within the target to proceed to the spectrometer. This technique will permit, where applicable, less complicated procedures for studies of the transition radiation component of the lamp's emissions.

---

1. W. Ginzburg and I. Frank, J. Phys. (USSR) 9, 363 (1945).

2. H. Boersch and G. Sauerbrey, Proceedings of the International Colloquium on Optical Properties and Electronic Structure of Metals and Alloys, F. Abelès, editor, North-Holland Publishing Co., Amsterdam (1966).

5. THEORETICAL NUCLEAR PHYSICS

INTRODUCTION AND OVERVIEW

The theoretical physics program in the Physics Division at ORNL involves research in both nuclear and atomic physics. These programs benefit from interactions with the various experimental programs in the Division, and from access to good computing facilities as discussed briefly below and in the section on HIRF facilities.

In nuclear physics there is extensive activity in the fields of direct nuclear reactions with light- and heavy-ion projectiles, the structure of nuclei far from stability and at elevated temperatures, and the microscopic and macroscopic description of heavy-ion dynamics, including the behavior of nuclear molecules and "super-nuclei." New research efforts in relativistic nuclear collisions and in the study of quark-gluon plasma have continued to grow this year.

The atomic theory program deals with a variety of ionization, multiple-vacancy production, and charge-exchange processes. Many of the problems are selected because of their relevance to the magnetic fusion energy program. In addition, there is a joint atomic-nuclear theory effort to study positron production during the collision of two high-Z numbers, i.e., U+U.

As this report is prepared, the theory program in the Physics Division is being significantly expanded. A new Distinguished Scientist program, sponsored jointly by the University of Tennessee and ORNL, has been initiated. Among the first appointments is G. F. Bertsch in theoretical physics. As a result of this appointment, Bertsch and an associated group of four theorists split their time between UT and ORNL. In addition, the State of Tennessee has established a significant budget to support the visits of outstanding scientists to the Joint Institute for Heavy Ion Research at ORNL. This budget should permit a significant improvement in the visitor program at ORNL. Finally, the Laboratory awarded a Wigner post-doctoral appointment to a theorist who will work in the theory group of the Physics Division. This significant expansion in the theory effort should be a stimulus to both the theory and experimental programs in the Physics Division.

The VAX-780/FPS-164 computer system has been in use for the whole report period. Our experience continues to be that the FPS-164 performs at a rate comparable or superior to a contemporary main frame computer such as the IBM-3033 or a DCD-7600 for the large, numerically intensive scientific calculations common to theoretical physics.

HEAVY-ION DYNAMICS

FOLDING-MODEL ANALYSIS OF ELASTIC AND INELASTIC α-PARTICLE SCATTERING USING A DENSITY-DEPENDENT FORCE[1]

A. M. Kobos[2] R. Lindsay[4]
B. A. Brown[3] G. R. Satchler

A folding model with a density-dependent form of the semi-realistic M3Y effective interaction was applied to α-particle scattering. A previous analysis of elastic scattering at 140 and 172 MeV was applied to data at other energies from 25 to 120 MeV. The model was also extended to inelastic scattering, using both the collective model and a valence-plus-core-polarization model for the transition densities. The proton transition densities were normalized to measured B(EL) values. When necessary, the neutron transition densities were rescaled to fit the (α,α') data, providing a source of information on the neutron contributions. The neutron transition multipole moments thus obtained were compared to those derived from (p,p') data at 800 MeV, as well as from other sources.

---

1. Abstract of paper: Nucl. Phys. A425, 205 (1984).
2. Oxford University, Oxford, England.
3. Michigan State University, East Lansing, Michigan.
4. SERC Daresbury Laboratory, Daresbury, Warrington, England.

POTENTIAL MODELS AND RESONANCES IN THE $^{16}O+^{28}Si$ SYSTEM[1]

A. M. Kobos[2] G. R. Satchler

Two recent papers have given optical potential descriptions for the elastic scattering of the $^{16}O+^{28}Si$ system at energies near the Coulomb barrier, both of which manifest partial-wave resonances. Our comment was that there is at least one other potential that reproduces the measurements but which does not result in such resonances.

---

1. Abstract of paper: Phys. Rev. C 30, 403 (1984).
2. Oxford University, Oxford, England.

A GLOBAL OPTICAL POTENTIAL ANALYSIS OF $^{16}O+^{28}Si$ ELASTIC SCATTERING[1]

A. M. Kobos[2] G. R. Satchler

The differential cross sections for $^{16}O+^{28}Si$ elastic scattering at many energies between 18 and 35 MeV in the center of mass are described very well over the whole angular range up to 180° by two optical potentials. One describes the data at twelve energies between 18 and 29 MeV and another one at two energies, 31.6 and 34.8 MeV. The two potentials differ in parameter values, but in both cases the real part consists of a folded potential supplemented in the surface with a double-peaked and energy-independent attractive correction which is parametrized as the derivatives of two Woods-Saxon form factors. The imaginary potential is a sum of Woods-Saxon volume and surface terms, and its radius increases linearly with energy. The excitation function for elastic scattering at 180° is also reproduced well up to about 32 MeV. The S-matrix elements generated by these potentials do not show any resonance features. The qualitative features of the scattering are discussed, especially in terms of the decomposition of the scattering amplitude into inner-wave and barrier-wave components.

---

1. Abstract of paper: Nucl. Phys. A427, 589 (1984).
2. Oxford University, Oxford, England.

ONE EFFECT OF USING RELATIVISTIC KINEMATICS IN THE ANALYSIS OF HEAVY-ION ELASTIC SCATTERING[1]

M. El-Azab Farid[2] G. R. Satchler

The ion-ion potential deduced from an optical model analysis of heavy-ion elastic scattering may be sensitive to whether the transformation from laboratory to center-of-mass system used is relativistic or not. For illustration, a semiclassical description is used to give a simple estimate of this effect and its dependence on energy and the masses of the nuclei. For example, the change in potential strength is larger than 20% for ^{40}Ar scattering from ^{208}Pb at an energy as low as 44 MeV per nucleon.

---

1. Abstract of paper: Physics Letters B (in press).
2. Guest assignee from Department of Physics, Faculty of Science, Assiut University, Assiut, Egypt, 8/1/83-8/1/84.

SOME OPTICAL-MODEL ANALYSES OF THE ELASTIC SCATTERING OF ^{40}Ar AT 1760 MeV[1]

M. El-Azab Farid[2] G. R. Satchler

The elastic scattering cross sections for ^{40}Ar on ^{60}Ni, ^{120}Sn, and ^{208}Pb at 1760 MeV were reanalyzed using both Woods-Saxon and folding model potentials. The latter required renormalizing by factors $N < 0.7$. This provides further evidence that the real potentials at this energy are substantially weaker than those obtained for other systems at lower energies. This was confirmed by comparison with data for $^{40}Ar + ^{208}Pb$ at 236 MeV. The 1760-MeV data appear to determine the values of both real and imaginary potentials in the vicinity of a strong absorption region, nearly one fermi inside the rainbow radius.

---

1. Abstract of paper to be submitted to Nuclear Physics A.
2. Guest assignee from Department of Physics, Faculty of Science, Assiut University, Assiut, Egypt, 8/1/83-8/1/84.

FOLDING-MODEL POTENTIALS FOR HEAVY-ION SCATTERING USING A SEMIREALISTIC DENSITY-DEPENDENT FORCE

M. El-Azab Farid[1] G. R. Satchler

The real part of the optical potential for heavy-ion scattering was calculated in a folding model using a density- and energy-dependent generalization, called DDM3Y, of the M3Y effective interaction. The interaction strength and density-dependence were calibrated against a realistic G-matrix. The resulting potentials must be reduced by factors $N \sim 0.8$ in order to fit 'low'-energy scattering data (~5 to 15 MeV per nucleon). High energy (44 MeV per nucleon) ^{40}Ar data required somewhat more reduction, $N = 0.65$, indicating that the energy dependence incorporated into the DDM3Y is insufficient. Further, the same DDM3Y interaction had been shown previously[2] to give a good account of α-particle scattering over the same range of energies per nucleon with a constant renormalization factor of $N = 1.3$. Consequently, the DDM3Y cannot simultaneously represent heavy-ion and α-particle scattering within the usual folding model.

1. Guest assignee from Department of Physics, Faculty of Science, Assiut University, Assiut, Egypt, 8/1/83-8/1/84.
2. A. M. Kobos et al., Nucl. Phys. A425, 205 (1984).

EFFECTS OF POTENTIAL VARIATIONS ON ONE-DIMENSIONAL BARRIER PENETRATION AND FUSION CROSS SECTIONS BELOW THE COULOMB BARRIER

M. M. Shalaby[1] G. R. Satchler

It is known[2] that coupling to non-elastic channels has very important effects on the fusion cross sections $\sigma_{fus}(E)$, below the Coulomb barrier, calculated using the simple one-channel potential barrier-penetration model. However, as a preliminary to such calculations, it is also of interest to know what effects result from the ambiguities in the one-channel potential itself. Measured fusion cross sections near the barrier determine the position, height, and curvature of the barrier, and hence its outer face, in a relatively unambiguous way, but leave uncertain the inner face and thus the shape of the potential at smaller radii. We explored a range of attractive nuclear potentials, from shallow (19 MeV) to very deep (8000 MeV), which gave the same barrier position, height, and curvature. There was very little effect on $\sigma_{fus}(E)$ until the attractive potential became so weak that the total potential exhibited only a shallow 'pocket' inside the barrier. This led to oscillations in $\sigma_{fus}(E)$, which could be associated with quasi-bound states in the pocket, but which are not like the effects seen experimentally in systems like Ni + Ni.

More important is the presence of a weak 'tail' of the absorptive potential under the barrier. The usual model assumes that absorption by direct (surface) reactions is taken into account explicitly by the coupled channels, while the fusion, or compound nucleus formation, is represented by a short-ranged absorption inside the barrier region. In practice, such a clear-cut division is unlikely, and we can expect some residual absorption under the barrier itself; i.e., the barrier becomes complex. Our calculations show that a relatively small imaginary part can produce dramatic changes. Figure 5.1 shows an example for $^{32}S + ^{26}Mg$ using the same potential as Ref. 2 but with a Woods-Saxon form for the imaginary part and its diffuseness increased to 0.635 fm. This results in an imaginary potential of -79 keV at 9.2 fm, the position of the barrier peak, which itself is 28 MeV high. The σ_{fus} at E_{cm} = 24 MeV is increased by a factor of 75. However, the shape of the $\sigma_{fus}(E)$ curve seen in this figure is not like that seen experimentally, so possibly the behavior of $\sigma_{fus}(E)$ observed at very low energies can be used to put limits on the amount of absorption that is present under the barrier.

1. Guest assignee from Faculty of Science, Ain Shams University, Cairo, Egypt, 6/83-12/83.

2. See, for example, M. Rhoades-Brown and P. Braun-Munzinger, Phys. Lett. 136B, 19 (1984).

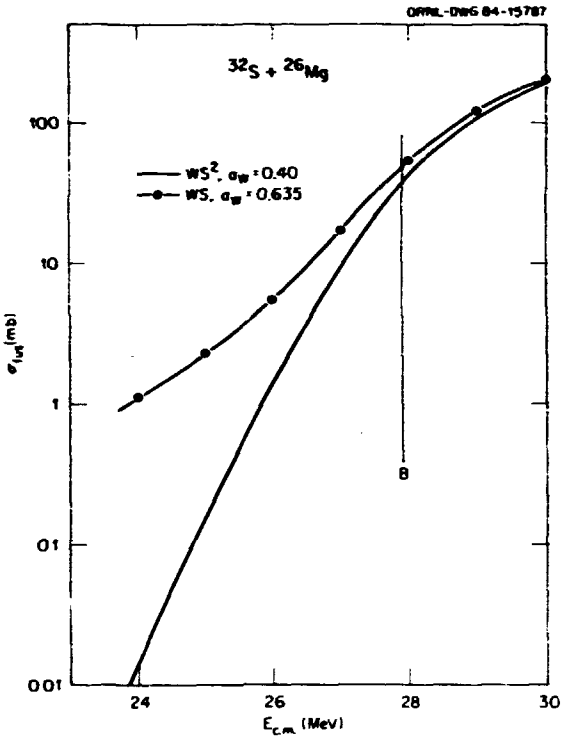

Fig. 5.1. Fusion cross section $\sigma_{fus}(E)$ versus center-of-mass energy. The solid curve was calculated using the optical potential from Ref. 2, in which the imaginary part was the square of a Woods-Saxon form, with diffuseness a_W = 0.4 fm. The broken curve used a similar potential except that the imaginary part had the Woods-Saxon form with a_W = 0.635 fm. The height of the Coulomb barrier is indicated by B. The two curves coincide for energies above 33 MeV.

COUPLED ELASTIC AND INELASTIC SCATTERING OF $^{16}O + ^{28}Si$ NEAR THE COULOMB BARRIER, WITH A WEAKLY ABSORBING OPTICAL POTENTIAL

M. M. Shalaby[1] G. R. Satchler

The effects of using a weakly absorbing optical potential on the elastic and inelastic scattering of $^{16}O + ^{28}Si$ near the Coulomb barrier were explored using both the DWBA and the full coupled-channels treatment. Strong coupling effects are important. A fit to the inelastic data at E_{cm} = 21.1 MeV appears to require a nuclear deformation length that is appreciably smaller than the Coulomb one.

1. Guest assignee from Faculty of Science, Ain Shams University, Cairo, Egypt, 6/83-12/83.

A DISPERSION RELATION AND THE ENERGY DEPENDENCE OF THE HEAVY-ION OPTICAL POTENTIAL

C. Mahaux[1] G. R. Satchler

The optical potential $U(E) = V(E) + iW(E)$ for the elastic scattering of two systems is, in general, complex and dependent on the energy E. Reaction theories imply a very general dispersion relation between the real and imaginary parts of the form

$$V(E) = V_0 - \frac{1}{\pi} P \int \frac{W(E')}{E-E'} dE', \qquad (1)$$

where P denotes the principal value and V_0 is independent of E. Consequently, if W(E) varies rapidly with E in some region, this equation implies that a corresponding rapid variation of V(E) should be observed in the same region of E. Empirically, W(E) for heavy ions appears to depend only weakly upon E for energies substantially above the Coulomb barrier. However, the magnitude of W(E) should decrease rapidly as the barrier is approached because the number of effectively open nonelastic channels is reduced drastically. This should be reflected in a corresponding change in V(E). Remembering that both V and W are attractive (negative), we see from Eq. (1) that V(E) should become more attractive as the Coulomb barrier is approached.

Such an effect has been observed at low energies for nucleon scattering, and interpreted[2] using Eq. (1). A similar behavior has now been seen[3] for $^{16}O + ^{208}Pb$ and possibly[4] for ^{16}O + Ni. A quantitative application of the dispersion relation (1) to these heavy-ion cases is underway.

Physically, $\Delta V(E) = V(E) - V_0$ arises from couplings to the nonelastic channels. If the dispersion relation can be used to reliably extrapolate V(E) to lower energies, the important coupled-channels effects on sub-barrier heavy-ion fusion can be re-expressed in terms of the one-dimensional barrier penetration model. This is being explored.

---

1. Consultant from Université de Liège, Liège, Belgium.
2. C. Mahaux and H. Ngô, Nucl. Phys. A378, 205 (1982).
3. J. S. Lilley et al., Physics Letters, to be published.
4. G. R. Satchler, Phys. Lett. 58B, 408 (1975).

PATH INTEGRAL APPROACH TO MULTIDIMENSIONAL QUANTUM TUNNELING AND SUB-BARRIER FUSION

A. B. Balantekin[1] N. Takigawa[2]

Recently, path integral approach to the coupled channel problem was formulated, transmission probabilities were worked out for some simple cases, and the properties of the dissipation factor were studied in the adiabatic limit.[3] We are now in the process of extending this work to include the effects of finite temperatures in the tunnelling process. In this context, calculations are being performed on temperature-dependent influence functionals for the three simple cases studied earlier, harmonic oscillators linearly or quadratically coupled to the translational motion and a system with a finite number of equidistant energy levels linearly coupled to the translational motion. Also, a simple many-body model to study microscopic effects is being developed.

---

1. Eugene P. Wigner Fellow.
2. Tohoku University, Sendai, Japan.
3. A. B. Balantekin and N. Takigawa, Annals of Physics (in press).

EFFECT OF DISSIPATION ON THE EIGENSOLUTIONS NEAR THE FISSION SADDLE POINT[1]

K. T. R. Davies J. R. Nix[2]
A. J. Sierk[2]

Two equivalent methods have been developed for solving the problem of small oscillations near equilibrium when dissipative forces are included in the dynamical equations of motion. One method relies on the Lagrangian formulation of the equations of motion, and the other method relies on the Hamiltonian formulation. The eigenvalues are, in general, complex, but for unstable or overdamped motion they are purely real. We have used the Lagrangian formulation to calculate the two lowest symmetric eigensolutions at the fission saddle point for nuclei with Z^2/A ranging from 18.0 to 44.6 for ordinary two-body viscosity, one-body wall-formula dissipation, and one-body wall-and-window dissipation. We find that two-body viscosity leads to relatively small changes in the directions of the eigenvectors, whereas one-body dissipation can lead to major changes in the directions of the eigenvectors. Also, with increasing dissipation, the fission eigenvalue λ_2 decreases in magnitude, and the stretching eigenvalue λ_4 changes from imaginary through complex to real and negative.

---

1. Summary of paper: Phys. Rev. C 28, 1181 (1983).
2. Los Alamos National Laboratory, Los Alamos, NM 87545.

STUDIES OF CONDITIONAL SADDLE POINT CONFIGURATIONS[1]

K. T. R. Davies A. J. Sierk[2]

We have developed a general method for determining an extremum on a potential energy surface subject to an arbitrary number of constraints. The basic equations are formulated using

Lagrange multipliers, and the extremum is obtained by iterating using a vector version of Newton's method. We then specialize the problem to a single constraint which can be, e.g., a multipole moment of the nuclear shape or a parameter specifying the mass asymmetry of the system. All of our calculations have been done for the constraint of mass asymmetry which might typically represent the initial value of mass asymmetry of a particular heavy-ion reaction. Such calculations then give the conditional saddle points which are thought to enable one to distinguish theoretically fast fission processes from true compound nucleus formation.[3-5] The advantage of the present method is that the conditional saddle points can be calculated when the mass asymmetry function is an arbitrary function of the generalized coordinates. This should be contrasted with other studies[3-6] in which the mass asymmetry variable is one of the chosen generalized coordinates, in which case the conditional saddle points can be determined by simply fixing the asymmetry coordinate.

Our results have been obtained mainly with the liquid-drop model[7] surface energy. A study comparing the results using the liquid-drop model with those of the Yukawa-plus-exponential nuclear energy[8,3] shows that, for the latter, one obtains a larger neck for a given mass asymmetry. However, the main conclusions of our work do not depend on the type of macroscopic energy considered. In order to describe the nuclear shape which is assumed to be axially symmetric, we use two different parametrizations: (i) a model consisting of smoothly joined portions of three quadratic surfaces of revolution,[10] and (ii) a Legendre polynomial expansion of the nuclear surface function.[11]

In Fig. 5.2 we display various saddle points on σ-r plots where σ and r represent respectively necking and separation degrees of freedom. By comparing the upper and lower parts of the figure, we see that, for a given fissility x, as we increase the mass asymmetry α, the moments of the system effectively behave like those of lighter nuclei. This occurs because, in a heavy-ion reaction appropriate to a given mass asymmetry, the effective entrance-channel Coulomb repulsion is proportional to $Z_1 \cdot Z_2$, where Z_1 and Z_2 are the projectile and target charges. Then, for a fixed total charge of the system, as α increases $Z_1 \cdot Z_2$ decreases, giving rise to a less repulsive system.

In Fig. 5.3 we display the conditional saddle point energy as a function of mass asymmetry α, for various values of the fissility x. The behavior of the energy depends upon whether the fissility is above or below the Businaro-Gallone point,[12] $x_{BG} = .396$. For $x < x_{BG}$ the energy always decreases monotonically with increasing α. On the other hand, for $x > x_{BG}$, as α increases, the energy first increases until it reaches a maximum corresponding to the Businaro-Gallone peaks, after which it decreases. In the neighborhood of $x = x_{BG}$, the saddle point energy with respect to α is very flat due to the coalescence at α = 0 of the Bohr-Wheeler mass symmetric saddle family with the Businaro-Gallone mass asymmetric saddle family. For α = 0 the conditional saddle point is always the Bohr-Wheeler saddle, while for α approaching 1 it corresponds to a single large sphere attached to an infinitesimally small sphere.

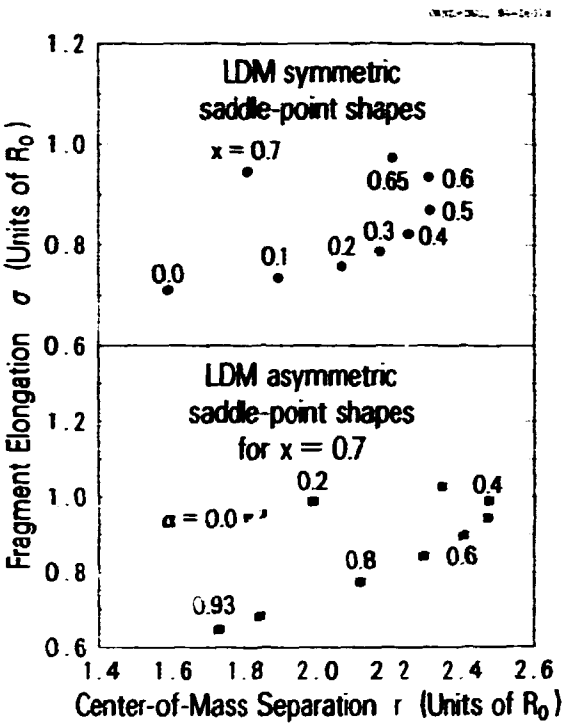

Fig. 5.2. Locations in σ-r space of the saddle points of liquid-drop nuclei. The upper portion of the figure shows the positions of the Bohr-Wheeler family of symmetric saddle points for selected values of the fissility parameter x. The lower portion shows the conditional saddle points as a function of constrained mass asymmetry α for x = 0.7; the α values are in increments of 0.1, except for the largest value (α = 0.93).

---

1. Summary of paper to be submitted to Physical Review.
2. Los Alamos National Laboratory, Los Alamos, NM 87545.
3. W. J. Swiatecki, Phys. Scr. 24, 113 (1981).
4. W. J. Swiatecki, Nucl. Phys. A376, 275 (1982).
5. S. Bjørnholm and W. J. Swiatecki, Nucl. Phys. A391, 471 (1982).
6. H. Feldmeier, p. 26 in Proceedings of the International Workshop X on Gross Properties of Nuclei and Nuclear Excitations, Hirschegg, Austria, 1982, ed. by H. Feldmeier, Technische Hochschule, Darmstadt, Report No. ISSN-0720-8715, 1982.
7. W. D. Myers and W. J. Swiatecki, Ark. Phys. 36, 343 (1967).

8. H. J. Krappe, J. R. Nix, and A. J. Sierk, Phys. Rev. Lett. 42, 215 (1979).
9. H. J. Krappe, J. R. Nix, and A. J. Sierk, Phys. Rev. C 20, 992 (1979).
10. J. R. Nix, Nucl. Phys. A130, 241 (1969).
11. S. Trentalange, S. E. Koonin, and A. J. Sierk, Phys. Rev. C 22, 1159 (1980).
12. U. L. Businaro and S. Gallone, Nuovo Cim. 1, 629 (1955); U. L. Businaro and S. Gallone, Nuovo Cim. 1, 1277 (1955).

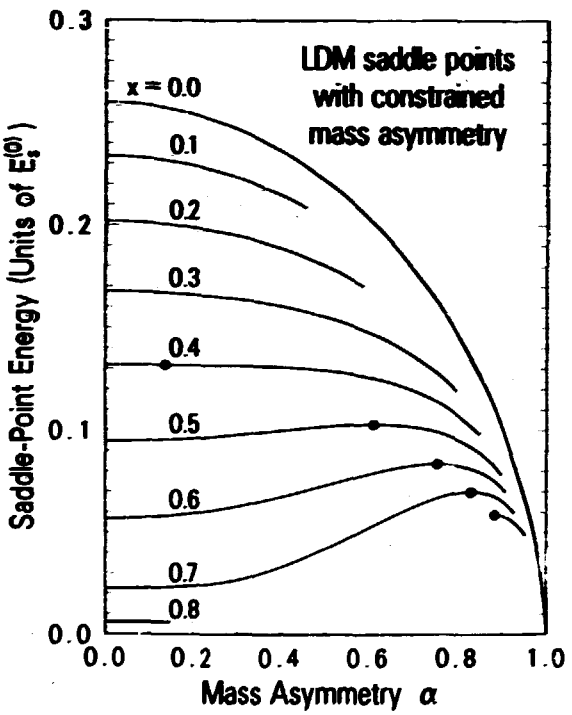

Fig. 5.3. Saddle-point energies as a function of constrained mass asymmetry α for various values of the liquid-drop model fissility parameter x. The solid points correspond to the Businaro-Gallone family of asymmetric saddle-point shapes with two unstable degrees of freedom. The solid lines terminate to the right at shapes with very small neck radii, beyond which we cannot calculate. The curve for x = 0.8 is not drawn where no constrained saddle point exists.

MACROSCOPIC AND MICROSCOPIC FUSION STUDIES OF THE $^{208}Pb+^{58}Fe$ REACTION

J. R. Nix[1] M. R. Strayer
A. J. Sierk[1] A. K. Dhar[2]
K. T. R. Davies A. C. Merchant[3]

Macroscopic[4] and microscopic calculations are being done for the reaction $^{208}Pb + ^{58}Fe$ at five bombarding energies corresponding to cases which have been studied experimentally.[5] In the macroscopic studies we examine the dependence upon angular momentum L of the mass transfer ΔA_{Fe} to the lighter ^{58}Fe nucleus from the heavier ^{208}Pb nucleus. Figure 5.4 displays ΔA_{Fe} vs. L for the five energies considered, using two-body viscosity[6] as the dissipation mechanism. This figure shows that, for a given bombarding energy, the mass transfer is zero for angular momenta larger than a critical value at which the nuclei first come into contact, at which point it jumps discontinuously in our calculations to a nonzero value. The mass transfer then increases with decreasing angular momenta until values corresponding to a mass-symmetric nuclear system are reached, below which some oscillations occur.

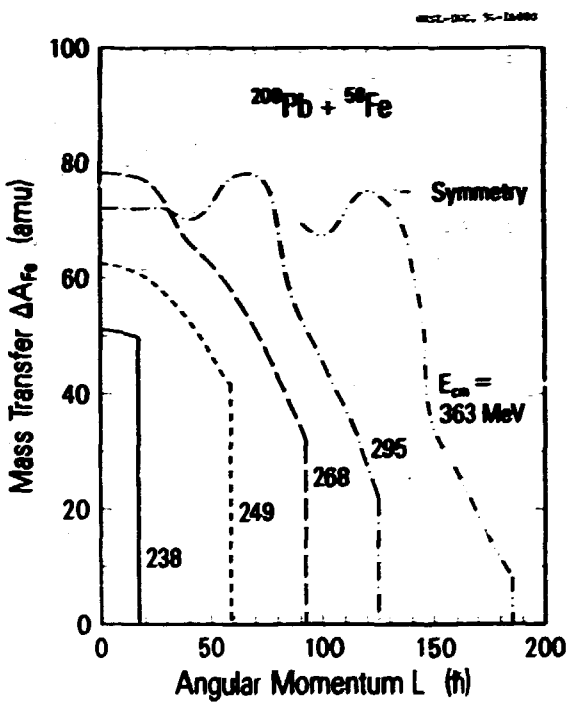

Fig. 5.4. Mass transfer ΔA_{Fe} vs. angular momentum L for the reaction $^{208}Pb + ^{58}Fe$. The calculations were done using two-body viscosity with viscosity coefficient μ = 0.02 TP.

In calculating the theoretical macroscopic capture cross section, we include all L values corresponding to mass transfers greater than 40 amu, and the results are displayed in Fig. 5.5. The error bars on the experimental points reflect the differences between two experimental procedures for calculating the cross section (one of which is identical to the theoretical method). Other than the lowest bombarding energy, our calculated curve for two-body viscosity lies substantially above the experimental points, with the deviation increasing to almost a factor of 2 at the highest bombarding energy.

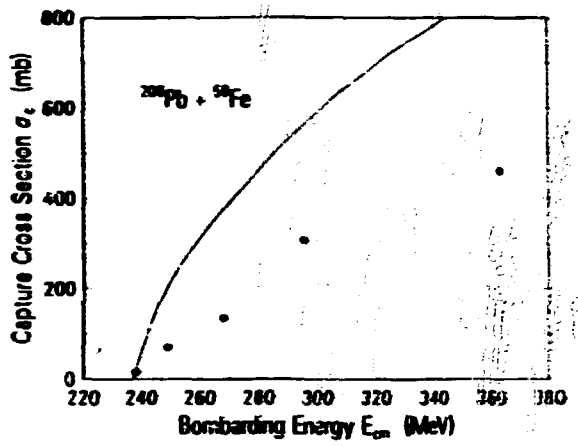

Fig. 5.5. Comparison of the experimental capture cross section with the theoretical results calculated for two-body viscosity, with viscosity coefficient μ = 0.02 TP. The full curve smoothly joins the theoretical points, while the full circles with error bars are the experimental results.

We regard this important discrepancy as experimentally demonstrating that two-body viscosity is *not* the complete dissipation mechanism in large-amplitude collective nuclear motion. Additional calculations are being done using one-body viscosity, taking into account the dissipation associated with a time rate of change of the mass asymmetry degree of freedom in the completed wall-and-window formula.[7]

Some preliminary time-dependent Hartree-Fock (TDHF) calculations of this reaction have also been done. For example, studies using the Skyrme III effective two-body interaction give the following results for the capture cross sections

$$\sigma_c(E_{cm} = 238 \text{ MeV}) = 196 \pm 100 \text{ mb}$$

$$\sigma_c(E_{cm} = 268) > 649 \text{ mb}$$

$$\sigma_c(E_{cm} = 363) = 780 \pm 111 \text{ mb},$$

where we have indicated the uncertainties in determining fusion. Comparing these microscopic cross sections with the macroscopic results shown in Fig. 5.5, we see that for E_{cm} = 238 and 268 MeV the TDHF limits are considerably above the macroscopic curve. On the other hand, the TDHF cross section for E_{cm} = 363 MeV may not be very different from the macroscopic value. In any case, the TDHF results strongly disagree with the experimental values, which are always below the macroscopic curve in Fig. 5.5. However, we have previously demonstrated that different effective two-body interactions can give widely varying fusion results.[8,9] Therefore, additional studies are being done using the modified Skyrme M interaction which correctly reproduces nuclear compressibilities and fission barrier heights.[10]

---

1. Los Alamos National Laboratory, Los Alamos, NM 87545.
2. Department of Physics, McGill University, Montreal PQ, H3A 2T8 Canada.
3. Present address: Centro Técnico Aeroespacial, Instituto de Estudos Avancados, São Paulo, Brazil.

4. J. R. Nix and A. J. Sierk, (invited paper) presented at the International Conference on Theoretical Approaches to Heavy Ion Reaction Mechanisms, Paris, France, May 14-18, 1984.
5. R. Bock, Y. T. Chu, M. Dakowski, A. Gobbi, E. Grosse, A. Olmi, H. Sann, D. Schwalm, U. Lynen, W. Müller, S. Bjørnholm, H. Esbensen, W. Wölfli, and E. Morenzoni, Nucl. Phys. A388, 334 (1982).
6. K. T. R. Davies, A. J. Sierk, and J. R. Nix, Phys. Rev. C 13, 2385 (1976).
7. J. Randrup and W. J. Swiatecki, Lawrence Berkeley Laboratory preprint LBL-17273 (1984).
8. K. T. R. Davies, K. R. S. Devi, and M. R. Strayer, Phys. Rev. C 24, 2576 (1981).
9. J. A. Maruhn, K. T. R. Davies, and M. R. Strayer, to be published.
10. J. Bartel, P. Quentin, M. Brack, C. Guet, and H. B. Håkansson, Nucl. Phys. A386, 79 (1982).

GEOMETRY AND DYNAMICS OF A ZERO-TEMPERATURE, FERMI-GAS MODEL FOR PRE-EQUILIBRIUM EMISSION OF NUCLEONS, WITH APPLICATION TO $^{16}O + ^{93}Nb$ AT E_{Lab} = 204 MeV[1]

K. T. R. Davies
B. Remaud[2]
M. R. Strayer
K. R. Sandya Devi[3]
Y. Raffray[2]

A detailed model for prompt, fast nucleon (pre-equilibrium) nucleon emission has been developed and analyzed. The basic scattering behavior in the early stages of the collision is described by a classical trajectory calculation, with particle emission arising from a zero-temperature, Fermi-gas approximation. The emission of a nucleon which has a velocity component normal to the reaction plane is taken into account in the formalism. The refraction of the nucleon trajectories passing through the mean field has been studied and different prescriptions for the absorption of nucleons have been carefully investigated. The method has been applied to the reaction $^{16}O + ^{93}Nb$ at E_{Lab} = 204 MeV, and various comparisons have been made with particle emission occurring in a recent TDHF calculation. It is found that the calculated multiplicity is greatest for head-on collisions. In addition, inclusive and in-plane energy spectra and angular distributions have been studied. The emission of forward-moving nucleons from the projectile (which pass through the target) takes place predominantly in the reaction plane and the angular distribution is

strongly peaked, approximately in the forward direction, with the energy spectrum centered about the beam energy per nucleon.

---

1. Summary of paper: Ann. Phys. 156, 68 (1984).
2. Institut de Physique, Université de Nantes, 44072 Cedex, France.
3. Department of Physics, University of Arizona, Tucson, AZ 85721.

TIME-DEPENDENT HARTREE-FOCK STUDIES OF THE SENSITIVITY OF DYNAMICAL FUSION THRESHOLDS TO THE EFFECTIVE TWO-BODY INTERACTION[1]

J. A. Maruhn[2] K. T. R. Davies
M. R. Strayer

There has been great interest in recent years in studies of dynamical thresholds which govern fusion behavior in heavy-ion reactions.[3-9] Two such thresholds can be identified. The first is the low-energy threshold which is associated with the phenomenon known in macroscopic studies as the extra push (or, in some cases, the extra-extra push).[4-6] This threshold can be characterized as follows. For head-on collisions of sufficiently light systems, fusion occurs for center-of-mass (CM) bombarding energies greater than or equal to the interaction barrier height. However, for a fixed CM energy, if one increases the repulsive potential energy of the system by increasing the charges of the target or projectile (or the orbital angular momentum), fusion becomes less probable. Thus, e.g., for head-on collisions of a system exceeding a critical fissility,[3-7] fusion will not occur unless the CM energy exceeds the barrier height by a certain threshold value known as the extra-push energy. This threshold occurs theoretically in both macroscopic[3-7] and microscopic[9] studies, and its existence is well established experimentally.[5-7]

The second type of dynamical threshold occurs only in TDHF calculations at relatively high energies,[8,9] where it is found that fusion abruptly disappears for head-on collisions. This threshold is known as the TDHF angular momentum window. For energies above this threshold, there exists a low-angular-momentum cutoff below which there is no fusion. This behavior is intimately associated with the transparency inherent in the mean-field approximation and its existence is thought to be very questionable experimentally.[10] We have completed TDHF calculations primarily devoted to the microscopic analogue of the macroscopic extra-push threshold, although we have also obtained some results for the window threshold.

TDHF studies of $^{86}Kr + ^{139}La$ show that the extra-push fusion threshold is very sensitive to the two-body effective interaction used. Figure 5.6 for head-on collisions, illustrates how the dynamical behavior depends upon the interaction. In this figure, we display the rms radius of the total system as a function of time for E_{lab} = 370 MeV for the five Skyrme forces considered.

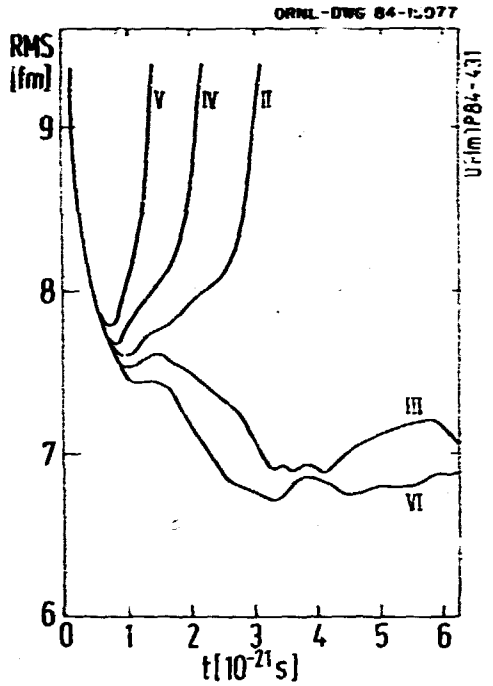

Fig. 5.6. The rms radius of the total system as a function of time for head-on collisions of $^{86}Kr + ^{139}La$ at E_{lab} = 370.0 MeV. The Roman numeral on each curve labels the Skyrme force used.

The general behavior shown in this figure is similar to that obtained at other energies. The initial minimum of the rms radius depends strongly on the force. Then the smaller the value of this minimum, the more likely the system is to fuse. For Skyrme forces II, IV, and V the initial coalesced system clearly reseparates, while it is our interpretation that the reactions for Skyrme forces III and VI lead to true compound nucleus formation. Thus, the tendency to fuse decreases according to the following sequence of Skyrme forces: VI, III, II, IV, and V.

We summarize the results for our fusion threshold studies in Fig. 5.7. The error bars in this figure show the uncertainties in determining the calculated thresholds. The calculations were performed in the laboratory energy range from 370.0 to 830.0 MeV. The lower energy limit was chosen because it is somewhat above the macroscopic interaction barrier, and we did not exceed the upper limit due to our concern both about numerical instability and about possible important corrections to TDHF at higher energies. For Skyrme forces III and VI, there is essentially no extra-push energy required since fusion occurs for all energies down to the interaction barrier. On the other hand, for Skyrme V, there is a large extra-push energy since the fusion threshold lies between 790.0 MeV and 830.0 MeV. This demonstrates that the extra-push thresholds for different Skyrme

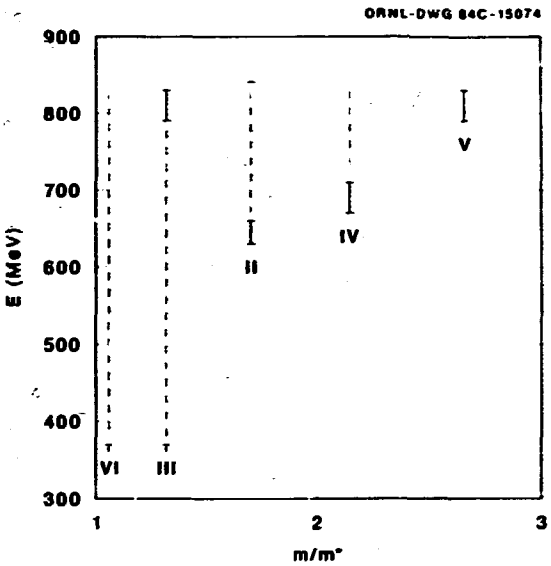

Fig. 5.7. Dynamical TDHF fusion thresholds for head-on collisions of $^{86}Kr + ^{139}La$. The laboratory energy thresholds for different Skyrme forces are plotted as a function of the inverse of the effective mass rat , m/m^*. The error bars indicate the uncertainties in determining the threshold. The lower error bars denote the extra-push fusion threshold, while the upper error bars, when present, indicate the window threshold. The dashed lines joining the lower and upper error bars denote the fusion region. The Roman numerals label the Skyrme forces.

forces can differ by almost 500 MeV. Also, for Skyrme forces IV and VI, after fusion occurs at lower energies, it continues up to 830.0 MeV, and no window threshold was determined in the energy range under consideration.

Also, studies of both $^{86}Kr + ^{139}La$ and $^{16}O + ^{16}O$ demonstrate that the relatively high-energy, angular momentum window threshold exhibits a pronounced force dependence. In particular, for $^{16}O + ^{16}O$ the thresholds for Skyrme II and IV differ by 20 MeV, with the threshold for Skyrme II only a few MeV below the energy used in the experiment[10] which seemed to rule out the existence of the window. We suggest that it would be desirable to reanalyze the experimental and theoretical information, taking into account more carefully the force dependence of the window threshold.

1. Summary of paper to be submitted to Physical Review.
2. Consultant from University of Frankfurt, Frankfurt, West Germany.
3. J. R. Nix and A. J. Sierk, Phys. Rev. C 15, 2072 (1977).
4. W. J. Swiatecki, Phys. Scripta 24, 113 (1981).
5. W. J. Swiatecki, Nucl. Phys. A376, 275 (1982).
6. S. Bjørnholm and W. J. Swiatecki, Nucl. Phys. A391, 471 (1982).
7. K. T. R. Davies, A. J. Sierk, and J. R. Nix, Phys. Rev. C28, 679 (1982). This paper contains additional theoretical and experimental refere relevant to dynamical fusion thresholds.
8. P. Bonche, K. T. R. Davies, B. Flanders, H. Flocard, B. Grammaticos, S. E. Koonin, S. J. Krieger, and M. S. Weiss, Phys. Rev. C 20, 641 (1979).
9. K. T. R. Davies, K. R. S. Devi, and M. R. Strayer, Phys. Rev. C 24, 2576 (1981).
10. A. Lazzarini, H. Doubre, K. T. Lesko, V. Metag, A. Scamster, R. Vandenbosch, and W. Merryfield, Phys. Rev. C 24, 309 (1981).

TIME-DEPENDENT HARTREE-FOCK CALCULATIONS OF NUCLEAR MOLECULAR RESONANCES[1]

M. R. Strayer
A. S. Umar[2]
R. Y. Cusson[3]
P.-G. Reinhard[4]

We have performed time-dependent Hartree-Fock (TDHF) calculations at bombarding energies near the Coulomb barrier for $^4He+^{14}C$ systems. The collective oscillations of the nuclear density are followed in time and analyzed in terms of their classical quasiperiodic behavior. Using the density constrained Hartree-Fock method, we have also calculated the position of the TDHF collective path with respect to the multidimensional energy surface of the compound nuclear system. In all of these cases the TDHF path is found to oscillate about the shape isomeric minimum of the compound system. The moments of the density are defined as

$$M_{LI}(t) = \int d^3r\, r^2\, Y_{L0}(\hat{r})\, \rho_I(\vec{r},t)$$

$$M_{LI}(\omega) = \int dt\, \exp(-i\omega t) M_{LI}(t)$$

where the index I identifies the isoscalar (I=0) and isovector (I=1) components. In Fig. 5.8 some of these moments are shown for the $^4He+^{14}C$ system. We clearly see an isoscalar octupole frequency at 4 MeV, two isoscalar quadrupole frequencies at 8 and 14 MeV, and an isovector dipole frequency at 4 MeV. The large deformations and characteristic clustering, observed in our calculations, suggest these collective states may correspond to molecular resonances observed in Ref. 5.

1. Summary of paper: Phys. Lett. 135B, 261 (1984).
2. Guest assignee from Wright Nuclear Structure Laboratory, Yale University, New Haven, CT 06511.
3. Consultant from Duke University, Durham, NC 27706.
4. Consultant from University of Frlangen, Erlangen, West Germany.
5. M. Gai et al., Phys. Rev. Lett. 50, 239 (1983).

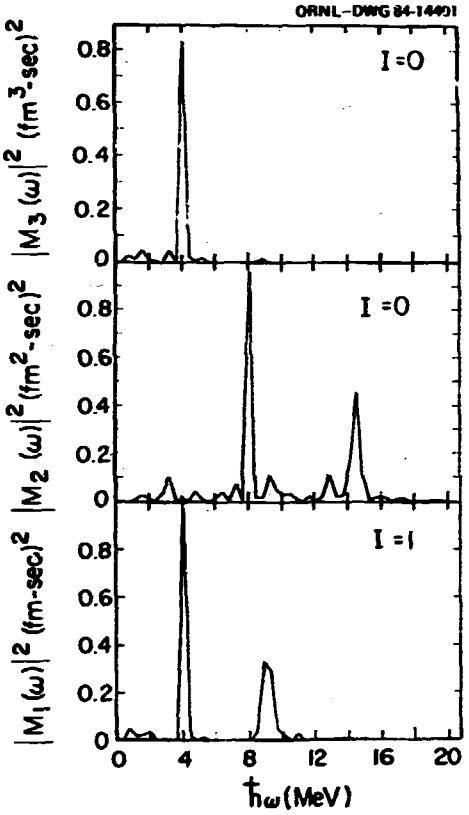

Fig. 5.8. The frequency dependence of the isoscalar quadrupole, isoscalar octupole, and the isovector dipole moments for the ^{18}O system.

A TIME-DEPENDENT MEAN-FIELD THEORY FOR PROMPT NUCLEON EMISSION IN HEAVY-ION REACTIONS[1]

A. S. Umar[2] M. R. Strayer
D. J. Ernst[3]

We have developed a time-dependent mean-field theory for the study of prompt nucleon emission in heavy-ion reactions. The model treats the relative motion of the ions classically while treating the internal excitations quantum mechanically. The motivation for the model comes from earlier time-dependent Hartree-Fock studies.[4] Here, we study emission from one of the heavy ions while we consider the other as a structureless particle, located at a distance R from the center of the emitting ion, producing a time-dependent field. This assumption is valid for mass asymmetric systems. Under these conditions, the Hamiltonian for the system becomes

$$H = H_0(\{\vec{r}_i\}) + T_{\vec{R}} + U(\vec{R},\{\vec{r}_i\})$$

where H_0 is the intrinsic Hamiltonian of the emitting ion and depends on the nucleon coordinates $\{\vec{r}_i\}$, T is the relative kinetic energy of the ions, and U is an external one-body field which induces the coupling between the two ions. The one-body nature of U is an assumption of our model. The wavefunction associated with H is taken to be a product form

$$\Psi(\{\vec{r}_i\},\vec{R},t) = G(\vec{R},t)\Phi(\{\vec{r}_i\},t)$$

where G describes the motion of the structureless particle and Φ is a time-dependent Slater determinant for the nucleons in the emitting nucleus. Variation of the action with respect to G^* and the single-particle states of Φ yields coupled equations governing the relative motion and the intrinsic dynamics of the emitting nucleus, respectively. The expression for the invariant single cross section is

$$\frac{d^3\sigma(1)}{dk^3} = \frac{1}{(2\pi)^2}\sum_{\lambda=1}^{A}\int_0^{b_{max}} db\; b\left|C_{\vec{k}\lambda}(t=\infty)\right|^2$$

where b denotes the impact parameter, and $C_{\vec{k}\lambda}$ denotes the probability for occupying the continuum state $\vec{k}$.

We have used as our external field a rank one separable potential having its range adjusted to contain the interaction within the strong absorption radius of the system and strength adjusted to the experimental multiplicity. We have studied neutron emission from the reaction $^{16}O + {}^{93}Nb$ at E_{lab} = 204 MeV.[5] In Fig. 5.9 we

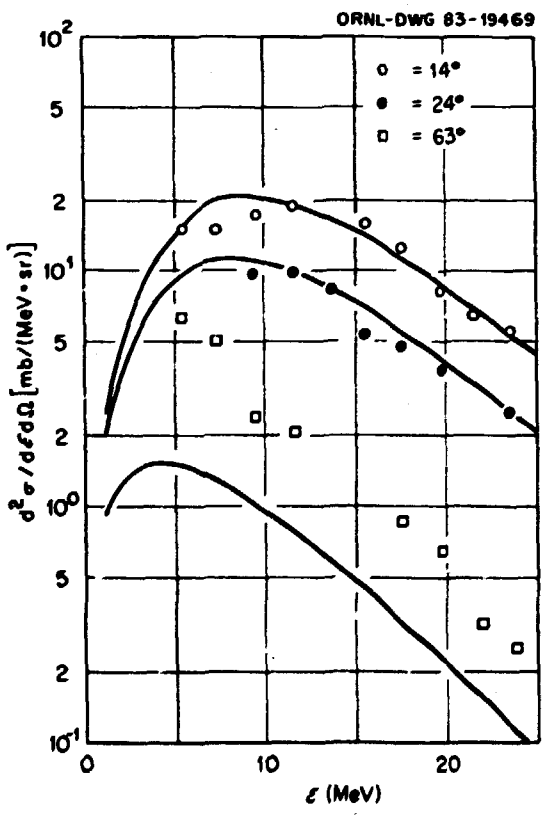

Fig. 5.9. Double differential cross sections as a function of laboratory energy for angles 14°, 24°, and 63°.

show the double differential cross sections together with the experimental results. The discrepancy at large angles may be due to the exclusion of emission from Nb.

---

1. Summary of paper: Phys. Lett. 140B, 290 (1984).
2. Guest assignee from Wright Nuclear Structure Laboratory, Yale University, New Haven, CT 06511.
3. Consultant from Texas A & M University, College Station, TX 77843.
4. K. R. S. Devi et al., Phys. Rev. C 24, 2521 (1981).
5. A. Gavron et al., Phys. Rev. Lett. 46, 8 (1981).

N-N CORRELATIONS IN INCLUSIVE NONEQUILIBRIUM PARTICLE EMISSION[1]

A. S. Umar[2] M. R. Strayer
D. J. Ernst[3]

Recent experiments[4] have shown pronounced nucleon-nucleon correlations in inclusive particle emission from heavy-ion reactions. Within the framework of Koonin's formalism[5] the associated spatial localization was calculated and interpreted as evidence for the formation of a "hot spot." We have recently developed a time-dependent mean-field model for prompt nucleon emission in heavy-ion reactions.[6] In this model the two-nucleon cross section is given by

$$\frac{d^6\sigma(2)}{d^3k d^3q} = \frac{1}{(2\pi)^5}\int_0^{b_{max}} db\, b \left\{ \sum_{\lambda,\mu=1}^{A} \left|C_{\lambda\vec{k}}\right|^2 \left|C_{\mu\vec{q}}\right|^2 - \left| \sum_{\lambda=1}^{A} C^*_{\lambda\vec{k}}\, C_{\lambda\vec{q}} \right|^2 \right\} \quad (1)$$

where b denotes the impact parameter, and $C_{\vec{k}}$ denotes the probability for occupying the continuum state $\vec{k}$.

Since we are working with a mean-field model, it is important to understand the source of these correlations. Our wavefunction is, at all times, a Slater determinant. The antisymmetry of the wavefunction leads to the second term on the righthand side of Eq. (1). Dynamical long-range correlations are included in the time-dependent field, and, as in time-dependent Hartree-Fock theory, the short-range correlations serve to renormalize the interaction and produce a mean field. Within this model, we ignore the contribution of the particle exchange and polarization to the mean field and determine it from the entrance channel configurations. The calculation of Eq. (1) was done for the neutron emission from the system ^{160} + ^{93}Nb at E_{lab} = 204 MeV. For this system we first adjusted the parameters of the external field to fit the singles neutron spectra. The details of the singles calculation are given in Ref. 6. We then calculated the two-neutron cross section of Eq. (1) as a function of the relative neutron velocity as shown in Fig. 5.10 (solid line). The results show the characteristics of the two-particle cross sections obtained for other systems.[5] A naive application of the uncertainty principle to the half-width of the two-neutron cross section of Fig. 5.10 yields a space localization of 2.5 fm, about the radius of the ^{16}O nucleus.

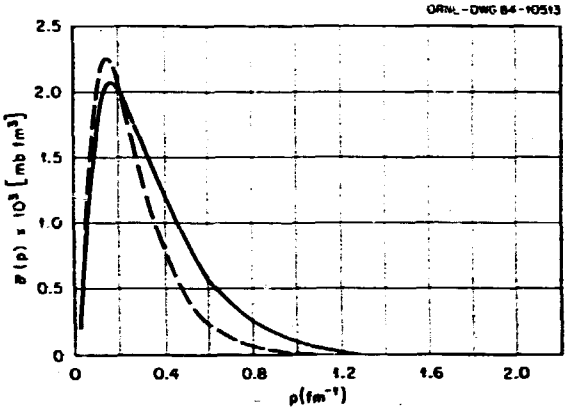

Fig. 5.10. Two-neutron cross section of Eq. (1) as a function of relative neutron momentum (solid line) and the same curve with the addition of final-state interaction (dashed curve). The dashed curve is divided by 100.

There is another type of correlation which we treat using a final-state interaction model. When two nucleons are emitted in nearly the same direction, then they can interact substantially before they reach the detector. This two-body interaction is short range and is dominated by the deuteron pole. We have used the separable interaction of Yamaguchi as our residual interaction. The dashed line of Fig. 5.10 shows the effect of this final-state interaction upon the two-neutron cross section. As we see, the effect of the final-state interaction leaves the momentum localization essentially unchanged.

---

1. Summary of papers to be published in Physical Review C and Proceedings of International Conference on Fusion Reactions below the Coulomb Barrier.
2. Guest assignee from Wright Nuclear Structure Laboratory, Yale University, New Haven, CT 06511.
3. Consultant from Texas A & M University, College Station, TX 77843.
4. W. G. Lynch et al., Phys. Rev. Lett. 51, 1850 (1983).
5. S. E. Koonin, Phys. Lett. 70B, 43 (1977).
6. A. S. Umar, M. R. Strayer, and D. J. Ernst, Phys. Lett. 140B, 290 (1984).

CHAOS IN TIME-DEPENDENT HARTREE-FOCK COLLISIONS OF HEAVY IONS[1]

M. R. Strayer
A. S. Umar[2]
R. Y. Cusson[3]
P.-G. Reinhard[4]

Recently we performed time-dependent Hartree-Fock (TDHF) calculations, at bombarding energies near the Coulomb barrier, for $^{4}He+^{14}C$, $^{12}C+^{12}C(0^{+})$, and $^{4}He+^{20}Ne$ systems. In particular, we examined the collective oscillations of the nuclear density in terms of its moments

$$M_{LI}(t) = \int d^3r\, r^2\, Y_{L0}(\hat{r})\rho_I(\vec{r},t)$$

$$M_{LI}(\omega) = \int dt\, \exp(-i\omega t) M_{LI}(t)$$

where the index I labels the isoscalar (I=0) and isovector (I=1) components. We have also calculated the classical frequencies associated with each of these collective degrees of freedom. The position of the TDHF path, with respect to the multidimensional energy surface of the compound system, was also calculated. In all of these cases the TDHF path was found to oscillate about the shape isomeric minimum of the compound system.

Depending on the amplitude of these oscillations, the motion can be identified as being chaotic or quasiperiodic. For a more elaborate identification, we plot the Poincaré projects for the motion of the $^{12}C+^{12}C(0^{+})$ system in Fig. 5.11. We see that both the isoscalar quadrupole and octupole modes seem to be filling most of the available phase space. The corresponding autocorrelation functions

$$C_{LI}(t) = \int \frac{d\omega}{2\pi} \exp(i\omega t) \left| M_{LI}(\omega) \right|^2$$

are small for all of the relevant modes suggesting that the motion is closer to being chaotic rather than harmonic. In order to improve the periodicity of the TDHF results, we have "cooled" the system, thus bringing it closer to the shape isomeric minimum. The "cooling" was done by performing a density-constrained Hartree-Fock calculation at a point on the TDHF path. This result was then used as the initial state for continuing the time evolution.

In Fig. 5.12 we show the time dependence of the moments for the "cooled" motion of the $^{12}C+^{12}C(0^{+})$ system. The correlation functions associated with these modes are large, indicating a quasiperiodic behavior. These results are important from the point of view that the quasiperiodic motion represents a known classical limit of quantum mechanics, whereas the chaotic motion does not. Figure 5.13 shows the classical frequencies for the "cooled" motion of

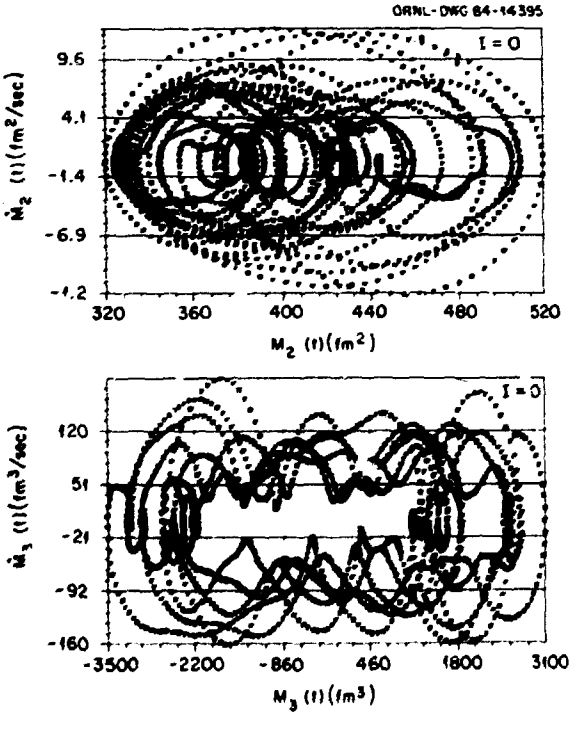

Fig. 5.11. Poincaré phase space plots of $M_{LI}(t)$ vs. $\dot{M}_{LI}(t)$ for the I=0, L=2,3 modes of the ^{24}Mg system.

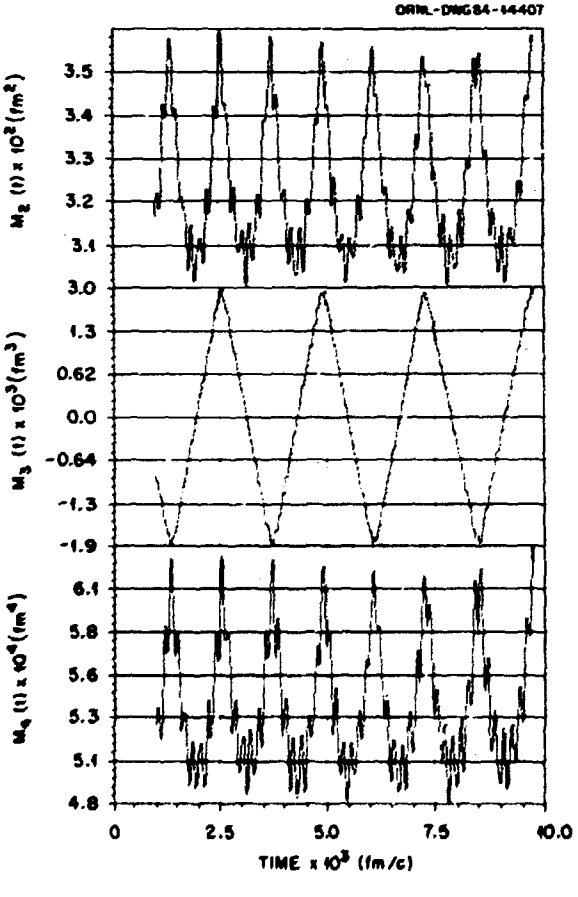

Fig. 5.12. Time dependence of the isoscalar quadrupole, octupole, and hexadecapole moments for the "cooled" modes of the ^{24}Mg system.

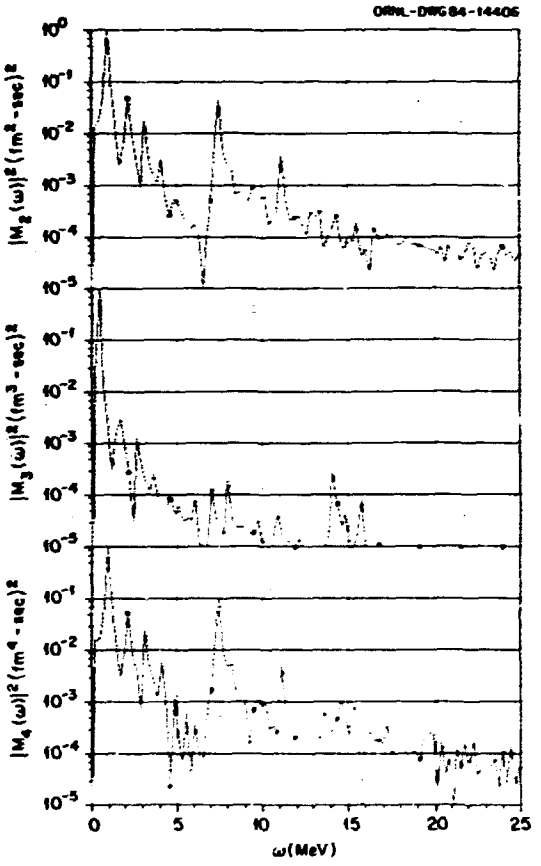

Fig. 5.13. The frequency dependence of the isoscalar quadrupole, octupole, and hexadecapole moments for the "cooled" modes of the ^{24}Mg system.

the $^{12}C+^{12}C(0^+)$ system. In this figure the first few harmonics are clearly visible suggesting that the motion is close to being harmonic.

---

1. Summary of paper to be published in Proceedings of the International Conference on Fusion Reactions Below the Coulomb Barrier, Cambridge, MA, June, 1984.
2. Guest assignee from Wright Nuclear Structure Laboratory, Yale University, New Haven, CT 06511.
3. Consultant from Duke University, Durham, NC 27706.
4. Consultant from University of Erlangen, Erlangen, West Germany.
5. M. R. Strayer et al., Phys. Lett. 135B, 261 (1984).

MEAN-FIELD CALCULATIONS OF FLUCTUATIONS IN NUCLEAR COLLISIONS[1]

J. B. Marston[2] S. E. Koonin[3]

We apply the new variational principle of Balian and Veneroni to calculate the fluctuations in final fragment mass, charge, and kinetic energy for the systems $^{16}O + ^{16}O$ (E_{LAB} = 160 MeV) and $^{40}Ca + ^{40}Ca$ (E_{LAB} = 278 MeV). The calculated fluctuations are larger than conventional TDHF results and, in the latter case, are consistent with the experimental fragment mass distribution.

---

1. Abstract of paper to be submitted for publication in Physical Review Letters.
2. Research Intern from California Institute of Technology, Pasadena, CA 91125, summer, 1984.
3. Consultant from California Institute of Technology, Pasadena, CA 91125.

ROTATING TOROIDAL NUCLEI IN HEAVY-ION REACTIONS[1]

Cheuk-Yin Wong

Recent experiemtnal measurements[2,3] on the correlation of the fragments in the bombardment of ^{32}S and ^{35}Cl on ^{58}Ni at an energy of about 11 MeV per (projectile) nucleon reveal interesting three-fragment events. These events are characterized by: (1) a bombarding energy threshold of slightly greater than 10 MeV per nucleon, (2) a cross section of 150 mb at about 11 MeV per nucleon, (3) approximately equal fragments in the reaction plane with momentum vectors making an angle of about 120° with respect to each other, (4) a value of Q_t, the difference of the estimated total final kinetic energy T_f of the three fragments and the initial kinetic energy T_i of about -150 MeV, and (5) a detected multiplicity lower than that for deep-inelastic collisions. The authors suggested that the scission configuration may be a closed configuration of oblate shape. We explore the possibility that the process of a three-fragment breakup observed in these reactions of ^{35}Cl and ^{32}S on ^{58}Ni may arise from an intermediate rotating toroidal nucleus with $\ell \sim 130\hbar$. Quantitative characteristics of the toroidal nuclei are presented and found to agree with those of the experiment. Further experimental investigation to search for a rotational symmetry of the three fragment events is suggested.

---

1. Summary of paper to be published in Physical Review C.
2. D. Pelte and U. Winkler, Nucl. Phys. A423, 164 (1984).
3. U. Winkler, B. Weissman, M. Bühler, A. Gorks, R. Novotny, and D. Pelte, Nucl. Phys. A425, 573 (1984).

LIMITS ON THE HIGH-DENSITY BEHAVIOR OF HEURISTIC NUCLEAR MATTER EQUATIONS OF STATE

J. A. Maruhn[1]

Both for hydrodynamic model calculations and for simple analysis of experimental data in high-energy, heavy-ion collisions, one has to employ a heuristic equation of state that is parametrized to reproduce some desirable properties near the ground state of nuclear matter while allowing flexibility at higher densities. In almost all calculations up to now the internal energy per nucleon as a function of density n and entropy s was set up as a sum of a zero-entropy contribution $W_0(n)$ and a thermal part W_t that is assumed to be given by a Fermi gas expression.

For the function $W_0(n)$ the usual requirements are those of correct ground-state binding energy $W_0(n_0) = B_0 = -18$ MeV, corresponding to a minimum in W_0, and a reasonable incompressibility $W_0''(n=n_0) = K/9n_0^2$ with $K = 200$ MeV.

The functions actually employed were either the quadratic equation of state

$$W_0(n) = \frac{K}{18n_0^2}(n-n_0)^2 + B_0$$

or the quasilinear one

$$W_0(n) = \frac{K}{18nn_0}(n-n_0)^2 + B_0 .$$

Both of these, however, face some problems at higher densities. As seen in Fig. 5.14, the speed of sound for the quadratic equation of state already exceeds the speed of light at about five times normal nuclear density while for the linearized one the compressional energy remains so small that in calculations it is very close to the ideal gas (i.e. $K = 0$).

It was therefore thought necessary to develop a new family of equations of state with more realistic properties at higher densities. After investigating a number of different functional forms, we propose the hyperbolic equation of state

$$W_0(n) = B_0 + \alpha\left[(n-n_0)^2/n_0^2 + \frac{\beta|\alpha^2}{K^2}\right]^{1/2} - \frac{9\alpha^2}{K} .$$

This reproduces all the ground-state properties and always approaches a sound speed equal to the speed of light at high densities.

The new parameter α characterizes the slope of $W_0(u)$ in the high-density limit; in fact

$$W_0(n) \sim \alpha\frac{n}{n_0} \quad \text{for } n \to \infty.$$

The curve for $W_0(n)$ interpolates between a parabola near n_0 and a linear behavior at large n. Because the speed of sound is related to the curvature of this curve, it still exceeds the speed of light for intermediate values of n if α becomes larger than a certain value depending on

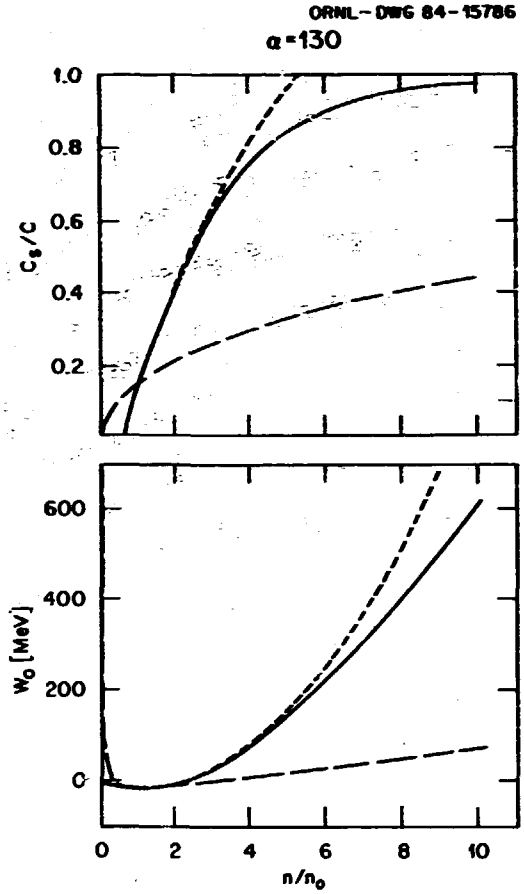

Fig. 5.14. Energy per nucleon and speed of sound in zero-temperature nuclear matter for the quadratic (short dashes), linearized (long dashes), and hyperbolic equation of state (full curve), the latter with $\alpha = 130$ MeV.

K. For $K = 200$ MeV, this value is $\alpha = 132.30$ MeV. This is not a fundamental limit on α; a different parametrization of W_0 might reduce the curvature in the transition region and thus allow slightly higher values of α. However, as seen in Fig. 5.14, for α close to this limiting value the resulting curve stays quite close to the quadratic equation of state up to almost $n = 5\ n_0$, where it has to deviate to avoid too large sound speeds. For small values of α, one can go to arbitrarily soft equations of state, up to and below the linearized one.

What emerges from these considerations is that, even aside from the particular form of $W_0(n)$ proposed here, the parameter α, the asymptotic slope of $W_0(n)$ is probably a necessary ingredient of any such equation of state and will play a more important role than K at the high densities.

---

1. Consultant from University of Frankfurt, Frankfurt, West Germany.

DENSITY AS A CONSTRAINT AND EXCITATION ENERGY IN TDHF[1]

R. Y. Cusson[2] M. R. Strayer
P.-G. Reinhard[3] J. A. Maruhn[4]
W. Greiner[4]

The time-dependent Hartree-Fock (TDHF) method aims at a mean-field description of the dynamics of a many-body system. Nevertheless, a TDHF trajectory describes not only collective motion but also a great deal of internal excitation. It is of considerable theoretical and practical interest to have a method which would allow us to disentangle both contributions to the motion.

The task is to find a fast iteration scheme for constrained Hartree-Fock, in particular for the case of multiple constraining conditions.

The Hartree-Fock state $|\Phi\rangle$ is an antisymmetrized product of single-particle states $|\phi_\alpha\rangle$. The most general gradient step can be written as

$$\left|\phi_\alpha^{(n+1)}\right\rangle = \mathcal{O}\left\{\left|\phi_\alpha^{(n)}\right\rangle - \hat{D}\left(\hat{W}^{(n)} + \underline{\lambda}^{(n)}\cdot\underline{\hat{Q}}\right)\left|\phi_\alpha^{(n)}\right\rangle\right\}$$

where $\hat{W}^{(n)}$ is the Hartree-Fock Hamiltonian to the $\left\{|\phi_\alpha^{(n)}\rangle\right\}$,

$$\hat{W}^{(n)} = \hat{T} + \mathrm{Tr}\left\{\hat{\rho}^{(n)}\hat{V}\right\}$$

and $\hat{T}$ is the kinetic energy, $\hat{V}$ is the interaction potential, and $\hat{\rho}^{(n)}$ is the one-body density matrix

$$\hat{\rho}^{(n)} = \sum_\alpha \left|\phi_\alpha^{(n)}\right\rangle\left\langle\phi_\alpha^{(n)}\right|.$$

The $\mathcal{O}$ means Gram-Schmidt orthogonalization of the single-particle wave functions. The $\hat{D}$ is a damping operator to ensure convergency of the iteration where

$$\langle\underline{Q}\rangle^{(n)} = \sum_\alpha \left(\phi_\alpha^{(n)}\left|\underline{\hat{Q}}\right|\phi_\alpha^{(n)}\right)$$

for $\underline{\hat{Q}}$ being a set of one-body operators. The straightforward way to adjust the constraint is simply to project out of the step $\hat{W}^{(n)}$ the component along $\underline{\hat{Q}}$ (which would drive to change its expectation value).

At the start of an iteration step we have now a set of occupied single-particle states $\{|\phi_\alpha^{(n)}\rangle\}$ and a constraining force $\underline{\lambda}^{(n)}$. First, we perform a trial step with $\hat{W}^{(n)} + \underline{\lambda}^{(n)}\cdot\underline{\hat{Q}}$. Since the $\underline{\lambda}^{(n)}$ has not yet reached the ideal value, this step will cause a change in $\langle\underline{\hat{Q}}\rangle$

$$\delta\underline{Q} = \sum_\alpha \left(\phi_\alpha\left|\underline{\hat{Q}}\right|\phi_\alpha\right) - \sum_\alpha \left(\phi^{(n)}\left|\underline{\hat{Q}}\right|\phi^{(n)}\right).$$

We correct $\underline{\lambda}^{(n)}$ to reduce the change

$$\lambda_i^{(n+1)} = \lambda_i^{(n)} + c_0 \frac{\delta\bar{Q}_i}{2\varepsilon \sum_\alpha \left(\phi_\alpha^{(n)}\left|\hat{Q}_i^2\right|\phi_\alpha^{(n)}\right)} + d_0$$

where c_0 and d_0 are numerical parameters to be adjusted such that optimal converging is achieved ($c_0 = 1$ and $d_0 = 0$).

We study two ^{16}O nuclei in the Hartree-Fock ground state placed at a distance of 10 fm and given an impact parameter zero.

For an initial energy of 1.56 MeV/nucleon we are in a situation slightly above the Coulomb barrier. In Fig. 5.15 we show the results for that case. The distance of the ions as a function of time shows that the two nuclei come into contact and merge until a distance of 4.4 fm is reached. Then they spring back, but they cannot escape because some relative energy is transferred to internal excitation and finally will flow into molecular vibrations. In order to give some impression about the process, we have added a few contour plots of equidensity lines

ORNL-DWG 84-15763

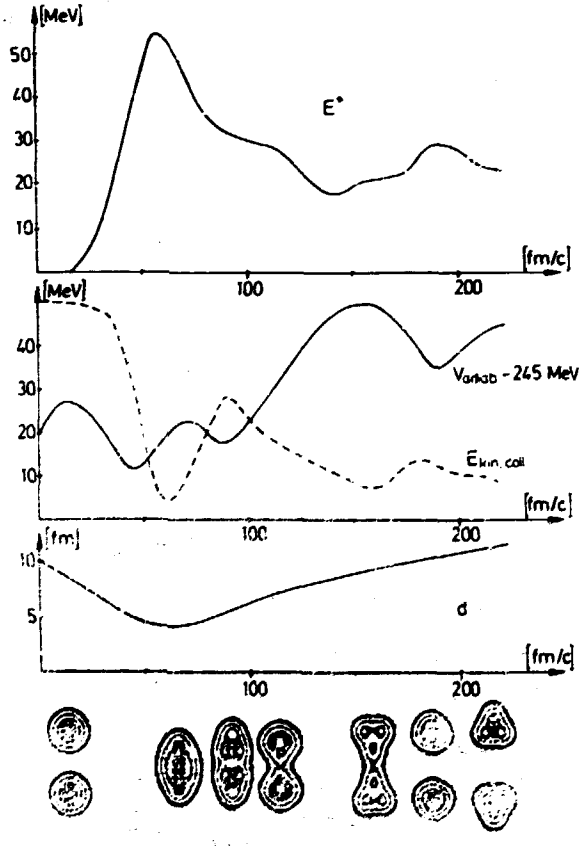

Fig. 5.15. Distance of the ions, adiabatic potential, collective kinetic energy and internal energy as functions of time for an initialization with 1.56 MeV/nucleon. As an illustration, a few contour plots of the equidensity lines are given.

at some typical stages. This behavior is reflected also by both collective energies, namely the adiabatic potential and the collective kinetic energy. Initially, the system needs some time to come across the Coulomb barrier. Then, at t = 80 fm/c, the nuclear attraction sets on and accelerates the ions drastically. With lowering separation, a repulsive force builds up which, at t = 158 fm/c, stops the relative motion and returns the process. Both the adiabatic potential and the collective kinetic energy are roughly symmetrical about the turning point. However, the deviations from an ideal collective motion are visible, namely the maxima of $E_{kin,coll}$ have unequal height, and these maxima do not precisely coincide with the minima of the adiabatic potential. This is due to the occurrence of strong internal excitations, as seen from the behavior of E^*.

In some sense, the internal energy behaves as expected; comparing the stages of small overlap initially and after the reflection, we observe that an internal excitation of about 3 MeV has been gathered during interaction time.

---

1. Summary of paper to be published in Zeitschrift für Physik.
2. Consultant from Duke University, Durham, NC 27706.
3. Consultant from University of Erlangen, Erlangen, West Germany.
4. Consultant from University of Frankfurt, Frankfurt, West Germany.

RELATIVISTIC MEAN-FIELD DYNAMICS APPLIED TO $^{16}O+^{16}O$ SCATTERING

R. Y. Cusson[1] H. Stöcker[3]
P.-G. Reinhard[2] M. R. Strayer
W. Greiner[4]

The time-dependent Hartree-Fock (TDHF) theory, using Skyrme forces, is widely used in microscopic descriptions of the mean-field dynamics of low-energy, heavy-ion reactions.[5] An approach which allows extensions to energies comparable to the nucleon rest mass raises questions of covariance and retardation in the mean-field propagation. We present here a microscopic model of relativistic nuclear mean-field dynamics. The model consists of nucleons obeying the time-dependent Dirac equation, a classical spin-zero attractive meson field (sigma), a spin-one repulsive mean field (omega), and a meson baryon interaction between them. The resulting coupled field equations are solved simultaneously in mean-field approximation. Similar models have been studied for the static case by Walecka and others.[6] The theory is treated in the Hartree approximation and this yields an effective Lagrangian. The masses and coupling constants for the mesons are phenomenological and are adjusted to fit static nuclear matter properties.[6]

An expression for the model Lagrangian density is obtained with model parameters as follows: baryon mass $m_b c^2$ = 938 MeV, scalar meson mass $m_S c^2$ = 500 MeV, vector meson mass $m_V c^2$ = 780 MeV, scalar coupling constant g_S = 18.030 MeV fm, vector coupling constant g_V = 33.141 MeV fm. The meson masses are taken from OBEP models, and the coupling constants are adjusted to reproduce the binding energy and density of nuclear matter.

The following equations of motion emerge from the Lagrangian density:

$$i\hbar \frac{\partial}{\partial t}\psi = \hbar c\left[-i\gamma_0\vec{\gamma}\cdot\vec{\nabla} + \frac{m_B c}{\hbar}\gamma_0 + g_S\gamma_0 + g_V \gamma^\nu \gamma_0\gamma_\nu\right]\psi$$

$$i\hbar \frac{\partial}{\partial t}\Pi = \left[-\hbar^2\Delta + (m_S c^2)^2\right]\Sigma + \hbar c\, g_S\langle\bar{\psi}\psi\rangle$$

$$i\hbar \frac{\partial}{\partial t}\Sigma = \Pi$$

$$i\hbar \frac{\partial}{\partial t}\mathcal{V}_\mu = \left[-\hbar^2\Delta + (m_V c^2)^2\right]V_\mu + \hbar c\, g_V \langle\bar{\psi}\gamma_\mu\psi\rangle$$

$$i\hbar \frac{\partial}{\partial t} V_\mu = \mathcal{V}_\mu$$

The gauge and continuity equations

$$\partial_\nu V^\nu = 0, \quad \partial_\nu \langle\bar{\psi}\gamma^\nu\psi\rangle = 0$$

are evaluated during the time evolution as a check of the numerical accuracy.

We use the classical equations of motion for the mesons in the mean-field theory. Thus the baryonic field can be treated exactly by single nucleon propagation and Slater determinants will remain so at all times. We restrict, in the present work, the progation to the A occupied bound states above the baryon vacuum. These approximations result in a theory free of mass and charge renormalization effects.

We represent the meson field and the baryon wavefunctions on a three-dimensional (32×32×32) mesh in both coordinate and momentum space, with a mesh spacing of 0.5 fm in coordinate space. The momentum space mesh is reached with the help of a fast Fourier transform. We employ isospin degenerate nucleon wavefunctions and treat the spin degrees of freedom in the usual four-component spinor formalism.

We use the relativistic static Hartree wavefunctions for each of the ^{16}O initial states, located at a separation distance of 10 fm from each other on the mesh, and Lorentz boosted to the appropriate initial energy in the center of velocity frame. The time evolution for the baryon wavefunction is done using a fifth-order predictor-corrector scheme in momentum space, and the meson equations are solved simultaneously using Green function techniques. The momentum space energy truncation was taken as 2 GeV. This limits the time step to less than 0.05 fm/c.

We have calculated head-on $^{16}O+^{16}O$ collisions at E/A_{Lab} = 300 MeV, 600 MeV, and 1200 MeV. The time evolution is followed until the expanding sideways flow of matter hits the outer edge of

the mesh. We show in Fig. 5.16 the time evolution of the baryon density, whose space integral is the total conserved baryon number (32 in this case), for E/A_{Lab} = 600 MeV. The early time behavior of the collision is similar to that of Skyrme TDHF. A compression zone and side splashing develops after about t = 6 fm/c. The system then proceeds to spallate in all directions. This can be contrasted with Skyrme TDHF where projectile-like fragments and target-like ones emerge after the reaction. The results of the present work are, in fact, reminiscent of fluid dynamical behavior. The behavior at the other two bombarding energies was found to be similar.

---

1. Consultant from Duke University, Durham, NC 27706.
2. Consultant from University of Erlangen, Erlangen, West Germany.
3. Michigan State University, East Lansing, MI 48824.
4. Consultant from University of Frankfurt, Frankfurt, West Germany.
5. Proceedings of the Workshop on 'TDHF and Beyond', ed. K. Goeke and P.-G. Reinhard, Lecture Notes in Physics, Vol. 171, Springer-Verlag, Berlin, 1981.
6. J. D. Walecka, Ann. Phys. (N.Y.) 83, 491 (1974).

ORNL-DWG 84-16177

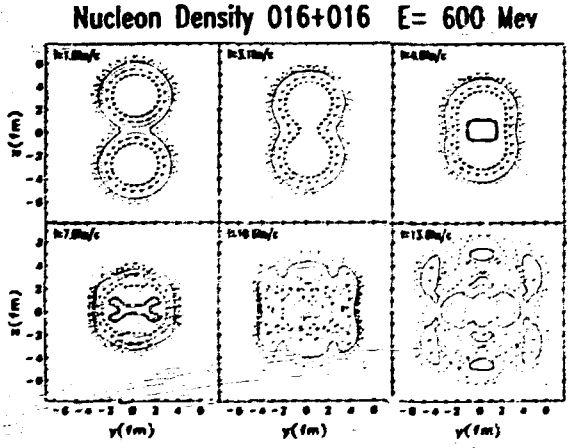

Fig. 5.16. The coordinate space baryon equidensity contours in the collision plane at various times during the 600-MeV collision. The time in fm/c is given in the upper left corner of each frame. Equidensity contours are taken at values of .245, .14, .08, .046, .026, .015, .0085, .005 nucleons/fm^3. The contour lines corresponding to these eight cuts have the styles thick (solid, dashed, dot-dashed, dotted) and thin (solid, dashed, dot-dashed, dotted) so that each contour line can be identified at a glance. The absolute maximum density reached was 0.29 n/fm^3.

SUBTHRESHOLD PION PRODUCTION IN HEAVY-ION COLLISIONS

D. J. Ernst[1] M. R. Strayer
A. S. Umar[2]

In heavy-ion collisions low energy pions have been detected[3] at bombarding energies below the free nucleon-nucleon threshold. The emission is thought to arise from a cooperative process in which the relative motion of the centers of the two ions is converted into the single degree of freedom of the produced pion. This makes subthreshold pion production a unique probe of the very early prethermalization stage of the collision.

We have developed a time-dependent, mean-field model of the emission process. In the model, nucleons in the target (projectile) are perturbed by the time-dependent mean field of the passing projectile (target). The time-dependent mass oscillations which are induced by the passing nucleus are coupled in lowest order to pion production using a standard nonrelativistic N+N+π coupling. Thus the relative motion is used to induce currents with bremstrahlung pions. Using the time-dependent reaction formalism developed in Refs. 4 and 5, the total inclusive pion emission cross section is found to be given by

$$\sigma = 2\pi \int_0^\infty b\, db\, \Sigma(b) \int \frac{d^3k}{(2\pi)^3} \frac{1}{(2\omega_k)} \int \frac{d^3p}{(2\pi)^3} \sum_h W_h$$

$$\times \left(\frac{f_o}{\mu}\right)^2 \left| \int \frac{d^3q\, d^3Q}{(2\pi)^6\, 2\omega_Q} \int \frac{dq_o}{2\pi} \vec{Q}\, \psi_{\vec{p}}^*(\vec{q},q_o) \right.$$

$$\left. \times \psi_h(\vec{q}+\vec{Q},\, q_o+\omega_k)\phi_{\vec{k}}^*(\vec{Q}) \right|^2 ,$$

where b is the impact parameter of the heavy-ion collision, $\Sigma(b)$ is classical transmission coefficient, W_h is a spin-isospin degeneracy factor for the occupied orbital h, $\psi_{\vec{p}}(\vec{p},q_o)\{\psi_h(\vec{q},q_o)\}$ is the space and time Fourier transform of the final-state nucleon (initial state nucleon), and $\phi_{\vec{p}}(0)$ is a distorted pion wave function.

If we approximate the final nucleon wave function by a plane wave and the pion wave function by a plane wave, the source current for the creation of the pion is proportional to the time-dependent Wigner function. That is, the time-dependent wave functions are Fourier transformed in the time variable and evaluated at the energy required by energy conservation. One then constructs a Wigner function for these wave functions and the double differential pion emission cross section is proportional to this function.

We have modeled the external time-dependent perturbation by a harmonic-oscillator, separable time-dependent field. This introduces two parameters into the model -- a strength function and a time scale. If we fit the strength to the total multiplicity for C+C collisions at 85 MeV,

we find empirically that the time scale $\tau^{-1} = E_{lab}/A$ produces the energy dependence for the pion multiplicity in C+C collisions as shown in Fig. 5.17. Preliminary estimates for sub-threshold kaon production indicate that these cross sections will be down many orders of magnitude as a result of the larger kaon mass and weaker coupling to the nucleon.

---

1. Consultant from Texas A & M University, College Station, TX 78712.
2. Guest assignee from Wright Nuclear Structure Laboratory, Yale University, New Haven, CT 06511.
3. T. Johannson et al., Phys. Rev. Lett. 48, 732 (1982); P. Braun-Munzinger et al., Phys. Rev. Lett. 52, 255 (1984).
4. A. S. Umar, M. R. Strayer, D. J. Ernst, and K. R. S. Devi, to be published in Physical Review C.
5. M. Baranger and I. Zahed, Phys. Rev. C 29, 1005 (1984).

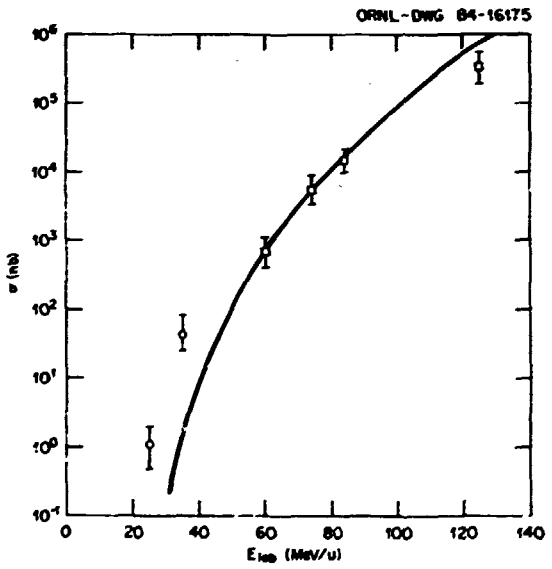

Fig. 5.17. The total $^{12}C+^{12}C$ pion production cross section as a function of the bombarding energy.

NUCLEAR STRUCTURE

THE UNISOR NUCLEAR STRUCTURE THEORY PROGRAM

Introduction

G. A. Leander[1]

A theory program is supported by UNISOR, the university isotope separator at ORNL. The aim is to conduct and stimulate theoretical research on nuclear structure, especially in areas where experiments at the Holifield facility have or potentially could have an impact. Such areas of current interest are: low-energy structure in nuclei far from stability, the cold or 'yrast' sequence of states at very high spin, and the warmer structures which are being studied by quasicontinuum spectroscopy. The focus lies on collectivity in nuclei, its basic principles, microscopic origin, and physical consequences. The most significant results from the past year pertain to intrinsic reflection asymmetry, which was previously established to occur in certain nuclides. In particular, octupole deformation was shown to exert a major influence on high-spin quasiparticles when it occurs, making nuclear rotation more regular and collective in character. Furthermore, intrinsic electric dipole moments have been shown to exhibit characteristic shell effects of their own, although they arise as a consequence of octupole deformation. These and other results are summarized below under four topical headings with reference to the respective publications.

Low-Energy Structure

A. F. Barfield[2]
F. Dönau[3]
J. Dudek[4]
B. E. Gnade[5]
W. M. Howard[6]
G. A. Leander[1]
P. Möller[7]
W. Nazarewicz[7,8]
J. R. Nix[9]
Ph. Quentin[10]
P. B. Semmes[11]
J. L. Wood[11]

Most microscopic theories for structure at low energies are based on single-particle orbits in a mean field, and an important activity is to follow up the results of spectroscopy in order to test and improve models for calculating such orbits. Data obtained during the last few years on the neutron-rich doubly magic nucleus ^{132}Sn have been evaluated[17] in terms of current models (Hartree-Fock with Skyrme III and Skyrme M forces, the Los Alamos-Lund folded Yukawa, and the Warsaw Woods-Saxon potentials). The successes and failures of each model in ^{132}Sn were significantly similar to what is obtained in ^{208}Pb. Assuming analogous correspondence between other doubly magic nuclei, the hitherto unobserved proton-rich nucleus ^{100}Sn can rather confidently be predicted to have a proton binding energy of 3-4 MeV.

An odd nucleon is an informative probe of collective as well as single-particle properties in the nucleus, and an on-going effort is therefore spent on the development and application of core-particle coupling models. In particular, the method of Dönau and co-workers for coupling BCS quasiparticles to dynamical fields of the core has been combined with the interacting boson model (IBM) developed by Arima, Iachello, Scholten, and co-workers. This dynamical BCS quasiparticle method has some obvious advantages over an alternative boson-fermion coupling model (IBFM) proposed by Iachello and Scholten: the BCS method can be applied with equal ease to any version of the IBM, methods exist to calculate the parameters of the coupling term microscopically, and there is no ambiguity in the form of

the particle-transfer operator. The first step has been to compare the BCS and IBFM coupling schemes on a phenomenological basis.[18] The difference lies in the way the Pauli principle is taken into account, and it is found that IBFM is more flexible if the strength of the exchange term is treated as a free parameter. There are specific values which give energy spectra similar to those of BCS.

The dynamical BCS quasiparticle method has been applied in the light Hg region, using the IBM2 cores with mixed boson numbers that were developed by the Tucson group. Odd-Hg $i_{13/2}$ spectra were adequately reproduced.[19] Calculations in progress for light Tl and Hg isotopes will provide a more crucial test of specific features in these cores.[20] The latter calculations are also expected to suggest how to test experimentally a hypothesis that has been made in connection with IBM, namely, that protons couple mainly to the quadrupole field of the neutron bosons and neutrons to the proton bosons. As an aside in this context, a claim in the literature that there is evidence for α-correlations in experimental binding-energy systematics resulting from this mechanism was shown to be unfounded.[21] Theoretical calculations for the light Hg cores are also being extended in connection with UNISOR measurements, using both models of prolate-oblate shape coexistence[22] and the IBM.[23,24]

The particle-triaxial rotor model was applied for a variety of purposes.[25,26] In particular, it was found that a very limited amount of spectroscopic data in certain isotopes might be enough to address the outstanding question of whether any well-deformed oblate nuclei exist beyond the sd shell. The prime candidate is the N=Z nucleus ^{72}Kr, and it was seen that all the low-lying bands in its odd-A neighbors would have clear signatures of either oblate or prolate shape. An example is shown in Fig. 5.18, where cascade to crossover ratios distinguish the two 3/2⁻ bands. Another calculation, for ^{185}Au, strongly suggests that the very high structure observed in-beam by Larabee et al. contains an "extra" $h_{9/2}$ band,[26] similar to the one previously indicated by low-spin UNISOR data on ^{187}Au.

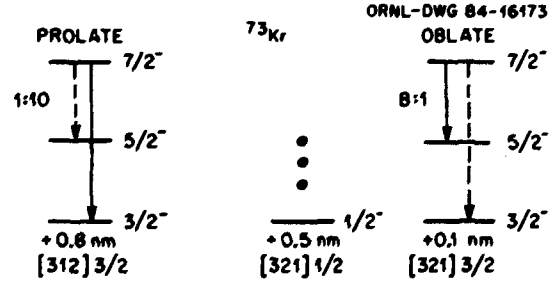

Fig. 5.18. Large oblate deformations are not known to occur except in light nuclei but have long been predicted in the region of ^{72}Kr. Oblate configurations would easily be recognized in spectroscopy on odd-mass neighbors. For example, the calculated odd-neutron 3/2⁻ bands shown here have distinct branching ratios.

In the region of the very heavy elements (Z > 100), the 1981 mass formula of Möller and Nix was applied[27] over a wider range of nuclei than in the original mass table, and lifetimes were calculated for α-decay and spontaneous fission. This work was motivated in part by the LEAP project, a joint ORNL-LANL-LBL-LLNL proposal to make a $^{254,255}_{99}$Es target for massive transfer and heavy-ion fusion reactions. The present predictions differ somewhat from earlier work, mainly due to the single-particle level scheme. One test of the level scheme would be a predicted kink in the α half-life curve at N = 162 due to a gap in the single-particle spectrum. It is similar to, but more pronounced than, the known kink at N = 152. In the superheavy region the β-stability line was obtained at lower N than previously, and the most favorable case for longevity is now ^{290}110 which could be reached from the LEAP target with a stable beam. The α half-life for ^{290}110 is 167 days, and for doubly magic ^{298}114 it is 1.2 minutes.

Intrinsic Reflection Asymmetry

G. F. Bertsch[16]
J. Dudek
G. A. Leander[1]
P. Möller[7]
W. Nazarewicz[7,8]
P. Olanders[7]
Ph. Quentin[10]
I. Ragnarsson[7]
E. Ruchowska[12,13]
M. R. Strayer

Octupole deformation which breaks the intrinsic reflection symmetry had previously been established in nuclei of the Ra-Th region, in part through an analysis of single-particle properties manifested by odd-A nuclei.[28] A somewhat different interpretation of the even-even nuclei in this region in terms of α clustering was tested,[18] using the case of ^{225}Ra where the decoupling factors of the $K^{\pi}=1/2^{\pm}$ bands are sensitive indicators of octupole deformation.[29] However, it was found that a potential resembling a core plus an α particle does not give the considerable modification of the decoupling factors which are observed in experiment and which are obtained with the smoother octupole-deformed equilibrium shape derived by the Strutinsky method. The Strutinsky calculations were also examined critically in order to see to what extent the development of an octupole-deformed minimum could be influenced by different choices of single-particle and liquid-drop models.[30] The most important single factor in the Ra region turned out to be the spacing between the proton $f_{7/2}$ and $i_{13/2}$ shells, and that value seemed to depend on whether the parameters of the single-particle potential were fitted to data in somewhat lighter and spherical or somewhat heavier and deformed nuclei.

For the neutron-rich nuclei around ^{146}Ba, where octupole deformation has been previously suggested but not investigated until now, all the models studied unanimously predict a soft, but nevertheless octupole-deformed, equilibrium shape.[30] Single-particle signatures of octupole deformation were calculated along the same lines as in the Ra region, and the still rather scanty

available data on odd-mass nuclei were found to support the predicted asymmetry.[31]

The consequences of octupole deformation at high spin were found to be significant.[32] Normally, high-spin properties are dominated by the spin alignment of a few quasiparticles from high-j shells. However, the octupole interaction mixes the high-j intruder shells with opposite-parity states in the valence shell, and thereby spreads the rotational strength over many valence orbitals. The in-band collective moment of inertia is increased and 'backbending' due to quasiparticle alignment no longer occurs, in agreement with experimental data for ^{222}Th (Fig. 5.19). The spin alignment of rotational

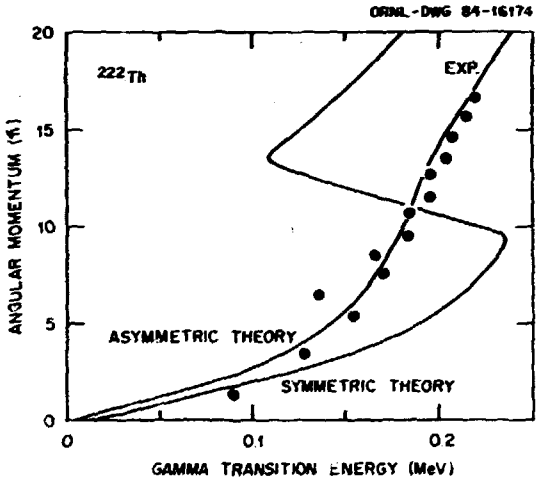

Fig. 5.19. The theoretical curves represent deformed shell-model-Bogoliubov-cranking calculations and the points experiment for the yrast line of ^{222}Th. The "symmetric theory" has the customary constraint to reflection symmetric intrinsic shapes and gives a backbend due to the alignment of $j_{15/2}$ neutrons. In the "asymmetric theory" the constraint is relaxed, ^{222}Th acquires an octupole deformed equilibrium shape, the $j_{15/2}$ orbitals are fragmented, and the yrast line is smooth, as observed in experiment.

quasiparticles, which could be extracted from sidebands and bands in odd-A nuclei, is expected to be rather uniform and smaller than the alignment typical for high-j quasiparticles. The "signature" quantum number commonly used at high spins is no longer relevant in the reflection asymmetric case, and instead a more generally applicable quantum number, "simplex", was proposed. Quasiparticle bands are expected to exhibit simplex splittings and occasional simplex crossings.

Octupole deformation is interesting not only per se but also because it leads to an "exotic state" of nuclear matter, where it is possible to observe phenomena whose existence requires broken reflection symmetry. One such phenomenon is an intrinsic collective E1 moment, which arises when there is no symmetry to make the proton and neutron centers of mass coincide exactly. Early estimates based on the liquid-drop model yielded E1 moments proportional to $\beta_2\beta_3$, but with conflicting results for the sign. An attempt is being made to resolve this conflict using the extended Thomas-Fermi formalism.[32] The calculation[33] shown in Fig. 5.20

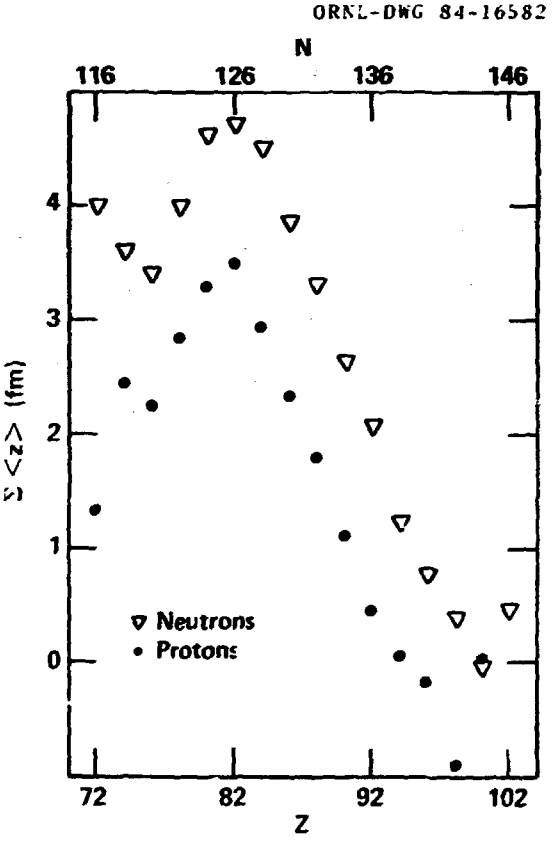

Fig. 5.20. A 'numerical experiment' which shows that single-particle effects on the E1 moment are neither random nor small. Single-particle states in a potential with fixed β_2 and β_3 are successively filled, and the accumulated <z> exhibits a coherent shell effect above the shell closures at Z = 82 and N = 126.

reveals another large contribution to the E1 moment which was not previously anticipated, namely, a single-particle shell effect at fixed $\beta_2\beta_3$. This shell effect must be Strutinsky renormalized to the liquid drop in a way that is consistent with the energy of the giant dipole resonance.[34] The E1 shell effect could account for a systematic dependence on nucleon number that is emerging from recent data, and the ambiguity mentioned above in the sign of the macroscopic contribution to the E1 moment would then be empirically resolved.[33]

High Spins

P. Arve[14] M. W. Guidry[16]
T. Bengtsson[7] G. A. Leander[1]
Y. S. Chen[15] W. Nazarewicz[7,8]
J. Dudek[4] P. Olanders[7]
S. Frauendorf[3] I. Ragnarsson[7]

The deformed shell-model-Bogoliubov-cranking theory was extended and explored for the case of reflection-asymmetric mean fields, as described in the previous section (c.f. Fig. 5.19).

Recent ORNL data on the yrast line of ^{158}Yb were found to have a remarkable interpretation in terms of a configuration-dependent cranking model.[35] Both the data and the model exhibit collective band structure with near-constant level spacings in the high-spin regime I=26-36, leading to collective angular momentum being generated much more efficiently than in well-deformed rotational nuclei like ^{168}Yb (Fig. 5.21). Above I = 36 there is an energy gap in

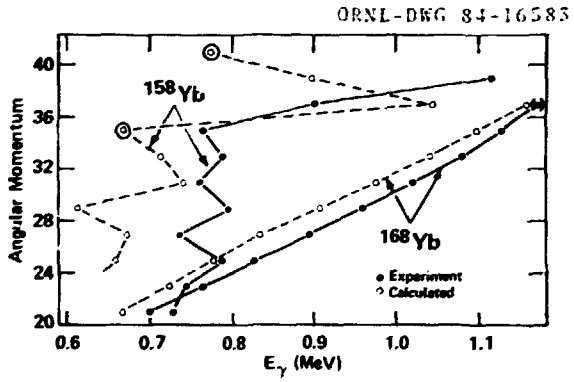

Fig. 5.21. Angular momentum versus E2 gamma-ray energy for theoretical (dashed) and experimental (solid) bands in ^{158}Yb and ^{168}Yb, respectively. The generation of collective angular momentum up to I = 36 is more energy efficient in transitional ^{158}Yb than in well-deformed ^{168}Yb. This results from a gradual shape transition followed by a band termination in ^{158}Yb.

the spectrum. In the model these features result from a gradual in-band transition from prolate shape at lower spins to a noncollective oblate state at I = 36 which terminates the collective band. Band terminations are commonplace in nuclei with only a few valence particles and also in the rotating harmonic oscillator model, but a band-terminating state had not previously been identified in experiment for such a large number of valence particles and such large angular momentum as in ^{158}Yb.

Several high-spin theory projects, such as the study of signature splitting[36] and the development of models for M1 radiation at high spin,[37] are unfortunately not being pursued in connection with ORNL at the present time, although warranted by the experimental situation.

Quasicontinuum Spectroscopy

T. Bengtsson[7] G. A. Leander[1]

The study of nuclear structure by means of the "quasicontinuum" of gamma rays which emanate from unresolved levels at very high spin and nonzero intrinsic excitation energy is a developing field. In particular, energy-energy correlations seem to contain valuable information, but both the extraction of the correlations from experimental data and the theoretical interpretation of ridge-valley structures are subject to controversy. An interesting finding has been that the ridge separations obtained in experiments on a sequence of nuclei around A=125 exhibit a systematic trend with nucleon number, which has a specific and semi-quantitative theoretical interpretation.[38,39] The data around ^{118}Xe indicate a dynamical moment of inertia $\mathcal{J}^{(2)}$ at high rotational frequencies that is well below the rigid-body estimate, whereas the data around $^{120}Ba_{72}$ give an effective $\mathcal{J}^{(2)}$ which increases up to or beyond the rigid-body value (Fig. 5.22). Previous cranking calculations suggested that the trend could be due to a well-deformed shape isomer which comes low in energy specifically around N=72. Configuration-dependent cranking calculations showed that the $\mathcal{J}^{(2)}$ values from the energy-energy correlations would indeed result if the decay pathways in the quasicontinuum resembled a representative sample of calculated near-yrast bands. More recently, the same kind of configuration-dependent cranking calculations were able to account for a cutoff in the quasicontinuum E2 spectrum of ^{158}Yb above ~800 keV.

Development has continued on a Monte Carlo code, GAMBLE, which provides a statistical model framework for the evaluation of quasicontinuum correlations. New technical and physical features have been incorporated which will be applied during the coming year to study structure-dependent aspects of the gamma cascade pathway.

---

1. UNISOR, Oak Ridge Associated Universities.
2. University of Arizona, Tucson, AZ 85721.
3. ZfK Rossendorf, Dresden, GDR.
4. Centre de Recherches Nucléaires, Strasbourg, France.
5. Texas Instruments, Dallas, TX.
6. Lawrence Livermore National Laboratory, Livermore, CA 94550.
7. Lund University, Lund, Sweden.
8. Technical University, Warsaw, Poland.
9. Los Alamos National Laboratory, Los Alamos, NM 87545.
10. Université de Bordeaux, Gradignan, France.
11. Georgia Institute of Technology, Atlanta, GA 30332.
12. KVI, Groningen, The Netherlands.
13. University of Warsaw, Warsaw, Poland.
14. NORDITA, Copenhagen, Denmark.
15. Institute of Atomic Energy, Beijing, China.
16. University of Tennessee, Knoxville, TN 37916.

17. G. A. Leander et al., Phys. Rev. C 30, 416 (1984).
18. G. A. Leander, P. B. Semmes, and F. Dönau, in "Interacting Boson-Boson and Boson-Fermion Systems," ed. by O. Scholten (World Scientific Publishers) in press.
19. P. B. Semmes, G. A. Leander, and J. L. Wood, ibid.
20. P. B. Semmes et al., current work.
21. G. A. Leander, Phys. Rev. Lett. 52, 311 (1984).
22. J. D. Cole et al., Phys. Rev. C 30, in press.
23. A. F. Barfield and B. R. Barrett, Phys. Lett. B, in press.
24. A. F. Barfield, current work.
25. B. D. Kern et al., Phys. Rev. C 28, 2168 (1983).
26. A. J. Larabee et al., Bull. Am. Phys. Soc. 29, 1049 (1984).
27. G. A. Leander, P. Möller, J. R. Nix, and W. M. Howard, Proc. Int. Conf. on Atomic Masses and Fundamental Constants, Darmstadt, 1984, in press.
28. G. A. Leander and R. K. Sheline, Nucl. Phys. A413, 375 (1984).
29. R. K. Sheline et al., Phys. Lett. 133B, 13 (1983).
30. W. Nazarewicz et al., Nucl. Phys. A, in press.
31. G. A. Leander, W. Nazarewicz, P. Olanders, I. Ragnarsson, and J. Dudek, to be published.
32. G. A. Leander, Ph. Quentin, and M. R. Strayer, current work.
33. G. A. Leander, in "Capture Gamma-Ray Spectroscopy and Related Topics," ed. by S. Raman (AIP Conference Series) in press.
34. G. A. Leander and G. F. Bertsch, current work.
35. I. Ragnarsson et al., to be published.
36. Y. S. Chen, S. Frauendorf, and G. A. Leander, Phys. Rev. C 28, 2437 (1983).
37. P. Arve, Y. S. Chen, and G. A. Leander, Physica Scripta T5, 157 (1983).
38. H. El-Samman et al., Proc. Int. Symp. on In-Beam Nuclear Spectroscopy, Debrecen, Hungary (Akadémiai Kiadó, Budapest) in press.
39. H. El-Samman et al., in press.

ACCIDENTAL DEGENERACIES AND DYNAMICAL SUPERSYMMETRIES[1]

A. B. Balantekin[2]

Recently, several Hamiltonians appeared in the literature[3] for which energy levels exhibit a degeneracy which cannot be associated with the known symmetry groups. We consider the two Hamiltonians motivated by the nuclear shell model

$$H = \frac{1}{2}(\vec{p}^2 + \vec{r}^2) + \lambda(\vec{\sigma}\cdot\vec{L} + 3/2) \qquad (1)$$

and

$$H = \frac{1}{2}(\vec{p}^2 + \vec{r}^2) + \frac{1}{2r^2} + \lambda\,\vec{\sigma}\cdot\vec{L} + \frac{3}{8r^2}. \qquad (2)$$

For the first Hamiltonian when we fix j, there is a degeneracy for the two cases $\lambda = +1$, $\ell = j+1/2$, and $\lambda = -1$, $\ell = j-1/2$. For the second Hamiltonian, the degeneracy is between $\lambda = +1$, $j = \ell+1/2$, and $\lambda = -1$, $j = \ell-1/2$ with ℓ fixed. It is shown that the degeneracy of such

ORNL-DWG 84-16476

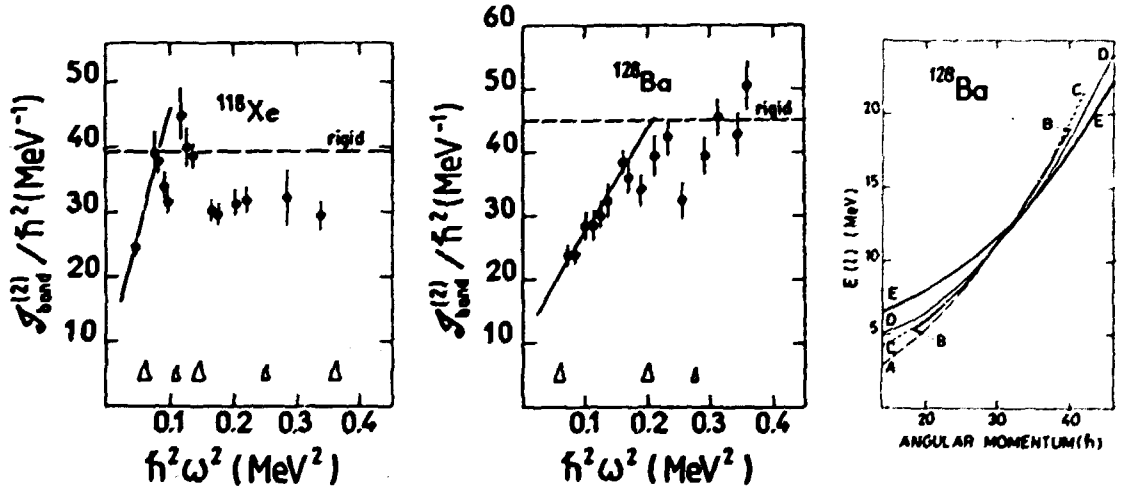

Fig. 5.22. These data for ^{118}Xe and ^{128}Ba provide some of the first evidence for connection between nuclear structure calculations at high spins and the dynamical moments of inertia, $\mathcal{J}^{(2)}$, derived from quasicontinuum energy-energy correlations at high rotational frequencies. The continued rise of $\mathcal{J}^{(2)}$ in ^{128}Ba could reflect an increasing population in bands of type E at high spins. Such bands are predicted in $^{128}Ba_{72}$ but not in $^{118}Xe_{64}$ due to a shell effect around N = 72.

Hamiltonians is due to an underlying supersymmetric quantum-mechanical structure, i.e., H can be written as an anticommutator of a fermionic conserved charge, Q, with its Hermitian conjugate, $Q^\dagger$

$$H = \frac{1}{2}\{Q, Q^\dagger\} \qquad (3)$$

To study such systems, spectrum-generating superalgebras are introduced and developed. In this context, one-parameter realization of the relevant noncompact superalgebras Osp(1/2) and Osp(2/2) are worked out. In both cases, the anticommuting charges are identified with the fermionic generators of the superalgebra Osp(2/2). The Hamiltonians (1) and (2) with $\lambda = +1$ and $\lambda = -1$ can be written together as

$$H = 2(K_0 + Y), \qquad (4)$$

where K_0 is the diagonal element of the subalgebra Sp(2) which acts on the bosonic subspace, and Y is the element of the subalgebra SO(2) which acts on the fermionic subspace.

Two-parameter realizations of Osp(2/2), which are potentially useful in nuclear and molecular physics, are currently under investigation.

---

1. Summary of paper submitted to Annals of Physics.
2. Eugene P. Wigner Fellow.
3. M. Moshinsky and C. Quesne, Ann. Phys. 148, 462 (1983); H. Ui and G. Takeda, Tohoku University preprint (1984).

CHARACTER EXPANSIONS FOR UNITARY GROUPS

A. B. Balantekin[1]

Character expansion techniques are used to calculate certain integrals, appearing in lattice gauge theories, to investigate the role of internal symmetries in certain high-energy reactions, to impose the colorlessness condition in the calculation of a quark-gluon gas, to calculate the partition functions in the statistical theory of nuclear reactions, and to calculate the level density of a spherical nucleus as a function of angular momentum. A very general formula was presented to generate expansions over U(N) characters.[2] We start from the power series expansion

$$G(x;t) = \sum_{n=0}^{\infty} A_n(x) t^n \qquad (1)$$

where we normalize $A_0 = 1$. Taking t_i, $i=1,\ldots,N$ to be the eigenvalues of the fundamental representation matrix U of U(N), we get the following character expansion

$$\left(\prod_{i=1}^{N} G(x;t_i)\right) = \sum_{n_1 \geq n_2 \geq \ldots \geq n_N} \det\left\{A_{n_j+i-j}\right\}(x) \, \chi_{[n_1 n_2 \ldots n_N]}(U) \qquad (2)$$

where $[n_1, n_2, \ldots, n_N]$ is the partition labeling the representations of U(N), $\chi_{[n_1,n_2,\ldots,n_N]}(U)$ is the character of the representation $[n_1, n_2, \ldots, n_N]$ and the ij-th element of the matrix, whose determinant is calculated, is shown.

The possible uses of this formula in lattice gauge theories and also in the statistical mechanical systems are currently under investigation.

---

1. Eugene P. Wigner Fellow.
2. A. B. Balantekin, J. Math. Phys. 25, 2028 (1984).

RELATIVISTIC HEAVY-ION PHYSICS

INITIAL ENERGY DENSITY OF QUARK-GLUON PLASMA IN RELATIVISTIC HEAVY-ION COLLISIONS[1]

Cheuk-Yin Wong

We estimate the initial rapidity distribution and the initial energy density in the central rapidity region of relativistic heavy-ion collisions by using a multiple-collision model and the nuclear-thickness function of Glauber. The parameter of the rapidity distribution is determined from the experimental multiplicity data of pα, dd, αα, pA, π^+A, K^+A, Si+Ag, and Ca+C reactions. We find that the initial energy density in the central rapidity region is high. For example, for the head-on collision of ^{238}U on ^{238}U at 30 GeV per nucleon in the center-of-mass system, the maximum energy density is about 10 GeV/fm^3, which may exceed the critical energy density for a phase transition from a confined hadron matter to an unconfined quark-gluon plasma. The initial energy density goes as $A^{1/3}B^{1/3}$ for the collision of two nuclei with mass numbers A and B, and is rather insensitive to impact parameters.

---

1. Abstract of paper: Phys. Rev. D 30, 961 (1984).

BARYON DISTRIBUTION IN ULTRA-RELATIVISTIC HEAVY-ION REACTIONS[1]

Cheuk-Yin Wong

Recent experimental results of high-energy nucleon-nucleus collisions reveal that a nucleon loses a large fraction of its energy in passing through a nucleus.[2] In high-energy nucleus-nucleus collision this energy loss may give rise to a substantial density of baryons in the central rapidity region.

In order to determine whether a pure quark-gluon plasma with no net baryon density can be formed in the central rapidity region in relativistic heavy-ion collisions, we estimate the baryon distribution by using a Glauber-type multiple-collision model in which the nucleons of one nucleus degrade in energy as they make collisions with nucleons in the other nucleus. As a test of this model, we study first nucleon-nucleus collisions at 100 GeV/c and compare the theoretical results with the experimental data of Barton et al.[3] The results are then generalized to study the baryon distribution in nucleus-nucleus collisions. It is found that in the head-on collision of two heavy nuclei ($A \geq 100$), the baryon rapidity distributions have broad peaks and extend well into the central rapidity region. The energy density of the baryon in the central rapidity region is about 5-6% of the total energy density at a center-of-mass energy of 30 GeV per nucleon and decreases to about 2-3% at a center-of-mass energy of 100 GeV per nucleon. The stopping power for a baryon in nuclear matter is extracted.

---

1. Summary of papers: Phys. Rev. Lett. 52, 1393 (1984) and Phys. Rev. D 30, 972 (1984).
2. W. Busza and A. S. Goldhaber, Phys. Lett. 139B, 235 (1984).
3. D. S. Barton et al., Phys. Rev. D 27, 2580 (1983).

NUCLEON-NUCLEUS REACTIONS AT ULTRA-RELATIVISTIC ENERGIES[1]

Cheuk-Yin Wong

In order to discern coherent processes from incoherent processes in nucleon-nucleus reactions at high energies, we study these reactions with an incoherent multiple collision model. In this model, the projectile nucleon makes successive inelastic collisions with nucleons in the target nucleus, the probability of such collisions being given by the thickness function and the nucleon-nucleon inelastic cross section. It is assumed that each baryon-baryon collision produces particles and degrade momenta just as a baryon-baryon collision in free space, and that there are no secondary collisions between the produced particles and the nucleons. We found that the inelastic proton data, the pseudo-rapidity distribution data $dN^{pA}/d\eta$, and the total nucleon-nucleus absorption data can be well explained by the incoherent multiple collision model. However, the single-particle fragmentation data for nonleading particles indicate that there is a reduction of the fragmentation cross section because of subsequent collisions of the leading baryon along the collision chain. Modification of the incoherent multiple collision model is suggested. The modified model gives cross sections for the reactions $pA \to \pi^+X$, $pA \to \pi^-X$, $pA \to K^+X$, $pA \to K^-X$, and $pA \to pX$ in the projectile fragmentation region in good agreement with experiment.

---

1. Abstract of paper submitted to Physical Review.

THE HYDRODYNAMIC PHASE IN ULTRA-RELATIVISTIC HEAVY-ION COLLISIONS

M.-C. Chu[1]

In recent years, there has been considerable interest in the subject of high-energy heavy-ion collisions, a major reason being that it offers the possibility of creating extended regions of extremely high-energy density. In fact, the energy density achievable may be high enough to carry matter through the deconfinement phase transition, thus forming a quark-gluon plasma.[2-6] Such an exotic state of matter is believed to simulate the conditions in the early universe and possibly in the interior of gravitationally collapsing astrophysical objects such as supernovae. The physics of quark-gluon plasma therefore interests not only nuclear and particle physicists but also astrophysicists as well.

If a quark-gluon plasma is indeed formed in ultra-relativistic heavy-ion collisions, all the quanta excited in the plasma will rapidly come into local thermal equilibrium, and a hydrodynamical description of the system will be valid. It is of interest to study the hydrodynamic evolution of a cylindrically symmetric quark-gluon plasma as formed in a central collision of two identical heavy ions.

At high enough energies, two nuclei in a central collision will pass through each other, producing three regions in phase space: the target fragmentation region (TFR), the projectile fragmentation region (PFR), and the central rapidity region (CRR). The TFR and PFR contain most of the net baryon number of the system and continue receding away from each other at close to the speed of light after the collision. In between TFR and PFR is the CRR with almost zero net baryon number but very high-energy density. Bjorken[2] has given a rough sketch of the space-time evolution of the CRR; immediately after the collision, particles will be only weakly interacting and undergo free streaming. Local thermal equilibrium will be established by a later proper time $\tau_0 \sim 1$ fm/c, and the subsequent hydrodynamic expansion of the plasma will then be determined by the initial conditions specified at $\tau = \tau_0$ and the laws of hydrodynamics. Further, assuming the existence of a central

plateau structure in the inclusive particle production versus rapidity, Bjorken argues that the CRR obeys Lorentz-invariant boundary conditions. In particular, this means a uniform initial energy density, ϵ_0, and a scaling form of the initial longitudinal velocity, $v_z = z/t$.

The laws of relativistic hydrodynamics can be derived from

$$\partial_\mu T^{\mu\nu}(x) = 0,$$

with the stress-energy tensor

$$T^{\mu\nu} = (\epsilon+P)u^\mu u^\nu - Pg^{\mu\nu},$$

neglecting viscous and transport terms. Here ϵ is the local energy density, P the pressure, $g^{\mu\nu}$ the metric tensor, and u^μ the four-velocity of the fluid.

Effective one-dimensional motion of the quark-gluon plasma with the above initial conditions has been investigated by Baym et al.[7] In the limit of an infinitely long cylinder of plasma, these calculations show that the predominantly longitudinal initial expansion is later modified by the transverse expansion. To study the more realistic case of a finite cylinder, a two-dimensional calculation is therefore necessary. Specializing to cylindrical coordinates, we obtain the following set of equations:

$$\frac{\partial}{\partial t}\left[(\epsilon+P)\gamma^2 - P\right] + \frac{1}{r}\frac{\partial}{\partial r}\left[r(\epsilon+P)\gamma^2 v_r\right] + \frac{\partial}{\partial z}\left[(\epsilon+P)\gamma^2 v_z\right] = 0 \tag{1a}$$

$$\frac{\partial}{\partial t}\left[(\epsilon+P)\gamma^2 v_z\right] + \frac{1}{r}\frac{\partial}{\partial r}\left[r(\epsilon+P)\gamma^2 v_r v_z\right] + \frac{\partial}{\partial z}\left[(\epsilon+P)\gamma^2 v_z^2 + P\right] = 0 \tag{1b}$$

$$\frac{\partial}{\partial t}\left[(\epsilon+P)\gamma^2 v_t\right] + \frac{1}{r}\frac{\partial}{\partial r}\left\{r\left[(\epsilon+P)\gamma^2 v_t^2 + P\right]\right\} + \frac{\partial}{\partial z}\left[(\epsilon+P)\gamma^2 v_t v_z\right] = 0. \tag{1c}$$

Here, $v_t(v_z)$ is the flow velocity perpendicular (parallel) to the collision axis. We shall use the equation of state for a relativistic ideal gas, $P = \epsilon/3$, which is shown by lattice Monte Carlo calculations[8,9] to be a good approximation at temperatures above the critical temperature of the hadronization transition. The Stefan-Boltzmann law relates ϵ to temperature, T,

$$\frac{\epsilon}{\epsilon_0} = \left[\frac{T}{T_0}\right]^4,$$

where T_0 is the initial temperature.

Two methods to solve Eqs. (1) have been tried. The first one utilizes a finite element method in the r-z plane and propagates with a fourth-order predictor-corrector method in time. In the second method, we rewrite Eq. (1) with the equation of state in a form resembling a Schroedinger equation and then solve the equations with the Peaceman-Rachford method.[10] Both methods are stable up to a time much later than when the temperature drops to the critical temperature for hadronization.

Preliminary results from these calculations show that the quark-gluon plasma, if formed in an ultra-relativistic heavy-ion collision, cools down very rapidly. For the head-on collision of ^{238}U on ^{238}U, the energy density in the plasma will be lowered from ϵ_0(~ 5 GeV/fm^3) (Ref. 6) to 2 GeV/fm^3, when hadronization is expected to start, after only about 1 fm/c. While the rate of cooling at z = 0 is found to agree with Baym's calculations, that at the ends of the cylinder is modified by a 'pile-up' effect, resulting in slower cooling at large z. Because of the rapid longitudinal expansion, the effect of the transverse expansion is very small prior to hadronization. The behavior of the system is also studied as a function of the highly uncertain parameter τ_0. We found that the expansion of the plasma slows down and becomes more uniform as the parameter τ_0 is increased. Evolution of the system after the onset of hadronization is an important problem which requires further study.

---

1. Guest assignee from California Institute of Technology, Pasadena, CA 91125, June-August, 1984.

2. J. D. Bjorken, Phys. Rev. D 27, 140 (1983).
3. R. Anishetty, P. Koehler, and L. McLerran, Phys. Rev. D 22, 2793 (1980).
4. L. McLerran, in Quark Matter Formation and Heavy-Ion Collisions, Proc. Bielefeld Workshop, ed. M. Jacob and H. Satz (World Scientific, Singapore, 1982), p. 63.
5. K. Kajantie, in Quark Matter Formation and Heavy-Ion Collisions, Proc. Bielefeld Workshop, ed. M. Jacob and H. Satz (World Scientific, Singapore, 1982), p. 39.
6. C. Y. Wong, Oak Ridge National Laboratory preprint, 1984.
7. G. Baym et al., Nucl. Phys. A407, 541 (1983).
8. J. Engels, F. Karsch, I. Montvay, and H. Satz, Nucl. Phys. B205 [FS5], 545 (1982).
9. I. Montvay and E. Pietarinen, Phys. Lett. 110B, 148 (1982).
10. R. Varga, Matrix Iterative Analysis (Prentice-Hall, Englewood Cliffs, 1962), p. 273.

THEORETICAL ATOMIC PHYSICS

MULTIPLE-VACANCY PRODUCTION IN THE INDEPENDENT-FERMI-PARTICLE MODEL[1]

R. L. Becker A. L. Ford[2]
J. F. Reading[2]

Measurements of K x-ray (or Auger) satellite intensities produced by ion impact have yielded

K^kL^v multiple-vacancy distributions which in most cases are nearly binomial. This implies that, statistically, the holes are nearly independent, which is surprising in view of the known influence of correlations on other collision processes. We give a detailed derivation of general expressions for ion-induced multiple-vacancy distributions in the independent-Fermi-particle collision model, based on the Hartree-Fock description of the target, which contains Pauli correlations. Our coupled-channels calculations employing these expressions have shown that the electron exchange terms tend to mutually cancel because of "random" phases, but need not cancel when a single channel, such as a resonant electron capture, is dominant.

---

1. Abstract of paper: Phys. Rev. A 29, 3111 (1984).
2. Texas A & M University, College Station, TX 77843.

INCLUSION OF ELECTRON TRANSFER IN THE CALCULATION OF K^kL^v MULTIPLE VACANCY PRODUCTION BY ION IMPACT[1]

R. L. Becker A. L. Ford[2]
J. F. Reading[2]

Measurements of K x-ray or Auger satellite (and hypersatellite) intensities provide information on KL^v (and K^2L^v) hole production in close collisions of ions with atoms. The L-shell vacancy distributions usually are nearly binomial. This distribution is specified by a single parameter, $\bar{p}_L$, the mean L-shell vacancy probability per electron, which can depend on the speed v, the nuclear charge Z_p and the ionic charge q of the projectile, and on the nuclear charge Z_T of the target. Almost all calculations of $\bar{p}_L$, aside from our work,[3-5] have been limited to first-order collision approximations. Moreover, all such calculations have included only impact ionization and, consequently, have neglected electron transfer to the projectile. The first-order calculations have had enough success for proton and alpha-particle impact to remain in vogue for a decade, but they predict that p_L is proportional to Z_p^2, whereas $\bar{p}_L$ must remain <1, which requires a unitary collision approximation. We have obtained the "saturation" of $\bar{p}_L$ with Z_p in two unitary schemes, the first Magnus approximation, and the more refined coupled-channels approximation.[4,5] In both schemes we used a single-centered expansion (SCE) in spin-orbitals representing bound and unbound states of the target. Typically, we employ ten radial functions for each of four angular momenta (s, p, d, and f states).

The SCE provides an accurate basis for asymmetric systems ($Z_p \ll Z_T$), but becomes inaccurate for nearly symmetric systems at intermediate energies for which electron transfer to the projectile is very probable. A full coupled-channel calculation with a two-center expansion (TCE) is still prohibitive for many-electron systems. We have previously developed an intermediate unitary scheme, referred to as the one-and-a-half center expansion (OHCE), which has been applied to light systems.[6] It includes electron transfer (so far, only to the 1s state) along with electron emission. We have now used the OHCE for calculations of inclusive K- and L-subshell vacancy cross sections and of $\bar{p}_L$ in F^{9+} + Ne collisions. Values at impact energy 1.5 MeV/amu are given in the table. The K-vacancy cross section is increased by 67%, but the L-shell vacancy cross section at this high energy ($v/v_L = 6.7$) is hardly changed by charge transfer.

Because the experimental L-shell vacancy distributions, $P(KL^v)$, for F^{9+} + Ne (Ref. 7) deviate strongly from the binomial at intermediate impact speeds, a multiple-vacancy theory which includes hole-hole correlations is required. We have developed such a theory[3,5,8] based on the independent-Fermi-particle model (IFPM), which includes Pauli correlations. We have calculated the effects of electron transfer on the deviations from the binomial distribution for $P(KL^v)$ for F^{9+} + Ne. It turned out that the charge transfer from the K-shell to the fluorine K-shell does not cause much deviation from binomial. The variance is given in Table 5.1. It remains to be seen what effect transfer to the

Table 5.1. Comparison of coupled-channels calculations of vacancy production with and without inclusion of charge transfer (C.T.) to the projectile K-shell: F^{9+} + Ne at 1.5 MeV/amu. Inclusive vacancy-production cross sections, σ_i in 10^{-20} cm^2. K x-ray satellite (j=1) and hypersatellite (j=2) information: (1) mean L-shell vacancy probability per electron, $\bar{p}_L^{(j)}$; (2) ratio, $R^{(j)}$ of IFPM to binomial variance (both from distributions with the IFPM value of $\bar{p}_L^{(j)}$).

	Without C.T.	With C.T.
σ_K	0.086	0.144
σ_{2s}	2.337	2.381
σ_{2p0}	7.831	7.966
$\sigma_{2p\pm1}$	7.038	7.058
σ_L	24.245	24.465
$\bar{p}_L^{(1)}$	0.759	0.754
$\bar{p}_L^{(2)}$	0.781	0.799
$R^{(1)}$	0.976	0.939
$R^{(2)}$	0.832	0.863

L-shell might have. Work has begun on that problem.

---

1. Summary of paper presented at "X84," the International Conference on X-Ray and Inner-Shell Processes in Atoms, Molecules and Solids, Leipzig, Aug. 20-24, 1984. See X84 Abstracts, p. 41.
2. Texas A & M University, College Station, TX 77843.
3. R. L. Becker, A. L. Ford, and J. F. Reading, Nucl. Instr. Meth. 214, 49 (1983).
4. R. L. Becker, A. L. Ford, and J. F. Reading, Nucl. Instr. Meth. B3, 43 (1984).
5. R. L. Becker, A. L. Ford, and J. F. Reading, Nucl. Instr. Meth. B4, 271 (1984).
6. J. F. Reading, A. L. Ford, and R. L. Becker, J. Phys. B: Atom. Mol. Phys. 14, 1995 (1981); ibid. 15, 3257 (1982); A. L. Ford, J. F. Reading, and R. L. Becker, ibid. 15, 3257 (1982).
7. R. L. Kauffman, C. W. Woods, K. A. Jamison, and P. Richard, Phys. Rev. A 11, 872 (1975).
8. R. L. Becker, A. L. Ford, and J. F. Reading, Phys. Rev. A 29, 3111 (1984).

THEORY OF MULTIPLE L-SHELL VACANCY PRODUCTION IN COINCIDENCE WITH ELECTRON TRANSFER[1]

R. L. Becker

Coincidence measurements of the final ionic charges of both the projectile and the target provide a clean separation between reactions involving, or not involving, charge transfer. Figure 5.23 shows such cross sections for H^+ + Ne.[2] They are dominated by L-shell processes. Each cross section is labeled by two or three subscripts. The first two are the initial and final ionic charges of the projectile. A third subscript signifies the final number of vacancies, v, in the target. The single-charge-transfer cross section with v L-shell vacancies can be calculated in the impact-parameter formalism, with the assumption that the transfer is to the K-shell of the projectile ($\overline{K}$) by

$$\sigma_v \equiv \sigma^{\overline{K},Lv}_{\overline{K},L^v} = 2\pi \int_0^\infty dB\, B\, P^{\overline{K},L^{8-v}}_{\overline{K},L^v}(B)$$

where superscripts label final occupancies and subscripts, final nonoccupancies. In the independent-Fermi-particle model (IFPM) the "number-exclusive hyperinclusive" (NEHI) probability in the integrand is given by an expression similar to that[3] for $P^{K,L^{8-v}}_{K,L^v}(B)$, appropriate for K_α satellites. Figure 5.23 contains coupled-channels values at E = 75 and 100 keV for σ_{10v}, v = 1,2,3 and their sum σ_{10}. The probability for v = 0, $P^{\overline{K},L^8}_{\overline{K},L^0}(B)$, is essentially zero in the IFPM. (There is a very small contribution from transfer from the K-shell.)

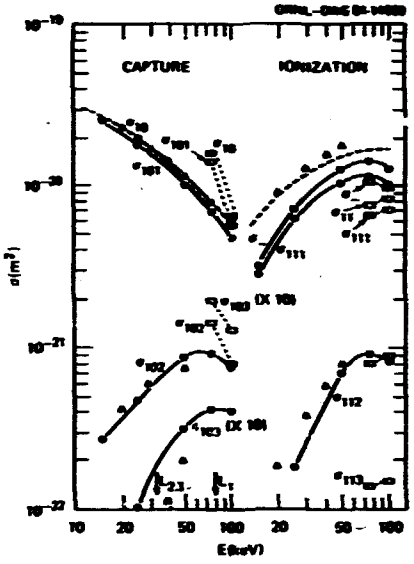

Fig. 5.23. Cross sections for the electron-capture and direct ionization channels in H^+ + Ne collisions. The data and curves through them are taken from Fig. 2a of Ref. 2. The open rectangles give OBCE-IFPM-coupled-channels values. The subscripts are defined in the text.

Figure 5.24 gives the binomial and IFPM distributions, $P^{K,L^{8-v}}_{K,L^v} \equiv \sigma_v \Big/ \sum_{v'=0} \sigma_{v'}$. The Pauli correlations of the IFPM permit the suppression of

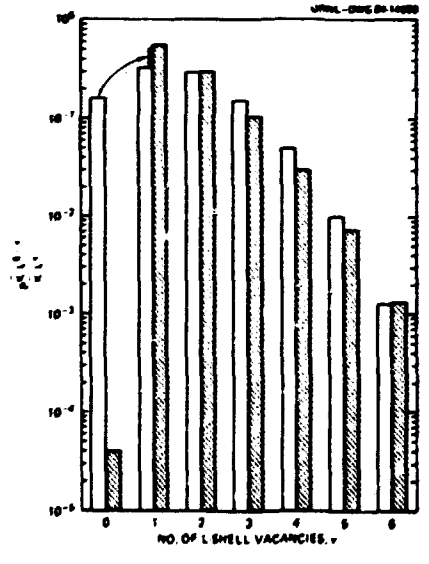

Fig. 5.24. L-shell vacancy distributions (integrated over the impact parameter) for single charge transfer in H^+ + Ne collisions at 100 keV. Shaded, IFPM calculations, unshaded, binomial distribution with the IFPM value of $\overline{p}_L$.

the v=0 components, in agreement with experiment. These measurements and IFPM calculations show for the first time a strikingly nonbinomial vacancy distribution explainable by Pauli correlations. Data and calculations[1] for $He^+ + Ne$ show the same features.

A more complicated coincidence experiment could measure the L-shell vacancy distribution for collisions in which there is a charge transfer to the $\bar{K}$-shell and also a K vacancy. Rødbro et al.[4] have, in fact, done this for the no-L-shell-vacancy case, v = 0, by resolving the diagram line in neon under He^{2+} impact. With Li^{3+} the diagram line was barely seen. Only a little more resolution would be needed to separate the satellites with various numbers of L-shell vacancies. The theory of such an experiment would involve the MEHI $p^{\bar{K},K,L^{8-v}}_{\bar{K},K,L^{v}}(8)$. It is now being evaluated.

---

1. A more extended discussion is given in Section 4.2 of R. L. Becker, "Multiple Vacancy Production by High Energy Heavy Ions," invited paper at the Second Workshop on High-Energy Ion-Atom Collision Processes, Aug. 27-28, 1984, Debrecen, Hungary, to be published (Akadémiai Kiadó, Budapest).

2. R. D. DuBois, Phys. Rev. Lett. 52, 2348 (1984).

3. R. L. Becker, A. L. Ford, and J. F. Reading, Phys. Rev. A 29, 3111 (1984).

4. M. Rødbro, E. Horsdal-Pedersen, C. L. Cocke, and J. R. Macdonald, Phys. Rev. A 19, 1936 (1979).

COLLISIONAL VACANCY-REARRANGEMENT IN THE FIRST MAGNUS AND COUPLED-CHANNELS COLLISION THEORIES[1]

R. L. Becker

Measurements of L-subshell cross sections in gold and neighboring heavy elements have shown variations with projectile charge, Z_p, and speed, v, which are not explained by first-order theories with higher-order corrections for Coulomb deflection of the projectile and increased binding of the electrons and polarization of their wave functions during the collision. Sarkadi and Mukoyama[2] took into account the collisional transfer of L-shell vacancies, from one subshell to another by a second interaction with the projectile, in a two-step model. They employ quantum-mechanical collision amplitudes to obtain probabilities for inclusive L-subshell ionizations and for excitations (transfers) from one subshell to another. But they combine these probabilities in a completely classical way in a set of kinetic equations. Calculations with the model did reproduce the decrease of $\sigma_{L_3}/\sigma_{L_2}$ with increasing Z_p at low v/v_{L_3}, but did not reproduce the ratio $\sigma_{L_1}/\sigma_{L_2}$, nor the alignment parameter $\mathcal{A}_{20}$ of the L_3 subshell.

We show that in the fully quantum-mechanical, unitary, first Magnus approximation, in semiclassical collision theory one finds collisional-vacancy-rearrangement terms analogous to those of the two-step model. It also contains nonclassical terms, which cannot be expressed as products of probabilities. We give results of numerical calculations for argon, in the first Magnus and in the coupled-channels approximation, which illustrate the deviations from first-order values of both ratios of subshell cross sections and $\mathcal{A}_{20}$. At the relatively low-impact speeds of interest, charge transfer can be important. We have begun calculations with our one-and-a-half-center version of coupled-channels theory to exhibit the effects of electron transfer.

---

1. Summary of paper: Proceedings of the Second Workshop on High-Energy Ion-Atom Collision Processes, Aug. 27-28, 1984, Debrecen, Hungary, to be published (Akadémiai Kiadó, Budapest).

2. L. Sarkadi and T. Mukoyama, J. Phys. B14, L255 (1981).

DEPENDENCE OF ION-RYDBERG ATOM CROSS SECTIONS ON THE ORIENTATION OF THE RYDBERG STATE

R. L. Becker A. D. MacKellar[1]

Classical trajectory Monte Carlo (CTMC) calculations have proved very useful and surprisingly accurate in estimating cross sections for collisions of charged particles (ions and electrons) with electrons in high Rydberg states. Aside from our work, the calculations have been for classical ensembles corresponding to complete n-shells. However, preparation of Rydberg states by multiphoton absorption allows for the selection of the ℓ value. We have derived[2] subensembles of the microcanonical hydrogenic ensemble which correspond to Rydberg states of given (n,ℓ) or given (n,ℓ,m). Results for the dependence of charge transfer, ionization, and excitation cross sections on the initial ℓ value have been published.[3] The dependence of the charge transfer cross section on the initial m value is even more striking.[4]

Figure 5.25 shows the CTMC charge transfer cross section for $H^+ + Na^*(n=28)$ with $\ell = 2$ and 27. Each m value corresponds to a classical range of values of a second Euler angle, θ. For $m = 0$ the range ends at $\theta = \pi/2$, while for $m = \ell$ the range ends at $\theta = 0$. The figure shows also cross sections for specified values of (ℓ,θ) and of $(\ell,|m|)$. For $\ell = 27$, specific m values correspond to such small intervals of θ that one value of θ in the interval represents m quite well. For $\ell = 2$, $\theta = \pi/2$ ceases to represent adequately $m = 0$, and $\theta = 0$ does not represent $m = 2$ sufficiently well. Notice that for the nearly circular orbits ($\ell = 27$) the ratio $\sigma(m=0)/\sigma(m=27)$ exceeds an order of magnitude at high-impact speeds.

1. University of Kentucky, Lexington, KY 40506.
2. R. L. Becker (unpublished).
3. R. L. Becker and A. D. MacKellar, J. Phys. B 17, 3923 (1984).
4. A. D. MacKellar and R. L. Becker, 13th ICPEAC (Berlin, 1983) Abstracts, p. 660; R. L. Becker and A. D. MacKellar, Bull. Am. Phys. Soc. 29, 795 (1984).

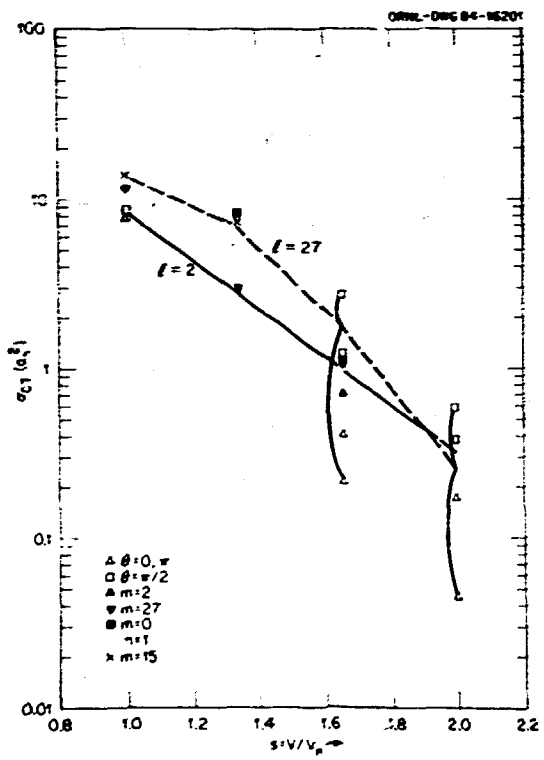

Fig. 5.25. CTMC charge transfer cross section for $H^+ + Na^*(n=28,\ell,m)$ in units of $a_n^2 = n^4 a_0^2$ versus scaled impact speed $s = v/v_n$ where $v_n = v_0/n$. The full (dashed) curve is for $\ell=2(27)$ and a uniform weighting of m values. Points: Δ, $\theta=0,\pi$; □, $\theta=\pi/2$; ▲, m=2; ▼, m=27; ■, m=0; +, $|m| = 1$; x, m=15.

NUMERICAL SOLUTION OF THE TIME-DEPENDENT DIRAC EQUATION[1]

C. Bottcher M. R. Strayer

A wide range of problems in atomic, nuclear, and particle physics can be reduced to the numerical solution of systems of relativistic fermion wave equations, possibly coupled via fields. We have developed a direct numerical method of propagating solutions of the Dirac equation in time, with particular application to electron-positron pair production in heavy-ion collisions. Our formulation contains a unified description of dynamical and spontaneous particle production, which have hitherto been treated as separate phenomena. We can also display pictures of the wavefunction to assist the interpretation of various physical phenomena.

It is generally accepted that electron-positron pairs should be excited from the vacuum in low-energy collisions of ions having a combined nuclear charge ≥ 173.[2] "Electrodynamic" positrons have indeed been observed;[3] the most striking feature of these emission spectra is the presence of sharp lines which suggest the formation of long-lived nuclear complexes.[4]

Calculation of positron spectra requires that probabilities be calculated for the following single-particle processes: creation of a K-shell vacancy, e.g.,

$$U^{q+} + Cm^{n+}(1s^2) \rightarrow U^{q+} + Cm^{(n-1)+}(1s) + e^-(E') \quad (1)$$

and excitation of an electron from the Dirac sea into the same vacancy

$$U^{q+} + Cm^{(n-1)+}(1s) + e^-(E < -mc^2) \rightarrow U^{q+} + Cm^{n+}(1s^2) \quad (2)$$

The net outcome is the creation of an electron-positron pair with energies $(E', -E)$, respectively. Given the nuclear trajectory, both probabilities are determined from the solutions of the time-dependent Dirac equation for the motion of a single electron.

Since pair production occurs at very small internuclear separations (<100 fm), we are justified in using a monopole approximation to the two-center electrostatic potential. The wavefunction then reduces to a two-component spinor, whose components depend on a single radial coordinate r (as well as time). These components are discretized by expanding in finite elements. Most of our calculations are performed with 85 elements distributed nonuniformly over the interval $r = (0, 12\alpha\ a_0)$, about one-third being inside the target nucleus. Propagation in time was achieved using a (1,1) Padé approximant to the evolution operator over a small time interval.

To obtain results, we have had to introduce several novel numerical techniques: (1) When the collision is complete, transition probabilities are computed by projecting on eigenstates of the final-state Hamiltonian in the finite element basis. (2) The accuracy of the solution at each time is controlled by iterated matrix inversion. (3) Fermion doubling (the pathological appearance of high momentum components at low energies) must be removed to calculate reliable transition probabilities; we have achieved this by modifying the matrix representation of the kinetic energy operator.

As a first test of the method, we calculated the probability P_K of ejecting a K-shell electron from Pb in a collision with Sm at a bombarding energy of 5.7 MeV/amu. The variation of P_K with impact parameter[2] is reasonable.

We next considered a U+Cm collision at 6.05 MeV per particle with no nuclear time delay (T=0), and with a long time delay (T=50 α^2 t_0, $t_0 = 2.42 \times 10^{-17}$ s). We denote the transition probabilities from the initially occupied $1s_{1/2}$ orbital to the positive and negative continua by P_{e-},P_{e+}: Figs. 5.26(a) and (b) show how P_{e-},P_{e+} evolves during the collision with and without a nuclear time delay. We note that one consequence of the delay is to increase the flux of emitted positrons and decrease the flux of emitted electrons. The effect of the delay on the wavefunction is shown in Figs. 5.26(c) and (d). The localized state in 5.26(c) decays into the outgoing waves seen to the right in Fig. 5.26(d).

We have investigated the dependence of the energy spectra of the ejected electrons and positrons on a nuclear time delay T. Figures 5.27(a)-(d) show that regular oscillations in the positron spectra are characteristic of short time delays, and that for $T > 10\ \alpha^2\ t_0$ these are superseded by a sharp peak. The total positron probability grows approximately linearly, reaching a value 0.28 when the time delay $T = 50\ \alpha^2\ t_0$, and thereafter does not change appreciably as T is increased. The width of the peak decreases as T increases and reaches a limiting value of 90 keV due to the finite extent of the finite element lattice; the position of the peak for this case is constant at 2.23 mc^2 regardless of T. In Fig. 5.26(d) we also indicate the position of the peak in head-on U+Pu collisions (1.90 mc^2) at about the same bombarding energy, and in U+Cm collisions at an impact parameter b = 19 fm (1.58 mc^2).

---

1. Summary of paper submitted to Physical Review Letters.

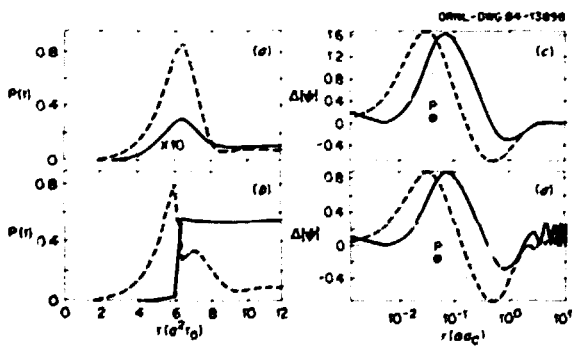

Fig. 5.26. U+Cm head-on collision at a bombarding energy of 6.05 MeV per particle. (a), (b): time evolution of the positron (full line) and electron (dotted line) in the finite element basis with and without a time delay of $T = 50\ \alpha^2\ t_0$ occurring at $t = 6\ \alpha^2\ t_0$. (c) and (d) shows the change in the modulus of the $1s_{1/2}$ wavefunction vs. the distance from the target nucleus before and after a time delay of $T = 50\ \alpha^2\ t_0$; full and dotted lines refer to the small and large wavefunction components G and F; P denotes the position of the projectile nucleus.

2. "Quantum Electrodynamics of Strong Fields," ed. W. Greiner, Plenum Press, New York, 1983.

3. J. Schweppe, et al., Phys. Rev. Letts. 51, 2261 (1983); M. Clemente, et al., Phys. Letts. 137B, 41 (1984).

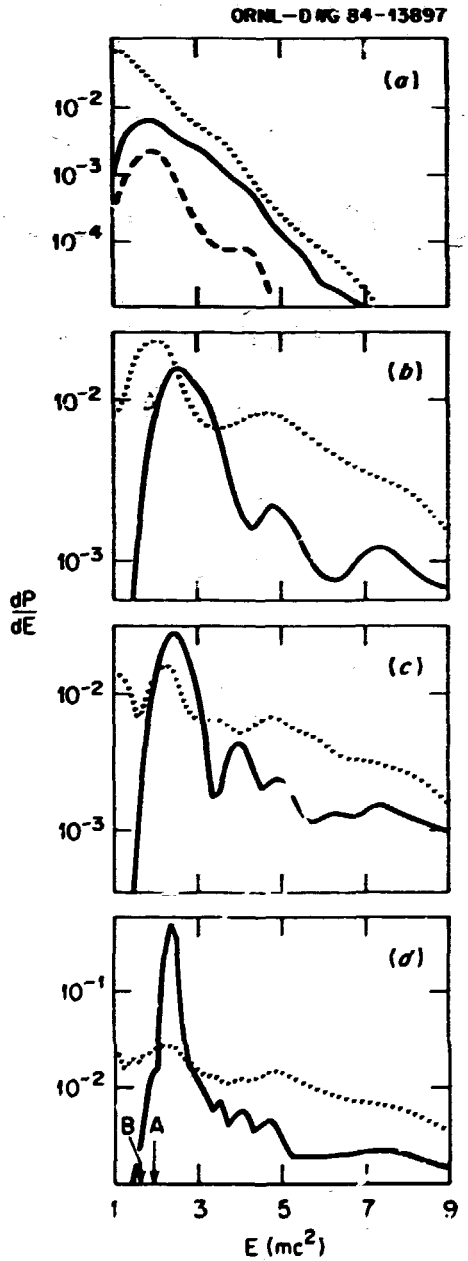

Fig. 5.27. U+Cm head-on collision at a bombarding energy of 6.05 MeV per particle. Positron (full line) and electron (dotted line) spectra in the target frame in units of $(mc^2)^{-1}$ per collision, for (a): no time delay; (b), (c), and (d), respectively, $T = 2.5, 5, 20\ \alpha^2\ t_0$. The positron spectrum for b = 19 fm is shown by the dashed line in (a).

4. U. Heinz, et al., Ann. Phys. (N.Y.) 151, 227 (1983); J. Reinhardt et al., Z. Phys. A303, 103 (1981); M. R. Strayer et al., Phys. Rev. C 28, 228 (1983); M. J. Rhoades-Brown et al., Z. Phys. A310, 287 (1983).

PHENOMENOLOGY OF NUCLEAR COLLISIONS WITH LONG TIME DELAYS

M. R. Strayer V. E. Oberacker[1]
C. Bottcher

We have used the methods described in another section to interpret experiments on positron production in U+Cm collisions.[2]

The energy spectrum of atomic positrons, integrated over nuclear scattering angles between 25° and 65° in the laboratory, consists of a broad structure (hump) between 0 and 1200 keV, on which is superimposed a small narrow feature (peak) at 316 keV in the center of mass. The peak is associated with angles close to 45°. We assume for the purposes of numerical estimation that the broad background is due to the undelayed Rutherford trajectories with impact parameters in the range b = (4.5,19) fm. The positron yield involves the probability of creating a K-shell hole in the target, and that for filling the hole from the negative energy sea, both being strong functions of the impact parameter. Averaging over impact parameters, we obtain a positron spectrum with a peak at 460 keV in the center-of-mass frame, and reaching a maximum yield of 2.0×10^{-7}/keV, in good agreement with the measurements and adiabatic basis calculations.[3]

We shall identify the sharp peak with an impact parameter b = 9 fm appropriate to 45° scattering of the heavy ions on a Rutherford trajectory. This simple assumption predicts a peak at 390 keV in the center of mass; a slightly modified trajectory would reproduce the experimental energy.

The ratio of the area under the peak to the area under the remaining part of the spectrum, $(P/H)_{expt} = 0.07$.[4] From our calculations, we know that the ratio λ = (total positron probability with a time delay)/(the same quantity without a time delay) is insensitive to the impact parameter, and ≈ 1.67. To derive $(P/H)_{theory}$, we adopt a model in which the nuclei have a probability f of coalescing in a range of relative orbital angular momenta $(\Delta L)_{peak}$, thereby giving

$$\left(\frac{P}{H}\right)_{theory} = \frac{\lambda f \Delta(L^2)_{peak}}{\Delta(L^2)_{hump}} .$$

Converting the angular momenta to scattering angles, we find $Tf(\Delta L)_{peak} \approx 55\hbar$. Since $\Delta b \approx 1$ fm corresponds to $L = 66\hbar$, our estimate is in harmony with the established models of the nuclear collision dynamics for this system.

We depart from earlier calculations in predicting sharp features in the ejected electron spectra for some ranges of nuclear time delay. An example is given in Fig. 5.28.

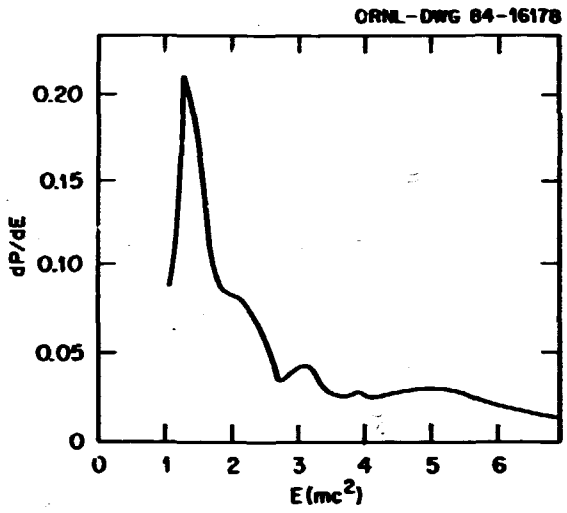

Fig. 5.28. Typical delta in electron spectrum as explained in the text.

The next stage in this investigation will be to synthesize the predicted spectrum using realistic nuclear trajectories. We have already constructed suitable trajectories using model nuclear interactions with attractive pockets and including energy transfer to nuclear excitations.[4]

---

1. Consultant from Vanderbilt University, Nashville, TN 37235.

2. J. Schweppe et al., Phys. Rev. Letts. 51, 2261 (1983).
3. J. Reinhardt et al., Z. Phys. A303, 103 (1981).
4. M. J. Rhoades-Brown et al., Z. Phys. A310, 287 (1983).

TIME-DEPENDENT HARTREE-FOCK THEORY FOR HEAVY ION-ATOM COLLISIONS

C. Bottcher

For several years, I have been able to study ion-atom collisions involving a single active electron, at intermediate energies (5-100 keV/amu), using numerical methods based on a finite-element representation of the wavefunction in positron space.[1] Other investigators have published studies on two-electron systems.[2] The extension to "heavy" systems (which I understand as those having 10 or more electrons) raises new problems. In particular, the rapid variation of the wavefunctions near the nuclei causes severe instabilities and violations of unitarity.

The time-dependent Hartree-Fock (TDHF) method can be formulated as follows. The wavefunction of A electrons is approximated by a Slater determinant of spin orbitals ϕ_α with occupancy

numbers ω_α. Each orbital satisfies an independent particle Schrödinger equation

$$h\,\phi_\alpha = i\,\frac{\partial \phi_\alpha}{\partial t} \qquad (1)$$

where (in atomic units)

$$h = -\frac{1}{2}\nabla^2 + V_n + V_d + V_x \qquad (2)$$

In Eq. (2), V_n is the nuclear potential, V_d the local electrostatic interaction due to the other electrons, and V_x the exchange interaction. We make the following approximations: (1) V_d is replaced by its average overall α, so that it is related to the electronic density by Poisson's equation,

$$\nabla^2 V_d = -2\left(\frac{A-1}{A}\right)D,\quad D = \Sigma\,\omega_\alpha |\phi_\alpha|^2 \qquad (3)$$

(2) V is replaced by the Hartree-Slater local approximation. (3) Axial decoupling is assumed, i.e., the wavefunction is taken to depend only on the cylindrical coordinates (ρ,z) referred to the rotating internuclear axis.

The numerical difficulties referred to above have been overcome by transforming to an orthogonal basis of finite elements and by using an exact exponential propagator at each time step. Orthogonal finite elements were also used to solve Poisson's equation. Excitation, capture, and ionization were distinguished by projecting on eigenstates of the initial and final Hamiltonians constructed in the same basis used for the time propagation.

The process

$$F^{9+} + Ne \rightarrow F^{(9-m)+} + Ne^{n+} + (n-m)e^- \qquad (4)$$

has been studied at two velocities, v = 1 and 2, and a range of impact parameters. Ionization and capture probabilities associated with the orbitals 2sσ, 2pσ, and 2pπ are shown in Fig. 5.29. An interesting feature of these results is the "shakeoff" of 2pσ electrons around b = 1 a_0. This interpretation is borne out by the final state density contours shown in Fig. 5.30. At impact parameters <0.5 a_0, shakeoff following quasi-resonant K-shell capture is important and will be addressed in future studies.

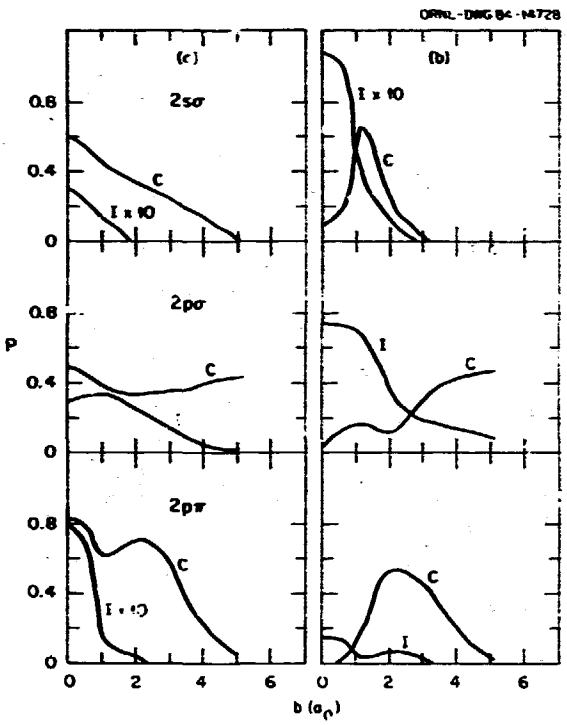

Fig. 5.29. The probabilities of capture (C) and ionization (I) for the 2sσ, 2pσ, and 2pπ orbitals are plotted vs. impact parameter for two relative velocities: (a) v = 1, (b) v = 2.

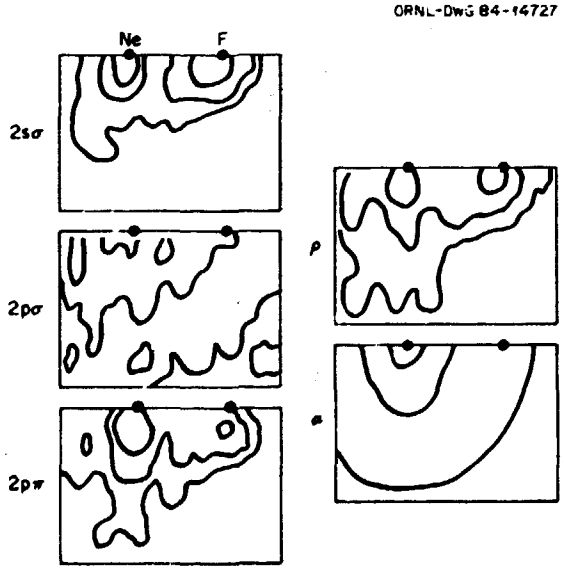

Fig. 5.30. The lefthand frames (see Fig. 5.29) show logarithmic density contours for the 2sσ, 2pσ, and 2pπ orbitals. The righthand frames show contours of the total density (logarithmic) and the electronic self-consistent field (linear).

1. C. Bottcher, Phys. Rev. Letts. 48, 85 (1982); C. Bottcher, in "Electronic and Atomic Collisions," eds. J. Eichler et al. (Elsevier Science Publishers B.V., 1984) p. 187.

2. D. Eichenauer et al., J. Phys. B 15, L17 (1982); K. C. Kulander et al., Phys. Rev. A 25, 2968 (1982); K.R.S. Devi and J. D. Garcia, J. Phys. B 16, 2837 (1983).

THRESHOLD IONIZATION THEORY

C. Bottcher

In earlier work on low-energy ionization I used wavepacket formulation and the time-dependent Schrödinger equation. Further progress requires a method of solving the stationary Schrödinger equation directly. This can be done by matching a set of solutions defined in a finite domain to asymptotic solutions on the boundary.

All calculations have so far been limited to the two-dimension model of the e+H system, in which the electrons move on a line passing through the proton at distances r_1, r_2 on opposite sides of the proton. Hyperspherical coordinates are defined by

$$r_1 = \rho \cos\alpha, \quad r_2 = \rho \sin\alpha \tag{1}$$

We have shown that eigenfunctions in a box r_1, $r_2 \leq 93\ a_0$ can be constructed with a finite element basis sufficiently large that the properties of breakup states near threshold are described. In particular, it is possible to compute certain moments of the energy distribution between the two electrons with knowledge of asymptotic solutions, and the values agree with those predicted by the Wannier theory of threshold ionization to within 10%.[1]

It is well recognized that asymptotic solutions are best obtained by semiclassical methods. If I write the wavefunction as $\psi = \exp(iS)$, S satisfies the Hamilton-Jacobi-Schrödinger equation

$$(\vec{\nabla}S)^2 = \left\{K^2 + \frac{2C(\alpha)}{\rho}\right\} + i\nabla^2 S \tag{2}$$

where we have written the potential energy as $-C/\rho$. If I drop the term $i\nabla^2 S$, I recover classical mechanics; the term discarded describes the diffraction of the deBroglie waves. Asymptotic solutions of (2) can always be described to a first approximation by a set of classical trajectories. I have found that all intuitively plausible solutions can be associated with sets of trajectories, each set having a common intersection (condensation point). Examples are given in Fig. 5.31: the set W correspond to a so-called Wannier solution, and the set T to a dipole (Temkin) solution.

In order to solve a scattering problem, I need a set of asymptotic functions $\psi(\rho,\alpha)$ complete in α for a fixed ρ. These can be obtained as follows for Wannier-type solutions. Suppose that at a very large distance

$$S \sim K\rho + \frac{C(\alpha)}{K} \ln\left(\frac{\rho}{a}\right) + \lambda F(\alpha) \tag{3}$$

where F is almost arbitrary, e.g., $F(\alpha) = i \ln \sin 2\alpha$ leads to wavefunctions which vanish rapidly as $\alpha \to 0$. As a,λ are varied, one obtains a double infinity of solutions suitable for matching at an inner boundary. The condensation point is determined by a, e.g., the orbits in Fig. 5.31 correspond to $a = 1$, $\rho_c = 25.02/K^2$; λ behaves like the index of a hyperspherical harmonic. However, it is permissible to consider any linear combinations of the $\psi(a,\lambda)$; e.g., $\psi(a,\lambda_0)$ could be expanded in $\psi(a_0,\lambda)$ where a_0, λ_0 have fixed values.

From a numerical perspective, (2) is a highly ill-conditioned nonlinear PDE, but some progress towards solutions has been made.

A related subject is the use of a two-dimensional model to obtain qualitative insight into the four-body Coulomb problem, i.e., two electrons in the field of two nuclei. This is discussed in another section of this annual report.

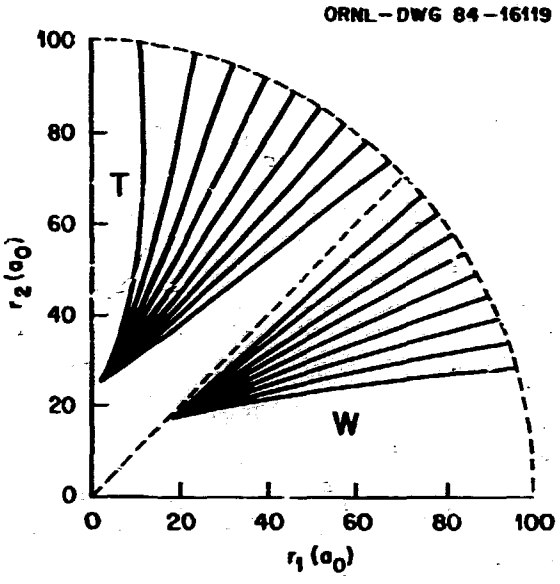

Fig. 5.31. Classical orbits corresponding to ionization in the e+p+e system. The axes correspond to the distances of the two electrons from the proton.

---

1. C. Bottcher, "Numerical Studies in Electron Impact Ionization," to appear in Advances in Atomic and Molecular Physics, 1985.

FORMAL RELATIONSHIP BETWEEN MASER THEORY AND QUANTUM FLUID MECHANICS

C. Bottcher C. Feuillade[1]

For several years we have been investigating the behavior of molecules coherently excited by radiation using the Bloch form of the density matrix equations. In particular we have studied the "ladder problem" in which the molecule is modeled by an anharmonic oscillator.[2] It seemed natural to apply our formalism in an attempt to resolve a long-standing controversy regarding the validity of classical solutions of this problem.[3]

We started with the density matrix $\rho(\alpha,\beta)$ in the representation of vibrational states and transformed to a new representation $\rho(m,n)$, where m,n are discrete eigenfunctions of the position operator q with eigenvalues q_m, q_n. Thus $\rho(m,n)$ approximates the density matrix in the position representation; diagonal elements correspond to particle density and off-diagonal elements can be related to the local current density, etc. Bloch equations in the position basis can be obtained from the usual Bloch equations by a linear transformation. The new equations can be related by a series of approximations to the classical Liouville equations of motion and hence to quantum fluid mechanics. Our analysis indicates that, unless the density of states is very large indeed, the inherently quantal effect of stimulated emission is too large to be discarded.

However, we have found that if the new equations are truncated at the level of coherence between adjacent points $|m-n| < 1$, a remarkably good approximation to the exact (quantal) solution is obtained.

Figure 5.32 plots the imaginary part of the dipole susceptibility in the model of Ref. 2

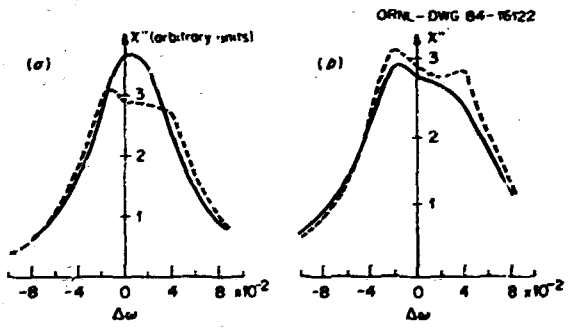

Fig. 5.32. Imaginary part of dipole susceptibility in the model of Ref. 2. (a) Original Bloch equations; full line, truncated to $\alpha-\beta < 1$; dashed line, exact. (b) New equations; full line, truncated to $m-n < 1$; dashed line, exact.

with a reduced laser field, $f = 0.5$. In Fig. 5.32(a) we show the drastic effect of truncating the original Bloch equations at the level $|\alpha-\beta| < 1$. Figure 5.32(b) shows that the effect on the new equations is much less severe. These equations are not equivalent to any previously recommended approximation, though their general structure resembles quantum fluid mechanics. We are considering applications to the dissociation of polyatomic molecules and to perturbed electron gases. The new approximation is sufficiently simple that it might be a competitive way of analyzing more complicated problems.

---

1. NORDA, N.S.T.L. Station, MS 39529.

2. C. Bottcher and C. Feuillade, Chem. Phys. Letts. 96, 279 (1983).
3. J. R. Ackerhalt et al., Optics Lett. 6, 377 (1981).
4. C. D. Cantrell et al., Optics Comm. 40, 413 (1982).

LOW-ENERGY CHARGE EXCHANGE

C. Bottcher T. G. Heil[1]

We have continued our studies of charge capture from hydrogen atoms by highly stripped ions using expansions in one-electron molecular eigenstates and a fully quantal description of the nuclear motion.[2] When the adiabatic potential energy functions and coupling matrix elements have been calculated, we can solve the resulting coupled equations with some facility, using fully vectorized programs developed for the Cray-1 and -1S.

In the past year, we have moved on to study more highly ionized projectiles, notably the 8+ isoelectronic sequence. Some results on O^{6+} and Ar^{8+} are shown in Fig. 5.33. We hope to study several members of this sequence with larger basis sets in order to make comparison with measurements in progress using the new ECRIS ion source at ORNL.[3]

Since we now routinely include π-states in our basis sets, we have found a number of cases where σ-π couplings affect the charge capture cross section by more than 30%. Figure 5.34 shows results for C^{4+} and O^{6+} projectiles. In

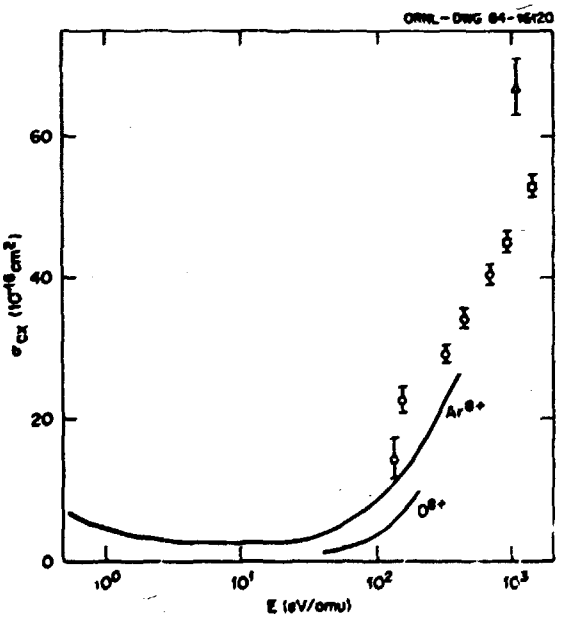

Fig. 5.33. Charge exchange cross sections for multicharged ions on hydrogen atoms. Full lines: calculated with a basis of 3 σ-states; open circles: measurement of Ref. 3 on O^{8+}; open triangle: measurement of Ref. 4 on Ar^{8+}.

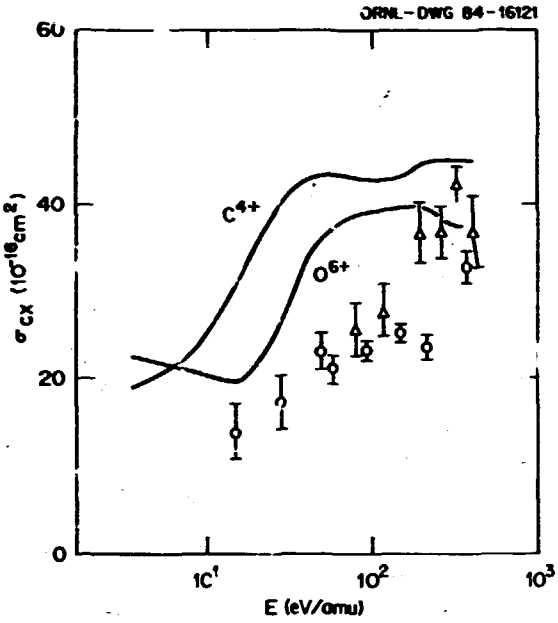

Fig. 5.34. Charge exchange cross sections for multicharged ions on hydrogen atoms. Full lines: calculated with a basis of 3 σ- and 3 π-states; open circles: measurements of Ref. 5 on C^{4+}; open triangles: measurements of Ref. 6 on O^{6+}.

the case of C^{4+} the disagreement with experiments appears to have worsened, a situation which merits further study.

We are also pursuing the more fundamental objective of a very accurate calculation on N^{5+} + H in which translation factors are included by matching to moving orbitals on some boundary. This matching requires an expansion in about 40 molecular eigenstates, for which we have now assembled the coupling matrix elements.

---

1. Consultant from University of Georgia, Athens, GA 30602.
2. C. Bottcher and T. G. Heil, Chem. Phys. Letts. 86, 506 (1982).
3. F. Meyer et al., private communication.
4. D. H. Crandall et al., Phys. Rev. A 22, 379 (1980).
5. R. A. Phaneuf, Phys. Rev. A 24, 1138 (1981).
6. R. A. Phaneuf et al., Phys. Rev. A 26, 1892 (1982).

SUMMARY OF CODE DEVELOPMENT FOR ELECTRON-ION SCATTERING

C. Bottcher D. C. Griffin[1]
M. S. Pindzola[2]

Between 1980 and 1983 we developed a program package to calculate distorted-wave excitation cross sections with intermediate coupling wavefunctions based on a single configuration of Hartree-Fock orbitals.[3] The structure eigenvectors and radiative branching ratios (for autoionizing states) are obtained from the Los Alamos atomic structure package developed by R. W. Cowan.

In the past year we have added codes to calculate direct ionization and dielectronic recombination. These codes are still based on Hartree-Fock orbitals for bound states and distorted waves for continuum states, but use "configuration-averaged" approximations in the structure calculations. They are well suited to surveys of, e.g., isoelectronic sequences, and we have the capacity to study in more detail individual cases where a breakdown of the approximations is suspected.

At the same time, a major effort has been devoted to extending the excitation code to handle configuration-interaction wavefunctions which describe effects omitted by single configuration Hartree-Fock theory, in particular, coupling between almost-degenerate configurations in the Hartree-Fock sea (e.g., $3s^23p^2$, $3p^4$, $3p^23d^2$), and pair excitations out of the sea ($3d^{10}$, $3d^84f^2$). The process of checking these new codes is almost complete, and application to transition metal ions will be made in the near future.

We have had for some time the capacity to perform close-coupling calculations, but progress on the complex targets we are interested in has been hindered by the lack of an efficient angular momentum algebra package in other groups as well as ours. This defect has been remedied by adapting our distorted-wave algebra package, and pilot calculations are in progress.

Particular applications of these codes are described in the following sections.

---

1. Consultant from Rollins College, Winter Park, FL 32789.
2. Consultant from Auburn University, Auburn, AL 36849.
3. C. Bottcher, D. C. Griffin, and M. S. Pindzola, J. of Phys. B 16, L65 (1983).

EXCITATION-AUTOIONIZATION PROCESSES IN THE ELECTRON IMPACT IONIZATION OF SINGLY-CHARGED IONS

D. C. Griffin[1] M. S. Pindzola[2]
C. Bottcher

We have examined the excitation-autoionization mechanism in electron impact ionization of alkaline earth ions,

$$e + np^6(n+1)s \rightarrow np^5\, nd(n+1)s + e \rightarrow np^6 + e + e \quad (1)$$

Our motives were to examine the data of Peart and Dolder[3] which have never been fully interpreted, and to compare distorted-wave with

close-coupling calculations, following a suggestion[4] that they might seriously disagree for processes of the type (1). We also felt that the term dependence of the nd-orbital should have the same large effect as in the xenon isonuclear sequence which we investigated earlier.[5]

Indeed, it is the case that term dependence has a serious effect on the highest-lying state, that with a $np^5nd(^1P)$ parent, e.g., with a term-dependent 3d orbital, the $3p^53d(^1P)4s^2P$ state of Ca^+ lies at 33.6 eV (37.6 eV) and has an excitation cross section at threshold of 25.4 Mb (106 Mb). The numbers in parentheses, just quoted, refer to the averaged-configuration 3d orbital.

We carried out unitarized distorted-wave calculations in intermediate coupling for Ca^+ and Ba^+.[6] The Ca^+ results can be compared with those of close-coupling calculations, and for impact energies twice threshold; the total excitation-autoionization cross sections agree to better than 20%. No comparison is possible near threshold, since the close-coupling calculations[4] retain only three out of nine possible levels of the multiplet and neglect term dependence; we find that the discarded levels make comparable contributions to the cross section near threshold. However, both methods predict a large peak near threshold due to the $(^1P)^2P$ state, of which there is no experimental indication.

No other calculations have been performed on Ba^+. Our results are shown in Fig. 5.35. As was the case in Ca^+, the large calculated peak at 22 eV due to $(^1P)^2P$ is not seen experimentally. We have, as yet, no explanation for this discrepancy, although we note that the peak is almost entirely due to a single outgoing partial wave ($\ell = 3$).

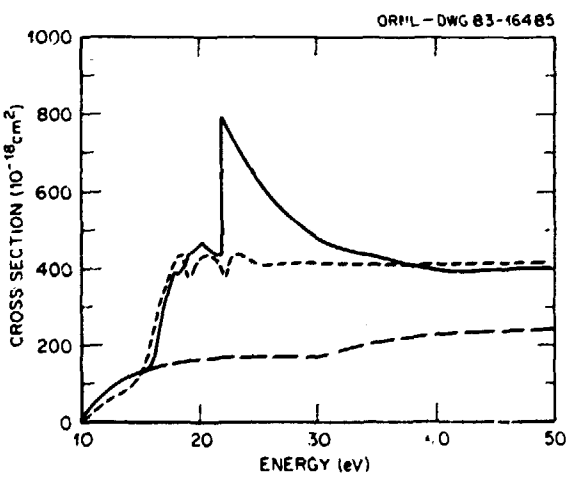

Fig. 5.35. Total ionization cross section for Ba^+. Dashed line, direct ionization cross sections calculated from the Lotz equation (unscaled); dotted line, experimental results of Peart et al. (1973); full line, unitarized, distorted-wave results (including transitions to all levels of $5p^55d6s$) added to the Lotz value for direct ionization.

We are now proceeding to close-coupling calculations on Ca^+ targets. The angular algebra part of our distorted-wave package has now been interfaced with the University College, London close-coupling package, (IMPACT), opening up the possibility of large calculations with many open shells. Exploratory studies suggest a high degree of mixing due to final-state interactions which may remove the spurious peaks.

---

1. Consultant from Rollins College, Winter Park, FL 32789.
2. Consultant from Auburn University, Auburn, AL 36849.
3. B. Peart and K. T. Dolder, J. Phys. B: At. Mol. Phys. 8, 56 (1975).
4. P. G. Burke et al., J. Phys. B: At. Mol. Phys. 16, L385 (1983).
5. D. C. Griffin et al., Phys. Rev. A 29, 1729 (1984).
6. D. C. Griffin et al., J. Phys. B: At. Mol. Phys. 17, 3183 (1984).

DIRECT AND INDIRECT IONIZATION OF TRANSITION METAL IONS

M. S. Pindzola[1] D. C. Griffin[2]
C. Bottcher

During the past year we completed a survey of experimental and theoretical electron-impact ionization cross sections for transition metal ions in low stages of ionization. The atomic ions Ti^+, Ti^{2+}, Ti^{3+}, Fe^+, Fe^{2+}, Fe^{3+}, Fe^{4+}, Ni^+, Ni^{2+}, Ni^{3+}, Cu^+, Cu^{2+}, and Cu^{3+} were examined using electron-ion crossed beams measurements and distorted-wave theory. In Fig. 5.36 we compare a single-configuration level to level distorted-wave calculation with experiment for Ti^{2+}.[3] The theory predicts a rapid change in the cross section for 30 eV to 35 eV followed by a 10-eV plateau and then further jumps in the cross section around 45 eV. On a smaller scale, the experimental measurements follow the same pattern. We believe that inclusion of configuration-interaction effects in the distorted-wave excitation calculations for Ti^{2+} will lower the cross section and thus improve the agreement between theory and experiment. In Fig. 5.37 we present the results of a single-configuration level to level distorted-wave calculation for Fe^{4+} (in this case, no experiment has yet been performed). From our survey work, we expect that the total cross section results and the direct cross section results will bracket expriment. In order for our predictions to be more precise, configuration-interaction effects in Fe^{4+} will need to be included in not only the indirect excitation process but also in the direct ionization calculation as well.

---

1. Consultant from Auburn University, Auburn, AL 36849.
2. Consultant from Rollins College, Winter Park, FL 32789.
3. D. W. Mueller et al., private communication.

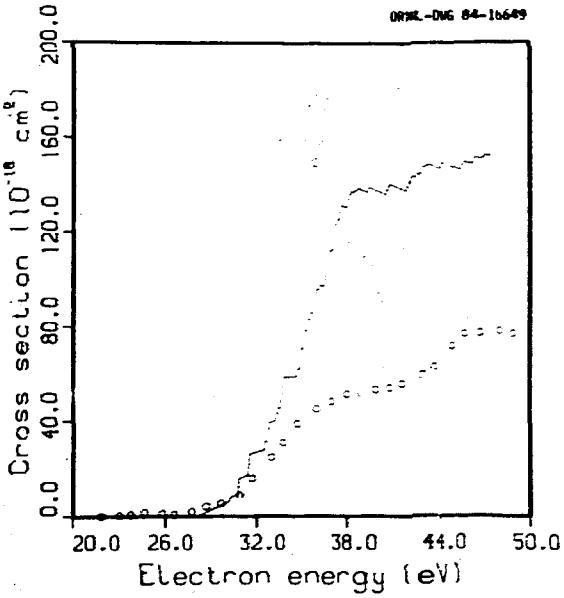

Fig. 5.36. Comparison of theory and experiment for electron impact ionization of Ti^{2+}. Dotted line: direct ionization; full line: sum of direct and excitation-autoionization; open circles: measurements of Ref. 3.

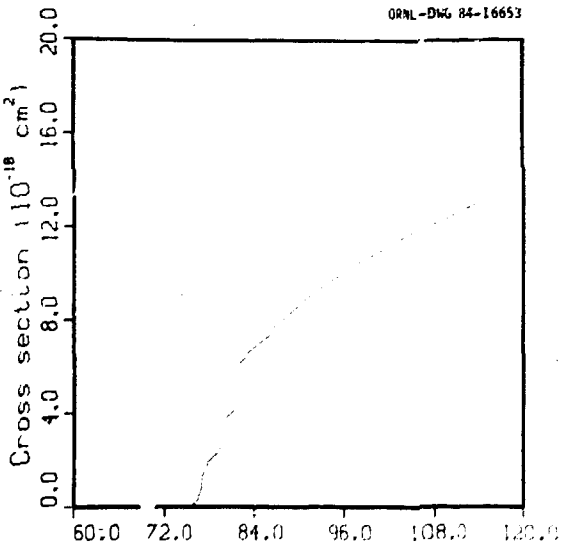

Fig. 5.37. Predictions for electron impact ionization of Fe^{4+}. Dotted line: direct ionization; full line: sum of direct and excitation-ionization.

DIELECTRONIC RECOMBINATION IN THE LITHIUM ISOELECTRONIC SEQUENCE

D. C. Griffin[1] M. S. Pindzola[2]
C. Bottcher

We have applied our recently developed distorted-wave code for dielectronic recombination to calculate the cross sections associated with the 2s-2p transition in the Li-like ions B^{2+}, C^{3+}, and O^{5+}.[3] We have compared calculated cross sections to selected configurations of the type 2pnℓ in pure LS coupling, intermediate coupling, and a configuration-averaged approximation. The most precise (intermediate coupling) results tend to be 50% higher than LS coupling, but agree fairly well with configuration-averaged results.

The explanation can be seen if we write the process, e.g. in B^{2+}, as

$$e(k'\ell') + B^{2+}(1s^2 2s) \rightleftarrows B^{+}(1s^2 2p n\ell, L) \rightarrow B^{+}(1s^2 2s n\ell) + h\nu \qquad (1)$$

In pure LS-coupling the total angular momentum $L = \ell \pm 1 = \ell'$ while in intermediate coupling; the spin-orbit interaction mixes $L = \ell \neq \ell' \pm 1$. The former states typically have autoionizing rates 10^3 - 10^5 times the radiative rate, so that if the latter are mixed to the extent of 1 part in 10^3, they will contribute equally to the cross section.

The interpretation of experiments on dielectronic recombination is presently in a state of flux. However, we note that measurements seem to be much larger than early theoretical predictions suggested, and that the effect of spin-orbit interactions and external fields is usually to enhance the calculated cross section.

The sensitivity of comparisons with experiment to assumptions about experimental conditions is illustrated in Fig. 5.38. Figure 5.38(a) shows the predicted cross section for B^{2+} as a function of experimental energy resolution, while Fig. 5.38(b) shows the variation with the field ionization cutoff.

---

1. Consultant from Rollins College, Winter Park, FL 32789.
2. Consultant from Auburn University, Auburn, AL 36849.
3. D. C. Griffin et al., Phys. Rev. A (1985) in press.
4. P. F. Dittner et al., Phys. Rev. Letts. 51, 31 (1983).

THE EFFECT OF ELECTRIC FIELDS ON DIELECTRONIC RECOMBINATION IN IONS OF THE LITHIUM AND SODIUM ISOELECTRONIC SEQUENCES

D. C. Griffin[1] M. S. Pindzola[2]
C. Bottcher

Dielectronic recombination (DR) is particularly sensitive to the presence of external

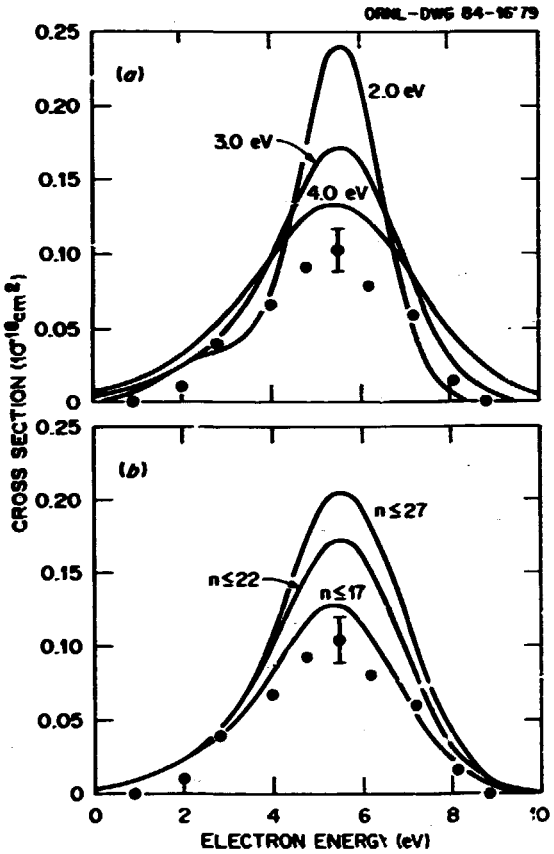

Fig. 5.38. Predicted cross section for dielectronic recombination of B^{2+}. (a) Variation of predicted cross section with electronic energy spread; (b) variation with analyzer field cutoff in principal quantum number, n; filled circles are measurements from Ref. 4.

electric fields. Such fields can cause a redistribution of angular momentum among the doubly-excited, resonant, Rydberg states which, in turn, increases the number of states for which the rate of resonant-recombination is appreciable. We have just completed a systematic study of the field enhancement of dielectronic recombination in the Li and Na isoelectronic sequences. In particular, we have applied the linear Stark approximation to examine these field effects for the dielectronic recombination transitions associated with the 2s → 2p excitation in the Li-like ions B^{2+}, C^{3+}, O^{5+}, and Fe^{23+}, and the 3s → 3p excitation in the Na-like ions Mg^{+}, S^{5+}, Cl^{6+}, and Fe^{15+}.

Although this technique does not allow one to determine field mixing as a function of electric field strength, it does provide physical insight into the nature of field effects in dielectronic recombination, and allows one to study important trends in the maximum field enhancement of the DR cross section as a function of ionization stage. We find that the magnitude of the field enhancement decreases as we move up an isoelectronic sequence, and is of the order of two or three in highly ionized systems. Furthermore, we show that DR transitions through doubly-excited states near threshold can produce large narrow peaks in the cross section at low energies, which are especially prominent in high stages of ionization, and are not affected by electric fields.

An especially striking example of the effect just referred to is provided by the DR cross section for Fe^{23+}, shown in Fig. 5.39 as a function of electron energy. In this plot, the narrow resonances associated with recombination

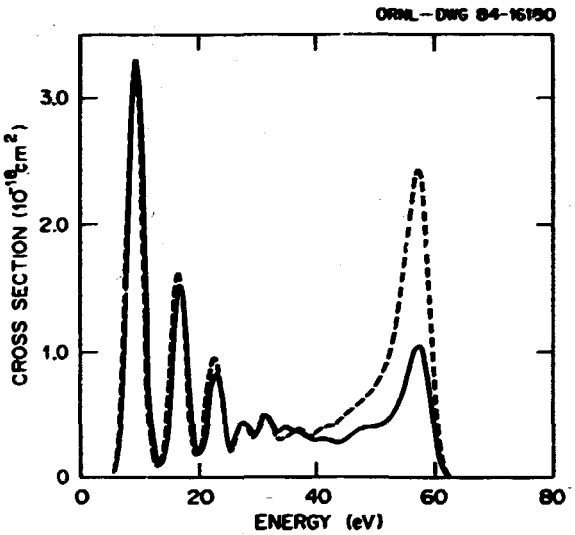

Fig. 5.39. Predicted dielectronic recombination cross section of Fe^{23+} convoluted into a 3-eV Gaussian electron energy distribution. The full and dashed lines pertain to the cross section with and without an external electric field.

transitions through the doubly-excited configurations 2pnℓ are convoluted with a 3.0-eV Gaussian to simulate an experimental electron-energy spread. The field enhancement in the high-energy peak is approximately equal to 2.3. The prominent low-energy peak is due to transitions through the resonant states for which the principal quantum of the Rydberg electron is n = 12.

---

1. Consultant from Rollins College, Winter Park, FL 32789.
2. Consultant from Auburn University, Auburn, AL 36849.

6. NUCLEAR SCIENCE APPLICATIONS

Nuclear science has common frontiers with other basic sciences. The current program concentrates on three areas. (1) In cooperation with the Engineering Physics and Mathematics, Analytical Chemistry, and Computing and Telecommunications Divisions, a program is currently underway to obtain verification of the neutronic and irradiation performance of higher actinides in fast spectrum reactors. This program utilizes the Dounreay Prototype Fast Reactor and will be completed by 1988. (2) In association with the Analytical Chemistry Division, the technique of studying the heavy-ion-induced x-ray satellite spectra has been advanced to the point that it can be applied to metal alloys and other materials of interest to the Metals and Ceramics Division. This program utilizes the EN Tandem and the HHIRF. Significant advances in this area are expected with the construction by early 1985 of an ultra-high-resolution Van Hamos spectrometer. (3) Working with personnel from the Aerospace Corporation, a program to study single-event upsets in integrated circuits has been started. With encouragement from NASA, plans are being drawn up to build a beam line at HHIRF dedicated to this program.

ACTIVITIES IN SUPPORT OF THE US/UK JOINT EXPERIMENT IN THE DOUNREAY PROTOTYPE FAST REACTOR

S. Raman — D. A. Costanzo[2]
H. L. Adair[1] — J. K. Dickens[2]
J. L. Botts[2] — J. F. Emery[2]
B. L. Broadhead[3] — R. L. Walker[2]

The United States and the United Kingdom are engaged in a joint research program in which samples of the higher actinides are irradiated in the Dounreay Prototype Fast Reactor in Scotland. The purpose of the program is (1) to study the materials behavior of selected higher actinide "fuels" and (2) to determine the integral cross sections of a wide variety of the higher isotopes. Samples of the actinides are incorporated in fuel pins inserted in the core. For the fuel study, the actinides selected are ^{241}Am and ^{244}Cm in the form of Am_2O_3, Cm_2O_3, and $Am_6Cm(RE)_7O_{21}$ where (RE) represents a mixture of lanthanides. For the cross-section determinations, the samples are milligram quantities of actinide oxides of ^{248}Cm, ^{246}Cm, ^{244}Cm, ^{243}Cm, ^{243}Am, ^{241}Am, ^{244}Pu, ^{242}Pu, ^{241}Pu, ^{240}Pu, ^{239}Pu, ^{238}Pu, ^{237}Np, ^{238}U, ^{236}U, ^{235}U, ^{234}U, ^{233}U, ^{232}Th, ^{230}Th, and ^{231}Pa encapsulated in vanadium. The development and application of the technology for preparing the actinide samples have been described in a report by Quinby, et al.[5] The characterization of the starting materials used in the samples for the cross-section determinations (denoted as physics specimens) and in the dosimeters has been described in a report by Walker, et al.[6] Preanalysis calculations were carried out[7] concerning actinide build-up and burnout in order to aid the experimentalists in the planning and preparation of their respective measurements.

The first fuel pin experiment was removed from the reactor in late 1983 after an irradiation of 63 effective full-power days and shipped to ORNL where subsequent analysis began in May 1984. The experimental results of gamma-ray characterization of fission products from several of the dosimeters have recently been completed. These results include fission product activities for ^{238}U, ^{235}U, and ^{239}Pu at each of the three dosimeter locations. Calculations were performed in a manner similar to the pre-analysis calculations reported in Ref. 7 with the following exceptions: (1) the actual operating history of the reactor was used; (2) all actinide and fission product cross sections were collapsed to one group with the spectrum near the axial centerline of the physics specimen section; and (3) the flux levels employed in the calculations were from the actual reactor run.

Shown in Table 6.1 are preliminary results for six different fission products produced by the fissioning of ^{238}U, ^{235}U, and ^{239}Pu at each of the three different dosimeter positions in fuel pin 1. The results are given as the ratio of the experimental value (E) to the calculated value (C). In all cases the agreement is very good with E/C values between 0.81 and 1.14. Also encouraging is that within each location a given dosimeter's E/C values are very nearly independent of the particular fission product. This indicates that some of the remaining discrepancies are systematic in nature. Thus, for example, if the flux used in the calculations was decreased 10% in the top (Positions 1 and 2) and middle (Positions 17 and 18) dosimetry locations, the resulting disagreements would then be 10% or less. The variation in E/C values as a function of the fission products for a given dosimeter is larger for the bottommost (Positions 33 and 34) locations than those of the top and middle locations. This is due to a known deficiency in the spectrum used to obtain the 1-group cross sections, and will be corrected in future analyses.

The US/UK joint program is ongoing with more detailed calculations and additional measurements underway. The preliminary results obtained thus far are very encouraging. The gamut of activities in support of this program involves not only several ORNL divisions but also close interaction and cooperation with Hanford Engineering Development Laboratory (HEDL) and the Dounreay Nuclear Power Development Establishment.

1. Operations Division, ORNL.
2. Analytical Chemistry Division, ORNL.
3. Computing and Telecommunications Division, ORNL.
4. Engineering Physics and Mathematics Division, ORNL.
5. T. C. Quinby et al., "Preparation of Actinide Specimens for the US/UK Joint Experiment in the Dounreay Prototype Fast Reactor," ORNL-5858 (1982).
6. R. L. Walker et al., "Characterization of Actinide Physics Specimens for the US/UK Joint Experiment in the Dounreay Prototype Fast Reactor," ORNL-5986 (1983).
7. B. L. Broadhead, W. B. Gove, and S. Raman, "Preanalysis Calculations in Support of the US/UK Joint Experiment in the Dounreay Prototype Fast Reactor," ORNL-6058 (1984).

Table 6.1. US/UK dosimeter results for Fuel Pin 1. Listed below are the ratios of experimental value to the calculated value.

Fission Product	^{238}U			^{235}U			^{239}Pu		
	Pos. #1	Pos. #17	Pos. #33	Pos. #1	Pos. #17	Pos. #33	Pos. #2	Pos. #18	Pos. #34
^{95}Nb	0.89	0.81	0.95	0.95	0.96	1.08	0.84	0.86	0.96
^{95}Zr	0.90	0.81	0.94	0.95	0.96	1.08	0.83	0.85	0.97
^{103}Ru	0.93	0.85	1.03	0.90	0.87	1.00	0.85	0.87	0.99
^{106}Ru	0.88	0.81	0.96	0.84	0.84	0.93	0.85	0.86	0.95
^{137}Cs	0.93	0.80	1.00	0.94	0.94	1.07	0.87	0.89	1.00
^{144}Ce	0.93	0.88	1.14	0.95	0.98	1.02	0.83	0.85	0.97

ULTRAHIGH-RESOLUTION STUDIES OF HEAVY-ION-INDUCED X-RAY SATELLITE EMISSION

C. R. Vane
E. Källne[1]
J. Källne[1]
G. Morford[2]
S. Raman
M. S. Smith[3]

When an energetic heavy ion collides with a target atom, several L-shell and M-shell electrons are ejected along with a K-shell electron. The initial vacancy distribution of, say, the L shell is altered by vacancy refilling prior to K_α x-ray emission. What is seen experimentally at moderately high resolution is a series of KL^n satellite peaks where n denotes the number of L-shell vacancies. Figure 6.1 shows sulfur $K_\alpha L^n$ for Na_2SO_4 and NaSCN excited by 36 MeV Cl^{9+} ions from the ORNL EN tandem. Experimental resolution here is ~7 eV FWHM. These peaks actually represent over a hundred individual transitions. We have studied this fine structure from six sulfur compounds when bombarded by 34-MeV ^{35}Cl ions. The data, composed of six normalized then pieced-together, narrow band spectra (20-to-40 eV each), are displayed in Fig. 6.2. These spectra were taken with a high-throughput, high-resolution Bragg crystal spectrometer[4] in the Van Hamos geometry. They show that the individual satellite peaks from S compounds not only differ in their gross shapes but also contain pronounced ~1-eV fine structures that exhibit intensity variations. For example, the area of the prominent sharp peak at ~2340 eV varies nearly linearly with target sulfur effective charge. It changes by +63% in going from NaSCN to Na_2SO_4, nearly 2.5 times the sensitivity found for the entire $K_\alpha L^2$ area measured earlier at lower resolution.[5] The observed profiles agree qualitatively with Hartree-Fock predictions[6] for the lower degrees of L-shell ionization (KL^0, KL^1, and KL^2), but less well for the higher degrees. In order to systematically investigate these remarkable fine structures, we have designed and begun construction of a new Van Hamos spectrometer[7] of much higher collection efficiency employing a large curved crystal (10 cm x 10 cm; 25.4 cm radius of curvature) and a position-sensitive detector. The main features of the spectrometer are shown schematically in Fig. 6.3. The design resolution was 1 eV at 2.5 keV with a dynamic range of 200-300 eV. The positions of the crystal and the detector are remotely variable on linear tracks allowing Bragg angle adjustment from 30° to 70° for a particular crystal. With this instrument, we intend to study both the chemically sensitive and temporal variations in x-ray spectra from a wide variety of targets bombarded with heavy ions from the Holifield Heavy Ion Research Facility.

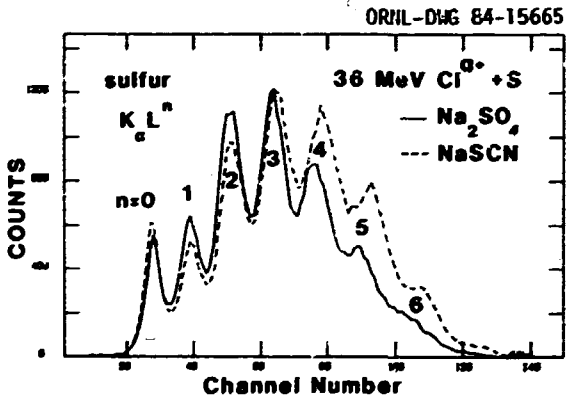

Fig. 6.1. Moderately high resolution (~7 eV FWHM at 2.3 keV) sulfur K_α x-ray spectra generated by 36 MeV Cl^{9+} ions on NaSCN and Na_2SO_4.

1. Now at JET Joint European Undertaking, Abingdon, England.
2. Undergraduate student from the Edinboro State College, Edinboro, PA, under the ORAU Summer Student Program.
3. Now a graduate student at Yale University, New Haven, CT 06511.

4. E. Källne and J. Källne, Physica Scripta T3, 185 (1983).
5. C. R. Vane et al., Nucl. Instrum. Methods Phys. Res. B3, 88 (1984); see Fig. 4 of this paper.
6. R. L. Watson, H.F. Calculations of Ne-like S, private communication.
7. C. R. Vane, M. S. Smith and S. Raman, ORNL report, in preparation.

ORNL-DWG 84-14557

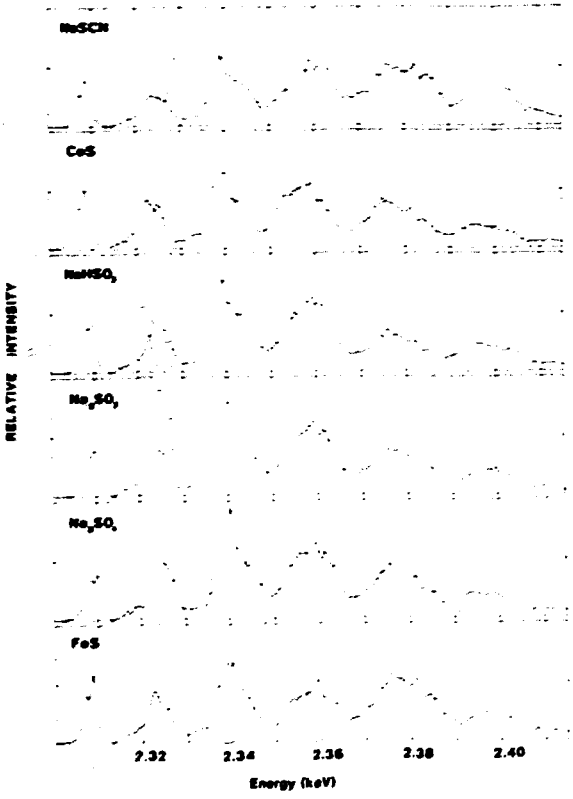

Fig. 6.2. Very high resolution (~1 eV FWHM at 2.3 keV) sulfur K_α x-ray spectra generated by 34-MeV Cl^{9+} ions on six compounds. Spectra were pieced together from 20- to 40-eV wide segments taken with narrow-bandwidth Van Hamos geometry spectrometer.

EFFECT OF THE CHEMICAL ENVIRONMENT ON THE L AND M HEAVY-ION-INDUCED X-RAY SATELLITE EMISSION SPECTRA

T. M. Rosseel[1] P. L. Pepmiller
J. M. Dale[1] S. Raman
L. D. Hulett[1] C. R. Vane
H. F. Krause J. P. Young[1]

The effect of the chemical environment on heavy-ion-induced K_α x-ray satellite yields has been studied extensively for a variety of second and third row elements.[2] Using high-resolution measurements, it has been shown that the sensitivity of the satellite lines to the chemical milieu is due to the modification of the vacancy distribution created at the time of collision by inter- and intra-atomic relaxation processes during the lifetime of the K vacancy. Because the relaxation processes depend primarily on the availability of weakly bound electrons, a change in the valence electron distribution due to a change in the chemical environment alters the vacancy transfer rates and thus alters the observed satellite yield.[3] Recently, similar investigations have been extended to the L x-ray satellites of transition metal elements.[4,5] Variations in the measured satellite intensity distribution were observed and correlated to chemical differences among a series of molybdenum alloys and compounds.[5] These results suggest that heavy-ion-induced x-ray satellite emission (HIXSE) is capable of analyzing the chemical nature of intermediate Z elements as effectively as low Z elements. As part of the effort to confirm the sensitivity of HIXSE to intermediate Z elements and to expand this method to new regions of the periodic table, we have examined the effect of the chemical environment on the Zr and Nb L and the Au and Pb M x-ray satellite lines at the Oak Ridge EN-Tandem Van de Graaff accelerator.

The Zr L x-ray satellite spectra of ZrO_2 and Zr produced by 36-MeV Cl ion bombardment are shown in

ORNL-DWG 84-14559R

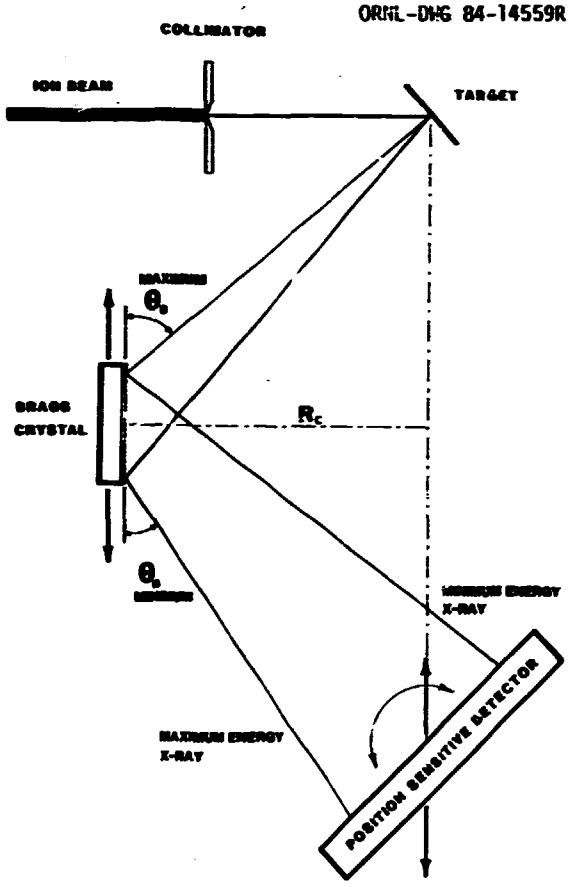

Fig. 6.3. Schematic of new Van Hamos spectrometer. Arrows indicate positioning of remotely adjusted components.

Fig. 6.4. Based on previous investigations[5] and Dirac-Fock calculations of transition energies,[6] the first band corresponds principally to the $L_\alpha^2 M^m$ satellite lines and the second band to the $L_{\beta_1} M^m$ transition. The smaller peaks following the L_{III} absorption edge at 2.22 keV are mainly due to the $L_{\beta_{2,15}}^2 M^m$ satellites. Clearly these spectra exhibit variations in their satellite intensity profile due to differences in the chemical environment of the Zr ion.

In order to amplify these variations and extract chemical information, difference spectra were generated using the Zr metal spectrum as the subtrahend. Two examples of these difference spectra are shown in Fig. 6.5. It can be seen that the deviation from zero (no chemical effect) is larger for ZrO_2 than $ZrAl_2$. This is in accord with calculated values of the bulk valence-electron densities. The valence-electron density, D_v, defined as the number of valence electrons/A^3, approximately describes the concentration of electrons available for vacancy refilling.[3,7] It is thus a measure of the effect of the chemical environment of the emitting target ion. The energy region which corresponds approximately to the $L_\alpha^2 M^m$ satellite lines (2.10-2.17 keV) was found to be particularly sensitive to changes in D_v. This is also in good accord with previous observations for Mo compounds,[5] and with data for Nb.

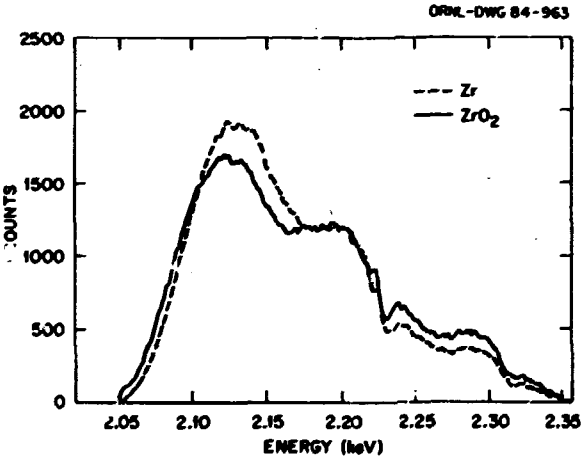

Fig. 6.4. The corrected and normalized Zr L x-ray satellite spectra produced by the bombardment of Zr metal (dashed line) and ZrO_2 solid line) with 36-MeV Cl ions.

In addition to examining compounds, a series of Zr-Ti alloys were also investigated. Although the difference spectra are dissimilar to the difference spectra of the compounds, as was observed for Mo-Ti alloys,[5] the alloy spectra exhibit a systematic decrease in the absolute value of the difference as the valence electron density of the minuend approaches the subtrahend. These results provide additional evidence that HIXSE can distinguish between different types of chemical bonding. Together with the Zr and Nb compound data, it confirms the sensitivity of the L x-ray satellites to the chemical environment of intermediate Z elements.

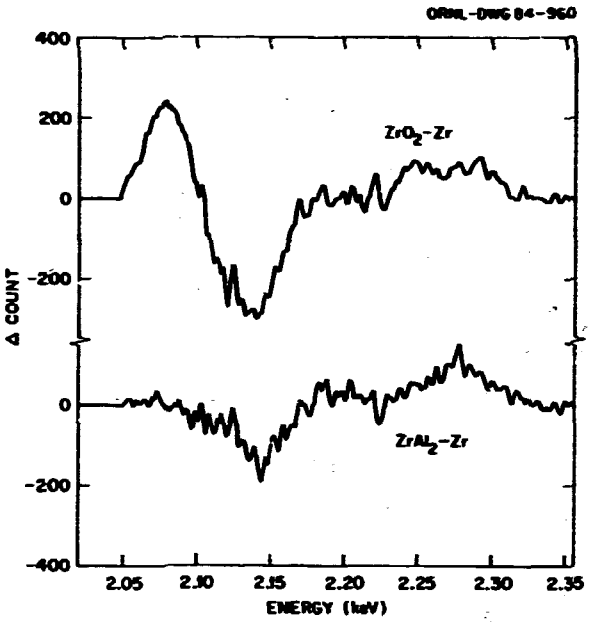

Fig. 6.5. The Zr x-ray satellite difference spectra of ZrO_2 and $ZrAl_2$. The Zr metal spectrum is the subtrahend. The projectile was 36-MeV Cl ions.

The Pb and Au M x-ray satellite spectra were also examined with 36-MeV Cl ions. The spectra, like those of Zr, Nb, and Mo, exhibit variations in the satellite intensity profile due to differences in the chemical environment of the target ion. Like the L spectra, the first two bands in the M spectra are composed of overlapping hypersatellites of the M_α and M_β transitions. Attempts to extract chemical information from these spectra are being pursued.

---

1. Analytical Chemistry Division.
2. S. Raman and C. R. Vane, Nucl. Instrum. Methods Phys. Res. B3, 71 (1984).
3. R. L. Watson et al., Phys. Rev. A15, 914 (1977).
4. M. Uda et al., Inner-Shell and X-ray Physics of Atoms and Solids, eds., D. J. Fabian, H. Kleinpoppen and L. M. Watson (Plenum, New York, 1981) p. 205.
5. T. M. Rosseel et al., Nucl. Instrum. Methods Phys. Res. B3, 94 (1984); J. Phys. F: Met. Phys. 14, L37 (1984).
6. C. W. Nestor, Modification of a Relativistic Hartree-Fock Program from J. P. Desclaux, Comp. Phys. Comm. 9, (1975).
7. A valence electron is defined here as any electron beyond the rare gas structure d and f electrons from a filled subshell.

SIMULATION OF COSMIC-RAY UPSET OF MICROELECTRONIC DEVICES

W. A. Kolasinski[1] M. Knoll[4]
J. Adolphsen[2] R. Koga[1]
G. Brucker[3] S. Raman
C. R. Vane

Several types of microelectronic chips have been bombarded with beams of Au, Ag, and C ions as part of a continuing investigation concerned with the effects of heavy cosmic rays on modern computers in space. With the present level of miniaturization, sensitivity of circuits in these computers has reached the point where individual energetic heavy ions such as those in the Fe or C-N-O peaks in the cosmic ray flux can produce upsets in the computer operation. These upsets, termed Single Event Upsets (SEU), can produce effects whose level of seriousness ranges from innocuous to disastrous.

The runs were carried out in collaboration with the NASA Goddard Space Flight Center, the Air Force Space Technology Center, Sandia National Laboratories, RCA, and the Aerospace Corporation. Various logic circuits representing several forms of silicon technology and different levels of complexity were irradiated to provide data needed in the design of devices resistant to SEU. Besides providing the needed data, the runs successfully demonstrated the feasibility of running diffuse, spatially uniform beams, with intensities appropriate for this type of experiment.

---

1. The Aerospace Corporation, Los Angeles, CA.
2. NASA Goddard Space Flight Center, Greenbelt, MD.
3. RCA, Princeton, NJ.
4. Sandia National Laboratory, Albuquerque, NM.

7. PLASMA DIAGNOSTICS FOR FUSION PROGRAM

MULTICHANNEL POLARIMETRY USING FARADAY ROTATION

C. H. Ma D. P. Hutchinson
P. A. Staats

Simultaneous measurements of electron density and Faraday rotation on all five channels of the FIR interferometer/polarimeter system on ISX-B tokamak have been achieved. The achievement is due mainly to two major improvements to the detectors and the Faraday modulator of the previous system: (1) The He-cooled Putley detectors are replaced by high responsivity Schottky diodes and (2) a novel technique is used to improve the performance of the polarization modulator. The use of the Schottky diodes in the present system has not only increased the detection sensitivity but has also eliminated the need for a wire-grid analyzer for polarization determination. The previous Faraday modulator utilized an air core coil. A ferrite disk was mounted in the center of the coil. The modulation frequency was limited to 3-5 kHz due to the high inductance and large stray capacitance of the 600-turn coil. In the present system, the multi-turn coil has been replaced by a single-turn copper coil which acts as the secondary of a radio frequency (rf) transformer. A modulation frequency of 92 kHz has been achieved by using a series resonant circuit for the primary winding. The increase of the modulation frequency has not only greatly improved the time resolution of the polarimeter but has also reduced the rf coupling between the modulator and the detection circuit.

A schematic diagram of the modified interferometer/polarimeter system is shown in Fig. 7.1. Briefly, the system consists of a pair of cw 447 μm iodomethane lasers, optically pumped by separate CO_2 lasers. The FIR cavities are tuned such that the two FIR lasers oscillate at frequencies differing by Δf of the order of 1 MHz. The linearly polarized beam of the source laser is passed through a ferrite polarization modulator, a mechanical polarization rotator into the dielectric waveguide, and is then divided into five beams which are projected through the plasma. Emerging from the plasma chamber, each beam enters again into a waveguide and is directed onto a signal detector. Part of the beam from the reference laser is mixed first in a reference detector with a portion of the source laser, which is split off before passage through the modulator, and the remainder is guided to the signal detector to mix with the plasma-probing beam. Schottky diodes are

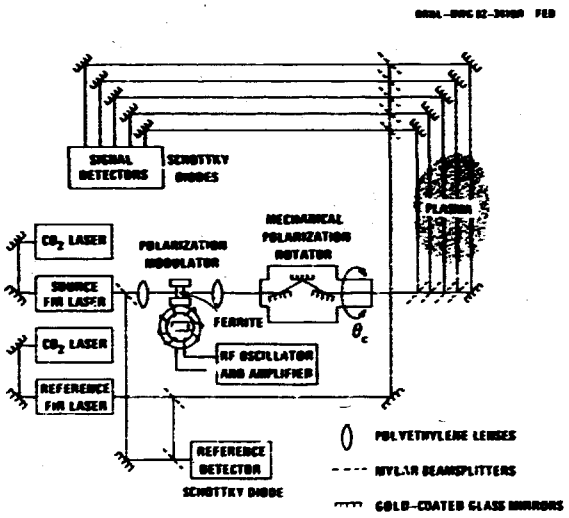

Fig. 7.1. Schematic of the multichord FIR interferometer/polarimeter system for simultaneous measurements of line-averaged electron density and Faraday rotation in ISX-B tokamak plasma.

utilized for all detectors. The output of the reference detector is a sinusoid at frequency Δf and is used as reference signal for phase detection. The output of each signal detector is filtered, amplified, and fed into a digital phase detection circuit to extract the phase shift due to plasma density. An envelope detection circuit is utilized to demodulate the phase-modulated signal, and provides a sinusoidal signal at the modulation frequency whose amplitude is proportional to $J_1(\theta_m)\cdot\sin(\theta)$, where θ_m is the amplitude of the modulation angle, θ is the sum of the rotation angles due to mechanical polarization rotator, θ_c, and Faraday rotation in plasma, θ_p. $J_1(\theta_m)$ is the Bessel function of the first kind with order one. This signal is synchronously detected by a lock-in amplifier, yielding an output voltage, $V_{out} = V_0 \cdot \sin(\theta)$. The calibration constant, V_0, can be obtained by setting the mechanical polarization rotator at a few degrees (<4°) and measuring the value of V_{out} without plasma in the chamber. The voltage V_0 as determined by this technique calibrates the polarimeter in a manner that does not require the absolute

knowledge of laser power, detector responsivity, modulation angle, or any system losses.

The system has been routinely employed to study the ohmic- as well as neutral-beam-heated plasma discharges in ISX-B tokamak for over one year. The standard deviation of the output of the interferometer of a constant phase shift is less than 5×10^{-2} fringe. Since one fringe corresponds to a line-averaged density of 9.2×10^{12} cm^{-3}, density variations as small as 4.6×10^{11} cm^{-3} can be measured. The polarimeter shows a sensitivity of the order of one milliradian and a time resolution of one msec. Figure 7.2 shows the time-resolved traces of (a) Faraday rotation and (b) line-averaged electron density of a typical tokamak plasma discharge. A neutral-hydrogen beam of approximately 1 MW was injected into the plasma 70 msec after the initiation of the plasma discharge. The position of each channel, relative to the center of the tokamak vacuum chamber is also indicated in the inset. The negative Faraday rotation on the central channel (channel 2) is due to the outward shift of the plasma centroid. The fast response of the system is demonstrated in Fig. 7.3. During this plasma discharge, a solid hydrogen pellet was injected into the

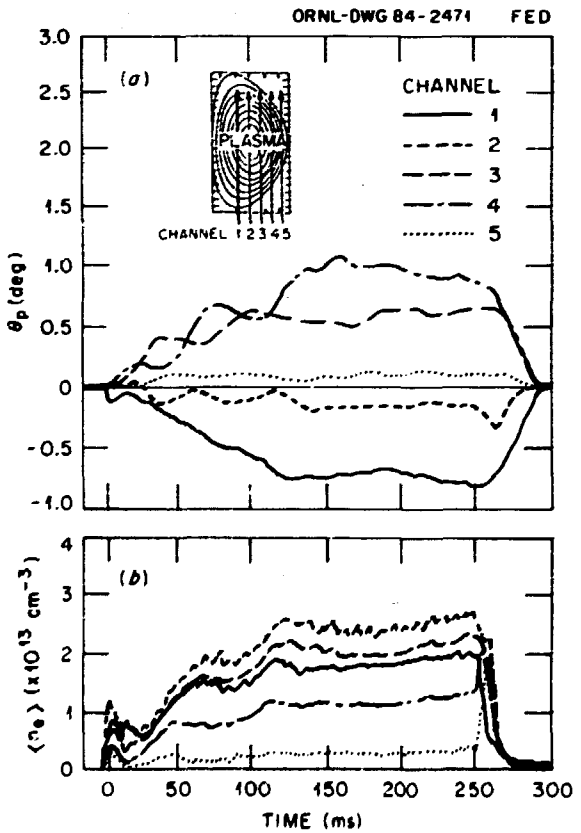

Fig. 7.2. Time variation of (a) Faraday rotation and (b) line-averaged electron density measured by the multichord FIR interferometer/polarimeter system on ISX-B tokamak.

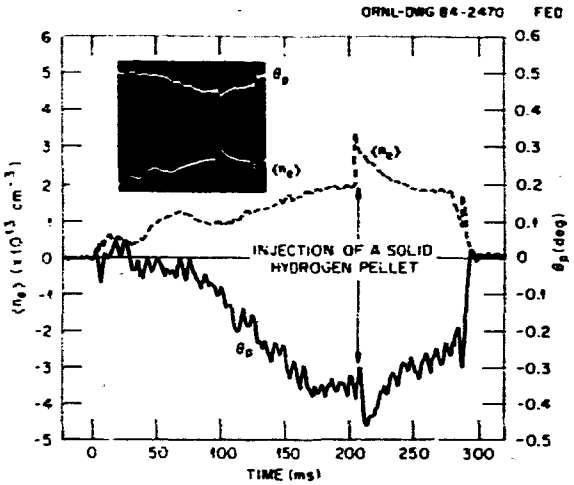

Fig. 7.3. Typical display of time-variation of line electron density and Faraday rotation signal on central channel of the FIR interferometer/polarimeter system. The abrupt changes of the line density and Faraday rotation are caused by the injection of a solid hydrogen pellet at the time of 204 msec after the beginning of the discharge.

plasma at the time of approximately 204 msec. The pellet caused an abrupt density increase of $\sim 1.4 \times 10^{13}$ cm^{-3}, and a change of Faraday rotation of $\sim 0.15°$ on the central channel. The changes of density and Faraday rotation occur during a period of approximately 400 μsec. The time delay (≈3 msec) between two curves is due to the RC constant of the lock-in amplifier (1 msec). It is believed that this is the first simultaneous measurement of electron density and Faraday rotation in pellet-injected discharges. Data analysis codes are under development to reconstruct the asymmetric spatial profiles of electron density and plasma current from the line-averaged chordal measurements.

We have continued to support the implementation of the FIR diagnostics on the TEXT tokamak at the University of Texas, Austin. T. Price has simultaneously measured both density and Faraday rotation on all six channels of the TEXT system. Although the system is not completely calibrated, the Faraday signals are of the proper polarity on all six channels and of roughly the proper magnitude.

C. H. Ma has been engaged in the development of the FIR polarimeter for the TFTR tokamak at Princeton Plasma Physics Laboratory. Experiments have been conducted to determine the performance characteristics of the polarimeter. A signal-to-noise ratio of 20 db has been achieved for a simulated Faraday rotation angle of 5° with four milliwatts of laser power. An analysis has also been carried out in order to identify some possible problems in the measurements, and to establish the calibration procedure for the system.

DIAGNOSTICS DEVELOPMENT CENTER

C. F. Barnett
E. W. Thomas[1]
K. O. Legg[1]
P. Bakshi[2]

A collaborative effort has been initiated with E. W. Thomas (Georgia Institute of Technology) and P. Bakshi (Boston College) to determine the feasibility of measuring plasma edge turbulence and electric fields in magnetically-confined plasmas. Fast-response diode arrays with H_α filters have been constructed to observe time correlations of H_α emission from adjacent locations in the plasma edge using techniques developed by Zweben et al.[3] The first series of measurements will establish the physical extent of coherent emission regions, both poloidally and toroidally. The second series will include the replacement of the H_α filter with a monochromator. By imaging a poloidal strip of the plasma on a vertical entrance slit and placing the diode array in the vertical detector plane we can determine the electric field from the Stark-broadened profiles or shifts of the H_α line. Since the conventional analysis of the Stark effect in plasmas is in terms of the static Holtsmark field, it is necessary to include the line shape and shifts due to quasistatic and high-frequency fields. Modeling of the line shape for different magnitudes and frequencies for these fields has been completed. In addition, the analysis indicates that by determining the polarization of the H_δ line the direction of the driving electric field can be determined. Two 8-diode arrays have been fabricated and tested with their associated amplifiers, circuitry, and signal recording. Computer programs are being written for cross-correlation analysis. Initial tests will be performed using a rapidly pulsed proton beam in H_2 gas, after which the apparatus will be moved to the TEXT tokamak at the University of Texas at Austin.

To measure the ion temperature in a high temperature D-D plasma, we have proposed to make use of the oxygen total neutron cross section which has a deep resonance at about 2.35 MeV.[4] At low plasma temperatures the 2.45-MeV D-D neutron spectra is narrow. As the plasma temperature increases, kinetic broadening increases the width of the neutron distribution with the low-energy tail spilling over into the oxygen resonance. By measuring the attenuation of the neutrons through a liquid oxygen cell, the plasma ion temperature can be obtained if the ions have a Maxwellian velocity distribution. Preliminary calculations[5] had shown the experiment to be feasible for a 2-keV plasma ion temperature using an available liquid oxygen cell. More precise calculations by Alsmiller et al.[6] for a global neutron source from a 6-keV D-D plasma indicated that the overall efficiency of the neutron detector at the rear of the absorption cell would be 4×10^{-11} counts per source neutron. This can be compared to a source strength on the ISX-B tokamak of 2×10^{10} neutrons/sec or approximately 0.16 counts/discharge at the rear detector. Since the calculations are believed to be accurate to within 20%, the technique does not appear to be feasible.

High speed (4000 fps) framing camera studies have been completed on the TEXT tokamak during stable and turbulent operation. Photographs were taken at three viewing ports: perpendicular to the plasma at the limiter port, longitudinal to the plasma viewing the inside of the toroidal limiter, and perpendicular to the plasma 180° from limiter. Semiquantitative data from the films were obtained by visual observation and frame-by-frame scanning with an optical densitometer. The observations are summarized as follows:

- Striations or particle density channels are always present at the beginning or termination of the discharge and during turbulent operation.
- During stable periods of operation, no fluctuations were observed.
- Spallation of macro-size particles or molten pieces of metal were observed during the formation of the discharge, at disruption or with unstable operation, and at the end of discharge.
- Macro-particles were observed at 180° from the limiter, apparently coming from the wall.
- Particles coming from the wall or limiter usually flowed in the direction of the plasma current with a luminous plume extending in front of and behind the particles.

A low-energy Cs neutral particle analyzer[7] has been loaned to the University of Wisconsin for use in the measurement of tokamak plasma ion temperature. In recalibrating the conversion and detection efficiency of the analyzer we found that the sensitivities of two of the channel multipliers were a factor of 2-5 less than the other two. The electrostatic analyzer is being rebuilt and the multipliers are being replaced. These changes in calibration demonstrate the need for periodic recalibration of analyzers after several months of operation.

---

1. Consultant, Georgia Institute of Technology, Atlanta, Georgia.
2. Consultant, Boston College, Boston, Massachusetts.
3. S. J. Zweben, J. McChesney, and R. W. Gould, Nuclear Fusion 23, 825 (1983).
4. P. H. Stelson and C. F. Barnett, "Plasma Ion Temperature Measured by Neutron Transmission Through Liquid Oxygen," Bull. Amer. Phys. Soc. 23, 882 (1978).
5. C. H. Johnson et al., "Measurement of the 2.35-MeV Window in O + n," National Bureau Special Publication 594, Nuclear Cross Section for Technology, 1980.
6. R. G. Alsmiller, Jr., et al., "Background Calculations for the Measurement of the Ion Temperature in a Deuterium Plasma," ORNL/TM-9230, July 1984.
7. D. M. Thomas, "Low Energy Neutral Particle Spectrometer," ORNL-6004, p. 266, Dec. 1983.

FEASIBILITY OF ALPHA PARTICLE DIAGNOSTICS BY CO_2 LASER THOMSON SCATTERING

D. P. Hutchinson
K. L. Vander Sluis
J. Sheffield[1]
D. J. Sigmar[1]

Introduction

The behavior of alpha particles in an ignited fusion plasma is of considerable importance in fusion research since it is the energy transferred to the D-T plasma from the energetic alphas that will be used to sustain the plasma temperature. Several methods have been proposed to measure the density and/or velocity distribution of the alphas.[2-5] Among the suggested techniques are the utilization of charge exchange reactions of the alphas with high energy neutral diagnostic beams,[2-4] the scattering of far-infrared radiation,[4] and the detection of the alphas that escape from the plasma.[4,5] We have evaluated a method that uses the scattering of a high power CO_2 laser by the Debye sphere of electrons associated with each alpha particle to determine both the density and velocity distribution of these energetic fusion products.

Scattered Power Spectrum

The incident radiation at the wavenumber $\bar{k}_i$ and frequency ω_i is scattered and Doppler shifted by electrons in the plasma to the scattered wavenumber $\bar{k}_s$ and frequency ω_s. The radiation of a particular $\bar{k}_s$ and ω_s reaching the detector come from a periodic distribution of electrons in the plasma with wavenumbers $\bar{k} = \bar{k}_s - \bar{k}_i$ and frequency $\omega = \omega_s - \omega_i$. The ions are massive and scatter relatively little of the incident radiation. However, when $|\bar{k}| > \lambda_D$, the Debye length, radiation is scattered from the electrons which are a Debye shield on each ion. For the conditions used in this diagnostic, the shift in frequency corresponds to the Doppler shift caused by the ion-thermal speed $v_i = \omega/k_i$, and the electron-thermal speed $v_e = \omega/k$. The scattered power in the frequency range $\omega \to \omega + d\omega$ and solid angle $d\Omega$ from a length L of the incident beam of electromagnetic radiation is given by Sheffield,[7]

$$P_s(\bar{R},\omega)d\Omega d\omega = P_i r_0^2 n_e L d\Omega \frac{d\omega}{2\pi} Q(\bar{k},\omega)$$

where

$$Q(\bar{k},\omega) = \frac{2\pi}{k}\left|1 - \frac{G_e}{\varepsilon}\right|^2 f_e(\omega/k)$$

$$+ \frac{2\pi}{k}\left|\frac{G_e}{\varepsilon}\right|^2 \sum_z Z f_i(\omega/k)$$

and where it is assumed that the scattered frequency shift $\omega \ll \omega_i$. The electron and ion velocity distribution functions are $f_e(\omega/k)$ and $f_i(\omega/k)$, respectively; r_0^2 is the Thomson cross section, 7.95×10^{-26} cm^2; n_e is the electron density; P_i is the incident laser power; and G_e is the electron susceptibility.

We assume that the electron and bulk ion velocity distributions of the plasma are Maxwellian and the bulk plasma is made up of isotopes of hydrogen (Z=1). The high energy spectrum of the alphas is assumed to be isotropically distributed in velocity space and $f_\alpha(v_\alpha)$ = constant for $v < v_{\alpha 0}$, the velocity of a 3.5 MeV α-particle. Above v_α the alpha distribution function is zero. Also, we ignore kinetic broadening of the alpha velocity distribution due to the finite energy of the interacting D-T ions.

In order to determine the range of scattering angles and frequencies over which more detailed calculations should be performed, we first place simplifying constraints upon the scattered spectrum: (1) consider only phase velocities near $\omega/k = v_\alpha$ and (2) pick a region where the alpha particle scattering and electron scattering are equal. Assuming a 10.6-μm wavelength laser, this corresponds to a scattering angle $\theta = 0.70°$. The signal received from the electron scattering for $v_e > v_\alpha$ will be used to calibrate the alpha-scattered signal, so that for known n_e, T_e we may determine n_α.

Based on this simplified calculation, the scattering geometry depicted in Fig. 7.4 was chosen. The scattered signal is assumed to emerge from the plasma device through an annular window centered on the input laser beam. The viewing window has an angular span from 0.5° to

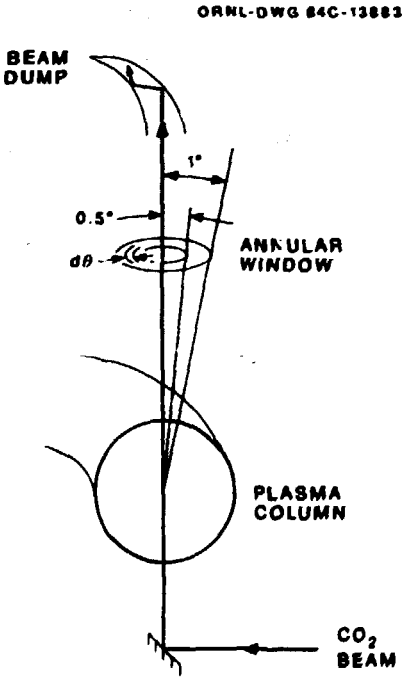

Fig. 7.4. The scattering geometry shown in this figure was chosen to accommodate the small scattering angle necessary to measure the alpha particle velocity distribution.

1.0°. A plot of the total scattered spectrum expected from a TFTR-like plasma as a function of scattered frequency shift based on the geometry depicted in Fig. 7.4 is shown in Fig. 7.5. This calculation assumes a flat alpha particle velocity distribution and indicates that alpha-particle produced scattering is dominant over a range of scattered frequencies from 6-22 GHz. Figure 7.6 depicts a calculation of the composite spectrum as a function of frequency in watts of scattered power per unit frequency for scattering frequencies δF from 0.1 to 25 GHz about the line center of the incident laser for three simple velocity distributions. The distributions modeled are (1) $f_\alpha(v) \equiv 1/v$; (2) $f_\alpha(v) \equiv$ constant; and (3) $f_\alpha(v) \equiv v$. The amplitude of the distributions was normalized to the value n_α/v_α at v_α. The first distribution proportional to 1/v would represent a buildup of particles toward zero velocity assuming little or no diffusion in real space; the second assumes a model based on calculations of TFTR-like[6] plasmas that predict a flat alpha velocity distribution; and the third distribution proportional to v could result if alpha particles were lost during the slowing down process. These distributions are not assumed to accurately model a true plasma case but were chosen to investigate the sensitivity of the proposed diagnostic technique to changes in the alpha-particle velocity distribution. Figure 7.6 shows the scattered power plotted for scattering frequencies greater than 6 GHz, the approximate frequency where the scattering from the injected beam components goes to zero. The composite scattered power from the electrons is constant

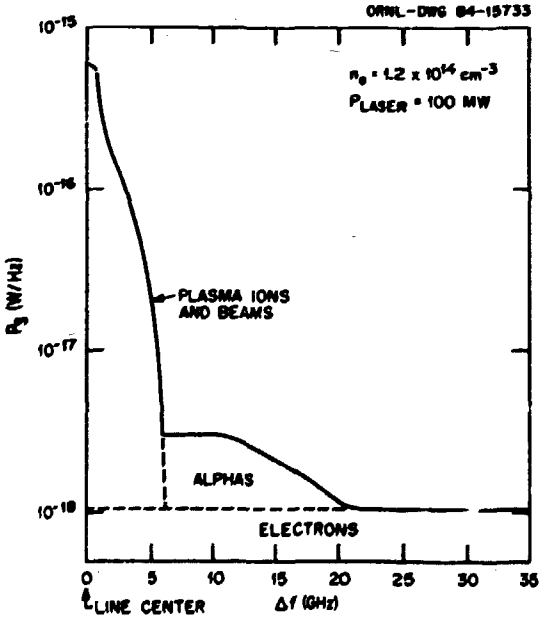

Fig. 7.5. A plot of the total scattered spectrum calculated from Eq. (6) is shown as a function of scattered frequency shift.

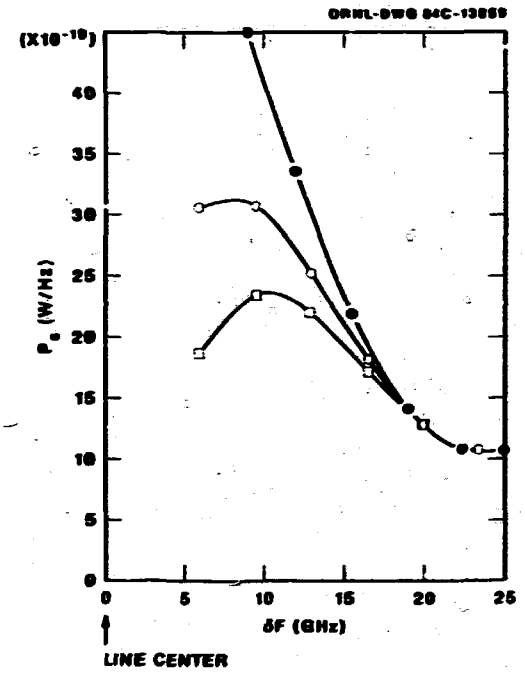

Fig. 7.6. The scattered power versus the shifted frequency δF is plotted for three simple α-particle distributions. The α-particle distribution proportional to 1/v is represented by the open circles, the f(v) = constant distribution by the open squares, and the distribution proportional to v is represented by the open triangles. The electron density assumed for these calculations is 1.2×10^{14} cm^{-3}.

over this range and has a value of approximately 1.05×10^{-17} W/Hz. The 1/f portion of the scattered spectrum from 10 to 20 GHz is due to averaging over the window. The scattering from the alpha particles is 2-3 times the scattering from the electrons over this frequency range.

Detection System

The scattered power from the alpha particles covers the frequency range from 6 to approximately 20 GHz on either side of the 10.6 μm line of the CO_2 laser, whose center frequency is approximately 28,306 GHz. The frequency resolution required is too high to use a grating for dispersion as in a conventional Thomson scattering measurement and too small to use a Fabry-Perot interferometer. Also, the noise level of a liquid-nitrogen-cooled HgCdTe detector operating in the video mode is too high to allow measurement of this power level. If we assume a required frequency resolution of 6 GHz, the video noise-equivalent-power $(NEP)_V$ of this detector is on the order of 5×10^{-8} watts.[8] Referring to Fig. 7.7, a bar graph is presented where the scattered power integrated over a 6-GHz bandwidth is plotted as a function of the frequency of a number of channels centered on the frequencies 7, 11, 17, and 53 GHz from the

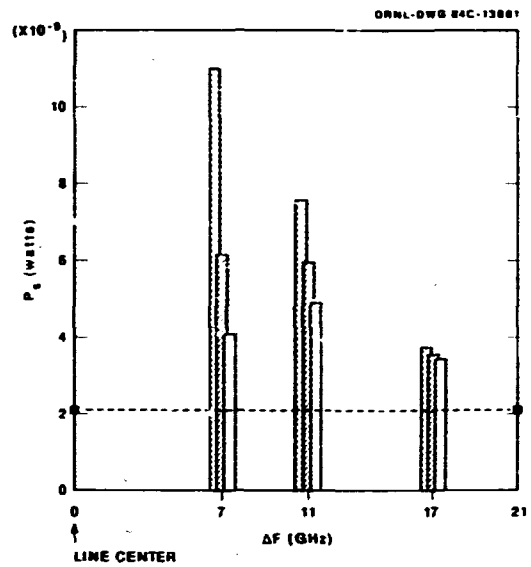

Fig. 7.7. The scattered power integrated over a 2 GHz bandwidth is plotted as a function of the shifted frequency of a number of channels centered on the frequencies 7, 11, 17 GHz from the center of the incident laser line. The channel at 53 GHz, which observes only the electrons, is shown as a dotted line. The 1/v distribution is represented by the bars slanted down to the right, the f(v) = constant distribution is depicted by the bars slanted up to the right, and the open bars represent the f(v) = v distribution.

center of the laser line. (The reason for this channel selection will be stated later.) The power level observed by the detectors varies from approximately 2×10^{-9} watts to 1×10^{-8} watts resulting in a signal-to-noise ratio (S/N) of 0.02 to 0.1. This S/N is clearly unacceptable. By using these detectors as mixers in a heterodyne mode, the NEP reduces to 1×10^{-19} W/Hz$^{1/2}$ resulting in a detector noise power of 2×10^{-10} watts over a 6-GHz bandwidth. This detector noise level translates into an input $(S/N)_i$ of 3 to 16 for a 100 MW CO_2 laser. The post-detection signal-to-noise ratio $(S/N)_{pd}$ for a heterodyne receiver is primarily determined by the post-detection averaging time and the input detector bandwidth. Assuming that the signal is averaged over a laser pulse width of 1 μs from a detector with a bandwidth of 6 GHz, the post-detection signal-to-noise ratio $(S/N)_{pd}$ will be improved by a factor $\sqrt{B\tau + 1}$, where B = predetection bandwidth = 6 GHz and τ = laser pulse width = 1 μs.

$$(S/N)_{pd} = \frac{(S/N)_i}{(S/N)_i + 1}\sqrt{B\tau + 1} = 77.5 ,$$

so that a system S/N of approximately 75 will be achieved.

In order to convert the system to heterodyne detection, a series of CO_2 laser local oscillators must be found whose frequencies differ from the incident laser frequency by only a few gigahertz. A CO_2 rotational line spacing of 53 GHz occurs in the vicinity of the highest gain transition, the 10P20 line. Fortunately, a number of c-w lasers are available within the required frequency range. We have constructed lasers operating on the first sequence bands of CO_2 and N_2O which produce power levels of several watts, far more than the 1-2 mW local oscillator requirement of the HgCdTe detectors.[9] It is expected that other useful local oscillator frequencies will become available when isotopic CO_2 lasers are considered.

Testing and Calibration

A very interesting and attractive feature of the proposed alpha particle diagnostic is that a simpler scattering experiment may be conducted on a non-ignited plasma device to determine the feasibility of the measurement. Referring to Fig. 7.6, since the scattered power due to the alpha particles is roughly equal to the small-angle Thomson scattering measurement of the electron scattering in the absence of alpha particles, the sensitivity of the diagnostic may be determined. In fact, since the electron density and temperature will be known from other diagnostics, an absolute calibration is possible. Also, because a detector observing frequencies shifted 53 GHz from line center will only see scattering from the electrons, even in a burning plasma with alphas present, the experiment will be self-calibrating for every measurement.

---

1. Fusion Energy Division.
2. D. E. Post et al., "Techniques for Measuring the Alpha-Particle Distribution in Magnetically Confined Plasmas," J. Fusion Energy, 1, 129-142 (1981).
3. U. Schumacher and E. Springmann, "Some Considerations Concerning Fusion Alpha Particle Diagnostics," IPP 1/215, Max-Planck-Institut Für Plasmaphysik Report, April 1983.
4. K. N. Sato and M. Sasao, "Alpha Particle Diagnostics for the R-Project," Institute of Plasma Physics, Nagoya University Annual Report, March 1982.
5. G. Gerdin and B. W. Wehring, Technical Progress Report on the TFTR Alpha Extraction and Measurement Project, DOE/ER/53197-1, U.S. DOE, September 1983.
6. Wayne Holberg, ORNL, private communication.
7. J. Sheffield, Plasma Scattering of Electromagnetic Radiation, Academic Press, NY, 1975.
8. Santa Barbara Research Catalog, p. 6 (1983).
9. B. J. Peyton et al., "High-Sensitivity Receiver for Infrared Laser Communications," IEEE J. Quantum Electronics, QE-8(2), Feb. 1972.

8. HIGH ENERGY PHYSICS

H. O. Cohn G. T. Condo[1]
J. E. Brau[1] T. Handler[1]
W. M. Bugg[1]

CHARM PHOTOPRODUCTION AT 20 GeV

The high energy physics program for this period has centered on a hybrid bubble chamber experiment at SLAC to study charm photoproduction with 20 GeV photons obtained from a backscattered laser beam. The project is a collaboration with groups from SLAC, LBL, MIT, Brown University, Tufts University, University of Tennessee, and other institutions in Great Britain, Japan, and Israel. Over 10% of the photographs obtained were scanned and measured on the spiral reader at ORNL. Charm candidates were selected by careful examination of the vertex of interactions in liquid hydrogen on high resolution photographs taken with special cameras where the lens was diffraction limited with a resolution of about 45 microns. Any event where one or more tracks did not extrapolate to the vertex were considered charm candidates. Geometric reconstruction and momentum determination was made from pictures taken with a three view conventional optics arrangement.

Several papers resulted from this experiment covering the charm photoproduction cross section,[2] charm lifetimes,[3] and inclusive photoproduction of neutral strange particles.[4] The inclusive charm cross section at a photon energy of 20 GeV was found to be 60 ± 8 - 21 nb. Here, the first error is due to the sensitivity of the experiment, while the second expresses the systematic errors, principally due to the lifetimes and 2-prong branching ratio uncertainties. Evidence was found for a non-D $\overline{D}$ component to charm photoproduction, consistent with (35 ± 20)% Λ_c^+ production and some $D^{*\pm}$ production.

CHARM LIFETIME

The charm-lifetime results are based on 42 neutral, 45 charged, and 13 topologically ambiguous decays of charmed mesons and were reported by the collaboration to be:

$$\tau_{D^0} = (6.4\ ^{+1.1}_{-0.9} \pm 0.5) \times 10^{-13} \text{ sec}$$

$$\tau_{D^\pm} = (8.2\ ^{+1.3}_{-1.1} \pm 0.6) \times 10^{-13} \text{ sec}$$

and their ratio $\tau_{D^\pm}/\tau_{D^0} = 1.3\ ^{+\ 0.5}_{-\ 0.3}$. The charged lifetime agrees well with the previously reported world average value, however, our neutral lifetime value is considerably longer than that of $(4.4\ ^{+0.8}_{-0.6}) \times 10^{-13}$ given by the data particle group.[5] One event with proper flight time of 55×10^{-13} sec has been observed in this experiment. This possibility of it not being a true charm event has been examined carefully with the conclusion that it is highly likely the event is genuine. The probability of observing such an event in our experiment is about 2%, based on our measured lifetime. On the other hand, the probability of observing this or a longer decay in this experiment is about 4×10^{-4} if the lifetime is taken to be the world average of 4.4×10^{-13} sec.

SEARCH FOR CROSS SECTION ENHANCEMENT NEAR THRESHOLD

It has been suggested[6] that an enhancement of several microbarns in cross section for $\gamma p \rightarrow$ charm baryon + charm meson exists a few hundred MeV above threshold. The collaboration has searched for such an enhancement[7] by exposing the SLAC one-meter hydrogen bubble chamber to a photon beam with energy peaked at 10.5 GeV, which is 700 MeV above the $\gamma p \rightarrow D^-\Sigma_c^{++}$ threshold. Except for reducing the beam energy, the experiment was performed in identical manner to the run at 20 GeV. A total of 98,000 pictures were taken. No charm decays were detected from which an upper limit to the charm cross section of 94 nb (90% confidence level) at E = 10 GeV was obtained.

PHOTOPRODUCTION OF THE CHARGED A_3 (1980) MESON

Little work has been done on the photoproduction of the spin 2 mesons. The only well-establisned observations have been of the charged A_2 through the reaction, $\gamma p \rightarrow A_2^+ n$. In a routine search of the data from a massive bubble chamber experiment, whose primary goal was to study charmed particle production, we have observed an enhancement in the bosonic spectrum of the reaction $\gamma p \rightarrow \pi^+\pi^+\pi^- n$, which is difficult to interpret other than photoproduction of the A_3.

For the current study, only the ~80,000 three-prong events have been examined. All events, for which a three-constraint fit was possible, were eliminated from further consideration ($\gamma p \rightarrow p\pi^+\pi^-$, pK^+K^-, $p\bar{p}p$). Further, if an

event contained an identified proton, either by ionization measurements or because it was a heavily ionizing particle which stopped in the chamber volume, it was removed from our sample. Finally, any event with an identified gamma in the downstream system was eliminated. Our data are derived from the sample of these events which fit the hypothesis $\gamma p \to \pi^+\pi^+\pi^-n$ with a photon energy in the momentum range 15-22 GeV/c. The full three-pion spectrum contains evidence only for A_2 production. However, when the restriction is made that $|t'_{\gamma,3\pi}|$ be less than 0.1 GeV^2, the three-pion spectrum displays clear evidence for not only the A_2^+ but also for a higher mass enhancement.

This spectrum can be fitted, in an acceptable fashion, to a polynomial background together with simple Breit Wigner resonances for the A_2 and a higher mass meson (A_3). Although the fitting program prefers a narrow A_3 resonance (Γ_{A_3} = 57 MeV). The fit quality is virtually undiminished for an A_3 whose width is constrained to be 200 MeV. The dipion mass spectrum for A_3^+ events shows that both ρ^0 and f^0 are present as the decay products of the A_3. Since the only known particle in the mass region with $I^G = 1^-$ is the A_3 and since the A_3^+ decays both to $\rho^0\pi^+$ and $f^0\pi^+$, the simplest assumption is that we are observing the photoproduction of the A_3. Because its production is enhanced at small t', it is suggested that the A_3 is produced by pion exchange. Such a conclusion would further imply that the A_3^+ has a finite decay width to $\pi^+\gamma$. Our initial estimate is that this width is ~1.5 MeV.

CAPTURE OF SLOW ANTIPROTONS

Another area of study concerned the behavior of slow antiproton capture by nuclei. The data were derived from an old bubble chamber exposure to slow antiprotons which stopped in plates of carbon, titanium, lead, and tantalum placed in the bubble chamber. Three papers variously reported the low energy antiproton-nucleus reaction cross sections,[8] Λ^0 production from low energy antiproton annihilations in complex nuclei,[9] and multinucleon captures of slow $\bar{p}$ in complex nuclei and search for the H dibaryon.[10] The later paper reports on a search for doubly strange final states which should become feasible in slow $\bar{p}$ captures in nuclei if the incident $\bar{p}$ interacts with clusters of nucleons. Because of the destruction of a unit of baryon number of the capturing cluster, the reactions possess comparable Q values to the ordinary strangeness producing annihilation reaction. Should double strangeness production occur in $\bar{p}$ annihilations, a doubly strange six-quark dibaryon (H) predicted by the MIT bag model[11] may occur. A sample of 80,000 $\bar{p}$ annihilations in nuclei with $\bar{p}$ momenta of less than 400 MeV/c were searched for the production of two Λ^0, two K^+ or a Λ^0 and K^- in a single interaction. No examples of such processes were found leading to upper limits for frequencies of production of final states containing $2\Lambda^0$, $2K^+$, $K^-\Lambda^0$ of 5 x 10^{-4} per $\bar{p}$ annihilation. If the H particle should exist as an object with mass less than $2m_\Lambda$, it would be stable against decay by the strong interaction, in which case the dominant weak decay mode would be the Σ^-p with a lifetime somewhat longer than the Λ^0. Such decay modes would leave a unique signature in a hydrogen bubble chamber of a "Vee" containing two baryonic prongs, and the negative prong would decay to a π^- or yield a Λ^0 from the reaction $\Sigma^-p \to \Lambda^0 n$. No such events were found leading to a H production upper limit of 9 x 10^{-5} assuming its lifetime is comparable to that of the Λ^0.

---

1. Adjunct staff members from the University of Tennessee, Knoxville, TN 37996.

2. K. Abe et al., Phys. Rev. 30D, 1 (1984).
3. K. Abe et al., Proceedings of XXII International Conference on High Energy Physics, Leipzig (1984), to be published.
4. K. Abe et al., Phys. Rev. 29D, 1877 (1984).
5. Review of Particle Properties, Rev. Mod. Phys. 56, No. 2, Part II, (April 1984).
6. H. Rubinstein and L. Stodolsky, Phys. Lett. 76B, 479 (1978).
7. K. Abe et al., Phys. Rev. 30D, 694 (1984).
8. H. O. Cohn et al., Phys. Rev. C29, 232 (1984).
9. G. T. Condo, T. Handler, and H. O. Cohn, Phys. Rev. C29, 1531 (1984).
10. G. T. Condo et al., Phys. Lett. 144B, 27 (1984).
11. R. L. Jaffe, Phys. Rev. Lett. 38, 195 (1977).

9. COMPILATIONS AND EVALUATIONS

CONTROLLED-FUSION ATOMIC DATA CENTER

C. F. Barnett
H. B. Gilbody[1]
D. C. Gregory
P. M. Griffin
C. C. Havener
A. M. Howald
H. T. Hunter
R. K. Janev[2]
M. I. Kirkpatrick
C. R. Mahon[3]
E. W. McDaniel[4]
R. H. McKnight[5]
F. W. Meyer
T. J. Morgan[6]
R. A. Phaneuf
M. S. Pindzola[7]
E. W. Thomas[4]

The data center continues to maintain a current annotated bibliography of atomic and molecular collision processes of interest in fusion research. During the 24-year history of the data center we have consistently been 1-2 years behind in entering current references into our data base. This year, references are entered directly into our computer file every three months and within a few months we anticipate a monthly input. A universal data storage and retrieval system (INQUIRE) has been implemented by M. Wright of the Computing and Telecommunications Division. Bibliographical information can now be retrieved on-line using ten different search elements. At the present time three outside users are experimenting with retrieval using telecommunications lines to determine the feasibility of extending the data base to a larger group of outside users. Over the years, as computer technology has advanced, we have used several different storage and retrieval programs, with the result that we are at present only able to conduct on-line searches of references entered since 1978. Efforts are being made to convert the various earlier bibliographic formats to one compatible with the INQUIRE format.

Cooperative efforts have continued with the Atomic Data Center for Fusion at the Institute of Plasma Physics (IPP, Nagova, Japan), Atomic and Nuclear Data Center of the Japan Atomic Energy Research Institute (JAERI, Tokai-mura, Japan), and the International Atomic Energy Agency Atomic Data Center (IAEA, Vienna, Austria). During this reporting period, an agreement was reached that the ORNL bibliography would serve as the major input to these centers. ORNL will provide computer tapes every three months. Our staff continues to meet with and advise the IAEA data center on their activities.

To increase the accuracy and efficiency of extracting numerical data from the literature, we have purchased a digitizer tablet and a small stand-alone computer with telecommunications capabilities. The required software has been written and implemented to perform the following steps: (1) digitize numerical data and store on floppy disc; (2) concatenate individual data sets for a given process into one set for comparison and evaluation; (3) redigitize the recommended cross section curve; (4) calculate Maxwellian reaction rate coefficients from cross section data; (5) provide a seven-parameter fit to rate coefficients as a function of temperature; and (6) prepare computer-generated curves of recommended data and data tables for publication. Interfacing the center's computer with the central PDP-10 permits steps 4-6 to be completed.

During the present reporting period the decision has been made to update and expand Vols. 1 and 2 of the present compilation, "Atomic Data for Controlled Fusion" (ORNL-5206 and -5207) to a new series with five or more volumes. Previously, the compilations contained only graphs and data tables of recommended numerical data. Future volumes will add tables and graphs of reaction rate coefficients for interactions of beam-Maxwellian or Maxwellian-Maxwellian distributions. Progress has been made on the first volume, "Heavy Particle Collisions," which will be done in-house. An interagency agreement with Jean Gallagher of the data center at the Joint Institute of Laboratory Astrophysics has been initiated to compile cross section data for "Electron Collisions." Reaction rate coefficient tables and graphs will be generated by the ORNL data center staff. Volume 3 of the series "Collision of Atomic Particles with Surfaces" has been completed and is now in the final stages of review before publication. Particle interactions with surfaces is still an inexact science and much of the data is qualitative. The fourth volume "Spectroscopic Data for Iron" has been compiled by W. Wiese and his colleagues at the National Bureau of Standards. We have received the compilation, except for one chapter on atomic energy levels, which awaits computer reformatting for compatibility prior to publication. Work has been initiated on volume 5, "Collisions of Carbon and Oxygen Ions with Electrons, H, H_2, and He," authored by R. A. Phaneuf of the ORNL Data Center, R. K. Janev, Institute of Physics-Belgrade, and M. S. Pindzola, Auburn University. Data have been compiled from the literature, digitized, evaluated, and cross sections have been recommended for electron capture by C^{q+} and O^{q+} ions from atomic hydrogen and helium. The completion date of these five volumes is anticipated to be

December 1985. Additional volumes are being planned for collisions of other impurity ions present in high temperature fusion plasmas.

---

1. Consultant, Queen's University, Belfast, Northern Ireland.
2. Consultant, Institute of Physics, Belgrade, Yugoslavia.
3. Summer student participant, 1984. Present address: University of Virginia, Charlottesville, Virginia.
4. Consultant, Georgia Institute of Technology, Atlanta, Georgia.
5. Consultant, National Bureau of Standards, Gaithersburg, Maryland.
6. Consultant, Wesleyan University, Middletown, Connecticut.
7. Consultant, Auburn University, Auburn, Alabama.

NUCLEAR DATA PROJECT

S. J. Ball
Y. A. Ellis-Akovali
M. J. Martin
M. R. McGinnis
M. R. Schmorak

The Nuclear Data Project (NDP) is one of five data evaluation centers comprising the U.S. Nuclear Data Network (USNDN). The Project is responsible for the evaluation of nuclear structure information in the mass region A > 195. The NDP maintains a complete computer-indexed library of reports and published articles in experimental nuclear structure physics as well as copies of the Evaluated Nuclear Structure Data and Nuclear Structure Reference files (ENSDF, NSR).

The Project houses the position of Editor-in-Chief of the Nuclear Data Sheets. All mass chains from the 14 centers in the International Nuclear Data Network are edited here, and the Editor-in-Chief has the ultimate responsibility for the quality of the mass chains entered into ENSDF and, thus, for what is published in the Nuclear Data Sheets.

Activities

Data Evaluation. During this report period, NDP staff members prepared revised evaluations for 9 mass chains. References to the publications based on these evaluations are given in the publications section of this report. ENSDF now includes:

1948 Adopted Level Properties data-sets (A = 1-263)

2396 decay scheme data sets

4257 reaction data sets

Mass Chain Editing and Review. NDP staff members edited and/or reviewed 12 mass chains.

Information Services. NNDP staff members responded to about 25 requests by researchers outside the evaluation center for specific information. Responses took the form of searches of the ENDSF and NSR files and personal consultation. A list of reports and preprints received by the NDP is prepared and distributed monthly to division staff members.

Research. NDP staff members have participated in research with other groups in the division. References to these activities are given in the publications section of this report.

10. ACCELERATOR-COLLIDER STUDY

G. D. Alton
W. H. Atkins[1]
C. Baktash
J. R. Beene
J. A. Biggerstaff
E. D. Hudson
C. M. Jones
R. C. Juras[2]
I. Y. Lee
J. A. Martin
J. W. McConnell
J. B. McGrory
W. T. Milner
S. W. Mosko
F. E. Obenshain
D. K. Olsen
F. Plasil
R. L. Robinson
M. R. Strayer
C. M. Thomas[3]
C. Y. Wong
G. R. Young

INTRODUCTION

This section describes a study done for an accelerator facility to be used to accelerate counter-rotating beams of heavy nuclei to kinetic energies of 10 GeV per nucleon and to bring these beams into head-on collision. The extreme conditions occurring in the resulting extended system of hot hadronic matter should result in creation in the laboratory of a qualitatively new form of matter, a quark-gluon plasma. This form of matter is thought to consist of quarks and gluons which are free to propagate over large space-time distances, in sharp contrast to the situation encountered in everyday experience in which quarks and gluons are confined to volumes the size of protons and neutrons. The production of very hot plasma could re-create in the laboratory conditions which have not existed in the universe since a short time, ~10 μs, after the Big Bang, at which time quarks and gluons were first confined in hadrons as the universe cooled. Production of very dense, as opposed to very hot, plasma could allow simulation in the laboratory of conditions thought to prevail today in the cores of neutron stars.

The proposed facility is designed to be able to scan through the expected phase transition separating the normal quark-confining, hadronic phase of nuclear matter and the quark-deconfining, plasma phase of nuclear matter. The nature of the phase transition, such as its order, latent heat, and location in temperature-density space, can be studied using this scanning capability of the facility. The conditions necessary to produce the phase transition, such as required collision energy as a function of the mass of the colliding partners, can be determined. All of this information constitutes essential experimental input to the theoretical description of the transition from hadronic to quark matter. This study is made all the more compelling by noting that such a transition represents the artificial reversal, in the laboratory, of one of the symmetry-breaking transitions postulated to be responsible for the observed hierarchy of forces in physics. Such symmetry-breaking transitions are one of the main cornerstones of modern gauge field theories of matter.

The facility is also well suited for the study of the baryon-rich manifestation of the quark-gluon plasma. This is due to good luminosity and energy variability of the accelerators in the region of 5 GeV/u. At about this collision energy, two heavy nuclei should overlap with maximum pileup of baryon density, creating a "cold" plasma which may be similar in structure to the matter in the cores of neutron stars.

The facility consists of a series of three accelerators optimized for the acceleration of heavy ions. The existing tandem electrostatic acclerator will be used as injector, providing beams of heavy ions ranging from ^{12}C to ^{197}Au at corresponding kinetic energies ranging from 10 MeV/u to 2 MeV/u. This will be followed by a small, room temperature, booster synchrotron with a bending product of 16 Tm. The size of this synchrotron is given by the requirement that all the above heavy ions be completely ionized by passage through a stripper foil after their exit from this accelerator. The third accelerator in sequence will be a pair of superconducting accelerator-collider rings. These will intersect at six points and have a bending product of 90.5 Tm, corresponding to 10 GeV/u for $^{197}Au^{79+}$ ions. Experimental halls will be located at (initially) four of the six intersection points and will have facilities for various type detectors ranging from single-arm spectrometers to large 4π detector facilities. A plan view of the facility as it would be located on the ORNL site is shown in Fig. 10.1.

The peak initial luminosity of the facility will range from $L_0 = 3.5 \times 10^{28}$ cm^{-2} sec^{-1} for $^{12}C + ^{12}C$ collisions to $L_0 = 3.3 \times 10^{26}$ cm^{-2} sec^{-1} for $^{197}Au + ^{197}Au$ collisions. Assuming that central collisions of heavy ions (the most likely ones to produce the transition to quark-gluon plasma) occur for impact parameters b of $b \leq 0.5$ fm, these values correspond to 275 central collisions per second for $^{12}C + ^{12}C$ and to 2.6 central collisions per second for $^{197}Au + ^{197}Au$. These rates are high enough to

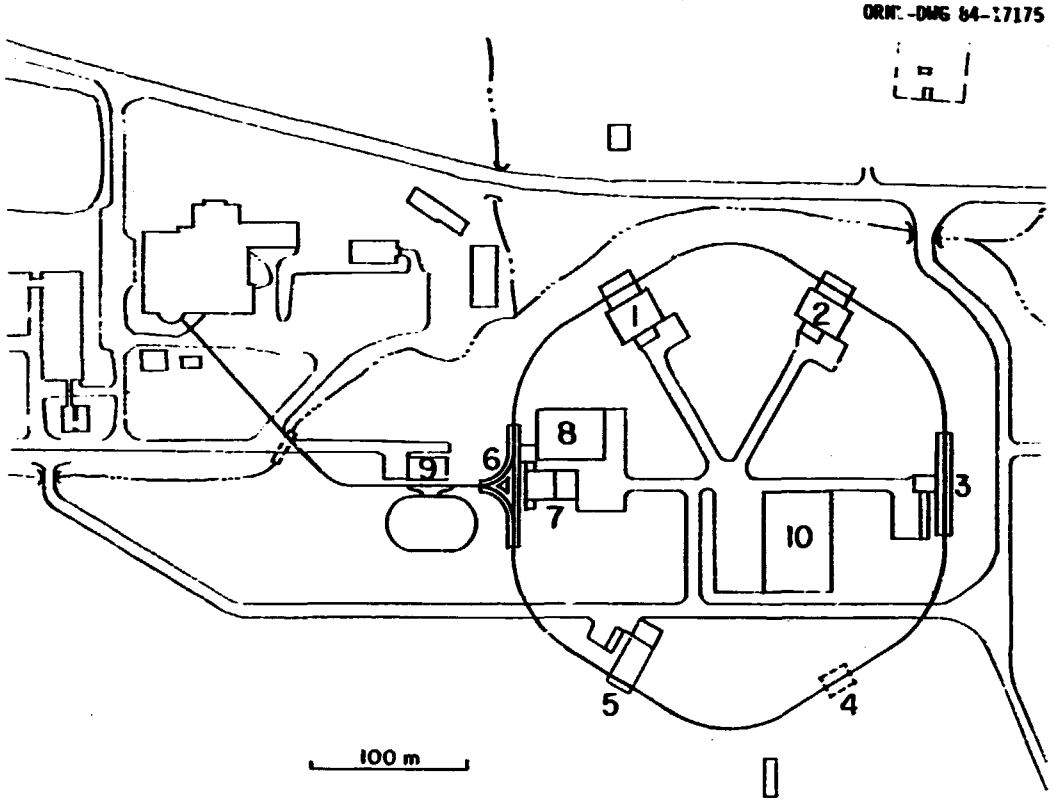

Fig. 10.1. ORNL Heavy-Ion Collider Building Layout

1	Large experiment area #1	7	Cryogenics and HVAC equipment buildings
2	Large experiment area #2	8	Control and office building
3	Narrow-angle experiment hall	9	Booster ring support building
4	Pad for future use	10	Magnet factory and warehouse
5	Wide-angle experiment hall	11	Electrical yard (not shown)
6	Beam injection hall		

allow thorough investigation of several exclusive reaction channels and to allow broad variation of beam parameters over reasonable running times for experiments.

SCIENTIFIC MOTIVATION

A. Theoretical Considerations

The primary scientific objective of the proposed facility is the formation and study of the quark-gluon plasma, which is predicted to be formed in collisions of relativistic heavy nuclei. In addition to the intrinsic interest of studies of the behavior of matter under extreme conditions of density and temperature, there are two specific motivations: (1) the production of the quark-gluon plasma addresses the problem of quark confinement, which is one of the most perplexing phenomena of modern physics; and (2) the production of the plasma may re-create in the laboratory conditions that are similar to those believed to have existed throughout the universe in the early stages (up to ~10 μs) after the Big Bang.

Confinement in QCD is believed to result from a process known as infrared slavery: when a quark tries to leave a nucleon, the potential energy of the color force field increases without bound. The quark is either pulled back into the nucleus or the color field is neutralized by the production of a quark-antiquark pair. In either event, the individual quark does not get free. When the quark is well within the confines of the nucleon, it moves relatively freely. For quarks in this regime, the color force field becomes weak. It has thus proved useful to model the nucleons as bags of quarks. The physical vacuum exterior to the bag exerts a confining pressure on the small region of space inside the bag. The quarks move freely within the bag, where they exist in a region of "perturbative QCD vacuum," but are unable to overcome the confining force of the exterior vacuum and escape from the bag. In more precise terms, phenomenological models of the strong interaction postulate "color confinement," so that the fundamental entities of QCD, quarks and gluons, are permanently confined in bound states. Only those states for which the net color quantum number is zero (colorless states, or color singlets) can exist separately; hence, colored particles like quarks and gluons cannot appear as free particles. In what could prove to be one

of the marked successes of QCD, recent calculations using the lattice-gauge approximation seem to show that color confinement is an inherent property of QCD, resulting from its basic structure. If this is correct, QCD actually predicts quark confinement, and the necessity of introducing it ad hoc disappears. These calculations show another remarkable property. At high temperatures (and presumably high densities), a transition occurs to a new phase in which color is no longer confined in individual hadrons. Instead, quarks and gluons are free to move nearly independently over the whole volume for which the conditions for the phase transition have been achieved. The resulting assembly of "asymptotically free" quarks and gluons is referred to as the quark-gluon plasma. These calculations are still in their infancy, however, and quark confinement remains the least understood aspect of QCD and therefore the most in need of experimental investigation.

At low baryon density and temperature, matter is composed of quarks confined in hadrons, but as the energy density is raised (by increasing the temperature or the baryon density or both), matter becomes deconfined into a quark-gluon plasma. The exact location and the nature of the deconfinement transition continue to be a subject of intense investigation.[4,5] In an SU(3) Yang-Mills system of gluons, Monte Carlo lattice calculations predict a critical temperature of T_c = 160-180 MeV and a phase transition of the first order.[6,7] Results for a system with quarks and gluons have been obtained by retaining only the leading term in the fermion coupling.[8] In this case, the phase transition is less sharp and becomes second order in nature. The energy density of the quark-gluon plasma is close to the Stefan-Boltzman value for an ideal gas of massless gluons and quarks, i.e., about 2.0 GeV/fm^3 at a temperature of about 190 MeV.

In general, the study of the quark-gluon plasma will help us understand the properties of matter under conditions of extreme temperature and density. Specifically, it may provide us with a good way to measure the momentum scale parameter Λ of QCD. Furthermore, by simulating primordial conditions, it may help our understanding of the evolution of the early universe, as well as the structure of neutron stars and the dynamics of supernova explosions. It has been suggested that, at an early epoch, matter in the universe was in the form of a quark-gluon plasma with very small net baryon density. Our familiar hadron-dominated world of the present epoch is the result of a phase transition from the quark-gluon plasma to hadronic matter. Of particular importance to the investigation of the early universe are the order of the phase transition and the temperature and density at which it occurs.[9] A first-order transition is accompanied by large fluctuations at the transition point and may produce planet-size black holes, which could have important implications for the question of the "missing mass" of the universe.

In contrast to the quark-gluon plasma associated with the evolution of the early universe, the plasmas in the interior of neutron stars and in supernova explosions have a large net baryon density but a relatively low temperature. The occurrence of quark-gluon plasma, however, depends on the critical density at the phase transition, and the possibility of a stable neutron star with a quark-gluon interior exists only if the critical density is less than about nine times the normal density of nuclear matter. In any case, it is clear that in view of their relevance to cosmology and to astrophysics, studies of quark-gluon plasmas with both low and high baryon densities would be of great interest.

The nature of the quark-gluon plasma is expected to vary as a function of the beam energy and of the region of rapidity at which it is produced. There result two basic experimental approaches to obtain deconfinement. The first concentrates on the pileup of baryon density such that the hadrons begin to overlap, leading to the formation of a relatively cool quark-gluon plasma. This situation corresponds to densities given by ~5-10 ρ_{nm} and by temperatures of less than 100 MeV. The optimum energies involved in this case must not be excessive in order to avoid the relativistic kinematical problems of longitudinal growth and of transparency. The former causes the hadrons produced in the collision to be formed over too large a region of space to attain high density. The latter reflects the increasing probability of one nucleus to pass through another with increasing relative energy. Various estimates[10,11] put this energy at around 5 GeV per nucleon in the c.m. system.

Alternatively, instead of compressing the matter, high hadron densities may be reached by raising the temperature of the system. This situation may be reached experimentally at higher energies. In this case, there are two separate regions: the mid-rapidity, central region, corresponding to a high hadron (pion) density but to a relatively low net baryon density, and the fragmentation regions at the extremes of the rapidity range, corresponding to high baryon densities. The critical bombarding energy needed for the formation of a quark-gluon plasma has been estimated by many authors.[11-13] One estimate[13] gives the energy density produced in a head-on collision of two equal nuclei, each with a mass number A as

$$\epsilon = 0.06\, A^{0.70}(0.48 \ln E_{c.m.} + 0.37)\ \text{GeV/fm}^3 ,$$

where $E_{c.m.}$ is the center-of-mass energy per nucleon in units of GeV. This estimate is based on multiplicity data obtained from a large number of nucleus-nucleus reactions. The region of collision energy and of mass number A leading to an energy density exceeding the critical energy density of about 2 GeV/fm^3 is indicated by the shaded region in Fig. 10.2. Thus, in a collision of two nuclei, each with $E_{c.m.}$ = 10 GeV per nucleon and $A \gtrsim 100$, the energy density produced will be high enough for the hadronic-matter to quark-gluon plasma phase transition to take place in the high temperature, low-baryon density mode.

The possible formation of a baryon-rich quark-gluon plasma at the extremes of the rapidity range, i.e., in the fragmentation region, is also of interest.[14] It was suggested that at $E_{lab} \gtrsim$ 25-50 GeV per nucleon, the baryons in the fragmentation region may be

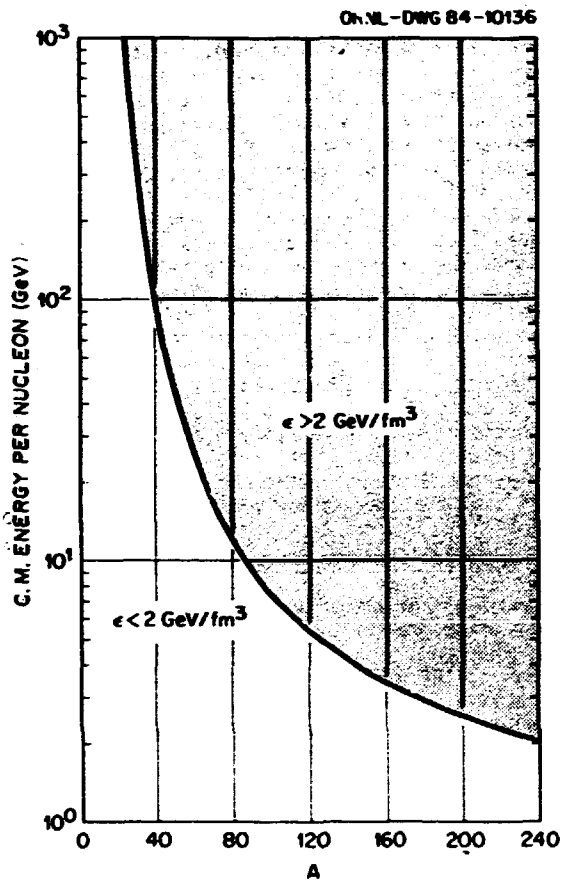

Fig. 10.2. In a head-on collision of two equal nuclei, the region of energy and mass combinations which lead to an energy density greater than 2 GeV/fm^3 is shown shaded.

compressed and excited. The excitation energy in the resulting nuclear fragments may reach 3.5 GeV/fm^3 and may thus exceed the critical energy required for a phase transition.

B. Experimental Considerations

The experimental investigation of the quark-gluon plasma that is expected to be created in collisions between relativistic nuclei is likely to be subject to several complications. In general, any specific signal from the quark-gluon plasma will have to be detected in the presence of a large background originating from the later stages of the decay of the system. Since the equilibrium, nonequilibrium, and critical behavior of the system dramatically affect the composition of the final-state particles and the character of their spectra, and since all of the processes involved are not well-known, the unambiguous isolation of the signals arising from the quark-gluon plasma from the signals arising from the hadronization and freezing-out processes is one of the major challenges that experimentalists have to face.

1. Observation of the Onset of the Quark-Gluon Plasma

Initially, the focus should be on those observables that carry the most unambiguous and direct signals from the quark-gluon plasma. Ideally, one would hope to observe such fingerprints of the plasma as fractionally charged fragments or long-lived exotic configurations of quarks and/or gluons. However, in the absence of any firm theoretical prediction for the existence of such exotic products, we should aim at the study of those penetrating probes that (a) have higher production rates in the quark-gluon plasma compared to the rates in hadronic matter and (b) survive through the hadronization and freezing-out processes with minimal interaction.

a. Direct Radiation

Due to the near absence of final-state interactions, the electromagnetic probes (leptons and photons) should provide a relatively clean signal from the early stages of the nucleus-nucleus collision. In a hot plasma, the $q\bar{q}$ annihilation process gives rise to a significant number of dileptons ($q\bar{q} \rightarrow l\bar{l}$), even beyond the kinematic limit for NN collisions.[15] Unfortunately, several sources of background are anticipated. At large invariant dilepton masses ($M \gtrsim 2$ GeV), the Drell-Yan process gives rise to a significant continuum background. Similarly, at lower masses, both the continuum lepton-pair creation (e.g., $\pi^+\pi^- \rightarrow l\bar{l}$ at $M = 0.8$ GeV, Dalitz-pairs from π^0, ω, and ζ, and Bethe-Heitler pair production at $M \lesssim 0.6$ GeV), and the discrete peaks due to the decay of vector mesons (ρ, ω, ϕ at $M = 0.7$-1.0 GeV) form sources of background. Shuryak[16] has suggested that the intermediate mass region $m_p < M < 2$ GeV is an ideal region to study dilepton production.

Similarly, direct photon production arising from q-q and q-g scattering processes provides a valuable source of information about the interior of the hot plasma. Here again, other sources of gamma rays (e.g., two-photon decay of π^0 and η^0) may interfere with a positive identification. However, one may take advantage of the distinguishing features of these sources of background in order to discriminate against them. For example, the π^0 decay photons are kinematically correlated with each other and have a Hagedorn distribution with an average kinetic energy of 160 MeV. In contrast, direct gammas measure the temperature or heat capacity of the quark-gluon plasma or of hadronic matter and are not limited in energy.

b. Freeze-Out Products

Observation of strange and charmed hadrons (and their antiparticles), which are produced only rarely in ordinary hadronic interactions, constitutes an alternative and complementary approach to the above identification technique. Ordinary nuclear matter contains only the up (u) and down (d) quarks. Therefore, because of the high chemical potential of these light quarks,

$s\bar{s}$ pair production proceeds much more easily in a quark-gluon plasma. According to Rafelski,[17] this results in the following approximate enhancement ratios:

$\frac{\langle s\rangle_{plasma}}{\langle s\rangle_{gas}} \approx 50\text{-}100$, and $\frac{\langle \bar{s}\rangle}{\langle \bar{u} \text{ or } \bar{d}\rangle} \approx 5$. Upon cooling down, the quark constituents of the plasma will freeze out into various hadrons, which are expected to reflect the composition of the hot plasma. Therefore, a large (relative to the gas phase) production cross section for strange, antistrange, and multiply strange hadrons would be a likely indication of the formation of the quark-gluon plasma. It should be noted that the shorter the plasma lifetime, or the smoother the phase transformation is, the more unique this signal becomes, compared to other indicators. Rafelski[17] has estimated that the decay of antihyperons formed in a plasma should provide several Vee's. When normalized to, for example, the cross section measured in pp interactions, high rates of decay of this type could constitute a signature of the onset of the formation of the quark-gluon plasma.

c. Discontinuities Associated with Phase Transitions

Should the transition from hadronic matter to the quark-gluon plasma be a first-order transition, many measurable properties are expected to exhibit a discontinuity across the phase transition. One obvious manifestation of a first-order phase transition is the constant temperature with increasing input energy (beam energy). This is due to the need to supply the latent heat for the formation of the quark matter. It has been suggested that the transverse momentum is a measure of the pressure of the central plasma and that the multiplicity, at a given rapidity, is a measure of energy deposition. On this basis, one may expect the transverse momentum ($P_\perp$) as a function of multiplicity (at a given rapidity) to show saturation effects similar to those seen in other first-order phase transitions.

In the quark-gluon plasma, the basic scattering processes are different from those of nucleon-nucleon scattering. Therefore, a change of the pattern of mass and energy flow of emitted particles may signal the formation of a new form of matter. Furthermore, the mid-rapidity ($y \approx 0$) region is expected to be especially rich in hadronized particles originating from the plasma. Thus, the multiplicity distribution, dn/dy, in the mid-rapidity region, might be directly related to the probability of plasma formation.

2. Properties and Dynamics of the Plasma

Complications associated with the characterization of the quark-gluon plasma are expected to result from the effects of dynamics and from the rapidly changing space-time evolution. For example, starting with a formation time of $\tau_0 \approx 1$ fm/c, the energy density is expected to subsequently drop by a factor of nearly 2 in 1 fm/c. It may take a few fm/c for the plasma to equilibrate (thermal phase). However, in the interim period, the plasma expands with a Hubble constant estimated to be 10^{17} larger than the cosmological Hubble constant, and its evolution will be governed by nonequilibrium processes. To study these complicated phases and their interfaces (initial compression and formation of a plasma, nonequilibrium expansion, thermalization, hadronization, and freezing-out processes), one needs to measure and correlate many hydrodynamical observables. The bulk properties of these systems may be characterized by temperature, volume, relaxation times, and energy and mass densities. However, many of these parameters with which we hope to characterize the plasma and its space-time evolution are, at best, only loosely connected to observables. A great deal of careful systematic work will have to be undertaken before acceptable diagnostic methods can be established. In the following, some possible experiments to determine a few basic properties of the quark-gluon plasma are discussed.

a. Spatial Characteristics

An important property is the size and the shape of the region over which the phase change has occurred. This quantity is primarily sensitive to the mechanism of energy deposition and thermalization in the reaction process; however, knowledge of the spatial extent of the plasma region will be important if we are to correctly interpret other measurements.

Intensity interferometry[18,19] is a well-established technique for studying the space-time structure of an emission source. Pairs of identical particles are detected, and a correlation $C(\vec{p}_1,\vec{p}_2)$ is determined. This function depends not only on the space-time extent of the source, but also on its degree of coherence, thus providing both geometrical and dynamical information on particle production in the reaction. The sensitivity of such measurements increases rapidly as the multiplicity of a particular species of particle increases. Since very large pion multiplicities are expected under conditions required for quark-gluon production, pion interferometry would appear to be a potentially important tool. Unfortunately, pions and other strongly interacting particles will carry little information about the hottest regions where the plasma can exist, because of absorption and rescattering effects in surrounding cooler matter. Therefore, two- and higher order interferometry of pions (speckle interferometry) will yield information only on the size and the shape of the system at the freeze-out time. Direct information, however, will be carried by electromagnetically interacting particles, i.e., by photons and leptons which are copiously produced in the plasma, as discussed in the previous section. Such experiments could yield reasonably direct information on plasma size, as well as provide a tool for investigating long-range order and correlation lengths in the plasma.

It is possible that K^+ correlations may also be an important tool. The K^+ satisfy the requirement of a weak interaction with normal hadronic matter and so can carry information out of the hot, dense region. It is possible that

these correlations could provide information on the space-time structure of the plasma region near the freeze-out, i.e., on the reconfinement process.

b. Temperature

It will be important to study the evolution of the temperature of the plasma as a function of bombarding energy. The best tool is probably provided by the measurement of the shapes of spectra of particles emitted at various stages of the reaction (e.g., photons and dileptons for the plasma and pions for the freeze-out stage). Once the critical energy density for the phase transition is reached, additional energy would go to "melting" hadrons into plasma, i.e., providing the latent heat of deconfinement rather than increasing the temperature. This effect is one of the potential signatures of the phase transition discussed in an earlier section. It would be of interest to continue an investigation of this temperature to higher c.m. energies until it again begins to rise. The length of this temperature plateau would be a measure of the latent heat of deconfinement.

Because of the complicated dynamics of the plasma, the interpretation of this type of data is also not expected to be straightforward. Since the observed particle spectra are space-time integrated, they receive important contributions from both the early stages (i.e., thermally unequilibrated) and later stages (hadronization and freeze-out) of the evolution. Proper deconvolution of these spectra requires not only a better theoretical understanding of the nonequilibrium process, but also a systematic experimental effort, in order to isolate the thermal component.

c. Lifetime

The quark-gluon plasma is expected to exist for a very short time. Its lifetime will depend on the dynamics of expansion and on energy transfer. A possible method to determine the plasma lifetime would consist of the measurement of the total yield of photons, leptons, and strange particles. The number of photons and leptons produced is related to the plasma size, temperature, and lifetime. If the size and temperature are determined independently, it may be possible to deduce the lifetime of the plasma. A similar method could be applied to the abundance of strangeness. It has been shown[17] that the time constant for the strange quarks to reach an equilibrium concentration is comparable to the lifetime of the quark-gluon plasma. Therefore, the lifetime can be derived from the ratio of the number of strange quarks to the number of baryons among the products.

ACCELERATOR FACILITY

The accelerator facility proposed here provides a means of accelerating heavy nuclei, with masses up to at least 200 atomic mass units (amu), to kinetic energies of at least 10 GeV per amu (GeV/u) and bringing two counter-rotating beams of such nuclei into collision. The resulting reaction energy available in the center-of-mass system corresponds to that produced by a beam of 255.6 GeV/u colliding with a stationary target. It is believed such center-of-mass energies and masses of collision partners are well in excess of the minimum values needed to produce a quark-gluon plasma.

The nuclei in each beam will thus have total energies up to at least 11.7 times their rest mass equivalent energy. The facility can easily vary the final kinetic energy of each beam down to a lower value of only half of a GeV/u. The facility can also accelerate a different type of nucleus in each of the two collider rings. A large number of nuclei, with masses spanning the entire periodic table, can be produced by the ion source and accelerated. It should thus be possible to vary the collision conditions sufficiently to produce systems which both do and do not exhibit the expected transition from hadronic matter to the quark-gluon plasma state.

Several collision points, or intersection regions, will be provided about the collider circumference so that up to four or possibly five experiments can proceed simultaneously. Although each group of experimenters must, of necessity, observe collisions between the same nuclei at the same energy, provisions will be made to tune the properties of each intersection region, such as luminosity and crossing angle, to the needs of specific groups and to integrate the experimental apparatus of each group into the structure of the collider.

The three accelerators required are arranged in a cascade with those preceding the collider rings serving to provide bunched beams of fully ionized heavy ions at sufficiently high energy for injection into the collider rings. In order, the facility will include an ion source to produce negative heavy ions, a tandem electrostatic accelerator to provide initial acceleration and first electron stripping of the heavy ions, a small booster synchrotron to bunch the beam and produce ions which may subsequently be completely ionized, and a pair of intersection accelerator collider rings to boost the ions to their final relativistic energies and bring them into collision. The collider will include additional large halls at the intersection regions to house experimental apparatus. Transfer lines connecting the various accelerators and a central control area complete the facility.

The generic advantages of a tandem accelerator as an injector in a multi-component system for the acceleration of heavy ions have been widely recognized. Specifically, they include:

(1) High beam quality (low emittance and energy dispersion, high energy and intensity).
(2) Flexibility (easily changed beam energy, species, intensity, and time structure).
(3) Long source lifetime and generally stable operation.
(4) Simplicity (beam extraction, time modulation, and control).

Operation of the HHIRF tandem accelerator (see Fig. 10.3) as an injector for the booster synchrotron requires acceleration of high intensity, low frequency beam pulses. Typical parameters used for the collider design calculations are: peak injected current, 200 μA; pulse

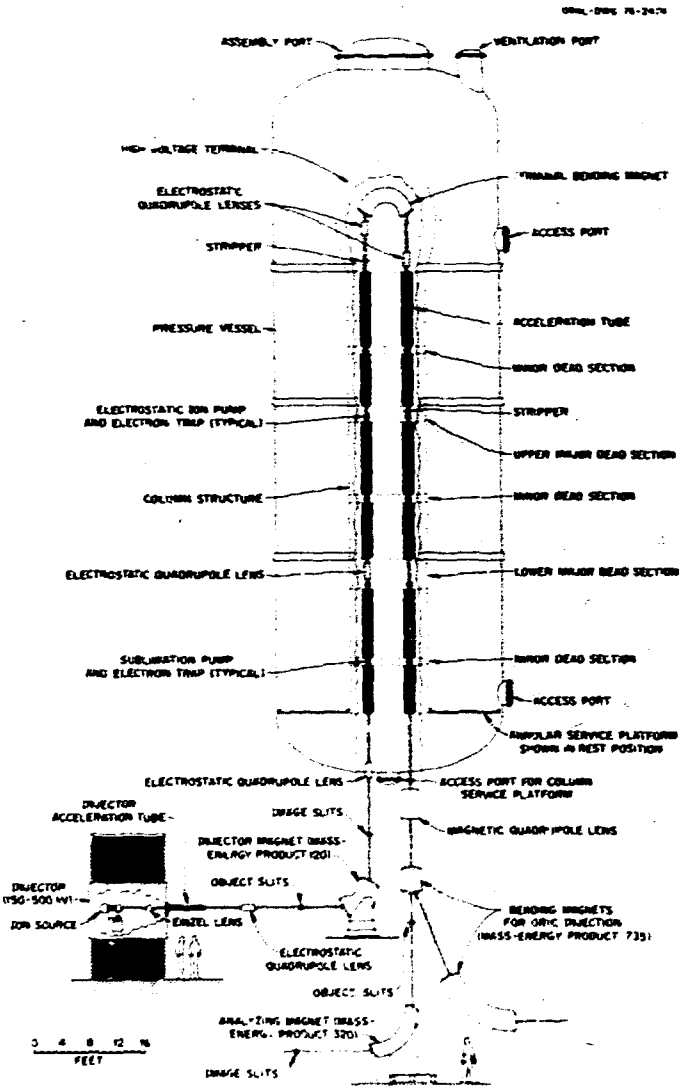

Fig. 10.3. HHIRF tandem electrostatic accelerator.

duration, 100 μsec; repetition rate, 1 Hz. Operation in this mode is made possible by the recent development of high-current, negative heavy-ion sources[20,21] and by the relatively large terminal capacitance of large tandem accelerators which allows acceleration of intense beam pulses without significant terminal voltage decrease.

The HHIRF tandem accelerator is well suited to operation in this mode for several reasons:

(1) Use of a quadrupole lens in the low-energy acceleration tube increases the acceptance of the accelerator by a factor of about two to a value of 16π mm-mrad $MeV^{1/2}$ at a terminal potential of 22 MV.[22] This may be important since high-current, pulsed sources may have higher emittance values than low-current sources. [Note, however, that the estimated emittance for a 70% beam fraction for the Middleton Mark VII axial geometry surface ionization source is 1.6π mm-mrad $MeV^{1/2}$ (Ref. 21).]

(2) Use of a 180° terminal magnet allows complete terminal charge-state separation. Thus, unused post-terminal charge states do not contribute to terminal voltage decrease.

(3) The large size of the terminal leads to a large terminal capacitance, 300 pF, which also reduces terminal voltage decrease.

As an example, we consider acceleration of $^{197}Au^{17+}$ with an injected beam pulse of 200 μA for a duration of 100 μsec. Assuming a 15% charge state fraction, the total charge perturbation will be

$$(200 \times 0.15 \times 17 \times 200) \times 10^{-6} \frac{\text{Coulomb}}{\text{sec}} \times 10^{-4} \text{ sec} = 7 \times 10^{-8} \text{ Coulomb} .$$

With a terminal capacitance of 300 pF, this leads to a terminal voltage decrease of

$$\Delta V = \frac{7 \times 10^{-8} \text{ Coulomb}}{300 \times 10^{-12} \text{ F}} = 240 \text{ V} ,$$

a value which will result in a beam energy change, $\Delta E/E$, of the order of 10^{-5} at both the

terminal and after acceleration through the entire accelerator. This is a negligible additional energy spread for injection into the booster synchrotron.

An important capability of tandem electrostatic accelerators as injectors for heavy-ion colliders is their ability to accelerate any species of negative ion for which a source may be developed. Table 10.1 lists several ions for which high dc current source operation has been demonstrated.[20] Also listed is the cube root of the mass number of the given nucleus. Since this is proportional to the nuclear radius, and since the probability of attaining conditions for producing a quark-gluon plasma also depends on nuclear radius, it is critical to have available a large range of nuclei of differing radii which can be accelerated by the tandem. It is seen from the table that this condition has been met in the ion source development already performed.

The booster synchrotron will be a small conventional machine, of circumference 144 m, employing warm iron magnets and a pair of ferrite-tuned rf cavities to accelerate all nuclei up to mass of 200 amu to kinetic energies of 500 MeV/u. At such kinetic energies, all electrons can be removed from greater than 80% of the nuclei in a beam of gold ions (mass 197) by passage through a thin stripping foil. Such a beam can then be accelerated and stored by the collider rings. For lighter ions the stripping efficiency improves at 500 MeV/u compared to that for gold, reaching nearly 100% for ions of 100 amu and lighter.

Table 10.1. Ions available from negative ion source

Ion	Z	$A^{1/3}$
H	1	1
C	6	2.29
O	8	2.52
S	16	3.17
Cl	17	3.27
Ni	28	3.87
Cu	29	3.98
Se	34	4.34
Br	35	4.33
Ag	47	4.78
I	53	5.03
Yb	70	5.58
Pt	78	5.79
Au	79	5.82

As the largest ion kinetic energies are required for the heaviest ions to remove all electrons by passage through a stripping foil, the necessary size of the booster is determined by the charge state of ^{197}Au ions (taken as the representative mass-200 beam in this report) after they pass through a thin carbon foil at the exit of the tandem accelerator. For a tandem terminal of 22 MV, ^{197}Au ions will strip to charge state 17^+ at the stripping foil inside the tandem terminal and exit the tandem at 396 MeV, or 2.01 MeV/u. Gold ions at this energy strip to a most probable charge state of 44^+, meaning a magnetic rigidity $B\rho$ = 16 T-m for the booster synchrotron will correspond to an exit energy of 488 MeV/u for $^{197}Au^{44+}$ ions.

The tandem beams will be transferred, after stripping at the exit, to the booster via an achromatic transfer line constructed of FODO cells with bending distributed symmetrically about points 180° apart in betatron phase. The required magnet strengths are quite low due to the small (<1 Tm) rigidities of the tandem beams. A combination of magnetic septum, electrostatic deflector, and collapsing orbit bump will be used to inject the beam into the booster ring.

A simple FODO cell lattice has been chosen for the booster, consisting of 18 cells, of which 12 incorporate two 2.6-m-long dipole magnets and of which the remaining 6 have no dipoles. The resulting free straight sections are used for injection, extraction, and acceleration of the beam. The lattice is arranged with six-fold periodicity as shown in Fig. 10.4.

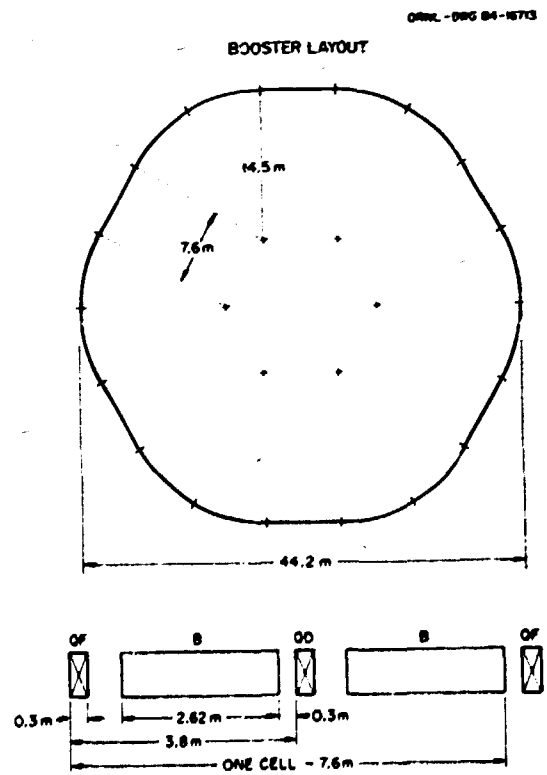

Fig. 10.4. Booster layout and full cell.

A layout of one of the full cells containing dipoles is also shown in Fig. 10.4. The betatron phase advance of each cell is chosen to be 87°, yielding betatron tunes $\nu_x \sim \nu_y \sim 4.3$. Parameters of the booster are given in Table 10.2.

The betatron acceptance in each plane is estimated to be greater than 40π mm-mrad while the emittance of beams produced by the tandem is measured to be less than 2π mm-mrad. By stacking in horizontal betatron space using a collapsing orbit bump, it should be possible to inject in excess of ten successive turns; to be conservative, in the following we have assumed ten such turns may be injected. The injected number of ions per booster cycle resulting from this assumption is then given in Table 10.3. An instantaneous source current of 200 μA, a tandem terminal potential of 22 MV, and selection of the optimum charge state after carbon foil stripping in the tandem terminal and at the tandem exit have been assumed. An overall transmission efficiency of 75% is used for the tandem, in accord with operational experience. The space-charge limit at injection into the booster for a time depression $\Delta\nu = 0.1$ and a bunching factor $B_f = 0.5$ is also given; it is seen that in no case is this limit exceeded.

Table 10.2. Booster parameters

Circumference	136.8 m
Number of cells	18
Cell length	7.6 m
Dipole length	2.62 m
Dipole field	1.6 T
Quadrupole length	0.3 m
Quadrupole poletip field	0.9 T
Phase advance/cell	87°
Tune, H and V	4.3
β_{max}/β_{min}	12.5 m/2.5 m
η_{max}/η_{min}	2.7 m/0.5 m
Max. $B\rho$	16 Tm
Bend radius	10 m

The booster synchrotron will employ conventional, room temperature, iron-dominated magnets. These are needed because of the rapid booster cycle (0.5 Hz) and are acceptable due to the modest power requirement of the booster. (Because the booster is needed only for a few minutes to refill the collider every few hours, it can be "turned off" between refills for further power savings.) A description of the standard dipole and quadrupole magnets is given in Table 10.4, and cross sections of each are shown in Fig. 10.5. To eliminate sagitta, the dipoles will be constructed of 1/16" laminations stacked along an arc of the proper radius. Other magnets included in small correction packages will include trim dipoles and quadrupoles, skew quadrupoles, and sextupoles. Orbit bump magnets, injection and ejection magnetic septum magnets, and the ejection kicker complete the set of magnets required for the booster.

The vacuum requirements of the booster are made especially severe by the need to avoid charge-changing reactions of the partly stripped heavy ions with residual gas atoms and molecules in the vacuum chamber. Since these cross sections are of the order of megabarns at injection, pressures of 10^{-11} torr at 20°C are required in the vacuum pipe of the booster. These will be obtained by having an all stainless steel vacuum system capable of withstanding 200°C bakeout. All possible joints will be field welded; those which must be demounted will be made with metal seal ultrahigh vacuum flanges. Metal-seal sector valves will be used to isolate each quadrant of the machine. Properly trapped roughing and turbomolecular pumps will be used for evacuating to 10^{-6} torr, followed by a combination of high-speed sputter ion pumps and titanium sublimator pumps for attaining the ultrahigh final vacuum of 10^{-11} torr. The vacuum chamber will be thermally insulated from the magnet laminations to prevent the

Table 10.3. Booster currents

Ion	Kinetic energy at tandem exit (MeV/u)	Charge state at tandem exit	Current at tandem exit (particle μA)	Number injected 10 turns ($\times 10^9$)	Space charge limit ($\times 10^9$)
^{12}C	11.0	6^+	75	14.75	42.9
^{32}S	7.56	15^+	22.5	5.32	12.7
^{32}Cu	4.89	24^+	9.0	2.64	6.32
^{127}I	2.77	35^+	5.4	2.11	3.38
^{197}Au	2.01	44^+	4.05	1.90	2.27

Table 10.4. Booster magnets

Dipole	
Length	2.0 m
Aperture	12 cm(h) x 5 cm(v)
Good field aperture	7 cm(h) x 5 cm(v)
Max field	1.57 T
Coil turns/pole	9
Max current	3472 A
Inductance	3.2 mH
Resistance	5.1 mΩ
Peak power	96.5 kW
Weight	2 Tons
Number	32
Quadrupole	
Length	0.3 m
Pole contour	xy = 10.5 cm^2
Max gradient	19.4 T/m
Pole tip field	0.63 T
Coil turns/pole	6
Max current	3899 A
Inductance	0.48 mH
Resistance	1.51 mΩ
Peak power	29.7 kW
Weight	0.36 Tons
Number	48

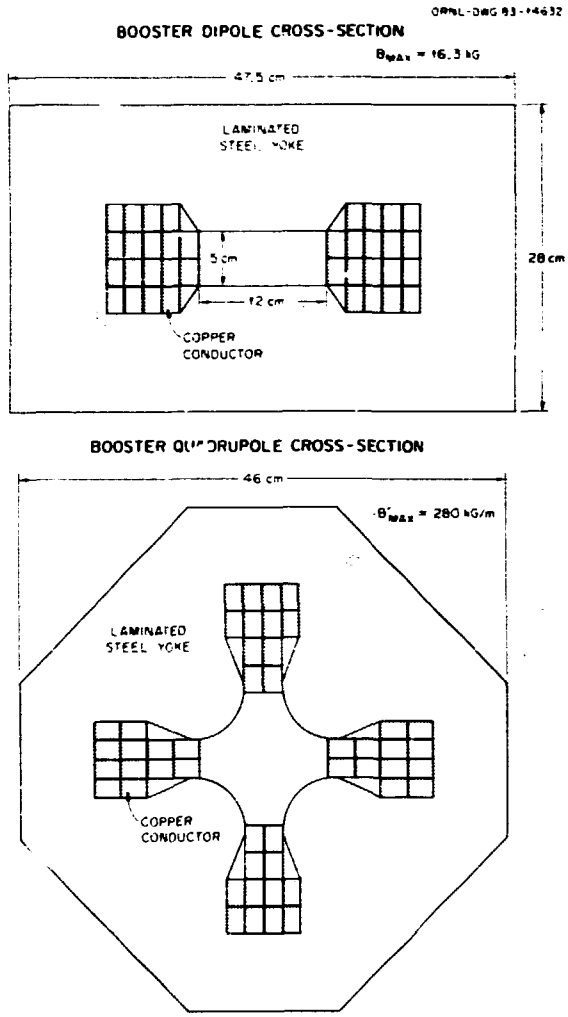

Fig. 10.5. Booster dipole and quadrupole cross sections.

latter's temperature from rising above 65°C to prevent damage to coil insulation and magnet lamination insulation.

After the beam has been accelerated by the booster and given its final bunching in rf phase, the ejector kicker is triggered to bring the beam across a magnetic septum and into an extraction channel. The beam is quickly brought to a focus in both planes and passed through a stripping foil (except for very light beams with A < 20 amu, which are already fully stripped upon injection into the booster). Such a foil must be ~100 mg/cm^2 of Cu (~0.1 mm thick) for heavy beams such as ^{197}Au and correspondingly thinner for less massive beams. The beam is then led through an achromatic transfer line to a splitter and septum magnet which deflects it into one of the two 90° bends leading to injection into the two rings of the collider.

The accelerator-collider consists of two interleaved, roughly hexagonal shape rings of magnets. The general site layout is shown in Fig. 10.1. The rings are each 864 meters in circumference (6 times the booster circumference) and cross at six equally spaced intersection regions. Each ring has a bending power of 90.535 Tm, sufficient to constrain $^{197}Au^{79+}$ of kinetic energy 10 GeV/u to the reference orbit. Each ring has ferrite-tuned rf cavities to accelerate the beams from the injection energy of 486 MeV/u to any desired final energy up to 10 GeV/u, which corresponds to a maximum revolution frequency change of 32%. The ring circumferences are divided roughly equally into six bending arcs, consisting of simple FODO cells, and six long straight sections containing necessary dispersion suppressors, matching quadrupoles, low beta insertions, and beam merging and reseparation magnets. The optical elements for the long straight sections must be designed to permit varying the crossing angle of the beams and thus the length of the luminous region and to permit varying the luminosity from one intersection region to another to accommodate different experimental requirements. A special building for experimental apparatus will surround four of the intersection regions, with two facilities for large detector arrays, one for wide-angle spectrometers and one for narrow-angle spectrometers. A fifth intersection region will be provided with an open pad beneath the collider rings for future development, and the sixth will have a somewhat enlarged tunnel to concentrate machine functions such as injection, ejection, rf cavities, and special equipment. A list of parameters is in Table 10.5.

The arcs are made up of six FODO cells each, 12 m in length. A phase advance near 90° per cell has been chosen, simplifying certain aspects of injection and extraction component

Table 10.5. Collider parameters

Circumference (6 x booster)	864 m
Number, length of arcs	6, 72 m
Number of cells/arc	6
Length of cell	12 m
Phase advance/cell	92°
Dipole length	4 m
Dipole field	2 T
Quadrupole length	0.8 m
Quadrupole poletip field	1.2 T
β_{max} in arcs	20 m
Number, length of IR's	6, 72 m
Free space at crossing	15 m
β_{max} at crossing	< 3 m
η at crossing	0 m
Maximum rigidity	90.53 Tm
Bending radius	45.3 m

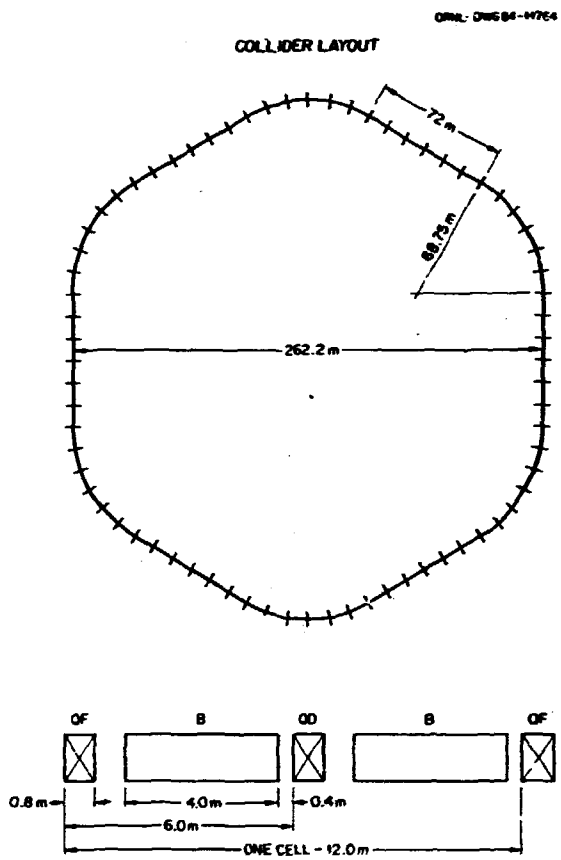

Fig. 10.6. Collider layout and full cell.

placement and yielding a maximum betatron amplitude of 20 m. The sixth cell in each arc contains the dispersion suppressing elements for the following intersection region. A matched cell with no bending follows this, followed by the matching and low beta sections leading to the beam-merging magnets and the crossing point. A layout of one sextant of the ring lattice is shown in Fig. 10.6, which also shows the layout of one full regular cell.

Because of the large normalized emittance (~9π mm·mrad) for light-ion beams just after injection into the booster and because of the need to have large emittances for heavy-ion beams in order to limit the emittance growth rates due to intrabeam scattering, the collider rings are designed to accommodate beams of 10π mm·mrad normalized emittance. Allowing ±5 mm for closed orbit distortion leads to a minimum aperture requirement of 4 cm good field, or a coil ID of 6 cm assuming good field extends to 2/3 of the coil ID. The magnets planned for the collider are of the type known generically as "super ferric" magnets, i.e., iron-dominated window frame magnets with superconducting coils. The dipoles are planned to be 4 meters long and to have a very conservative field of 2 T. The magnets will be constructed with a curvature of 45 m to remove the 4.4 cm sagitta that would result otherwise in straight dipole magnets. The small aperture required and high-current density of present superconductor will result in a compact yoke design. It is therefore planned to assemble two dipoles in a common yoke. Quadrupoles will be kept separate from one another to allow independent positioning of the quadrupoles in the two rings. Development work will also concentrate on mounting dipoles, quadrupoles, correction packages, and beam pick-up elements for one-half cell into a common cryostat. This will simplify transfer of helium between ring elements and minimize the number of cold to warm joints needed for power and control leads.

In order to provide for short bunches for collider operation, the rf system in the collider will run at a harmonic of that in the booster. Given the ratio of circumferences between booster and collider (1:6), matching rf frequencies at transfer (1.572 MHz) results in a harmonic 6 system in the collider. Since this corresponds to a 636-ns separation between bunches and since injection kickers can be made to operate much faster, ~100 ns for a 500-G field, a higher harmonic choice is favored. Present plans call for an h = 144 system operating between 37.73 MHz at injection (β = 0.7549) and 49.78 MHz at top energy (β = 0.9964). With a 106-ns injection kicker, every fourth rf bucket would be filled in the system, resulting in 36 bunches distributed about the circumference of each ring. Thus 72 booster cycles, or 144 seconds, would be required to refill both collider rings. Ferrite-tuned single-gap cavities will be provided in each ring for accelerating and maintaining the length of each beam bunch. An acceleration cycle of one minute to full energy is planned, followed by storage for several hours in collider mode.

The collider magnets will be of the cold iron, cold bore type. This conserves space inside the coil for beam pipe, compared to warm bore designs due to the lack of extra insulation. The vacuum attained in such magnets is 10^{-11} torr at 4°K (based on FNAL experience).

This is adequate to provide for beam survival times of more than one day for the process of electron capture by the beam ions from residual gas ionized by the beam. However, the beam gas background at experiments will be rather high at such pressures, so transitions to a warm bore, baked stainless steel vacuum system are planned for the intersection regions of the machine. The components of this part of the vacuum system will be similar to those used in the booster ring.

Projected performance of the facility for five representative heavy ions is given in Table 10.6. Listed therein are maximum energy, number of stored ions, and maximum initial luminosity for head-on collisions in the intersection regions. Preliminary estimates of luminosity lifetime due to intrabeam scattering indicate that for gold beams the luminosity will decay to 25% of this value after 2 hours; for light beams the projected decay times for luminosity are in excess of one day. The principal loss mechanism for light beams (carbon, sulfur, copper) will be nuclear cross sections which are of the order of 1-5 barns. For very heavy beams such as gold, the cross sections for electromagnetic Coulomb disintegration and K-shell pair production are the dominant loss modes. They increase with collision energy and total more than 50 barns at 10 GeV/u x 10 GeV/u.

EXPERIMENTAL FACILITIES AND SUPPORT BUILDINGS

The present design of the collider ring accommodates six straight sections, one of which will be used for beam injection and rf systems. The remaining straight sections will provide for up to five intersection regions (IR). Four of the IR will be equipped with shielded experimental halls, while the fifth one will be left as a large open pad. This open area is reserved for second generation detectors whose space requirements cannot be foreseen at present. The physical dimensions of the five experimental areas are given in Table 10.7, while Figs. 10.7 and 10.8 show plan and elevation views of the large hall; Fig. 10.1 shows their location on the ring.

A brief survey of existing large collider detectors shows their dimensions are about 11 m long by 8 m high by 8 m wide. Such detectors are easily accommodated between the last insertion quadrupoles, as there will be 15-m free space along the beams centered at the intersection point. Furthermore, to allow for forward-angle instrumentation, the accelerator tunnel will be enlarged for a considerable distance about the intersection point so that counters can be placed at small angles to the colliding beams. To achieve a high luminosity, it is necessary to use near the detectors special low beta insertion quadrupole magnets other than those used in the standard lattice. If the magnetic field in the detectors is not collinear with the beams, special compensating dipoles will be needed to avoid beam-optics disturbances. The beam tube in the center of the IR will be of thin-wall beryllium to reduce interaction with the scattered particles, notably conversion of electrons and photons. A vacuum of 10^{-11} torr at 20°C will be maintained in the IR.

The experimental halls will be equipped with standard laboratory facilities such as clean and general power, lighting, climate control, communications, cooling water, gas handling equipment, fire alarms and sprinkler systems, radiation monitors, and drainage. If room temperature magnets are used for the detectors, one or two megawatts of power may be needed. But if superconducting magnets are used, little power will be needed to energize the magnets. However, liquid helium refrigeration equipment will then be needed to cool the magnets to 4°K. Up to several hundred kilowatts of power will be provided to power the large number of detector modules and the associated electronics that comprise a typical detector system to be housed in the intersection region halls.

Provisions will be made for a large staging area adjacent to each of the two large experimental halls, to allow for the assembly, testing, modification, and repair of the detector systems. The staging areas will have the same elevation as the experimental halls. Loading docks and service roads provide for the access and transport of equipment to and from these areas. Each area will also have laboratory space to handle work on smaller detectors, office space for experimentalists, and a large counting room adjacent for readout electronics and computers. Signals corresponding to machine

Table 10.6. Collider performance

Ion	ε_N π mm mrad	Ions/Bunch	T/A_{max} (GeV/u)	L_0 (head-on) $\beta^* = 3m$ (cm^{-2} sec^{-1})
^{12}C	10	$1.1\ 10^{10}$	12.7	$3.6\ 10^{28}$
^{32}S	10	$4.0\ 10^{9}$	12.7	$4.6\ 10^{27}$
^{63}Cu	10	$2.0\ 10^{9}$	11.6	$1.1\ 10^{27}$
^{127}I	10	$1.6\ 10^{9}$	10.4	$5.0\ 10^{26}$
^{197}Au	10	$1.2\ 10^{9}$	10.0	$3.3\ 10^{26}$

Table 10.7. Locations, dimensions (m), and crane capacities (tons) of the experimental areas

Area	Location	Length	Width	Beam height	Ceiling height	Crane capacity
Large #1 and 2	1&11 o'clock	14	12	5	10	-
Forward bldg. (2)		3	5	3	6	-
Staging area		20	20	5	15	40
Narrow-angle	3 o'clock	10	12	2	7	10
Forward stubs (2)		25	12	2	7	10
Open pad (future use)	5 o'clock	20	15	3	-	-
Wide-angle	7 o'clock	15	30	4	10	20
Injection hall	9 o'clock	72	6	1.2	3	-

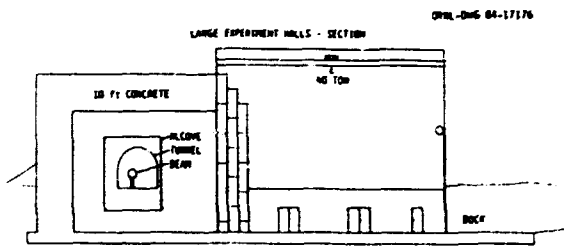

Fig. 10.7. Large facility hall — section view.

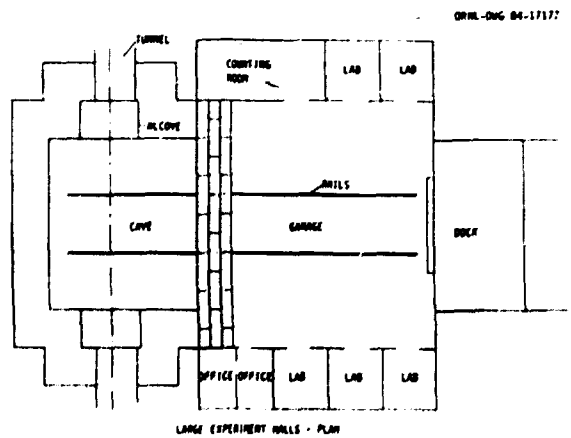

Fig. 10.8. Large facility hall — plan view.

parameters such as beam crossing time, beam position and profile, luminosity, vacuum, radiation level, and status (filling, ramping, colliding, and dumping) will be provided for each counting area.

It is envisioned that the 4π detectors will be assembled on railroad-type carriages in the staging area, and rolled into position on rails. This will minimize the shielding and crane-coverage requirements. The shielding between the hall and staging area will be easily movable. In this scheme, the detector removal from and installation on the beam line will take a short time and have minimal impact on the accelerator operation. The total weight of a typical 4π detector may be a few hundred tons, and some parts may weigh as much as 30 tons. Therefore, a crane of appropriate size will be installed in the staging area. The average floor loading for a completely assembled detector will be approximately 10 tons/m^2.

---

1. Computing and Telecommunications Division.
2. Instrumentation and Controls Division.
3. Oak Ridge Associated Universities, Oak Ridge, Tennessee.
4. For a review, see J. Kogut, Nucl. Phys. A418, 381c (1984).
5. G. Baym, Nucl. Phys. A418, 433c (1984).
6. J. Engels et al., Nucl. Phys. B205, 545 (1982); I. Montvay and E. Pietarinen, Phys. Lett. 110B, 148 (1982).

7. J. Kogut et al., Phys. Rev. Lett. 48, 1140 (1982).
8. J. Engels, F. Karsh, and H. Satz, Phys. Lett. 113B, 398 (1982).
9. D. Schramm and K. Olive, Nucl. Phys. A418, 289c (1984).
10. W. Busza and A. S. Goldhaber, Phys. Lett. 139B, 235 (1984).
11. M. Gyulassy, Proceedings of the Bielefeld Workshop, World Scientific, 1982, p. 81.
12. J. D. Bjorken, Phys. Rev. D 27, 140 (1983).
13. C. Y. Wong, Phys. Rev. D (in press).
14. R. Anishetty, P. Koehler, and L. McLerran, Phys. Rev. D 22, 2793 (1980).
15. K. Kajantie and H. I. Miettinen, Z. Phys. C14, 357 (1982); J. Badier et al., Proc. Bielefeld Workshop, World Scientific (1982), p. 463.
16. E. Y. Shuryak and O. V. Zhirov, Phys. Lett. 89B, 253 (1980).
17. J. Rafelski, Nucl. Phys. A418, 215c (1984).
18. M. Gyulassy, S. K. Kauffmann, and L. W. Wilson, Phys. Rev. C 20, 2267 (1979) and references therein; H. Boggid and I. Otterlund, Proc. Bielefeld Workshop, World Scientific (1982), p. 485 and references therein.
19. W. A. Zjac et al., Proc. 5th High Energy Heavy Ion Summer Study, LBL-12652.
20. G. D. Alton and G. C. Blazey, Nucl. Instrum. Methods 166, 105 (1979).
21. R. Middleton, Nucl. Instrum. Methods Phys. Res. 214, 139 (1983).
22. J. D. Larson and C. M. Jones, Nucl. Instrum. Methods 149, 489 (1977).

11. PUBLICATIONS

List Prepared by Shirley J. Ball

The following list of publications includes primarily those articles by Physics Division staff members and associates which appeared in print from October 1983 through September 1984. Articles pending publication as of September 30, 1984, are listed immediately following this section.

BOOK, JOURNAL, AND PROCEEDINGS ARTICLES

Abe, K., T. C. Bacon, J. Ballam, L. Berny, A. V. Bevan, H. H. Bingham, J. E. Brau, K. Braune, D. Brick, W. M. Bugg, J. Butler, W. Cameron, J. T. Carroll, C. V. Cautis, J. S. Chima, H. O. Cohn, D. C. Colley, G. T. Condo, S. Dado, R. Diamond, P. J. Dornan, R. Erickson, T. Fieguth, R. C. Field, L. Fortney, B. Franek, N. Fujiwara, R. Gearhart, T. Glanzman, J. J. Goldberg, G. P. Gopal, A. T. Goshaw, E. S. Hafen, V. Hagopian, G. Hall, E. R. Hancock, T. Handler, H. J. Hargis, E. L. Hart, P. Haridas, K. Hasegawa, T. Hayashino, D. Q. Huang, R. I. Hulsizer, S. Isaacson, M. Jobes, G. E. Kalmus, D. P. Kelsey, J. Kent, T. Kitagaki, J. Lannutti, A. Levy, P. W. Lucas, M. MacDermott, W. A. Mann, T. Maruyama, R. Merenyi, R. Milburn, C. Milstene, K. C. Moffeit, J. J. Murray, A. Napier, S. Noguchi, F. Ochiai, S. O'Neale, A.P.T. Palounek, I. A. Pless, M. Rabin, P. Rankin, W. J. Robetson, A. H. Rogers, E. Ronat, H. Rudnicka, T. Sato, J. Schneps, S. J. Sewell, J. Shank, A. M. Shapiro, C. K. Sinclair, R. Sugahara, A. Suzuki, K. Takanashi, K. Tamai, S. Tanaka, S. Tether, H. B. Wald, W. D. Walker, M. Widgoff, C. G. Wilkins, S. Wolbers, C. A. Woods, Y. Wu, A. Yamaguchi, R. K. Yamamoto, S. Yamashita, G. Yekutieli, Y. Yoshimura, G. P. Yost, and H. Yuta
"Charm Photoproduction at 20 GeV," Phys. Rev. D 30, 1-21 (1984)

Abe, K., T. C. Bacon, J. Ballam, A. V. Bevan, H. H. Bingham, J. E. Brau, K. Braune, D. Brick, W. M. Bugg, J. Butler, W. Cameron, J. T. Carroll, C. V. Cautis, J. S. Chima, H. O. Cohn, D. C. Colley, G. T. Condo, S. Dado, R. Diamond, R. Erickson, T. Fieguth, R. C. Field, B. Franek, N. Fujiwara, K. Furuno, R. Gearhart, D. Gershoni, J. J. Goldberg, G. P. Gopal, A. T. Goshaw, E. S. Hafen, G. Hall, E. R. Hancock, T. Handler, H. J. Hargis, P. Haridas, E. L. Hart, K. Hasegawa, T. Hayashino, I. Hideta, R. I. Hulsizer, M. Jobes, G. E. Kalmus, D. P. Kelsey, J. Kent, T. Kitagaki, A. Levy, P. W. Lucas, W. A. Mann, R. Merenyi, R. Milburn, C. Milstene, K. C. Moffeit, J. J. Murray, A. Napier, S. Noguchi, F. Ochiai, S. O'Neale, Y. Ohtani, A.P.T. Palounek, I. A. Pless, P. Rankin, A. H. Rogers, E. Ronat, H. Rudnicka, H. Sagawa, T. Sato, J. Schneps, J. Shank, A. M. Shapiro, R. Sugahara, A. Suzuki, K. Takahashi, K. Tamai, S. Tanaka, S. Tether, W. D. Walker, M. Widgoff, C. G. Wilkins, S. Wolbers, C. A. Woods, A. Yamaguchi, R. K. Yamamoto, S. Yamashita, Y. Yoshimura, G. P. Yost, and H. Yuta
"Inclusive Photoproduction of Neutral Strange Particles at 20 GeV," Phys. Rev. D 29, 1877-87 (1984)

Abe, K., T. C. Bacon, J. Ballam, A. V. Bevan, H. H. Bingham, J. E. Brau, K. Braune, D. Brick, W. M. Bugg, J. M. Butler, W. Cameron, H. O. Cohn, D. C. Colley, S. Dado, R. Diamond, P. Dingus, R. Erickson, R. C. Field, B. Franek, N. Fujiwara, R. Gearhart, T. Glanzman, J. J. Goldberg, A. T. Goshaw, G. Hall, E. R. Hancock, T. Handler, H. J. Hargis, E. L. Hart, K. Hasegawa, R. I. Hulsizer, M. Jobes, G. E. Kalmus, D. P. Kelsey, T. Kitagaki, W. Kowald, A. Levy, P. W. Lucas, W. A. Mann, E. McCrory, R. Merenyi, R. Milburn, C. Milstene, K. C. Moffeit, J. J. Murray, A. Napier, S. Noguchi, F. Ochiai, S. O'Neale, A.P.T. Palounek, I. A. Pless, P. Rankin, W. J. Robertson, H. Sagawa, T. Sato, J. Schneps, F. J. Sewell, J. Shank, A. M. Shapiro, R. Sugahara, A. Suzuki, K. Takahashi, K. Tamai, S. Tanaka, S. Tether, W. D. Walker, M. Widgoff, C. G. Wilkins, S. Wolbers, C. A. Woods, A. Yamaguchi, R. K. Yamamoto, S. Yamashita, Y. Yoshimura, G. P. Yost, and H. Yuta
"Study of the $\rho'(1600)$ Mass Region Using $\gamma p \to \pi^+\pi^- p$ at 20 GeV," Phys. Rev. Lett. 53, 751-754 (1984)

Abe, K., T. C. Bacon, H. H. Bingham, J. E. Brau, K. Braune, D. Brick, W. M. Bugg, J. M. Butler, W. Cameron, H. O. Cohn, D. C. Colley, S. Dado, P. Dingus, R. Erickson, R. C. Field, B. Franek, R. Gearhart, T. Glanzman, I. M. Godfrey, G. Hall, E. R. Hancock, H. J. Hargis, E. L. Hart, M. J. Harwin, K. Hasegawa, R. I. Hulsizer, M. Jobes, T. Kafka, G. E. Kalmus, D. P. Kelsey, T. Kitagaki, A. Levy, R. Merenyi, J. J. Murray, V. O'Dell, I. A. Pless, P. Rankin, E. Ronat, H. Sagawa, S. J. Sewell, J. Shank, J. Shimony, K. Tamai, S. Tanaka, D. A. Waide, M. Widgoff, S. Wolbers, C. A. Woods, A. Yamaguchi, R. K. Yamamoto, G. P. Yost, and H. Yuta
"Search for a Threshold Enhancement in the $\gamma p \to$ Charmed Baryon + Charmed Meson Cross Section," Phys. Rev. D 30, 694-96 (1984)

Alton, G. D.
"Ionization Phenomena and Sources of Ions," pp. 44-178 in Applied Atomic Collision Physics, Vol. 4: Condensed Matter, Academic Press, Orlando, Florida, 1983

Alton, G. D. (Invited Paper)
"Ionization Phenomena and Sources of Negative Ions," p. 85 in Vol. I, Proceedings, International Ion Beam Engineering Congress, Kyoto, Japan, September 12-16, 1983

Andersen, L. H., M. Frost, P. Hvelplund, H. Knudsen, and S. Datz
"Correlated Two-Electron Effects in Highly Charged Ion-Atom Collisions: Transfer Ionization and Transfer Excitation in 20-MeV Au^{15+} + He Collisions," Phys. Rev. Lett. 52, 518-21 (1984)

Arve, P., Y. S. Chen, and G. A. Leander
"Microscopic Calculations of Nuclear Wobbling Rotation," Proceedings, Nordic Symposium on Nuclear Physics, Fuglso, Denmark, August 16-20, 1982, Phys. Scr. T5, 157-61 (1983)

Atkins, W. H.
"Data Acquisition Software for the Holifield Heavy Ion Research Facility," Proceedings, Conference on Real-Time Computer Applications in Particle and Nuclear Physics, Berkeley, California, May 16-19, 1983, IEEE Trans. Nucl. Sci. NS-30, 3797-801 (1983)

Auble, R. L.
"Nuclear Data Sheets for A = 198," Nucl. Data Sheets 40, 301-83 (1984)

Auble, R. L., Editor
"Holifield Heavy Ion Research Facility Newsletter," Issue No. 25 (1984)

Auble, R. L., J. B. Ball, F. E. Bertrand, C. B. Fulmer, D. C. Hensley, I. Y. Lee, R. L. Robinson, P. H. Stelson, C. Y. Wong, D. L. Hendrie, H. D. Holmgren, and J. D. Silk
"Light-Ion Emission from Reactions Induced by 0.8-2.4 GeV ^{16}O Projectiles," Phys. Rev. C 28, 1552-64 (1983)

Austin, S. M., G. A. Baym, F. Boehm, D. A. Bromley, H. H. Chen, D. Cline, K. A. Erb, H. A. Grunder, C. M. Hoffman, A. K. Kerman, M. H. Macfarlane, P. G. Roos, J. P. Schiffer, A. Z. Schwarzschild, I. Sick, and E. W. Vogt
"Report of the Panel on Electron Accelerator Facilities," DOE/NSF Nuclear Science Advisory Committee Report, DOE/ER-0164 (April 1983)

Austin, S. M., G. A. Baym, F. Boehm, D. A. Bromley, H. H. Chen, D. Cline, K. A. Erb, H. A. Grunder, C. M. Hoffman, A. K. Kerman, M. H. Macfarlane, P. G. Roos, J. P. Schiffer, A. Z. Schwarzschild, I. Sick, and E. W. Vogt
"A Long Range Plan for Nuclear Science," DOE/NSF Nuclear Science Advisory Committee Report (December 1983)

Awes, T. C., R. L. Ferguson, R. Novotny, F. E. Obenshain, F. Plasil, S. Pontoppidan, V. Rauch, G. R. Young, and H. Sann
"Energy Division in Damped Reactions," Phys. Rev. Lett. 52, 251-54 (1984)

Awes, T. C., R. L. Ferguson, R. Novotny, F. E. Obenshain, F. Plasil, V. Rauch, H. Sann, and G. R. Young (Invited Paper)
"Projectile Fission in ^{58}Ni-Induced Reactions at 15.3 MeV/u," pp. 101-04 in Proceedings, Workshop on Nuclear Dynamics III, Copper Mountain, Colorado, March 5-9, 1984, Indiana University Nuclear Chemistry Report, INC-40007-24 (April 1984)

Ball, J. B., and R. L. Auble (Invited Paper)
"Emission of High-Energy Light Particles from Intermediate-Energy Heavy-Ion Reactions," pp. 359-73 in Proceedings, Second Indo-U.S. Symposium on Nuclear Physics at Cyclotron and Intermediate Energy, Bombay, India, May 24-28, 1982, Bhabha Atomic Research Centre, Bombay, India, 1983

Barnett, C. F.
"Preface," in Applied Atomic Collision Physics, Vol. 2: Controlled Fusion, Academic Press, New York, 1984

Barnett, C. F.
"Introduction," pp. 1-25 in Applied Atomic Collision Physics, Vol. 2: Controlled Fusion, Academic Press, New York, 1984

Barnett, C. F.
"Particle Plasma Diagnostics," pp. 249-305 in Applied Atomic Collision Physics, Vol. 2: Controlled Fusion, Academic Press, New York, 1984

Barnett, C. F., and D. C. Gregory
"ORNL's Controlled Fusion Atomic Data Center," pp. 156-59 in Proceedings, Workshop on Electronic and Ionic Collision Cross Sections Needed in the Modeling of Radiation Interaction with Matter, Argonne, Illinois, December 6-8, 1983, Argonne National Laboratory Report, ANL-84-28 (May 1984)

Becker, R. L., A. L. Ford, and J. F. Reading
"Multiple-Vacancy Production in the Independent-Fermi-Particle Model," Phys. Rev. A 29, 3111-21 (1984)

Becker, R. L., A. L. Ford, and J. F. Reading
"Rate of Saturation of Target L-Shell Vacancy Probability, p_L, with Projectile Charge as Given by Coupled-Channels Calculations," Proceedings, Third International Conference on Particle-Induced X-Ray Emission, Heidelberg, West Germany, July 18-22, 1983, Nucl. Instrum. Methods Phys. Res., Sect. B, 231 [B3], 43-46 (1984)

Becker, R. L., A. L. Ford, and J. F. Reading (Invited Paper)
"The Roles of Pauli Correlations, Channel Couplings, and Shake-Off in Ion-Induced KL^V and K^2L^V Multiple-Vacancy Production," Proceedings, Third Workshop on Inner Shell Ionization by Light Ions, Linz, Austria, August 4-5, 1983, Nucl. Instrum. Methods Phys. Res., Sect. B, 232 [B4], 271-78 (1984)

Beene, J. R., R. L. Auble, F. E. Bertrand, M. L. Halbert, D. C. Hensley, D. J. Horen, R. L. Robinson, R. O. Sayer, and T. P. Sjoreen (Invited Paper)
"Neutron and Gamma Decay of Giant Resonances in ^{208}Pb Excited by 381-MeV ^{17}O Ions," pp. 161-78 in Nuclear Physics with Heavy Ions (Proceedings, International Conference on Nuclear Physics with Heavy Ions, Stony Brook, New York, April 14-16, 1983), Harwood Academic, New York, 1984

Bemis, C. E., Jr., J. R. Beene, J.L.C. Ford, Jr., D. Shapira, and B. Shivakumar (Invited Paper)
"Development of Optically Pumped Polarized Jet Targets for Use in Heavy-Ion Reaction Studies," pp. 141-[illegible] in Proceedings, Workshop on Polarized Targets in Storage Rings, Argonne, Illinois, May 17-18, 1984, Argonne National Laboratory Report, ANL-84-50 (August 1984)

Berman, B. L., S. Datz, R. W. Fearick, R. L. Swent, R. H. Pantell, H. Park, J. O. Kephart, and R. K. Klein
"Planar Channeling Radiation from Relativistic Positrons and Electrons in LiF," Proceedings, 10th International Conference on Atomic Collisions in Solids, Bad Iburg, F.R.G., July 18-22, 1983, Nucl. Instrum. Methods Phys. Res., Sect. B, 230 [B2], 90-94 (1984)

Bertrand, F. E.
"Giant Resonances — Why Protons?," pp. 181-232 in Proceedings, Conference on Studying Nuclei with Medium Energy Protons, Edmonton, Canada, July 11-13, 1983, TRIUMF Meson Facility Report TRI-83-3 (1983)

Bertrand, F. E., J. R. Beene, and T. P. Sjoreen
"Heavy-Ion Excitation and Photon Decay of Giant Resonances," Proceedings, International Symposium on Highly Excited States and Nuclear Structure, Orsay, France, September 5-8, 1983, J. Phys. (Paris) Colloq. 45, C4-99-114 (1984)

Blecher, M., K. Gotow, R. L. Burman, M. V. Hynes, M. J. Leitch, N. S. Chant, L. Rees, P. G. Roos, F. E. Bertrand, E. E. Gross, F. E. Obenshain, T. P. Sjoreen, G. S. Blanpied, B. M. Preedom, and B. G. Ritchie
"Isospin Effects in $\pi^{\pm}$ Elastic Scattering from ^{12}C, ^{13}C, and ^{14}C at 65 and 80 MeV," Phys. Rev. C 28, 2033-41 (1983)

Bottcher, C. (Invited Paper)
"Numerical Solution of the Few-Body Schrödinger Equation," pp. 187-200 in Proceedings, XIII International Conference on the Physics of Electronic and Atomic Collisions, Berlin, West Germany, July 27-August 2, 1983, Elsevier, Amsterdam, 1984

Bottcher, C.
"Numerical Calculations on Electron-Impact Ionization," pp. 241-66 in Advances in Atomic and Molecular Physics, Vol. 20, Academic Press, New York (1984)

Braga, R. A., B. E. Gnade, R. W. Fink, and H. K. Carter
"Half-Life of the $h_{9/2}$ Shell-Model Intruder-State Isomer ^{187m}Au," Nucl. Phys. A410, 441-44 (1983)

Braun-Munzinger, P., P. Paul, L. Ricken, J. Stachel, P. H. Zhang, G. R. Young, F. E. Obenshain, and E. Grosse
"Pion Production in Heavy-Ion Collisions at E_{lab}/A = 35 MeV," Phys. Rev. Lett. 52, 255-58 (1984)

Breinig, M., G. J. Dixon, P. Engar, S. B. Elston, and I. A. Sellin
"First Observation of the Thomas Peak in Continuum Capture: Capture of H Atoms from CH_4 Molecules by Fast Ar^+ Projectiles," Phys. Rev. Lett. 51, 1251-54 (1983)

Brick, D., H. Rudnicka, A. M. Shapiro, M. Widgoff, R. E. Ansorge, W. W. Neale, D. R. Ward, B. M. Whyman, R. A. Burnstein, H. A. Rubin, E. D. Alyea, Jr., L. Bachman, C.-Y. Chien, P. Lucas, A. Pevsner, J. T. Bober, T. Frank, E. S. Hafen, P. Haridas, D. Huang, R. I. Hulsizer, V. Kistiakowsky, P. Lutz, S. H. Oh, I. A. Pless, T. B. Stoughton, V. Suchorebrow, S. Tether, P. C. Trepagnier, M. von Randow, Y. Wu, R. K. Yamamoto, F. Grard, J. Hanton, V. Henri, P. Herquet, J. M. Lesceux, R. Windmolders, H. DeBock, F. Crijns, W. Kittel, W. Metzger, C. Pols, M. Schouten, R. Van de Walle, H. O. Cohn, F. Carminati, R. Dolfini, S. Ratti, R. DiMarco, P. F. Jacques, M. Kalelkar, R. J. Plano, P. Stamer, T. L. Watts, E. B. Brucker, E. L. Koller, S. Taylor, S. Dado, J. Goldberg, G. Alexander, O. Benary, J. Grunhaus, R. Heifetz, A. Levy, J. E. Brau, W. M. Bugg, G. T. Condo, T. Handler, E. L. Hart, A. H. Rogers, Y. Eisenberg, U. Karshon, A. Shapira, T. Ludlam, R. Steiner, and H. Taft
"Search for Long-Lived +2 Hadrons," Phys. Rev. D 30, 1134-36 (1984)

Brick, D., H. Rudnicka, A. M. Shapiro, M. Widgoff, R. E. Ansorge, W. W. Neale, D. R. Ward, B. M. Whyman, R. A. Burnstein, H. A. Rubin, E. D. Alyea, Jr., L. Bachman, C.-Y. Chien, P. Lucas, A. Pevsner, J. T. Bober, T. Frank, E. S. Hafen, P. Haridas, D. Huang, R. I. Hulsizer, V. Kistiakowsky, P. Lutz, S. H. Oh, I. A. Pless, T. B. Stoughton, V. Suchorebrow, S. Tether, P. C. Trepagnier, Y. Wu, R. K. Yamamoto, F. Grard, J. Hanton, V. Henri, P. Herquet, J. M. Lesceux, P. Pilette, R. Windmolders, F. Crijns, H. DeBock, W. Kittel, W. Metzger, C. Pols, M. Schouten, R. Van de Walle, H. O. Cohn, F. Carminati, R. Dolfini, S. Ratti, R. DiMarco, P. F. Jacques, M. Kalelkar, R. J. Plano, P. Stamer, T. L. Watts, E. B. Brucker, E. L. Koller, S. Taylor, L. Berny, S. Dado, J. Goldberg, S. Toaff, G. Alexander, O. Benary, J. Grunhaus, R. Heifetz, A. Levy, J. E. Brau, W. M. Bugg, G. T. Condo, T. Handler, E. L. Hart, A. H. Rogers, Y. Eisenberg, U. Karshon, A. Shapira, T. Ludlam, R. Steiner, and H. Taft
"Planar Events in Hadron-Proton Collisions at 147 GeV/c and Their Jet-Like Structures," Z. Phys. C24, 19-29 (1984)

Burgdörfer, J., M. Breinig, S. B. Elston, and I. A. Sellin
"Calculation of Electron-Loss-to-Continuum Cusps: An Algebraic Approach," Phys. Rev. A 28, 3277-90 (1983)

Carlton, R. F., J. A. Harvey, and C. H. Johnson
"s- and p-Wave Neutrons on ^{30}Si and ^{34}S: Spherical Optical Model Analysis," Phys. Rev. C 29, 1988-92 (1984)

Carter, H. K.
"Laser Spectroscopy on β-Unstable Nuclei and Future Directions for Laser Spectroscopy," pp. 906-11 in Vol. II, Proceedings, Third LAMPF II Workshop, Los Alamos, New Mexico, July 18-20, 1983, Los Alamos National Laboratory Report LA-9933-C (1983)

Carter, H. K., P. Juncar, J. A. Bounds, C. R Bingham, D. J. Pegg, and W. Fairbank, Jr.
"Sensitive Collinear Laser Spectroscopy on Fast Atom and Ion Beams," Proc. Soc. Photo-Optical Eng. 426, 60-64 (1983)

Castel, B., and A.G.M. van Hees
"Distribution of El Spin-Flip Strength," Phys. Rev. C 28, 2571-73 (1983)

Chen, Y. S., S. Frauendorf, and G. A. Leander
"Shape of Rotating Quasi-Particle Orbits and Signature Splitting in La, Ce, and Pr Nuclei," Phys. Rev. C 28, 2437-46 (1983)

Church, D. A., K. W. Jones, B. M. Johnson, M. Meron, and I. A. Sellin
"Production and Storage of Highly Charged Ions at Room Temperature," J. Phys. B17, L401-06 (1984)

Church, D. A., R. A. Kenefick, W. S. Burns, C. S. U, R. Holmes, S. Huldt, S. Berry, M. Breinig, S. Elston, J.-P. Rozet, I. A. Sellin, D. Taylor, and B. Thomas
"Charge Transfer to Multicharged Recoil Ions in a Penning Trap," Phys. Rev. Lett. 51, 1636-39 (1983)

Cohn, H. O., J. E. Brau, W. M. Bugg, G. T. Condo, T. Handler, and E. L. Hart
"Low-Energy $\bar{p}$-Nucleus Reaction Cross Sections," Phys. Rev. C 29, 332 (1984)

Condo, G. T., W. B. Bugg, T. Handler, and H. O. Cohn
"Multinucleon Captures of Slow Antiprotons in Complex Nuclei and a Search for the H Dibaryon," Phys. Lett. 144B, 27-29 (1984)

Condo, G. T., T. Handler, and H. O. Cohn
"Λ^0 Production from Low-Energy Antiproton Annihilations in Complex Nuclei," Phys. Rev. C 29, 1531-33 (1984)

Datz, S.
"Atomic Collisions in the High-Energy Regime," pp. 369-94 in Atomic Physics, Vol. 8, Plenum, New York, 1983

Datz, S., Editor
Applied Atomic Collision Physics, Vol. 4: Condensed Matter, Academic Press, Orlando, Florida, 1983

Datz, S. (Invited Paper)
"Dielectronic Recombination: An Introduction," pp. 795-800 in Proceedings, XIII International Conference on the Physics of Electronic and Atomic Collisions, Berlin, West Germany, July 27-August 2, 1983, North-Holland, Amsterdam, 1984

Datz, S., R. W. Fearick, H. Park, R. H. Pantell, R. L. Swent, J. O. Kephart, and B. L. Berman
"Electron and Positron Channeling Radiation from Type-Ia and Type-IIa Diamonds," Proceedings, 10th International Conference on Atomic Collisions in Solids, Bad Iburg, F.R.G., July 18-22, 1983, Nucl. Instrum. Methods Phys. Res., Sect. B, 230 [B2], 74-79 (1984)

Davies, K.T.R., B. Remaud, M. Strayer, K.R.S. Devi, and Y. Raffray
"Geometry and Dynamics of a Zero-Temperature Fermi-Gas Model for Preequilibrium Emission of Nucleons with Application to ^{160} + ^{93}Nb at E_{lab} = 204 MeV," Ann. Phys. (N.Y.) 156, 68-109 (1984)

Davies, K.T.R., A. J. Sierk, and J. R. Nix (Invited Paper)
"Dynamical Fusion Thresholds in Macroscopic and Microscopic Theories," pp. 57-76 in Nuclear Physics with Heavy Ions (Proceedings, International Conference on Nuclear Physics with Heavy Ions, Stony Brook, New York, April 14-16, 1983), Harwood Academic, New York, 1984

Dittner, P. F., S. Datz, P. D. Miller, C. D. Moak, P. H. Stelson, C. Bottcher, N. Neskovic, and C. M. Fou (Invited Paper)
"Cross Sections for Dielectronic Recombination of B^{2+} and C^{3+} via $1s^22s \rightarrow 1s^22p$ Excitation," pp. 819-26 in Proceedings, XIII International Conference on the Physics of Electronic and Atomic Collisions, Berlin, West Germany, July 27-August 2, 1983, North-Holland, Amsterdam, 1984

Donangelo, R., M. W. Guidry, R. E. Neese, and M. J. Rhoades-Brown
"Angular Localization and Approximations to the Deformed Nuclear Potential in Heavy-Ion Reactions," Phys. Rev. C 29, 1925-27 (1984)

Ellis-Akovali, Y. A.
"Nuclear Data Sheets for A = 230," Nucl. Data Sheets 40, 385-423 (1984)

Ellis-Akovali, Y. A.
"Nuclear Data Sheets for A = 234," Nucl. Data Sheets 40, 523-603 (1983)

Gaarde, C., J. S. Larsen, H. Sagawa, N. Ohtsuka, J. Rapaport, T. N. Taddeucci, C. D. Goodman, C. C. Foster, C. A. Goulding, D. Horen, T. Masterson, and E. Sugarbaker
"Spin Dipole Strength in ^{12}N," Nucl. Phys. A422, 189-204 (1984)

Gavron, A., P. Eskola, A. J. Sierk, J. Boissevain, H. C. Britt, K. Eskola, M. M. Fowler, H. Ohm, J. B. Wilhelmy, S. Wald, and R. L. Ferguson
"New Evaluation of Fission-Fragment Angular Distributions in Heavy-Ion Reactions," Phys. Rev. Lett. 52, 589-92 (1984)

Gomez del Campo, J., J. A. Biggerstaff, R. A. Dayras, D. Shapira, A. H. Snell, P. H. Stelson, and R. G. Stokstad
"Comparison of Fusion Cross Sections for the ^{10}B + ^{16}O and ^{12}C + ^{14}N Systems," Phys. Rev. C 29, 1722-34 (1984)

Gomez del Campo, J., R. W. Fearick, J. A. Biggerstaff, C. D. Moak, P. D. Miller, N. Neskovic, D. Shapira, and J.P.F. Sellschop (Invited Paper)
"Crystal Blocking Measurements in Heavy-Ion Reactions," Proceedings, Sixth Symposium on Nuclear Physics, Oaxtepec, Mexico, January 4-7, 1983, Notas de Fisica 6, 115-26 (1983)

Griffin, D. C., C. Bottcher, M. S. Pindzola, S. M. Younger, D. C. Gregory, and D. H. Crandall
"Electron-Impact Ionization in the Xenon Isonuclear Sequence," Phys. Rev. A 29, 1729-41 (1984)

Griffin, D. C., M. S. Pindzola, and C. Bottcher
"Calculations of the Contributions of Excitation-Autoionization to the Electron-Impact Ionization of Ca^+ and Ba^+ in the Distorted-Wave Approximation," J. Phys. B17, 3183-92 (1984)

Groeneveld, K. O., W. Meckbach, I. A. Sellin, and J. Burgdorfer
"Collisional Electron Transfer into the Continuum of Ionic Projectiles," Comments At. Mol. Phys. 4, 187-200 (1984)

Gross, E. E., T. P. Cleary, J.L.C. Ford, Jr., D. C. Hensley, K. S. Toth, F. T. Baker, A. Scott, C. R. Bingham, and J. A. Vrba
"Nuclear Moments of the First Excited State of ^{22}Ne from ^{22}Ne (132 MeV) + ^{208}Pb Scattering," Phys. Rev. C 29, 459-63 (1984)

Gross, E. E., and M. P. Fewell
"Resolution of a Coulomb Reorientation Ambiguity in ^{18}O," Nucl. Phys. A411, 329-36 (1983)

Hamilton, J. H., A. V. Ramayya, C. F. Maguire, R. B. Piercey, R. Bengtsson, P. Moller, J. R. Nix, J.-Y. Znang, R. L. Robinson, and S. Frauendorf
"Effects of Reinforcing Shell Gaps on the Competition Between Spherical and Highly Deformed Shapes," J. Phys. G10, L87-L91 (1984)

Helmer, R. G., and C. W. Reich
"Levels in $^{204}_{84}$Po from the Decay of $^{204}_{85}$At," Phys. Rev. C 27, 2248-60 (1983)

Hensley, D. C.
"Parallel Processor for Fast Event Analysis," Proceedings, Conference on Real-Time Computer Applications in Particle and Nuclear Physics, Berkeley, California, May 16-19, 1983, IEEE Trans. Nucl. Sci. NS-30, 3913-16 (1983)

Horen, D. J., F. E. Bertrand, E. E. Gross, T. P. Sjoreen, D. K. McDaniels, J. R. Tinsley, J. Lisantti, L. W. Swenson, J. B. McClelland, T. A. Carey, S. J. Seestrom-Morris, and K. Jones
"Excitation of E2 Transitions in ^{40}Ca by 334-MeV Protons," Phys. Rev. C 30, 709-11 (1984)

Horen, D. J., R. L. Macklin, J. A. Harvey, and N. W. Hill
"Measurements of the Neutron Transmission and Capture Cross Sections in ^{204}Pb," Phys. Rev. C 29, 2126-34 (1984)

Hudson, E. D., R. S. Lord, M. L. Mallory, and T. A. Antaya
"Dual Arc Penning Ion Source Gas Flow Experiments," pp. 130-32 in Proceedings, Tenth International Conference on Cyclotrons and Their Applications, East Lansing, Michigan, April 30-May 3, 1984, IEEE Conf. Record 84CH1996-3, Institute of Electrical and Electronics Engineers, New York, 1984

Huyse, M.
"Ionization in a Hot Cavity," Nucl. Instrum. Methods Phys. Res. 215, 1-6 (1983)

Hynes, M. V., J.L.C. Ford, Jr., T. P. Sjoreen, J. L. Blankenship, and F. E. Bertrand
"Design and Performance of a Vertical Drift Chamber for Heavy-Ion Applications," Nucl. Instrum. Methods Phys. Res., Sect. A, 224, 89-96 (1984)

Itikawa, Y., S. Hara, T. Kato, S. Nakazaki, M. S. Pindzola, and D. H. Crandall
"Recommended Data on Excitation of Carbon and Oxygen Ions by Electron Collisions," Report IPPJ-AM-27, Institute of Plasma Physics, Nagoya University, Nagoya, Japan (June 1983), 135 pp.

Johnson, C. H., N. M. Larson, C. Mahaux, and R. R. Winters
"Reply to 'Calculation of the Lorentz-Weighted Average S Matrix from High-Resolution Low-Energy Neutron Scattering Data'," Phys. Rev. C 29, 1563-65 (1984)

Johnson, N. R., C. Baktash, and I. Y. Lee (Invited Paper)
"Bismuth Germanate's Role in the New Revolution in Gamma-Ray Spectroscopy," Proceedings, 1983 Nuclear Science Symposium, San Francisco, California, October 19-21, 1983, IEEE Trans. Nucl Sci. NS-31, 243 (1984)

Jones, C. M. (Invited Paper)
"Large Electrostatic Accelerators, pp. 496-503 in Proceedings, Tenth International Conference on Cyclotrons and Their Applications, East Lansing, Michigan, April 30-May 3, 1984, IEEE Conf. Record 84CH1996-3, Institute of Electrical and Electronics Engineers, New York, 1984

Jones, C. M., G. D. Alton, J. B. Ball, J. A. Benjamin, J. A. Biggerstaff, K. A. Erb, E. D. Hudson, R. C. Juras, P. K. Kloeppel, R. S. Lord, C. A. Ludemann, J. E. Mann, J. A. Martin, S. W. Mosko, E. G. Richardson, R. O. Sayer, and N. F. Ziegler
"Status Report on the Holifield Heavy Ion Research Facility," Proceedings, Sixth Tandem Conference, Chester, England, April 18-22, 1983, Nucl. Instrum. Methods Phys. Res. 220, 1-9 (1984)

Kahane, S., S. Raman, G. G. Slaughter, C. Coceva, and M. Stefanon
"Electric Dipole Transitions from Neutron Capture in ^{167}Er Resonances," Phys. Rev. C 30, 807-19 (1984)

Kern, B. D., K. S. Toth, D. M. Moltz, J. Lin, F. T. Avignone III, H. Noma, and G. A. Leander
"Beta Decay of ^{75}Rb to Low-Lying Levels in ^{75}Kr," Phys. Rev. C 28, 2168-70 (1983)

Kobos, A. M., B. A. Brown, R. Lindsay, and G. R. Satchler
"Folding Model Analysis of Elastic and Inelastic α-Particle Scattering Using a Density-Dependent Force," Nucl. Phys. A425, 205-32 (1984)

Kobos, A. M., and G. R. Satchler
"Potential Models and Resonances in the ^{16}O + ^{28}Si System," Phys. Rev. C 30, 403-04 (1984)

Larabee, A. J., L. H. Courtney, S. Frauendorf, L. L. Riedinger, J. C. Waddington, M. P. Fewell, N. R. Johnson, I. Y. Lee, and F. K. McGowan
"Shape Effects in $h_{11/2}$ and $g_{7/2}$ Bands in ^{159}Tm," Phys. Rev. C 29, 1934-37 (1984)

Leander, G. A.
"Comment on 'Nuclei: A Superfluid Condensate of α Particles? A Study Within the Interacting-Boson Model'," Phys. Rev. Lett. 52, 311 (1984)

Leander, G. A., J. Dudek, W. Nazarewicz, J. R. Nix, and Ph. Quentin
"Single-Particle Levels in the Doubly Magic ^{132}Sn and ^{100}Sn Nuclei," Phys. Rev. C 30, 416-19 (1984)

Leander, G. A., and R. K. Sheline
"Intrinsic Reflection Asymmetry in Odd-A Nuclei," Nucl. Phys. A413, 375-416 (1984)

Lee, I. Y., C. Baktash, and J. X. Saladin
"γ-γ Energy Correlations and the Moments of Inertia in ^{176}W," Phys. Rev. C 29, 837-42 (1984)

Leitch, M. J., R. L. Burman, R. Carlini, S. Dam, V. Sandberg, M. Blecher, K. Gotow, R. Ng, R. Auble, F. E. Bertand, E. E. Gross, F. E. Obenshain, J. Wu, G. S. Blanpied, B. M. Preedom, B. G. Ritchie, W. Bertozi, M. V. Hynes, M. A. Kovash, and R. P. Redwine
"Pion-Nucleus Elastic Scattering at 80 MeV," Phys. Rev. C 29, 561-68 (1984)

Lönnroth, T., and C. Baktash
"In-Beam Study of ^{213}Rn, ^{215}Ra, and ^{217}Ra: Strongly Enhanced E3 Transitions in Odd-A N = 127 Isotones," Phys. Scr. 28, 459-66 (1983)

Ludemann, C. A.
"A Microprocessor Multi-task Monitor," Proceedings, Conference on Real-Time Computer Applications in Nuclear and Particle Physics, Berkeley, California, May 16-19, 1983, IEEE Trans. Nucl. Sci. NS-30, 3858-63 (1983)

Lynch, W. G., C. B. Chitwood, M. B. Tsang, D. J. Fields, D. R. Klesch, C. K. Gelbke, G. R. Young, T. C. Awes, R. L. Ferguson, F. E. Obenshain, F. Plasil, R. L. Robinson, and A. D. Panagiotou
"Formation and Decay of a Localized Region of High Excitation in Heavy-Ion-Induced Reactions," Phys. Rev. Lett. 51, 1850-53 (1983)

Lynch, W. G., C. B. Chitwood, M. B. Tsang, D. J. Fields, D. R. Klesch, C. K. Gelbke, G. R. Young, T. C. Awes, R. L. Ferguson, F. E. Obenshain, F. Plasil, R. L. Robinson, and A. D. Panagiotou
"Response to Comment on 'Formation and Decay of a Localized Region of High Excitation in Heavy-Ion-Induced Reactions'," Phys. Rev. Lett. 52, 2302 (1984)

Ma, W. C., A. V. Ramayya, J. H. Hamilton, S. J. Robinson, M. E. Barclay, Z. Zhao, J. D. Cole, E. F. Zganjar, and E. H. Spejewski
"Ground-State Shape and Crossing of Near Spherical and Deformed Bands in ^{182}Hg," Phys. Lett. 139B, 276-78 (1984)

MacKellar, A. D., and B. Castel
"s- and p-Wave Neutrons on ^{30}Si and ^{34}S: Coupled Channels Optical Model," Phys. Rev. C 29, 1993-95 (1984)

MacKellar, A. D., G. R. Satchler, and C.-Y. Wong
"An Exploratory Study of Antiproton-Nucleus Scattering," Z. Phys. A316, 35-42 (1984)

Maguire, C. F., G. L. Bomar, M. E. Barclay, R. B. Piercey, A. V. Ramayya, J.L.C. Ford, Jr., D. Shapira, E. R. Flynn, J. D. Moses, J. C. Peng, and N. Stein
"Systematic Spectroscopic-Factor Discrepancy in Heavy-Ion Proton-Pickup Reactions on ^{40}Ca," Phys. Rev. Lett. 52, 743-46 (1984)

Martin, J. A. (Invited Paper)
"The International Cyclotron Conference's Twenty-Five Years of Progress," pp. 1-2 in Proceedings, Tenth International Conference on Cyclotrons and Their Applications, East Lansing, Michigan, April 30-May 3, 1984, IEEE Conf. Record 84CH1996-3, Institute of Electrical and Electronics Engineers, New York, 1984

McVoy, K. W., and G. R. Satchler
"Nuclear Rainbows and Heavy-Ion Scattering," Nucl. Phys. A417, 157-73 (1984)

Mehta, R., T. L. Duggan, F. D. McDaniel, M. C. Andrews, G. Lapicki, P. D. Miller, L. A. Rayburn, and A. R. Zander
"Direct Ionization and Electron Capture in M-Shell X-Ray Production by Fluorine Ions," Phys. Rev. A 28, 2722-26 (1983)

Migneréy, A. C., C. Merouane, S. Bradley, D. Benton, H. Breuer, J. D. Silk, K. Kwiatowski, V. E. Viola, Jr., T. C. Awes, F. E. Obenshain, and S. Pontoppidan
"Quasi-Elastic Structure in the Reaction $^{56}Fe + {}^{56}Fe$ at 14.6 MeV/Nucleon," pp. 76-79 in Proceedings, Workshop on Nuclear Dynamics III, Copper Mountain, Colorado, March 5-9, 1984, Indiana University Nuclear Chemistry Report, INC-40007-24 (April 1984)

Nazarewicz, W., P. Olanders, I. Ragnarsson, J. Dudek, and G. A. Leander
"High-Spin Consequences of Octupole Shape in Nuclei Around ^{222}Th," Phys. Rev. Lett. 52, 1272-75 (1984)

O'Kelley, G. D., R. L. Auble, L. D. Hulett, H. J. Kim, W. T. Milner, S. Raman, O. Shahal, C. R. Vane, J. P. Young, and G. Lapicki
"Implications of Heavy-Ion-Induced Satellite X-Ray Emission II: Production of K and L X-Rays by 0.9-2.6 MeV/u Argon Ions in Thick Targets of Vanadium, Copper, Niobium, Tantalum, and Platinum," Proceedings, Third International Conference on Particle-Induced X-Ray Emission, Heidelberg, West Germany, July 18-22, 1983, Nucl. Instrum. Methods. Phys. Res., Sect. B, 231 [B3], 78-87 (1984)

Park, H., R. H. Pantell, R. L. Swent, J. D. Kephart, B. L. Berman, S. Datz, and R. W. Fearick
"Comparison of Channeling Radiation from Diamonds with and without Platelets," J. Appl. Phys. 55, 358-64 (1984)

Phaneuf, R. A.
"Atomic Processes Involving Impurities in the Plasma Edge," Proceedings, Workshop on Impurity Control Physics, Atlanta, Georgia, May 30-31, 1984, pp. 101-25 in Report ETR-INTOR/ICP/3 (1984)

Pindzola, M. S., D. C. Griffin, C. Bottcher, D. H. Crandall, R. A. Phaneuf, and D. C. Gregory
"Electron-Impact Double Ionization of Rare-Gas Ions," Phys. Rev. A 29, 1749-56 (1984)

Plasil, F.
"Comment on 'Fission-Fragment Angular Distributions'," Phys. Rev. Lett. 52, 1929 (1984)

Plasil, F., T. C. Awes, B. Cheynis, D. Drain, R. L. Ferguson, F. E. Obenshain, A. J. Sierk, S. G. Steadman, and G. R. Young
"Angular-Momentum-Dependent Fission Barriers in the Rare-Earth Region," Phys. Rev. C 29, 1145-48 (1984)

Plasil, F., T. C. Awes, B. Cheynis, D. Drain, R. L. Ferguson, F. E. Obenshain, A. J. Sierk, S. G. Steadman, G. R. Young, A. Gavron, J. Boissevain, H. C. Britt, K. Eskola, P. Eskola, M. M. Fowler, Z. Fraenkel, H. Ohm, J. van der Plicht, and S. Wald (Invited Paper)
"Recent Results in Heavy-Ion-Induced Fission," pp. 1-4 in Proceedings, Workshop on Nuclear Dynamics III, Copper Mountain, Colorado, March 5-9, 1984, Indiana University Nuclear Chemistry Report, INC-40007-24 (April 1984)

Pontoppidan, S., P. R. Christensen, O. Hansen, F. Videbaek, H. C. Britt, B. H. Erkkila, Y. Patin, R. H. Stokes, M. P. Webb, R. L. Ferguson, F. Plasil, and G. R. Young
"Quasielastic Transfer Reactions Induced by ^{56}Fe on ^{58}Ni, ^{64}Ni, and ^{122}Sn," Phys. Rev. C 28, 2299-311 (1983)

Poskanzer, A., H-G. Ritter, B. Ludewigt, K. Foley, S. Borenstein, E. Platner, W. Love, D. Keane, and F. Plasil
"Event Parameters — Fixed Target," pp. 38-44 in Proceedings, Workshop on Detectors for Relativistic Nuclear Collisions, Berkeley, California, March 26-30, 1984, Lawrence Berkeley Laboratory Report, LBL-18225 (August 1984)

Raman, S.
"Ion-Induced X-Ray Emission," pp. 407-28 in Applied Atomic Collision Physics, Vol. 4: Condensed Matter, Academic Press, Orlando, Florida, 1983

Raman, S., Editor
"Actinide Newsletter," Issue No. 7 (March 1984)

Raman, S., E. Kallne, J. Kallne, T. Nakajima, C. W. Nestor, Jr., P. H. Stelson, C. R. Vane, and T. A. Walkiewicz
"Implications of Heavy-Ion-Induced Satellite X-Ray Emission V: Fine Structure of the Sulfur K X-Ray Satellite Peaks," Proceedings, Third International Conference on Particle-Induced X-Ray Emission, Heidelberg, West Germany, July 18-22, 1983, Nucl. Instrum. Methods Phys. Res., Sect. B, 231 [B3], 100-03 (1984)

Raman, S., W. Ratynski, E. T. Jurney, M. E. Bunker, and J. W. Starner
"$^{36}S(n,\gamma)^{37}S$ Reaction with Thermal Neutrons and Decay of ^{37}S to Levels in ^{37}Cl," Phys. Rev. C 30, 26-30 (1984)

Raman, S., and C. R. Vane (Invited Paper)
"Implications of Heavy-Ion-Induced Satellite X-Ray Emission I: Introduction," Proceedings, Third International Conference on Particle-Induced X-Ray Emission, Heidelberg, West Germany, July 18-22, 1983, Nucl. Instrum. Methods Phys. Res., Sect. B, 231 [B3], 71-77 (1984)

Rapaport, J., T. Taddeucci, T. P. Welch, C. Gaarde, J. Larsen, D. J. Horen, E. Sugarbaker, P. Koncz, C. C. Foster, C. D. Goodman, C. A. Goulding, and T. Masterson
"Excitation of Giant Spin-Isospin Multipole Vibrations in $^{54,56}Fe$ and $^{58,60}Ni$," Nucl. Phys. A410, 371-98 (1983)

Reading, J. F., A. L. Ford, J. S. Smith, J. Alexander, and R. L. Becker (Invited Paper)
"Progress in Numerical Calculations of Ion-Atom Collisions," Proceedings, Third Workshop on Inner Shell Ionization by Light Ions, Linz, Austria, August 4-5, 1983, Nucl. Instrum. Methods Phys. Res., Sect. B, 232 [B4], 266-70 (1984)

Reading, J. F., A. L. Ford, J. S. Smith, and R. L. Becker (Invited Paper)
"Learning from Numerical Calculations of Ion-Atom Collisions," pp. 201-11 in Proceedings, XIII International Conference on the Physics of Electronic and Atomic Collisions, Berlin, West Germany, July 27-August 2, 1983, North-Holland, Amsterdam, 1984

Riedinger, L. L.
"Aligned Bands and Nuclear Shapes in the N = 90 Region," Proceedings, Nordic Symposium on Nuclear Physics, Fuglso, Denmark, August 16-20, 1982, Phys. Scr. T5, 36-44 (1983)

Rosseel, T. M., J. M. Dale, H. W. Dunn, L. D. Hulett, S. Kahane, H. F. Krause, S. Raman, G. G. Slaughter, C. R. Vane, and J. P. Young
"Implications of Heavy-Ion-Induced Satellite X-Ray Emission IV: Chemical Effects in L X-Ray Satellites of Molybdenum Compounds and Alloys," Proceedings, Third International Conference on Particle-Induced X-Ray Emission, Heidelberg, West Germany, July 18-22, 1983, Nucl. Instrum. Methods Phys. Res., Sect. B, 231 [B3], 94-99 (1984)

Rosseel, T. M., J. P. Young, J. M. Dale, A. DasGupta, L. D. Hulett, H. F. Krause, C. T. Liu, S. Raman, and C. R. Vane
"Application of Heavy-Ion-Induced X-Ray Satellite Emission to Alloys," J. Phys. F14, L37-L41 (1984)

Satchler, G. R. (Invited Paper)
"Nucleus-Nucleus Potentials," Proceedings, International Conference on Heavy-Ion and Nuclear Physics, Catania, Italy, March 21-26, 1983, Nucl. Phys. A409, 3c-20c (1983)

Satchler, G. R.
"The Distorted-Waves Theory of Direct Nuclear Reactions with Spin-Orbit Effects," [Nucl. Phys. 55, 1-33 (1964)], Current Contents (Citation Classics Section) 23, No. 36, 18 (1983)

Satchler, G. R., and W. T. Pinkston
"Properties of the Transition Amplitude for Two-Nucleon Transfer Reactions," Nucl. Phys. A411, 144-50 (1983)

Satchler, G. R., and W. T. Pinkston
"Comment on J Dependence in (α,d) Transfer Reactions," Phys. Lett. 134B, 7-10 (1984)

Sayer, R. O.
"RIP — General Purpose Interactive Display at HHIRF," Proceedings, Conference on Real-Time Computer Applications in Particle and Nuclear Physics, Berkeley, California, May 16-19, 1983, IEEE Trans. Nucl. Sci. NS-30, 3833-37 (1983)

Schmorak, M. R.
"Nuclear Data Sheets for A = 231, 235, and 239," Nucl. Data Sheets 40, 1-147 (1984)

Schuck, C., N. Bendjaballah, R. M. Diamond, Y. Ellis-Akovali, K. H. Lindenberger, J. O. Newton, F. S. Stephens, J. O. Garrett, and S. Herskind
"Evidence for Reduced Neutron Pairing Correlations in ^{165}Yb," Phys. Lett. 142B, 253-57 (1984)

Seiwert, M., W. Greiner, V. Oberacker, and M. J. Rhoades-Brown
"Test of the Proximity Theorem for Deformed Nuclei," Phys. Rev. C 29, 447-85 (1984)

Shapira, D., and K. A. Erb (Invited Paper)
"Molecular Degrees of Freedom: Resonances and Orbiting," pp. 305-28 in Nuclear Physics with Heavy Ions (Proceedings, International Conference on Nuclear Physics with Heavy Ions, Stony Brook, New York, April 14-16, 1983), Harwood Academic, New York, 1984

Shapira, D., K. A. Erb, J.L.C. Ford, Jr., J. Gomez del Campo, B. Shivakumar, R. Novotny, D. Schull, S. T. Thornton, R. L. Parks, and R. Cecil (Invited Paper)
"Orbiting in Collisions Between Light Heavy Ions (A_T + A_P < 50)," Proceedings, Sixth Symposium on Nuclear Physics, Oaxtepec, Mexico, January 4-7, 1983, Notas de Fisica 6, 325-54 (1983)

Sheline, R. K., D. Decman, K. Nybo, T. F. Thorsteinsen, G. Lovhoiden, E. R. Flynn, J. A. Cizewski, D. K. Burke, G. Sletten, P. Hill, N. Kaffrell, W. Kurcewicz, G. Nyman, and G. A. Leander
"Evidence for Near-Stable Octupole Deformation in ^{225}Ra," Phys. Lett. 133B, 13-16 (1983)

Sjoreen, T. P., F. E. Bertrand, R. L. Auble, E. E. Gross, D. J. Horen, D. Shapira, and D. B. Wright
"Inelastic Excitation of Giant Resonances by 400-MeV ^{16}O," Phys. Rev. C 29, 1370-76 (1984)

Sjoreen, T. P., J.L.C. Ford, Jr., J. L. Blankenship, R. L. Auble, F. E. Bertrand, E. E. Gross, D. C. Hensley, D. Schull, and M. V. Hynes
"The Vertical Drift Chamber as a High Resolution Focal Plane Detector for Heavy Ions," Nucl. Instrum. Methods Phys. Res., Sect. A, 224, 421-31 (1984)

Strayer, M. R., R. Y. Cusson, A. S. Umar, P.-G. Reinhard, D. A. Bromley, and W. Greiner
"Time-Dependent Hartree-Fock Picture of Nuclear Molecular Resonances," Phys. Lett. 135B, 261-65 (1984)

Swent, R. L., R. H. Pantell, H. Park, J. O. Kephart, R. K. Klein, S. Datz, R. W. Fearick, and B. L. Berman
"Planar and Axial Channeling Radiation from Relativistic Electrons in LiF," Phys. Rev. B 29, 52-60 (1984)

Tabor, S. L., G. Neuschaefer, J. A. Carr, F. Petrovich, C. C. Chang, A. Guterman, M. T. Collins, D. L. Friesel, C. Glover, S. Y. Van der Werf, and S. Raman
"The (^{3}He,t) Reaction at 197 MeV on ^{12}C, ^{24}Mg, ^{28}Si, and ^{40}Ca," Nucl. Phys. A422, 12-44, 1984)

Taddeucci, T. N., T. A. Carey, C. Gaarde, J. Larsen, C. D. Goodman, D. J. Horen, T. Masterson, J. Rapaport, T. P. Welch, and E. Sugarbaker
"Measurement of the Transverse Spin-Transfer Coefficient $D_{NN}(0°)$ for (p_{pol},n_{pol}) Reactions at 160 MeV," Phys. Rev. Lett. 52, 1960-63 (1984)

Taddeucci, T. N., J. Rapaport, C. C. Foster, C. D. Goodman, C. Gaarde, J. Larsen, C. A. Goulding, D. J. Horen, T. Masterson, and E. Sugarbaker
"Spin Excitations in ^{40}Ca(p,n)," Phys. Rev. C 28, 2511-14 (1983)

Thornton, S. T., R. L. Parks, D. Shapira, D. Schull, J.L.C. Ford, Jr., B. Shivakumar, and J. Gomez del Campo
"Observation of a Critical Angular Momentum for Deep Inelastic Processes with Light Heavy Ions," pp. 97-100 in Proceedings, Workshop on Nuclear Dynamics III, Copper Mountain, Colorado, March 5-9, 1984, Indiana University Nuclear Chemistry Report, INC-40007-24 (April 1984)

Toth, K. S., D. M. Moltz, E. C. Schloemer, M. D. Cable, F. T. Avignone, III, and Y. A. Ellis-Akovali
"Beta-Delayed Proton Activities: ^{147}Dy and ^{149}Er," Phys. Rev. C 30, 712-14 (1984)

Umar, A. S., M. R. Strayer, and D. J. Ernst
"A Time-Dependent External-Field Model for Particle Emission in Heavy-Ion Reactions," Phys. Lett. 140B, 290-94 (1984)

van der Plicht, J., H. C. Britt, M. M. Fowler, Z. Fraenkel, A. Gavron, J. B. Wilhelmy, F. Plasil, T. C. Awes, and G. R. Young
"Fission of Polonium, Osmium, and Erbium Composite Systems," Phys. Rev. C 28, 2022-32 (1983)

Vane, C. R., L. D. Hulett, Jr., S. Kahne, F. D. McDaniel, W. T. Milner, G. D. O'Kelley, S. Raman, T. M. Rosseel, G. G. Slaughter, S. L. Varghese, and J. P. Young
"Implications of Heavy-Ion-Induced Satellite X-Ray Emission III: Chemical Effects in High-Resolution Sulfur K_α X-Ray Spectra," Proceedings, Third International Conference on Particle-Induced X-Ray Emission, Heidelberg, West Germany, July 18-22, 1983, Nucl. Instrum. Methods Phys. Res., Sect. B, 231 [B3], 88-93 (1984)

Willett, S. J., S. K. Korotky, R. L. Phillips, D. A. Bromley, and K. A. Erb
"Spin Alignment and Phase Angles in $^{12}C + ^{12}C$ Inelastic Scattering," Phys. Rev. C 28, 1986-2000 (1983)

Willis, R. D., S. L. Allman, C. H. Chen, G. D. Alton, and G. S. Hurst
"Pumping of Inert Gases by Electron-Impact Ionization Sources and Associated Memory Effects," J. Vac. Sci. Technol. A2, 57 (1984)

Wong, C. Y.
"Baryon Distribution in Relativistic Heavy-Ion Collisions," Phys. Rev. Lett. 52, 1393-96 (1984)

Wong, C. Y.
"Initial Energy Density of Quark-Gluon Plasma in Relativistic Heavy-Ion Collisions," pp. 207-10 in Proceedings, Workshop on Nuclear Dynamics III, Copper Mountain, Colorado, March 5-9, 1984, Indiana University Nuclear Chemistry Report, INC-40007-24 (April 1984)

Wong, C. Y. (Invited Paper)
"Baryon Distribution in Relativistic Heavy-Ion Collisions," pp. 203-06 in Proceedings, Workshop on Nuclear Dynamics III, Copper Mountain, Colorado, March 5-9, 1984, Indiana University Nuclear Chemistry Report, INC-40007-24 (April 1984)

Wong, C. Y.
"Initial Energy Density of Quark-Gluon Plasma in Relativistic Heavy-Ion Collisions," Phys. Rev. D 30, 961-71 (1984)

Wong, C. Y.
"Baryon Distribution in Relativistic Heavy-Ion Collisions," Phys. Rev. D 30, 972-84 (1984)

Wong, C. Y., A. K. Kerman, G. R. Satchler, and A. D. MacKellar
"Ambiguity in Antiproton-Nucleus Potentials from Antiprotonic-Atom Data," Phys. Rev. C 29, 574-80 (1984)

Young, G. R., J. A. Martin, and J. B. Ball
"A 10-GeV on 10-GeV Heavy-Ion Collider," Proceedings, Third International Conference on Ultra-Relativistic Nucleus-Nucleus Collisions, Upton, New York, September 26-30, 1983, Nucl. Phys. A418, 361c-69c (1984)

PROGRESS REPORT

Ball, J. B., Division Director
Physics Division Progress Report for Period Ending September 30, 1983, ORNL-6004 (December 1983)

TOPICAL REPORTS

Barnett, C. F., D. H. Crandall, H. B. Gilbody, D. C. Gregory, M. I. Kirkpatrick, E. W. McDaniel, R. H. McKnight, F. W. Meyer, T. J. Morgan, R. A. Phaneuf, M. S. Pindzola, and E. W. Thomas
1982 Bibliography of Atomic and Molecular Processes, ORNL-6052 (May 1984)

Bottcher, C., D. C. Griffin, M. S. Pindzola, and R. A. Phaneuf
Indirect Processes in Electron-Ion Scattering, ORNL/TM-8868 (October 1983)

Halbert, M. L.
New Vistas of Heavy-Ion Reactions with the Spin Spectrometer, ORNL/TM-8986 (January 1984)

Olsen, D. K., J. A. Martin, and D. J. Horen
A Preliminary Study of Possible ORELA Replacement Options, ORNL/TM-8669 (June 1984)

ARTICLES PENDING PUBLICATION AS OF SEPTEMBER 30, 1984

Abe, K., R. Armenteros, T. C. Bacon, J. Ballam, H. H. Bingham, J. E. Brau, K. Braune, D. Brick, W. M. Bugg, J. M. Butler, W. Cameron, H. O. Cohn, D. C. Colley, G. T. Condo, P. Dingus, R. Erickson, R. C. Field, B. Franek, R. Gearhart, T. Glanzman, I. M. Godfrey, J. J. Goldberg, G. Hall, E. R. Hancock, H. J. Hargis, E. L. Hart, M. J. Harwin, K. Hasegawa, M. Jobes, T. Kafka, G. E. Kalmus, D. P. Kelsey, T. Kitagaki, W. A. Mann, R. Merenyi, R. Milburn, K. C. Moffeit, J. J. Murray, A. Napier, V. R. O'Dell, P. Rankin, H. Sagawa, J. Schneps, S. J. Sewell, J. Shank, A. M. Shapiro, J. Shimony, K. Tamai, S. Tanaka, D. A. Waide, M. Widgoff, S. Wolbers, C. A. Woods, A. Yamaguchi, G. P. Yost, and H. Yuta
"Charm Photoproduction at 20 GeV Including Preliminary Lifetime Results with Improved Optical Resolution," Proceedings, XXII International Conference on High-Energy Physics, Leipzig, East Germany, July 19-25, 1984

Abe, K., R. Armenteros, T. C. Bacon, J. Ballam, H. H. Bingham, J. E. Brau, K. Braune, D. Brick, W. M. Bugg, J. M. Butler, W. Cameron, H. O. Cohn, D. C. Colley, G. T. Condo, P. Dingus, R. Erickson, R. C. Field, B. Franek, R. Gearhart, T. Glanzman, I. M. Godfrey, J. J. Goldberg, G. Hall, E. R. Hancock, H. J. Hargis, E. L. Hart, M. J. Harwin, K. Hasegawa, M. Jobes, T. Kafka, G. E. Kalmus, D. P. Kelsey, T. Kitagaki, W. A. Mann, R. Merenyi, R. Milburn, K. C. Moffeit, J. J. Murray, A. Napier, V. R. O'Dell, P. Rankin, H. Sagawa, J. Schneps, S. J. Sewell, J. Shank, A. M. Shapiro, J. Shimony, K. Tamai, S. Tanaka, D. A. Waide, M. Widgoff, S. Wolbers, C. A. Woods, A. Yamaguchi, G. P. Yost, and H. Yuta
"Comparison of Lambda and Antilambda Inclusive Photoproduction at 20 GeV with Quark-Diquark Fusion Model," Proceedings, XXII International Conference on High-Energy Physics, Leipzig, East Germany, July 19-25, 1984

Alton, G. D., R. N. Compton, and D. J. Pegg
"Electron Detachment Spectroscopy of 20 → 120 keV H^- and He^- Projectiles Interacting with Thin He and Ar Targets," Physical Review A

Awes, T. C., R. L. Ferguson, F. E. Obenshain, F. Plasil, G. R. Young, P. Braun-Munzinger, R. Freifelder, P. Paul, L. Ricken, J. Stachel, P. de Young, and P.-H. Zhang
"A Large Acceptance Spectrometer for π^0 Mesons," Proceedings, Conference on Instrumentation for Heavy-Ion Nuclear Research, Oak Ridge, Tennessee, October 22-24, 1984

Balantekin, A. B.
"Accidental Degeneracies and Supersymmetric Quantum Mechanics," Annals of Physics (New York)

Becker, R. L.
"Vacancy-Rearrangement Theory in the First Magnus Approximation," Proceedings, Second Workshop on High Energy Ion-Atom Collisions, Debrecen, Hungary, August 27-28, 1984

Becker, R. L., A. L. Ford, and J. F. Reading (Invited Talk)
"Multiple Vacancy Production by High-Energy Heavy Ions," Proceedings, Second Workshop on High Energy Heavy-Ion Collisions, Debrecen, Hungary, August 27-28, 1984

Becker, R. L., and A. D. MacKellar
"Theoretical Initial-(n,ℓ) Dependence of Ion-Rydberg Atom Collision Cross Sections," Journal of Physics B

Bemis, C. E., Jr., J. R. Beene, J.L.C. Ford, Jr., D. Shapira, and B. Shivakumar (Invited Paper)
"Development of Polarized Targets for Subbarrier Fusion Studies," Proceedings, International Conference on Fusion Reactions Below the Coulomb Barrier, Cambridge, Massachusetts, June 13-15, 1984

Berman, B. L., and S. Datz
"Channeling-Radiation Experiments," Topics in Current Physics, "Coherent Radiation Sources"

Berry, S. D., G. A. Glass, I. A. Sellin, K.-O. Groeneveld, D. Hofmann, L. H. Andersen, M. Breinig, S. B. Elston, P. Engar, M. M. Schauer, N. Stolterfoht, H. Schmidt-Bocking, G. Nolte, and G. Schiwietz
"Shape of the Electron Capture to the Continuum Cusps for H, H_2, and He Targets in the Velocity Range 6.3 to 18.0 a.u.," Physical Review A

Bertrand, F. E., and J. R. Beene
"Giant Resonance Gamma Decay in ^{208}Pb," Physics News in 1984

Bertrand, F. E., J. R. Beene, and M. L. Halbert
"Photon Decay of Giant Resonances," Proceedings, International Symposium on Nuclear Spectroscopy and Nuclear Interactions, Osaka, Japan, March 21-24, 1984

Bertsch, G. F. (Invited Paper)
"Nonrelativistic Theory of Heavy-Ion Collisions," Proceedings, School on Heavy-Ion Physics, Erice, Sicily, July 17-23, 1984

Bottcher, C.
"Transition State Theory for Nonstationary Atomic and Molecular Systems," Proceedings of the Royal Society of London A

Britt, H. C., M. M. Fowler, Z. Fraenkel, A. Gavron, J. Van der Plicht, J. B. Wilhelmy, F. Plasil, T. Awes, and G. R. Young (Invited Paper)
"Heavy-Ion-Induced Fission Reactions," Proceedings, International School-Seminar on Heavy-Ion Physics, Alushta, Crimea, U.S.S.R., April 14-21, 1983

Carlton, R. F., J. A. Harvey, and C. H. Johnson
"Optical Model Scattering Functions for Low Energy Neutrons on ^{86}Kr," Proceedings, Neutron-Nucleus Collisions: A Probe of Nuclear Structure, Glouster, Ohio, September 5-8, 1984

Casson, W. H., D. P. Hutchinson, C. H. Ma, P. A. Staats, and J. B. Wilgen
"Far-Infrared Laser Diagnostic on EBT and Extreme Far-Forward Laser Scattering on ISX," Proceedings, 5th Topical Conference on High Temperature Plasma Diagnostics, Tahoe City, California, September 16-20, 1984

Chitwood, C. B., J. Aichelin, D. H. Boal, G. Bertsch, D. J. Fields, C. K. Gelbke, W. G. Lynch, M. B. Tsang, J. C. Shillcock, T. C. Awes, R. L. Ferguson, F. E. Obenshain, F. Plasil, R. L. Robinson, and G. R. Young
"Final State Interactions Between Noncompound Light Particles for ^{16}O Induced Reactions on ^{197}Au at E/A = 25 MeV," Physical Review Letters

Cole, J. D., J. H. Hamilton, A. V. Ramayya, W. Lourens, B. van Nooijen, H. Kawakami, L. A. Mink, E. H. Spejewski, H. K. Carter, R. L. Mlekodaj, G. A. Leander, L. L. Riedinger, C. R. Bingham, E. F. Zganjar, J. L. Wood, R. W. Fink, K. S. Toth, B. D. Kern, and K.S.R. Sastry
"The Decay of ^{188}Tl and Observed Shape Coexistence in the Bands of ^{188}Hg," Physical Review C

Cusson, R. Y., P.-G. Reinhard, M. R. Strayer, J. A. Maruhn, and W. Greiner
"Density as a Constraint and the Separation of Internal Excitation Energy in TDHF," Zeitschrift fur Physik A

Datz, S., and C. D. Moak
"Heavy-Ion Channeling," Heavy-Ion Science

Davies, K.T.R., K.R.S. Devi, S. E. Koonin, and M. R. Strayer
"TDHF Calculations of Heavy-Ion Collisions," Heavy-Ion Science

Demas, N. G., C. H. Ma, D. P. Hutchinson, and P. A. Staats
"Determination of Spatial Distribution of Plasma Electrons by Multi-beam FIR Interferometry," IEEE Journal of Plasma Science

Dennis, L. C., and S. Raman
"Location of a Doorway State Using the Channel n + ^{207}Pb," Proceedings, Fifth International Symposium on Gamma-Ray Spectroscopy and Related Topics, Knoxville, Tennessee, September 10-14, 1984

El-Samman, H., V. Barci, T. Bengtsson, A. Gizon, J. Gizon, L. Hildingsson, D. Jerrestam, W. Klamra, R. Kossakowski, Th. Lindblad, Y. Gono, T. Bengtsson, and G. A. Leander
"Dynamic Moments of Inertia in Xe, Cs, and Ba Nuclei," Proceedings, International Symposium on In-Beam Nuclear Spectroscopy, Debrecen, Hungary, May 30-June 1, 1984

El-Samman, H., V. Barci, A. Gizon, J. Gizon, L. Hildingsson, D. Jerrestam, W. Klamra, R. Kossakowski, Th. Lindblad, T. Bengtsson, and G. A. Leander
"On the Difference of the Dynamic Moment of Inertia $\mathcal{J}_{band}^{(2)}$ for Xe and Ba Nuclei," Nuclear Physics A

Elston, S. B., S. D. Berry, M. Breinig, R. DeSerio, C. E. Gonzalez Lepera, I. A. Sellin, K.-O. Groeneveld, D. Hoffman, P. Koschar, I. B. Nemirovski, and L. I. Liljeby
"Doubly Differential Emission Distributions from Electron Loss to the Continuue from Fast Heavy Projectiles in Gas Targets," Proceedings, Symposium on the Physics of Electron Ejection in Ion-Atom and Ion-Solid Collisions, Aarhus, Denmark, June 29-30, 1984

Erb, K. A. (Invited Paper)
"Quasi-Molecular Single-Nucleon Effects in Heavy-Ion Collisions," Proceedings, 5th Adriatic International Conference on Nuclear Physics: Fundamental Problems in Heavy-Ion Collisions, Hvar, Yugoslavia, September 24-29, 1984

Erb, K. A., and D. A. Bromley
"Heavy-Ion Resonances," Heavy-Ion Science

Farid, M. E., and G. R. Satchler
"One Effect of Using Relativistic Kinematics in the Analysis of Heavy-Ion Elastic Scattering," Physics Letters B

Farid, M. E., and G. R. Satchler
"Some Optical-Model Analyses of the Elastic Scattering of ^{40}Ar at 1760 MeV," Nuclear Physics A

Fewell, M. P., N. R. Johnson, F. K. McGowan, J. S. Hattula, I. Y. Lee, C. Baktash, Y. Schutz, J. C. Wells, L. L. Riedinger, M. W. Guidry, and S. C. Pancholi
"The Collectivity of $^{160,161}Yb$ at High Spin," Physics Letters B

Ford, J.L.C. (Invited Paper)
"Heavy Ions, Targets, and Research at HHIRF," Proceedings, 1983 Workshop of the International Nuclear Target Development Society, Argonne, Illinois, September 7-9, 1983

Fulmer, C. B., G. R. Satchler, K. A. Erb, D. C. Hensley, R. L. Auble, J. B. Ball, F. E. Bertrand, and E. E. Gross
"Elastic and Inelastic Scattering of 158 MeV ^{9}Be Ions," Nuclear Physics A

Gavron, A., J. Boissevain, H. C. Britt, K. Eskola, P. Eskola, M. M. Fowler, H. Ohm, J. B. Wilhelmy, T. C. Awes, R. L. Ferguson, F. E. Obenshain, F. Plasil, G. R. Young, and S. Wald
"Fission Cross Sections up to 20 MeV/amu," Physical Review C

Glass, G. A., P. Engar, S. D. Berry, M. Breinig, R. DeSerio, S. B. Elston, and I. A. Sellin
"Electron Capture to the Continuum from Atomic Hydrogen," Proceedings, Eighth Conference on the Application of Accelerators in Research and Industry, Denton, Texas, November 12-14, 1984

Goodman, C. D., R. C. Byrd, I. J. Van Heerden, T. A. Carey, D. J. Horen, J. S. Larsen, C. Gaarde, J. Rapaport, T. P. Welch, E. Sugarbaker, and T. N. Taddeucci
"Measurements of Gamow-Teller Strength Distributions in Mass 13 and 15," Physical Review Letters

Gregory, D. C. (Invited Paper)
"Indirect Processes in Electron-Impact Ionization of Multiply Charged Ions," Proceedings, Eighth Conference on the Application of Accelerators in Research and Industry, Denton, Texas, November 12-14, 1984

Griffin, D. C., M. S. Pindzola, and C. Bottcher
"Distorted Wave Calculations of Dielectronic Recombination Cross Sections in the Li Isoelectronic Sequence," Physical Review A

Guidry, M. W., R. E. Neese, C. R. Bingham, L. L. Riedinger, J. A. Vrba, I. Y. Lee, N. R. Johnson, G. R. Satchler, P. A. Butler, R. Donangelo, J. O. Rasmussen, D. L. Hillis, and H. H. Kluge
"Heavy-Ion Inelastic Scattering from Deformed Nuclei," Nuclear Physics A

Horen, D. J.
"Isotopes," McGraw-Hill Encyclopedia of Science and Technology, Sixth Edition

Hutchinson, D. P., C. H. Ma, P. A. Staats, and K. L. Vander Sluis
"Far-Infrared Interferometry/Polarimetry on the ISX-B Tokamak," Proceedings, Third International Conference on Infrared Physics, Zurich, Switzerland, July 23-27, 1984

Hutchinson, D. P., K. L. Vander Sluis, and J. Sheffield
"Feasibility of Alpha Particle Measurement by CO_2 Laser Thomson Scattering," Proceedings, Ninth International Conference on Infrared and Millimeter Waves, Takarazuka, Osaka, Japan, October 22-26, 1984

Hutchinson, D. P., K. L. Vander Sluis, J. Sheffield, and D. J. Sigmar
"Feasibility of Alpha Particle Measurement by CO_2 Laser Thomson Scattering," Proceedings, 5th Topical Conference on High Temperature Plasma Diagnostics, Tahoe City, California, September 16-20, 1984

Johnson, C. H. (Invited Paper)
"Optical Models from Low-Energy s-, p-, and d-Wave Cross Sections," Proceedings, Neutron-Nucleus Collisions: A Probe of Nuclear Structure, Glouster, Ohio, September 5-8, 1984

Juncar, P., H. K. Carter, R. L. Mlekodaj, J. A. Bounds, C. R. Bingham, D. J. Pegg, and J. D. Cole
"New Method to Measure Doppler Shift: First Results and a Proposal," Physical Review Letters

Kim, H. J., T. C. Awes, J. R. Beene, C. E. Bemis, Jr., R. L. Ferguson, I. Y. Lee, F. K. McGowan, F. E. Obenshain, F. Plasil, V. Rauch, R. L. Robinson, and S. Steadman
"Calibration and Initial Experiments with the ORNL-MIT Recoil Mass Spectrometer," Proceedings, International Conference on Fusion Reactions Below the Coulomb Barrier, Cambridge, Massachusetts, June 13-15, 1984

Klein, R. K., J. O. Kephart, R. H. Pantell, H. Park, B. L. Berman, R. L. Swent, S. Datz, and R. W. Fearick
"Electron Channeling Radiation from Diamond," Physical Review B

Kobos, A. M., and G. R. Satchler
"A Global Optical Potential Analysis of ^{16}O + ^{28}Si Elastic Scattering," Nuclear Physics A

Leander, G. A.
"Shell Effects on the El Moments of Ra-Th Nuclei," Proceedings, Fifth International Symposium on Capture Gamma-Ray Spectroscopy and Related Topics, Knoxville, Tennessee, September 10-14, 1984

Leander, G. A., P. Möller, J. R. Nix, and W. M. Howard
"Calculated Masses and Half-Lives for Nuclei in the Region $100 < Z < 110$," Proceedings, Seventh International Conference on Atomic Masses and Fundamental Constants, Darmstadt, West Germany, September 3-7, 1984

Leander, G. A., P. B. Semmes, and F. Donau (Invited Paper)
"Unpaired Nucleons as Probes of Core Collective Fields," Proceedings, International Workshop on Interacting Boson-Boson and Boson-Fermion Systems, Gull Lake, Michigan, May 28-30, 1984

Lisantti, J., J. R. Tinsley, D. M. Drake, I. Bergqvist, L. W. Swenson, D. K. McDaniels, F. E. Bertrand, E. E. Gross, D. J. Horen, T. P. Sjoreen
"Analyzing Power for the Inelastic Continuum with 200-MeV Protons," Physics Letters B

Ludemann, C. A., and B. J. Casstevens
"Operator Interface to the URIC Control System," Proceedings, European Physical Society Conference on Computing in Accelerator Design and Technolgy, Berlin, West Germany, September 20-23, 1983

Ma, C. H., D. P. Hutchinson, P. A. Staats, and K. L. Vander Sluis
"FIR Interferometer/Polarimeter System on ISX-B Tokamak," Proceedings, 5th Topical Conference on High Temperature Plasma Diagnostics, Tahoe City, California, September 16-20, 1984

Marston, J. B., and S. E. Koonin
"Mean-Field Calculations of Fluctuations in Nuclear Collisions," Physical Review Letters

Martin, M. J.
"Nuclear Decay Data for Selected Radionuclides," National Council on Radiation Protection and Measurements Report, Appendix

McDaniels, D. K., J. R. Tinsley, J. Lisantti, D. M. Drake, I. Bergqvist, L. W. Swenson, F. E. Bertrand, E. E. Gross, D. J. Horen, T. Sjoreen, R. Liljestrand, and H. Wilson
"Cross Section and Analyzing Power Measurements for the Giant Resonance Region in ^{208}Pb with 200-MeV Protons," Physical Review C

Meyer, F. W.
"The ORNL ECR Multicharged Ion Source," Proceedings, International Conference on the Physics of Highly Ionized Atoms, Oxford, England, July 2-5, 1984

Moltz, D. M., J. P. Sullivan, R. E. Tribble, C. A. Gagliardi, K. S. Toth, and F. T. Avignone
"Neutron-Deficient Mass Surface Between the $1f_{7/2}$ and $1g_{9/2}$ Shells: The Masses of ^{77}Kr and ^{79}Kr," Proceedings, Seventh International Conference on Atomic Masses and Fundamental Constants, Darmstadt, West Germany, September 3-7, 1984

Moltz, D. M., K. S. Toth, F. T. Avignone, III, H. Noma, B. D. Kern, R. E. Tribble, and J. P. Sullivan
"Beta Decay of ^{76}Rb and the Level Structure of ^{76}Kr," Nuclear Physics A

Nazarewicz, W., P. Olanders, I. Ragnarsson, J. Dudek, and G. A. Leander
"Octupole Shapes in Nuclei and Some Rotational Consequences Thereof," Proceedings, XIX Winter School on Physics Selected Topics in Nuclear Structure, Zakopane, Poland, April 13-15, 1984

Nazarewicz, W., P. Olanders, I. Ragnarsson, J. Dudek, G. A. Leander, P. Moller, and E. Ruchowska
"Analysis of Octupole Instability in Medium Mass and Heavy Nuclei," Nuclear Physics A

Neskovic, N.
"The Effect of Transverse Correlations in Ion Channeling in Very Thin Crystals," Physical Review Letters

Park, H., J. O. Kephart, R. K. Klein, R. H. Pantell, B. L. Berman, S. Datz, and R. L. Swent
"Electron Channeling Radiation from Diamonds with and without Platelets," Journal of Applied Physics

Phaneuf, R. A.
"Electron Capture by Multiply Charged Ions from Hydrogen Atoms at Low Energies," Proceedings, VIII International Seminar on Ion-Atom Collisions, Utrecht, The Netherlands, August 4-5, 1983

Phaneuf, R. A., and D. H. Crandall
"Collisions of Low-Energy Multiply Charged Ions," Proceedings, Atomic Physics Contractors' Workshop, Gaithersburg, Maryland, April 26-27, 1984

Plasil, F. (Invited Paper)
"Recent Advances in Fusion-Fission Reactions," Proceedings, Tsukuba International Symposium on Heavy-Ion Fusion Reactions, Ibaraki, Japan, September 3-5, 1984

Ragnarsson, I., T. Bengtsson, W. Nazarewicz, J. Dudek, G. A. Leander, and C. Baktash
"Evidence for Band Termination at Very High Spin in ^{158}Yb," Physical Review C

Raman, S., R. F. Carlton, J. C. Wells, E. T. Jurney, and J. E. Lynn
"Thermal Neutron Capture Gamma Rays from Sulfur Isotopes: Experiment and Theory," Physical Review C

Raman, S., and B. Fogelberg (Invited Paper)
"Overlapping β Decay and Resonance Neutron Spectroscopy," Proceedings, International Symposium on Nuclear Spectroscopy and Nuclear Interactions, Osaka, Japan, March 21-24, 1984

Ramayya, A. V., W. C. Ma, J. H. Hamilton, S. J. Robinson, K. Zhao, J. D. Cole, E. F. Zganjar, and E. H. Spejewski
"Competing Nuclear Structures in $^{182-188}$Hg," Proceedings, International Symposium on In-Beam Nuclear Spectroscopy, Debrecen, Hungary, May 14-18, 1984

Rapaport, J., R. Alarcon, B. A. Brown, C. D. Goodman, D. Horen, T. Masterson, E. Sugarbaker, and T. N. Taddeucci
"The ^{51}V(p,n)^{51}Cr Reaction at E_p = 160 MeV," Nuclear Physics A

Rapaport, J., C. Gaarde, J. Larsen, C. Goulding, C. D. Goodman, C. Foster, D. J. Horen, T. Masterson, E. Sugarbaker, and T. N. Taddeucci
"The ^{19}F(p,n)^{19}Ne and ^{39}K(p,n)^{39}Ca Reactions at Intermediate Energies and Quenching of the Gamow-Teller Strength," Nuclear Physics A

Remaud, B.
"A Linearized Kinetic Equation for the Transport of Fast Nucleons Through Nuclei," Physics Letters B

Sellin, I. A.
"Forward Electron Production in Heavy Ion-Atom and Ion-Solid Collisions," Proceedings, International Conference on X-Ray and Inner Shell Processes in Atoms, Molecules, and Solids, Leipzig, East Germany, August 20-24, 1984

Sellin, I. A.
"Convoy Electron Production by Heavy Ions in Solids," Proceedings, Eighth Conference on the Application of Accelerators in Research and Industry, Denton, Texas, November 12-14, 1984

Sellin, I. A., S. D. Berry, M. Breinig, C. Bottcher, R. Latz, M. Burkhard, H. Folger, H.-J. Frischkorn, K.-O. Groeneveld, D. Hofmann, and P. Koschar
"Anomalous Mean Free Paths for Scattering of Convoy Electrons Generated by Fast, Highly Ionized Ions in Thin Solid Targets," Proceedings, Symposium on the Physics of Electron Ejection in Ion-Atom and Ion-Solid Collisions, Aarhus, Denmark, June 29-30, 1984

Sellin, I. A., S. B. Elston, and S. D. Berry
"Recent Advances in Forward Electron Production Studies in Ion-Atom and Ion-Solid Collisions," Proceedings, Second Workshop on High-Energy Ion-Atom Collision Processes, Debrecen, Hungary, August 27-28, 1984

Semmes, P. B., G. A. Leander, and J. L. Wood (Invited Paper)
"Particle-Core Coupling Calculations for the Positive Parity States in the Odd-Mass Hg Isotopes as a Test of IBA Core Descriptions," Proceedings, International Workshop on Interacting Boson-Boson and Boson-Fermion Systems, Gull Lake, Michigan, May 28-30, 1984

Shapira, D., Conference Chairman
"Program and Abstracts for Conference on Instrumentation for Heavy-Ion Nuclear Research," Oak Ridge, Tennessee, October 22-24, 1984

Shapira, D., J.L.C. Ford, Jr., R. Novotny, B. Shivakumar, R. L. Parks, and S. T. Thornton
"The HHIRF Supersonic Gas-Jet Target Facility," Nuclear Instruments and Methods in Physical Research, Section A

Shapira, D., J. Gomez del Campo, J.L.C. Ford, Jr., B. Shivakumar, P. H. Stelson, B. A. Harmon, R. A. Parks, and S. T. Thornton
"Nuclear Physics Experiments with the ORNL-HHIRF Supersonic Gas-Jet Target," Proceedings, Eighth Conference on the Application of Accelerators in Research and Industry, Denton, Texas, November 12-14, 1984

Shapira, D., D. Schull, J.L.C. Ford, Jr., B. Shivakumar, R. L. Parks, R. A. Cecil, and S. Thornton
"Observation of Angular Momentum Saturation in Deep-Inelastic Processes Involving Light Heavy Ions," Physical Review Letters

Stone, R. E., C. R. Bingham, L. L. Riedinger, R. W. Lide, H. K. Carter, R. L. Mlekodaj, and E. H. Spejewski
"The Decay of Mass-Separated ^{199m}Po and ^{199g}Po," Physical Review C

Strayer, M. R. (Invited Paper)
"Chaos near the Coulomb Barrier? — Nuclear Molecules," Proceedings, International Conference on Fusion Reactions Below the Coulomb Barrier, Cambridge, Massachusetts, June 13-15, 1984

Strayer, M. R. (Invited Paper)
"Nuclear Molecules in TDHF," Proceedings, 5th Adriatic International Conference on Nuclear Physics: Fundamental Problems in Heavy-Ion Collisions, Hvar, Yugoslavia, September 24-29, 1984

Thorn, C. E., J. W. Olness, E. K. Warburton, and S. Raman
"^{36}S(d,p)^{37}S and ^{34,36}S(d,^{3}He)^{33,35}P Reactions," Physical Review C

Toth, K. S., Y. A. Ellis-Akovali, C. R. Bingham, D. M. Moltz, H. K. Carter, R. L. Mlekodaj, E. H. Spejewski, and D. C. Sousa
"Decay Properties of ^{186}Pb and the Lead Alpha-Decay Rate Anomaly," Proceedings, Seventh International Conference on Atomic Masses and Fundamental Constants, Darmstadt, West Germany, September 3-7, 1984

Toth, K. S., Y. A. Ellis-Akovali, C. R. Bingham, D. M. Moltz, D. C. Sousa, H. K. Carter, R. L. Mlekodaj, and E. H. Spejewski
"Evidence from α Decay That Z = 82 Is Not Magic Midway Between N = 82 and N = 126," Physical Review Letters

Toth, K. S., D. M. Moltz, E. C. Schloemer, M. D. Cable, F. T. Avignone, III, and Y. A. Ellis-Akovali
"Beta-Delayed Proton Activities: ^{147}Dy and ^{149}Er," Proceedings, Seventh International Conference on Atomic Masses and Fundamental Constants, Darmstadt, West Germany, September 3-7, 1984

Tsang, M. B., W. G. Lynch, C. B. Chitwood, D. J. Fields, D. R. Klesch, C. K. Gelbke, G. R. Young, T. C. Awes, R. L. Ferguson, F. E. Obenshain, F. Plasil, and R. L. Robinson
"Azimuthal Correlations Between Light Particles Emitted in ^{16}O-Induced Reactions on ^{12}C and ^{197}Au at 400 MeV," Physics Letters B

Uchai, W., C. W. Nestor, Jr., S. Raman, and C. R. Vane
"Energy Shifts of L X Rays from 70 < Z < 90 Elements due to Multiple M Vacancies," Atomic Data and Nuclear Data Tables

Umar, A. S.
"A Time-Dependent Mean-Field Theory for Prompt Nucleon Emission in Heavy-Ion Reactions," Proceedings, International Conference on Fusion Reactions Below the Coulomb Barrier, Cambridge, Massachusetts, June 13-15, 1984

Umar, A. S., M. R. Strayer, D. J. Ernst, and K.R.S. Devi
Mean-Field Theory of Prompt, High-Energy Nucleon Emission," Physical Review C

Wells, J. C., N. R. Johnson, J. Hattula, M. P. Fewell, D. R. Haenni, I. Y. Lee, F. K. McGowan, J. W. Johnson, and L. L. Riedinger
"Evidence for Collective Behavior in ^{128}Ce from Lifetime Measurements," Physical Review C

Welton, T. A.
"Fluctuation as Explanation in Quantum Electrodynamics," Annals of Physics (New York)

Winters, R. R., C. H. Johnson, and A. D. MacKellar
"Optical Model for Low-Energy Neutrons on ^{60}Ni," Physical Review C

Wong, C. Y.
"Nucleon-Nucleus Reactions at Ultra-Relativistic Energies," Physical Review D

Wong, C. Y.
"Rotating Torodial Nuclei in Heavy-Ion Reactions," Physical Review C

Young, G. R. (Invited Paper)
"Near-Threshold Production of Neutral Pi Mesons in Heavy-Ion Reactions," Proceedings, 7th Oaxtepec Symposium on Nuclear Physics, Oaxtepec, Mexico, January 4-6, 1984

Ziegler, N. F., E. G. Richardson, J. E. Mann, P. K. Kloeppel, R. C. Juras, C. M. Jones, J. A. Biggerstaff, J. A. Benjamin, and G. D. Alton
"Status of the Oak Ridge 25 URC Accelerator," Proceedings, Symposium of Northeastern Accelerator Personnel, Rochester, New York, October 3-5, 1983

Ziegler, N. F., E. G. Richardson, J. E. Mann, R. C. Juras, C. M. Jones, D. L. Haynes, J. A. Benjamin, and G. D. Alton
"Status Report on the ORNL 25 URC Accelerator," Proceedings, 1984 Symposium of Northeastern Accelerator Personnel with Postaccelerator Workshop, Stony Brook, New York, October 15-18, 1984

Zumbro, J. D., E. B. Shera, Y. Tanaka, C. E. Bemis, Jr., R. A. Naumann, M. V. Hoehn, W. Reuter, and R. M. Steffen
"E2 and E4 Deformations in $^{233,234,235,238}U$," Physical Review Letters

12. PAPERS PRESENTED AT SCIENTIFIC AND TECHNICAL MEETINGS

October 1983 Through September 1984

List Prepared by Shirley J. Ball

1983

Symposium of Northeastern Accelerator Personnel, Rochester, New York, October 3-5, 1983

N. F. Ziegler, E. G. Richardson, J. E. Mann, P. K. Kloeppel, R. C. Juras, C. M. Jones, J. A. Biggerstaff, J. A. Benjamin, and G. D. Alton
"Status of the Oak Ridge 25URC Accelerator"

American Physical Society Meeting, Notre Dame, Indiana, October 13-15, 1983

C. Baktash, Y. Shutz, I. Y. Lee, F. McGowan, N. R. Johnson, M. P. Fewell, M. L. Halbert, D. C. Hensley, L. Courtney, A. Larabee, L. L. Riedinger, and D. G. Sarantites
"Study of the Spin-Induced Shape Changes in ^{158}Yb," Bull. Am. Phys. Soc. 28, 991 (1983)

M. E. Bunker, J. W. Starner, and S. Raman
"Decay of ^{37}S," Bull. Am. Phys. Soc. 28, 968 (1983)

C. B. Chitwood, W. G. Lynch, M. B. Tsang, D. Fields, D. Klesch, A. D. Panagiotou, C. K. Gelbke, T. C. Awes, R. Ferguson, F. Obenshain, F. Plasil, R. Robinson, and G. R. Young
"Two-Proton Correlations at Small Relative Momentum for ^{16}O-Induced Reactions on ^{197}Au at E/A = 25 MeV," Bull. Am. Phys. Soc. 28, 973 (1983)

L. H. Courtney, L. L. Riedinger, A. J. Larabee, C. R. Bingham, C. Baktash, M. Halbert, D. Hensley, N. R. Johnson, I. Y. Lee, Y. Schutz, J. Hattula, J. Waddington, B. Herskind, D. Haenni, D. Sarantites, A. Dilmanian, M. Rajagopalan, S. Hjorth, and A. Johnson
"Discrete Gamma-Ray Studies Using Spin Spectrometer," Bull. Am. Phys. Soc. 28, 982 (1983)

Y. A. Ellis-Akovali, K. S. Toth, D. M. Moltz, and D. C. Sousa
"Single-Particle States near N = 82; Search for the N = 81 Isotope, ^{149}Er," Bull. Am. Phys. Soc. 28, 981 (1983)

J. Gomez del Campo (Invited Talk)
"Measurements of Nuclear Deexcitation Times Using the Crystal Blocking Technique," Bull. Am. Phys. Soc. 28, 987 (1983)

M. L. Halbert (Invited Talk)
"New Vistas of Heavy-Ion Reactions with the Spin Spectrometer," Bull. Am. Phys. Soc. 28, 964 (1983)

H. Ikezoe, D. G. Kovar, G. Rosner, G. Stephens, E. Ungricht, B. Wilkins, T. Awes, G. R. Young, C. Maguire, Z. Kui, W. C. Ma, S. Robinson, D. Watson, and G. Word
"Coincidence Measurements Between Evaporation Residues and Light Particles Produced in ^{16}O + ^{40}Ca at $E_{lab}(^{16}O)$ = 160 MeV," Bull. Am. Phys. Soc. 28, 974 (1983)

C. H. Johnson, N. W. Hill, J. A. Harvey, and D. J. Horen
"Afterpulses of Several μsec for an RCA-8854 Multiplier," Bull. Am. Phys. Soc. 28, 992 (1983)

D. Klesch, C. B. Chitwood, D. Fields, C. K. Gelbke, W. G. Lynch, M. B. Tsang, A. D. Panagiotou, T. C. Awes, R. Ferguson, F. Obenshain, F. Plasil, R. Robinson, and G. R. Young
"Single and Two-Particle Measurements for Light Particle Emission of ^{16}O-Induced Reactions at 400 MeV," Bull. Am. Phys. Soc. 28, 973 (1983)

A. J. Larabee, L. H. Courtney, S. Frauendorf, L. L. Riedinger, J. C. Waddington, M. P. Fewell, N. R. Johnson, I. Y. Lee, and F. K. McGowan
"Shape Effects in $h_{11/2}$ and $g_{7/2}$ Bands in ^{159}Tm," Bull. Am. Phys. Soc. 28, 982 (1983)

W. C. Ma, A. V. Ramayya, K. Zhao, J. H. Hamilton, M. E. Barclay, S. Robinson, J. D. Cole, E. F. Zganjar, and E. H. Spejewski
"High Spin States in ^{182,184}Hg," Bull. Am. Phys. Soc. 28, 989 (1983)

A. D. MacKellar and C. H. Johnson
"Coupled Channel OMP Analysis with Parity Dependence for n + ^{40}Ca," Bull. Am. Phys. Soc. 28, 982 (1933)

D. M. Moltz, K. S. Toth, J. P. Sullivan, R. E. Tribble, C. A. Gagliardi, and F. T. Avignone III
"Mass of ^{75}Kr," Bull. Am. Phys. Soc. 28, 970 (1983)

S. Raman (Invited Talk)
"Overlapping β Decay and Resonance Neutron Spectroscopy," Bull. Am. Phys. Soc. 28, 972 (1983)

A. V. Ramayya, W. C. Ma, J. H. Hamilton, M. E. Barclay, K. Zhao, S. Robinson, J. D. Cole, E. F. Zganjar, and E. H. Spejewski
"Identification of ^{182}Hg with Near-Spherical and Deformed States," Bull. Am. Phys. Soc. 28, 989 (1983)

Zhao Kui, C. F. Maguire, J.L.C. Ford, Jr., D. Shapira, F. E. Bertrand, E. Gross, R. O. Sayer, and T. P. Sjoreen
"The ^{28}Si(^{11}B, ^{10}B and ^{10}B*)^{29}Si Reactions as a Test of the Spin-Orbit Potential for Heavy Ions," Bull. Am. Phys. Soc. 28, 994 (1983)

1983 Nuclear Science Symposium, San Francisco, California, October 19-21, 1983

D. C. Hensley
"Data Acquisition with the Event Handler

N. R. Johnson, C. Baktash, and I. Y. Lee (Invited Talk)
"Bismuth Germanate's Role in the New Revolution in Gamma-Ray Spectroscopy"

1983 Annual Meeting of the Southeastern Section of the American Physical Society, Columbia, South Carolina, November 3-5, 1983

B. D. Kern, K. S. Toth, D. M. Moltz, J. Lin, F. T. Avignone, III, and G. Leander
"Beta Decay of ^{75}Rb," Bull. Am. Phys. Soc. 28, 130 (1984)

R. A. Phaneuf (Invited Talk)
"Electron Capture by Multiply Charged Ions from Hydrogen Atoms at Low Energies," Bull. Am. Phys. Soc. 29, 123 (1984)

I. A. Sellin (Invited Talk)
"Some Old, New, Borrowed, and Blue Topics in Accelerator-Related Atomic Physics," Bull. Am. Phys. Soc. 29, 123 (1984)

American Physical Society Meeting, San Francisco, California, November 20-23, 1983

B. L. Berman, S. Datz, J. O. Kephart, R. K. Klein, R. H. Pantell, H. Park, R. L. Swent, M. J. Alguard, and M. V. Hynes
"Channeling Radiation from LiH," Bull. Am. Phys. Soc. 28, 1322 (1983)

H. Park, R. H. Pantell, R. L. Swent, J. O. Kephart, R. K. Klein, B. L. Berman, S. Datz, and R. W. Fearick
"Comparison of Channeling Radiation from Diamonds with and without Platelets," Bull. Am. Phys. Soc. 28, 1323 (1983)

Workshop on Electronic and Ionic Collisions Cross Sections Needed in the Modeling of Radiation Interaction with Matter, Argonne, Illinois, December 6-8, 1983

D. C. Gregory
"The Controlled Fusion Atomic Data Center"

1984

7th Oaxtepec Symposium on Nuclear Physics, Oaxtepec, Mexico, January 4-6, 1984

G. R. Young (Invited Talk)
"Near-Threshold Production of Neutral Pi Mesons in Heavy-Ion Reactions"

International Workshop on Hyperfine Interactions, Kanpur, India, January 16-25, 1984

C. E. Bemis, Jr. (Invited Talk)
"Laser Optical Pumping in Nuclear Physics: Fission Isomers, Oriented Targets, and Hyperfine Pumping in Single-Electron Atoms"

International Winter Meeting on Nuclear Physics, Bormio, Italy, January 23-27, 1984

T. C. Awes, R. L. Auble, F. E. Bertrand, M. L. Halbert, D. C. Hensley, I. Y. Lee, V. O. Rauch, R. L. Robinson, D. G. Sarantites, and G. R. Young
"Fast Particles in Coincidence with γ Rays from the $^{12}C + ^{60}Ni$ and $^{12}C + ^{120}Sn$ Reactions"

Workshop on Nuclear Dynamics III, Copper Mountain, Colorado, March 4-9, 1984

T. C. Awes, R. L. Ferguson, R. Novotny, F. E. Obenshain, F. Plasil, V. Rauch, H. Sann, and G. R. Young (Invited Talk)
"Projectile Fission in ^{58}Ni-Induced Reactions at 15.3 MeV/u"

A. C. Mignerey, C. Merouane, S. Bradley, D. Benton, H. Breuer, J. D. Silk, K. Kwiatowski, V. E. Viola, Jr., T. C. Awes, F. E. Obenshain, and S. Pontoppidan
"Quasi-Elastic Structure in the Reaction $^{56}Fe + ^{56}Fe$ at 14.6 MeV/Nucleon"

F. Plasil, T. C. Awes, B. Cheynis, D. Drain, R. L. Ferguson, F. E. Obenshain, A. J. Sierk, S. G. Steadman, G. R. Young, A. Gavron, J. Boissevain, H. C. Britt, K. Eskola, P. Eskola, M. M. Fowler, Z. Fraenkel, H. Ohm, J. van der Plicht, and S. Wald (Invited Talk)
"Recent Results in Heavy-Ion-Induced Fission"

S. T. Thornton, R. L. Parks, D. Shapira, D. Schull, J.L.C. Ford, Jr., and B. Shivakumar
"Observation of a Critical Angular Momentum for Deep Inelastic Processes with Light Heavy Ions"

C. Y. Wong (Invited Talk)
"Initial Energy Density of Quark-Gluon Plasma in Relativistic Heavy-Ion Collisions"

C. Y. Wong (Invited Talk)
"Baryon Distribution in Relativistic Heavy-Ion Collisions"

International Symposium on Nuclear Spectroscopy and Nuclear Interactions, Osaka, Japan, March 21-24, 1984

F. E. Bertrand, J. R. Beene, and M. L. Halbert
"Photon Decay of Giant Resonances"

S. Raman (Invited Talk)
"Overlapping β Decay and Resonance Neutron Spectroscopy"

Workshop on Detectors for Relativistic Nuclear Collisions, Berkeley, California, March 26-30, 1984

A. Poskanzer, H-G. Ritter, B. Ludewigt, K. Foley, S. Borenstein, E. Platner, W. Love, D. Keane, and F. Plasil
"Event Parameters — Fixed Target"

American Chemical Society, Division of Nuclear Chemistry and Technology, St. Louis, Missouri, April 8-13, 1984

R. L. Ferguson (Invited Talk)
"Heavy-Ion-Induced Fission of Medium-Energy Compound Systems with Projectile Energies up to 25 MeV per Nucleon"

XiX Winter School on Physics Selected Topics in Nuclear Structure, Zakopane, Poland, April 13-15, 1984

W. Nazarewicz, P. Olanders, I. Ragnarsson, J. Dudek, and G. A. Leander
"Octupole Shapes in Nuclei and Some Rotational Consequences Thereof"

American Physical Society Meeting, Washington, D. C., April 23-26, 1984

J. R. Beene (Invited Paper)
"Crystal Ball Studies of Giant Resonance Decay," Bull. Am. Phys. Soc. 29, 620 (1984)

P. Braun-Munzinger, P. Paul, L. Ricken, J. Stachel, P. H. Zhang, G. R. Young, F. E. Obenshain, and E. Grosse
"Collectivity in Subthreshold Pion Production," Bull. Am. Phys. Soc. 29, 672 (1984)

Y. A. Ellis-Akovali, K. S. Toth, D. M. Moltz, F. T. Avignone, E. C. Schloemer, and M. D. Cable
"Search for the M4 Isomeric Transition in ^{149}Er," Bull. Am. Phys. Soc. 29, 718 (1984)

C. B. Fulmer, D. C. Hensley, R. L. Auble, J. B. Ball, K. A. Erb, E. E. Gross, G. R. Satchler, D. Shapira, and Y-d. Chan
"Elastic Scattering of 140-MeV ^{9}Be on ^{12}C and ^{16}O," Bull. Am. Phys. Soc. 29, 624 (1984)

J. Gomez del Campo, R. Ribas, N. Neskovic, D. Shapira, J. A. Biggerstaff, C. D. Moak, P. D. Miller, J.P.F. Sellschop, and R. W. Fearick
"Crystal Blocking Measurements for Elastic Transfer Reactions and α-Particle Emission for the ^{16}O + ^{nat}Ge System," Bull. Am. Phys. Soc. 29, 688 (1984)

D. J. Horen, F. E. Bertrand, E. E. Gross, T. Sjoreen, J. B. McClelland, T. A. Carey, S. J. Seestrom-Morris, K. Thomas, D. K. McDaniels, J. R. Tinsley, J. Lisantti, and L. Swenson
"Excitation of E2 Transitions in ^{40}Ca by 334-MeV Protons," Bull. Am. Phys. Soc. 29, 628 (1984)

C. H. Johnson, N. W. Hill, J. A. Harvey, and D. J. Horen
"Afterpulses from Residual Gases in RCA-8854 and RCA-4522 Multipliers," Bull. Am. Phys. Soc. 29, 664 (1984)

G. A. Leander (Invited Talk)
"Learning to Read the Nuclear Structure Story Told by Yrast γ Rays," Bull. Am. Phys. Soc. 29, 726 (1984)

W. G. Lynch, C. B. Chitwood, D. J. Fields, C. K. Gelbke, D. R. Klesch, M. B. Tsang, G. R. Young, T. C. Awes, R. L. Ferguson, F. E. Obenshain, F. Plasil, and R. L. Robinson
"Large-Angle Correlations Between Nonequilibrium Light Particles Emitted in ^{16}O-Induced Reactions at E/A = 25 MeV," Bull. Am. Phys. Soc. 29, 672 (1984)

A. D. MacKellar, C. H. Johnson, and R. R. Winters
"Deformed Optical Model Potential for s-Wave Neutrons on ^{60}Ni in the Kilovolt Energy Region," Bull. Am. Phys. Soc. 29, 636 (1984)

G. A. Petitt, A. Gavron, J. R. Beene, B. Chenis, R. L. Ferguson, F. E. Obenshain, F. Plasil, G. R. Young, M. Jääskeläinen, D. G. Sarantites, and C. F. Maguire
"Systematics of Nonequilibrium Neutron Emission in Inelastic Reactions ^{12}C + ^{158}Gd and ^{20}Ne + ^{150}Nd," Bull. Am. Phys. Soc. 29, 673 (1984)

R. V. Ribas, N. R. Johnson, I. Y. Lee, D. R. Haenni, L. L. Riedinger, R. M. Diamond, F. S. Stephens, S. Shih, and H. Kluge
"Coulomb Excitation of ^{160}Dy with Lead Ions," Bull. Am. Phys. Soc. 29, 688 (1984)

D. Shapira, B. Shivakumar, J. Gomez del Campo, J.L.C. Ford, Jr., P. H. Stelson, B. A. Harmon, and S. T. Thornton
"On the Equilibration of the Mass Degree of Freedom in Orbiting Processes," Bull. Am. Phys. Soc. 29, 626 (1984)

B. Shivakumar, D. Shapira, J. Gomez del Campo, J.L.C. Ford, Jr., P. H. Stelson, B. A. Harmon, and S. T. Thornton
"Backward Angle Yields of Products from ^{28}Si + ^{14}N Collisions," Bull. Am. Phys. Soc. 29, 626 (1984)

K. S. Toth, D. M. Moltz, F. T. Avignone, E. C. Schloemer, M. D. Cable, and Y. A. Ellis-Akovali
"Identification of ^{149}Er via Its β-Delayed Proton Activity," Bull. Am. Phys. Soc. 29, 718 (1984)

D. Wang, R. Alarcon, P. Welch, J. Rapaport, D. Horen, T. N. Taddeucci, C. D. Goodman, E. Sugarbaker, and C. Saarde
"The ^{57,58}Fe(p,n)^{57,58}Co Reactions at 120 MeV," Bull. Am. Phys. Soc. 29, 717 (1984)

R. R. Winters, C. H. Johnson, and A. D. MacKellar
"A Spherical Optical Potential for s-Wave Neutrons on ^{60}Ni in the Kilovolt Energy Region," Bull. Am. Phys. Soc. 29, 636 (1984)

J. D. Zumbro, R. A. Naumann, E. B. Shera, M. V. Hoehn, W. Reuter, C. E. Bemis, Jr., Y. Tanaka, and R. M. Steffen
"Precision Muonic-Atom Determinations of the Charge Parameters for ^{233,234,235,238}U," Bull. Am. Phys. Soc. 29, 720 (1984)

Atomic Physics Contractors' Workshop, Gaithersburg, Maryland, April 26-27, 1984

R. A. Phaneuf and D. H. Crandall
"Collisions of Low-Energy Multiply Charged Ions"

Tenth International Conference on Cyclotrons and Their Applications, East Lansing, Michigan, April 30-May 3, 1984

E. D. Hudson, R. S. Lord, M. L. Mallory, and T. A. Antaya
"Dual Arc Penning Ion Source Gas Flow Experiments," Bull. Am. Phys. Soc. 29, 837 (1984)

C. M. Jones (Invited Talk)
"Review of the Current Status of Large Electrostatic Accelerators," Bull. Am. Phys. Soc. 29, 849 (1984)

J. A. Martin (Invited Talk)
"Conference Introduction: The International Cyclotron Conference's Twenty-Five Years of Progress," Bull. Am. Phys. Soc. 29, 833 (1984)

International Symposium on In-Beam Nuclear Spectroscopy, Debrecen, Hungary, May 14-18, 1984

H. El-Samman, V. Barci, T. Bengtsson, A. Gizon, J. Gizon, L. Hildingsson, D. Jerrestam, W. Klamra, R. Kossakowski, G. A. Leander, and Th. Lindblad
"Collective Moment of Inertia of ^{118,122}Xe and ^{128,130}Ba"

A. V. Ramayya, W. C. Ma, J. H. Hamilton, S. J. Robinson, K. Zhao, J. D. Cole, E. F. Zganjar, and E. H. Spejewski
"Competing Nuclear Structures in $^{182-188}$Hg"

Workshop on Polarized Targets in Storage Rings, Argonne, Illinois, May 17-18, 1984

C. E. Bemis, Jr., J. R. Beene, J.L.C. Ford, Jr., D. Shapira, and B. Shivakumar (Invited Talk)
"Development of Optically Pumped Polarized Jet Targets for Use in Heavy-Ion Reaction Studies"

Thirteenth International Colloquium on Group Theoretical Methods in Physics, College Park, Maryland, May 21-25, 1984

H. M. Khalil and M. M. Shalaby
"An Alternative Residue Expansion for the Scattering Amplitude"

Conference on the Intersections Between Particle and Nuclear Physics, Steamboat Springs, Colorado, May 23-30, 1984

G. R. Young (Invited Talk)
"Accelerator-Colliders for Relativistic Heavy Ions or in Search of Luminosity"

International Workshop on Interacting Boson-Boson and Boson-Fermion Systems, Gull Lake, Michigan, May 28-30, 1984

G. A. Leander, P. B. Semmes, and F. Donau (Invited Talk)
"Unpaired Nucleons as Probes of Core Collective Fields"

P. B. Semmes, G. A. Leander, and J. L. Wood (Invited Talk)
"Particle-Core Coupling Calculations for the Positive Parity States in the Odd-Mass Hg Isotopes as a Test of IBA Core Descriptions"

Workshop on Impurity Control Physics, Atlanta, Georgia, May 30-31, 1984

R. A. Phaneuf
"Atomic Processes Involving Impurities in the Plasma Edge"

American Physical Society (Division of Electron and Atomic Physics), Storrs, Connecticut, May 30-June 1, 1984

R. L. Becker and A. D. MacKellar
"Calculations of Collisions of Ions with Rydberg Atoms in High |m| States," Bull. Am. Phys. Soc. 29, 795 (1984)

C. Bottcher
"A Classical Theory of Recombination in Perturbed Environments," Bull. Am. Phys. Soc. 29, 792 (1984)

C. Bottcher
"Time-Dependent Self-Consistent Field Study of a Heavy-Ion Collision: F^{9+} Ne," Bull. Am. Phys. Soc. 29, 813 (1984)

C. Bottcher and T. G. Heil
"Charge Transfer in Few-Electron Systems Using One-Electron Eigenstate Expansions," Bull. Am. Phys. Soc. 29, 810 (1984)

S. Datz (Invited Talk)
"Beams Experiments on Dielectronic Recombination," Bull. Am. Phys. Soc. 29, 784 (1984)

S. B. Elston, M. Breinig, I. Sellin, S. Berry, D. Hofmann, P. Koschar, and I. B. Nemirovsky
"Two-Dimensional Energy/Angular Distributions of ELC Electrons for 41-MeV and 82-MeV O^{5+} Projectiles on He and Ne," Bull. Am. Phys. Soc. 29, 777 (1984)

P. Focke, I. B. Nemirovsky, E. Gonzalez Lepera, W. Meckbach, I. A. Sellin, and K. O. Groeneveld
"Beam Foil Convoy Electron Distribution as a Function of Energy and Angle of Emission," Bull. Am. Phys. Soc. 29, 817 (1984)

A. M. Howald, R. A. Phaneuf, D. H. Crandall, and D. C. Gregory
"Single, Double, and Triple Ionization of Xe^{6+} by Electron Impact," Bull. Am. Phys. Soc. 29, 804 (1984)

F. W. Meyer
"The ORNL ECR Multicharged Ion Source," Bull. Am. Phys. Soc. 29, 810 (1984)

R. A. Phaneuf, C. C. Havener, and H. F. Krause
"Ion-Atom Merged Beams," Bull. Am. Phys. Soc. 29, 812 (1984)

M. S. Pindzola, D. C. Griffin, and C. Bottcher
"DRACULA - A Dielectronic Recombination Cross Section Code," Bull. Am. Phys. Soc. 29, 805 (1984)

J. F. Reading (with A. L. Ford and R. L. Becker) (Invited Talk)
"Charge Transfer and the Development of Techniques for Numerical Calculations of Ion-Atom Collisions," Bull. Am. Phys. Soc. 29, 821 (1984)

Conference of the Belgian Physical Society, Louvain-la-Neuve, Belgium, June 7-8, 1984

P. DeFrance, D. Belic, F. Brouillard, S. Chantrenne, D. Gregory, J. Jureta, and S. Rachafi
"Experimental Study of the Ionization of Multicharged Ions"

International Conference on Fusion Reactions Below the Coulomb Barrier, Cambridge, Massachusetts, June 13-15, 1984

C. E. Bemis, Jr., J. R. Beene, J.L.C. Ford, Jr., D. Shapira, and B. Shivakumar (Invited Talk)
"Development of Polarized Targets for Subbarrier Fusion Studies"

H. J. Kim, T. C. Awes, J. R. Beene, C. E. Bemis, Jr., R. L. Ferguson, I. Y. Lee, F. K. McGowan, F. E. Obenshain, F. Plasil, V. Rauch, R. L. Robinson, and S. Steadman
"Calibration and Initial Experiments with the ORNL-MIT Recoil Mass Spectrometer"

M. R. Strayer (Invited Talk)
"Chaos near the Coulomb Barrier? — Nuclear Molecules"

A. S. Umar
"A Time-Dependent Mean-Field Theory for Prompt Nucleon Emission in Heavy-Ion Reactions"

Symposium on the Physics of Electron Ejection in Ion-Atom and Ion-Solid Collisions, Aarhus, Denmark, June 29-30, 1984

S. B. Elston, S. D. Berry, M. Breinig, R. DeSerio, C. E. Gonzalez Lepera, I. A. Sellin, K.-O. Groeneveld, D. Hoffman, P. Koschar, I. B. Nemirovski, and L. I. Liljeby
"Doubly Differential Emission Distributions from Electron Loss to the Continuum from Fast Heavy Projectiles in Gas Targets"

I. A. Sellin, S. D. Berry, M. Breinig, C. Bottcher, R. Latz, M. Burkhard, H. Folger, H.-J. Frischkorn, K.-O. Groeneveld, D. Hofmann, and P. Koschar
"Anomalous Mean Free Paths for Scattering of Convoy Electrons Generated by Fast, Highly Ionized Ions in Thin Solid Targets"

International Conference on the Physics of Highly Ionized Atoms, Oxford, England, July 2-5, 1984

F. W. Meyer
"The ORNL ECR Multicharged Ion Source"

School on Heavy-Ion Physics, Erice, Sicily, July 17-23, 1984

G. F. Bertsch (Invited Talk)
"Nonrelativistic Theory of Heavy-Ion Collisions"

XXII International Conference on High-Energy Physics, Leipzig, East Germany, July 19-25, 1984

K. Abe, R. Armenteros, T. C. Bacon, J. Ballam, H. H. Bingham, J. E. Brau, K. Braune, D. Brick, W. M. Bugg, J. M. Butler, W. Cameron, H. O. Cohn, D. C. Colley, G. T. Condo, P. Dingus, R. Erickson, R. C. Field, B. Franek, R. Gearhart, T. Glanzman, I. M. Godfrey, J. J. Goldberg, G. Hall, E. R. Hancock, H. J. Hargis, E. L. Hart, M. J. Harwin, K. Hasegawa, M. Jobes, T. Kafka, G. E. Kalmus, D. P. Kelsey, T. Kitagaki, W. A. Mann, R. Merenyi, R. Milburn, K. C. Moffeit, J. J. Murray, A. Napier, V. R. O'Dell, P. Rankin, H. Sagawa, J. Schneps, S. J. Sewell, J. Shank, A. M. Shapiro, J. Shimony, K. Tamai, S. Tanaka, D. A. Waide, M. Widgoff, S. Wolbers, C. A. Woods, A. Yamaguchi, G. P. Yost, and H. Yuta
"Charm Photoproduction at 20 GeV Including Preliminary Lifetime Results with Improved Optical Resolution"

K. Abe, R. Armenteros, T. C. Bacon, J. Ballam, H. H. Bingham, J. E. Brau, K. Braune, D. Brick, W. M. Bugg, J. M. Butler, W. Cameron, H. O. Cohn, D. C. Colley, G. T. Condo, P. Dingus, R. Erickson, R. C. Field, B. Franek, R. Gearhart, T. Glanzman, I. M. Godfrey, J. J. Goldberg, G. Hall, E. R. Hancock, H. J. Hargis, E. L. Hart, M. J. Harwin, K. Hasegawa, M. Jobes, T. Kafka, G. E. Kalmus, D. P. Kelsey, T. Kitagaki, W. A. Mann, R. Merenyi, R. Milburn, K. C. Moffeit, J. J. Murray, A. Napier, V. R. O'Dell, P. Rankin, H. Sagawa, J. Schneps, S. J. Sewell, J. Shank, A. M. Shapiro, J. Shimony, K. Tamai, S. Tanaka, D. A. Waide, M. Widgoff, S. Wolbers, C. A. Woods, A. Yamaguchi, G. P. Yost, and H. Yuta
"Comparison of Lambda and Antilambda Inclusive Photoproduction at 20 GeV with Quark-Diquark Fusion Model"

9th International Conference on Atomic Physics, Seattle, Washington, July 23-27, 1984

C. Bottcher and M. R. Strayer
"Numerical Solutions of the Dirac Equation Describing Collisions Between Very Heavy Ions"

C. Bottcher, R. Latz, M. Burghardt, H.-J. Frischkorn, K.-U. Groeneveld, D. Hofmann, P. Koschar, S. D. Berry, M. Breinig, and I. A. Sellin
"Anomalous Mean Free Paths of Convoy Electrons in Foils: A Coulomb Focussing Effect?"

P. Engar, M. Breinig, R. DeSerio, I. A. Sellin, C. E. Gonzalez-Lepera, S. D. Berry, M. Bloemer, and T. Underwood
"Field-Ionization of Foil-Excited Rydberg States of Fast Oxygen Ions"

P. M. Griffin and C. C. Havener
"EUV Radiation from keV Electron Impact on Tantalum"

Third International Conference on Infrared Physics, Zurich, Switzerland, July 23-27, 1984

D. P. Hutchinson, C. H. Ma, P. A. Staats, and K. L. Vander Sluis
"Far-Infrared Interferometry/Polarimetry on the ISX-B Tokamak"

Tenth International Conference on Particles and Nuclei, Heidelberg, West Germany, July 30-August 3, 1984

C. S. Mishra, G. S. Blanpied, B. M. Preedom, B. G. Ritchie, R. S. Moore, M. Blecher, K. Gotow, R. L. Burman, M. V. Hynes, E. Piasetzky, N. S. Chant, P. G. Roos, F. E. Bertrand, T. P. Sjoreen, F. E. Obenshain, and E. E. Gross
"Elastic $\pi^{\pm}$ Scattering from ^{14}C at 50 MeV"

B. Fick, M. Blecher, K. Gotow, D. Wright, G. Blanpied, J. A. Escalante, C. S. Mishra, B. M. Preedom, R. L. Burman, M. Hynes, C. Ciangaru, N. Chant, P. Roos, B. G. Ritchie, F. E. Bertrand, E. E. Gross, F. E. Obenshain, and W. Burger
"$\pi^{\pm}$ Elastic Scattering Sensitivity to the Neutron Radius"

International Conference on X-Ray and Inner Shell Processes in Atoms, Molecules, and Solids, Leipzig, East Germany, August 20-24, 1984

R. L. Becker, A. L. Ford, and J. F. Reading
"Inclusion of Electron Transfer in the Calculation of K^0L^v Multiple Vacancy Production by Ion Impact"

I. A. Sellin
"Forward Electron Production in Ion-Atom and Ion-Solid Collisions"

American Chemical Society, Division of Nuclear Chemisty and Technology, Philadelphia, Pennsylvania, August 26-31, 1984

G. A. Leander (Invited Talk)
"Spectroscopy of Rotating Reflection-Asymmetric Nuclei"

Second Workshop on High Energy Ion-Atom Collisions, Debrecen, Hungary, August 27-28, 1984

R. L. Becker
"Vacancy-Rearrangement Theory in the First Magnus Approximation"

R. L. Becker, A. L. Ford, and J. F. Reading (Invited Talk)
"Multiple Vacancy Production by High-Energy Heavy Ions"

I. A. Sellin
"Horizons of Forward Electron Production in Ion-Atom and Ion-Solid Collisions"

INS-RIKEN International Symposium on Heavy-Ion Physics, Mt. Fuji, Japan, August 27-31, 1984

J. R. Beene, F. E. Bertrand, M. L. Halbert, D. C. Hensley, R. L. Auble, D. J. Horen, R. L. Robinson, T. P. Sjoreen, and R. O. Sayer (Invited Talk)
"Crystal Ball Studies of Giant Resonance Decay"

Tsukuba International Symposium on Heavy-Ion Fusion Reactions, Ibaraki, Japan, September 3-5, 1984

F. Plasil (Invited Talk)
"Recent Advances in Fusion-Fission Reactions"

H. Yamada, D. G. Sarantites, R. L. Robinson, M. L. Halbert, D. C. Hensley, V. Rauch, R. L. Auble, F. E. Bertrand, and J. H. Hamilton
"Partial Fusion Reaction in Crystal Ball Spin Spectrometer"

Seventh International Conference on Atomic Masses and Fundamental Constants, Darmstadt, West Germany, September 3-7, 1984

G. A. Leander, P. Möller, J. R. Nix, and W. M. Howard
"Calculated Masses and Half-Lives for Nuclei in the Region $100 < Z < 110$"

D. M. Moltz, K. S. Toth, F. T. Avignone, J. P. Sullivan, R. E. Tribble, and C. A. Gagliardi
"Neutron-Deficient Mass Surface Between the $1f_{7/2}$ and $1g_{9/2}$ Shells"

K. S. Toth, Y. A. Ellis-Akovali, C. R. Bingham, D. M. Moltz, H. K. Carter, R. L. Mlekodaj, E. H. Spejewski, and D. C. Sousa
"Decay Properties of ^{186}Pb and the Lead Alpha-Decay Rate Anomaly"

K. S. Toth, D. M. Moltz, E. C. Schloemer, M. D. Cable, F. T. Avignone, III, and Y. A. Ellis-Akovali
"Beta-Delayed Proton Activities: ^{147}Dy and ^{149}Er"

Neutron-Nucleus Collisions: A Probe of Nuclear Structure, Glouster, Ohio, September 5-8, 1984

R. F. Carlton, J. A. Harvey, and C. H. Johnson
"Optical Model Scattering Functions for Low Energy Neutrons on ^{86}Kr"

C. H. Johnson (Invited Talk)
"Optical Models from Low-Energy s-, p-, and d-Wave Cross Sections"

Fifth International Symposium on Gamma-Ray Spectroscopy and Related Topics, Knoxville, Tennessee, September 10-14, 1984

J. R. Beene, F. E. Bertrand, M. L. Halbert, D. C. Hensley, R. L. Auble, D. J. Horen, R. L. Robinson, T. P. Sjoreen, and R. O. Sayer (Invited Talk)
"Crystal Ball Studies of Giant Resonance Neutron and Gamma Decay"

L. C. Dennis and S. Raman
"Location of a Doorway State Using the Channel $n + ^{207}$Pb"

B. Fogelberg, J. Harvey, M. Mizumoto, and S. Raman
"Observation of Extremely Low s-Wave Strength in the Reaction ^{136}Xe + n"

Z. Gacsi, J. Sa, J. L. Weil, E. T. Jurney, and S. Raman
"Decay Scheme of ^{116}Sn from $(n,n'\gamma)$ and (n,γ) Results"

G. A. Leander
"Nuclear Structure of Neutron-Rich Fission Products"

G. A. Leander
"Shell Effects on the E1 Moments of Ra-Th Nuclei"

N. K. Sherman, W. F. Davidson, S. Raman, W. Delbianco, G. Kajrys
"Comparison of Photoabsorption by ^{16}O and ^{18}O"

5th Topical Conference on High Temperature Plasma Diagnostics, Tahoe City, California, September 16-20, 1984

C. A. Bennett, D. P. Hutchinson, K. L. Vander Sluis, and P. A. Staats
"Development of Sequence and Regular Band Lasers for Use as Local Oscillators in Thomson Scattering Alpha Particle Diagnostics"

W. H. Casson, D. P. Hutchinson, C. H. Ma, P. A. Staats, and J. B. Wilgen
"Far-Infrared Laser Diagnostic on EBT and Extreme Far-Forward Laser Scattering on ISX"

D. P. Hutchinson, C. H. Ma, K. L. Vander Sluis, and P. A. Staats
"Feasibility of Alpha Particle Measurement by CO_2 Laser Thomson Scattering"

C. H. Ma, D. P. Hutchinson, P. A. Staats, and K. L. Vander Sluis
"FIR Interferometer/Polarimeter System on ISX-B Tokamak"

1984 Federation of Analytical Chemistry and Spectroscopy Societies, Philadelphia, Pennsylvania, September 16-21, 1984

C. R. Vane
"Environmental Effects in High-Resolution X-Ray Satellite Spectra"

5th Adriatic International Conference on Nuclear Physics: Fundamental Problems in Heavy-Ion Collisions, Hvar, Yugoslavia, September 24-29, 1984

K. A. Erb (Invited Talk)
"Quasi-Molecular Single-Nucleon Effects in Heavy-Ion Collisions"

M. R. Strayer (Invited Talk)
"Nuclear Molecules in TDHF"

13. GENERAL INFORMATION

ANNOUNCEMENTS

A. Baha Balantekin was appointed Eugene P. Wigner Fellow effective September 10, 1984.
George F. Bertsch was appointed UT/ORNL Distinguished Scientist effective August 6, 1984.

PERSONNEL CHANGES

New Staff Members

A. Scientific Staff

M. Breinig, University of Tennessee, Knoxville, Tennessee (part-time)
B. L. Burks, University of North Carolina, Chapel Hill, North Carolina
D. T. Dowling, Tennessee Technological University, Cookeville, Tennessee
K. A. Erb (transferred from Central Management Offices)
C. W. Glover, Indiana University, Bloomington, Indiana
D. L. Haynes (transferred from Engineering Division)
H. T. Hunter, University of Washington, Seattle, Washington

B. Administrative and Technical Staff

M. R. Dinehart, Accelerator Operations
J. R. Ellis, Secretary (transferred from Central Management Offices)
J. R. Heath, Secretary
C. A. Irizarry, Accelerator Operations
R. L. McPherson, Accelerator Operations

Staff Transfers and Terminations

A. Scientific Staff

J. A. Benjamin (present address: Brookhaven National Laboratory, Upton, New York)
J. L. C. Ford, Jr. (deceased)
C. B. Fulmer (deceased)
R. S. Lord (retirement)
J. E. Mann (retirement)
T. P. Sjoreen (transferred to Solid State Division)
C. L. Viar (retirement)

B. Administrative and Technical Staff

V. K. Hill, Secretary (retirement)
J. C. Sharp, Laboratory Technician (transferred to Laboratory Protection Division)
P. T. Singley, Accelerator Operations (transferred to Energy Division)

TEMPORARY ASSIGNMENTS

Short-Term Assignments

Scientific Staff

N. B. Neskovic, Boris Kidric Institute of Nuclear Science, Belgrade, Yugoslavia

Guest Assignments

A. Graduate Students

S. D. Berry, University of Tennessee, Knoxville, Tennessee
M. J. Bloemer, University of Tennessee, Knoxville, Tennessee
M. P. Carpenter, University of Tennessee, Knoxville, Tennessee
M-C. Chu, California Institute of Technology, Pasadena, California
L. H. Courtney, University of Tennessee, Knoxville, Tennessee
M. E-A. H. Farid, Assiut University, Assiut, Egypt
G. A. Glass, University of Tennessee, Knoxville, Tennessee
R. W. Kincaid, University of Tennessee, Knoxville, Tennessee
A. J. Larabee, University of Tennessee, Knoxville, Tennessee (on leave from McMaster University)
S. E. Lasley, University of Tennessee, Knoxville, Tennessee
X. T. Liu, University of Tennessee, Knoxville, Tennessee
R. S. Moore, Indiana University, Bloomington, Indiana
K. J. Nyberg, University of Tennessee, Knoxville, Tennessee (on leave from Research Institute for Atomic Physics, Stockholm, Sweden)
J. Shimony, University of Tennessee, Knoxville, Tennessee
B. Shivakumar, Yale University, New Haven, Connecticut
R. T. Short, University of Tennessee, Knoxville, Tennessee
K. M. Teh, Vanderbilt University, Nashville, Tennessee
J. S. Thompson, University of Tennessee, Knoxville, Tennessee
W. Uchai, Emory University, Atlanta, Georgia
S. A. Umar, Yale University, New Haven, Connecticut
T. A. Underwood, University of Tennessee, Knoxville, Tennessee

B. Co-op Students

D. E. Hoglund, Virginia Polytechnic Institute and State University, Blacksburg, Virginia
M. A. Walker, Morehouse College, Atlanta, Georgia

C. ORAU Graduate Research Participant

J. A. Bounds, University of Tennessee, Knoxville, Tennessee

D. ORAU Postgraduate Research Training Program

C. C. Havener, North Carolina State University, Raleigh, North Carolina
A. M. Howald, University of Wisconsin, Madison, Wisconsin

E. ORAU Faculty Research Participant

C. A. Bennett, Jr., University of North Carolina, Asheville, North Carolina

F. ORAU Student Research Participants

J. W. Cooke, Eckerd College, St. Petersburg, Florida
L. T. Daly, Mount Holyoke College, South Hadley, Massachusetts
F. A. Harrison, Dartmouth College, Hanover, New Hampshire
L. B. Lurio, Columbia University, New York, New York
G. L. Morford, Edinboro University of Pennsylvania, Edinboro, Pennsylvania
D. H. Olive, Carson-Newman College, Jefferson City, Tennessee
D. Thomson, Lawrence University, Appleton, Wisconsin

G. Great Lakes College Association Science Program

D. R. Shepard, Lawrence University, Appleton, Wisconsin

H. Southern Colleges and Universities Union Science Program

T. L. Hart, Centenary College of Louisiana, Shreveport, Louisiana

Summer Assignments

A. Undergraduate Student

E. M. Lee, Massachusetts Institute of Technology, Cambridge, Massachusetts

B. Graduate Students

E. A. Goode, University of Tennessee, Knoxville, Tennessee
C. R. Mahon, University of Virginia, Charlottesville, Virginia
J. B. Marston, Princeton University, Princeton, New Jersey

PHYSICS DIVISION SEMINARS: OCTOBER 1983-SEPTEMBER 1984

Those seminars arranged by the Physics Division and announced in the ORNL Technical Calendar are listed below. During the period of this report, I. Y. Lee served as Seminar Chairman.

Date	Speaker	Title
1983		
Oct. 6	Birger Fogelberg, Studsvik Science Research Laboratory, Sweden	What do we Know About Shell Model States in the Tin Region
Oct. 20	Karl L. Kratz, Univ. of Mainz, Mainz, Federal Republic of Germany	Beta Strength Function Phenomena of Short-Lived Neutron-Rich Isotopes
Oct. 27	Cheuk-Yin Wong Physics Division Staff	Energy Density of Quark-Gluon Plasma in Relativistic Heavy-Ion Collisions
Nov. 3	Julrich Heinz, Vanderbilt University, Nashville	Quark-Gluon Transport Theory
Nov. 10	G. F. Bertsch, Michigan State University, East Lansing	From TDHF to Newtonian Mechanics in Heavy Ion Collisions
Nov. 16	Erhard Salzborn, Justus Liebig University, Giessen, F.R.G.	Experiments with Multiply Charged Ions: Transfer Ionization and Electron Impact Ionization
Dec. 7	Gunther Rosner, Argonne National Laboratory	Complete and Incomplete Fusion
Dec. 8	Rolf Scharenberg, Purdue University, Lafayette, Indiana	Nuclear Fragmentation as a Critical Phenomena
Dec. 15	F. T. Avignone, University of South Carolina, Columbia	Double Beta Decay: Status and Future Projections
1984		
Feb. 2	J. Wilcyznski, Michigan State University, East Lansing	Role of the Entrance-Channel Angular Momentum in the Mechanism of Heavy-Ion Reactions at Low Energy
Feb. 3	Cheuk-Yin Wong, ORNL Staff Member	Stopping Power of Nuclear Matter
Feb. 23	S. Pontoppidan, Niels Bohr Institute, Copenhagen, Denmark	Angular Momentum Transfer in Deeply Inelastic Heavy-Ion Collisions
March 2	Mark J. Rhoades-Brown, State University of New York at Stony Brook, New York	A Self-Consistent Description of Low Energy Heavy-Ion Reactions
March 13	Helmut O. Oeschler, Institut für Kernphysik, Darmstadt, F.R.G.	Linear Momentum Transfer Studies at Energies Around 100 MeV/u
March 15	T. Døssing, Lawrence Berkeley Laboratory	Dynamics of Angular Momentum in Damped Nuclear Reactions
March 16	U. Winkler, University of Heidelberg, F.R.G.	Three-Nuclei Fragmentation in Light-Ion Reactions at 11 MeV/n
March 20	Peter Twin, Daresbury Laboratory Warrington, U.K.	Probe the γ-Ray Continuum with TERESA
March 22	Rainer Novotny, University of Giessen, F.R.G.	Recent Results from the Darmstadt-Heidelberg Crystal Ball
April 10	Surrender Saini Argonne National Laboratory	Resonance Phenomena in Heavy-Ion Reactions

Date	Speaker	Title
April 5	W. U. Schroeder University of Rochester	Mass and Energy Transport in Heavy Ion Collisions
April 9	Frederick E. Mills Fermi National Accelerator Laboratory	Electron Beam Cooling
April 12	Indrek Martinson University of Lund, Sweden	Optical Studies of Ion-Atom Interactions
April 19	Fred Petrovich Florida State University Tallahassee	Overview of the Scattering of Elementary Probes from Nuclei
May 17	Teng Lek Khoo Argonne National Laboratory	Entrance Channel Dependence in Compound Nucleus Decay
May 18	Armon McPherson North Carolina State University Raleigh	A New Radiometric Standard for the EUV
May 24	Mike W. Guidry University of Tennessee & Oak Ridge National Laboratory	Direct Reactions and High-Spin Physics
May 31	Flemming Videbaek Niels Bohr Institute, Copenhagen	Strong Coupling Effects in Heavy-Ion Quasi-Elastic Reactions
June 1	Michel Vergnes Institute of Nuclear Physics Orsay, France	Change of Structure in the Germanium Region & the Interacting Boson Model
June 7	Cheuk-Yin Wong Physics Division Staff	Incoherent Multiple Collision Description of Nucleon-Nucleus Reactions at Ultra-Relativistic Energy
June 11	Roland A. Dayras Center for Nuclear Study (CEN) Saclay, France	Projectile Fragmentation at GANIL Energies
June 14	Peter Morsch Institute for Nuclear Physics Nuclear Research Installation (KFA) Jülich, F.R.G.	New Giant Resonance Results from Jülich
June 19	I. Hertel Free University of Berlin Berlin, F.R.G.	Collision of Laser Excited Atoms
June 26	K. Goeke Nuclear Research Installation (KFA) Julich, F.R.G.	Quantized ATDHF for Low-Energy Heavy-Ion Reactions
June 28	D. Guerreau GANIL, Caen, France	Present Status of GANIL and Recent Experimental Results
July 12	Claire Schuck Orsay, France	Rotational Inertia and Pairing in good Rotors of the Rare Earth Region
July 17	Robert L. Varner University of North Carolina	A Global Parameterization of the Nucleon-Nucleus Optical Model
July 19	K. D. Hildenbrand GSI, Darmstadt, F.R.G.	Aspects of Deep-Inelastic Reactions Between Mo and Mo at Incident Energies from 12 to 18 MeV/u
July 26	Hans Ströher University of Giessen, F.R.G.	Electrofission of Pre-actinide Nuclei

Date	Speaker	Title
Aug. 2	Peter Möller Lund Institute of Technology Lund, Sweden	Mass Formula Combining the best Features of the Droplet Model and the Finite Range Model
Aug. 9	Volker E. Oberacker Vanderbilt University	A Microscopic Approach to the Calculations of Heavy Ion Potentials
Sept. 4	M. Klapisch Racah Institute of Physics Hebrew University of Jerusalem Israel	An Efficient Program for Relativistic Distorted Waves for Highly Ionized Heavy Atoms
Sept. 6	D. M. Nadkarni Bhabha Atomic Research Center Trombay, Bombay, India	Results of Recent Fission Experiments from Trombay
Sept. 13	Jim Feagin California State University Fullerton	Wannier Threshold Theory
Sept. 18	H. V. Klapdor Max Plank Institute Heidelberg, F.R.G.	Neutrino Spectra in the Reactor Core & Reactor Decay Heat
Sept. 20	Patrick J. Daly Purdue University	Spectroscopy of N~82 Nuclei Near the Proton Drip Line
Sept. 25	Osamu Miyamura Osaka University Toyonaka, Osaka, Japan	Cosmic Ray Events Above TeV/amu: Is There Any Phase Transition?

SCIENTIFIC MEETINGS SPONSORED BY THE PHYSICS DIVISION AND HELD DURING THE REPORTING PERIOD

Fifth International Symposium on Capture Gamma-Ray Spectroscopy and Related Topics

Knoxville, Tenn., September 10-14, 1984

S. Raman, organizer

Information Meeting, December 1983

The most recent Physics Division Information Meeting was held on December 12-14, 1983. The members of the Advisory Committee were:

S. E. Koonin, California Institute of Technology

E. Merzbacher, University of North Carolina

R. E. Pollock, Indiana University

D. K. Scott, Michigan State University

PHYSICS DIVISION

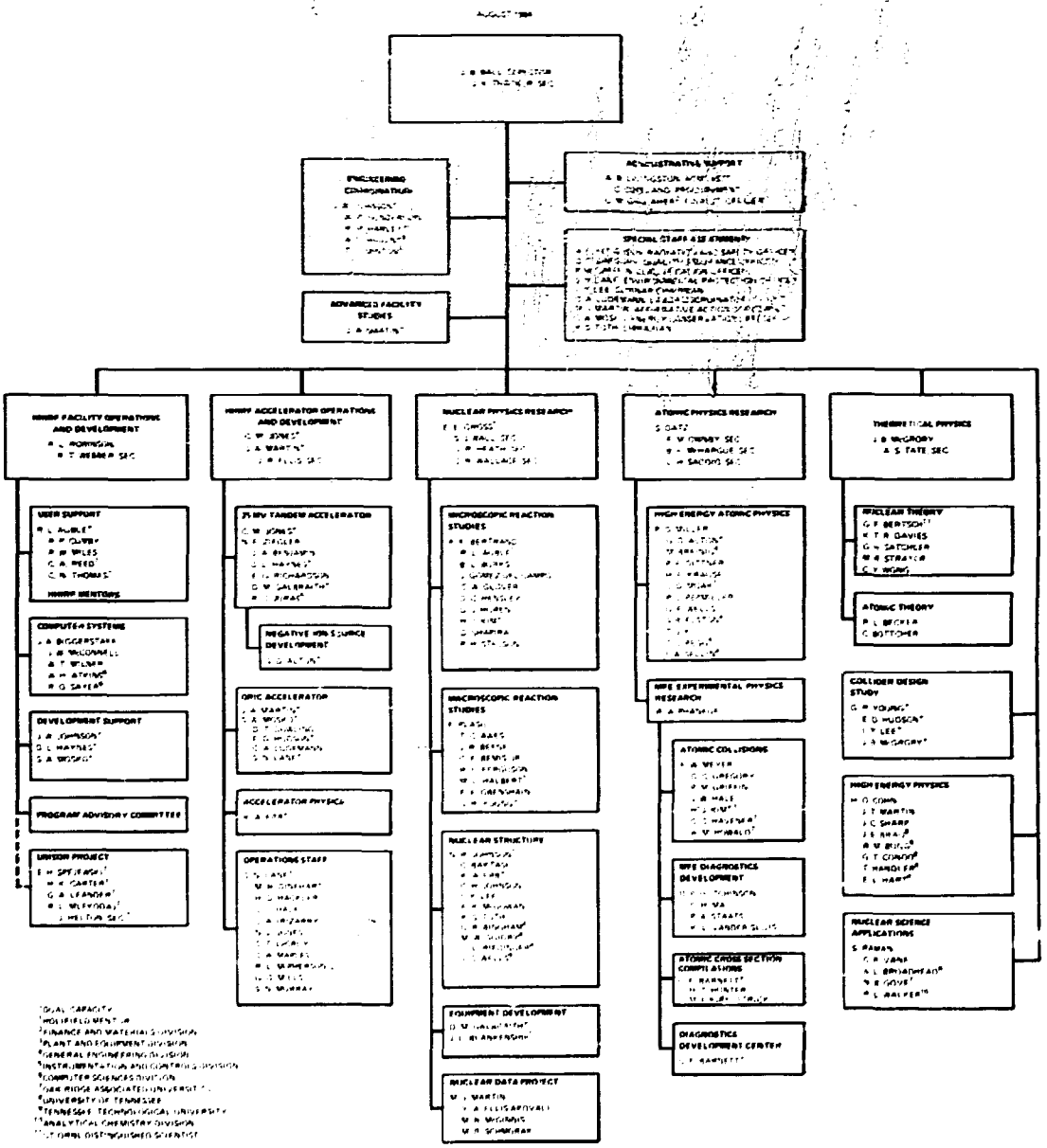

ORNL-6120
Distribution Category
UC-34

INTERNAL DISTRIBUTION

1. G. D. Alton
2. T. D. Anderson
3. B. R. Appleton
4. R. L. Auble
5. S. I. Auerbach
6. T. C. Awes
7. C. Baktash
8. A. B. Balantekin
9-129. J. B. Ball
130. S. J. Ball
132. C. F. Barnett
132. R. L. Becker
133. J. R. Beene
134. C. E. Bemis, Jr.
135. J. A. Benjamin
136. F. E. Bertrand
137. G. F. Bertsch
138. J. A. Biggerstaff
139. C. R. Bingham
140. Biology Library
141. C. Bottcher
142. J. E. Brau
143. W. M. Bugg
144. B. L. Burks
145-146. Central Research Library
147. H. O. Cohn
148. G. T. Condo
149. R. P. Cumby
150. S. Datz
151. K. T. R. Davies
152. P. F. Dittner
153. D. T. Dowling
154. B. G. Eads
155. J. R. Ellis
156. Y. A. Ellis-Akovali
157. S. B. Elston
158. K. A. Erb
159. R. L. Ferguson
160. C. W. Glover
161. J. Gomez del Campo
162. D. C. Gregory
163. P. M. Griffin
164. E. E. Gross
165. M. W. Guidry
166. R. L. Hahn
167. M. L. Halbert
168. T. Handler
169. B. A. Harmon
170. E. L. Hart
171. J. A. Harvey
172. L. J. Hawkins-Saddiq
173. D. L. Haynes
174. J. R. Heath
175. D. C. Hensley
176. R. O. Hippler
177. D. J. Horen
178. E. D. Hudson
179. D. P. Hutchinson
180. L. H. Jenkins
181. C. H. Johnson
182. J. W. Johnson
183. N. R. Johnson
184. C. M. Jones
185. P. R. Kasten
186. S. V. Kaye
187. H. J. Kim
188. H. F. Krause
189. E. H. Krieg, Jr.
190-191. Laboratory Records Department
192. Laboratory Records, ORNL R.C.
193. G. A. Leander
194. I. Y. Lee
195. A. B. Livingston
196. R. S. Lord
197. C. A. Ludemann
198. C. H. Ma
199. J. E. Mann
200. J. A. Martin
201. M. J. Martin
202. J. W. McConnell
203. F. K. McGowan
204. J. B. McGrory
205. B. F. McHargue
206. G. S. McNeilly
207. F. W. Meyer
208. R. W. Miles
209. P. D. Miller
210. W. T. Milner
211. R. L. Mlekodaj
212. S. W. Mosko
213. F. R. Mynatt
214. F. E. Obenshain
215. D. K. Olsen
216. ORNL - Y-12 Technical Library
Document Reference Section
217. F. M. Ownby
218. D. C. Parzyck
219. R. W. Peelle
220. D. J. Pegg
221. P. L. Pepmiller
222. F. G. Perey
223. R. A. Phaneuf
224. J. J. Pinajian
225. F. Plasil
226. H. Postma
227. M. L. Poutsma
228. S. Raman
229. E. G. Richardson, Jr.
230. L. L. Riedinger
231. R. L. Robinson
232. T. M. Rosseel
233. M. J. Saltmarsh
234. G. R. Satchler
235. R. O. Sayer
236. M. R. Schmorak
237. W. D. Schults
238. I. A. Sellin
239. D. Shapira
240. J. Sheffield
241. B. Shivakumar
242. T. P. Sjoreen
243. A. H. Snell
244-246. E. H. Spejewski
247. P. A. Staats
248. P. H. Stelson
249. M. R. Strayer

250. A. S. Tate
251. J. K. Thacker
252. K. S. Toth
253. D. B. Trauger
254. K. L. Vander Sluis
255. C. R. Vane
256. C. R. Wallace
257. R. T. Webber
258. G. F. Wells
259. J. C. Wells, Jr.
260. M. K. Wilkinson
261. C-Y. Wong
262. G. R. Young
263. N. F. Ziegler
264. A. Zucker

EXTERNAL DISTRIBUTION

265. B. J. Allen, Physics Division, Australian Atomic Energy Commission, Sutherland, N.S.W., Australia
266. C. H. Annett, U.S. Army - CAORA (Physics), 5445 Charlotte, Kansas City, Missouri 64110
267. Charles A. Barnes, Division of Physics and Astronomy, California Institute of Technology, Pasadena, California 91125
268. G. A. Bastin, Centre de Spectrometrie Nucleaire et de Spectrometrie de Masse, B. P. 104, 91405 Orsay, France
269. H. Behrens, Zentralstelle fur Atomkernenergie-Dokumentation, Kernforschungszentrum Karlsruhe 7514, Eggenstein-Leopoldshafen-2, Federal Republic of Germany
270. Ingmar Bergstrom, Nobel Institute of Physics, Stockholm 50, Sweden
271. Biblioteca do Depto. de Fisica Nuclear, Instituto de Fisica da USP, Caixa Postal 20516, 0100 - Sao Paulo, SP, Brasil
272. Bibliotheque - Madame Belle, Universite de Grenoble, Institut des Sciences Nucleaires, 53, rue des Martyrs, B. P. 21, 38 Grenoble, France
273. J. P. Blaser, Swiss Institute for Nuclear Research (SIN), CH-5234 Villigen, Switzerland
274. S. D. Bloom, University of California, Lawrence Livermore National Laboratory, P. O. Box 808, Livermore, California 94550
275. H. G. Blosser, Cyclotron Laboratory, Michigan State University, East Lansing, Michigan 48824
276. H. Bohn, Physik-Department E12, Technische Universitat, 8046 Garching bei Munchen, Federal Republic of Germany
277. A. Bohr, Copenhagen University, Niels Bohr Institute, Blegdamsvej 17, Copenhagen, Denmark
278. J. S. Briggs, Theoretical Physics Division, Atomic Energy Research Establishment, Harwell, Didcot, Oxfordshire OX 11 ORA, England
279. J. A. Brink, Library Division, The Merensky Institute of Physics, University of Stellenbosch, Stellenbosch, Republic of South Africa
280. D. A. Bromley, Nuclear Structure Laboratory, Yale University, New Haven, Connecticut 06520
281. T. A. Cahill, Director, Crocker Nuclear Laboratory, University of California, Davis, California 95616
282. Jose L. S. Carvalho, Instituto de Radioprotecao e Dosimetria, C.N.E.N., Av. das Americas km 11,5 Barra de Tijuca - R. J., 22700 - Rio de Janeiro, R. J. Brazil
283. David Clark, Lawrence Berkeley Laboratory, University of California, Berkeley, California 94720
284. D. H. Crandall, Branch Chief for Experimental Research, Applied Plasma Physics Division, Office of Fusion Energy, ER 542, G-226, GTN, U.S. Department of Energy, Washington, D.C. 20545
285. F. L. Culler, Office of the President, Electric Power Research Institute, P. O. Box 10412, 3412 Hillview Avenue, Palo Alto, California 94303
286. T. J. Curtin, Director, Office of Research and Grants Administration, Texas Women's University, Box 22939, TWU Station, Denton, Texas 76204
287. R. Y. Cusson, Physics Department, Duke University, Durham, North Carolina 27706
288. Solange de Barros, Head, Department of Nuclear Physics, Universidade Federal do Rio de Janeiro, Instituto de Fisica - Department Fisica Nuclear, Centro de Technologia - Bloco A, Ilha do Fundao - Rio de Janeiro, Brasil
289. Adriano de Lima, Physics Laboratory, University of Coimbra, Coimbra, Portugal
290. R. M. Diamond, Chemistry Division, Lawrence Berkeley Laboratory, Berkeley, California 94720
291. Olacio Dietzsch, Depto. de Fisica Experimental, Instituto de Fisica, Universidade de Sao Paulo, Cx. Postal 20516, Sao Paulo, S.P., Brazil
292. U. Facchini, Physics Department, University of Milan, Via Saldini 50, Milan, Italy
293. H. Faraggi-Mathieu, Centre d'Etudes Nucleaires de Saclay, B. P. No. 2, Gif-Sur-Yvette (S. and O.), France
294. M. P. Fewell, Australian National University, Canberra, 2600 Australia
295. G. N. Flerov, Laboratory for Nuclear Reactions, Dubna Joint Institute for Nuclear Research, Dubna, Moscow Oblast, U.S.S.R.

296. J. D. Fox, Department of Physics, Florida State University, Tallahassee, Florida 32306
297-306. GLCA-ORS, Attention: R. R. Winters, Denison University, Granville, Ohio 43023
307. H. E. Gove, Nuclear Structure Laboratory, University of Rochester, Bldg. 510A, Rochester, New York 14627
308. Walter Greiner, Institut fur Kernphysik der Johann Wolfgang Goethe Universitat, Frankfurt am Main, Federal Republic of Germany
309. H. Grunder, Lawrence Berkeley Laboratory, Berkeley, California 94720
310. M. Grypeos, University of Thessaloniki, Department of Theoretical Physics, Thessaloniki, Greece
311. J. H. Hamilton, Department of Physics, Vanderbilt University, Nashville, Tennessee 37203
312. K. Harada, Division of Physics, Japan Atomic Energy Research Institute, Tokai Research Institute, Postal Area Number 319-11, Tokai-mura, Naka-gun, Ibaraki-ken, Japan
313. J. S. Hattula, Department of Physics, University of Jyvaskyla, Seminaarinkatu 15, SF-40100 Jyvaskyla 10, Finland
314. R. L. Heath, Idaho National Engineering Laboratory, EG&G Idaho, Inc., P. O. Box 1625, Idaho Falls, Idaho 83401
315. H. R. McK. Hyder, Nuclear Physics Laboratory, Oxford University, Keble Road, Oxford OX1 3RH, England
316. Institute for Energy Analysis, P. O. Box 117, Oak Ridge, Tennessee 37830
317. Institute of Physics, High Energy and Nuclear Physics Library, C. Postal 20.516,0100 - Sao Paulo, S.P., Brasil
318. Beth Jinkerson, ORAU/UPD
319. R. Kamermans, Fysisch Laboratorium, Rijksuniversiteit Utrecht, P. O. Box 80.000, 3508 TA UTRECHT, The Netherlands
320. H. Kamitsubo, Head, Cyclotron Laboratory, Institute of Physical and Chemical Research, Wako-shi, Saitama, 351 Japan
321. D. G. Kamke, Ruhr-Universitat Bochum, Dynamitron Tandem Laboratory, Universitattstr, 150 Gibaunde NT, Postfach 1021 48, 4360 Bochum 1, Federal Republic of Germany
322. H. Kawakami, Institute for Nuclear Study, University of Tokyo, Midori-cho, Tokyo, Japan
323. P. K. Kloeppel, Associate Professor, Department of Physics, Monmouth College, Monmouth, Illinois 61462
324. M. Langevin, Institut de Physique Nucleaire, B. P. No. 1, 91406 Orsay Cedex, France
325. J. A. Lenhard, DOE-ORO, Federal Office Building, Oak Ridge, Tennessee 37830
326. Michel Letournel, Centre de Recherches Nucleaires, Service des Accelerateurs, B. P. 20 CRO, 67037 Strasbourg Cedex, France
327. Librarian, Atomic Energy Centre, P. O. Box No. 164, Ramna, Dacca, Bangladesh
328. Librarian, Chen Kin-hai, Institute of Modern Physics, Academia Sinica, P. O. Box 31, Lanzhou, People's Republic of China
329. Librarian, Cyclotron Laboratory, Michigan State University, East Lansing, Michigan 48824
330. Librarian, Cyclotron Laboratory, RIKEN (The Institute of Physical and Chemical Research), Wako-shi, Saitama 351, Japan
331. Librarian, Department of Physics, Georgia State University, Atlanta, Georgia 30303
332. Librarian, GANIL, B. P. No. 5027, 14004 Caen Cedex, France
333. Librarian, GSI, Postfach 11 05 41, 6100 Darmstadt, Federal Republic of Germany
334. Library of the Institute of Atomic Energy, Beijing, People's Republic of China
335. Librarian, MERT Division Library, Oak Ridge Associated Universities, P. O. Box 117, Oak Ridge, Tennessee 37831-0117
336. Librarian, Physics Department, 374 Bausch and Lomb Building, University of Rochester, Rochester, New York 14627
337. Librarian, Institut des Sciences Nucleaires, B. P. No. 257 - Centre de Tri, 38044 Grenoble Cedex, France
338. A. D. MacKellar, Department of Physics and Astronomy, University of Kentucky, Lexington, Kentucky 40506-0055
339. G. Madurga, Departameto de Fisica Atomica y Nuclear, Facultad de Ciencias, Universidad de Sevilla, Sevilla, Spain
340. Mario Mariscotti, Comision Nacional de Energia Atomica, Departmento de Fisica, Avenida del Libertador 8250, 1429 Buenos Aires, Argentina
341. Niels Marquardt, Institut fur Experimentalphysik III der Ruhr-Universitat Bochum, Postfach 102148 Gebaude NB/3, 4630 Bochum, Federal Republic of Germany
342. J. V. Martinez, Division of Chemical Sciences, Mail Stop J309 CTN, U.S. Department of Energy, Washington, D.C. 20545
343. W. R. McMurray, Deputy Chief Scientist, Kerninstituut Van Die Suidelike Universiteite, Southern Universities Nuclear Institute Republic of South Africa
344. G. K. Mehta, Professor of Physics, Van de Graaff Laboratory, Indian Institute of Technology Kanpur, Kanpur 208 016, India
345. A. Michaudon, Chef du Service de Physique Nucleaire, Commissariat a l Energie Atomique, Centre d'Etudes de Bruyeres le Chatel, P. O. Box 61, Montrouge 92120, France
346. R. Middleton, Department of Physics, University of Pennsylvania, Philadelphia, Pennsylvania 19104
347. E. Migneco, INFN Laboratorio Nazionale del Sud, Corso Italia 57, 95127 Catania, Italy

348. J. C. D. Milton, Physics Division, Atomic Energy of Canada Ltd., Chalk River, Canada KOJ 1J0
349. G. C. Morrison, Department of Physics, University of Birmingham, Birmingham B15 2TT, England
350. S. C. Mukherjee, Librarian, Saha Institute of Nuclear Physics, 92, Acharya Prafulla Chandra Road, Calcutta - 9, India
351. K. Nagatani, Institute for Nuclear Study, University of Tokyo, Tanashi, Tokyo, 188 Japan
352. Y. Nakamura, JPL, Systems Analysis Section, California Institute of Technology, 4800 Oak Grove Drive, Pasadena, California 91103
353. Ranier W. Novotny, University Giessen, II. Physical Institute, Heinrich-Buff-Ring 16, 6300 Giessen, Federal Republic of Germany
354. Masumi Oshima, Japan Atomic Energy Research Institute, Tokai Establishment, Tokai-mura, Naka-gun, Ibaraki-ken 319-11, Japan
355. Peter Paul, Department of Physics, S.U.N.Y. at Stony Brook, Stony Brook, New York 11794
356. Max Peisach, Southern Universities Nuclear Institute, P. O. Box 17, Faure, 7131, Republic of South Africa
357. Elliott S. Pierce, Assistant Director, Molecular Sciences, Department of Energy, Washington, D.C. 20545
358. A. A. Pilt, Tandem Accelerator Laboratory, McMaster University, Hamilton, Ontario, Canada L8S 4K1
359. R. E. Pollock, Department of Physics, Indiana University, Bloomington, Indiana 47405
360. B. Povh, Max Planck Institut fur Kernphysik, 69 Heidelberg, Saupfercheckweg, Postfach 1248, Federal Republic of Germany
361. James Purcell, Department of Physics, Georgia State University, Atlanta, Georgia 30303
362. Jacobo Rapaport, Department of Physics, Ohio University, Athens, Ohio 45701-0640
363. John Rasmussen, Lawrence Berkeley Laboratory, Building 70A, Berkeley, California 94720
364. Patrick Richard, Physics Department, Kansas State University, Manhattan, Kansas 66506
365. E. T. Ritter, Division of Nuclear Physics, ER 23, Mail Station J-309, U.S. Department of Energy, Washington, D.C. 20545
366. L. Rosen, Los Alamos National Laboratory, P. O. Box 1663, Los Alamos, New Mexico 87544
367. Ranier Santo, Sektion Physik der Universitat Munchen, 8046 Garching, Beschleuigerlaboratorium (Forschungsgelande), Federal Republic of Germany
368. D. G. Sarantites, Department of Chemistry, Washington University, St. Louis, Missouri 63130
369. V. Sarantseva, Head, Publishing Department, Joint Institute for Nuclear Research, Head Post Office, P. O. Box 79, Moscow, U.S.S.R.
370. J. P. Schiffer, Physics Division, Argonne National Laboratory, 9700 South Cass Avenue, Argonne, Illinois 60439
371. A. Schwarzschild, Brookhaven National Laboratory, Upton, New York 11973
372. Hermann Schweickert, Cyclotron Laboratory, Kernforschungszentrum Karlsruhe, Institut fur Applied Physik, P. O. Box 3640, D-7500 Karlsruhe 1, Federal Republic of Germany
373. S. Seki, Tandem Accelerator Center, University of Tsukuba, Ibaraki 305, Japan
374. J. C. C. Sharp, Information Officer, Daresbury Laboratory, Science Research Council, Daresbury, Warrington WA4 4AD, England
375. R. H. Siemssen, Kernfysisch Versneller Instituit der Rijksuniversiteit Zernikelaan 25, 9747 AA Groningen, The Netherlands
376. C. Signorini, INFN Laboratorio Nazionale di Legnaro, Via Romea 4, 35020 Legnaro-Padova, Italy
377. S. J. Skorka, Tandem Accelerator Laboratory, University of Munich, Munich, Federal Republic of Germany
378. Hsu Loke Soo, Department of Physics, Nanyang University, Singapore 22, Republic of Singapore
379. C. Speth, Institut fur Kernphysik, KFA, Julich, Postfach 1913, D-5170 Julich, Federal Republic of Germany
380. T. Springer, Institut Max von Laue - Paul Langevin, 156 X Centre de Tri, 38402 Grenoble Cedex, France
381. R. G. Stokstad, Lawrence Berkeley Laboratory, Bldg. 88, Berkeley, California 94720
382. T. T. Sugihara, College of Science, Oregon State University, Corvallis, Oregon 97331
383. Kazusuke Sugiyama, Department of Nuclear Engineering, Faculty of Engineering, Tohoku University, Sendai, Japan
384. Shigyea Tanaka, Japan Atomic Energy Research Institute, Tokai-mura, Ibaraki-ken, Japan
385. J. Teillac, Laboratoire de Physique Nucleaire d'Orsay, Facultes des Sciences, B. P. No. 1, Orsay (S. and O.), France
386. S. T. Thornton, Physics Department, University of Virginia, Charlottesville, Virginia 22901
387. T. A. Tombrello, Division of Physics and Astronomy, California Institute of Technology, 106-38, Pasadena, California 91125
388. P. J. Twin, Daresbury Nuclear Physics Laboratory, Daresbury, Nr. Warrington, Lancashire, England
389. J. P. Unik, Argonne National Laboratory, Building 200, Argonne, Illinois 60439
390. Robert Vandenbosch, Department of Chemistry, University of Washington, Seattle, Washington 98195
391. A. van der Woude, Kernfysisch Versneller Institut der Rijksuniversiteit, Universiteitscomplex Paddepoel, Groningen, The Netherlands
392. H. Verheul, Natuurkundig Laboratorium der Vrije Universiteit de Boelelaan 1081, Amsterdam, The Netherlands

393. VICKSI, Sekretariat, Hahn-Meitner Institut fur Kernforschung Berlin GmbH, Postfach 39 01 28, D-1000 Berlin 39, Federal Republic of Germany
394. W. von Oertzen, Hahn-Meitner Institut fur Kernforschung, Berlin GmbH, Federal Republic of Germany
395. George Vourvopoulos, Department of Physics, Western Kentucky University, Bowling Green, Kentucky 42101
396. A. H. Wapstra, Institute Voor Kernphysisch Onderzoek, Ooster Ringdijk 18, Amsterdam, The Netherlands
397. Harlan L. Watson, Deputy Staff Director, Subcommittee on Energy Development and Applications, Committee on Science and Technology, U.S. House of Representatives, B374 Rayburn House Office Building, Washington, D.C. 20515
398. H. E. Wegner, Department of Physics, 901A, Brookhaven National Laboratory, Upton, New York 11973
399. O. C. Weisser, Department of Nuclear Physics, Institute of Advanced Studies, The Australian National University, P. O. Box 4, Canberra ACT 2600, Australia
400. W. G. Weitkamp, Nuclear Physics Laboratory, G-10, University of Washington, Seattle, Washington 98195
401. Joseph Weneser, Department of Physics, Bldg. 510, Brookhaven National Laboratory, Upton, New York 11973
402. E. P. Wigner, Department of Physics, Princeton University, Princeton, New Jersey 08540
403. B. H. Wildenthal, Department of Physics, Drexel University, Philadelphia, Pennsylvania 19104
404. H. B. Willard, Program Director for Intermediate E ergy Physics, National Science Foundation, 1800 G Street NW, Washington, D.C. 20050
405. H. Yamada, School of Physics, The University of Melbourne, Parkville, Victoria, Australia 3052
406. Takashi Yamazaki, Research Center for Nuclear Physics, Osaka University (Suita Campus), Ibaraki, Osaka, 567 Japan
407. D. Youngblood, Cyclotron Institute, Texas A&M University, College Station, Texas 77940
408. Alexander Xenoulis, Van de Graaff Laboratory, Nuclear Research Center, Demokridos, Aghia Paraskevi Attikis, Athens, Greece
409. E. F. Zganjar, Department of Physics and Astronomy, Louisiana State University, Baton Rouge, Louisiana 70803
410. K. Ziegler, Hahn-Meitner Institut fur Kernforschung Berlin GmbH, Postfach 39 01 28, D-1000 Berlin 39, Federal Republic of Germany
411-506. Given distribution as shown in TID-4500 under Physics categor/ (25 copies - NTIS)